Universidade de Évora - Instituto de Investigação e Formação Avançada

Programa de Doutoramento em História

Tese de Doutoramento

"CALIPH: Comprehensive Archaeological and laboratory investigation of Islamic pottery in Portuguese History"

Massimo Beltrame

Orientador(es) | Fernando Branco Correia

Jose Mirao

Luís Jorge Gonçalves

Évora 2022

Universidade de Évora - Instituto de Investigação e Formação Avançada

Programa de Doutoramento em História

Tese de Doutoramento

"CALIPH: Comprehensive Archaeological and laboratory investigation of Islamic pottery in Portuguese History"

Massimo Beltrame

Orientador(es) | Fernando Branco Correia

Jose Mirao

Luís Jorge Gonçalves

Évora 2022

A tese de doutoramento foi objeto de apreciação e discussão pública pelo seguinte júri nomeado pelo Diretor do Instituto de Investigação e Formação Avançada:

Presidente	|	António José Candeias (Universidade de Évora)
Vogais	|	Elena Salinas (Universidad de Almeria) Jose Mirao (Universidade de Évora) (Orientador) João Pedro Botelho Veiga (Universidade Nova de Lisboa - Faculdade de Ciências e Tecnologias) Stefano Columbu (Universita Cagliari) Susana Gómez Martínez (Universidade de Évora)

Évora 2022

UNIVERSIDADE DE ÉVORA
INSTITUTO DE INVESTIGAÇÃO
E FORMAÇÃO AVANÇADA

Contactos:

Universidade de Évora

Instituto de Investigação e Formação Avançada - IIFA

Palácio do Vimioso | Largo Marquês de Marialva, Apart. 94

7002-554 Évora | Portugal

Tel: (+351) 266 706 581

Acknowledgments

This thesis is the result of a long, hard and challenging work, and the credits are not just mine because many people helped me. One in particular was always very close to me, and she was always there when I needed. I will not dwell on too long acknowledgements, as they would not be sincere; a page or two will be more than enough.

This Ph. D. thesis is dedicated to my new family, to Ginevra and Amália. The past few months spent in these pandemic times have been very hard, but nevertheless I do not regret all the sleepless nights nor the terrible headaches. Ginevra has been a wonderful partner in this journey, and many more adventures with our baby girl are still to come.

No academic research would be successful without fundings and trust. Thus, I want to collectively thank the "Triad", namely Prof. José Mirão, Prof. António Candeias (who helped me find the most appropriate title for my thesis), and Prof. Cristina Dias. They warmly welcomed me in Hércules Laboratory in March 2014 and made this research begin.

A special thanks goes to Prof. Felipe Themudo Barata, for all his support and mostly for funding my research project through the Ph. D. scholarship of the UNESCO Chair in Intangible Cultural Heritage of the University of Évora.

I wish to also thank Prof. José Mirão for the "second time". He always helped and financially supported me by including me in many projects, to which I often gave just a minor contribution. I must be honest. His observations to my work have always been important, though very long awaited; this may be due to his background, as geologists are used to thinking in "millions of years".

I would then like to thank Prof. Luís Jorge Gonçalves, who has always proven to be available and interested in my project, despite me being sometimes a bit too absent.

Nothing about this work could have been done without the ceramics. Therefore, I would like to warmly thank Susana Goméz Martínez – nowadays Professor at the University of Évora – and all the colleagues of the "CIGA" group, who gave me access to all the Islamic ceramics that I wished to work on, many of which I still wish and have to study.

I also want to thank Marco Liberato and Prof. Ana Margarida Arruda, who provided me with the "*scalabitane*" ceramics. Thanks to them, it has been possible to carry on an exhaustive work on the medieval ceramics of Santarém.

The Sardinian experience. I cannot forget to thank Prof. Columbu Stefano, Stefano Noli and most of all Fabio Sitzia, who helped me during my mobility period at University of Cagliari. Fabio, in particular, has been a true colleague and friend.

Finally, I am grateful to all those friends and colleagues who helped and supported me throughout this journey; among them, Carlo Bottaini, Lorenzo Bottaini, Mattia Bottaini, Marianna Sautariello, Egidio Marino, Prof. Nicola Schiavon, Prof. Patrícia Moita, Sara Valadas, Luis Dias, Sandra Velez, Pedro Barrulas, Carla Lisci, Catarina Miguel, Luis Almeida, Mafalda Costa, Ana Cardoso, Nuno Carriço, Anne-France Maurer, Ian White, Lucia White, Patricia Branco, Sergio Moleta, Jorge Farias, Rui Bordalo, Sergio Martins, Marina Gonzales, Mara Silva, Miriam Pressato, Sriradha Bhattacharya, Penka Girginova e Rebecca MacRoberts, Marlon Pazan and Nicasio Jiménez.

Massimo

Abstract

In this PhD thesis Islamic ceramics characteristics (i.e. ceramic paste and decoration) and provenance from Santarém (Portugal)were considered to understand how the "Portuguese *Reconquista*" (12th century) affected ceramics craftsmanship. A set of possible raw materials and ceramic wastes were included in the study. Middle ages ceramics from Santarém have also been compared with traditional ceramics produced at Muge (15 -20 Km far from Santarém) to evaluate if similar technological criteria were employed. To compare Islamic ceramics productions in a different city, several ceramics and kiln rods from Mértola were selected. The methodological protocol involved firing experiment and petrographic, mineralogic, chemical, micro-structural, physical and mechanical tests, both on ceramics and raw materials.

During the Islamic period imported ceramics with lime ceramic body could be present at Santarém. White painted, red painted, monochromatic, honey and black and partial/total *corda seca* glazed ceramics were produced at Santarém during the Islamic period. At least, two different local raw materials were utilized to produce decorated and not decorated ceramics. The same raw materials have been exploited uninterruptedly until the 15th-16th century. Moreover, results evidenced that the Portuguese Reconquista did not affect ceramic technology, and ceramics were produced following specific functional chriteria in all period, still valid nowadays for the production of traditional ceramics.

At Mértola, some green and brown, partial *corda seca* and honey and black glazed ceramics were locally produced. The analyses evidenced the extensive use of bone (or bone ashes), glass/frit and limestone fragments in local ceramic bodies. Similar characteristics were also observed in some imported samples. Moreover, bones (or bone ashes) were also utilized to opacify some glazed decorations, as it happens in Byzantine mosaic tiles and some Islamic glasses. In all cases, a technological transfer from the Middle East is suggested.

Caliph: Estudo arqueológico e laboratorial da cerâmica Islâmica na história Portuguesa

Resumo

A presente tese centra-se no estudo das cerâmicas Islâmica de Santarém (Portugal), com o objetivo de compreender como a "Reconquista" (século XII) afetou a sua produção. Um conjunto de possíveis matérias-primas e de cerâmica recuperada em contexto de produção foram também incluídas no estudo. As cerâmicas Medievais de Santarém foram ainda comparadas com as cerâmicas tradicionais produzidas em Muge (15 -20 Km de Santarém), para se perceber se foi utilizada uma tecnologia de produção semelhante. Além disso, a fim de se comparar com a produção de uma cidade Islâmica diferente, foram selecionadas várias cerâmicas e de Mértola.

O protocolo experimental envolveu ensaios petrográficos, mineralógicos, químicos, microestruturais, físicos e mecânicos, além de experiências de cozimento.

Durante o período Islâmico, cerâmicas importadas com pasta cerâmica enriquecida em cálcio estão presentes em Santarém. Durante o mesmo período, na cidade produziam-se cerâmicas pintadas a branco, vermelho, vidradas monocromáticas, a melado e manganês e a corda seca parcial e total. Duas matérias-primas diferentes de origem local foram utilizadas para produzir cerâmica decorada, e não decorada. Os mesmos recursos naturais foram utilizados até oo século XV-XVI.

Além disso, os resultados evidenciaram que a Reconquista Portuguesa não afetou a produção cerâmica local durante diversos os período históricos, e que os mesmos critérios são utilizados atualmente na produção de cerâmicas tradicionais.

Em Mértola, produziam-se cerâmicas decorada a verde e manganês, corda seca parcial e melado e manganês, sendo também documentadas cerâmicas importadas. As análises evidenciaram o extensivo uso de osso/cinza de osso, vidro/*frita* e fragmentos de calcário na produção da cerâmica vidrada local. Características semelhantes também foram identificadas em algumas amostras de cerâmicas importadas. Ossos/cinzas de ossos foram utilizados para opacificar alguns vidrados, de acordo com uma tecnologia utilizada em mosaicos Bizantinos e alguns vidros Islâmicos. Em todos os casos, é sugerida uma transferência tecnológica do Oriente Médio.

General Index

Abbreviations

LTCB: Lower Tagus Cenozoic Basin

GMC: "*verde e manganês/verde y morado*" or green and black glazed ceramics

CSP: Partial corda seca glazed ceramic

CST: Total corda seca glazed ceramic

PLM: Polarized light microscopy

CGW: Coptic glaze ware

YGF: Yellow glaze family

OM: Optical microscopy

XRF: X-Ray Fluorescence spectroscopy

ICP-MS: Inductively coupled plasma mass spectrometry

FT-IR: Fourier-transform infrared spectroscopy

µRaman: Micro Raman spectroscopy

XRD: X-Ray diffraction

XRPD: X-Ray powder diffraction

µXRD: Micro X-Ray diffraction

km: Kilometre

m: Meter

cm: Centimetre

µm: Microns

URM: Untreated raw material

ASTM: American Society for Testing and Materials

m_D: Dry mass

V_R: Real volume

V_S: Solid volume

m_W: Wet solid mass

V_B: Bulk volume

m_{HY}: Hydrostatic mass

ρ_{TWX}: Water density

$\Phi_O H_2O$ (%): Open porosity to water

$\Phi_O He$ (%): Open porosity to helium

$\Phi_C He$ (%): Closed porosity to helum

Φ_T (%): Total porosity

ρ_B: Bulk density

ρ_R: Real density

ρ_S: Solid density

$IC_W(\%)$: Weight imbibition coefficient

$SI(\%)$: Saturation index

HeP: Helium pycnometry

PL: Point load

PRM: Permeability test

Is: Not normalized point load strength index

Is_{50}: Normalized point load strength index

P: failure point (N)

D_e^2: Equivalent core diameter

A: Minimum cross-sectional area through the platen contact points

W: Medium value for W_1 and W_2

Perm: Water vapour permeability

Perm norm: Thickness normalized water vapour permeability

REE: Rare earth element

REE_{CN}: Chondrite normalized rare earth element

$\sum LREE_{CN}$: Sum of chondrite normalized light rare earth element

$\sum MREE_{CN}$: Sum of chondrite normalized meddle rare earth element

$\sum HREE_{CN}$: Sum of chondrite normalized high rare earth element

IPB: Iberian Pyrite Belt

SPZ: Southern Portuguese Zone

VSC: Vulcano Sedimentary Complex

PQ: Phyllite-Quartzite Group

BH: *Barranco do Homen* Formation

Fr: *Freixial* Formation

βTCP: β-Tricalcium phosphate

GYA: Greish-yellowis anhedral inclusion

SE: Secondary electrons

BSE: Back scattered electron

List of Figure

List of Tables

List of Annexes

1. Introduction

Caliph: Comprehensive archaeological and laboratory investigation of Islamic pottery in Portuguese History

This section describes the structure of the PhD thesis

The present PhD thesis presents an ***Archaeological Science*** approach to ***History*** and several scientific techniques and methodologies have been applied to understand *Islamic Pottery in Portuguese History*. Archaeological Sciences have greatly influenced history, archaeology and anthropology in the last decades. Thanks to this approach, it is now possible to extract significant additional data from an artefact using different and complementary natural sciences methods. Besides, the integrated data interpretation combined with the historical, archaeological, and anthropological background has the potential to ***improve our understanding of the past***.

This dissertation aims to determine the characteristics of Islamic ceramic production in the city of Santarém (Portugal), identify the main commercial routes to import and export ceramics and show how the two previous issues have been affected by the "Portuguese *Reconquista*". Consequently, ceramics (decorated and undecorated) from different archaeological sites and with different chronology (Islamic, post-Islamic and with Christian-Portuguese characteristics) were considered in this research. Moreover, to evaluate Islamic pottery characteristics geographically, ceramic samples from the city of Mértola were also selected for analysis. Five more chapters has been put together in the PhD thesis.

Chapter 2, ***"Goals and objectives"***, describes the general goals of the dissertation as well as the subsidiary objectives.

Chapter 3, ***"Research context"***, contains three different sections. The first one (3.1), *"The city of Santarém and its context"*, describes the area from the natural and the historic-archaeological point of view. It is further divided into two different sub-sections. The 3.1.1 is entitled *"Geomorphological and geological description"*. The geomorphology and geology of Santarém and Muge areas are described with the aid of topographic and geological maps. The data from this subsection were essential in the development of the thesis, to evaluate and discuss ceramic provenance and for raw material sampling. The geological description of the area of Mértola was only inserted in the result section (i.e. section 5.4) of the thesis, to improuve the compression and reading of the manuscript. The 3.1.2 subsection is entitled *"Historical background"*, and it gives some generic, but essential, information regarding the historical context during the Late Antiquity-Early Middle Ages around the Mediterranean Sea. Subsequently subsection 3.1.2 has been further subdivided into two different parts. The first one (3.1.2.1) entitled *"Location and functions of the city of Santarém during the Islamic occupation"* describes the importance of the city during the Islamic domination. The second one (3.1.2.2) entitled *"The City of Santarém from the Islamic domination (8th century) to the Portuguese Kingdom (16th century)"* describes the historical context of the city between the

beginning of the Islamic domination, 8th century, and the 16th century. The second section (3.2), *"Archaeology and Archaeological Science of Islamic ceramics"*, is a synthesis of the most significant publications regarding archaeological and archeometric study of Islamic ceramics in the *al-Andalus,* with a special attention for the *Garb al-Andalus*.

Section 3.2 is subdivided into 4 sub-sections which summarize the rise of the Islamic glazed ceramic in the Middle East and the technological transfer to the *al-Andalus* (3.2.1), the most significant archaeological and archaeometric information for the Emiral period (3.2.1), the Caliphal and *Taifa* Kingdoms periods (3.2.2) and finally *the African period: Almoravid and Almohad* (3.2.3).

Chapter 4, ***"Methodology"***, defines ceramics and raw materials selection criteria and the work methodology. In total, four different ceramic assemblages and eleven different raw materials have been studied. They have been organized into 4 different scientific contributions. A multi-analytical approach was always used in the material characterization of the artefacts, but different chemical, physical or mechanical tests methods could be integrated. At the beginning of the chapter, a table will synthesize the experimental protocol developed for every contribution. The chapter is further divided into ten different sections which describe raw materials and ceramic sampling strategy and the principles of *granulometric analysis, polarized light microscopy (PLM), X-Ray diffraction (XRD), chemical analysis (XRF, ICP-MS), Raman spectroscopy, FT-IR spectroscopy, micro-chemical/morphological microscopy (SEM-EDS) and physical/mechanical tests*. In every section, when needed, the general principles of every method and the experimental condition are briefly described.

Chapter 5, ***"Results"***, is the central part of the PhD thesis. In this chapter, all results, different goals and objectives are presented and discussed. The chapter is subdivided into four different sections:

5.1 The Islamic ceramics of the Santarém Alcaçova: Raw material technology and trades;

5.2 The Islamic and post-Islamic ceramics from Santarém: The continuity of ceramic technology in a transforming society;

5.3 Comparative pottery technology between the Medieval period and Modern time in the Santarém area;

5.4 Islamic glazed ceramic from Mértola, Southern Portugal: provenance and technology.

The sections are organized similarly. In the beginning, an abstract briefly describes the most important information contained in the topic. This initial unit is followed by the

archaeological questions, the goals, archaeological material presentation, results and discussion and by a final remarks section. The experimental protocol is not included in the topic, as it is described in chapter 3. In the case of section 5.4, it is also included the geological description of the area of Mértola.

Chapter 6, **"Conclusions"**, discuss the general output of the thesis and future perspectives in the field of the Islamic ceramic studies in the *Garb al-Andalus*.

After chapter 6, the bibliographic references and annexes can be consulted.

2 Goals

Caliph: Comprehensive archaeological and laboratory investigation of Islamic Pottery in Portuguese History

This chapter describe the main goals of the thesis and the subsidiary objectives that will be accomplished.

This PhD thesis's main goal is to contribute to the understanding of ceramic production and the societies that manufacture and trade it in the *Garb al-Andalus* (Western Iberia during Islamic time). The relation of the population with the environment, namely with the raw-materials' availability, is especially important. The study uses archaeometric methods and it is focused on Medieval Islamic ceramic.

Two different variables are important: time and space. *Time,* because it is essential to evaluate the characteristics and evolution of utilitarian and decorated ceramic production during the Islamic period, and the influence of the "Portuguese *Reconquista*" on ceramic craftsmanship after the end of the Islamic domination of the *Garb al-Andalus*. Of course, it is impossible to develop this goal in a large territory. Thus, a specific city was chosen. *Space*, because it is important to compare decorated glazed ceramic from different Islamic cities to understand whether they were imported from a different Islamic territory, or locally produced.

The work is mainly dedicated to the Islamic ceramics of Santarém (Portugal). Their characteristics and provenance were considered to understand how the "Portuguese *Reconquista*", occurred in the middle of the 12th century, affected ceramics craftsmanship. Decorated and undecorated ceramics, from different archaeological sites and diverse chronologies (Islamic, post-Islamic and with Christian-Portuguese) were considered. The evaluation of the Islamic ceramics recovered at Mértola was utilized to compare *Islamic glazed ceramics* productions in a different city from Santarém. To achieve the main goal different periods of the history of Santarm were considered, and three subsidiary objectives have to be accomplished separately.

First of all, the ***Islamic pottery characteristics and provenance*** is examined. Santarém, since the beginning of the 8th century, was included in the *Garb al-Andalus* (Western Iberia during Islamic time), and it was an important political, military and economic city, like Lisbon, Coimbra, Palmela, Silves, Mértola, Beja and Évora. These cities had river (Mondego, Tagus, Sado, Arade and Guadiana) ports and were indirectly connected to the Atlantic Ocean and the Mediterranean Sea. In contrast, Évora and Beja were a crossroad between the Iberian Peninsula inland and the Atlantic coast.

So, Santarém was connected to the most important Islamic cities in the *al-Andalus*. So, different kinds of goods could be imported and exported, including ceramics. In the last twenty-thirty years, several archaeological excavations were carried out in the city's historical centre, and different types of ceramics have been recovered, including undecorated and decorated ceramics. The recovering of different types of glazed ware, especially *corda seca* glazed ceramics, clearly suggested that they could be imported. So a group of ceramic fragments have

been further compared with nine local ***raw materials*** to recognise possible local produced and imported goods.

By the end of the 11th – first half of the 12th century, Santarém was in the northernmost border of the Islamic territory (*marca*), holding the "Tejo military line" against the Portuguese armies. In the middle of the 12th century (1147 AD), the fall of the city was a crucial step in the *Reconquista* of the Tagus valley by *D. Afonso Henriques,* the first King of Portugal. For this reason, special emphasis has also been given to the study of the ***continuity of ceramic production in a transforming society*** during a transition period, when the socio-political set-up of the city radically changed. Undecorated and decorated ceramics (including partial and total *corda seca* glazed ceramics) with a chronology comprised between the 8th-9th and the 15th-16th centuries were selected for analysis. The archaeological sites chosen were located in the historical centre of the city (*Rua 5 de Outubro, Rua João Afonso*) and on the Ribeira de Santarém (*Necropole de Santa Iria*), the riverine neighborhood. Selected ceramics have also been compared with ceramics wastes recovered inside different medieval ceramic kilns (Islamic and post-Islamic).

Moreover, Middle Ages utilitarian ceramics from Santarém (Islamic, Post-Islamic and Portugues-Christian – 11th/12th to 15th-16th century), recovered in the archaeological site *Rua 5 de Outubro,* were then compared with traditional utilitarian ceramics, produced in Muge (a small village located at 15 km from Santarém, in the Municipality of Salvaterra de Magos) by an elderly artisan called Mr. Domingos, using a holistic approach. Two different raw materials utilised by the artisan were considered for analysis. The objective is ***to understand, considering ceramic characteristics and function, whether similar technical principles were still followed since the Islamic period*** on ceramic production. The Islamic legacy is at the centre of the discussion. This topic was crucial for the UNESCO Chair in Intangible Heritage and Traditional Know-How: Linking Heritage objectives. Every year, fewer people choose pottery manufacturing as a profession, and the combined study of archaeological and traditional ceramics is a way to document and preserve local ceramic tradition.

Finally, to expand the geographic limits of this dissertation within the Islamic period, a group of ceramic samples from the city of Mértola have been selected and analysed. In this case, Mértola represented one of the most important river ports of the Islamic period of the southern *Garb al-Andalus*. The city was included in the Portuguese Kingdom only in 1238 AD, roughly one century after the fall of Santarém. Many papers have been published regarding its ceramics, in the last thirty years, by Claudio Torres and Susana Gómez Martínez. The study of its rich and diversified ceramic collection, which cover the whole Islamic domination, gave a fundamental

contribution to the Islamic ceramics studies in Portugal. Mértola was an important centre, connected to the Mediterranean Sea and the Atlantic Ocean thanks to its port, located on the Guadiana river bank. Moreover, the city markets distributed different kinds of products in a vast territory. But, it is not clear *if* ***decorated ceramics were locally produced and traded or imported and traded.*** In this case, a set of honey and black, green and black (*verde e manganês/verde y morado*) and partial *corda seca* glazed ceramics recovered in different archaeological sites of the city (*Alcaçova-Criptoportico*, *Alcaçova*, *Largo Vasco da Gama*, Castle, Castle hillside) have been analysed and compared with kiln bars and waste burnt ceramics recovered in two different production sites (*Rua Dr. Afonso Costa*, *Rua 25 de Abril*). Ceramics chronology spans from the 10th century to the beginning of the 13th century. The green and black glazed ceramics group is the most represented, and it offers the opportunity to evaluate the evolution of the technique over almost three centuries.

3. Research context

Caliph: Comprehensive archaeological and laboratory investigation of Islamic pottery in Portuguese History

The chapter describes the geomorphological and geological setting of the area of Santerém as well as the historical and archaeological context of the city with special emphasis to the Medieval period. Moreover, the chapter summarize the state of the art regarding the scientific investigation developed on Islamic ceramic in the ancient territories of the al-Andalus, and abroad, with special attention to Islamic ceramic technology.

3.1 The city of Santarém and its context

3.1.1 Geomorphological and Geological description

Santarém is a Portuguese city located in the western part of the Iberian Peninsula (Fig. 1). It is located at 75-80 km north-east of Lisbon, in central Portugal. The geomorphological and

Figure 1 Geographic position of Santarém and Muge in the Iberian Peninsula

geological description of the area also includes the small village of Muge (Municipality of Salvaterra de Magos), where traditional/modern ceramic was sampled. In the current administrative subdivision of the Portuguese territory, Santarém is the capital of the district which includes 21 different municipalities (Fig. 2), including Santarem itself and Salvaterra de Magos.

The district corresponds to a large fraction of the Portuguese Tagus sedimentary basin, establishing the transition between the coast and the inland. With the new administrative subdivision of the Portuguese territory, created in 1976, the district of Santarém substituted the early Portuguese Province called *Ribatejo*, with Santarém as capital, but with a slightly different extension. The name "*Ribatejo*" is still quite used nowadays in Portugal, and it is fixed in the memory of the inhabitants due to cultural and historical reasons, especially due to the Portuguese *Reconquista*.

The fall of Santarém under Portuguese control in the middle of the 12th century meant an important step forward for the conquest of Lisbon, the future capital of the Kingdom, which happened shortly after. The name *Ribatejo* can be divided into two different parts: *Riba* which

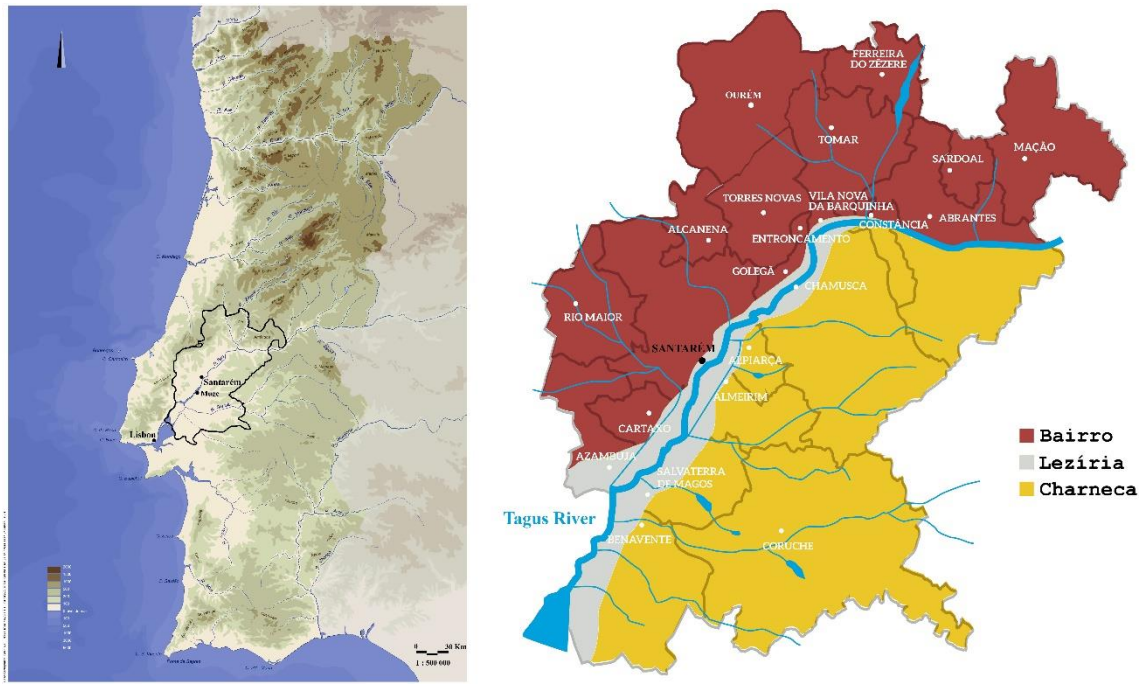

Figure 2 Geographical extension and altitudes representation of the district of Santarém in the Portuguese territory (left), and the geomorphological subdivision of the district territory basing on landscape characteristics (right).

means "margin or until", and *Tejo* (Tagus), which is the name of one of the most important rivers of the Iberian Peninsula. So, this is the land around Tagus River, which crosses most of the Iberian Peninsula from west to east, connecting the city to the Atlantic Ocean. Different geological events, the action of the river stream and of the man moulded this territory along thousands of years, and different landscapes/geomorphological characteristics are visible (from north-west to south-east), they are the *"Serra"*, the *"Bairro"*, the *"Lezíria"* and the *"Charneca"* (Fig. 2). In the northwestern part, the district is bordered by the Mounts (*Serra*) of *Aire* and *Candeeiros.* This represents the highest area of the municipality (350-400 m a.s.l.). In this territory, the natural vegetation, mainly composed of olive (*Olea europaea*) and oak (*Quercus faginea, Quercus ilex rotundifolia*) trees is predominant, but in some cases it is interrupted by natural spaces dedicated to agricultural activities or by stone queries (mostly limestone). Heading in the direction of the River Tagus, the *"Bairro"* represent the most extended area of the municipality. It is characterised by the presence of numerous hills, and the altitude progressively decreases, if compared to the *"Serra"*, being roughly comprised between 250 and 100 m a.s.l.. The vegetation is mainly composed by olive (*Olea europaea*), oak (*Quercus faginea*, *Quercus suber*) and pines (*Pinus pinea*, *Pinus pinaster*) trees which coexist with different farming activities for the production of wine and cereals. In this portion of the territory, just by the River Tagus, the city of Santarém stands on the top of a 100 m high plateau. It is a prime position (Fig. 3) over the flat fertile wetland region, the River Tagus valley, one of

Figure 3 View of the river Tagus from Santarém. The "Leziria" is visible on the river borders.

the nation's richest agricultural land. The *"Lezíria"* (Fig. 3) is mainly identified by a natural depression occupied by the River stream, the altitude is very low, between 7 and 10 m a.s.l.. It also includes the land portion usually flooded by the river in the past (Azevêdo et al., 2004). The *"Lezíria"* is mainly used for agriculture activities because of its fertility, in particular for wine, cereals and fruits production. The *"Charneca"* is an area with intermediate altitude, which progressively increase heading south-east from the "*Leziria"*, from 10-15 m to roughly 150 m a.s.l.. It occupies different municipalities and it also continues to different districts (e.g. Évora and Portalegre). In this area the vegetation can be quite dense, and it is highly exploited for the silviculture of pine (*Pinus pinaster*) and eucalyptus (*Eucalyptus spp*) trees which coexist with different agricultural activities.

From the geological point of view the district of Santarém is included in the Lower Tagus Cenozoic Basin (LTCB), and it constitutes the continuation of the oriental huge Upper Tagus Basin, cantered at Madrid (Pais et al., 2013; Cunha, 2019; Pais, 2004). The real extension of the LTCB is bigger than the district of Santarém. It is also included fractions of the districts of Castelo Branco, Portalegre, Lisbon and Setubal (just by the Atlantic Ocean). The filling of the basin started in the Cenozoic (Middle Eocene), thanks to the combination of several factors such as the erosion of proximal rocks, the evolution of the drainage system (endorheic to exorheic) of the river, climatic changes and different eustatic sea level during the Miocene (Cunha et al., 2005; Cunha, 2019). In the LTCB three different sectors have been distinguished. The Proximal, the Middle and the Distal sector. The Proximal sector is located on the north-eastern part of the

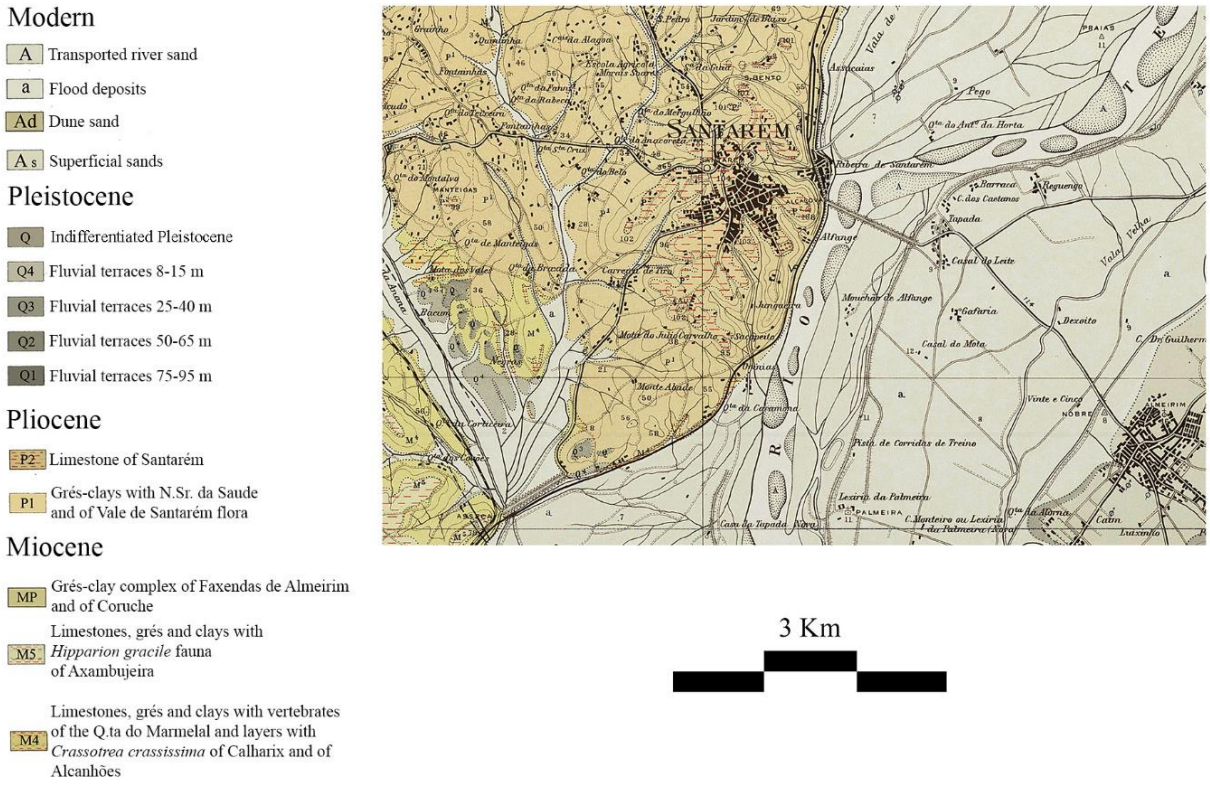

Figure 4 Adapted Geological map of the area of Santarém after Zbyszewsky (1953).

basin between the districts of Portalegre (*Alto Alentejo*) and Castelo Branco (*Beira Baixa*) and in Spanish territory. It only contains continental facies. In this area the valley is very narrow, and Cenozoic sediments overlay several igneous and metamorphic rock of the Hercynian massif, formed during the Variscan orogeny (Romão et al., 2013). They are mainly composed of slates and metagreywakes of the Beira Group (Pre-Cambrian - Lower Cambrian) and quartzites (Ordovician). Granitic rocks also appear in Nisa and Castelo Branco. This area is also known as the Uranium province of the *Alto Alentejo* (Neiva, 2003; Marques Prazeres, 2011). The proximal sector feed the western the oldest sedimentary deposits since the Palaeogene, which mainly filled the basement of the basin in every sector (Barbosa, 1995). Nevertheless, sediments transportation has never stopped. The Middle sector includes the district of Santarém (*Ribatejo*) and part of the district of Portalegre (*Alto Alentejo*), while the Distal sector includes the estuarine area of the river Tagus, the Lisbon area, close to the Atlantic Ocean. These two sectors are very similar, and the valley spread out but the distal sector is/was more affected by different tidal sea levels. Both of them were completely covered by different Miocene and Pliocene sedimentary deposits and, afterwards, by Pleistocene fluvial terraces. Since the later-middle Miocene the fluvial sedimentation is well represented and overlay the older Palaeogene deposits. The presence of oysters on similar sedimentary record in both sectors, suggest high eustatic sea levels. So, brackish water arrived roughly 130 km far from the present coast line

(Pais, 2004), in the proximity of Santarém. In the upper Miocene-Pliocene the sedimentary condition changed, and it favoured the formation of lacustrine limestone and calcareous deposits. In the middle sector Miocene and Pliocene sedimentary deposits are known as Almoster Formation and Tomar Formation. The combination of these two formations is called Almoster Aloformation (Pais et al., 2013). In figure 4, we present the geological map (adapted) of Santarém, and in figure 5 the stratigraphic column of Santarém and Muge obtained by the analysis of the respective geological maps (Zbyszewsky, 1953; Zbyszewsky and Da Viega Ferreira, 1968). Both places pertain to the middle sector of the Tagus basin. The city lays at the top of a small Pliocene plateau with a total thickness of 90 m located on the right margin of the river. The plateau can be subdivided into two different geological units (Zbyszewsky, 1953). The most recent (*P2 – Limestone of Santarém*), with a thickness of around 3-4 m, is made of grey limestone with gastropods followed by a layer of clayey material and a layer of marly-limestone. The oldest one (*P1*), with a total thickness of 80-85 m, is mainly composed by several interlayers (*C1* to *C8* to the top) of clay, claystone and sandstone (i.e. *grés*) enriched in micas and/or lime concretions (i.e. calcretes) and with a different fossil content. The interlayer *C2* can be enriched in kaolinite, and it was identified in several outcrops close to the railway line. The Miocene geological units outcrop at some kilometres from the city

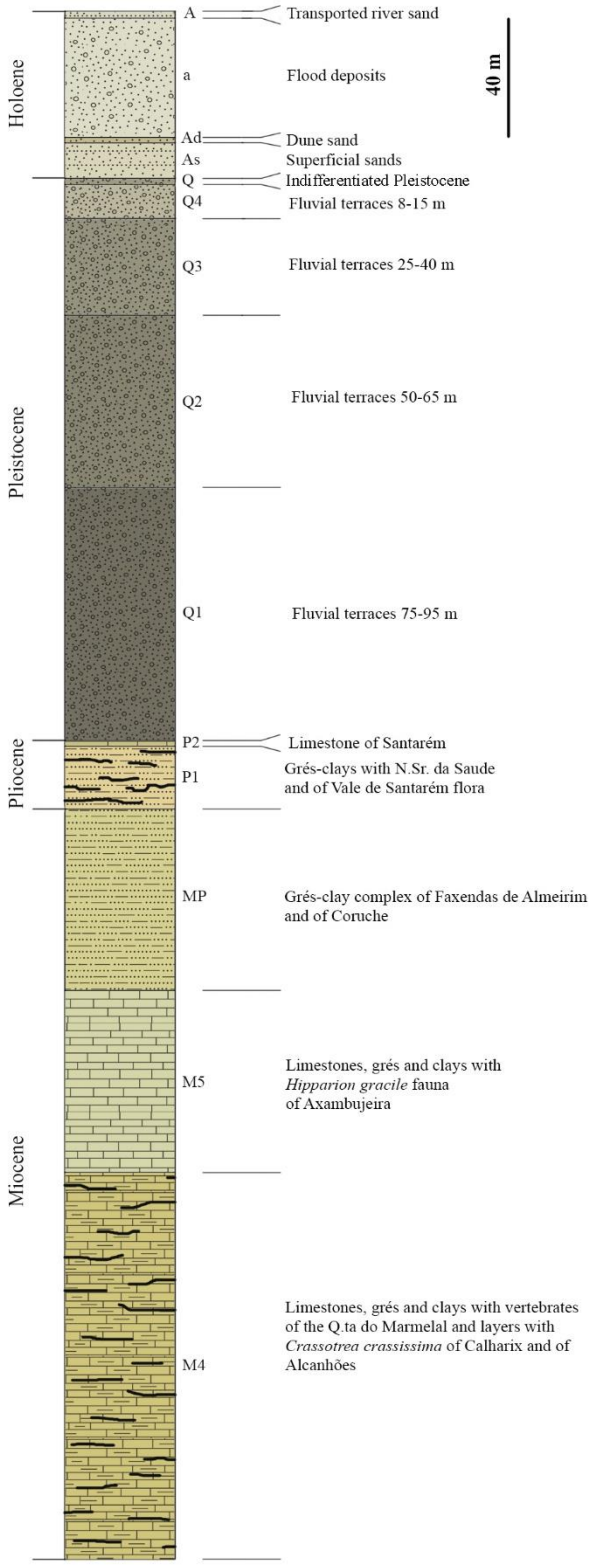

Figure 5 Stratigraphic column of the area of Santarém and Muge. Picture elaborated by Fabio Sitzia (Hercules Laboratory, UE)

(layers MP, M4, M5). They represent a succession of limestone, sandstone, and clay. The alluvial plain is located in front of the city (total width approximately 10 km), on the left side of the river. It is composed by modern deposits (*A, a, Ad, As*) and by Pleistocene alluvial terraces (*Q, Q1, Q2, Q3, Q4*). The area of Muge lay on the left margin of the river bank. The geology is very uniform (Zbyszewsky and Da Viega Ferreira, 1968) and composed by modern flooded deposits (*a*), superficial sands (*As*) and by different Pleistocene fluvial terraces (*Q2-Q3*), which outcrop at approximately at 4-5 km from the village. In the same area, some Miocene sedimentary deposits (*MP*) also outcrop.

3.1.2 Historical background

Before the description of the city of Santarém and its context it is important to give some generic but essential information regarding the historical context during the Late Antiquity-Early Middle Ages around the Mediterranean Sea.

Different historical events, wars and political instability led to an extensive modification of the socio-economic balances in the Mediterranean area. In these cases, ceramic material culture can be one of the most important indicators of these modifications. Besides, different researchers see long-distance shipping as an indicator of Mediterranean unity, and the intense study of ceramics evidence the trade and economic activity (Cameron, 2015).

By the last quarter of the 5th century, the Western Roman Empire reach at its end. Since the beginning of the 5th century the barbaric invasions, spread westward and southward mainly from central Europe. In 476 AD, *Odoacer* forced the deposition of the young emperor *Romulus Augustulus*, becoming the first King of Italy (Wickham, 2005). With the barbaric invasions, the Western Roman Empire was subsequently fragmented in many Kingdoms. In the Iberian Peninsula, the Visigoth replaced the Roman power until the beginning of the 8th century while the Vandals established their Kingdom for almost one century in the North of Africa (mostly in the present Tunisia, Algerian and Libyan coasts) including the Balearic Islands, and the islands of Sardinia, Corsica and part of Sicily (Wickham, 2005).

The Eastern Roman Empire (lately Byzantine Empire) did not disappear. Still, it faced several threats during the end of the 5th century and the 7th century, losing and recovering different territories in the Middle-East against the Sassanian Empire. Only *Justinian the I°* (or the Great) partially restored the ancient Roman rule, including part of Southern Iberian, and to control most of the Mediterranean area during the second half of the 6th century (Cameron, 2015). In the same century he also signed a peace treaty with the Sassanian Empire to guarantee peace and stability in the Middle East. Nevertheless, the Byzantine-Sassanian contraposition did never really stop, and at the beginning of the 7th century, Persians declared war to Byzantium again. The Byzantine Emperor *Heraclius* defeated the Persians in 628 AD, but both Kingdoms were very weak after almost three decades of war.

In the meantime, another dynasty was growing in the Arab Peninsula, the followers of *Muhammad*. He was a religious, political, and social reformer. *Muhammad* was the founder of the "Islam", and he united Arabia into a single Muslim polity unit based in the *Quran*, as well as his teachings and practices, forming the basis of Islamic religious belief. From the perspective of the Islamic faith, he was a God's Messenger (*rasūl Allāh*), a prophet, called to be a "warner,"

first to the Arabs and then to all humankind (Moussalli et al., 2016). He rapidly established his power all over the Arabian Peninsula, and he died in 632 AD. After the death of the prophet, two successive Caliphates, *Rashidun* and *Umayyad*, consistently increased the territory of the new Islamic Empire. At the end of the 7th century and the beginning of the 8th century the *Umayyad* Caliphate easily absorbed the powerful Sassanian Kingdom and it conquered most of the Byzantine lands. By the middle of the 8th century a new and powerful *Umayyad* Caliphate controlled all the former Sassanian/Persian territories, the former Roman provinces in the east, Arabia, Egypt, much of Anatolia (or Asia minor), the *Ifriqiya* (actual Tunisia), all the North of African Mediterranean coast including the Gibraltar strait and most of the Iberian Peninsula, or *al-Andalus* during the Islamic domination (Fig. 6).

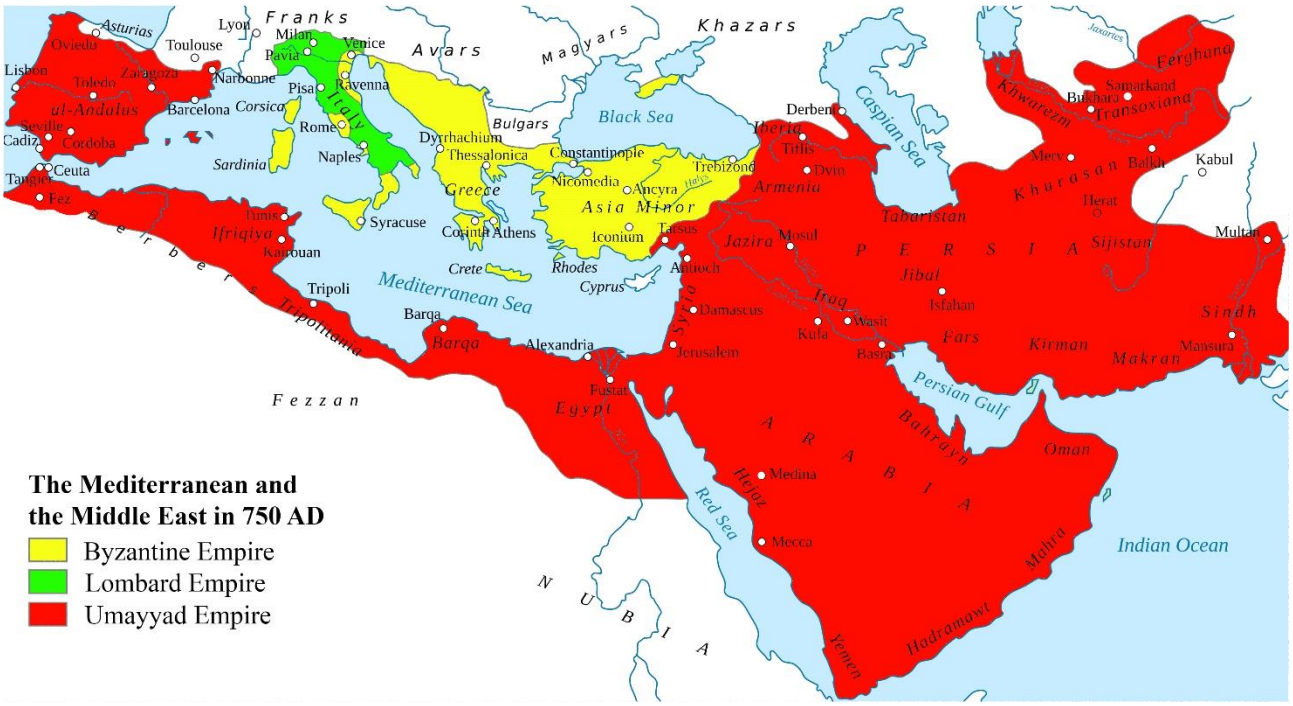

Figure 6 Geographic extension of the Umayyad Caliphate in the middle of the 7th century.

3.1.2.1 Location and functions of the city of Santarém during the Islamic occupation

The city of Santarém, also knew as *Scallabis* (Roman name) - *Sesserigo* (Visigoth name) – *Shantarīn* (Islamic name), was part of the *Garb al-Andalus*. Its geographical location was always considered strategic by its inhabitants or invaders. The most ancient traces of human occupation go back to the first millennium BC, and it is related to the Phoenician colonisation of the Tagus estuary (Arruda, 1993).

The ancient Islamic town, as the Roman one, settled into two different nuclei (Almeida, 2002). The first one is located at an elevated position compared to the alluvial plain (Fig. 7). It included the old Islamic Castle, the *Alcaçova*, the *Marvilla* plateau (*Alpran* during the Middle Ages), the *Madina*, and the area of the *San Francisco* Church. The visual control of the valley was assured from the *Alcaçova,* and the town could be easily protected from military attacks. The second one, just by the river Tagus[1], included the neighbourhoods of the *Ribeira of Santarém* and of the *Alfange*.

The bibliography described Santarém as a "peripheric" town of the *al-Andalus* (the Iberian Peninsula during Islamic time) especially from the city of Córdova, which was the capital of the Emirate and, after, of the Calipphate . Therefore the town was geographically far away from the most important political, cultural, social and religious centres of the *al-Andalus* (Fernandes, 2002). At the same time, the control of the town was strategic for historical, administrative, military, and commercial/economic reasons. The town was already a *conventus iuridicus* of the Roman Lusitania (Viegas, 2003), with capital in *Emerita Augusta* (Merida, Spain).

With the inclusion of most of the Iberian Peninsula under the Caliphate of Damascus (early 8th century), the new juridical and administrative subdivision of the territory reflected almost completely the one used by the Visigoth, inherited, from the Romans. Thus, the *al-Andalus* was subdivided into provinces, 6 in total, and subsequently divided in *Kuwar* (military districts, singular → *kura*). Santarém becomes a *kura* of the province of Merida, and until the end of the Caliphal period (beginning of the 11th century), it administrated a big territory (Catarino, 1999). The administration of the territory of the *kura* was strategic for the control of the *Gharb al-Andalus*[2]. The conquest of Santarém could guarantee easy access to an army to the whole Tagus valley (Fig. 7) and especially to the city of Lisbon.

[1] In this place, almost certainly was located the river harbour of the town, which worked as commercial hub and interface with the Atlantic Ocean (V. da Rocha Beirante, 1980; Almeida, 2002).

[2] The town was connected to many places both by river and/or by terrestrial routes (Mantas, 2002). Indeed, it was a crossroads for many terrestrial paths leading to different places such as Leiria (North-West), Braga (North),

Figure 7 View of the River Tagus from the Islamic Alcaçova of Santarém.

Nevertheless, during the first centuries of the Islamic domination, this territory was partially neglected by the central power (Branco, 2013), and it caused a generalised political instability during the Emiral period. Therefore, since the Caliphal period (10th century), the *alcaçova* and the *madina* underwent several and successive fortification phases to improve their defences against military attacks (Branco, 2010). The strengthening of the town also continued during the 11th century after the end of the *Taifa* kingdoms, and with the arrival in the *al-Andalus* of the new Berber dynasty from Medieval Morocco, the *Almoravids* (end of the 11th century – beginning of the 12th century). The bibliography also attests that the *alcaçova* was quite big compared to similar fortresses of the *Gharb al-Andalus*, and it could include many soldiers (Fernandes, 2002). After the inclusion of the town in the Portuguese Kingdom, the reinforcement of the *alcaçova* continued, and it was extended to the riverine area (Custodio, 2002). This testifies that the function of the town gradually changed, especially during the 11th and the 12th century when the Islamic and Christian ariems disputed Santarém.

The proximity to the river and of the alluvial valley were other factors that characterised Santarém. First, the river Tagus was navigable, and it was possible to easily rich Lisbon. So, the town was indirectly linked to the Atlantic coast and consequently opened to long-haul trades also from the Mediterranean basin as evidenced by Phoenicians and Romans archaeological evidence (Arruda, 2002a, Arruda, 2002b; Viegas et al., 2005). Secondly the Tagus valley have

Coimbra (North), Tomar (North-East), Merida (East) and Évora (South-East) mainly following ancient Romans paths.

been widely described on different Arabs agricultural treatises (Santos, 2011), and agriculture surelly was one of the most important economic activity of the area. The description of Santarém by *Al-Idrisi*[3] (Idrisi, 1866) an Arab geographer, underlines the importance of the town within the regional economic frame, being mainly the results of the cultivation of cereals, legumes, and fruits as evidenced by an archaeobotanical study published by Paula Fernanda Queiroz (2001).

[3] The Arab geographer also give a different description of the administrative subdivision of the territory. In this case Santarém was included in an administrative territory called "Balata ", which also included the areas of Lisbon and Sintra during the Almoravid period.

3.1.2.2 The city of Santarém during the Middle Ages

Since the beginning of the Islamic domination (8th century), the Iberian Peninsula was space to an uninterrupted opposition between two different powers/societies: The Christians, initially consigned to the North of the Peninsula and divided into different Kingdoms, and the Muslim in the Centre-South, which transformed most of the *al-Andalus* (Iberian Peninsula during the Islamic domination) in an Emirate of the Umayyad Caliphate from Damascus (Syria). From that moment onwards, Christians will fight for the *Reconquista* of the ancient Visigoth Kingdom of Toledo, as they considered themselves their legitimate heirs (Alves Conde, 2005). Nowadays, the term has a strong political and nationalist meaning, different from that of the Middle Ages (García Fitz, 2009; García Sanjuán, 2019; García Fitz, 2019).

The invasion of the Iberian Peninsula started at the beginning of the 8th century and matched a social and political crisis, within the Visigoth Kingdom for succession to power

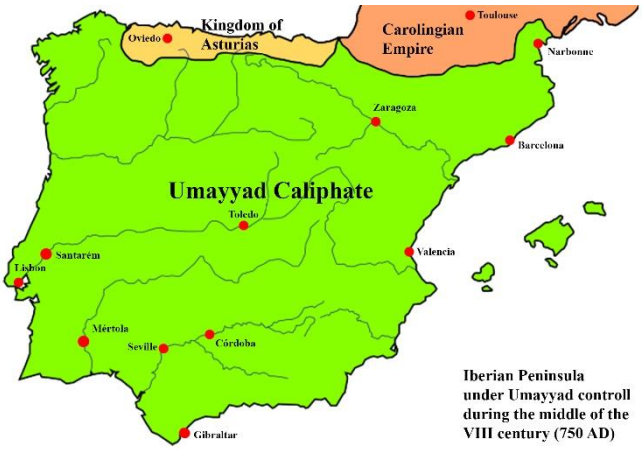

Figure 8 Extension of the territory under the control of the Umayyad Caliphate of Damascus in the middle of the 8th century.

(Catarino, 1995; Acién Almansa, 1984). The first exploratory mission occurred at the beginning of the 8th century, 710 AD, under the command of *Tarif Ibn Malluk* with approximatelly 500 men. In 711 AD the Emir of *Ifriqiya*, *Mūsà Ibn Nusayr*, order to its general *Tāriq ibn Ziyād,* to cross the Gibraltar Straits with its Berber army of roughly 12000 men and to start the conquest of the Iberian Peninsula. In the following year, in 712 AD, also *Mūsà Ibn Nusayr* disembarks with an army of 18000 Arabs. The conquest was almost concluded in 714 AD (Fig. 8), and Abd al-Aziz *Mūsà Ibn Nusayr* become the first governor of the *al-Andalus* (Catarino, 1995) with Seville as the provisional capital[4].

The town of Santarém, located in the *Garb al-Andalus*, peacefully agreed to its submission in the same year, maintaining several privileges such as its social, religious and

[4] The Capital of the Emirate will be moved to Córdova in the middle of the 8th century.

economic autonomy and paying taxes to the new ruling power (Catarino, 1995; Sidarus, 2007). As a result of this agreement, at least for the first's centuries of the Emiral period, the local population was composed by local Christians and, by some Arabs-Berbers (Sidarus, 1996; Gutiérrez Lloret, 2007). The assimilation of the Islamic culture as well as of the new political and economic structure by the local population led to the formation of a numerous *"moçárabe"* (Sidarus, 2007), Arabized Christians, and *"muladi"* (converted Christians) communities.

In the middle of the 8th century (750 AD), the *Umayyad* dynasty in Damascus crumbled, and it was substituted by the *Abassid* dynasty, which moved the capital of the empire first in Cufa (750-762 AD), and after to Bagdad (762 AD). *Abd al- Rahmân I*, the only survivor of the previous dynasty, escaped, and he disembarked in the Iberian Peninsula in 756 AD. In the same year, he declared himself Emir of the *al-Andalus,* and he moved the capital of the Emirate to Córdova. In the following century the Emirate, underwent a period of political instability. When it reached its end, it was followed by a short period of civil war (*fitna*).

The peace was re-established under *Abd al-Rahmân III* in 929; this was the beginning of the *Umayyad* Caliphate of Córdova. This was a period of prosperity and stability in the *al-Andalus* that allowed the formation of a homogeneous and autochthone Islamic cultural identity defined by some authors "*Andalusi*", which distinguished Iberian Muslim from foreign Arabs or Berbers (Sidarus, 1996). In Santarém, a mosque, a symbol of political and juridical power, was also built but without significant changes in the composition of the local population (Sidarus, 2007), confirming the cosmopolitan characteristics of this city during the Middle Ages.

When the dynasty crumbled during the first half of the 11th century, the political disgregation led to the creation of small independent "*Taifa*" kingdoms (Fig. 9), and Santarém

Figure 9 Subdivision of the al-Andalus during the Taifa Kingdom period following the end of the Caliphate of Córdova.

was included in the *Taifa* of Badajoz (1022). During the 11th century, after the fall of Coimbra (1064) and of Toledo (1085), thanks to *Fernando I* and *Afonso VI of León*, Santarém became the northernmost militarised border (*marca*) of the *Gharb al-Andalus*. By the end of the 11th century, the last king of the Badajoz *Taifa*, *Umar al-Mutawakkil*, could not fully control the territory. Following the continuous pressure from the north and the arrival to the Iberian Peninsula of a fanatic Berber dynasty from Morocco, the *Almoravid*[5], he sought protection from *Afonso VI* of *León* and delivered the cities of Santarém, Lisbon and Sintra to the Christian King of *León*. For the first time, after centuries, the Tagus valley became Christian again.

The conflict between Christianity and the Islam in the 12th century assumed a different religious connotation after the arrival in Iberian Peninsula of foreign fighters, under the protection and benediction of the Roman Church to support the Iberian crusade for the *Reconquista* (Garcia y Garcia, 2007): the Christians Military and Religious orders (Sidarus, 2007; Costa, 2005). They acted in favour of the Christians Kings, and won influence and properties, being responsible for the protection of the territory, for the construction of new castles, to favour the colonisation and the conversion of local populations to Christianism.

Nevertheless, the *Almoravids* took again the control of the Tagus valley defeating the Count *Raimundo* of Burgundy in Lisbon (1096 AD), and after a decade (1111 AD), Santarém was under Islamic control again. After the arrival of the new Berber dynasty, the local population of Santarém changed significantly, especially due to the installation of the *Almoravid* army, to protect the borders of the territory. Historical sources attested that due to religious intolerance and mistrust of the new Berbers against the local population, part of the local community decided to leave Santarém (Sidarus, 1996). From this moment onward the *Taifa* kingdoms disappeared completely, and the remains of the *al-Andalus* were included in the *Almoravid* African Empire.

After the loss of Lisbon, *Afonso VI* of *Leão* created the County of Portugal following the marriage of his daughter *Infanta D. Teresa* with *Henrique* of Burgundy. After *Henrique* death, his son, *D. Afonso Henriques*, took control of the County, moved definitely to Coimbra, and in 1139 AD, he declared himself King of Portugal (Barroca, 2003). With the aid of the Religious and Military order of Solomon's Temple, he control over the whole Tagus Valley in 1147 AD, including Lisbon and Santarém. In the subsequent years, another Berber dynasty, the *Almohad*, substituted the *Almoravid*. Still, they were never able to restore the ancient borders in the Tagus valley and especially to takeover it back. In the middle of the 13th century, *Afonso III*

[5] This was the beginning of the African Kingdom period.

concluded the Portuguese *Reconquista* and annexed the Algarve. Regarding the Tagus Valley and the city of Santarém, King *Afonso Henrique* and its successors favoured the settlement of Christian communities from the north and settled several Religious and Military orders (Solomon's Temple, Calatrava-Avis, Santiago, Hospital).

In 1179, Santarém received the "*Foral*", a Royal document that regulates the political, economic, fiscal, and social set up of the city, as well as the rights of the King. In this document, it was also granted protection to all the inhabitants, including the Islamic community. This suggests that they had an active and important role in the city of that time, just after the *Reconquista*. Nevertheless, during the 12th and 13th centuries, the structure of the society radically changed passing from urban, trading and tax-based society during the Islamic period to a rural, feudal and stratified society (Alves Conde, 2005) in the Portuguese Kingdom.

Between the end of the 12th and the 16th century, the city expanded, especially to the neighbourhood of the *Alfange* and *Sesserigo,* close to the river Tagus, becoming an important river arbour opened not only to the Mediterranean but also to the Atlantic Ocean (Casimiro et al., 2018; Liberato, 2016; V. da Rocha Beirante, 1980). From the social point of view, during the 13th century, the Islamic population lived freely in the city but with fewer rights than Christians. The historical sources attested that there were several marriages between Christians and Muslims in the 14th century and conversion to Christianism, suggesting a progressive assimilation of the Islamic population in the Christian society. Nevertheless, since the middle of the 15th century, the Muslims, as well as the Jewish, were segregated in a specific neighbourhood of the city (V. da Rocha Beirante, 1980).

3.2 Archaeology and Archaeological Science of Islamic ceramics

With the development of the modern Islamic archaeological research in the Iberian Peninsula (Zozaya, 1978; Rosselló-Bordoy, 1978; Rosselló-Bordoy, 1991; Rosselló-Bordoy, 2002a; Rosselló-Bordoy, 2002b; Retuerce Velasco and Zozaya, 1986; Retuerce Velasco and Zozaya, 1991) different types of decorated glazed wares have been recovered including monochromatic, painted, bichromatic and polychromatic glazed ceramic such as for example green and black glazed ceramics (GMC, *verde e manganês/verde y morado*), honey and black (HB), lustre[6] ceramics and *corda seca* glazed ceramics, partially (CSP) or totally (CST) covered by glaze. These almost unique ceramics are complemented with more common ones, as undecorated or painted pottery

In this framework, Islamic ceramics became one of the most studied archaeological evidence. Researchers with distinct academic backgrounds (Gómez Martínez, 2019 and references therein) widely addressed different archaeological questions about the typological/stylistical characteristics, decoration, production technology, distribution and commercialization.

Special attention has been paid to the interaction with the north of Africa (i.e. Maghreb), to understand the Islamization process during the firsts centuries of the Islamic domination of the Iberian Peninsula (Gutierrez Lloret, 2011; Alba Calzado and Gutierrez Lloret, 2008). The Middle-Near East, Syria, Egypt, Mesopotamia (Arabic Peninsula, modern Iraq), with similarities observed on some ceramic assemblages (Salinas and Zozaya, 2015), are essential to understand the technological transference, in the case of glaze and lustre technology (Mason and Tite, 1997; Tite et al., 2015; Matin et al., 2018; Ting and Taxel, 2020; Salinas et al., 2019a; Hill et al., 2004; Pradell et al., 2008; Gutierrez et al., 2010).

So, archaeologist and archaeological science scientist (using different tools) must understand the socio-economic setup, the cultural and technology development available to the societies that produced and used these ceramics. The stability of ceramic sherds in the soils and the constant increase of archaeological excavations, in the last twenty/thirty years, makes this material easily available for these studies. In this framework, archaeological sciences disciplines have been fundamental for archaeologist to determine ceramic provenance and to

[6] Islamic lustre ceramic and technology will not be treated in this thesis, because no samples have been considered for analysis. In any case it will be mentioned along the manuscript because it represented one of the most important and studied Islamic ceramic wares.

evaluate the production technology in different territories[7]. The collaboration between archaeologist and archaeological sciences specialists included the analysis of glazed decorations, of the ceramic pastes, or the study of wastes recovered within islamic ceramic workshops, including, for examples, fritting vessels, slags, frit, ceramic tools, kiln rods and ceramics (Salinas et al., 2019; Molera et al., 2009; Coll Conesa and García Porras, 2010; Molera et al., 1999a).

The firsts prototypes of high lead glaze ceramics were produced at Pechina (Almeria, Spain) and Córdova during the Emirate (Salinas et al., 2019b; Salinas et al., 2021) in the middle of the 9th century, although important recent developments indicate that lead ore was already utilized at the beginning of the Emirate, 8th-9th century, for glass production (Schibille et al., 2020). Conequently, the technology was already available.

Shortly after, by the end of the 9th century-beginning of the 10th century, tin ore started to be extensively used as opacifier to produce white glazes, and it could also be used on different glazed wares characteristics of Islamic *al-Andalus* (González García et al., 1992; Molera et al., 1999a; Coll et al., 1999; Perez-Arantegui et al., 1999; Roqué et al., 2008; Molera et al., 1998; Molera et al., 1999; Molera et al., 1997; Molera et al., 2001c; Molera et al., 1993; Vendrell-Saz et al., 2000; Di Febo et al., 2018; Molera et al., 2013; Molera et al., 2001b; Molera et al., 1996; Molera et al., 2018; Molera et al., 2001a; Roqué et al., 2008; Pradell et al., 2016; Pradell et al., 2012; Pradell et al., 2008a; Pradell et al., 2010; Pradell et al., 2013; Lapuente and Pérez-Arantegui, 1999; Pérez-Arantegui and Castillo, 2000; Pérez-Arantegui et al., 1999; Déléry, 2006; Salinas and Pradell, 2018; Salinas et al., 2019b; Salinas et al., 2019c; Garofano et al., 2015; Peréz-Arantegui et al., 2004; Valdés Fernandés, 1985; González García et al., 1992).

Unfortunately, the geographic distribution of these publications is mainly focused on ceramic samples recovered in Spain and few data are available in the case of Portugal, the *Garb al-Andalus* during Islamic times (Christine Henry, 2012; Karagiannopoulou, 2017; Chapoulie et al., 2005; Déléry, 2006; Ferreira et al., 2016).

By studying the ceramic paste, several researchers tried to identify ceramic provenance (*i.e.* the centres or the regions of production) and understand the commercial trade routes. These studies combined formal/stylistic ceramic analysis with different archaeometric techniques such as polarized light microscopy (PLM) and/or chemical (X-Ray Fluorescence -

[7] One of the first researchers that used natural scieneces approaches to study Islamic ceramic during the nineties stated (Berti and Mannoni, 1991): *"The recognition and precise definition of some ceramic techniques, also with the use of analytical methods, can be helpful for the differentiation of production areas and for the differentiation of diffusion routes"*.

XRF) and mineralogical (X-Ray diffraction - XRD) analyses. Ceramics from Spain, Portugal, Italy and the North of Africa with different chronology were analysed (Berti and Mannoni, 1995; Berti et al., 1986; Berti and Mannoni, 1991; Berti and Mannoni, 1997; Berti et al., 2009; Berti, 2010; Capelli et al., 2011; Bazzana and Picon, 1981; Louhichi and Picon, 1983; Picon and Navarro Palazon, 1986; Bazzana et al., 1986; Demians D'Archimbaud et al., 1986; Bazzana et al., 1986; Bonifay et al., 2002; Zozaya et al., 1995; Zozaya and Aparicio Yague, 2003; Gómez Martínez, 2003; Capelli et al., 2005; Bridgman, 2007; Bridgman et al., 2009; Albero Santacreu et al., 2019; Carvajal and Day, 2013; Carvajal López and Day, 2015; Carvajal López et al., 2018).

Unfortunatelly, the scientific research was discontinuos, and the low number of samples analysed was probably the main limitation of this approach. Moreover, in many *al-Andalus* workshops, ceramic was continuously produced since the end of the Emirate or the beginning of the Caliphate (Coll Conesa and García Porras, 2010), sometimes using slightly different raw materials in each location.

In any case, this approach gave some general but important results. Most of the decorated glazed wares, GMC, CSP, CST and lustre ceramics, were mainly produced in southern/south-eastern *al-Andalus*. Besides, in this area most of the ceramic kilns of the *al-Andalus* have been identified (Coll Conesa and García Porras, 2010).

In Portugal, a conspicuous number of Islamic ceramics have been analysed by a team of the Institute of Nuclear Technology (ITN). The analysis were mainly focused in ceramics from Lisbon, but some from Sintra, Santarém and Alcaçer do Sal ceramics were also studied (Prudêncio et al., 2006; Dias et al., 2001; Dias et al., 2009; Dias et al., 2008; L. Fernandes et al., 2015; Gomes et al., 2009). In these studies, it was possible to recognise local and imported ceramic productions, considering the ceramic paste chemical and mineralogical characteristics.

The utilitarian wares productions show chemical and mineralogical compositions compatible with the local raw materials, pointing to the use of local resources. In the *Garb al-Andalus*, just in Lisbon, the local production CSP and CST ceramics were also established since the 11th-12th century[8]. Islamic ceramics have also been analysed at the University of Évora and

[8] Corda seca glazed ceramic started to be produced in Lisbon during the *Taifa* Kingdom period and the production continued until the fall of the city under Christian control in the middle of the 12th century.

Aveiro in the framework of different Master thesis (Christine Henry, 2012; Markovic, 2016; Karagiannopoulou, 2017).

The historical, archaeological, and archaeological science contributions regarding the Islamic ceramics in the *al-Andalus* will be summarized[9] in the following sections. The presentation has been organized following the chronological-temporal subdivision typically applied in Middle Ages Islamic archaeology, in the Iberian Peninsula. The Emiral period (beginning of the 8th–10th centuries) will be followed by the Caliphal period (beginning of the 10th– beginning of the 11th century) the *Taifa* Kingdoms period (11th century), and by the African period (end of the 11th - middle of the 13th centuries), with the Almoravid and the Almohad Magrebine Caliphates. Some periods have been merged in the same chapter, like the Caliphal plus the *Taifa* Kingdom periods and the African occupation (*Almoravid* and *Almohad*) of the Peninsula.

These sections will be preceded by the description of the origin of Islamic glazed ceramic in the Middel East.

[9] It is not a major goal of this thesis to focus in the formal and stylistical diversity of Islamic ceramic in the *al-Andalus*. Just the most important aspects, and useful for the dissertation, have been revised and included.

3.2.1 Islamic glazed ceramic origin in the Middle East and the technological transfer to the al-Andalus

The historiography regarding the rising and development of Islamic glazed ceramic in the *al-Andalus* is constantly developing during the last twenty years. Several authors suggest that glazing technology was not an independent creative field, but it was probably linked to metal, and especially to glass expertise (Matin, 2019; Schibille et al., 2020).

Two different technologies were introduced in the *al-Andalus* during the Islamic period. The first one, and the most ancient, is the exploitation of lead ores and the introduction of lead technology to produce high-lead glazes in the middle of the 9th century (Salinas et al., 2019b; Salinas et al., 2021), during the Emiral period. The second one is the introduction of alkali metal oxides (i.e. Na_2O, K_2O) and tin oxide (SnO_2) in the production of lead-alkali tin opacified glazes (Vendrell-Saz et al., 2000; Molera et al., 2001; Molera et al., 2018; Salinas and Pradell, 2018; Salinas et al., 2019), by the end of the Emiral period or the beginning of the Caliphate, 9th-10th centuries[10].

Presently, it is generally supposed that lead glaze technology was introduced in the *al-Andalus* in the middle of the 9th century (Salinas et al., 2019b). Probably, the trade between the Southern Iberian cities (e.g. Pechina) and the territories of the *Aghlabid* Emirate in *Ifriqiya* (North of Africa) played a key role in the transmission of the knowledge (Acién Almansa and Martínez Madrid, 1989; Acién Almansa, 1993; Salinas, 2013). It is supposed that this region acted as an intermediary between Iberian Penisula and the *Abbasid* Caliphate of Bagdad (modern Iraq), where the Islamic glaze technology first developed. Nevertheless,none of the most recent theories completely explain the introduction of high-lead glezes in the Iberian Peninsula during the Islamic period (i.e. the introduction of lead technology).

The knowledge regarding the rising and development of glazed ceramics in the Islamic world has also been recently revisited (Watson, 2014). The most outstanding examples of Islamic ceramic, considering its beauty, decoration characteristics and production technology, were represented by the palatial "***Samarra* type pottery**".

In the paper *"Revisiting Samarra: the Rise of Islamic Glazed Pottery"*, Oliver Watson (Watson, 2014) argued that Islamic glazed ceramics did not blossom in Abbasid Iraq during the 9th century as a response to the Chinese imports (Hallett, 2011; Northedge, 2001; Wood et al.,

[10] The bibliography suggest that high lead silica glazes and lead-alkali tin opacified glazes were introduced in roughfly 50 years.

2007), as it is also suggested by the discovery of the Belitung Shipwreck[11] (Flecker, 2001). Actually, Chinese ceramics recovered in the remmants of Belitung reflects the commissioning to Chinese workshops by Middle-Eastern importers (Watson, 2014) for a market of glazed ceramics already produced in Egypt, in the Levant, and in Mesopotamia, since the 8th century.

Only in a second moment, during the 9th century, in *Abbasid* Iraq, a wide range of white tin-opacified glazed wares, known as "*Samarra* type pottery", started to be produced at Basra (Mason, 1995; Mason and Keall, 1991; Mason, 1991). These outstanding examples of Islamic ceramic, considering beauty, decoration characteristics and technology of production, were excavated in the city of Samarra (Iraq), before the first world war, and it was securely dated at the 9th century (Sarre, 1925). It included opaque white tin-glazed ceramics inspired, in shape and decoration, to Chinese importations of stoneware and porcelain (Mason and Tite, 1997).

The first examples of Islamic glazed ceramics initially appeared, in the territories of present Egypt and Syria, during the 8th century. They were characterized by the extensive utilization/application, amongst other, of an **opaque yellow glaze**. This ceramic ware substituted typical Roman fine ceramic tableware generally unglazed and covered by a gloss or slipped surface, making the object smooth, lustrous and impermeable, resembling a glaze cover.

They were produced in different places around the central and eastern Mediterranean until the 6th-7th century. African red slip ware (ARS) produced in Carthage, and Phocaean (also known as Late Roman C) red slip ware produced in Western Anatolia were the most diffuse all over the Mediterranean Basin (Wickham, 2005). The strong demand for fine tableware did not cease with the crisis of the Byzantine Empire and the blossom of the *Umayyad* Caliphate. Still, they were not anymore regularly distributed in former Roman provinces. Some authors suggested that ceramic workshops were probably destroyed by the firsts Arabs armies (Hayes, 1972) during the conquest of Byzantine territory in the Eastern Mediterranean area.

In this context, the strong demand for fine ceramics favoured the appearance of the first Islamic glazed ceramics. These ceramics usually appeared above late Roman-Byzantine archaeological sequences. The first type is the **Coptic Glazed Ware (CGW)**. It appeared first in Alexandria, Egypt, probably during the first half of the 8th century (Rodziewicz, 1976; Rodziewicz, 1983) and in many other Egyptian archaeological sites (Matin et al., 2018). A recent study also suggests an early chronology for the CGW, mainly centred in the second half of the 7th century (Ting and Taxel, 2020). Mainly dishes, partially covered by a glaze with two different decorative solutions were produced. Decorations could be painted underglaze in

[11] The Belitung shipwreck was excavated in 1998/9 off the Indonesian island of Belitung between Sumatra and Borneo.

brown or black, or were based in a combination of colourless, green, brown, opaque yellow or white broad glazed bands.

Afterwards, in the second half of the 8th century, CGW spread to Raqqa (Syria) and to many other archaeological sites in Syria (Matin et al., 2018), where the **Yellow Glaze Family (YGF)** ware developed (Watson, 1999). Bowls and dishes were normally decorated, but the use of a distinctive opaque yellow glaze, often with in-glazing green painting decorations was the most important characteristic of YGF. Opaque white glazed wares with green and/or brown decorations could also appear.

By the second half of the 8th century to the beginning of the IX (i.e. during the *Abbasid* Caliphate) YGF tradition spread to Mesopotamia. In the same period, the *Abbasid* moved the capital of the Caliphate from Damascus (Syria) to Bagdad (Iraq). The most significant archaeological evidences are represented by the **"Samarra type pottery"**. Ceramic typology and glaze characteristics could be very similar to YGF from Syria, but in addition they showed a different decoration: with cobalt blue painting in an opaque-white glaze or with luxury metallic lustre decorations (Watson, 2014).

These archaeological observations were also supported by further research. Data obtained by the archaeometric analysis of several glazed ceramic samples established a technological connection between CGW, YGF and Samarra type pottery (Tite et al. 2015; Matin et al. 2018; Matin, 2019; Ting and Taxel, 2020). CGW was first produced in Egypt. It was the result of the combination of different ceramic tradition such as the Egyptian red and white slip wares, the Coptic painted ware and the Byzantine high lead glaze tradition. If compared to the Byzantine glaze tradition, Egyptian potters had also introduced new glaze colours on CGW, in addition to copper and iron oxides colourant, namely manganese and tin-based pigments to obtain brown/black and opaque yellow/white glazes respectively (Ting and Taxel, 2020).

As opacifier, Islamic artisans employed different lead/tin compounds, prepared by the simultaneous calcination of lead and tin minerals (lead-tin calx) mixed in different ratios. In the case of lead-tin calx with $Pb/Sn<3.5$ the calcination produce a greyish powder composed of lead oxide (PbO), tin dioxide (SnO_2), with some tin oxide (SnO) and metallic lead and tin. The calx could then be mixed with silica, silica plus alkali, or a glassy preparation (i.e. frit) to produce white glazes[12] opacified by SnO_2 particles (Molera et al., 1999b; Vendrell-Saz et al., 2000).

[12] As evidenced by Matin et al. (2018) lead-tin calx with $Pb/Sn<3.5$ was normally utilized in the production of alkali-lead glazes from Samarra and Susa where the PbO concentration is rather low.

Otherwise, for lead-tin calx with Pb/Sn>3.5 the calcination would produce orthorhombic lead stannate (Pb_2SnO_4) in addition to lead oxide (PbO), tin dioxide (SnO_2) and some metallic lead and tin. The calx could then be mixed with silica, or silica plus alkalis, and heated at approximately 750-800 °C, to obtain lead-tin anime[13] (Moretti and Hreglich, 1984) or lead-tin alkali frit.

In the first case, the mixture was heated in the absence of alkalis, causing the crystalline conversion of orthorhombic lead stannate (Pb_2SnO_4) to cubic lead stannate [$Pb(SiSn)O_3$)] where some SiO_2-SnO_2 substitution occurred. Lead-tin anime could then be used to produce opaque yellow glazes or glasses. Heating the lead-tin anime at a temperature higher than 800 °C would cause the dissolution of cubic lead stannate [$Pb(SiSn)O_3$)], with the consequent precipitation of tin dioxide (SnO_2) and the colour conversion from opaque yellow to opaque white.

In the second case, if the original mixture was heated at approximately 750-800 °C in the presence of alkalis, orthorhombic lead stannate (Pb_2SnO_4) dissolved and tin oxide (SnO_2) would precipitate to produce high lead-alkali opaque white frit (Matin, 2019).

These two methods were used to produce of CGW and YGF wares (Tite et al., 2015; Matin et al., 2018). So, artisans had different options to obtain yellow and white glazes, using and mixing different ingredients. The complete control of the kiln temperature was essential, especially when preparing yellow glaze with lead-tin calx with Pb/Sn>3.5. Moreover, the introduction of alkalis, and especially the increase of the PbO/SnO_2 ratio, favoured the dissolution of lead stannate (Pb_2SnO_4) to tin oxide (SnO_2), responsible for the opaque white colour of the glaze (Molera et al., 1999b; Vendrell-Saz et al., 2000) and further reduced the maturing temperature of the glaze (Matin et al., 2018).

Afterwards, specialized craftsman exported these technologies from Egypt and Levant to Mesopotamia, for the production of opaque yellow glazed ceramics and, as referred, for the production of opaque white glazed ceramic (Mason and Tite, 1997; Matin et al., 2018), the "Samarra type" pottery, (Watson, 2014). In the followings decades, tin opacified white glaze technology migrated westward and it arrived in *al-Andalus,* by the end of the 9th century – beginning of the 10th century (Molera et al., 2018; Salinas and Pradell, 2018; Salinas and Pradell, 2020), being employed for the production of the so-called *"verde y morado / verde e manganês"* (i.e. green and brown) decorated glazed ceramic (Molera et al., 2001c).

[13] Anime was a specific material utilized by glass artisans in Venice to obtain and colour their glass transparent in the range of colours from lemon-yellow to brown. It was a glassy coloured material, prepared separately. The opaficfing and colouring constituents of anime are lead stannate and/or lead antimoniate.

In any case, this general model does not explain how lead glaze technology arrived in the Iberian Peninsula. Conversely, it explained how lead-alkali tin opacified white glazes were obtained and diffused, using exhaustive archaeological and archaeometric evidences. In this specific case, the difference in chronology between the first appearance of opaque white tin opacified glazed ceramic in Mesopotamia (9th century) and in the Iberian Peninsula (end of the 9th – beginning of the 10th century) support the model that the Abbasid world is the most probable source, at least for the technological transmission of white tin opacified white glazes to the Iberian Peninsula.

In the case of the high lead glazes, recently, a new research paper suggest an alternative (Schibille et al., 2020), for the introduction lead technology in the *al-Andalus*[14]. It was recently demonstrated that lead glaze technology was not introduced in the middle of the 9th century (Salinas et al., 2019b) for the production of glazed ceramics at Pechina (Spain). Actually, the analysis of glass samples recovered in the *Rabad of Šaqunda* (Córdova), dated between the middle of the 8th century and the first 20 years of the 9th century, have been directly linked to the exploitation of local raw materials.

The research established the development of two new glass technologies that used local lead slags from silver and lead mining. Slags were processed in the region around Córdova for the production of a low alkali high lead glasses ($47.5 < PbO\ wt\% < 55.8$), and (just one sample) of soda ash lead glass ($Na_2O = 7.63$ wt%, $PbO = 33.7$ wt%). Soda ash lead glasses continued to be produced during the *Umayyad* Caliphate in the *al-Andalus* (Duckworth et al., 2015; De Juan Ares and Schibille, 2017).

The authors justify these new innovations as the result of the demise of glass supplies from the Eastern Mediterranean area, probably following the *Abbasid* revolution, in the middle of the 8th century. Before this date, glass/raw glass chunk were normally imported from Egypt and Levant to the Visigothic Iberia between the 5th century and the end of the 7th – beginning of the 8th century (De Juan Ares et al., 2019; De Juan Ares et al., 2018).

So the glass samples of the *Rabad of Šaqunda* in Córdova represent the best example of an independent decentralized economic system, previously focused in the Eastern Mediterranean, which uses new raw materials and technologies that marked the emancipation of the *Umayyad* Iberia from the Middle East. Moreover, these are the oldest Islamic archaeological glasses discovered with these characteristics, within the Iberian Peninsula.

[14] See European project "Mapping the First Millennium Glass Economy (https://cordis.europa.eu/project/id/647315)

The closest match, in term of chemical composition with the glass samples of the *Rabad of Šaqunda*, have been encountered with high-lead glazed ceramic produced at Pechina (Almeria, Spain) and Córdova (Salinas et al., 2019; Salinas and Pradell, 2018), dated to the second half of the 9th century. Consequently, the archaeological and archaeometric discovery of the *Rabad of Šaqunda* might predates of about half a century the introduction of transparent high lead glaze ceramics in the Iberian Peninsula (Salinas et al., 2019; Salinas and Pradell, 2018; Molera et al., 2018). At this point, it can be argued that lead glaze technology developed independently, in the *al-Andalus,* from the Middle East.

Besides, a recent research developped on archaeoleogical findings from Córdova, established the technological connection and transfere between local glass and glaze ceramic expertise (Salinas et al., 2021), confirming that the production of high lead glaze ceramic in the *al-Andalus* was an authoctonous innovation.

Thus, it is now defenitly escluded the transmission of the knowledge from the territories of the *Aghlabid* Emirate in *Ifriqiya* (North of Africa) (Acién Almansa and Martínez Madrid, 1989; Acién Almansa, 1993; Salinas, 2013).

3.2.2 The Emiral period

The most ancient Islamic ceramic productions of the *al-Andalus* are from the Emiral period. In the *Garb al-Andalus,* Emiral ceramic is less known if compared with the more recent Islamic periods (Gómez Martínez et al., 2015). The main reason is the simplicity of these productions and of the low number of archaeological sites identified with this chronology. Ceramics were normally handmade, and with low-technology characteristics.

The transition period between the Late Antiquity (5th-7th century), the Visigoth period included, and the beginning of the Emirate (8th-9th century) is especially hard to study. This is the period of the Barbarian invasions of the Iberian Peninsula , of the end of the Western Roman Empire (476 AD) and of the creation of the Visigoth Kingdom, in the centre-south of the Iberian Peninsula (Acién Almansa, 1984). During this historical phase, the material culture is not evident, and some authors define it as the age of the "reuse" or call it the "invisible middle ages. On the Eastern Mediterranean, the Eastern Roman Empire (future Byzantine Empire) survived, with Constantinople (nowadays Istanbul, Turkey) as capital.

The decline of the Western Roman Empire during Late Antiquity was the result of a diffuse and internal political instability. This was amplified by the conquest of Northern Tunisia (*Ifriqiya*) and of Carthage by the Vandals (439 AD) and the consequent breakdown of the fiscal and economic-commercial system based on the "*annona*[15]*"* (Wickham, 2005). This led to the socio-economic instability and the consequent crisis of the 5th century, contributing to the end of Rome supremacy on the Western Mediterranean[16].Moreover, *Ifriqiya* was also an important centre of productions of fine ceramic like the African Red Slip ware (ARS), exported all over the Mediterranean basin (Watson, 2014), making this event very visible in the archaeological record.

The fiscal and economic-commercial disarticulation of the Western Roman Empire by the end of the Late Antiquity resulted in the commercial isolation of the Western Mediterranean area (Iberian Peninsula included) between the second half of the 5th century and the beginning of the 7th century. Different archaeological and archaeometrical evidences testify this. During the Visigoth period raw glass chunk and finished glass objects continued to be imported in the

[15] The term had a general meaning, that is, of supplies of grain collected in public granaries. Subsequently, due to the financial difficulties of the state it took the form of a tax in kind. This tax was owed by the major producing provinces, such as Africa and Egypt, and which were therefore called "*annonarie*" provinces. Moreover also the salaries of officials and soldiers began to be paid first in money and in kind, then mainly in kind and the term *annona*, especially in the expression "*annona militaris"*, came to mean the unit of wages of wheat used to pay salaries.

[16] These historic dynamics are well described and explained in the book "*Framing the Early Middle Ages*" (Wickham, 2005 - section four).

Iberian Peninsula from the east (De Juan Ares et al., 2019; De Juan Ares and Schibille, 2017), but not so much as during the Roman period. Moreover, the decrease of commercial exchanges within the western Mediterranean area is also corroborated by the disappearance, from the Iberian archaeological records, of typical North African late Roman ceramic productions (Bonifay, 2004; Alba Calzado and Gutiérrez Lloret, 2008), imported from *Ifriqiya*, in particular from the Túnez area, as food/liquid containers (amphoras) or kitchen ceramics.

North African ceramic productions are accurately dated at the source and well-characterized from the archaeometric point of view (Capelli and Bonifay, 2014; Capelli and Bonifay, 2007; Gragueb et al., 2011; Bonifay et al., 2002). The ceramic paste of these productions is distinguished by the presence of aeolian[17] grains of quartz as temper, easily found in regions close to the desert, especially in the North of Africa. Similar characteristics have also been noted on Islamic ceramics of the 10th-11th century (Capelli et al., 2011) from the same area[18]. Also, imports of Late Roman Phocaean ceramics from the far east Mediterranean area decreased considerably and/or completely stopped (Gómez Martínez, 2019).

The collapse of the commercial routes with central-southern Iberia resulted in a modification of the local economy in these reagions, now less focus on urban areas and on their markets, and converted on a rural economy with local-domestic interactions and a clear tendency to self-sufficiency (Alba Calzado and Gutierrez Lloret, 2008; Gómez Martínez, 2019). So, independent ceramic productions and local distribution pattern prevail and almost completely substituted the long-distance commercial routes and more advanced artefacts (Gómez Martínez, 2019). This transformation has been noted on the archaeological record and the ceramic collections of the 6th-7th century. Late Roman ceramic standardization and typological and functional diversification decreased or almost vanished.

Simple and everyday objects did not disappear, and they were constantly recovered within the ceramic archaeological record. Some objects have shown a noticeable continuity along time. Amongst them, several pots and pans (with many similarities with African kitchen ceramics), imitation of the of Roman Terra Sigillata bowls (also known as African Red Slip-ARS), or objects from the Roman-Visigoth tradition such as vases or two-handled bottles can be included (Gutiérrez Lloret, 2015a). This tendency was maintained during the early Islamic

[17] For the definition of aeolian quartz grain read the following publication (Thomas, 1987).

[18] The ceramic production from Tunisia and Algeria are well characterized. Many thin sections, from different archaeological sites, with a different chronology, have been prepared and analysed by PLM. So, the texture and mineralogical composition are well known and have been utilized by archaeologist and archaeological science researchers to evaluate the provenance of different Islamic ceramics in the Iberian Peninsula.

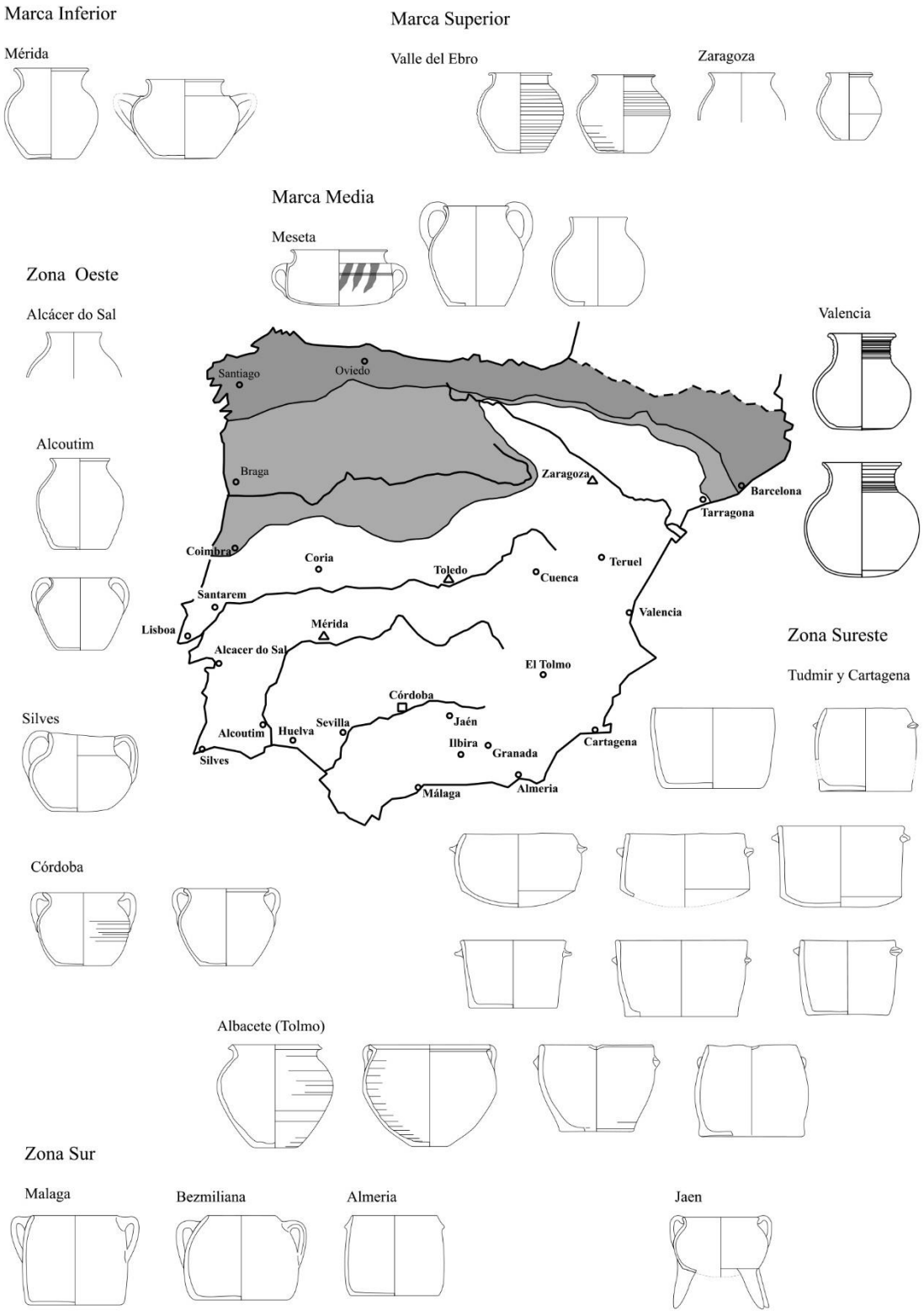

Figure 10 Examples of the geographic distribution fire ceramics (i.e. cooking pots), centuries 8th-9th, as a consequence of the formal evolution from visigoth prototypes, of the influence of the new emiral prototypes in different areas of the Iberian Peninsula (Alba Calzado and Gutiérrez Lloret, 2008).

periods in South eastern Iberia. This suggests that the first wave of Islamization did not correspond to a radical change in the habits of the local population.

The first episodes of Islamic ceramic production was particularly clear on cooking pots, as evidenced by the archaeological and archaeometric investigation developed in Granada (Vega de Granada). In this case, the authors combine ceramic typology and Polarizing Light Microscopy (PLM) to study this specific ceramic ware (Carvajal and Day, 2013) and discuss the early Islamization of the area. During this period (7th-9th centuries) the diffusion of handmade ceramics was significant, being greater in rural areas than in to urban ones (Gómez Martínez, 2019), where the utilization of the potter wheel was still significant.

The typological study of cooking pots from the 6th and the 9th century also revealed a strong regional diversification among different parts of the Peninsula (Alba Calzado and Gutiérrez Lloret, 2008). On South eastern Iberia (Fig. 10), handmade cooking pots have a flat base, cylindric body and horizontal handles (Alba Calzado and Gutiérrez Lloret, 2008). They are very common in archaeological contexts since the Late Antiquity (6th century) until post-Caliphal (11th century) archaeological contexts. Similar ceramic productions, with comparable chronology, were also identified in North Africa related to the late Roman-Byzantine archaeological record (Gutiérrez Lloret, 2011), suggesting that these ceramics probably developed from a common pottery tradition with its origins in the Late Antiquity.

On the contrary, in Western Iberia (including the *Garb al-Andalus*) and northern territories, this kind of cooking pot is not so common, probably because the ceramics developped from a different tradition, most likely Visigoth (Alba Calzado and Gutiérrez Lloret,

Figure 11 Cooking pot from Santarém - Emiral period (Liberato and Santos, 2018). *Picture and drawing by Marco Liberato*

2008). The most widespread cooking pot has an "S profile" (Fig. 11), which is mainly prevalent in rural settlements between the 6th and the 8th century (Gómez Martínez et al., 2015).

Since the beginning/middle of the 9th century, the most important urban centres started to recover importance. They became more active, and new technological solution and object were introduced in the ceramic repertoire of the *al-Andalus*. The archaeological site of Pechina (Almeria, Spain) is the best example. Formal similarities of Iberian wares with ceramics from the Middle East regions were also recently observed (Salinas and Zozaya, 2015), suggesting that commercial contacts with different territories returned to be safe and usual. In the beginning, rural settlements were not involved in this formal renovation. Handmade productions did not disappear, but their abundance decrease if compared to ceramics produced using the potter wheel. This was the result of the political decisions of the Emirate that reactivate the economy begun by the main urban centres.

The socio-economic set-up of the Islamic society developed, it was changing, but this time in the opposite direction, from rural/domestic to urban. This evolution has also been observed by ceramic petrography ran on several cooking pots and water containers from the Vega of Granada archaeological site (Carvajal López et al., 2018; Carvajal and Day, 2013; Carvajal López and Day, 2015). The study focused on different rural settlements and the major cities of *Ilbirah* and Granada. The authors showed how the importance of local ceramic production on rural settlements decreased, while the production on the main centres of Granada and *Ilbirah* increase accordingly. This general trend became evident by the end of the Emirate (9th century) and the beginning of the Caliphate (10th century).

Moreover, the reactivation of urban workshops is associated with the introduction in the *al-Andalus* of new decorative solutions and the technological diversification of the ceramic. The workshops of Pechina and Malaga (Castillo Galdeano and Martínez Madrid, 1993; Iñiguez and Mayorga, 1993) and probably Córdova (Salinas, 2013; Salinas and Pradell, 2018) were certainly the most involved during the 9th century in this decorative revolution. Aplastic application and incised or impressed motifs could be flanked by the introduction of painted decorations, painted decoration applied above an engobe or by glaze application (Gómez Martínez, 2019; Salinas and Zozaya, 2015).

The Iberian Emirate was one of the the last Islamic territory where the glaze was applied on ceramics. It is commonly accepted that Islamic glazed ceramic tradition developed first in the Middle East (section 3.1.2). Afterwards, it spread eastward and westward. In any case, glazed ceramics from the Iberian Peninsula, North of Africa, Egypt, the Levant and Mesopotamia

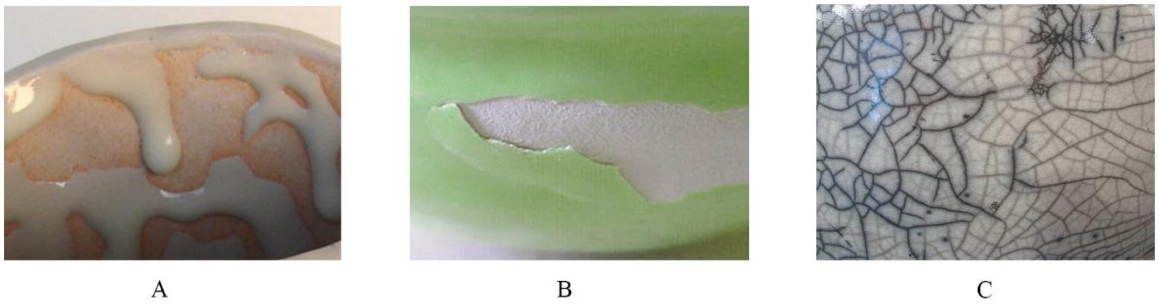

Figure 12 Defects on glazed ceramics A, crawling; B, Shivering; C, Crazing. Pictures obtained from http://www.lakesidepottery.com/index.html.

have common characteristics like the utilization of lead oxide (PbO) as the main fluxing agent combined to silicon oxide (SiO_2). The PbO/SiO_2 ratio may differ (Tite et al., 1998; Molera et al., 2001c).

The utilization of lead oxide in glazes production can give several advantages to the ceramist. The mixture is easy to prepare and to apply on the ceramics body using different recipes and methods. Moreover, the resulting melt is less viscous, and the glaze has higher optical brilliance (Tite et al., 1998). Alkali metals oxides (i.e. Na_2O, K_2O), and alkaline earth metal oxides (i.e. CaO, MgO) could also be added as secondary fluxing agents and/or stabilizers.

In some glazing traditions, the concentration of alkali metals is significant (alkali-lead glazes). For example, Islamic glazes produced in Syria and Egypt, between the late 7th and 9th century, were of the high-lead type (PbO = 55-60 wt%) or of the high lead-alkali type (PbO= 40-45 wt%), while glazes produced in Mesopotamia during the 9th century were mainly of the alkali-lead type (PbO = 2-5 wt%)(Tite et al., 1998; Mason and Tite, 1997; Tite et al., 2015; Matin et al., 2018), and more similar to the Parthian and Sassanian glazing tradition from Iran (Hill et al., 2004; Pace et al., 2008).

Moreover, every type of glaze has different wetting properties and thermal expansion-contraction coefficient rate. Generally, high-lead and lead-alkali glazes are less susceptible to crawling[19], shivering and crazing[20] (Fig. 12) than the alkali-lead type (Tite et al., 1998).

[19] Crawling is represented by the effect which leave unglazed area on the ceramic body (extended areas of the ceramic body are exposed). Normally the effect of crawling is reduced by a lower surface tension of the glaze during firing which favoured glaze dispersion on the ceramic body surface. This is also known as glaze wetting property.

[20] Any fired ceramic object experiences expansion as it is heated, and contraction as it is cooled. A typical piece of functional ware is a two-part system in that body and glaze possess independent expansion characteristics. However, the glaze is fixed to the underlying body and is therefore obliged to conform to the body's thermally induced size changes. So, they must have similar thermal expansion coefficient and similar contraction during cooling. Shivering and crazing are directly influenced by the interaction of the glaze with ceramic body, which is intense below the glass transition temperature, which is normally around 500 °C. If the contraction of the glaze is greater than that of the ceramic body, then the glaze would be under tensile stress and crazing of the glaze surface would occur. If the contraction of the glaze is less than that of the ceramic support it is not a big problem, since

Glazes could also be applied on different ceramic bodies, namely produced using a calcareous (i.e. CaO rich) or a silica (i.e. SiO_2 rich) rich clay, which normally has a very different thermal behaviour. Whatever raw material was selected, to obtain good results, the ceramic paste and the glaze must have similar thermal expansion coefficient - contraction rate, normally within 5-15% difference (Lawrence and West, 1982). If this difference is too high, shattering[21] might be present.

Lead, for glaze production, was normally extracted from naturally occurring minerals such as galena (PbS), litharge (PbO), minium - red lead (Pb_3O_4), hydrocerussite ($PbCO_3 . Pb(OH)_2$), cerussite ($PbCO_3$) and anglesite ($PbSO_4$). The technology developed in the Mediterranean basin and Europe for lead mineral extraction, mineral treatment, glaze mixture preparation and mixture application on ceramic vessels was not an Islamic discovery. It was already known before the appearance of the first attested examples of Islamic ceramics, during the 7th-8th century (Watson, 2014).

Lead has been utilized for the production of glazed ceramic since the 10th century BC (Marzo et al., 2009), and the application of the high-lead glaze on ceramic has been uninterrupted since then. Romans[22] utilized two different techniques to apply lead glaze on ceramics, depending on the enrichement in CaO or SiO_2 of the ceramic raw material. The lead compounds could be directly apply on the ceramic body and subsequently fired in the case of SiO_2-rich ceramic pastes. Differently, in the case of CaO-rich ceramic paste a lead-silica frit was prepared and then applied on the ceramic body and fired (Walton and Tite, 2010). This was a technological adaptation to the raw materials because the amount of SiO_2 was not sufficient to allow glaze formation in the secon case.

High-lead glazed ceramics were rediscovered/readopted by the Byzantines since the 7th century, and later for the production of the first Byzantine glazed white wares (Waksman et al., 2008;Waksman et al., 2007; Armstrong et al., 1997; Palamara et al., 2016). Consequently, it is plausible that early Islamic glazed ceramic renew the Hellenistic, Roman and subsequent Byzantine tradition in the utilization of high-lead glazes to decorate/impermeabilize ceramic vessels.

glazes better resist to compression than tension. If the contraction of the glaze is much smaller than that of the ceramic support the compression stress would significantly increase and the glaze would peel of from the body. This effect is known as shivering by ceramists (Tite et al., 1998).

[21] When the ceramic/glaze thermal expansion coefficient and contraction rate is to different cracking and fragmentation of the fired body might happen.

[22] Examples of high lead glaze application during Roman times have been found in the East as well as in Italy, France, within the Balkans and possibly in Spanish Iberia (Greene, 2007; Walton and Tite, 2010; Pérez-Arantegui et al., 1996; Capelli et al., 2007; Medeghini et al., 2018; Pérez-Arantegui et al., 1995; Paz Peralta, 2008; Tite et al., 1998).

Undoubtly, the introduction of high lead glaze technology in Islamic Iberia represented a huge step forward, and its application to decorate/impermeabilize vessels was the most important innovation for the Islamic ceramic in the *al-Andalus*.

Early Emiral glazed ceramics normally appear only sporadically on the archaeological record, if compared to undecorated wares. So, its rarity is proportional to its prestigious and representative nature. Initially ceramic vessels were covered by a homogeneous transpaternt monochromatic (green, brown, honey) glazed layer, by a bichromatic glaze with two different colours in the interior and on the exterior walls of the object or, by the end of the Emiral period, by a polychromatic glaze in one side (Salinas and Pradell, 2018).

Emiral glazed ceramics has been identified on archaeological sites usually located close to the Mediterranean and Atlantic coastline of the Iberian Peninsula. So archaeologists supposed that these materials were mainly traded by sea (Salinas and Zozaya, 2015). Just in

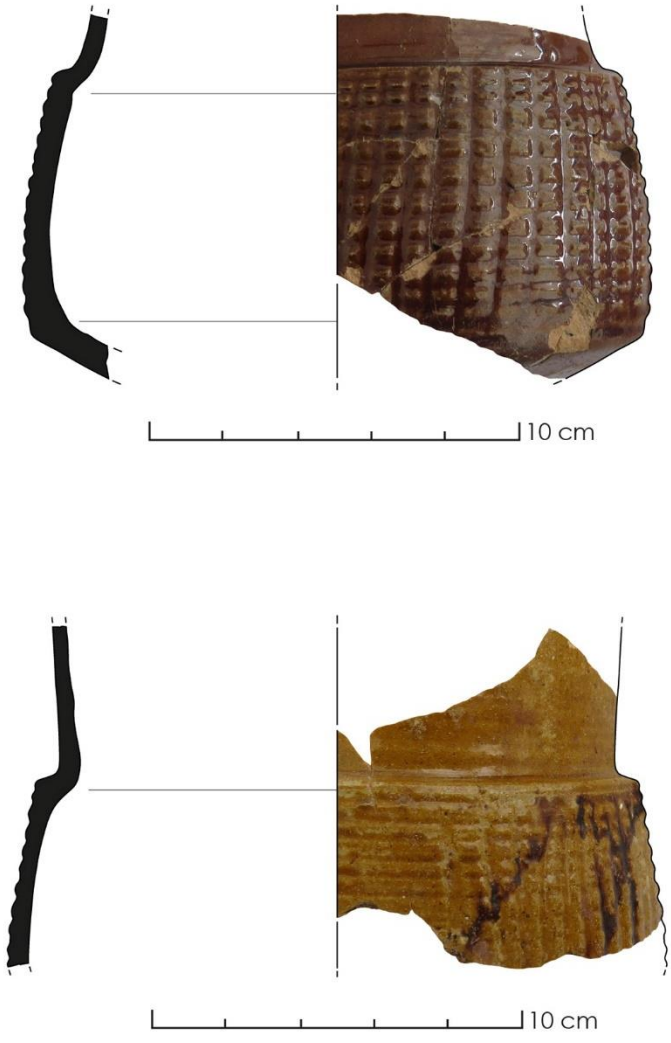

Figure 13 Islamic Emiral glazed ceramics (9th century) recovered in the city of Silves (Portugal), monochromatic (upper picture) and polychromatic (lower picture). All fragments have underglaze incised decoration and traces of manganese can be seen in one samples. Picture by Maria Gonçalves – Municipality of Silves

the capital of the Emirate, Córdova, it was identified on different archaeological sites (Salinas, 2013; Salinas and Pradell, 2018). Some fragments (Fig. 13) have been identified in Portuguese territory, namely in Lisbon, Silves, Alcoutin, Castelo Velho de Reliquias and Mértola but, at present, do not exist any available archaeometric data.

Analyses have been performed just on ceramic samples recovered at Pechina, Granada and Córdova, southern *al-Andalus* (Salinas and Pradell, 2018; Salinas et al., 2019; Molera et al., 2018; Salinas et al., 2021). Ceramics, both open and/or closed shapes (bowl, big bowl, plates, pitcher/jug, oil lamp, glass, bottle), were covered by a high lead-silica glaze (PbO 45-65 wt% roughly), typically poor in alkali, usually Na_2O+K_2O below 2-3 wt%, and with calcium oxide concentration (CaO) generally below 5 wt%. Cations such as copper (Cu^{2+}), manganese (Mn^{2+}) and iron (Fe^{2+}, Fe^{3+})[23] were responsible for the green, black and honey/yellow/green/brown colour respectively. When present, on polychromatic Emiral glazed ceramics, decorations were commonly applied overglaze.

The ceramic paste characteristics pubblished data shows that calcium oxide concentration (CaO) is comprised between 12 and 20 wt %. Thus, the clayey raw material exploited was probably a marl with a calcitic or dolomitic component, widely available in southern Spain on Mesozoic and/or Cenozoic geological sequences (Vera, 2004).

The workshop of Pechina (Almeria, Spain) represents the best example of this production. In this case, it was possible to characterize kiln waste, frit, fritting vessels, wasters, slags, tripods, and different objects such pitchers, serving dishes, one oil lamp and understand the whole productive ceramic cycle (Salinas et al., 2019b).

This study presents all the different aspects of raw material processing (i.e. lead ore), options (i.e. clay raw material selection) and glaze application. Lead source (i.e. probably galena, PbS) was roasted until a temperature of approximatelly 1000 °C (Abdel-Rehim, 2006) to obtain lead oxide (PbO). Afterwards, it was milled, mixed with sand, and fired to obtain a raw compound with a chemical composition close to 70-90 % PbO and 30-10 % SiO_2. In the following step, the resulted compound was extracted, milled another time and re-fired in a second fritting vessel to favour sand melting and glass homogenization. The resulting frit was then crushed and applied on pre-fired ceramic bodies[24] using a liquid medium and subsequently fired, to allow glaze adhesion on the vessel surface.

[23] When iron oxide appears in the glaze with a significant concentration gives different colour to the glaze depending on its oxidation state (Fe^{2+}, Fe^{3+}). The oxidation state in conditioned by the applied ceramic firing cycle and conditions (Molera et al., 1998; Molera et al., 1997)

[24] The double firing technique was widelly utlized by Islamic ceramist, but a single firing cycle could also be adopted. In this case the glazed decoration was applied on an unfired ceramic body. Afterward they were fired at

The study (Salinas et al., 2019b) also put in evidence that glazed ceramic bodies and the fritting vessels had different chemical composition. The main difference resided in the notable depletion in calcium oxide (CaO) and enrichement in silicon (SiO_2) and aluminium (Al_2O_3) oxides of the fritting vessels. So, the ancient ceramist deliberately chose a calcium-rich raw material for glazed ceramic manufacturing. These technological choices (pre-fired ceramic body with high calcium oxide content) characterized most lead glaze ceramics in antiquity (Tite et al., 1998), including Islamic ceramics from *al-Andalus*.

Frit preparation and glaze application were probably prepared/applied in a temperature range between 650 and 720 °C considering the chemical composition of the mixture (Di Febo et al., 2018). It is interesting to note that similar procedures were also done/developed on the Islamic workshop of San Nicolás (Murcia, Spain), dated from the 10th century (Molera et al., 1999a; Molera et al., 2009). This suggests that the same ceramic technology continued to be used during the Caliphal period.

the same time. Single and double firing technique have been widelly investigated by different scholars (Molera et al., 2001b; Pradell and Molera, 2020; Molera et al., 1993). Normally, glaze adhesion to the ceramic support involve chemicals excahange between the glaze and the ceramic body, and new crystalites generally nucleate in the glaze-ceramic interface. This process is stronger when the glaze is aplied on an unfired ceramic body (sinlge firing cycle). Consequently more crystalites develop, and the interface is usually more thick.

3.2.3 The Caliphal and Taifa Kingdoms period

The end of the Emirate and the beginning of the Caliphate of Córdova, under *Abd al-Rahmân III* rule, in 929 (10th century), marked a significant change in the Islamic ceramic repertoire of the *al-Andalus*. It was a period of peace, political stability, cultural/scientific development and of the construction of masterpieces of *al-Andalus* architecture such as the huge palace of *Madīnat az-Zahrā*, the fortified residence of the Caliph, located at some kilometres from Córdova. At the beginning of the 11th century, the Caliphate of Córdova crumbled, and it was substituted by numerous independents political units called *Taifa* Kingdoms (Fig. 9) until roughly the end of the 11th century. Several differences were noted in ceramic characteristics (formal, stylistic and technical) compared to the Emiral period. Most of the innovations introduced during the Caliphate continue to appear in *Taifa* Kingdoms period ceramics.

Since the first half of the 10th century and during the 11th century, there was a progressive reactivation of the urban workshops, in continuity with Emiral period. The reinforced consolidation and dynamization of regional distribution networks and commercial trade routes (terrestrial and maritime) between cities lead to widespread economic growth and prosperity. Therefore compared with Emiral ones, Caliphal and *Taifa* ceramics acquired a clear identity from the formal, stylistic, and technical prospective (Gómez Martínez, 2019).

During the 10th and the 11th century, some ceramics characteristics reflected high handcraft skills, coexisting with less technological productions, with a local/regional diffusion. This tendency was particularly evident in rural settlements[25]. In urban workshops, the production increased and it was probably able to satisfy the request of the local markets and supply the surrounding territories. A specific paper (Coll Conesa and García Porras, 2010) also evidenced that the number of workshops substantially increased, especially in the most important urban centres located in the centre-south of the *al-Andalus*.

Regarding firing technology, the two-chambers kiln of Roman tradition was the most diffuse during the Caliphate. A vent holed floor separated the fire chamber (for fuel) from the firing chamber (ceramic compartment). Between the 10th and the 11th century, it was also introduced a new type of kiln (of Middle East tradition), normally associated with the utilization of kiln bars[26]. They were normally inserted on specific slots in the kiln to form a shelf, in which

[25] During the Caliphate and the *Taifa* Kingdom period rural settlement were not included in the most important commercial networks. Consequently local/regional ceramic production dominate the archaeological scenario.
[26] This type of kiln was normally associated to the production of decorated glazed ceramic, especially tin opacified decorated glazed ceramic.

the ceramic was placed during the firing process (Coll Conesa and García Porras, 2010)[27]. In this case, the fire chamber and firing chamber were not separated.

Archaeologist also noted that the ceramic repertoire was highly diversified, specialized (every piece had a specific function) and formally homogeneous in different territories in most cases. For example formal similarities were observed between different territories of the *al-Andalus* in the production of small liquid containers (jugs) with a globular body and high neck or on some kitchen ceramics.

Figure 14 Caliphal GMC glazed ceramic from Mértola, picture by Susana Gómez Martínez.

In other cases the formal charcteristics evolved between the Caliphate and the *Taifa* period. The typological analysis of open shaped ceramics recovered in the *Garb al-Andalus* (Gonçalves et al., 2015) showed that Caliphal bowls generally do not have the foot at the base (Fig. 14) if compared to the same object produced during the *Taifa* period (Fig. 16).

Ceramics were frequently decorated. The most common was the application of aplastic decorations (especially on big earthen pots) or the creation of singular or parallel incised motifs in the object surfaces close to the neck (especially on big jar) using thin sticks. White, red and black painted decorations became widespread all over the *al-Andalus.* In particular white-

[27] To have a complete overview of the different type of kiln and structures identified in the *al-Andalus* all the information can be found on Coll Conesa and García Porras (2010). On this article it can also be noted that in the 10th and 11th century pottery was manufactured all over the Islamic land in the Iberian Peninsula. So this period was characterized by a strong technological transfer including ceramic manufacturing techniques and firing structures.

painted decorations in the *Garb al-Andalus,* become the fingerprint of the Islamic community in south-western Iberia for the whole Islamic period (Martínez, 2014; Liberato, 2016).

But the biggest difference between the Emiral and the Caliphal period was the generalized diffusion in the territories of the *al-Andalus* of different kind of glazed ceramics. This tendency was stronger in the most important cities. Since the end of the Caliphate and the beginning of the *Taifa* kingdoms (10^{th}-11^{th} century), glazed ceramics have become quite common also in secondary centres such as small towns, villages and fortress. It is important to stress that the presence of glazed ceramics is considerable in the centre-south of the Iberian Peninsula, but in the northernmost Islamic territories, it is only sporadic (Gómez Martínez et al., 2015).

Ceramics could be covered by a monochromatic glaze (green, yellow, brown, white) or by a bichromatic glazed decoration with different motifs (geometric, epigraphic, phytomorphic). One of the most diffuse and recovered was the so-called "honey and manganese/black" glazed ceramic. Black patterns were normally drawn using manganese and/or iron oxide rich minerals (Molera et al., 2013; Di Febo et al., 2017b; Di Febo et al., 2017a) on a honey-coloured background. Less frequently, copper oxide could substitute manganese and/or iron oxides to make green glazed motifs, or the background could be white and subsequently decorated with black motifs as evidenced in Mértola (Gómez Martínez, 2014).

Scarce archaeometric data, regarding monochromatic and bichromatic glazed ceramics are available from the Caliphal and *Taifa* kingdom period (Lapuente and Peréz-Arantegui, 1999; Peréz-Arantegui and Lapuente, 2003; Molera et al., 1999a; Molera et al., 2018; Molera et al., 2009). The main components of the glaze were lead oxide (PbO=45-55 wt%) and silicon oxide (SiO_2=30-35 oxide wt%), with low amount of alkalis ($Na_2O+K_2O \leq$ 2-3 wt%). Calcium oxide (CaO), iron oxide (FeO) and aluminium oxide (Al_2O_3) could have a concentration of 5-6 wt% in total. Manganese oxide (Mn^{2+}), copper (Cu^{2+}) and iron ($Fe^{2+, 3+}$) were utilized to obtain black, green and honey/brown/yellow/green decorations, respectively. A specific publication[28] describes how the chemical composition of the ceramic paste could influence the final glaze colours (Molera et al., 1997).

The technology of raw material treatment for glaze production and its application on ceramic vessels did not change if compared to the Emiral period (Salinas et al., 2019b; Molera et al., 2009; Molera et al., 1999a). Glaze was applied on biscuit fired ceramic bodies, produced using a calcium oxide rich raw materials (CaO > 7-8 wt%). As during the Emirate, in the

[28] This publication did not analyse Islamic glazed ceramics, but *hispano-moresque* glazed ceramics. In any case it fully describes how different glaze colour were could be obtained during the middle ages in the Iberian Peninsula.

Caliphate and the *Taifa* period ceramics with different function (i. e. cooking pots) were generally manufactured using silica-rich raw materials (Salinas et al., 2019b; Molera et al., 2009; Molera et al., 1999a; Peréz-Arantegui and Lapuente, 2003; Lapuente and Peréz-Arantegui, 1999).

By the end of the 9th century – beginning of the 10th century an important innovation was represented by the introduction of a new variety of decorated glazed ceramic, the so-called *"verde y morado / verde e manganês/ green and brown"* (GMC) polychromatic glazed ceramics (Salinas, 2013; Gómez-Martínez et al., 2018). Recently, different papers estblished that the first prototypes of GMC ceramics started to be produced during the late Emiral period (Salinas and Pradell, 2018; Molera et al., 2018; Carvajal López, 2008; Salinas, 2013) in the cities of Granada and Cordoba, slightly before the beginning of the Caliphate. In this period tin ores started to be utilized, as opacifier, to produce white glazes.

Both closed shapes, such as medium/small liquid container (i.e. jugs, pitchers), or open shapes such as bowls (Gómez-Martínez et al., 2018; Gómez-Martínez, forthcoming) were decorated. The glaze colours included white, green, brown and honey. Normally, the decoration was developed overglaze (Molera et al., 2001c) in green and brown on a white background (the most widespread). The undecorated side (i.e. reverse side) of the objects were also normally white, but it could also be covered by a honey glaze.

Archaeologists have studied GMC glazed ceramic since the 19th century. But during the 20th century a conspicuous ceramic assemblage was discovered at *Madīnat az-Zahrā* in Córdova. Then, researchers supposed that GMC was an exclusive palatial ceramic production, and from that moment onward it was defined as *Madīnat az-Zahrā* or Caliphal ceramics. Associated with *Umayyad* Caliphate, the ornamental style and the iconographic meaning spread the political messages of the ruling dynasty (Barceló, 1993; Rosselló-Bordoy, 1987). The white glaze represented the colour of the prophet *Muhammad* while the green glaze represented the colour of the *Umayyad*.

Vessels were decorated with different ornamental themes, which might include geometrics, epigraphic (Fig. 15B), phytomorphic, zoomorphic or anthropomorphic (Fig. 15A) compositions (Gómez-Martínez et al., 2018; Santos, 2015; Santos, 2016). A recent study has demonstrated the existence in the northeast

Figure 15 GMC glazed ceramic samples from Évora with anthropomorphic (A) and epigraphic (B) glazed decorations.

sector of Córdova of a workshop area that manufactured GMC ceramics during the Caliphal period. Two different productions with different quality were recognized. A high-quality ware was produced for the palaces (the palatial production) and the less-quality ones for the urban populations (Salinas and Pradell, 2020).

By the end of the 10th century, GMC ceramics were already produced in different workshops (Zaragoza, Valencia, Almeria, Murcia and probably Malaga), in eastern and south-eastern *al-Andalus* (Bazzana and Picon, 1981; Demians D'Archimbaud et al., 1986; Bazzana et al., 1986; Peréz-Arantegui and Lapuente, 2003; Lapuente and Pérez-Arantegui, 1999; González García et al., 1992; Molera et al., 2001c; Molera et al., 1999a). At present, no evidences attest the production of caliphal GCM in the *Garb al-Andalus*, but these materials were identified in several archaeological sites, especially in the centre-southern of *Garb al-Andalus*[29]. Probably, the most significant GMC ceramic assemblage have been recovered at Mértola, Cerro da Vila (Vilamoura), Faro and Silves.

During the 11th century, and especially in the *Taifa* Kingdom period, artisans tested different chromatic, stylistic, and iconographic solutions. The iconographic composition is usually more elaborated compared to the Caliphal GMC glazed ceramics. It could occupy almost entirely the surface of the piece, with a central theme (usually epigraphic or phytomorphic) surrounded by concentric bands or radial motifs (Gómez Martínez et al., 2018). From the formal point of view, bowls and washbasins (*jofainas*) were the most diffuse. They all present a vertical cylindrical foot at the base, semi-oval or spheric body, a slightly faired ceramic body and a circular/semi-circular lib.

Yellow and honey glaze were also introduced in the decoration during the *Taifa* period. The white background could also be substituted by a honey-coloured glaze in the decorated side, or, in a more recent discovery, the white background could be substituted by a black coloured glaze (Fig. 16). In this specific case, the decoration was made using white and green coloured glazes (Beltrame et

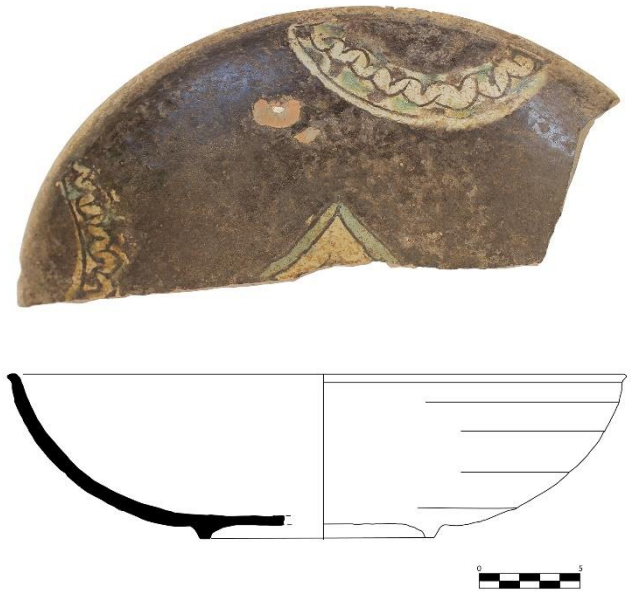

Figure 16 GMC glazed ceramics from Évora (Portugal). Picture José Rui Santos.

[29] In the Garb al-Andalus GMC glazed ceramics has been recovered in many places. A complete list can be found in Gómez Martínez et al. (2018)

al., 2015). The undecorated side could be covered by a transparent, honey, green or white glaze with different hues.

During the *Taifa* kingdoms, GMC glazed ceramics became more common if compared to the Caliphal period in the *al-Andalus*. GMC ceramics were produced in many other workshops, like Mallorca and Denia, in addition to the workshops active during the Caliphate (Molera et al., 2001c).

In the northernmost areas of the *Garb al-Andalus,* such as in the Tagus Valley (Gómez Martínez et al., 2018), it was also identified on several archaeological sites[30]. Moreover, the results obtained by the POLIX project (Bugalhão et al., 2008b) suggested the production of GMC ceramics in Lisbon during the *Taifa* kingdoms period (Dias et al., 2008), using a raw material generally exploited for the production of local undecorated and white painted ceramics. Nevertheless, just a few ceramic fragments have been identified and analysed until now, so these data must be considered with caution (Gómez Martínez et al., 2018).

At Mértola, southern *Garb al-Andalus* , PLM studies suggest the exploitation of local natural resources for the production of GMC ceramics during the *Taifa* Kingdom period (Zozaya and Aparicio Yague, 2003). Local ceramic production of tin opacified polychromatic glazed ceramic in Mértola will be discussed in this thesis in the results section.

GMC ceramic paste and glaze also show specific characteristics (Molera et al., 2001c; Salinas and Pradell, 2018; Molera et al., 2018; Coll Conesa et al., 1999; González García et al., 1992; Perez-Arantegui et al., 1999; Molera et al., 1999a; Salinas and Pradell, 2020, González-García et al., 1999). In all cases, GMC ceramics produced since the late Emirate period has a calcium-rich ceramic paste, with CaO concentration between 8 and 20 wt%. The exploitation of calcareous clays (i.e. marls) to produce GMC ceramics is convenient for several reasons. Foremost, the firing process of calcareous clays favours the incorporation of iron atoms into the crystal structure of pyroxenes (Trindade et al., 2009; Heimann and Maggetti, 2019; Heimann and Maggetti, 2014). Consequently, the colour of the ceramic paste become "buffy/cream" (the colour of the paste is not seen through the glaze), and it is easier to make a white glaze. Moreover, the thermal expansion coefficient of calcium-rich ceramic paste is similar to that of lead-tin opacified glazes, avoiding glaze defects during heating and cooling (Kreimeyer, 1987; Vendrell-Saz et al., 2000; Tite et al., 1998).

[30] For the Taifa kingdom period the geographic distribution of GMC ceramics in the *Garb al-Andalus* can be evaluated in Gómez Martínez et al. (2018). Most of the samples have been recovered in the centre-south of the region.

The analyses developed on decorations evidenced that GMC glazes are normally of the high-lead type, or with low-alkali content (Na_2O+K_2O < 2-3 wt%). The main components are PbO (36-58 wt%), SiO_2 (33-46 wt%) and SnO_2 (4-14 wt%). In particular, the utilization of tin dioxide was essential to obtain white glazes. Besides, the addition of tin to the glaze mixture favour the precipitation of small cassiterite crystals into the glaze favouring opacification[31] (Berti and Mannoni, 1991; Molera et al., 1999b; Vendrell-Saz et al., 2000).

In some cases, such as glazes produced in Zaragoza, alkali content (Na_2O+K_2O) might be higher (maximum 5 wt%) with lower PbO content. In Córdova, it has also been suggested the utilization of plant ash in the glaze preparation process (Salinas and Pradell, 2018; Salinas and Pradell, 2020) as fluxing agent. The undecorated side (i.e. the reverse of the object) could be covered by the same kind of glaze, or by a honey-coloured glaze. In this case, SnO_2 was not included, and the result was a honey-transparent glaze enriched in Al_2O_3, FeO and with a higher concentration of PbO.

Regarding glaze application, two different glaze mixtures/frits could be prepared, with or without SnO_2 (opacified or not). The transparent glaze mixture was prepared following the technology adopted during the Emirate period. In the case of white tin opacified glazes, a lead-tin calx with Pb/Sn>3.5 (Matin, 2019) was probably prepared and subsequently mixed and roasted with silica (sand). Big grains of quartz could be observed within the glaze, suggesting less care in the mixture/frit preparation. Alternatively, unmelted quartz crystals could also act as opacifier agent in addition to tin[32].

Subsequently, the obtained mixture/frit was milled and applied on pre-fired[33] object using a liquid medium. Green and brown decorations were usually applied/painted over the the unfired glaze (Molera et al., 2001c) with the addition of copper oxide(CuO) for green glaze, and manganese oxide (MnO) for the black glaze.

By the middle/end of the 10th century (Déléry and Gómez Martínez, 2006) another kind of polychromatic glazed decoration appeared in the *al-Andalus*. This is *corda seca* (*cuerda seca* in spanish) glazed ceramics. This decorative technique has been utilized even after the Islamic domination for the production of "*Azulejos*" (glazed tiles), the Hispano-Moresque ceramic tiles

[31] This technique was introduced directly from the Middle East, as explained in section 3.1.1 (Matin et al., 2018; Salinas and Pradell, 2018; Salinas and Pradell, 2020).
[32] The double opacification method has been widely adopted through the Islamic world. In the Iberian Peninsula it has been also utilized in the production of *corda seca* glazed ceramics (Chapoulie et al., 2005).
[33] Glazed ceramic could be single or double fired. These two processes are easily identifiable by the study of the interface ceramic paste / glaze. This interaction has been studied experimentally (Molera et al., 2001b), and doubled fired ceramics normally show a very small interface.

utilized in the Iberian Peninsula to decorate important historical building (Coentro et al., 2014; Coentro et al., 2017).

During this period, the *Umayyad* Caliphate of Córdova reached its apex, and the commercial trade network established during the Emirate (maritime and terrestrial) was extremely developed. The most active area of the *al-Andalus* was probably the south-eastern part of the kingdom. From there, the Mediterranean harbour cities of Almeria, Pechina and Murcia distributed imported and locally produced ceramics, even in the Atlantic facade of the *al-Andalus* (I. C. Fernandes et al., 2015).

Two different decorative variants of *corda seca* glazed ceramics can be identified: partially (CSP) and totally (CST) covered by glaze. In the first case, just one side of the piece has decoration. While in CST, one side of the piece is decorated using the *corda seca* technique, and monochromatic glaze commonly cover the reverse side.

The *corda seca* technique, both on CSP and CST ceramics, is characterized by a design normally drawn mixing MnO and /or FeO rich minerals; this was the "*corda*" line. It could be applyied on unfired or fired ceramic bodies generally using a liquid medium (probably a fatty substance) that favoured its adhesion. Subsequently, the black outline of the pattern was filled with distinct coloured glazing preparations (white, green, yellow, honey, turquoise) to complete the decorative pattern. The function of the *corda seca* line was to prevented the raw glazing materials from mixing with each other (Peréz-Arantegui et al., 1999b).

During the Caliphate and the *Taifa* Kingdom period, on CSP glazed ceramics just one coloured glaze preparation was generally chosen. In contrast, CST glazed ceramics had a multicoloured glazed decoration. Thus, technically, it is much more difficult to produce CST glazed ceramics than GMC glazed ceramics. The artisans must produce glazes and succeed in reaching the vitrification state[34] with materials with different chemical composition, maturing temperature[35] and different behaviour during firing. A detailed description of *corda seca* glazed ceramics can also be found elsewhere (Déléry, 2006; Chapoulie et al., 2005).

Different authors have widely debated the origin of *corda seca* glazed ceramic in the last thirty years by different authors, and two different theories existed nowadays. For some authors, *corda seca* glazed ceramic was created in the *al-Andalus,* probably at *Madīnat Ilbīra*

[34] The vitrification state is reached when chemical elements mobility of a melt during cooling is sufficiently limited to forbid the formation of an ordered crystal structure. This led to the formation of aa amorphous inorganic material, a glass.

[35] For a glaze the "maturing temperature" corresponds to a temperature interval at which the viscosity of the formed melt is sufficiently low to allow the escape of bubbles and the filling of pinholes, and sufficiently high to prevent the glaze running of the ceramic body (Tite et al., 1998).

Figure 17 Ceramic vase with palm tree, decorated with the corda seca technique recovered in Susa (Iran), 8th-9th century. (Ref. MAOS 383/Louvre Museum)

(Granada) or *Madīnat al-Zahrā* (Córdova). This is supported by the abundance of *corda seca* glazed ceramics recovered in these cities, and more generally in the Iberian Peninsula, if compared to other Islamic territories. Other authors (e.g. Déléry, 2006; Déléry, 2009; Déléry and Gómez Martínez, 2006) claim that this decorative technique originated in the Middle-Near East, between the 7th and the 9th century, and subsequently was introduced and re-elaborated in the *al-Andalus*.

This model is supported by the formal, stylistic and technical comparison of ceramics produced in the Iberian Peninsula and the eastern Islamic territories. Thus, several ceramic samples/objects (jugs) retrieved in Samarra (Iraq), Susa (Iran) and Antioquía (Turkey) and Mesopotamia, stored at the Louvre Museum (Paris, France), Museum für Islamische Kunst (Berlin, Germany), Princeton University Art Museum (Princeton, USA) and Victoria Albert Museum (London, UK) respectively, are considered the ancestors of, or at least the ceramic object that directly influenced, Iberian *corda seca* glazed ceramics (Déléry and Gómez Martínez, 2006; Déléry, 2006).

These ceramics are partially glazed using yellow and/or green glazes, with the decoration eventually surrounded by black paint, like in *corda seca* glazed ceramics from the *al-Andalus* (Fig. 17). Most of these objects have not a secure archaeological stratigraphic contextualization, but they preceded the production of the Samarra type pottery described by O. Watson (2014). Thus, they were contemporaneous to the Coptic glazed ware (CGW) and the Yellow glazed family (YGW) from Egypt and Syria.

The same author (Watson, 2006) also argued that the Islamic YGF ceramics (Watson, 1999) recovered at *Tall Aswad* (Raqqa, Siria), dated from the early 9th century, are technically related to Iberian *corda seca* glazed ceramics. The similitudes are especially evident with two variants of the YGF, the "yellow glazed ware with painted decoration" and the "sparse decorated

ware", from the beginning of the 9th century. On the first one, the glazed decoration might be applied directly on the ceramic object, previously covered by a slip, and subsequently bordered by a black paint. On the second one, the glazed decoration might be applied directly on the ceramic body, partly covering the surface of the object. Subsequently, the glaze could be bordered or not by black paint (Déléry and Gómez Martínez, 2006; Déléry, 2006).

So, from the technical point of view, ceramics stored in museums and recovered at *Tall Aswad* and *corda seca* glazed ceramics from the *al-Andalus* have common characteristics, especially the utilization of black paint and the application of glazed decoration. Nevertheless, the main difference is in the function of the black paint. In the Iberian *corda seca* glazed ceramics, the black paint prevented the mixing of different coloured glazed preparations, while on eastern YGF ceramics it just bordered the glazed decorations. At present, any imported glazed ceramics of the YGF ware in the Iberian Peninsula have been identified.

It is impossible to know whether ceramic was directly imported and subsequently "revisited" or whether artisans migrated to the *al-Andalus.* In any case, commercial trade routes within the Mediterranean Sea could have played an important role (Zozaya, 1993; Constable, 1996) and, even if *corda seca* glazed ceramics from the *al-Andalus* inherited some characteristics from the eastern YGF glazed productions, it never appeared in the eastern Mediterranean area, pointing to a local re-elaboration of eastern prototypes or an Iberian technique.

The CSP decorative variant was the first to appear, by the end of the Caliphate, in the South eastern *al-Andalus*, and it was surely produced in the Mediterranean Islamic citie of Pechina, Almeria and Murcia. Moreover the production of CSP ceramics is also suggested in the cities of Seville, Zaragoza, Lérida, Toledo (Iberian Peninsula inland), Córdova, Valencia and Málaga (Déléry, 2006; Déléry, 2009).

In the *Garb al-Andalus* (I. C. Fernandes et al., 2015), the diffusion of CSP was linked to the main maritime and terrestrial routes established since the Emirate of Córdova. Seaports and river arbours located on the most important riverbanks (i.e. Guadiana, Sado, Tago, Arade and Mondego) were directly involved on maritime trades with Islamic cities of Pechina, Almeria and Murcia (I. C. Fernandes et al., 2015).

Caliphal imported CSP ceramics have been identified in the cities of Silves, Castelo Velho de Alcoutim, Castelos das Relíquias, Mesas do Castelinho, Mértola and Évora. The most common recovered objects included small jugs (with one or two handles), jars and pitchers, with no foot, decorated with phytomorphic or epigraphic motifs. Afterwards, CSP strongly developed since

the beginning of the *Taifa* Kingdoms period (11th century), being quite diffuse all over the Peninsula.

The archaeological evidences indicate that the beginning of *Taifa* kingdoms corresponded an increase and diversification of CSP production. Besides, in addition to the previous ones, workshops were also identified in Toledo, Badajoz, Zaragoza and indirect archaeological evidences suggest CSP production also in the cities of Tortosa, Málaga, Niebla, Balaguer, Valencia, Seville and in the Iberian Peninsula inland – central Iberia (possibly Alcala´ la Vieja, Talavera de La Rainha, Soto Blanco, Gormaz, Calatalifa, Madrid) (Déléry, 2009; Déléry, 2006).

In the *Garb al-Andalus*, *Taifa* CSP ceramics were identified in several archaeological sites, and continued to show strong similarities with the CSP production from the South eastern *al-Andalus* (I. C. Fernandes et al., 2015). Geometric, epigraphic or phytomorphic motifs usually decorated jugs, jars, pitchers (all of them with a foot at the base), glasses or small lantern.

Nevertheless, the diffusion of specific CSP ceramics could be limited to the territory of a specific *Taifa* Kingdom. The small lanterns with phytomorphic motifs recovered in different Islamic centres of the *Garb al-Andalus* (e.g. Mértola, Faro, Moura, Cerro da Vila, Évora, Castelo Velho de Alcoutim, Silves) and included in the *Taifa* of Sevilla are an example.

In the city of Lisbon, the production of CSP during the *Taifa* kingdom was also established. The discovery of different workshops and Islamic houses on the archaeological sites of *Rua dos Correeiros* and of *Mandarim Chinese* allowed an extensive archaeological and archaeometric investigation (Bugalhão and Folgado, 2001; Bugalhão et al., 2008). Stylistic and formal ceramic characteristics have been influenced by Caliphal CSP ceramic productions from Alicante, Pechina and Alméria (I. C. Fernandes et al., 2015).

The archaeometric analyses developed on numerous ceramic samples with different decoration (Dias et al., 2001; Dias et al., 2008; Déléry, 2006) evidenced that CSP ceramics recovered in Lisbon have a high concentration of silicon oxide (SiO_2), aluminium oxide(Al_2O_3) and low concentration of calcium oxide (CaO) if compared to CSP glazed ceramics supposedly imported from Southern Iberia. Visually, ceramics are also different. The ceramic paste of CSP from Lisbon is usually reddish, while the ceramic paste of CSP ceramics from southern Iberia is normally buffy. The diffusion of this local/regional production is restricted to the lower Tagus basin, and it was identified on the archaeological sites of Sintra, Frielas, Vila Franca de Xira and Palmela.

The CST ceramics started to be widely produced and diffused in the *al-Andalus* only (Gómez Martínez, 2019) at the end of the *Taifa* Kingdoms (11th century). Producing CST

workshops were identified in Toledo, Badajoz, Saragoza and Murcia (Déléry, 2009; Déléry, 2006). But the production in different unidentified centres was quite probable. During this period has also been observed a difference between *corda seca*, both CSP and CST, glazed ceramic recovered in the central or southern territories of the *al-Andalus*. On glaze ceramics from the central Iberian Peninsula, *Taifa* of Toledo and Badajoz (Valdés Fernandés, 1985), the decoration is dominated by a honey-coloured glaze flanked by different coloured glazed preparation (black, dark green or white), or by black paint in the case of CSP (Déléry, 2006a). As a result, the honey-black glaze colour gives an overall darker hue to these ceramic productions. By the other side, southern ceramic productions have usually lighter colours.

In the *Garb al-Andalus,* CST glaze ceramics were imported and possibly locally produced. The production was confirmed in Lisbon (Gomes et al., 2009), on ceramic samples recovered at the Saint Jorge Castle. Moreover, the decoration of several CST glazed ceramics from Coimbra, Lisbon and Évora are characterized by an extensive application of honey and black-glaze in the decoration. As evidenced by Gomes et al. (2009), these artefacts probably represent a regional copy of similar CST ceramics, produced within the *Taifa* of Badajoz and Toledo.

Different archaeometric studies have been developed on glaze of Caliphal and *Taifa corda seca* glazed ceramics (CSP and CST) from various archaeological sites of the *al-Andalus* such as Badajoz[36], Pechina, Almeria, Malaga, Mércen, La Iglesita (Úson), Zaragoza, Lisbon (Valdés Fernandés, 1985; Déléry, 2006; Chapoulie et al., 2005; Peréz-Arantegui et al., 1999c). Nevertheless, if compared to GMC glazed ceramics, fewer data are available. Consequently, we are probably far from a real understanding of the diversity of *corda seca* glazed ceramics in the Iberian Peninsula.

The most extensive technical, provenance and chronological study was developed by Claire Déléry, on her PhD thesis (Déléry, 2006a) and partly published on Chapoulie et al. (2005). The data available show that glaze composition is different in different sites, evidencing that the technology transfer within the *al-Andalus* was not easy. Different ateliers produced glazed ceramic using different ratios of the same raw materials (i.e. PbO, SiO_2, alkalis, alkaline earth) utilizing different manufacture cycles (Déléry, 2006; Chapoulie et al., 2005; Peréz-Arantegui et al., 1999c). Nevertheless, some general trends can be identified. Generally, glazes are high-lead type with PbO (35-65 wt%) and SiO_2 (24-48wt%). The higher PbO content is a fingerprint of the first *corda seca* glazes in the *al-Andalus*.

[36] The available data for the city of Badajoz are not complete. The author just published qualitative data and it is impossible to extract any quantitative information regarding glaze characteristics.

Alkalis content on glazes was commonly low ($Na_2O+K_2O < 2$-3 wt%), but on glazes from Zaragoza (Peréz-Arantegui et al., 1999b) it could be higher[37]. Moreover, on one sample from Lisbon Na_2O or K_2O were not detected (Déléry, 2006), pointing to differentiation of ceramic production on different workshops. The concentration of Al_2O_3 and CaO could be very different depending on the characteristics of the ceramic body, or because the addition of some clay to the glaze mixture. Glazes could also be opacified using SnO_2. In particular, one sample from Almeria can be considered representative of the introduction of the tin glaze technique on *corda seca* decorated ceramics (Chapoulie et al., 2005).

Copper (Cu^{2+}) and iron (as Fe^{2+}) were the main colourant to get turquoise, dark green or green glazes. Yellow glazes were obtained with the addition of some clay or iron oxides (as Fe^{3+}). Regarding white and black glazes, few samples were analysed from the workshops of Zaragoza and from the *Alcazaba* of Badajoz (Peréz-Arantegui et al., 1999c; Valdés Fernandés, 1985). In the first case, data were not presented because glazes were highly weathered, while just histograms have been presented in the second case. In both cases, black glazes were obtained by adding manganese oxide and some iron oxide to the glaze mixture, while white glazes were obtained thanks to the addition of tin oxide as evidenced for GMC ceramics (Molera et al., 1999b).

[37] With the addition of more alkalis, PbO concentration consistently decreases. This is a characteristics of *corda seca* glaze ceramics produced at Zaragoza.

3.2.4 The African period: Almoravid and Almohad

By the end of the 11th century, the *al-Andalus* ceramic repertoire significantly changed, marking a clear difference with the ceramic productions of *Umayyad* tradition (Caliphal and *Taifa*). The new period coincided with the end of the *Taifa* Kingdom diversity and the beginning of the African period, when two Berber dynasties from Morocco, the *Almoravid* (end of the 11th century) and the *Almohad* (middle of the 12th century), ruled on the *al-Andalus*. These events radically changed the political and social set-up of Islamic Iberia, being more connected to the north of Africa – Maghreb. The political unification increased the trade between the two sides of the Mediterranean thanks to the control of the Maritime commercial routes of the western Mediterranean and of the close Atlantic facade.

In any case, in this timeframe, between the middle of the 12th century and the middle of the 13th century, most of the territories of the *al-Andalus* will be included in the Christian Kingdoms. Just the *Nazarí* Kingdom of Granada will survive until the end of the 15th century. This tendency is evident in the ceramic repertoire. Besides, decorated ceramics distribution in the *al-Andalus* have been influenced by the Christian *Reconquista* of the Iberian Peninsula, and it tendentially disappeared in central Iberia. During the *Almoravid* and *Almohad* period, the production was mostly concentrated in southern territories (Coll Conesa and García Porras, 2010), especially in the most important urban centres.

Workshops were generally able to produce every kind of utilitarian ceramics for the urban markets and for the surroundings territories[38], with some general formal similarities among different areas of the Peninsula. Besides, differently from the Caliphal and *Taifa* Kingdoms period, some general tendencies on decorated ceramic productions have been noted.

During the African domination, some cities – ceramic centres, were specialized in the manufacturing of distinct kinds of glazed decorated ware. This was the case[39] of the city of Palma de Mallorca during the *Almoravid* domination, for the production of GMC glazed ceramics (Berti et al., 1986; Berti and Mannoni, 1997; Berti et al., 2009). Or the cities of Almería, Granada and probably Murcia for the production of *corda seca* glazed ceramics during the same period (Flores Escobosa et al., 1998; Rodríguez Aguilera, 1997; Rodríguez Aguilera, 1999; Déléry, 2006; Berti and Mannoni, 1995). Or, yet, of the cities Murcia, Málaga, Calatrava la Vieja and Mértola, as suggested by Zozaya and Aparicio Yague (2003), for the production of lustre

[38] As evidenced by a recent article (Albero Santacreu et al., 2019) many workshops during the African period developed a large capacity to distribute their products throughout the territory of the *al-Andalus* as well as in rural area (García Porras, 2001).

[39] This is partial list. Many other workshops produced decorated ceramics during the African domination, and they are not reported in detail. We reported just the workshops who supposedly exported decorated ceramics.

ceramics during both the *Almoravid* and *Almohad* period (Demians D'Archimbaud et al., 1986; Picon and Navarro Palazon, 1986; Zozaya et al., 1995).

Ceramics were also exported to other Mediterranea regions, as, possibly, green and brown ceramics produced during the *Almoravid* period in the *al-Andalus*. Similar prototypes are represented by the ceramic "*Bacini*[40]", supposedly imported from the Iberian Peninsula, and recovered in the Italian Peninsula (mainly in Liguria and Tuscany region) and in Corsica Island, utilised to decorated churches facades (Berti and Mannoni, 1991; Berti and Mannoni, 1995; Berti and Mannoni, 1997; Berti et al., 2009) and on urban settlements (Baldassarri and Berti, 2009).

In the *Garb al-Andalus,* the continuity of the ceramic production during the *Almoravid* period was confirmed in Lisbon (L. Fernandes et al., 2015; Prudêncio et al., 2006; Dias et al., 2009), and new workshops were discovered in the city of Santarém (Gómez-Martínez et al., 2015; Liberato, 2012; Liberato, 2016), associated to the production of utilitarian ceramics (undecorated and white painted) and probably of *corda seca* glazed ceramics (I. C. Fernandes et al., 2015).

In the city of Mértola, additional archaeological evidences of ceramic production during the African period have been documented. Several kiln rods/bars have been recovered outside the city walls, on the river banks neighbourhood, with a chronology between the *Almoravid* and *Almohad* period (Gómez Martínez, 2016). Moreover, an *Almohad* kiln was also identified (Gómez Martínez, 2006). As in other cities, the production of utilitarian ceramics such as undecorated and white painted ceramics and monochromatic glazed ceramics[41] is evident.

Archaeological ceramics studies evidenced some general trends in ceramic typology and characteristics, weakly observed since the end of the *Taifa* Kingdom period. This tendency strongly typifies the whole African period, *Almoravid* and *Almohad*. Standardized ceramic productions almost completely substituted manual and less technological ones. Also, raw materials were accurately decanted, and ceramics were generally lighter if compared to the previous periods (i.e. Caliphal and *Taifa* period).

Moreover, during the *Almolravid* period, typology was tightly connected to the object function. This aspect of ceramic production became even stronger during the *Almohad* period (Lafuente Ibáñez, 1994; Gómez Martínez, 2019).

[40] The diffusion of different kind of decorated glazed ceramics produced on Islamic Iberia within the Mediterranean area have been treated by Graziella Berti and Liana Tongiori in several different publication (Berti and Tongiori, 1981; Berti and Tongiori, 1980; Berti and Tongiori, 1985; Berti, 2010).

[41] The archaeological material correlated to ceramic production from the city of Mértola have been analysed within this PhD thesis to evaluate the production of different kind of decorated glazed ceramics during the Islamic period.

Almohad decorated ceramics also show slightly different characteristics if compared to the *Almoravid* ceramics. Monochromatic glazed ceramic, unglazed ceramic with relief (moulded, incised, stamped or *calado*[42]) decorations, or a combination of these two techniques become generalized.

An example of this tendency can be found in the typological and stylistic characterization of big earthen vessel in the *Garb al-Andalus* (Costança dos Santos et al., 2016)[43] or in different lustre moulded glazed ceramics recovered at Mértola, Alcácer do Sal, Silves, Córdova, Jerez de La Frontera and Almería (Gómez Martínez, 2014 and references therein)[44]. *Sgraffito* decorated ceramics also became quite diffuse[45].

Moreover, during the *Almohad* period, the production cycle of monochromatic glazed ceramic could be simplified. The glaze could now also be applied on unfired ceramic bodies[46], as happened in the Islamic workshop of Denia (Molera et al., 1999a). Still, in the large glazed ceramic container, biscuit fired ceramic bodies were preferred (Karagiannopoulou, 2017).

During the *Almoravid* period a new version of GMC ceramic appeared, completely different from *Umayyad* and *Taifa* tradition exemplars. Bowls were normally decorated using this technique. From the formal point of view, they usually have a convex base with a slightly vertical foot. The foot section can be triangular or square, and the overall diameter is quite small compared to the dimension of the bowl. The body is hemispherical, and the lib/rim can have a triangular section, or it develops in a semi-horizontal wing. The decorative style has been defined "geometric" by archaeologist (Gómez-Martínez et al., 2018; Gómez Martínez, 2019; Gómez-Martínez, n.d.), and could develop anthropomorphic, zoomorphic (Fig. 18A) or naval

[42] Calado decorations, also knew as "openworks", is a term adopted in Art History and related fields to define a decorative technique which produces decorative patterns/motifs with the creation of holes. This decorative technique has been widely used during Islamic times in architecture decoration, ceramic decoration as well as in metalworks.

[43] A recently discussed Master Thesis in Archaeological Material Science (Karagiannopoulou, 2017) supervised by Prof. José Mirão, Dr. Maria José and the PhD candidate analysed several large decorated vessels from the city of Silves (Portugal).

[44] The archaeological problematic regarding the production of this particular kind of decorated ceramic is widely discussed in the book titled *"Cerámica Islámica de Mértola"* (Gómez Martínez, 2014) pg. 255-257. The author of this PhD thesis started the analysis of several ceramic samples (12) from Mértola. Results are unpublished, but different publications (Gómez Martínez, 2003; Zozaya and Aparicio Yague, 2003) already pointed to a local production in the city of Mértola.

[45] The diffusion of Sgraffito decorated ceramics can be found in the publication of Navarro Palazon (1986)

[46] Monochromatic glazed ceramic during the Caliphal and *Taifa* Kingdom period was produced by glaze application on biscuit fired ceramic bodies (double firing). The difference resided on the interaction between the ceramic paste and the glaze, higher in the case of single firing thechnique (Molera et al., 2001b).

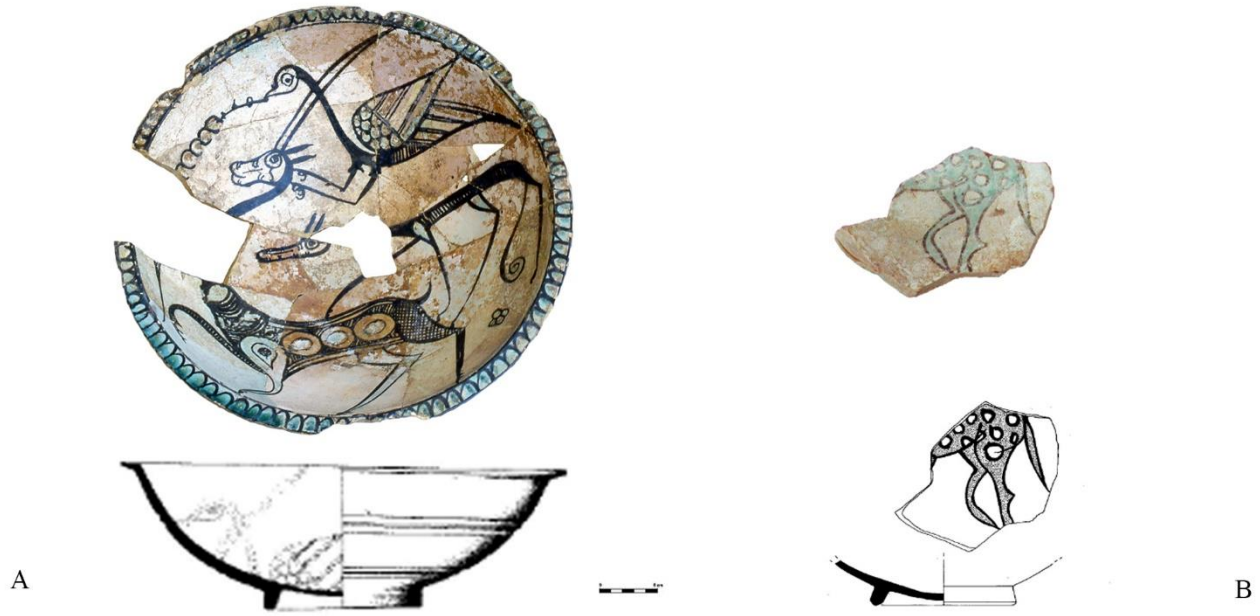

Figure 18 GMC glazed ceramic from the Almoravid (A) and Almohad (B) period from Mértola. Picture and drawings by Susana Gómez Martínez.

themes. GMC ceramics with these characteristics have been just recovered in the most important city harbours of the western Mediterranean, namely in Ceuta, Denia, Palma de Mallorca, Almería, Cartagena and Pisa[47] (i.e. the so called *Bacini*). In the *Garb al-Andalus, Almoravid* GMC ceramics were identified in Santarém, Lisbon, Silves, Mértola and Palmela.

Initially, the typological and stylistic similarity with North African (*Ifriqiya*) glazed ceramics production from the 10th and 11th century recovered in Kairawan (Daoulatli, 1979) and Cartago (Vitelli, 1981), suggested they were produced in *Ifriqiya* (i.e. actul Tunisia), and subsequently traded within the Mediterranean area (Rosselló-Bordoy, 1985).

Nevertheless, the petrographic analysis of several ceramic samples excluded this hypothesis, suggesting they were produced on the Balearic Island (Berti et al., 1986; Berti and Mannoni, 1991; Berti and Mannoni, 1997; Berti et al., 2009), but not only. They could also be produced in different un-identified workshops of southern al-*Andalus* (Berti et al., 2009; Gómez artínez, 2003; Gómez Martínez, 2006[48]). For example at Silves (Gonçalves, 2010; Gonçalves, 2012), located in southern *Garb al-Andalus,* on the right bank of the Arada river, dozens of *Almoravid* GMC glazed ceramic fragments were recovered, pointing to the existence of local production. Nevertheless, this new hypothesis has still to be confirmed by archeometry.

[47] The Chronology of the Islamic ceramic recovered in Pisa, studied by Graziella Berti and Liana Tongiori and published on several different publication, have been recently debated. A later chronology have been proposed basing on different archaeological considerations (Azuar López, 2005; Azuar López, 2010; Meo, 2018).

[48] On the PhD thesis of Susana Gómez Martínez the results of the petrographic analysis performed on Islamic ceramics from Mértola are presented in the appendix F. Analysis were developed by Alfredo Aparicio Yague at the Madrid University (Spain).

Considering the *Almoravid* GMC glazed ceramic geographic distribution, some important archaeological consideration can be done. They have never been recovered in archaeological sites located in the Iberian Peninsula inland, but just in archaeological sites positioned close to the coastline (Mediterranean or Atlantic), or connected to it by a river. So it can be argued that these ceramics were just produced in cities with a harbour and afterwards traded by sea. Thus, they represent the archaeological evidence of the trade routes that Islamic merchants followed at the beginning of the 12th century (Gómez Martínez, 2019).

In the second half of the 12th century, a new version of GMC ceramics (Fig. 18B) with different formal and stylistic characteristics were also produced by the *Almohad* ruled populations, but with a lower diffusion if compared to the previous period. It is difficult to differentiate *Almohad* from *Almoravid* GMC ceramics. Just after the publication of a GMC ceramic assemblage recovered at Calatrava La Vieja and Alarcos (Retuerce Velasco and De Juan García, 1998), it was possible to disclose the *Almohad* GMC characteristics.

The petrographic analysis carried out on several samples confirmed the existence of a local production on both archaeological sites[49]. Other examples of *Almohad* GMC ceramic have been identified at Medellín, Denia and Priego de Cordoba (Retuerce Velasco et al., 2009 and references therein). Moreover, petrographic analysis also suggests the production of *Almohad* GMC ceramic at Jerez de La Frontera (Martín Patino et al., 1987). In the *Garb al-Andalus,* several samples were identified in Mértola and Arge (Gómez Martínez et al., 2018; Gómez Martínez, n.d.).

If compared to *Almoravid* GMC ceramic bowls, *Almohad* exemplares have a smoothly faired ceramic body with a vertical edge and a triangular lib. The ornamental composition is also different, and ceramics are usually decorated with phytomorphic or zoomorphic motifs (Fig. 18B). In particular, several similarities have been observed with Caliphal zoomorphic compositions, where the animal body was decorated with circular white spots.

Unfortunately, few samples of GMC glazed ceramics from the African period have been analysed. They were recovered at Denia, in a 13th century Islamic workshops (Gisbert, 1990; Gisbert et al., 1992) from the *Almohad* period. In this case several ceramic vessel[50] and frits have been sampled and analysed (Molera et al., 1999a; Molera et al., 2001c). Ceramics were manufactured using a CaO rich raw-materials. The analyses developed on decorations

[49] Previous archaeometric analyses already established the production of lustre ceramic at Calatrava la Vieja (Zozaya et al., 1995).

[50] On the archaeometric study of the workshop of Denia just the analysis of the decorated vessels side have been published.

evidenced that glazes were of the high lead type with low alkali content ($Na_2O+K_2O < 2$-3 wt%) and opacified using SnO_2 (6-7 wt%). Green and brown decorations were usually painted on the unfired glaze (Molera et al., 2001c). Cu^{2+} and Mn^{2+} were the main colourant of green and black glazes, respectively.

C*orda seca* glazed ceramics reached the apex of their diffusion, beauty, formal and decorative diversification during the *Almoravid* period[51]. Partial *corda seca* (CSP) ceramics could be decorated with one, two or three different coloured glazed preparation, with a combination of glazed decoration and relief pattern made with a mould, or with a combination

Figure 19 CSP (A) and CST (B) glazed ceramic from the Almoravid period recovered at Mértola. Picture and drawings by Susana Gómez Martínez.

[51] A complete overview of *Almoravide* ceramics (recoveries, characterization, production and geographic distribution) can be found Claire Déléry PhD thesis (Déléry, 2006a), Tome II - chapter 2/C and Tome IV – chapter 7.

of glazed and "*sgraffito*[52]" decorations. CST glazed ceramic could be associated to underglaze relief pattern decorations. Closed shapes (Fig. 19A) such as jars, jugs, pitchers, and cups could be partially (CSP) or totally (CST) covered by glaze, while open (Fig. 19B) shapes such as plates, terrines, bowls and lids were generally totally covered by glaze (CST).

In the *Garb al-Andalus, Almoravid corda seca* glazed ceramics were quite common[53], and were identified in several archaeological sites. The typological and stylistic studies evidenced high formal and decorative ceramic diversification. Most of *corda seca* ceramics were probably imported and show strong formal and stylistic similarities with ceramics from the workshops of Almería (Flores Escobosa et al., 1998) and from several different archaeological sites, located on southern Iberia such as Málaga, Palma de Mallorca and Denia (I. C. Fernandes et al., 2015).

Nevertheless, imported ceramics could also coexist with regional variants (I. C. Fernandes et al., 2015), such as in the Lisbon region and at Santarém (Fig. 20A, B). CSP ceramics could be decorated with different motifs including phytomorphic, epigraphic, pointed continue bands, or downturned wave-shaped continue patterns. It is interesting that CSP ceramics with multichromatic glazed decoration were just recovered in the city of Mértola (Gómez Martínez, 2014) and Silves.

Figure 20 Almoravid corda seca glazed ceramic from the Tagus valley. Picture and drawings of CST ceramic from Santarém (A) by Marco Liberato; picture and drawings of CSP ceramic from Lisbon (B) by José Paulo Ruas and Maria João Sousa.

[52] *Sgraffito* is a decorative technique obtained by the application of one or two different and contrasting slip layers on the surface of the ceramic body. Afterward the surface is scratched, revealing parts of the underlaying layer. Different decorative motifs could be obtained. This ceramic could be also manufacture without any glazed decoration. It was a typical ceramic production of the southern *al-Andalus* traded all over the Iberian Peninsula, including in northern Christian territories (Gómez Martínez, 2019; Fernández et al., 1989). This specific kind of glazed decorated ceramics have been documented in the *Garb al-Andalus* just since the *Almohad* period.

[53] A detailed geographic distribution of *corda seca* glazed ceramic in the *Garb al-Andalus* can be found in I. C. Fernandes et al. (2015)

In the *Almoravid* CST ceramics, epigraphic, phytomorphic and zoomorphic motifs were developed on object surface. A paradigmatic case is represented by a group of bowls (Fig. 19B) with phytomorphic decorations, created based on a floral radial geometric composition (Déléry, 2006; Gómez Martínez, 2019). A detailed study about this specific variant of *Almoravid* CST ceramics with floral radial motif has already been developed (Déléry, 2006a). Results evidenced that decorated bowls can be grouped into different typological groups linked to different decorative styles, suggesting that it was probably produced simultaneously in different workshops.

Similarly to *Almoravid* GMC ware, these ceramic have been mostly found in archaeological sites located close to the coastline or connected to it by a river such Almería, Málaga, Granada, Alcoy, Mallorca, Ceuta, Gádor, Cartagena, Pisa, Lisbon, Santarém, Silves, Faro and Mértola. Less frequently, few samples were also recovered far from the coastline, in the cities of Juromenha, Évora, Beja, Moura, Cidade das Rosas (Serpa) and Mesas do Castelinho.

The only attested *corda seca* glazed ceramic workshops have been documented in Granada and Almeria, and probably in Murcia (Berti and Mannoni, 1995) and Lorca (Déléry, 2006a)[54]. At Málaga, *corda seca* glazed ceramic was probably also produced (Demians D'Archimbaud et al., 1986), but samples characteristic and chronology were not included on published data.

Almohad corda seca glazed ceramic was produced in different places. Its diffusion was quite generalized on southern *al-Andalus*[55]. Different workshops have been identified in Valencia, Dénia, Murcia, Priego de Córdova, Seville[56], Córdova and, probable, also in Jerez de La Frontera and Calatrava La Vieja (Martín Patino et al., 1987; Déléry, 2006). The city of Almeria fell under Christian control in the middle of the 12th century and the production of decorated ceramics ceased (Tapia Garrido, 1981) and it was not exported anymore in the *al-Andalus*.

On both CSP and CST *corda seca* glazed ceramics some stylistic innovation were introduced[57]. *Sgraffito* decorations could be associated with CSP glazed decorations in the same piece. In the case of CST ceramics, decorations started to be also applied to bigger ceramic

[54] A more specific description of this topic with bibliography can be found on Claire Déleéry PhD thesis (Déléry, 2006a) on Tome II - chapter 2C.
[55] The Geographic distribution of *Almohad corda seca* glazed ceramics can be evaluated on Claire Déléry PhD Thesis (Déléry, 2006a) on Tome IV - chapter 8.
[56] Different kind of ceramic were produced and imported to Seville during the Almohad period. An overview of ceramic fabric characteristic can be found in Bridgman (2007) and Bridgman et al. (2009).
[57] Formal and stylistical characteristics of the ceramics produced in each workshop can be consulted on Claire Déléry PhD Thesis (Déléry, 2006a) on chapter 2-D.

objects (Gómez Martínez, 2019), related to ablution rituals ("*pia de abluções"* in Portuguese), or to protect the top of the wells (*"boca de poço"* in Portuguese).

In the *Garb al-Andalus,* it has never been identified any archaeological evidence correlated to *corda seca* glazed ceramic production during the *Almohad* period. Moreover, the fall of Lisbon and Santarém under Christian control permanently discontinued the production *corda seca* glazed ceramics within Tagus Valley. At present, CSP and/or CST glazed ceramics have been identified in the Islamic cities of Évora, Beja, Castro da Cola, Mértola, Silves, Castelo de Paderne, Tavira and Cacela Velha (I. C. Fernandes et al., 2015).

From the formal point of view, *Almohad* CSP and CST glazed ceramics, inherit many formal and stylistic characteristics from *Almoravid* ceramics. This tendency is well represented in Mértola, on the river neighbourhood (Gómez Martínez, 2016). In the case of CSP glazed ceramics, the jar with a ring-shaped base, globular body and tight neck or the glass (Fig. 21B) with a piriform body decorated with epigraphic or phytomorphic motifs are good examples. At Mértola, a group of jugs with globular body and cylindrical neck with *sgraffito* technique associated to CSP decoration (Gómez Martínez, 2014) have also been recovered.

In the case of CST ceramics, the most common ceramic objects are big ceramic vases with a flat base, cylindrical body (it can also be hexagonal, octagonal or rectangular) which ended with a square-shaped lib (Fig. 21A). As already mentioned the characteristics of the decoration, mainly epigraphic or with religious connotation, indicated they were water container correlated to ablution rituals (I. C. Fernandes et al., 2015). CSP and CST Almohad ceramics could also be imported, probably from Seville (Bridgman, 2007), as in the case of Mértola, or produced locally. This hypothesis will be tested by the present PhD thesis in the case of Mértola.

Figure 21 CST (A) and CSP (B) Almohad corda seca glazed ceramic from Mértola. Picture and drawings by Susana Gómez Martinez.

In the case of CSP decorated ceramics associated with *sgraffito* decoration, archaeologists think that this production was imported from southeastern *al-Andalus* (Gómez Martínez, 2014; I. C. Fernandes et al., 2015). Its production has been attested in different workshops in that territory, such as Palma de Maiorca and Denia, and probably also Valencia and Murcia (Déléry, 2006a). Nevertheless, these indications are not conclusive.

The archaeometric data for *Almoravid* and *Almohad corda seca* ceramics available is rather reduced. Few samples have been analysed, and just from the cities of Mértola, Lisbon[58], Malaga[59] and Córdova[60] (Déléry, 2006; Chapoulie et al., 2005, González-García et al., 1999). Most of the data have been obtained by the analysis of ceramic samples from Mértola. Thus, the sampling is limited if compared with the geographic dispersion of *corda seca* glazed ceramic in the *al-Andalus* (I. C. Fernandes et al., 2015; Déléry, 2006).

In all cases, ceramics were normally produced using a CaO rich raw material, similar to what happened during the Caliphal and the *Taifa* Kingdom period. The ceramic paste is normally buffy-cream after firing, due to high CaO content (Molera et al., 1998). On samples from Mértola, an anomalous concentration of P_2O_5 have been registered (associated with CaO) accompanied by a high concentration of Fe_2O_3. These data suggestthe exploitation or the mixing of different raw materials[61].

Regarding glazes, some important differences have been registered if compared with the Caliphal and *Taifa* Kingdom ceramics. In the *corda seca* multicoloured technique ceramists could use both tin-opacified and transparent glaze on the same piece. Moreover, the utilization of tin to opacify glazes become a common practice, and it could also be used on darker glazes (i.e. green and black), although it was not essential to obtain them. In this specific case different researchers supposed (Chapoulie et al., 2005; Tite et al., 1998) that tin might effect glazes maturing temperature. Consequently, the application of different preparetions with different chemical compositions and glaze maturing temperature required a high level of expertise, and especially a strict control of firing condition and raw material mixing.

In other cases, depending on the characteristics of the ceramic paste, green glazes could also be opacified by the addition of unmelted quartz crystals, in addition to tin (Chapoulie et al.,

[58] Just one sample has been considered from Lisbon (Déléry, 2006). It corresponds to CST ceramic bowl with phytomorphic decorations, created on the basis of a floral radial geometric composition. The sample is similar to CST sample of figure 19B recovered at Mértola from the formal and stylistical point of view.
[59] Just one sample have been analysed from Malaga (Déléry, 2006; Chapoulie et al., 2005).
[60] Just one sample from Córdova have been analysed (González-García et al., 1999). Moreover, glazes were not analysed using a scanning electron microscope, like most samples, but by atomic absorption spectroscopy (AAS). Alkalis have not been quantified and consequently just some general consideration can be made regarding the chemical composition of different glaze colours.
[61] This hypothesis was testes by the present PhD thesis.

2005). This method was utilized in the case of red ceramic pastes to hide the red colour of the fired clay and obtain glazes with the desired shade. The frits preparation process most probably followed the same process utilized during the Emiral, Caliphal and *Taifa* Kingdoms periods, and described in previous paragraphs.

Regarding the firing cycle, during the *Almoravid* and the *Almohad* period, glazed ceramics were typically double fired. So, the glaze suspension was applied on biscuit fired bodies (Chapoulie et al., 2005)[62]. Subsequently, the "*corda*" line could be drawn directly on fired ceramic bodies similar to what happened in the previous periods (Peréz-Arantegui et al., 1999b).

Published data (Déléry, 2006; Chapoulie et al., 2005, González-García et al., 1999) for glaze chemical composition show slightly heterogeneous results. Glazes could be of the high lead or of the lead-alkali type with different PbO (52.2-28.1 wt%) and SiO_2 (51-33.9wt%) concentration. On glazes from Cordoba SiO_2 concentration could be as much as 55-60 wt%. Depending on ceramic provenance, alkali content could be different.

Glazes from Lisbon and Mértola are enriched in alkali ($Na2O + K_2O$= 5-6 wt% maximum) while glazes from Malaga are poor in alkali ($Na2O + K_2O$ < 2-3wt%). The concentration of Al_2O_3 could vary because of the addition of some clay to the glaze mixture to obtain different colours, but on white glazes Al_2O_3 concentration was quite low and SnO_2 was normally identififed.

Copper (Cu^{2+}) with the addition of some iron (in the form of Fe^{2+}) were utilized to obtain turquoise and green glazes. In the first colour, tin was routinely included. In the case of black glazes manganese (Mn^{2+}) and iron (Fe^{2+}) were the main chromophores and tin could be added as an opacifier. Yellow and secondary glazes (i.e. the undecorated side of the object) had similar shade, and iron (Fe^{3+}) was the principal colourant.

[62] Differently from the previous periods the double firing method was an answer to a specific technical problem, that is the reduction or the oxidation of iron (Molera et al., 1997). In the single firing method, the glaze is directly applied on the unfired ceramic body. In this way the glaze would act as insulating barrier and a reduction environment would form in the ceramic paste with the formation of Fe^{2+}. In this case a transparent glaze would turn green. In the case of double firing technique iron would be oxidized to Fe^{3+}, and in the case of a transparent glaze it would turn yellow. On CST glazed ceramic from the African period both iron rich yellow glaze and tin opacified white, green, and black glazes could coexists supporting the hypothesis of the double firing method.

4. Methodology

Caliph: Comprehensive archaeological and laboratory investigation of Islamic pottery in Portuguese History

This chapter describes ceramics and sediments sampling criteria and methods. A table summarizes methodology utilized in the development of each topic. Every analytical method and experimental condition will be briefly described.

4.1 Ceramic and raw material sampling strategy

As already described in chapter 2, four different ceramic assemblages (152 samples in total) and eleven different raw materials have been considered. Their analysis will be treated in chapter 5 (sections 5.1 to 5.4). Ceramics were accurately selected to develop each of the four sections. Three groups were ceramics from the city of Santarém, while one ceramics group was recovered in the city of Mértola. In all cases, several archaeological publications (Arruda and Viegas, 1999; Liberato and Santos, 2018; Liberato, 2012; Liberato, 2016; Liberato et al., 2019; Gómez Martínez, 2006; Gómez Martínez, 2016; Gómez Martínez, 2014) precede the archaeometric work of the present thesis. The production of traditional ceramic from Muge has also been studied by different authors (Lepierre, 1899; Santos Júnior, 1932; Gomes Pinto, 2012).

Ceramic sampling has been planned in cooperation with the archaeologist who did the excavation and previously studied the materials. Different aspects of ceramic characteristics, as availability, typology, function, decoration and chronology, have been considered. Typology and function were related and particularly important, because ceramics were normally produced to accomplish a specific function. Usually, ceramic objects related to everyday activities such as consumption (kitchen ceramic), preparation (fire ceramic) and storage of liquid/food (container ceramic) are always the most abundant, in every archaeological site.

Thus, ceramic related to everyday activities are important to assess the relationship between ceramic function and raw materials or the technology used.

These ceramics can be undecorated or incised and white or red painted decorated. White painted ceramics were quite common, while the red-painted ones were less represented. Moreover, slip application could be combined or not with white paint. Slip could be applied for different reasons, as to mitigate the deep red-colour of the ceramic paste, or to smooth and impermeabilize the object surface.

Glazed ceramics are a different category of ceramic objects, and they are less abundant than unglazed ceramics. Sometimes they are defined as luxury ceramic because of their scarcity. Their presence, in some cases, can point to long-distance trade. In these decorated ceramics, the artisan must “harmonise” two different composite materials (ceramic paste – and glaze). Ceramics with monochromatic, dichromatic (i.e honey and black) and polychromatic glazes (i.e. green and black – partial and total corda seca) were sampled. Different glaze preparation could be applied simultaneously depending on the decortive style to obtain a specific decorative motif. Distinct motifs were developed during the Islamic period, and the style of the

composition might be different, considering the ceramic chronology. Ceramic typology also changed. Thus, also, glazed ceramics were sampled considering the fragments availability, decoration, typology, and chronology.

The archaeological context was also an important issue that was considered, both in Santarém and Mértola. Several productive archaeological structures were identified with ceramic wastes associated with the kiln firing chamber/corridor. Tools (i.e. kiln bars) associated with pottery production activities were also recovered. All these materials have been included in the study, and they allowed a direct comparison with ceramics to evaluate ceramic provenance.

In the case of sediment sampling, eleven different raw materials were collected. None of them was retrieved in the area of Mértola. Nine were collected close to Santarém, to identify the raw material source/s utilized in the city, during the middle ages. Samples were selected based on the observations carried out during different field trips, using geological maps (Zbyszewsky, 1953) and consulting historical sources (Lepierre, 1899).

Two raw material have been collected close to the village of Muge (Salvaterra de Magos) with the help of Mr. Domingos (a local potter). They are still employed nowadays to produce diverse traditional ceramics. All the specific information regarding ceramics and raw materials (including pictures and sampling position) will be furnished in chapter 5.

Table 1 summarizes the scientific methods and procedure utilized in the analysis of ceramics and sediments, reported in sections 5.1 to 5.4. A brief description of the different techniques employed, accompanied by the instrumental conditions applied, follows it.

Table 1 The table summarizes the scientific methodology applied and the materials utilized in the development of sections 5.1 to 5.4

Materials		**5.1**	**5.2**	**5.3**	**5.4**
Samples chronology / centuries		11^{th}-12^{th}	8^{th}-9^{th} to 15^{th}-16^{th}	11^{th}-12^{th} to 15^{th}-16^{th}	10^{th} to 13^{th}
Undecorated – incised - painted ceramic		X	X	X	X
Glazed ceramic		X	X		X
Traditional ceramics				X	
Manufacturing evidence (kiln wastes)			X		X
Total number samples considered		42	35	41	34
Methods					
Sediments sampling		X (9)		X (2)	
Granulometry	Grain size distribution	X		X	
	Sieving experiment	X			
Microscopy	PLM	X	X	X	X
	SEM-EDS	X	X		X
Mineralogy	XRPD	X	X	X	X
	µXRD		X		
	Oriented aggregate mount	Just sediments		Just sediments	
	µRaman spectroscopy		X		X
	FT-IR-ATR spectroscopy		X		
Chemistry	XRF spectroscopy	X	X	X	X
	ICP-MS spectroscopy	X	X		X
Physical and mechanical test	Helium pycnometry			X	
	Mechanical test			X	
	Permeability test			X	
Experimental firing test	Muffle furnace			X	

4.2 Sediment particle size distribution and sieving experiment

Particle-size distribution was evaluated for all raw materials collected (i.e. 11 in total). Sediment analysis were included in sections 5.1 (9 out of 11) and 5.3 (2 out of 11). The raw materials, ≈ 1 kg, was roughly disaggregated in a porcelain mortar. Afterwards, particles distribution of sediments were determined using 2mm, 1 mm, 500 μm, 250 μm, 125 μm and 63 μm (which included silt+clay) sieves by dry sieving.

For Particle-size distribution, the Udden-Wentworth scale was used (Adams et al. 1984). Just in the case of sediments samples of section 5.1, two different sediments portions were treated. The first one was utilized to evaluate sediments particle size distribution. The second one was further divided into 5 sub-samples, to test the effect of sieving in the chemical and mineralogical composition of raw materials.

The first subsample was marked as untreated raw material (URM), while the remnant four sub-samples were sieved, using only one sieve to isolate the fractions with less than 500 μm, 250 μm, 125 μm and 63 μm. Sieved sediments were then marked as <500μm, <250μm, <125μm and <63μm respectively preceded by the raw material reference. Subsequently, on these 5 sub-samples, for each raw material, XRPD, XRF and ICP-MS analysis were performed. The fraction <63μm was also utilized for the preparation of oriented aggregate mounts, for clay minerals identification (section 4.4.1).

The sieving tests remove sand, depurate, and homogenize raw materials, to establish a correlation between mineralogical and chemical composition with particles size. Conversely, the ceramic process contemplates the addition of temper and/or clay mixing. As a result of this process, the final mixture can be similar, or different to the original one, depending on the characteristics of the added material (Arnold et al., 1991), and/or the overall chemical composition can be diluted by temper addition preserving specific characteristics (Rollinson, 1993). These different datasets has been utilized to evaluate raw material selection/processing, ceramic technology, and provenance.

4.3 Microscopy

4.3.1 Polarized light microscopy - PLM

PLM is usually known for its extensive application in geological sciences, mainly focusing on the study and identification of minerals and rocks. Nowadays, it is widely employed to study cultural heritage objects such as pottery, mortars, wall paintings, and building stones. A thin-section has to be made, and a slice of sample must be cut, englobed, consolidated (if necessary), lapped[63] to obtain a flat surface and glued (using glue or resin) on a standardized glass slide[64]. The surplus of the sample is then cut off. The remaining unglued sample side is slightly ground with an automatic grinding machine, lapped, and eventually polished[65].

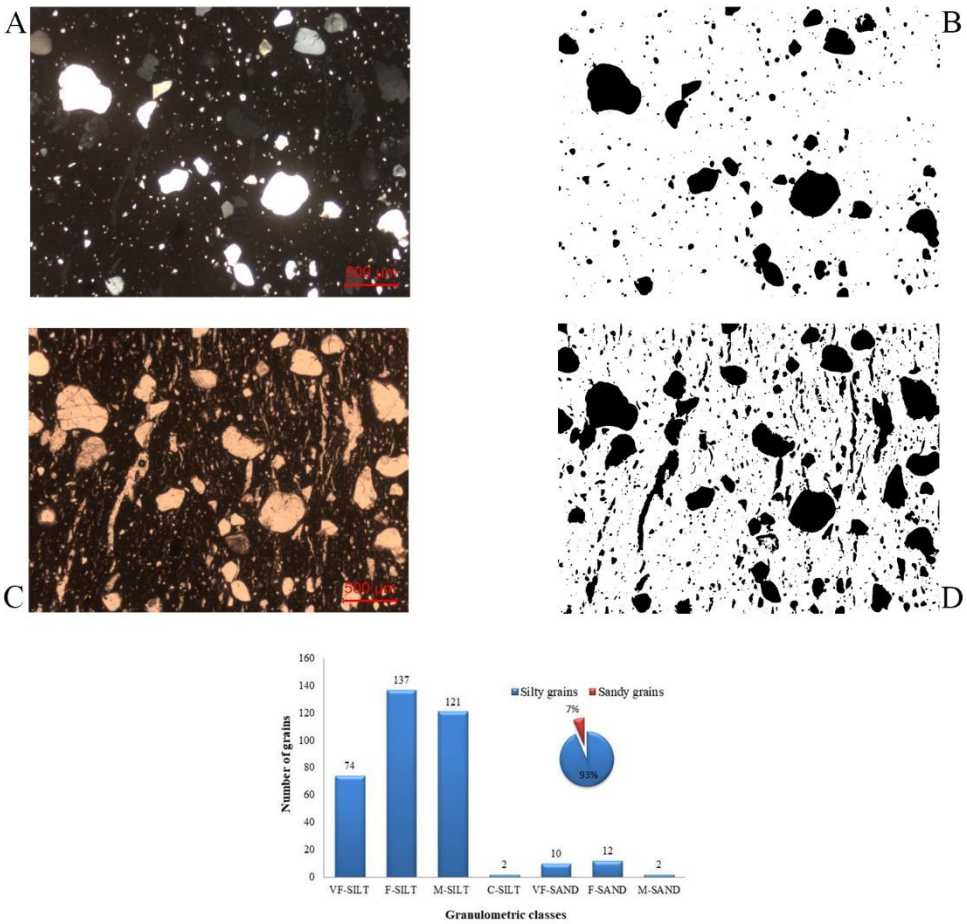

Figure 22 Images collected at the optical microscope at crossed (A) and parall (C) nichols, and their conversion into binary images (B-D) for temper, porosity, clay matrix and grain size distribution evaluation.

[63] Lapping is usually performed using a silicon carbide powders with different granulometry, roughly from 600 to 1200 grit (15 to 9 μm). The process can be done automatically or manually.

[64] Before the sample is cemented, the glass slide must be standardized. This is to say that one side must be as plane as possible. This operation is normally performed using an automatic grinding machine with high precision. Usually a standard thickness is also required to fasten the preparation process.

[65] Polishing is normally performed on an automatic polishing machine using specific liquid medium, cloth and very fine powders (from 15 μm to 0.25 μm in granulometry). The most used polishing compounds are composed by aluminium oxide or diamond paste.

The specimen is considered ready when its thickness is 30 μm. Most minerals are transparent at this thickness, they can be studied using a polarized[66] light microscope, and can be identified according to their optical properties. The principles of PLM (polarized light microscopy) can be found elsewhere (e.g. Klein, 2002; Gribble and Hall, 1985; Peccerillo and Perugini, 2005).

In ceramic studies polarized light microscopy is utilized to get the mineralogical composition and the microstructural characteristics of the sample. Once a ceramic thin section is positioned on the microscope rotating stage, different components and features can be observed. The more important are the clay matrix, mineral and rock inclusions (i.e. temper), diverse inclusions (organic or inorganic in nature), the porosity and eventually the presence of a slip, glaze or paint layers.

All these characteristics are related to the raw material exploited, raw material characteristics, raw material treatment, the vessel forming method and decoration, to the ceramic vessel function and the firing history of the piece. To sum up, thanks to PLM, it is possible to extract many different information, which cannot be collected by any other analytical method.

PLM was applied to all ceramic fragments studied in this thesis. Observations have been performed using a transmitted light petrographic microscope, model Leica DM-2500-P, equipped with an acquisition camera model Leica MC-170-HD. The mineralogy, presence of rock fragments, characteristic of the matrix, porosity, sorting and packing were described following the scheme proposed by P.S. Quinn (Quinn, 2013). The degree of sphericity and grain size characteristics of temper were described following the terminology utilized in the characterization of sedimentary rocks and classified using the Udden-Wentworth grain size scale (Adams et al., 1984).

Textural analysis, including temper percentage and modal analysis (through the estimations of the different grain size classes) have been performed using ImageJ free software 1.51k (https://imagej.nih.gov/ij/), starting from images obtained under crossed nicols (XPL) and converted into binary images (Fig. 22 A-B).

The results of image analysis is generally summarized in an excel file where it is reported the total area occupied by temper, in addition to the area occupied by each temper grain.

[66] Recent scientific theories consider light as a form of energy characterized by a double nature, corpuscular and of an electromagnetic wave. In the second case natural light radiation propagates vibrating in all direction, but at right angles to the direction of propagation. When light vibration is restricted just to one plane it is defined “polarized”.

Subsequently, grains are divided in different grain size classes, counted, and the total area that each grain size class is evaluated. The result is a binary plot (ordinate/y = total area occupied by each gran size class – abscissa/x = grain size class), where it is possible to evaluate temper grain size distribution in the sample (unimodal/bimodal/polymodal).

On section 5.4, porosity and the clay matrix were also estimated. To evaluate porosity by image analysis 2 different picture were collected and converted into binary images. The first one is collected at crossed Nichols (XPL), which include temper (Fig. 22A, B), and at parallel nicols (PPL), which includes temper and porosity (Fig. 22C, D). Porosity amount was calculated as the difference between the picture collected at PPL and XPL. Results are reported in percentage (%). The area occupied by the clay matrix was calculated by subtracting to 100 % the amount of temper and porosity.

4.3.2 Scanning electron microscopy (SEM-EDS)

The scanning electron microscope (SEM) is a powerful analytical instrument used to study different materials. It is a versatile instrument that can offer various types of information according to the user's requirements. When an electron beam hits the sample, the instrument combines high-resolution and high-magnification imaging by the detection of back-scattering (BSE) and secondary (SE) electrons, with the analysis of characteristic X-ray produced detect by Energy Dispersive Spectrometer (EDS). This combination allows analysis of very small areas or points to obtain chemical data and evaluate the spatial distribution of the chemical elements (compositional mapping).

The physical principles of the technique can be found elsewhere (e.g. Goldstein et al., 2003). This technique is widely employed in material cultural heritage (Tite, 1991; Froh, 2004; Schreiner et al., 2007; Freestone and Middleton, 1987).

In this thesis, ceramic pastes and decorations (glazed / painted) of samples included in section 5.1, 5.2 and 5.4 were characterized using a variable pressure HITACHI S3700N SEM coupled with a Quantax EDS microanalysis system. The Quantax system was equipped with a Bruker AXS XFlash® Silicon Drift Detector (129 eV Spectral Resolution at FWHM/MnKα). PhiRhoz quantitative elemental analysis was performed using the Bruker ESPRIT software. The system was checked using 7 Standard Reference Materials (SRM), namely 5 glasses (CMOG B, CMOG C, SGT5, SGT7, SGT8) and 2 microanalytical reference materials (BIR-1G, BCR-2G). For oxides concentration below 0.3 wt% the variations between certified and obtained values could be higher than 20%; for oxides concentration between 0.3 and 1 wt% the variation was a maximum of 10% of the certified values; for oxides concentration higher than the 1 wt% the variation was included between 2 and 5 % of the certified values. The operating conditions for analysis were as follows: backscattering mode (BSEM), 20 kV accelerating voltage, 10 mm working distance, 100 μA emission current and 40Pa pressure in the chamber. Scanning electron microscopy was utilized to characterize the ceramic body, temper inclusions and the decorative layers (slip, paint and glazed when present).

Uncoated polished thin-section or polished blocks were utilized. Considering compositional heterogenity of the ceramic paste, of some mineral inclusion and of glazed and painted decoration, at average of 3 different analytical spots was considered for chemical analysis. Elemental concentrations were afterwards converted to oxides by stoichiometry and normalized to 100%. The instrumental statistical uncertainty was 1σ.

4.4 Mineralogical composition

4.4.1 X-ray diffraction - XRD

X-ray Diffraction (XRD) is a method used to identify minerals and different chemical compounds who present crystal structure (Klein, 2002). XRD technique is based on the three-dimensional periodic crystal lattice capability to give a characteristic diffraction patterns when subjected to an incident monochromatic X-ray beam of known wavelengths. In this case, the Bragg law ($n\lambda=2d \sin \theta$)[67] must be satisfied.

In the present thesis, XRD was applied to all ceramic and sediment samples. The equipment utilized was Bruker AXS D8 Discover XRD with the Da Vinci design. A Cu Kα source operating at 40 kV and 40 mA and a Lynxeye 1-dimensional detector were used. Scans were run from 3 to 75 º 2θ, with 0.05 2θ step and 1s/step measuring time by point.

When sampling was possible, a small ceramic fragment was cleaned (the decoration was removed as well), finely powdered and mounted in a sample holder for analysis. In this case, XRPD (powder X-ray diffraction) was employed for bulk analysis.

When sampling was not possible and/or not necessary (i.e. paint or glaze layers), the analysis was performed directly on the sample surface with the aid of a Goebel mirror and a 1 mm laser collimator. So, the micro X-ray diffraction (μXRD) setting was utilized.

In the case of raw materials, oriented-aggregate mounts were also prepared for clay mineral identification. Experiments conditions were the same used for XRPD. Clay minerals[68] were remouved by decantation (gravity settling of particles in a suspension) in a glass tube, and extracted using a pipette. For every raw material-oriented aggregates, two different samples were prepared. Once completely dried, they were both analysed to register the original spectrum. Afterwards, one sample was treated by ethylene glycol vapours for one day, while the second one underwent two different firing cycles, at 400 °C and at 550 °C for 30 minutes in a muffle furnace. After every treatment/firing cycle, an XRD pattern was registered.

Diffract-EVA software with PDF-2 mineralogical database (International Centre for Diffraction Data - ICDD) was utilized to interpret XRD patterns. For clay mineral identification, a Clay Mineral Identification Flow Diagram was used (https://pubs.usgs.gov/of/2001/of01-041/htmldocs/flow/index.htm) in addition to specialized bibliography (Moore and Reynolds, 1997).

[67] In the Bragg law n is an integer number and λ is the wavelength of incident x-ray beam. It varies depending on the characteristics of the X-ray tube. Θ is the angle of incidence of the beam in the specimen.
[68] Clay minerals were extracted and mounted for analysis following the procedure of the U. S. Geological Survey. All the information can be found at: https://pubs.usgs.gov/of/2001/of01-041/index.htm

4.4.2 µRaman spectroscopy

Raman spectroscopy is an analytical technique utilized to examine vibrational, rotational and other low-frequency modes in a system. It provides detailed information regarding molecular vibration, chemical structure, phase and polymorphism, crystallinity and molecular interaction. The method is based on the interaction of light with a material chemical's bonds, and it is normally defined as a scattering technique, whereby a molecule scatters incident light from a high-intensity laser light source.

The light-matter interaction can be either elastically (wavelength does not change) or inelastically (wavelength does change). The first one is normally called Rayleigh effect, while the second one is called Raman Scatter. The energy emitted by Raman scattering can be higher (anti-stoke) or lower (stoke) than the incident beam energy.

The spectrum acquired by the instrument is a distinct chemical fingerprint for a particular molecule or material. Consequently, it can be used for material identification. A detailed description of the method can be found elsewhere (e.g. Jones et al., 2019; Nasdala et al., 2004; Frezzotti et al., 2012).

In the present thesis, a µRaman spectrometer was utilized to identify specific mineralogical inclusion observed in thin-sections or polished blocks in section 5.2 and 5.4. The analytical work was performed using a HORIBA XPlora spectrometer equipped with a diode laser of 28 mW operating at 785 nm, coupled to an Olympus BX41 microscope.

Raman spectra were acquired in an extended mode in the 100–1400 cm-1 region. The equipment was previously calibrated using a quartz reference sample. The laser was focused with an Olympus 100x lens, 10% of the laser power on the sample surface, 15s of exposure, 20 cycles of accumulation. Results were acquired and interpreted using LabSPEC5 software with the aid of specialized bibliography and exploring RRUFF database (Lafuente et al., 2016).

4.4.3 FT-IR-ATR spectroscopy

Fourier Transform Infrared spectroscopy is an analytical technique which is used to obtain infrared spectrum of absorption, reflection and emission of organic or inorganic materials.

The infrared (IR) signal originated when vibrating atomic group absorb a specific amount of energy in the IR range, satisfing the Bohr law. So, they are promoted to a different vibrational energy level. The result is an absorption spectrum.

Molecules, atomic groups and even crystal lattices can interact with the electron magnetic field of light. The energy at which any peak in an absorption spectrum appears corresponds to the frequency of vibration of a sample component.

To show infrared absorption, the electric dipole moment of a molecule must change due to vibration. This is the selection rule for IR. The raw signal (interferogram) is afterwards treated by the computer using a well-known mathematical technique called Fourier Transformation to obtain a frequency spectrum.

A detailed description of the method can be found elsewhere (e.g. Coates, 2006; Beran et al., 2004). In the present thesis, FT-IR spectroscopy was applied on samples from section 5.2. Analyses were performed in the medium infrared region (4000–650 cm-1) using a Brüker Hyperion 3000 Tensor 27 equipped with a single point MCT detector cooled with liquid nitrogen. The spectra were collected in ATR mode using a 20x ATR objective (Germanium crystal with 80 μm of diameter) and the pressure sensor at position 1. Spectra were collected using OPUS 7.2 software with a spectral resolution of 4 cm-1 and 64 scans in absorbance mode. The same software was utilized for interpretation with the aid of specialized bibliography (Chukanov, 2014; Chukanov and Chervonnyi, 2016) and exploring the RRUFF database (Lafuente et al., 2016).

4.5 Chemical composition

4.5.1 XRF spectroscopy: Major chemical oxides composition

XRF (X-ray fluorescence) spectroscopy is an analytical technique applied to analyse different materials such as soils, rocks, glasses, ceramics and alloys. According to the Beer's law, when atoms of a sample are irradiated by X-ray, generated by high-intensity X-Ray tube, they can be absorbed by the matter[69]. During the absorption process, electrons of an atomic inner shell gain sufficient energy to escape from the attractive force of the nucleus. So, a vacancy is created.

These vacancies are filled by electrons located in an outer shell. Consequently, the electron moves from higher to lower energy levels. The difference in energy is emitted (i.e. a photon), and it is characteristics of a specific electronic transition and of a specific chemical element. Because there are several electronic transitions in the same atom, numerous spectra lines occurred for the same chemical element. The result is an X-ray emission spectrum that is characteristics of each chemical element in the sample. A detailed description of the method can be found elsewhere (e.g. Van Grieken and Markowicz, 2001).

XRF is used to perform quantitative bulk chemical analysis of a sample. In the present thesis, XRF spectroscopy was applied to all ceramic and sediment samples and it allowed the quantification of different major oxides (Na_2O, MgO, Al_2O_3, SiO_2, P_2O_5, SO_3, K_2O, CaO, TiO_2, MnO, FeO). Analyses were performed using an Energy Dispersive X-Ray Spectrometer (EDS-XRF) Bruker S2 Puma, adopting a methodology already tested by different scholars Georgiou (Georgiou et al., 2015). Before the analysis the sample must be homogenized.

Samples were fused on a Claisse LeNeo using a flux (Li-tetraborate): sample ratio of 10:1 to form fused beads. Quantifications were obtained using a regression method with 19 standard reference materials (SRM) namely GSP-2, SBC-1, BCR-2, BHVO-2, BIR-1A, DTS-2B, SGR-1B, SDC-1, QLO-1, AVG-2, COQ-1, W2A (USGS SRM), SARM-52 (MINTEK SRM), STSD-3 (Natural Resource Canada SRM), SXO7-10 (LGC SRM), DC 60105, DC 73020, DC 61101, DC 62108c, DC 73309 (NCS SRM). Some SRM were combined to increase the concentration of specific oxides such as CaO, MgO, MnO and P_2O_5 in the calibration. SRM mixtures were DTS-2B (50%)/COQ-1 (50%), DTS-2B (10%)/DC73020 (90%), DC73309 (80%)/COQ1 (20%), DC73309

[69] When a monochromatic light passes through an absorbing medium its intensity decreases exponentially as the concentration of the absorbing medium increases. The relationship can be expressed as $A = \varepsilon lc$ where A is absorbance, ε is the molar extinction coefficient (which depends on the nature of the chemical and the wavelength of the light used), l is the length of the path light must travel in the solution in centimetres, and c is the concentration of a given solution.

(95%)/COQ-1 (5%), NOD-1A (25%)/ QLO-1A (75%), NOD-1A (12.5%)/ QLO-1A (87.5%), QLO-1A (25%)/Bone Ash (75%) and QLO-1A (75%)/Bone Ash (25%). The Spectra Elements 2. software was utilized for acquisition and data processing, and it reports the final oxides concentration and the instrumental statistical error associated. The loss on ignition was evaluated by calcination (on crucibles) of roughly 1g of dry sample in a muffle furnace for 1 hour at 1050 °C.

For interpretation, the correlation between chemical elements was established using both binary and ternary plots. Particularly important was the evaluation of lime and magnesia content. Calcium/magnesium-rich raw materials can be associated to the exploitation of raw materials formed by the weathering of limestone or dolostone, and significant differences in concentration might influence the firing process with the formation of specific high-temperature mineralogical phases (Trindade et al., 2009; Heimann and Maggetti 2014).

In ceramic studies, various authors made a distinction between lime-rich and lime-poor ceramics just with the evaluation of CaO content. This boundary was established between 3wt% (Maggetti and Galletti, 1982) and 6 wt% (Maniatis and Tite, 1981). Nevertheless, in this thesis, ceramic paste composition was described following the classification proposed by Heimann and Maggetti (Heimann and Maggetti 2014; Heimann and Maggetti, 2019), and ceramic paste composition was plotted in the SiO_2, Al_2O_3 and CaO+MgO triangular space. The triangular space is“forecast” of the mineralogical assemblage stable above 950 °C, considering the chemical composition of the sample.

4.5.2 ICP-MS spectroscopy: Trace chemical elements analysis

ICP-MS (inductively coupled plasma mass spectrometry) is a powerful analytical technique to measure very small (sub-part per million) concentrations of most chemical elements. The acronym also specified that it is a compound technique, with two different segments, consisting of an inductively coupled plasma[70] system connected to a mass spectrometer. If the sample is solid, it must be digested using an appropriate mix of acids and/or heat and/or pressure.

Subsequently, the digested sample is injected and ionized in the plasma torch. As the last step ions are separated and identified using their mass to charge ratio (m/c), in a mass spectrometer. Ionic masses measurement is performed by a device that filters ions with a specific m/c ratio. Quadrupoles are the most used, and they consist of four metal rods to which radio frequency and direct current voltages are applied. Frequency and current determine which ion, with a specific m/c ratio, will pass through the quadrupole and rich the detector. A detailed description of the methods and of the physical principles can be found elsewhere (e.g. Neff, 2017; Sader and Ryan, 2020; Wilschefski and Baxter, 2019).

In the present thesis, ICP-MS analysis were performed on ceramic and sediment samples included in sections 5.1, 5.2 and 5.4. Samples were prepared following the methods previously used by Egging (Eggins et al., 1997), Ottley (Ottley et al., 2003) and Finlay (Finlay et al., 2012) with some modifications. Briefly, the method consisted of the hotplate acidic digestion of 100 mg of powdered sample in PFA Savillex® beakers using a solution made of 2 mL 47% HF (OPTIMA grade) and 0.5 mL of 65% HNO_3 (Suprapur grade), for 48h at 150ºC, followed by evaporation but not to the complete dryness to avoid the stabilization of fluorides that could precipitate. The crude was then re-suspended in 2 mL of freshly prepared aqua-regia solution and was allowed to digest over 24h at 140ºC. After the solution was dried over the hotplate, 2 mL of pure HNO_3 (65%) were added and allowed to digest under reflux for 24h. The final solution was prepared, after drying, with 1.6 mL of HNO_3 (65%) and fulfilled with milliQ water up to a final volume of 50 mL, to reach a solution matrix of $HNO_3 \cong 2\%$. Elemental content determination was performed on an Agilent 8800 ICP Triple Quad (ICP-QQQ). Prior to the analysis, the equipment was daily calibrated with a tune solution from Agilent, and the sensitivity and resolution was optimized as well as the doubly charged ions ($< 1.84\%$) and

[70] Plasma is a state of matter, it has not a defined shape, but it is similar to a gas. In the plasma a significant portion of the constituent particles are ionized. Ionization is normally produced by heat application, which determine the dissociation of molecular bonding and the conversion of the original material on its elemental constituents. In addition, heat can also ionize the atoms (loosing and acquiring electrons) and the plasma contain free charged particles.

oxides (<1.17%) were minimized. All the ceramic samples were analysed for Rb, Sr, Y, Zr, Nb, V, Cr, Co, Ni, Zn, As , Sc, Cu, Ga, Ge, Sn, Sb, Cs, Ba, La, Ce, Pr, Nd, Sm, Eu, Gd, Tb, Dy, Ho, Er, Tm, Yb, Lu, Hf, Th and U. For the quantification of the analytes, a multi-elemental solution from High Purity Standards was used and a solution with Ru, Rh and Ir was online added to each sample to be used as internal standards and to correct for possible drifts and matrix effects. Precision of analysis was achieved running each solution in triplicate reporting for each sample the relative standard deviation (RSD). The accuracy of the analysis and stability of the instrument was ensured through running certified reference materials (AGV-2 and W2-a) with the same matrix as our samples every 10 samples measurements. Experimental detection limits were performed by measuring a blank and a 200 ppb's standard solution in 11 replicates each. Quantification limits of the analysis were obtained from 10 times the detection limit obtained before. For interpretation, rare earth chemical elements (REE) were normalized to chondrite (McDonough and Sun, 1995).

4.6 Physical, mechanical and permeability tests

4.6.1 Helium pycnometry (HeP)

HeP is a method used to measure the volume, and consequently the density (when the weight is known), of different kind of porous or not porous materials. Organic and inorganic materials can be tested by this method. Besides, it also possible to evaluate which kind of porosity (closed or open) makes it up.

Different types of instruments exist. They take advantage of Archimede's principles of fluids displacement or the Boyle's Law of gas expansion whether the sample volume is determined using a liquid or a gas. Nowadays, inert gases (especially helium – He - and nitrogen - N) are widely employed because they do not react with the sample, and they can easily penetrate even in the smallest porous of the sample.

The method itself is very simple. A sealed sample chamber of known volume is pressurized to a target pressure with the displacement of a gas. Once stabilized, this pressure is recorded. A valve is then opened allowing the gas to expand into a reference chamber whose volume is also known. Once stabilized, the pressure is recorded a second time. The pressure drop is then compared to the behaviour of the system when a known volume standard underwent the same process. A complete description of the physical principle of the method and of the components can be found elsewhere (e.g. Tamari, 2004; Lowell et al., 2004).

In the present thesis, ceramic samples, included in section 5.3, have been tested. Fragments with dimension 1x1x1[71] cm were cut, washed and dried at 105 $\pm$ 5 °C for one day. After that the dry masses (m_D) was measured using an analytical balance model Sartorius R9. The real volume of dry cubes (V_R) was determined by helium pycnometer using an Ultra-pycnometer 1000 model of Quantachrome Instruments.

Subsequently, the wet solid mass (m_W) of the samples was determined after water absorption by immersion for 10 days. The same analytical balance was also utilized to evaluate the hydrostatic mass, m_{HY}, of wet specimens. Afterwards, the bulk volume V_B was calculated as:

$$V_B = [(m_W - m_{HY}) \div \rho_{TWX}] \times 100$$

In the previous formula, ρ_{TWX} is the water density (0.9970 g/cm^3) at 25 °C. Subsequently, the ceramic cubes were dried at 105 $\pm$ 5 °C for one day, to determine the Point Load strength index (section 4.6.2), and to be finely milled to evaluate the solid volume (V_S) by pycnometry.

[71] In the present work samples size could vary. Not always ceramics presented a wall thickness of 1 cm. So slightly irregular specimens were prepared.

Open porosity to water and helium ($\Phi_O H_2O, \Phi_O He$), closed porosity helium ($\Phi_C He$), total porosity (Φ_T), bulk density (ρ_B), real density (ρ_R) and solid density (ρ_S), were computed as:

$$\Phi_O H_2O\ (\%) = \{[(m_W - m_D)\ \div \rho_{TW°25C}] \div V_B\} \times 100$$

$$\Phi_O He\ (\%) = [(V_B - V_R) \div V_B)]\ \times 100$$

$$\Phi_C He\ (\%) = [(V_R - V_S) \div V_S)]\ \times 100$$

$$\Phi_T = \Phi_C He + \Phi_O He$$

$$\rho_S\ (\frac{g}{cm^3}) = m_D \div V_S$$

$$\rho_R\ \left(\frac{g}{cm^3}\right) = m_D \div V_R$$

$$\rho_B\ \left(\frac{g}{cm^3}\right) = m_D \div V_B$$

Weight imbibition coefficient (IC_W) and the saturation index (SI) were computed as:

$$IC_W(\%) = [(m_W - m_D) \div m_D] \times 100$$

$$SI\ (\%) = (\Phi_O He \div \Phi_O H_2O) \times 100$$

4.6.2 Mechanical test – Point Load Test (PLT)

PLT has been invented to characterize rock materials in terms of strength (ASTM International, 2021), but it is also utilized in the field of cultural heritage (Columbu et al., 2015; Sitzia, 2020), especially in the analysis of mortars.

It is an index test, meaning that it can be performed relatively quickly and without sophisticated equipment. In this case, it has been applied in the analysis of ceramic samples included in section 5.3, on the same specimens[72] utilized for helium pycnometry (HeP) tests.

The sample is subjected to an increasingly concentrated point load, applied through a pair truncated, conical steel platens until failure (Franklin, 1985). The observed failure load is used to calculate the normalized point load strength index, $Is_{(50)}$. The apparatus consists of a rigid loading frame, a loading measuring system, and a simple system of measuring the distance between the two platens. Samples of various size can be tested (1 to 10 cm thick maximum). Normalized point load strength index (Is_{50}) was determined with a Controls D550 Instrument, in accordance with the ASTM recommendations (ASTM International, 2021).

When specimens do not respect the standard size (i.e. 1x1x1 cm), the sample has to be tested perpendicularly to the longest and widest specimen side. Thus, prior the beginning of the test, in the case of "irregular lump testing specimens" (ASTM International, 2021), the size of the lower and upper base (W_1 and W_2) and the thickness of each sample (D) must be measured. Afterwards, the medium value for W $[(W_1+W_2)/2]$ must be calculated. Not normalized point load strength index has been calculated as:

$$Is\ (MPa, \frac{N}{mm^2}) = P/D_e^2$$

Where P is the failure point registered during the experiment, and D_e^2 is the equivalent core diameter calculated as:

$$D_e^2\ (mm^2) = 4 * \frac{A}{\pi}$$

Where A is equal to:

$$A\ (mm^2) = W * D$$

[72] Samples sizes were smaller than the advisable size because of sampling restriction on ceramics samples. They measured roughly 1x1x1 cm and they were considered as "irregular lump testing" specimens with a trapezoid geometric shape.

Considering that Is vary as a function of D and of D_e^2, the normalized value of point load strength index is normally calculated for a standard D size of 50 mm as:

$$Is_{(50)} = F * Is$$

Where F is the correction factor, and it is calculated as:

$$F = (\frac{D_e}{50})^{0.45}$$

4.6.3 Permeability test (PRM)

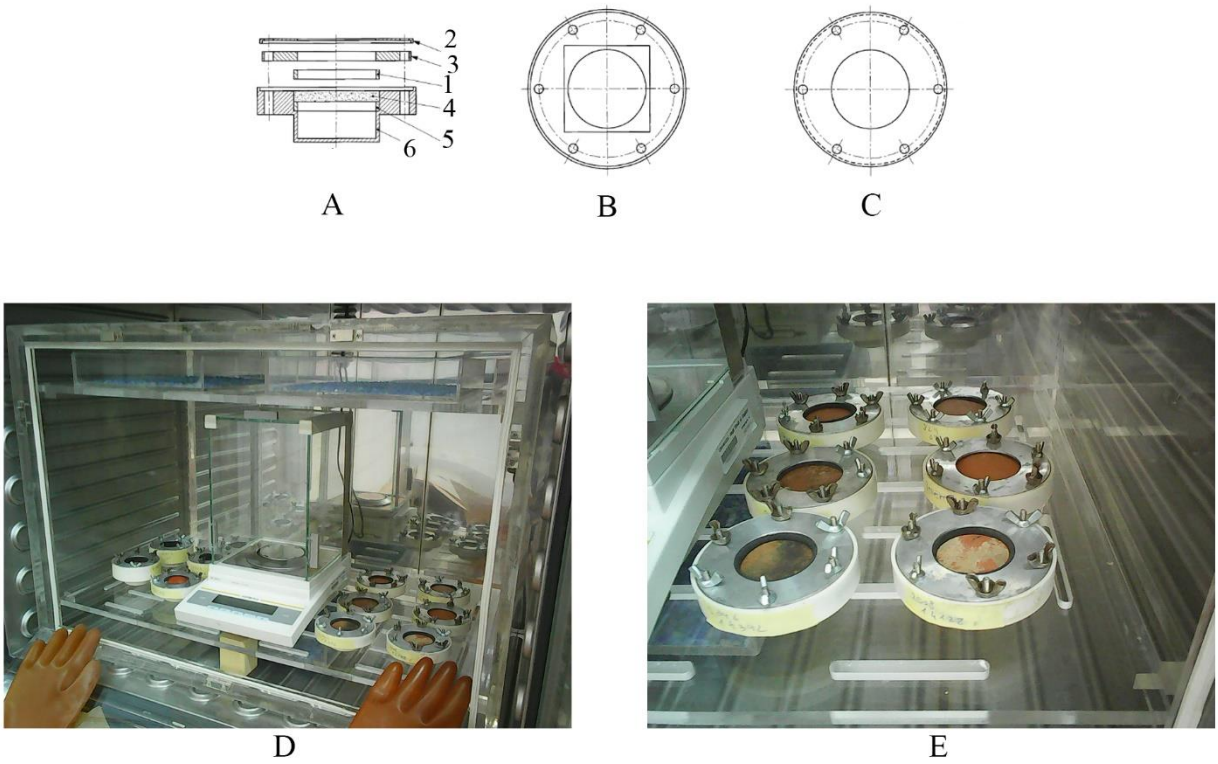

Figure 23 View of the PVC sample holder with the specimen. 1, joint rubber; 2, aluminium disc; 3, upper trimming; 4, sample; 5, lower trimming; 6, PVC sample holder (A); View of the sample holder from the top (B); View of the aluminium disc that covers the sample (C); View of the inside of the thermostatic chamber, of the samples, of the analytical balance and of the containers with silica gel (D); View of the samples inside the thermostatic chamber (E).

A PRM test is generally performed to determine the water vapour permeability of porous inorganic materials either untreated or subjected to any treatment or ageing. According to Recommendations 21/85 of the Italian research council (Normal, 1985), the vapour permeability was determined in samples roughly sized 5x5x1 cm.

Samples[73] were mounted on specific PVC sample holders[74] (Fig. 23 A, B, C), in between two different trimming and sealed. The bottom part of the PVC sample holder contained cotton wool with roughly 10 g of water, which are supposed to evaporate and cross the samples during the experience[75].

Afterwards, samples plus samples holder were positioned inside a specific thermostatic chamber[76] made of plexiglass (Fig. 23 D, E). The same chamber also holds an analytical balance (resolution equal to 0.0001 g) and three containers with silica gel. Silica gel is normally utilized

[73] Before any test samples are dried overnight at 105 °C.
[74] Before any test samples are dried overnight at 105 °C. Sample holders are normally built using inert material, which it is not corrodible and impermeable to water.
[75] In total, sample holder, sample, water and cotton wool do not weight more than 250 g
[76] The thermostatic chamber is normally mounted inside a laboratory stove.

to maintain the relative humidity stable during the experience. Once the thermostatic chamber was loaded, closed, and set to 25 °C.

The technique measures the mass of water vapour diffused through the flat sample with a specific thickness, in static condition and at regular intervals of time (24h), until the steady-state is reached. The water vapour is diffused thanks to a gradient of partial vapour pressure between the two parallel surfaces of the specimen. The steady-state is achieved if the average value of the weight variation (ΔM), between two successive measures (considering a minimum of four values), shows an oscillation of - 5% maximum. The vapour permeability is then calculated as:

$$Perm = [(\Delta M_i + \Delta M_{i-1}) \div 2] \div \pi r^2$$

The first part of the equation represents the media of two values recorded on steady-state, while πr^2 represent the circular surface area crossed by the water vapour. The permeability to water vapour is expressed in g/m^2 x 24 h (according to ANSI-ASTM C355- 64) and normalized to 20 °C.

In the present thesis, permeability tests were performed just on ceramic samples studied in section 5.3. Nowadays, permeability to vapour is usually measured in conservation of cultural heritage and building materials (Columbu et al. 2017a; Dondi et al. 2003; Silva et al. 2009) using standardized samples. In our case, it was not always possible. Traditional and archaeological ceramics had not flat and straight walls, and the thickness could be variable. So, permeability was also normalized to the fragment thickness as:

$$Perm\ norm. = Perm \div d$$

Where d is the sample thickness and the normalized value is expressed as (g/m^2 x 24h)/ mm), considering that the firing process might influence the vitrification of the ceramic paste. Consequently, its porosity (open and closed porosity), permeability to vapour can give a valuable indication of ceramic technology.

4.7 Experimental firing tests

Experimental firing tests (Fig. 24) were developped only in section 5.3, to evaluate different traditional ceramic and sediments properties such as:

- To quantify the evolution of physical and mechanical properties of traditional ceramic after different firing tests (750 and 1000 °C);
- To evaluate traditional ceramic mineralogical (XRPD) transformation after different firing steps (750 and 1000 °C);
- To evaluate raw materials (fraction < 63 μm) mineralogical (XRPD) transformations after different firing steps (400, 500, 600, 700, 800, 900, 1000 and 1100 °C). The two different raw materials employed by Mr. Domingos, on his atelier for traditional ceramic production, are especially important.

Tests were planned and performed following a predetermined firing cycle, like that adopted by the ceramist on his atelier. Samples were positioned inside porcelain crucibles and then positioned in the muffle chamber. The muffle furnace took 2 hours to reach the desired temperature, the maximum temperature was maintained for 5 hours and with a cooling time of 5 hours. At the end of each cycle, crucibles with samples were positioned inside a desiccator with silica gel in the bottom part to avoid humidity absorption after the test.

Figure 24 Extraction of calcined samples from the muffle furnace

5 Results

Caliph: Comprehensive archaeological and laboratory investigation of Islamic pottery in Portuguese History

This chapter present the result of this PhD thesis in 4 different sections

5.1 The Islamic ceramics of the Santarém Alcaçova: Raw materials, technology, and trade

The results obtained by the study developed in this section have been published on Archaeometry, an international Journal published by John Wiley & Sons, Inc.. Section 5.1 focuses on the archaeometric analysis of Islamic ceramics from the Alcaçova of Santarém, Portugal. The archaeological site has been excavated for many years by Prof. Ana Margarida Arruda from the University of Lisbon. To establish the ceramic provenance and the technology used, raw materials were sampled and compared with the archaeological ceramics. The results showed that two raw materials were selected for local ceramic production of unpainted and white-painted ceramic, and for monochromatic glazed ceramic. Five artefacts were imported from two different undefined regions of Southern Iberia. Including two samples of undecorated ceramic, one sample of monochromatic glazed ceramic and two samples of total *corda seca* glazed ceramics.

5.1.1 Introduction and goals of the section

The archaeological studies carried out in the *Garb al-Andalus* during the last 20 years, evidenced that the beginning of the Islamic domination represented a significant step forward in ceramic technology. Simultaneously, several archaeological questions arose regarding the characteristics of local ceramic production and the trade of polychromatic glazed ceramics, between the main towns of the *al-Andalus* (Islamic Iberia).

The most common wares, (i.e. unpainted and white-painted ceramics) were widely produced and utilized for everyday needs. In particular, the wide distribution of white-painted ceramic, in most rural and urban centres, is considered a fingerprint of the Islamic communities living in the *Gharb al-Andalus* since the Caliphal period (Gómez-Martínez et al. 2015). The distribution of dichromatic and polychromatic glazed ceramics in the firsts centuries of the Islamic domination, especially of the most remarkable ones, considering the ornamental diversity and decoration quality like honey and black (*melado e manganês* in Portuguese), green and brown (the so called *verde e manganês* in Portuguese) and *corda seca* decorated ceramics (CSP and CST), follow a different distribution pattern (Fernandes et al. 2015; Gómez-Martínez et al. 2018).

Initially, these ceramics were mainly recovered in towns close to rivers, such as the Guadiana (Mértola), Arade (Silves), Sado (Palmela, Alcaçer do Sal), Tagus (Lisbon, Santarém) and Mondego (Coimbra) or close to important terrestrial routes (e.g. Évora, Beja). The most up-to-date model suggests that these materials were mainly imported into the *Gharb al-Andalus* from different Islamic towns located on Southern Iberia or on the Iberian Peninsula inland (Gómez Martínez, 2009a).

Though artifacts seem typologically and stylistically similar, the identification by polarized light microscopy (PLM) of microfossils, limestone fragment, specific rock fragments/mineral (Berti et al. 2009; Capelli et al. 2005; Zozaya and Aparicio Yague 2003; Lapuente and Pérez-Arantegui 1999) or aeolian quartz grains (Capelli et al., 2011) may constrain the interpretation of ceramics provenance (Southern Iberia *vs* Northern Africa).

Thus, for archaeologists, decorated ceramics are considered the proof of sea and/or terrestrial trade (Fernandes et al. 2015; Gómez-Martínez et al. 2018). Subsequently, the imported goods were locally and regionally redistributed, and the biggest centres of the *Gharb al-Andalus* supposedly contributed to the spread of such materials. This situation seems to become slightly different during the *Taifa* kingdom-Almoravid period (11th-12th century) to a specific ceramic ware, *corda seca* glazed ceramics. This technique is characterized by a

design/composition (i.e. the *corda*) drawn on a pre-fired clay body using a mixture of manganese oxide (MnO or MnO_2) and/or iron oxide (FeO) (Déléry 2006; Peréz-Arantegui et al. 1999). Subsequently, the composition was completed using distinct coloured glazing preparations (Chapoulie et al., 2005). Ceramics could be totally (CST) or partially (CSP) covered by glazed decorations.

The diffusion of CST and CSP ceramics within the *Garb al-Andalus* pointed to the existence of local productions in several Islamic centres (I. C. Fernandes et al., 2015). In the Portuguese territory, workshops were just discovered in Lisbon, Santarém[77] and Mértola (Bugalhão and Folgado 2001; Liberato 2012; Gómez Martínez 2016), but none of those is associated to the production of polychromatic glazed ceramic. In Portugal, most of the archaeometric data were obtained by the analyses on archaeological ceramics collected in the Tagus valley, or very close to it.

In Lisbon, ceramic samples recovered from different Islamic workshops and in some domestic contexts have been compared with local raw materials (Bugalhão et al., 2008b). In this case, the local production of unpainted, painted (white and red), monochromatic and CSP ceramics were assessed. Unpainted, as well as white and red-painted ceramic production, were also confirmed in the Islamic *Alcaçova* of Lisbon (Dias et al., 2009).

In the *Garb al-Andalus*, raw material characteristics and selection procedures for local ceramic productions are almost unknown. In this framework, the local natural resources characterization is the best solution to understand pottery technology, to establish similarity in ceramic tradition[78], and to identify imported goods.

This study aims to understand these selection criteria concerning the choice and use of raw materials, and to define technological characteristics to address provenance issues in the town of Santarém (Portugal). The Islamic ceramics recovered in the Islamic *Alcaçova* have been sampled, analysed, and compared with local raw materials. Archaeological samples included unpainted, white-painted, with incised decoration, monochromatic and *corda seca* style ceramics (Arruda and Viegas, 1999).

[77] Workshops from the city of Santarém have been analysed in this PhD thesis. Results are presented on section 5.2.
[78] This aspect of ceramic production will be treated on section 5.3.

5.1.2 Ceramic and raw material sampling

Ceramic samples were recovered during different archaeological excavations conducted in the Islamic Alcaçova of Santarém, from 1984 to 1987 (Arruda and Viegas, 1999). The excavation covered an area of roughly 36 m^2 in sector 2 (Fig. 25). The Islamic level (4.5 m below the present topography) was characterized by the presence of a considerable number of "*silos*", ovoid or circular depressions with variable depth and diameter, excavated in the limestone bedrock. *Silos* were probably utilized to store food in the domestic space. In a second moment, they were filled with different materials (i.e., garbage) including ceramics. The typological

Figure 25 Picture of the archaeological excavation sector 2 carried out in the Alcaçova of Santarém (Portugal). Ovoid and circular depressions (i.e. silos) are visible

characterization of ceramics (Arruda and Viegas, 1999) indicated that *silos* were filled in a short period of time. The morphological diversity, the presence of glazed cooking pan as well as of polychromatic total *corda seca* ceramics suggest a chronology comprised between the end of the 11th and the first half of the 12th century, during the Almoravid occupation of the town. The ceramic assemblage (Table 2) includes fire ceramics (i.e. cooking pots), kitchen ceramics, container ceramics and objects with specific functions. Ceramics can be undecorated or present different decorative solutions such as incised decorations, white-paint, monochromatic or CST ceramics (Fig. 26). A description of *corda seca* glazing technique can be found elsewhere (Déléry, 2006a). Moreover, nine different raw materials were collected considering the geological information and outcrops availability (Zbyszewsky, 1953). Most of them pertain to

the *P1* (Pleistocene) geological unit and just one in the *M4* (Miocene). For each raw material, the most important information are reported with the following order: Sample name / Close village / Field description / Geological unit, layer / Geographic coordinates / Altitude (a.s.l.). Google Earth Pro[79] was utilized to collect georeferenced data for raw materials (Fig. 27):

- **Ca1** / Fonte da Pipa-Vale de Santarém / grey clay / P1, layer C1-C2 / 39°11'8.84''N, 8°43'31.36''W / 23 m
- **Ca2** / Ómnias-Santarém / beige clay with lime concretion / M4 / 39°12'45.05''N, 8°41'15.30''W / 20 m;
- **Ca3** / Ómnias-Santarém / grey clay / P1, layer C1-C2 / 39°13'7.01''N, 8°40'59.29''W / 19 m;
- **Ca4** / Santarém / yellow clay with sand / P1, layer C6 / 39°14'20.06''N, 8°40'36.09''W / 70 m;
- **Ca5** / Santarém / yellow clay / P1, layer C4 / 39°14'18.3''N, 8°40'36.13''W / 47 m
- **Ca6** / Santarém_SRib / yellow clay with calcretes / P1, layer C8 / 39°14'42.95''N, 8°41'3.75''W / 86 m;
- **Ca7** / Santarém_Rib3 / white siltstone / P1, layer C3 / 39°14'42.95''N, 8°41'3.75''W / 54 m;
- **Ca8** / Santarém_Rib3a / red clay with sand / P1, layer C2 / 39°14'42.95''N, 8°41'3.75''W / 57 m;
- **Ca9** / Santarém_Rib3b / yellow clay with sand / P1, layer C2 / 39°14'42.95''N, 8°41'3.75''W / 53 m.

[79] Data degree of reliability extracted using Google Earth Pro, such as elevation and horizontal accuracy, are discussed on specialized bibliography (Goudarzi and Landry 2017; Pulighe et al. 2016; Wang et al. 2017).

Table 2 Ceramic samples list with description and archaeological references (Arruda and Viegas 1999)

L.N.	Typology	Function	Decoration	Archaeological Reference
1	Jug	Kitchen ceramic	Pb	Alc. Sant., 2080, corte 2, I9, fossa 1
.2	Glass	Kitchen ceramic	Pb	Alc. Sant., 2079, corte 2, I9, fossa 1
3	Bottle	Container ceramic	Mon.Glaze	Alc. Sant., 2106, corte 2, I9, fossa 1
4	Bottle	Container ceramic	Cc	Alc. Sant.,2082, corte 2, I9, fossa 1
5	Jar	Container ceramic	Mon.Glaze	Alc. Sant., 2087, corte 2, I9, fossa 1
6	Jar	Container ceramic	Cc	Alc. Sant., 2105, corte 2, I9, fossa 3
7	Bowl	Kitchen ceramic	Mon.Glaze	Alc. Sant., 2062, corte 2, I9, fossa 1
8	Bowl	Kitchen ceramic	Mon.Glaze	Alc. Sant., 2063, corte 2, I9, fossa 1
9	Bowl, CST	Kitchen ceramic	Poly.Glaze	Alc. Sant., 2085, corte 2, I9, fossa 1
10	Bowl, CST	Kitchen ceramic	Poly.Glaze	Alc. Sant., 2086, corte 2, I9, fossa 1
11	Bowl	Kitchen ceramic	Cc	Alc. Sant., 2055, corte 2, I9, fossa 1
12	Bowl	Kitchen ceramic	Cc	Alc. Sant., 2016, corte 2, I9, fossa 1
13	Cup	Kitchen ceramic	Pb	Alc. Sant., 1998, corte 2, I9, fossa 1
14	Big bowl	Kitchen ceramic	Mon.Glaze	Alc. Sant., 2068, corte 2, I9, fossa 1
15	Big bowl	Kitchen ceramic	Mon.Glaze	Alc. Sant., 2070, corte 2, I9, fossa 1
16	Big bowl	Kitchen ceramic	Mon.Glaze	Alc. Sant., 2066, corte 2, I9, fossa 1
17	Big bowl	Kitchen ceramic	Cc	Alc. Sant., 2012, corte 2, I9, fossa 1
18	Big bowl	Kitchen ceramic	Cc	Alc. Sant., 2017, corte 2, I9, fossa 1
19	Cooking pan	Fire ceramic	Mon.Glaze	Alc. Sant., 2061, corte 2, I9, fossa 1
20	Cooking pan	Fire ceramic	Mon.Glaze	Alc. Sant., 2067, corte 2, I9, fossa 1
21	Cooking pan	Fire ceramic	Cc	Alc. Sant., 1994, corte 2, I9, fossa 1
22	Cooking Pot	Fire ceramic	Pb	Alc. Sant., 1911, corte 2, K9, fossa 3
23	Cooking Pot	Fire ceramic	Pb	Alc. Sant., 1926, corte 2, K9, fossa 2
24	Cooking Pot	Fire ceramic	Pb	Alc. Sant., 2025, corte 2, I9, fossa 1
25	Cooking Pot	Fire ceramic	Cc	Alc. Sant., 2020, corte 2, I10, fossa 4
26	Cooking Pot	Fire ceramic	Cc	Alc. Sant., 2004, corte 2, I10, fossa 4
27	Cooking Pot	Fire ceramic	Cc	Alc. Sant., 2041, corte 2, I10, fossa 4
28	Big Jar	Container ceramic	Cc	Alc. Sant., 2081, corte 2, I9, fossa 1
29	Big Jar	Container ceramic	Pb	Alc. Sant., 2026, corte 2, I9, fossa 1
30	Big earth. pot	Container ceramic	Id	Alc. Sant., 2039, corte 2, I10 banq. sul, fossa 4
31	Big earth. pot	Container ceramic	Id	Alc. Sant., 2022, corte 2, I10, banq. sul, fossa 4
32	Big earth. pot	Container ceramic	Cc	Alc. Sant., 2046, corte 2, I9, fossa 1
33	Earth. pot	Container ceramic	Cc	Alc. Sant.,1953, corte 2, J8, fossa 1
34	Earth. pot	Container ceramic	Cc	Alc. Sant., 2036, corte 2, I9, fossa 3
35	Basine	Kitchen ceramic	Cc	Alc. Sant., 2050, corte 2, I9, fossa 1
36	Lid	Fire ceramic	Cc	Alc. Sant., 2056, corte 2, I9, fossa 1
37	Small lantern	Spec. Function	Mon.Glaze	Alc. Sant., 2094, corte 2, K9, fossa 1
38	Clay charcoal braizer	Fire ceramic	Cc	Alc. Sant., 2091, corte 2, I9, fossa 1
39	Pot support	Spec. Function	Cc	Alc. Sant., 2093, corte 2, I9, fossa 1
40	Glass	Kitchen ceramic	Pb	Alc. Sant., 2078, corte 2, I9, fossa 1
41	Glass	Kitchen ceramic	Pb	Alc. Sant., 1937, corte 2, K9, fossa 3
42	*Alcatruz*	Container ceramic	Cc	Alc. Sant., 2097, corte 2, I9, fossa 1

Figure 26 Pictures of some samples analysed in this section.

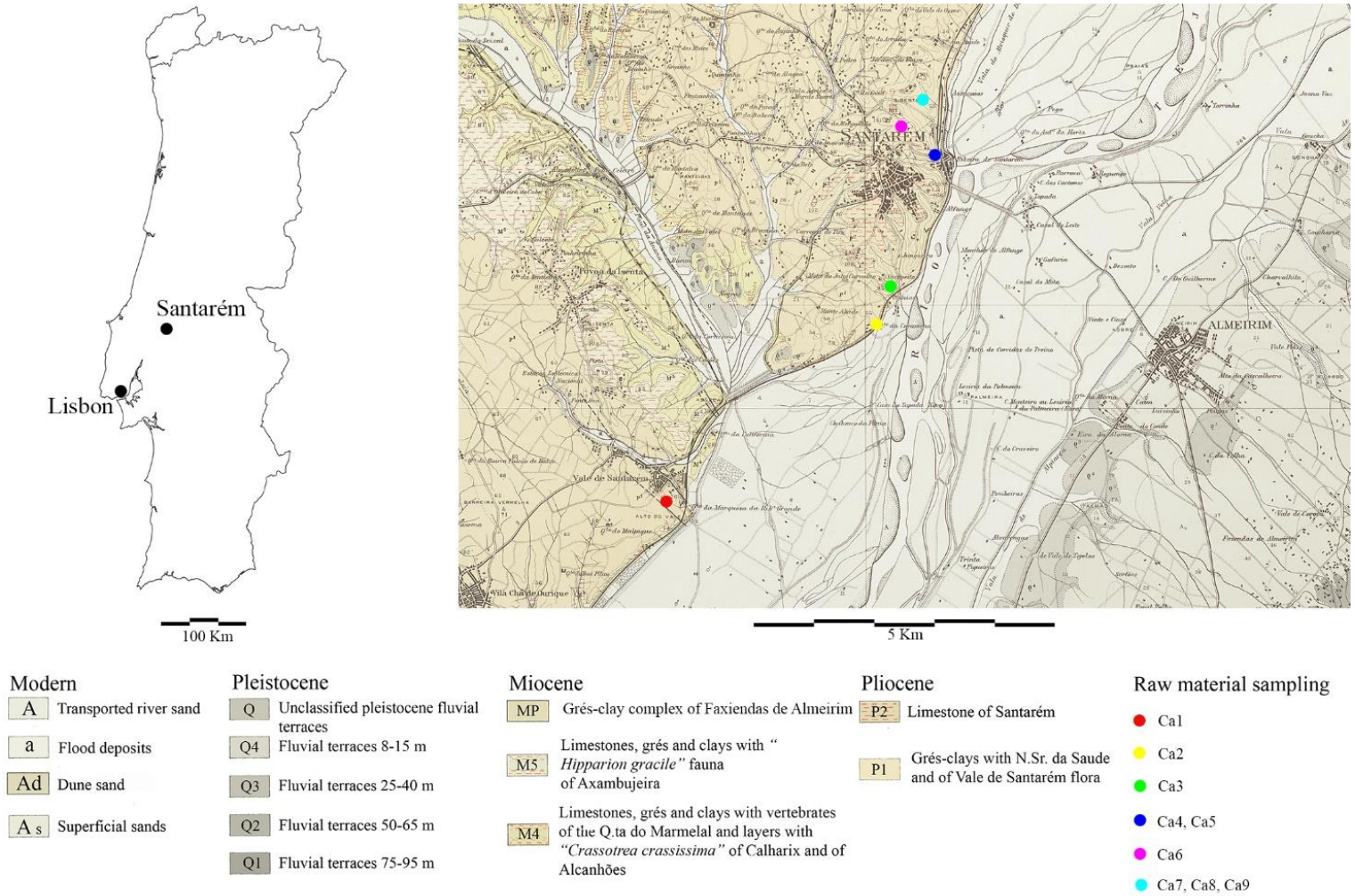

Figure 27 Geological map of Santarém area, after Zbyszewsky 1953. Raw material sampling position is showed by coloured circles

5.1.3 Analytical methods employed in this section

This section lists, with the aid of a small table, the analytical methods employed on ceramic and sediment analysis. For a detailed description of each method and regarding instrumental conditions, all information can be found in chapter 4. Several tables have been prepared from data collection. Because of their excessive size, XRPD, oriented aggregate mounts, XRF and ICP-MS results have been included at the end of the thesis in annex 1.

Table 3 List of the analytical methods employed in this section

Method		Samples analysed	Data tables added as annexe
Granulometry	*Grain size distribution*	Sediments	
	Sieving experiment	Sediments	
Microscopy	*PLM*	Ceramics	Ceramic paste and temper
	SEM-EDS	Ceramics	X
Mineralogy	*XRPD*	Ceramics and sediments	Ceramics and sediments
	Oriented aggregate mount	Sediments	
Chemistry	*XRF*	Ceramics and sediments	Major oxides
	ICP-MS	Ceramics and sediments	Trace elements

5.1.4 Results and discussion

5.1.4.1 Characterization of raw materials

5.1.4.1.1 Grain size distribution and the sieving experiment

Sediments are mostly composed of sand (>63µm), with values between 68.7 and 98.6% of the total weight. Gravels were rarely present. Very coarse (1.99-1mm) and coarse sand (0.99-0.5 mm) are usually not abundant, but the sum of these two fractions could rich up to 43.7%. Medium (0,49-0,25mm), fine (249-125µm) and very fine sand (124-63µm) are generally more abundant. In all cases, silt+clay (<63µm) percentage does not exceed 31.3 % (Table 4). On samples Ca4 and Ca8 the total sand percentage is very high (98.6% and 97%), and medium and fine sand are more than 60% of the total weight sieved sediment. On samples Ca2, Ca3, Ca6, Ca9, sand is between 79.6% (Ca2) and 89.1% (Ca9). On samples Ca3 and Ca9, very coarse and coarse sand represent more than 42% of the sediment. On samples Ca1, Ca5, Ca7, sand percentage is still very high, 68.7% (Ca7), 71.1% (Ca1) and 70.3% (Ca5), but the silt+clay is the more abundant, roughly around 30% of the total sediment. So, some raw materials were probably not appropriate for pottery production considering the high amount of sand (such as Ca8 and Ca4), while raw materials Ca2, Ca3, Ca6 and Ca9 could be slightly more suitable. Nevertheless, sand content is still very high. Conversely, raw materials Ca1, Ca5, Ca7 could be easily selected for ceramic production. In all cases, these raw materials must be treated before their use to increase clay content.

Table 4 Granulometric analysis results expressed in weight percentage, W%. VCS, very coarse sand; CS, coarse sand; MS, medium sand; FS, fine sand; VFS, very fine sand; S+C, silt plus clay; TS, total sand.

		Weight percentage, w%						
		VCS	CS	MS	FS	VFS	S + C	TS
Sediment Sample	Closest village	1.99-1 mm	0.99-0.5 mm	0.49-0.250 mm	0.249-0.125 mm	0.124-0.063 mm	> 0.063 mm	%
Ca1	Fonte da Pipa - Vale de Santarém	4.4	12.4	24.6	15.5	14.2	28.9	71.1
Ca2	Omnias - Santarém	10.9	16.4	16.2	21.1	15.0	20.4	79.6
Ca3	Omnias - Santarém	17.5	25.1	19.1	14.2	9.2	14.9	85.1
Ca4	Santarém	13.1	15.8	18.7	43.9	7.1	1.4	98.6
Ca5	Santarém	6.6	19.5	20.9	13.2	10.1	29.7	70.3
Ca6	Santarém	9.5	10.0	16.5	32.0	17.9	14.2	85.8
Ca7	Santarém	11.0	14.5	10.1	11.7	21.4	31.3	68.7
Ca8	Santarém	3.1	7.3	35.9	44.7	6.0	3.0	97.0
Ca9	Santarém	23.2	20.5	19.4	16.5	9.5	10.9	89.1

5.1.4.1.1 Mineralogical composition: XRPD and oriented aggregate mounts

All XRPD data can be found in the annexe 1 (Table 8 and 9). Results show that on raw material quartz is the dominant mineral phase, followed by potassium-rich feldspars and sodium-rich plagioclase, in all the fraction of each sample. On raw material Ca6 and Ca8, the amounts of sodium-rich plagioclases are slightly higher. In some cases, anatase (Ca1, Ca7, Ca8), calcite (Ca2, Ca3, Ca6) and halite (Ca2, Ca4) were identified. Among phyllosilicates, illite/muscovite was dominant, with lower amounts of kaolinite (particularly abundant on samples Ca1, Ca7), chlorite (Ca2), smectite (Ca2, Ca4, Ca6, Ca7, Ca8, Ca9), vermiculite (Ca4, Ca5, Ca6, Ca8, Ca9) and interstratified chlorite-smectite (Ca7). As expected, the tectosilicates/phyllosilicates ratio decreases from the URM (untretaed raw material) to the <63 μm sub- samples. On raw materials Ca1, Ca5 and Ca7, this effect is weak or inexistent due to the originally high clay content, and more clay could be extracted for ceramic production.

The analyses of oriented aggregate mounts further confirmed illite/muscovite (the most abundant), kaolinite, chlorite, vermiculite, and smectite identification. Raw material Ca3 is mostly composed of illite/muscovite, Ca2 by chlorite, while raw materials Ca1 and Ca7 are quite enriched in kaolinite. In all other cases, illite/muscovite was accompanied by a smaller amount of kaolinite, smectite, vermiculite or interstratified chlorite-smectite.

5.1.4.1.2 Chemical composition: XRF and ICP-MS analysis of raw materials

All the results of XRF and ICP-MS analysis can be found in annexe1 (Table 22 to 32). On raw materials, from the URM samples to the < 63 µm samples, SiO_2/Al_2O_3 ratio almost always decreases. This behaviour can be explained by higher clay content in the silt+clay fraction, as evidenced by XRPD patterns. SiO_2/Al_2O_3 ratio is higher on raw materials Ca3, Ca4, Ca8 and Ca9. Raw materials Ca2 and Ca6 show intermediate values. On the contrary, on raw materials Ca1, Ca5 and Ca7, it is lower and quite constant. Also, L.O.I. values do not change significantly, indicating stable sand content in these samples considering particle size.

Raw material Ca2 is enriched in Na_2O and MgO, and halite and chlorite have been identified on XRPD patterns. Raw material Ca6 is also enriched in Na_2O, and sodium-rich plagioclase concentration increased on XRPD patterns. The CaO content is usually low (< 1 wt%), but on raw materials Ca2, Ca3 and Ca6 can be higher (maximum 6.81 wt%), and calcite could be identified.

By decreasing the particle size, Al_2O_3 increase and SiO_2 decrease. This general trend is more evident in the sand-rich samples (i.e. Ca4 and Ca8), and doubtful in clay-rich samples (i.e. Ca1, Ca5 and Ca7) as can be realized by the rather constant SiO_2/Al_2O_3 ratio. Fe_2O_3 is negatively correlated to SiO_2/Al_2O_3 ratio, and its concentration increase from the URM to the < 63 µm samples. Fe_2O_3 does not clearly follow this path on clay-rich raw materials (i.e Ca1, Ca5 and Ca7). This is especially clear on raw material Ca1 (Fig. 28).

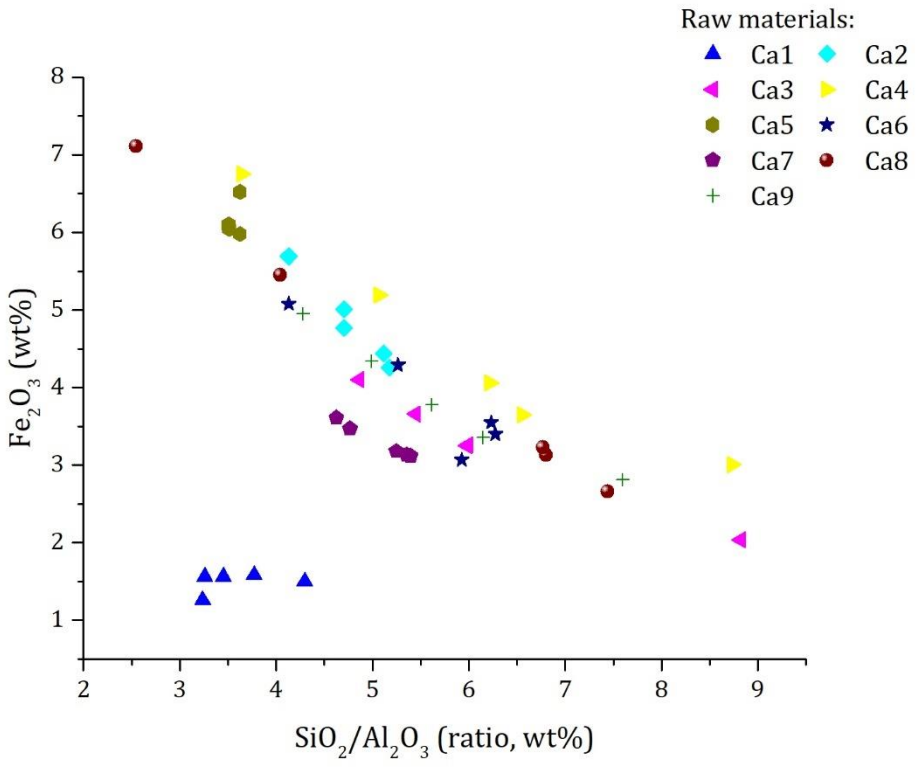

Figure 28 Binary plot SiO_2/Al_2O_3 ratio vs Fe_2O_3

Besides, the linear relation between Fe_2O_3 and TiO_2 (and most of the transition metals) divides raw materials into two main groups, titanium oxide-rich/iron oxide-poor (i.e., Ca1, anatase detected by XRPD, $Fe_2O_3/TiO_2<1.56$), and with iron+titanium oxides (i.e., Ca2, Ca3, Ca4, Ca5, Ca6, Ca7, Ca8 and Ca9, $2.97<Fe_2O_3/TiO_2<8.50$), where ilmenite ($FeTiO_3$) is probably a critical phase.

Zirconium concentration roughly increases when particle size decreases (SiO_2/Al_2O_3 ratio decrease). The only exceptions are raw materials Ca3 and Ca7 suggesting that zircon ($ZrSiO_4$) is more abundant in the sandy fraction of these sediment samples. Moreover, the relation between Zr-U (Fig. 29) showed 2 different patterns in zircon mineral population (Fedo et al., 2003) with different Zr/U-Hf/U ratios. These ratios distinguish raw material Ca1 ($Zr/U<25.87$; $Hf/U<0.73$) from the others ($Zr/U>34.31$; $Hf/U>0.96$).

Regarding REE, all raw materials are enriched in $\sum LREE_{CN}$ if compared to $\sum MREE_{CN}$ and $\sum HREE_{CN}$, and they present a significant negative Eu_{CN} anomaly, which indicates Eu^{2+} fractionation at the source (Henderson, 1984). The Ce_{CN} anomaly is absent or small. The sieving experiments show that $\sum REE_{CN}$ has similar behaviour to Zr in all raw materials. REE tend to increase in the <63 μm fractions because sand content (i.e., quartz) mainly dilute REE_{CN} abundance in the sand rich sub-samples. So, the overall REE_{CN} profile is generally preserved but with small differences depending on grain size (Fig. 30). Considering all different sub-samples, raw materials Ca1, Ca5 and Ca7 have relatively stable SiO_2/Al_2O_3 ratio and $\sum REE_{CN}$ abundance

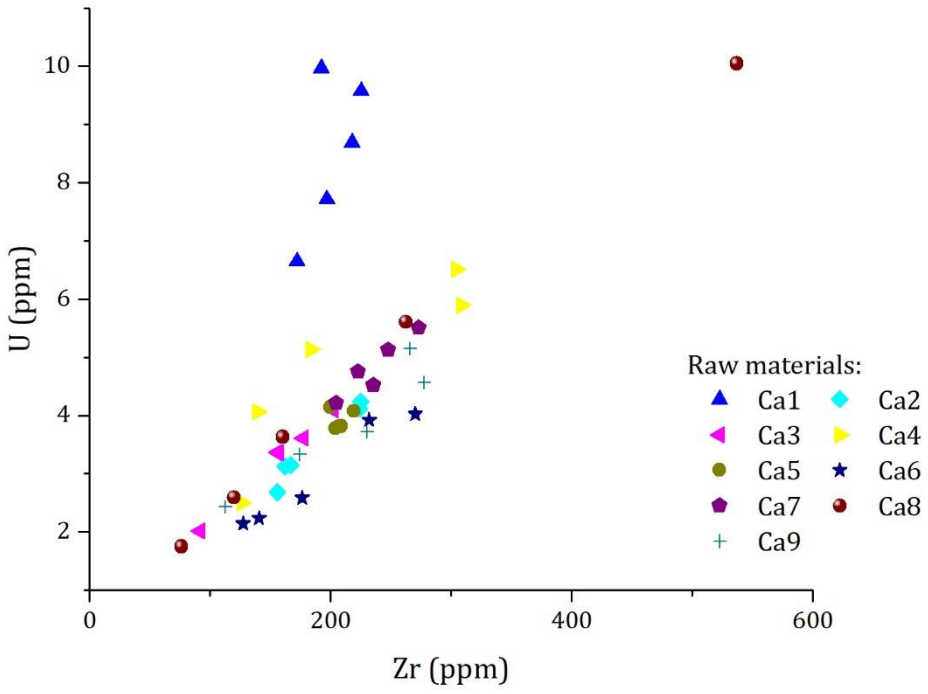

Figure 29 Zr vs U binary plot of sediment samples.

and patterns. If raw materials REE_{CN} patterns are compared to that of the European shale (Bau et al., 2018), the result shows that clay-rich raw materials are more similar to the standard profile than the sand-rich ones. So, as expected, the fine fraction of these raw materials are quite mature sediments with contributions from different source rocks.

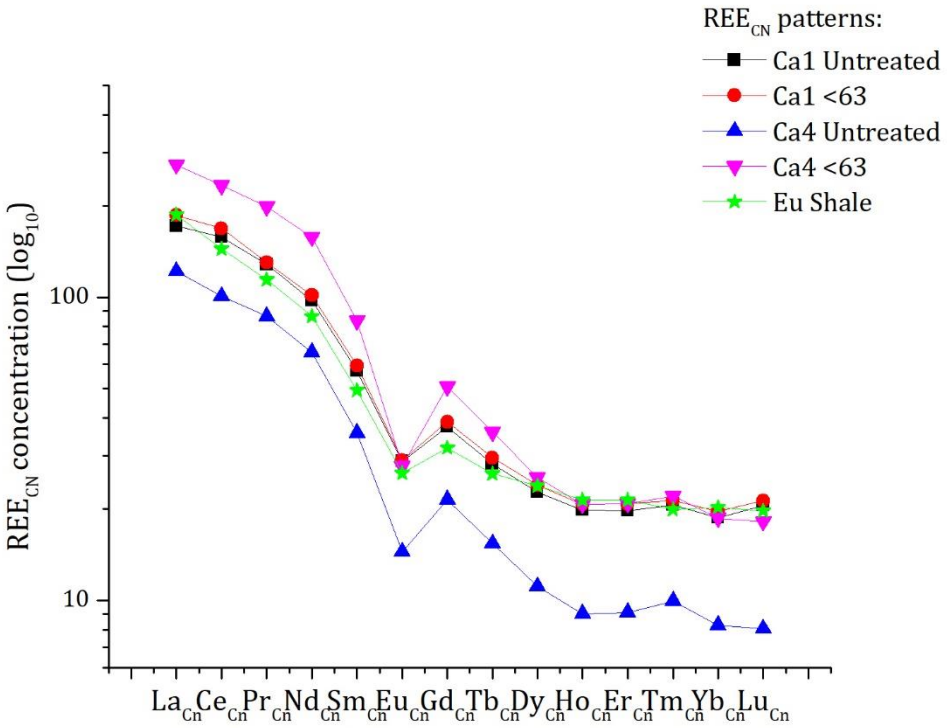

Figure 30 REE_{CN} profiles of the sediment samples Ca1 and Ca4. The graph also reports the profile of the Eu shale (Bau et al., 2018)

5.1.4.2 Archaeological ceramics

5.1.4.2.1 Microscopy: PLM on ceramic thin-sections

PLM observations (Annexe 1 / table 2 to 6, Fig. 31) showed that inclusions are mainly composed of quartz, potassium-rich feldspar, few plagioclase feldspars (mainly sodium-rich), muscovite, green-brown tourmaline, biotite, brown-green amphibole, clay pellets and, in some cases, by post-depositional calcite (contamination from the soils) and/or secondary calcite (recrystallized after firing). Rock fragments were identified as quartzite, sandstone, slate, granite and micritic limestone, sometimes thermally altered. In some cases, *microforaminifera* bioclasts were also detected. Regarding secondary calcite, it usually surrounds thermally altered limestone fragments. Post-depositional calcite, mainly in monochromatic glazed ceramic and in some unpainted and white-painted ceramics, could also appear dispersed in the ceramic paste or inside pores, suggesting contamination from the soil.

Pores size and shape is quite variable, and bigger pores have been observed on big container ceramics with thicker walls (i.e., big jars, earthen pots). Just in some cases, pores are parallel to the vessel wall. Grain size distribution can be unimodal or bimodal. Inclusions' shape varies from angular to sub-rounded. The most rounded and abundant fraction is composed of very fine sand and silt.

The characteristics observed by PLM allowed the identification of three different fabrics (Fig. 31). An iron-rich ceramic paste characterizes fabric 1, usually red/brown/dark brown in colour and poorly sorted inclusion sized up to 2.2 mm. Temper concentration is between 5 and 20%. The lower amount of temper is typical of thin walled pottery, and sorting is poor to moderate. The alignment of the inclusion is weak to moderate, in rare cases, strong. The main temper minerals are quartz, K-feldspar, plagioclase, muscovite, and occasional green-brown tourmaline. Quartzite is frequent, and limestone, sandstone and granite can be present. The fabric has been further subdivided into 3 different sub-groups. Subgroup *1A* has a red ceramic paste with inclusion concentration ranging from 5.39 to 18.40 %. In subgroup *1B*, the ceramic paste is brown-dark brown and inclusion concentration ranging from 14.01 to 20.81 %. Subgroup *1C* was utilized for object with thinner walls, and inclusion concentration is comprised between 8.08 and 13.24 %.

Fabric 2 has a grey/brown ceramic paste, slightly enriched in post-depositional calcite (samples n. 3-37), temper is moderately sorted and sized up to 1 mm. Temper concentration ranges between 5.49 and 12%. The mineralogy is very similar to fabric 1, but the amount of rock inclusions is lower if compared to fabric 1.

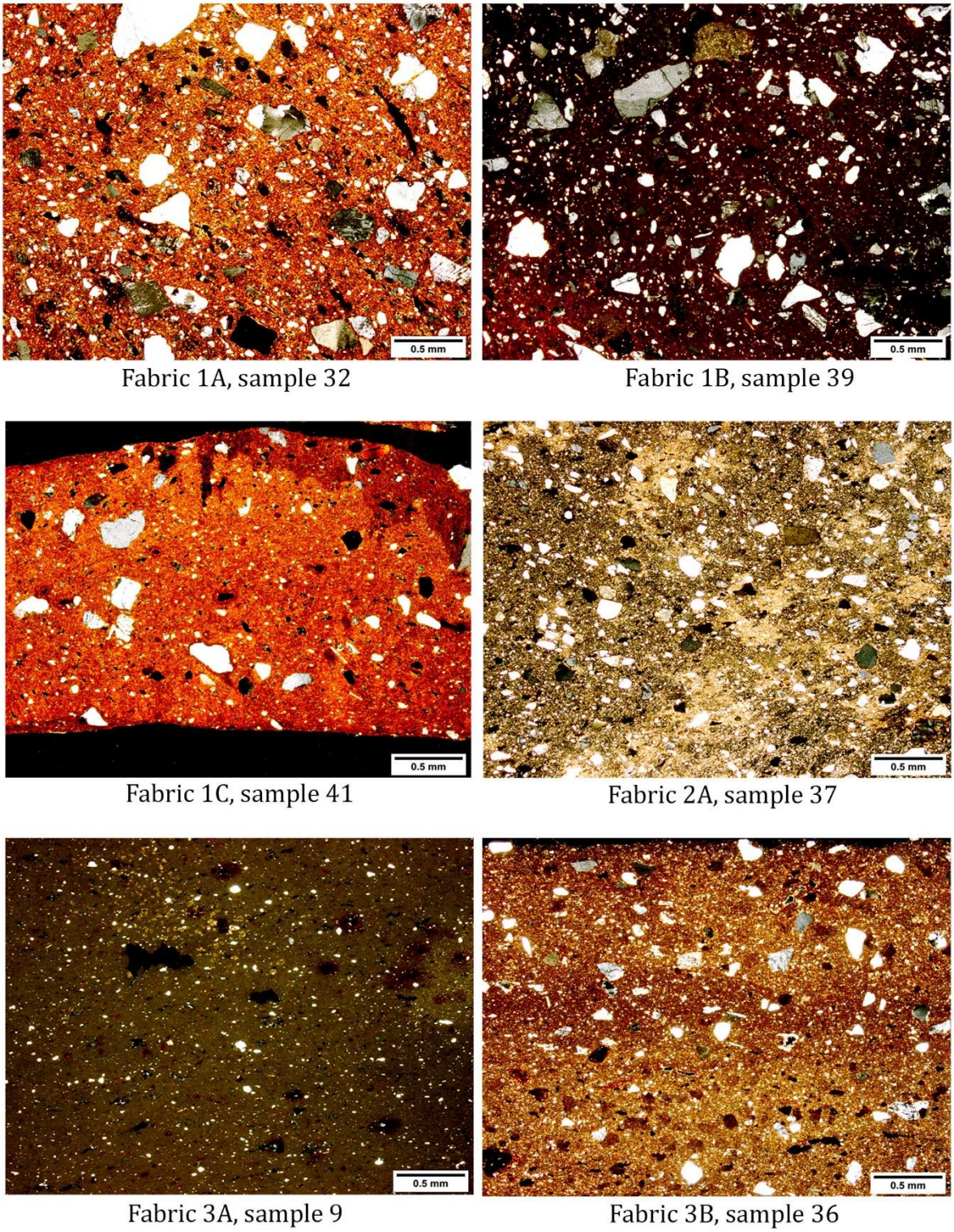

Figure 31 Pictures captured during PLM analysis of the different fabrics and subgroups

Fabric 3 has grey/grey-brown calcium-rich ceramic paste, with well-moderate sorted inclusion sized up to 0.95 mm. On samples 11 and 36 (undecorated ceramics) the granulometric distribution is bimodal. Secondary calcite, thermally altered limestone fragments and *microforaminifera* bioclasts were also identified (samples 5, 10, 11, 36). Temper ranges between 2 and 8%. Nevertheless, the fabric was divided into two different sub-groups.

On sub-group *3A,* temper size is generally smaller (maximum 0.45 mm) if compared to sub-group *3B* (maximum 0.95 mm). Moreover, also temper concentration is slightly different, up to 6.67% on sub-group *3A*, and up to 8.35% on sub-group *3B*.

The results obtained by PLM analysis indicate that fabrics have different characteristics due to the use of distinct raw materials. Fabric 1 (with subgroups A, B, C) was utilized to produce different functional objects, including white-painted ceramics, undecorated ceramics, ceramics with incised decoration, as well as two samples of monochromatic glazed ceramic (samples n. 19-20). Fabric 2 was just utilized to produce monochromatic glazed ceramic. All ceramics included in fabrics 1 and 2 are compatible with the local geology, so they were probably locally produced.

The identification of thermally altered limestone fragments and *microforaminifera* bioclasts in the ceramic paste distinguishes fabric 3 (subgroups *A*, *B). Microforaminifera* have been previously observed by PLM on different samples from Malaga, Almeria and Mallorca in the Mediterranean area (Berti et al. 2009; Capelli et al. 2005; Zozaya and Aparicio Yague 2003). Moreover, the absence of aeolian quartz inclusions suggests they were not imported from the North of Africa (Capelli et al., 2011). Samples n. 5-11-36 (undecorated and mono-chromatic glazed ceramics) and samples n. 9-10 (*corda seca* style ceramics) are included in this category.

5.1.4.2.2 Mineralogical composition: XRPD of ceramic samples

XRPD data (Annex 1, table 7) shows that ceramic samples can be divided into two different groups, A and B. On group A, all sub-group of fabrics 1 and fabric 2 are included. Group B is just composed by ceramic samples included in fabric 3 (samples n. 5-9-10-11-36). On group A, quartz, potassium-rich feldspars and illite-muscovite were the dominant mineralogical phases followed by sodium-rich feldspars. Hematite was identified in most samples, and calcite can also be present in small amounts. In minor amounts, tourmaline, anatase, mullite, and traces of smectite have also been identified. On group B, quartz and potassium-rich feldspars are less abundant, and illite/muscovite peak is absent in some samples. Calcium-rich phases such as calcium-rich plagioclase, pyroxene (i.e. diopside) and gehlenite-akermanite were more abundant. Ca-rich plagioclase and pyroxene were not detected by PLM, so they formed during the firing process. Calcite is ubiquitous, and it is a major phase in sample n. 36. Minor amounts of hematite were also identified.

The estimated firing temperature of group A ceramics can vary. The identification of smectite (sample 1), vermiculite (sample 32), calcite, hematite, illite-muscovite and mullite indicate that ceramic were probably fired in a temperature range comprised between 500 and 1050 °C (Maritan et al. 2006; Nodari et al. 2007; Cultrone et al. 2004; Cultrone et al. 2001; Rodriguez-Navarro et al. 2003; Riccardi et al. 1999; Jordán et al. 1999). The low firing temperature of samples 1 and 32 was probably due to the ceramic position inside the kiln, sample thickness or of a short duration firing cycle. The presence of smectite can also be explained by a recrystallization process in the buried artefact.

On group B, high-temperature calcium-rich mineralogical phases usually form above 800 °C (Trinidade et al., 2009) at the expense of calcite and clay minerals. On sample n. 36 both calcite, which usually disappears above 750 °C, and clay minerals were abundant while lower amount of pyroxenes were identified. Moreover, on two samples, illite/muscovite was not identified, suggesting a firing temperature higher than 1000 °C. Thus, ceramic samples from group B were probably fired between 700 and 1050 °C.

5.1.4.2.3 Chemical composition: XRF and ICP-MS analysis of ceramics

Major oxides (annexe1, table 10 to 12) content reflects the general subdivision obtained by PLM (fabrics 1, 2, and 3), with the identification of 3 main groups. Groups have a different chemical composition and SiO_2/Al_2O_3 ratio (mean=3.63, 4.58, 3.53) becomes smaller when temper content decreases and the clay fraction increase. Similar behaviour has been observed during sediment analysis on different raw material sub-samples.

From the chemical point of view group 1 have low CaO (mean=0.79 wt%) and high Fe_2O_3 (mean=5.58 wt%) concentration. The relation between SiO_2/Al_2O_3 ratio *vs.* Fe_2O_3 (Fig. 32) indicated that Al_2O_3 is associated with Fe_2O_3 in the enriched clay fraction. Samples 19 and 20 are an exception. They have lower Fe_2O_3 content as well as SiO_2/Al_2O_3 ratio if compared to temper content (around 20%). In this case, possibly, the original raw material of group 1 was partly mixed with a different Al_2O_3 rich raw material, probably potassium-rich feldspars, as evidenced by XRPD patterns. The relations between Fe_2O_3 and TiO_2 on group 1 ($5.71<Fe_2O_3/TiO_2$ ratio<9.26) suggests that ilmenite ($FeTiO_3$) is an important phase.

Group 2 has low Fe_2O_3 (mean=1.49 wt%) and low CaO (mean=0.89 wt%) concentration, and it is enriched in TiO_2 (mean=1.13 wt%). In particular, the low Fe_2O_3/TiO_2 ratio (<1.39) suggests that titanium oxides are probably abundant in the ceramic paste.

Group 3, which includes *corda seca* style ceramics, is enriched in Na_2O, CaO (mean=17.18 wt%) and Sr (mean=357.18 ppm) and poorer in SiO_2 (mean=46.04 wt%).

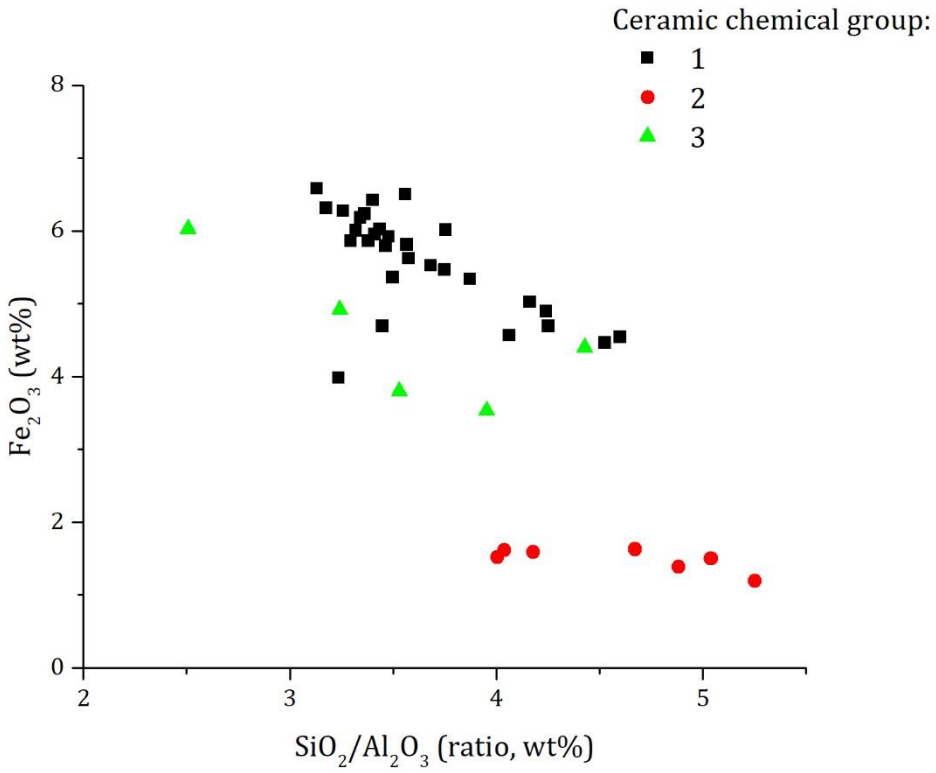

Figure 32 SiO_2/Al_2O_3 ratio vs. Fe_2O_3 binary plot of ceramic group identified after chemical analysis

Nevertheless, within this group, samples 5, 9 and 10 present higher Sr content (>421.89 ppm) and Fe_2O_3/TiO_2 ratio (>8.03) if compared to samples 11 and 36 Sr (Sr<242.36 ppm; Fe_2O_3/TiO_2<4.67).

Regarding trace elements (annexe 1, table 13 to 15), the linear correlation between Zr/U and Hf/U (Fig. 33) evidenced that different populations of zircon ($ZrSiO_4$) minerals are present. On group 1, samples have Zr/U>36.30 and Hf/U>1.18, while on group 2, samples have Zr/U<32.16 and Hf/U<1.03. Moreover, some samples of group 1 (i.e. 19, 20, 25, 27, 28, 33) have similar ratios to group 2 samples. On group 3, samples could have similar ratios to groups 1 or 2, suggesting differences in zircon mineral composition within the group.

The REE analyses (annexe 1, table 16 to 21) showed that all samples are enriched in $LREE_{CN}$ if compared to $MREE_{CN}$ and $HREE_{CN}$ and present a negative Eu_{CN} anomaly (Fig. 34). The overall $\sum REE_{CN}$ abundance is generally higher on ceramic samples of group 2. Samples of groups 1 and 3 have a similar abundance of $\sum REE_{CN}$, but they differ in major oxides concentration. Result also showed that $\sum REE_{CN}$ abundance within groups usually increase when SiO_2/Al_2O_3 ratio decreases due to the presence of less temper in the ceramic paste. This suggests that quartz (i.e. the major inclusion) has a dilute effect on REE_{CN} abundance.

On group 1, 2 and 3 $\sum LREE_{CN}/\sum MREE_{CN}$ ratios (mean=4.8, 4.87, 4.35), $\sum LREE_{CN}/\sum HREE_{CN}$ ratio (mean=8.68, 9.40, 8.21) and Eu_{CN} anomaly (mean=0.58, 0.58, 0.61) are slightly similar. The mean REE_{CN} groups profiles are also comparable to the European shale

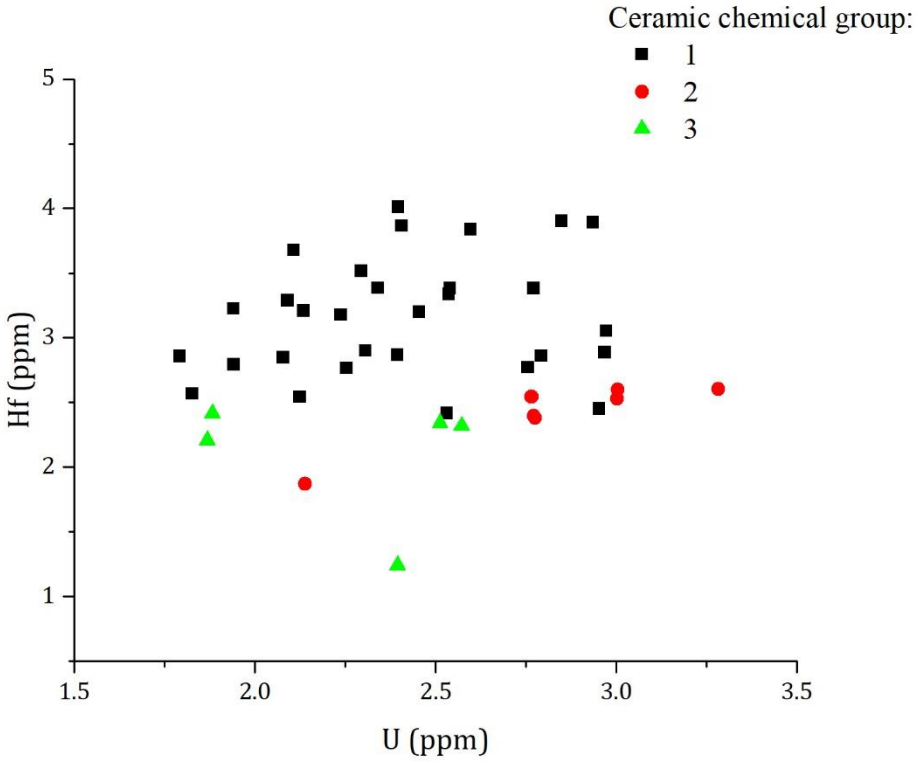

Figure 33 Hf vs U binary plot of ceramic group identified after chemical analysis

profile (Bau et al., 2018), $\sum LREE_{CN}/\sum MREE_{CN}$ ratio=4.49, $\sum LREE_{CN}/\sum HREE_{CN}$ ratio=7.15 and Eu_{CN} anomaly=0.66 pointing to the exploitation of mature clay-rich sediments for ceramic production in each case (Fig. 34) but they generally have less $HREE_{CN}$.

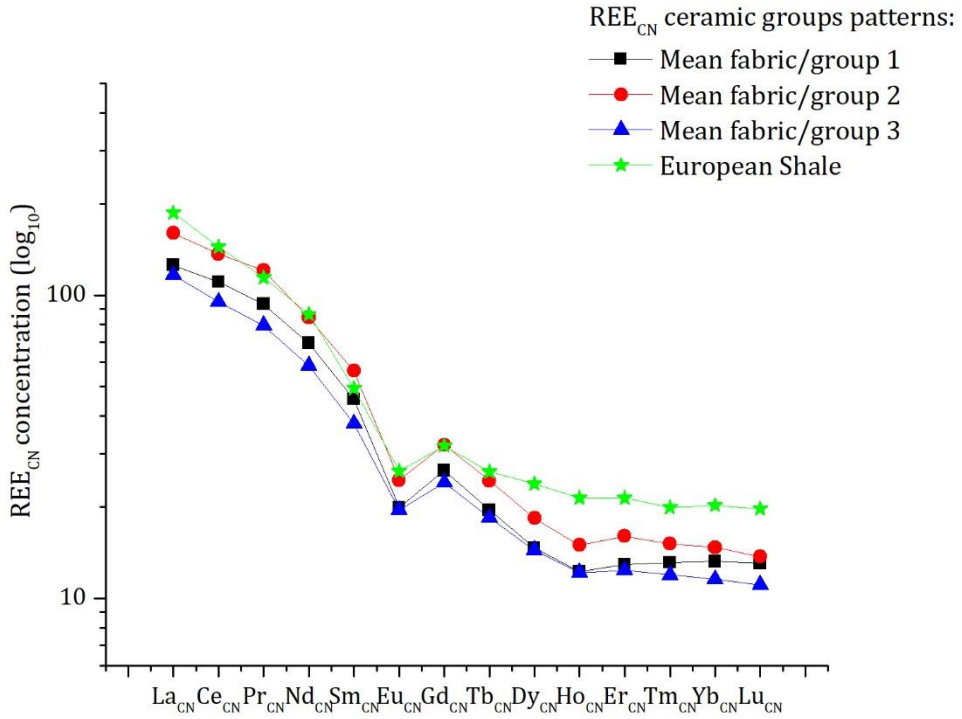

Figure 34 REE_{CN} profiles of fabrics/groups 1, 2 and 3 compared to the European shale (Bau et al., 2018)

5.1.4.2.4 Microscopy: SEM-EDS micro-analysis of the ceramic paste

Micro-analysis by SEM-EDS of ceramic pastes were developed in all samples, to understand chemical elements distribution (chemical mapping) in the matrix, and the chemical composition of specific temper inclusion by spot/area analysis.

Results evidenced that Al_2O_3, Fe_2O_3 and MgO are abundant in the ceramic paste of fabric 1, Al_2O_3 on fabric 2 (Fig. 35A/B), while Cao and MgO on the ceramic paste of fabric 3. These data corroborate previous tests, pointing to the exploitation of 3 different raw materials for ceramic production. Temper grains, mainly sand and silt, are composed of muscovite, quartz, potassium-rich feldspars and sodium-rich plagioclase (Fig. 35D). Punctual analysis of feldspar minerals evidenced that the anorthitic component in sodium-rich plagioclases is rarely higher than 25% (Fig. 36). Among micro-sized silty inclusions ilmenite (sometimes enriched in Mn), iron oxides, barite, monazite and zircon have been identified. Titanium oxides such as anatase and/or rutile were particularly represented on ceramic samples of fabric 2 as suggested by XRPD and chemical analyses (Fig. 35C).

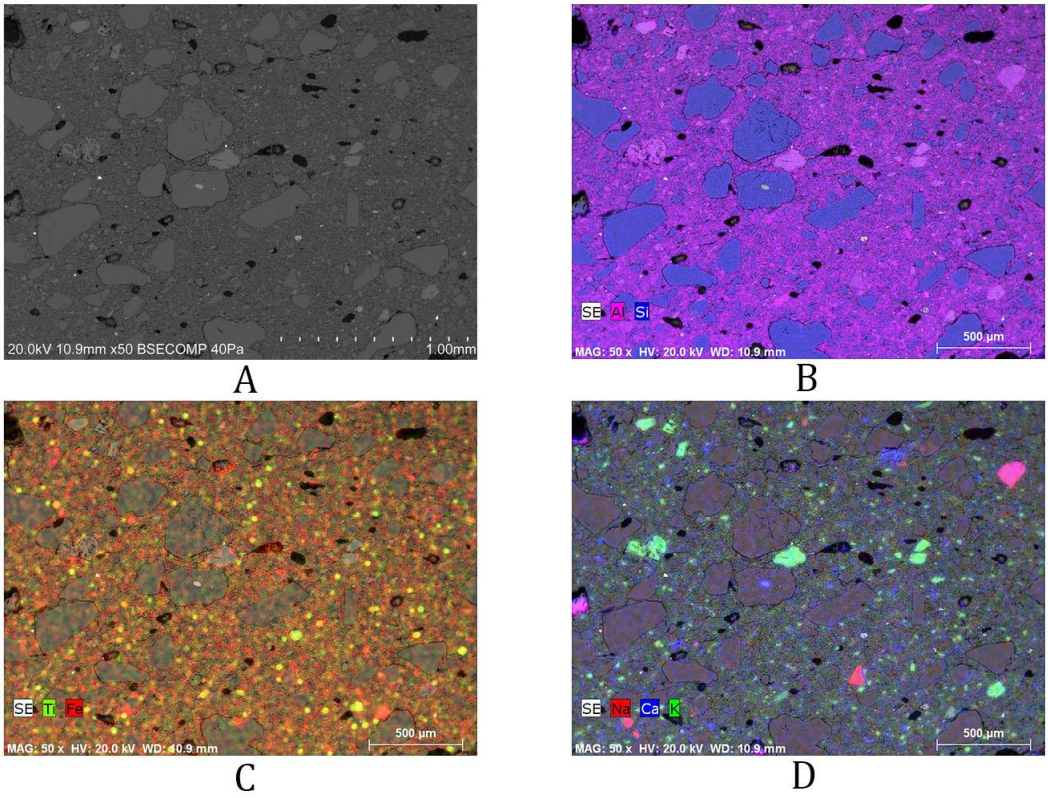

Figure 35 Elemental mapping distribution obtained from the analysis of sample 14 included in fabric 2.

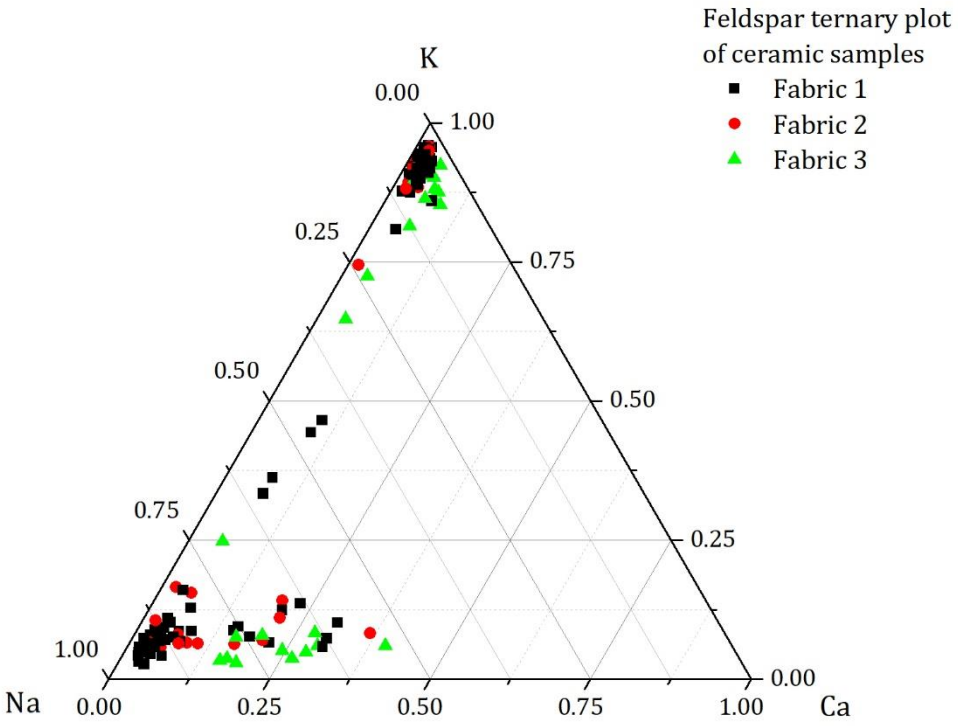

Figure 36 Feldspars ternary plot obtained of the ceramic samples included in the different farics.

5.1.4.2.5 Microscopy: SEM-EDS micro-analysis of glazed decorations

Glazed decorations were studied on 13 out of 42 samples (Table 5). All samples are covered by a high lead (fabric 1 and 2) or by a lead-alkali glaze (fabric 3). Alkaline earth metals concentration (i.e. MgO and CaO) is also significant. The main colouring agents were FeO (yellow, honey, black), MnO (black) and CuO (green). In sample 14, a small amount of MnO gave a light pink colour. White glazes (samples 9, 10) were achieved by opacification (Vendrell-Saz et al., 2000) using SnO_2. It appears as dispersed small acicular or sub-rounded inclusion.

In all cases, considering the model developed by Walton and Tite (2010)[80] and the guidelines of Tite et al. (1998), glazes were applied using SiO_2 and PbO together in the form of frit, with SnO_2 (fabric 3) or without (all fabrics). In addition, the absence of unmelted quartz crystals indicate that frit was accurately prepared and milled before application.

Regarding *corda seca* glazed ceramics, the "*corda line"* (Fig.37) was directly drawn on the ceramic body using MnO rich mineral. Some clay was also probably added (Peréz-Arantegui et al. 1999b) as evidenced by the significant concentration of FeO (Table 7). In another case, it formed a heterogeneous layer with a significant concentration of MnO, FeO, and PbO pointing to the addition of some frit on the top of the *corda line* (Peréz-Arantegui et al., 1999b). This is evident in sample 9 by the position of manganese-rich inclusions inside the glaze, located close to the interface and below SnO_2 inclusions (Fig. 38A/B/C).

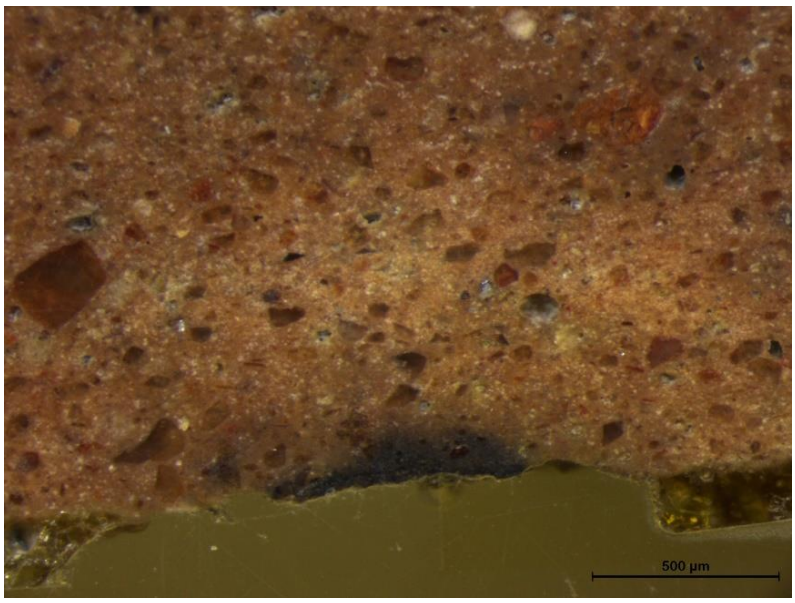

Figure 37 Picture collected using an optical microscope of the corda line of sample 10

[80] The model developed by Walton and Tite (2010) compares ceramic pastes and glazes chemical compositions after the remouval of PbO (ceramic paste and glaze), colourants such as CuO and MnO (glaze) and opacifier like SnO_2 (glaze). In both cases resulted values are recasted to 100%. When ceramic pastes and glazes resulted values are very similr, PbO was probably applied by itself on the ceramic body. On the contrary when SiO_2 was applied in combination with PbO, ceramic pastes and glazes chemical composition normally are substantially different.

Differences in glaze chemical composition, firing technique, in the interface and in glaze inclusions (Molera et al. 2001; Déléry 2006; Peréz-Arantegui et al. 1999; Chapoulie et al. 2005) subdivided samples into 3 groups.

Glazes of fabric 1 (Fig. 39D/E/F; Table 6) are poor in alkalis, homogeneous, unaltered, with rare bubbles and cracks. Glaze thickness is comprised between 70 and 120 μm. PbO/SiO_2 ratio is high as on similar monochromatic glazed ceramics from the 11th to the 14th century (Molera et al., 1999; Molera et al. 1997). The low diffusion of PbO in the ceramic paste and the formation of a 15-35 μm interface with K-Pb feldspars indicate that ceramics were doubled fired and underwent a slow cooling rate. The identification of Al_2O_3 rich inclusions points to the addition of some clay to the glaze mixture;

Glazes of fabric 2 (Fig. 39A/B/C; Table 6) are also poor in alkalis, homogeneous, unaltered with rare bubbles and cracks. Glaze thickness is comprised between 100 and 200 μm. PbO/SiO_2 ratio is high as on similar monochromatic glazed ceramics from the 11th to the 14th century (Molera et al., 1999; Molera et al. 1997). The high diffusion of PbO in the ceramic paste indicates that ceramics were single-fired, and they underwent a slow cooling rate. The formation of a thin interface (2-8 μm) enriched on K-Pb feldspars is the result of the ceramic paste composition, enriched in Al_2O_3 which act as a stabilizer (Molera et al., 2001b). Also, in this case, some clay was added to the glaze;

Glazes of fabric 3 (Fig. 38D/E/F; Table 7) are enriched in alkali and lime. They are normally well preserved (excluding green glazes), and with rare bubbles PbO/SiO_2 ratio is lower if compared to fabric 1 and 2 ceramic samples. The low diffusion of PbO in the ceramic paste indicates that ceramics were doubled fired. Glaze thickness is comprised between 180 and 220 μm, and just on sample 5 (i.e. bottle) glaze thickness can be 400-500 μm thick. Moreover, on the interface (5-25 μm thick) K-Pb feldspars and Na-Pb plagioclase were observed. Ca-Pb pyroxenes (especially on secondary glazes/undecorated side) appeared as isolated crystals dispersed in the middle of the glaze (Molera et al., 2001b). These pieces of evidence suggest that glazes underwent a slow cooling rate. Considering glaze chemical composition and characteristics from previous published data (Déléry 2006), decorations are similar to samples from Lisbon (white glaze, BDX8785), Malaga (honey glaze, BDX8780) and La Iglesieta (green glaze, BDX9542) with different chronology and decoration (CSP and CST). Nevertheless, basing on glazes chemical compositions, the closest match (secondary, white, green and honey glazes) was found on *Almoravid corda seca* glazed ceramics from Mértola (Déléry 2006; Chapoulie et al. 2005).

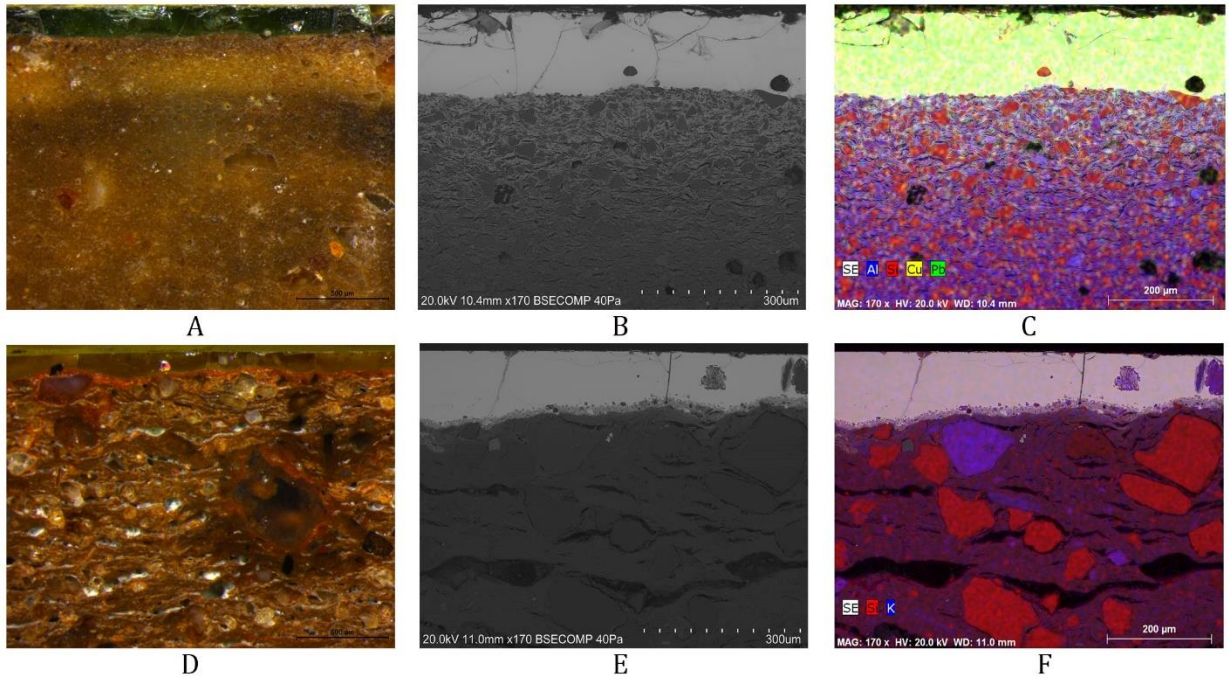

Figure 38 Picture of samples 15 (A, B, C) and 20 (D, E, F). Picture A and D were collected by optical microscopy. Picture B and E were collected by SEM-EDS in BSE mode. Picture C and F represent the result of elemental mapping distribution analysis.

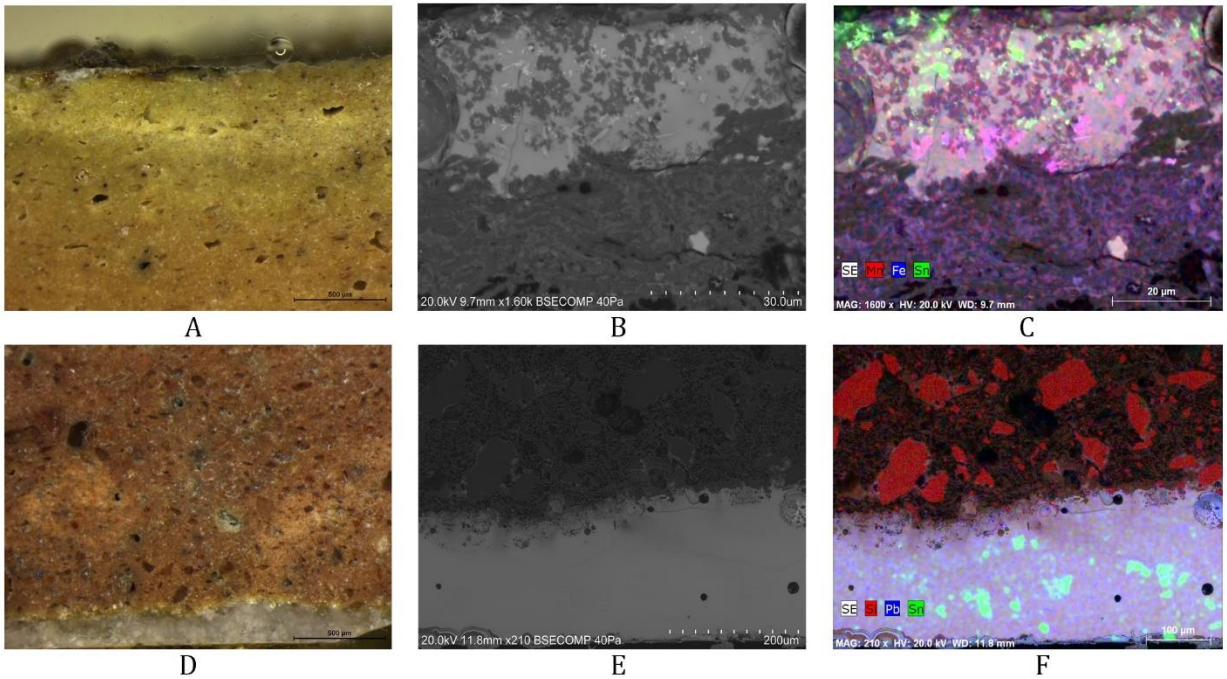

Figure 39 Picture of samples 9 (A, B, C) and 10 (D, E, F). Picture A and D were collected by optical microscopy. Picture B and E were collected by SEM-EDS in BSE mode. Picture C and F represent the result of elemental mapping distribution analysis.

Table 5 List of colours of the glazes, firing technique and glazing technique for each decorated sample.

L.N.	Fabric	Typology – Dec. style	Colour	Glaze side	Firing technique	Glaze technique
3	2	Bottle - MG	Yellow	Outside	Single	Frit
3	2	Bottle - MG	Yellow/Green	Inside	Single	Frit
5	3	Jar - MG	Honey/Green	Outside	Double	Frit
7	2	Bowl - MG	Yellow	Outside	Single	Frit
7	2	Bowl - MG	Green	Inside	Single	Frit
8	2	Bowl - MG	Yellow	Outside	Single	Frit
8	2	Bowl - MG	Yellow	Inside	Single	Frit
14	2	Big bowl - MG	Light Pink	Outside	Single	Frit
14	2	Big bowl - MG	Yellow	Inside	Single	Frit
15	2	Big bowl - MG	Yellow	Outside	Single	Frit
15	2	Big bowl - MG	Green	Inside	Single	Frit
16	2	Big bowl - MG	Yellow	Outside	Single	Frit
16	2	Big bowl - MG	Yellow	Inside	Single	Frit
19	1	Cooking Pan - MG	Brown	Outside	Double	Frit
19	1	Cooking Pan - MG	Brown	Inside	Double	Frit
20	1	Cooking Pan - MG	Brown	Outside	Double	Frit
20	1	Cooking Pan - MG	Brown	Inside	Double	Frit
37	2	Small lantern - MG	Yellow	Outside	Single	Frit
37	2	Small lantern - MG	Yellow	Inside	Single	Frit
9	3	Bowl - PG- CST	Honey	Secondary - Outside	Double	Frit
9	3	Bowl - PG- CST	Green	Decorated - inside	Double	Frit
9	3	Bowl - PG- CST	Black	Decorated - inside	Double	Frit
9	3	Bowl - PG- CST	White	Decorated - inside	Double	Frit
10	3	Bowl - PG- CST	Honey	Secondary - Outside	Double	Frit
10	3	Bowl - PG- CST	Green	Decorated - inside	Double	Frit
10	3	Bowl - PG- CST	Black-*Corda line*	Decorated-Paint	Double	Frit
10	3	Bowl - PG- CST	White	Decorated - inside	Double	Frit
10	3	Bowl - PG- CST	Honey	Decorated - inside	Double	Frit
L.N.	**Fabric**	**Typology - Decoration style**	**Colour**	**Position**	**Firing technique**	**Glaze technique**

Table 6 Glazes chemical composition of monochromatic glazed samples from fabric 1 and 2 obtained by SEM-EDS. Results are normalized to 100%. Uncertainty is 1σ.

L.N.	Fabric	Position	Na_2O	MgO	Al_2O_3	SiO_2	K_2O	CaO	TiO_2	MnO	FeO	CuO	SnO_2	PbO	PbO/ SiO_2	Na_2O +K_2O
3	2	Outside	0.58	0.43	6.23	25.31	0.82	1.01	0.74		1.98			62.9	2.49	1.4
3	2	Inside	0.6	0.44	7.41	27.63	0.67	0.8	0.8		1.77			59.88	2.17	1.27
5	3	Outside	2.6	0.8	3.79	38.59	2.95	4.36	0.73		1.92	1.52		42.76	1.11	5.55
7	2	Outside	0.9	0.53	8.56	42.31	1.54	1.21	1.12		1.68			42.15	1.00	2.44
7	2	Inside	0.26	0.38	2.8	35.69	0.67	1.26	0.92		0.36	4.57		53.08	1.49	0.93
8	2	Outside	0.63	0.5	6.53	28.34	0.92	0.97	0.99		2.22			58.89	2.08	1.55
8	2	Inside	0.85	0.58	7.83	34.23	1.55	1.79	0.64		1.77			50.77	1.48	2.4
14	2	Outside	1.21	0.48	6.34	34.66	1.19	1.39	0.91	0.6	1.71			51.5	1.49	2.4
14	2	Inside	0.63	0.48	6.15	27.82	0.78	0.8	1		1.71			60.63	2.18	1.41
15	2	Outside	0.62	0.35	5.93	26.92	0.96	1.21	1.87		3.54			58.6	2.18	1.58
15	2	Inside	0.22	0.31	3.2	31.8	0.57	0.47	0.99		1.87	3.45		57.12	1.80	0.79
16	2	Outside	0.86	0.69	6.98	31.96	0.97	0.82	1.02		2.5			54.2	1.70	1.83
16	2	Inside	0.48	0.52	6.45	29.32	0.99	0.56	0.92		1.72			59.04	2.01	1.47
19	1	Outside	1.04	0.96	8.33	28.97	1.19	1.41	1.01		1.83			55.26	1.91	2.23
19	1	Inside	0.65	0.56	7.71	25.99	1.04	0.81	1.38		1.62			60.24	2.32	1.69
20	1	Outside	0.41	0.54	6.16	26.18	0.9	1.13	1.01		1.53			62.14	2.37	1.31
20	1	Inside	0.76	0.68	5.27	25.68	1.02	1.08	1.12		1.59			62.79	2.45	1.78
37	2	Outside	0.84	0.72	4.55	24.13	0.62	1.64	0.78		1.6			65.11	2.70	1.46
37	2	Inside	0.62	0.49	6.24	31.15	0.75	1.56	0.72		2.13			56.35	1.81	1.37
L.N.	**Fabric**	**Position**	**Na_2O**	**MgO**	**Al_2O_3**	**SiO_2**	**K_2O**	**CaO**	**TiO_2**	**MnO**	**FeO**	**CuO**	**SnO_2**	**PbO**	**PbO/ SiO_2**	**Na_2O +K_2O**

Table 7 Glazes chemical composition of corda seca style decorated samples from fabric 3 obtained by SEM-EDS. Results are normalized to 100%. uncertainty is 1σ.

L.N.	Fabric	Side	Na_2O	MgO	Al_2O_3	SiO_2	K_2O	CaO	TiO_2	MnO	FeO	CuO	SnO_2	PbO	PbO/ SiO_2	Na_2O +K_2O
9	3	Outside	2.06	0.78	5.44	37.64	3.11	3.73	0.9		2.99			43.34	1.15	5.17
9	3	Decorated - inside	2.63	1.27	2.21	44.03	2.67	4.45	0.84		1.21	2.06	1.94	36.69	0.83	5.3
9	3	Decorated - inside	3.22	0.87	4.27	43.79	3.89	4.35	0.27	1.42	7.73	0.82	1.18	28.2	0.64	7.11
9	3	Decorated - inside	3.08	1.18	1.46	46	3.23	2.84	0.98		1.11		2.5	37.6	0.82	6.31
10	3	Outside	1.13	0.6	4.91	36.15	2.19	4.4	0.96		2.51			47.14	1.30	3.32
10	3	Decorated - inside	3.31	0.65	1.32	43.08	1.49	2.68	0.74		1.07	2.86	1.8	41	0.95	4.8
10	3	Decorated – *Corda seca* line	0.34	1.37	10.15	38.98	2.25	22.76	1.12	6.25	5.91			10.87	0.28	2.59
10	3	Decorated - inside	2.99	0.84	2.11	39.47	1.96	3.15	0.96		1.12		3	44.4	1.12	4.95
10	3	Decorated - inside	1.43	0.44	4.19	39.43	2.58	3.99	1.1	0.12	3.14			43.58	1.11	4.01
L.N.	**Fabric**	**Position**	**Na_2O**	**MgO**	**Al_2O_3**	**SiO_2**	**K_2O**	**CaO**	**TiO_2**	**MnO**	**FeO**	**CuO**	**SnO_2**	**PbO**	**PbO/ SiO2**	**Na_2O +K_2O**

5.1.4.3 Comparing ceramic samples with raw materials

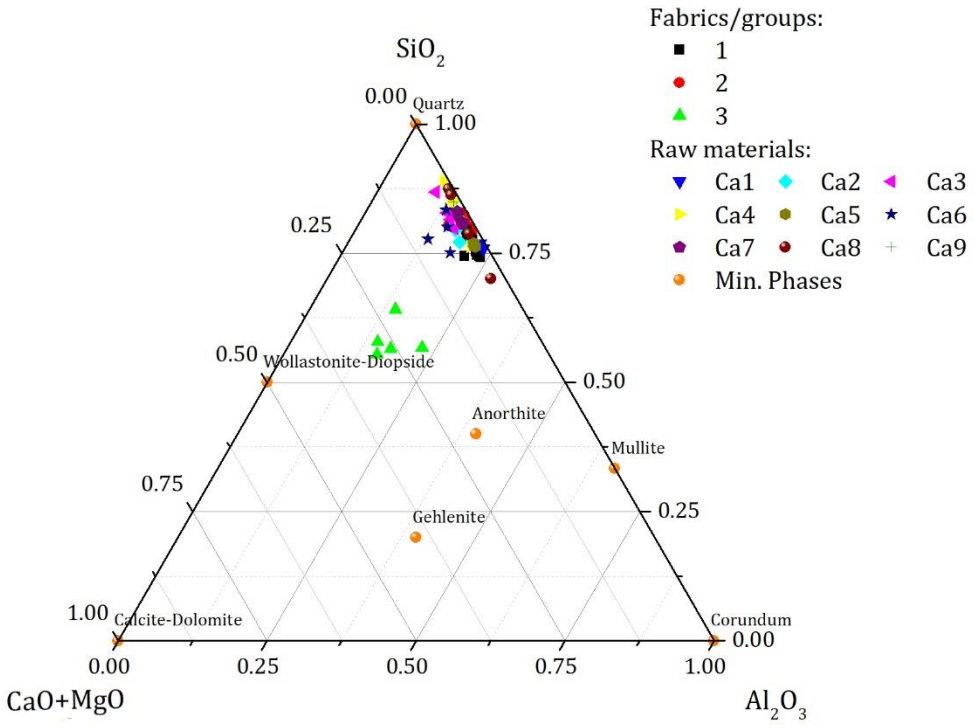

Figure 40 Raw materials and ceramics ternary plot (Al_2O_3-SiO_2-CaO+MgO)

The raw materials and ceramics ternary plot (Fig. 40), Al_2O_3, SiO_2, CaO+MgO (Heimann and Maggetti 2014; Heimann and Maggetti 2019), showed that group 3 falls in the triangular space be limited by quartz, anorthite and wollastonite/diopside (identified on XRPD patterns) normally occupied by CaO and MgO rich materials. Thus, none of the raw materials can explain the composition of fabric/group 3 characteristics.

Microforaminifera bioclasts (samples 5, 10, 11, 36) and thermally altered limestone fragments were identified by PLM but not typical aeolian quartz inclusions normally observed in North African productions. Moreover, SEM-EDS analyses evidenced that Ca and Mg are concentrated in the ceramic paste. These data indicate that the raw materials exploited for the production of fabric/group 3 result from the alteration of a marl, and they were imported from an unknown production site located in Southern Iberia. Moreover, as explained on section 5.1.4.2.3, samples 5, 9, and 10 have completely different Sr concentrations and Fe_2O_3/TiO_2 ratios if compared to 11 and 36, suggesting they were also produced in different workshops.

The result obtained by the chemical analysis of sediment samples (section 5.1.4.1.2) evidenced that basing on the evaluation of Zr/U, Hf/U and Fe_2O_3/TiO_2 ratios, similar host phases were present on raw materials Ca2, Ca3, Ca4, Ca5, Ca6, Ca7, Ca8 and Ca9 and raw material Ca1. In any case, if granulometry and mineralogical/chemical analysis results of the sedimentssub-samples (URM to <63 µm) are considered, some raw materials were discarded

as a possible natural resource for ceramic production. On raw materials, Ca4-Ca8 sand content is too high (98.6-97%), and roughly only 2-3 % of silt+clay could be extracted. On raw materials Ca3-Ca6, CaO concentration (mean=2.17, 3.16 wt%) was also high when compared to ceramics fabric/group 1 and 2 (mean=0.79, 0.89 wt%). On raw materials Ca7-Ca9, Fe_2O_3 concentration (mean=3.26, 3.88 wt%) was rather low if compared to fabric/groups 1 (mean=5.58 wt%) and high if compared to fabric/group 2 (mean=1.49 wt%). On raw material Ca2, Na_2O (mean=1.15 wt%) and MgO (mean=1.71 wt%) concentration are not compatible neither with fabric/group 1 (Na_2O mean=0.37 wt%; MgO mean=0.98 wt%) nor with fabric/group 2 (Na_2O mean=0.40 wt%; MgO mean=0.53 wt%) ceramics.

Fabric/group 2 ceramics and raw material Ca1 have consistent mineralogy of iron and titanium oxides and are distinct from fabric/group 1 ceramics and raw material Ca5 (Fig. 41A). In these ceramics and raw materials, iron and titanium oxides are probably associated with the mineral ilmenite considering Fe_2O_3/TiO_2 ratio. In raw materials Ca1 and group 2 ceramics, the Fe_2O_3/TiO_2 ratio points to the presence of TiO_2 (i.e. anatase) minerals as detected in XRPD.

The Zr *vs* U plot (Fig. 41B) corroborates previous observations about raw materials and ceramics. On the binary plot, fabric/group 2-raw material Ca1 and fabric/group 1-raw material Ca5 show a good coefficient of correlation (R^2=0.87; 0.71). In any case, if compared with the raw materials, ceramics are generally more enriched in sand (after temper addition), as evidenced by SiO_2/Al_2O_3 ratio (Fig. 41A), but quite depleted in zirconium (Fig. 41B). The amount of quartz has a dilution effect on zirconium, as discussed in the raw material section (section 5.1.4.1.2). So, the relation of fabric/group 2 and Ca1 or fabric/group 1 and Ca5 is done by similar Zr/U ratios, after dilution by quartz temper addition. Furthermore, some samples of fabric/group 1 (25, 27, 28, 33), including glazed samples (19, 20), overlap with fabric/group 2, suggesting that raw materials Ca1 and Ca5 were partially mixed.

REEs (Fig. 42A/B) follow the zirconium trend, and they are less abundant in archaeological ceramics (Annexe 1, table 16 to 21)when compared with raw materials (Annex 1, table 30 to 32). Group 2 ceramics and raw material Ca1 (Fig. 42A) have compatible $\sum LREE_{CN}/\sum MREE_{CN}$ ratio (mean= 4.87, 4.52) and Eu_{CN} anomaly (mean= 0.58, 0.61), but ceramics are depleted in $HREE_{CN}$ as evidenced by $\sum LREE_{CN}/\sum HREE_{CN}$ ratio (mean= 9.40, 7.66). This ratio tends to increase during sieving. At present, it is not possible to establish whether it is an effect of raw material treatment (decantation), temper addition, or raw material mixing. Fabric/group 1 and raw material Ca5 (Fig. 42B) have very similar profiles, with respect to

$\sum LREE_{CN}/ \sum MREE_{CN}$ ratio (mean= 4.8, 4.78), Eu_{CN} anomaly (mean= 0.58, 0.58) and $\sum LREE_{CN}/\sum HREE_{CN}$ ratio (mean= 8.68, 8.12).

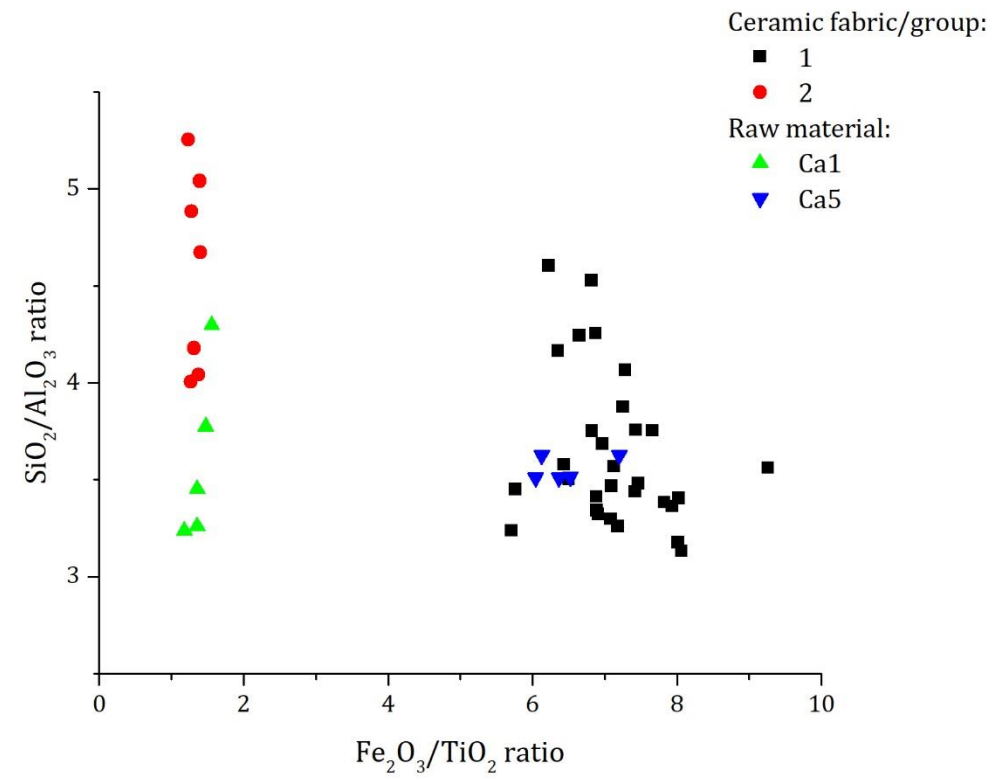

A

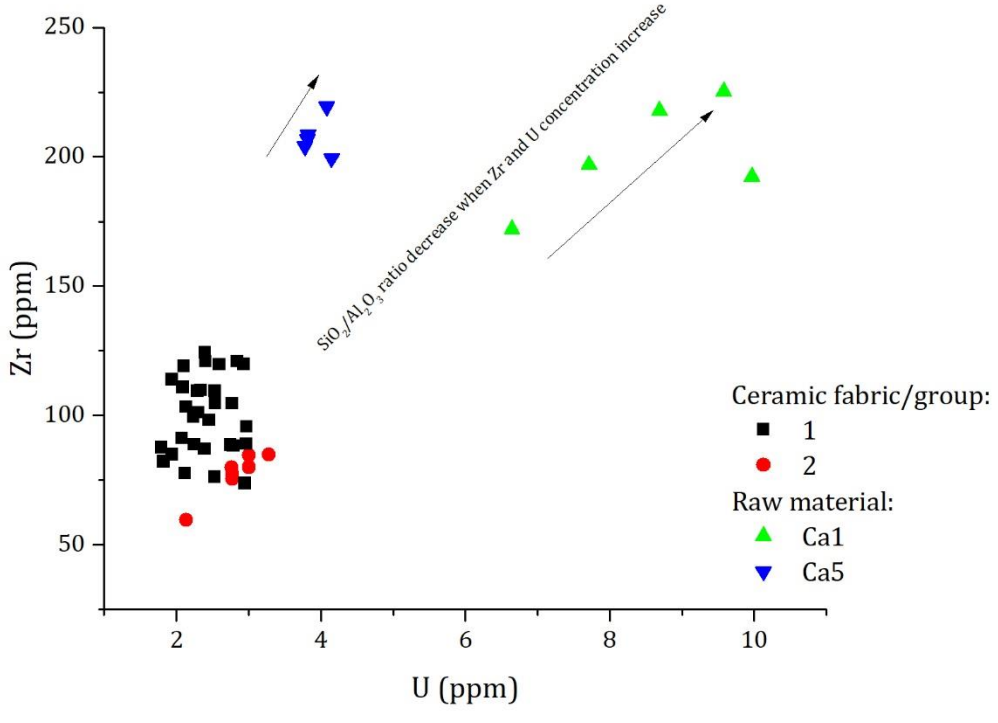

B

Figure 41 SiO_2/Al_2O_3 vs Fe_2O_3/TiO_2 (A) and Zr vs U (B) binary plots of fabric/group 1, 2 and raw material Ca1, Ca5.

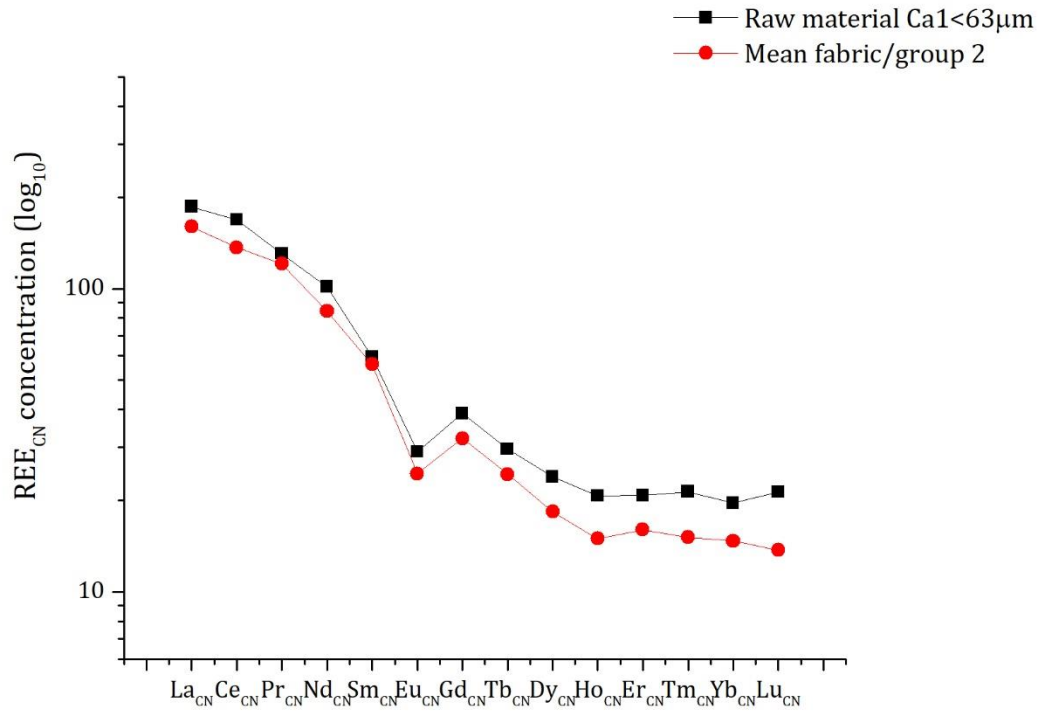

A

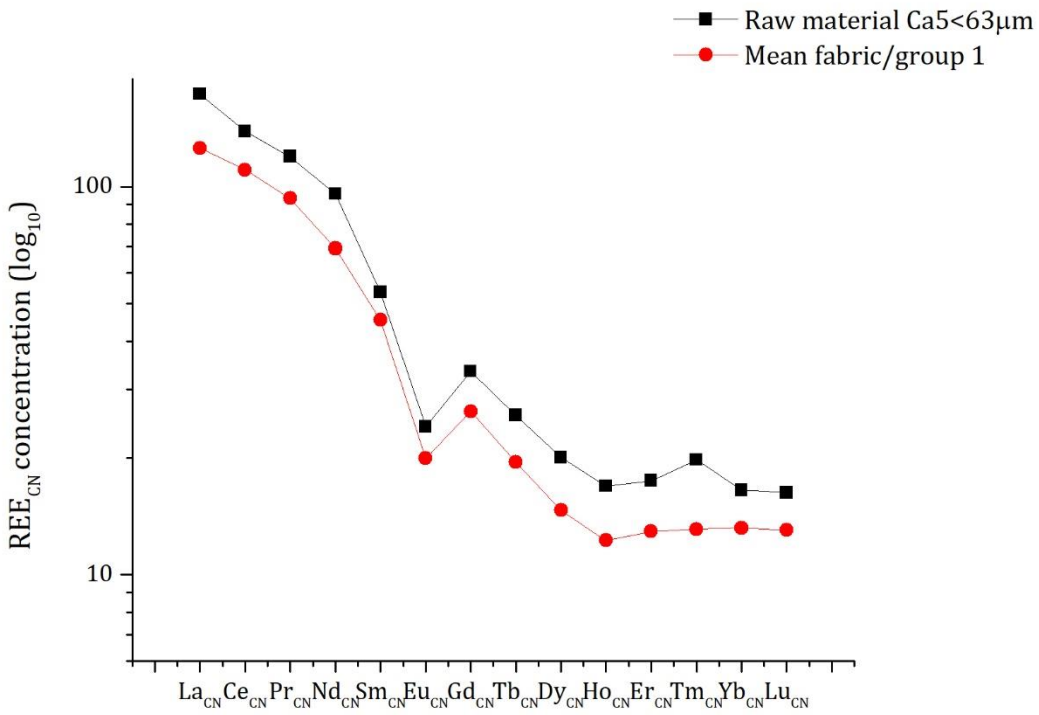

B

Figure 42 REE$_{CN}$ profiles of fabric/group 2 – raw material Ca1<63 µm (A), and fabric/group 1 – raw material Ca5<63µm (B).

5.1.5 Final remarks the section

A set of raw materials were collected on Pleistocene and Miocene geological formations close to Santarém as possible candidate for the production of the ceramic under study.

Remarkably, samples from the same geological formations have dissimilar mineralogical and chemical compositions. Moreover, these compositions change during sieving with sand extraction, and it usually increases the amount of clay-minerals and associated elements in the fine fractions of the sediment (e.g. Zr, Ti, Hf, U and REE). Thus, for the interpretation of the ceramic technology, it is essential to recognize the distribution of the minerals and the chemical elements by the different size fractions.

This allowed the identification of two different raw materials (Ca1, Ca5) exploited for the production of unglazed (fabric/group 1) and monochromatic (fabric/group 1 and 2) glazed ceramics at Santarém. Raw materials were treated, and temper was added in a second moment. Moreover, the sieving experiment showed that detrital chemical elements and REE concentrations usually increased in the finer fraction, and it was subsequently diluted by the addition of quartz temper during ceramic manufacturing.

The study has also established that ceramics of fabric/group 3 were imported in the city, and they were produced using a typical calcareous raw material, probably from Southern Iberia. Differences in Sr concentration and Fe_2O_3/TiO_2 ratio supported PLM results and evidenced that samples were imported in the city from two not identified locations (sub-group of fabric/group 3: 3A and 3B).

In all cases, glazes were prepared using a frit, finely prepared and milled before application. Glazes of fabric/group 1 and 2 are of the high lead type, and they have similar chemical composition. However, ceramics from group 1 underwent a doubled firing while those from group 2 were single fired. This shows that ceramist/s in Santarém was/were able to adapt the different stages of the production process to the raw materials available.

Glazes of fabric/group 3 (samples 5, 9, 10) are of the lead-alkali type enriched in lime. Decorations showed similarities with samples from other archaeological sites, especially with *Almoravid corda seca* glazed ceramics from Mértola. These results indicate that a similar glaze recipe was employed in different parts of the al-Andalus between the end of the 10th and the 12th century. The close similarities observed with glazes from Mértola point to an active commercial network able to trade glazed ceramics from southern to western Iberia.

5.2 Islamic and post-Islamic ceramics from Santarém: The continuity of ceramic technology in a transforming society

The results of this section have been fully published in the Journal of Archaeological Science: Report edited by Elsevier. The same data were presented at the *European Meeting on Ancient Ceramics* (Bordeaux, France – 6/9 September 2017). Some prelimiray results were also published in the journal "*O Arqueologo Portugues"* edited by the National Museum of Archaeology (Portugal).

The study presented in this section discuss the results obtained by the archaeometrical investigation carried out on Islamic and post-Islamic ceramics recovered at Santarém (Portugal). They were recovered on different archaeological excavations covering a chronological timeframe between the 8th and the 15th-16th centuries, before and after the conquest of the town by Christian armies in the middle of the 12th century.

The collection includes unpainted, white painted, red painted and glazed ceramics of Islamic and Post Islamic chronology. Amongst glazed specimens, 2 samples of "*corda seca*" style glazed ceramics (CSP and CST) were recovered in two different archaeological sites, in one case associated to kiln tools like stilts and kiln bars. Archaeologist supposed they could be both regionaly produced.

The main goal of this section was to assess the continuity in raw material exploitation and production technology in the city in different period, to understand how the Portuguese Reconquista affected ceramic production. Moreover the local production of "*corda seca*" glazed ceramics will also be assesed during the Islamic period.

Results indicated that all ceramics were locally produced, including *corda seca* style ceramics, in two different workshops. Ceramic technology did not change with the Portuguese Reconquista, confirming that a modification in the political power did not correspond to a change in ceramic technology.

5.2.1 Introduction and goals of the section

The Iberian Peninsula became part of the Islamic territory when Berbers armies crossed the Gibraltar strait at the beginning of the 8th century and defeated the Visigoth. Since then, the the *al-Andaluz* was ruled by different Muslim powers.

Due to the continuous incursion of the northern Christians kingdoms, after the 10th century, the border between Muslim and Christian territories regularly mouve to south during the so colled "*Reconquista"*. This includes the fall of the Tagus valley in the middle of the 12th century, with the submission of the cities of Santarém and Lisbon in the same year (1147 AD) during the *Almoravid* domination of the *al-Andalus*.

This permanent contact between Islamic and Christian societies in the *Marca* (the unstable border splitting Christians and Muslims) imparted unique characteristics to the frontier territories. Despite the almost persistent confrontation between the two military and political powers, some agreements are historically documented and commercial, and cultural exchanges remained unbroken.

Moreover, in the territories ruled by Islamic and Christian powers, important communities of other religious faith still persisted. The more important were the Christian communities (i.e. *mozarabs*) and converted Christians (i.e. *muladi*) in muslins territories, and the Islamic communities in Christian territories (i.e. *mudejar*).

In our case, material culture such as pottery might reflect the diversified composition of the society or show homogeneous characteristics. At the same time, it can be influenced by a modification in the ruling power of the city and/or by a modification in the composition of the society. Thus, it is important to evaluate ceramic characteristics to understand local social dynamics and modifications and to estimate how political changes might influenced the material culture, namely in what concerns pottery production.

During the Islamic-Reconquista-Christian period, the uninterrupted occupation of the city of Santarém is widely attested in many archaeological sites inside the old Islamic *Alcaçova,* in the historical centre of the city, and on the riverine neighbourhood, the *Ribeira* and *Alfange*.

In addition, archaeological sites diversity[81], in terms of space utilization, allowed the recovery and identification of potteries assemblages linked to ceramic production, during and

[81] A complete list of archaeological sites can not be presented in the present thesis. A complete overview can be found at the website https://arqueologia.patrimoniocultural.pt/. On this website, it is possible to obtain information regarding each archaeological site excavated in Santarém including the archaeological reports of each excavation.

after the Islamic occupation (Liberato, 2012a), and consumption (Arruda and Viegas, 1999) activities. Several Islamic necropolises were also identified (Liberato, 2012b).

As expected unpainted (i.e. undecorated), white painted and monochromatic glaze ceramic were frequently recovered. On the contrary, red painted ceramic, dichromatic (honey and black), CSP and CST glazed ceramics were less frequent. During the late 15th century, there was also a strong revival of white painted ceramic in the *Mudejar* ceramic tradition of the city (Liberato, 2012; Liberato et al., 2019).

This section, as described on section 4.1, do not provide sediments, but includes several ceramic wastes recovered on different productive archaeological context. These ceramics wastes have been utilized as a reference of local production, and include fragments of burnt CST glazed ceramics recovered in association with kiln bars and stilts.

The identification of CST ceramic in a production context represents a relevant archaeological discovery, pointing to a local production of this specific ceramic ware. So far, the production of CSP and CST ceramics has been attested only in the Lisbon area between the *Taifa* Kingdom period and the Almoravid domination (Bugalhão et al., 2008a; Dias et al., 2008; Gomes et al., 2009) as already explained on chapter 3. This local/regional *corda seca* ceramic production were influenced and coexisted (I. C. Fernandes et al., 2015) with similar imported ceramics from Southern Iberia (i.e. Almeria, Murcia, Pechina, Alicante).

In this section, a set of ceramic samples were selected and analysed in order to: *a*) determine the characteristics of the local ceramics; *b*) compare local unglazed and glazed ceramic ware with Islamic and early Christian chronology; *c*) to characterize "*corda seca*" glazed ceramic from Santarém and to contextualize the results in the general productions frame of the Western Islamic Iberia; *d*) test the continuity or assimilation of the Islamic ceramic tradition after the Reconquista (1147 A.D.) and during Portuguese Kingdoms.

5.2.2 Ceramics sampling

Ceramic samples were recovered in three different preventive archaeology interventions in the town historical centre and in the riverine neighbourhood (Fig. 43). They

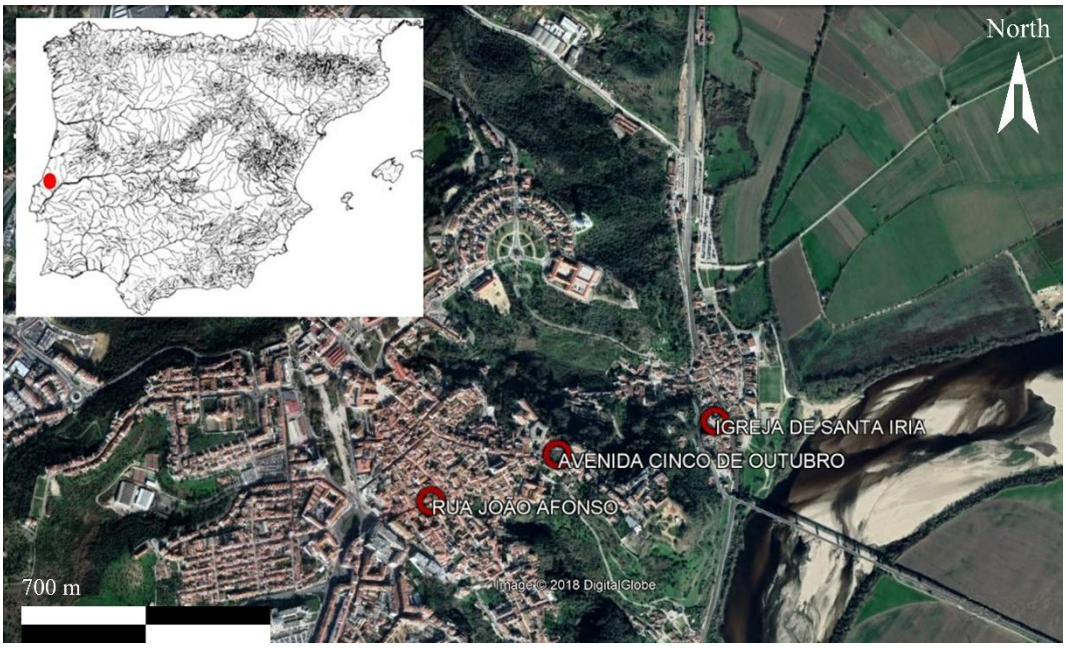

Figure 43 Position in the city of Santarém of the archaeological sites under investigation in this section.

cover a chronological period comprised between the 8th-9th and 16th centuries (Table 8, Fig. 44). The last filling of *silos* was selected in most cases, because they can give high reliably chronological contexts as they were usually filled with domestic waste in a short period of time.

The first archaeological site is located at the *Ribeira* de Santarém, by the right riverbank, next to the church of *Santa Iria* (SICh). A total of five closed shaped kitchen ceramic containers, excavated from the interior of a *silo* opened on the bedrock (Batata et al., 2004) have been selected. Their characteristics, namely the poor treatment of the surfaces, the noticeable formal monotony, typical of western Iberia (Alba Calzado and Gutiérrez Lloret, 2008; Gutiérrez Lloret, 2015b), and the low-rotation modelling process make it possible to date the samples in Emiral period of the Iberian Peninsula, from 8th to 9th century (Liberato and Santos, 2018).

On the contrary, samples from the 11th and 12th centuries (*Taifa* Kingdom/*Almoravid* period) are well represented. Late Islamic *Almoravid* and early Christian ceramics were mostly obtained from the excavation of the archaeological site *Avenida 5 de Outubro, n.º 2*-8 (RCO).Within this intervention, it was possible to register a complete stratigraphic sequence dated from the beginning of the Iron Age until the 18th century in an area of roughly 1000 square meters.

In addition, samples from 4 production archaeological contexts, 3 from the RCO (3 kilns) and 1 from the *Rua João Afonso* (RJA) archaeological sites were also selected. In the case of the

RCO archaeological site samples, of ceramic containers broken during the firing process and recovered inside the kilns tunnels were selected.

For the Islamic period, 11th-12th centuries, samples from kiln 1 (U.S. [1720]) and from kiln 2 (U.S. [2046]), as well as ceramic fragments with similar chronology recovered in *silos* have been sampled. In this period/site, along with unpainted or white painted pottery, the presence of monochromatic glazed pottery is fairly frequent. Moreover, rarer productions, such as red painted ceramics or polychromatic glaze ceramic, in particular *corda seca* glazed ceramics (CSP and CST) are present.

In the case of post-Islamic ceramics from the RCO site, 12th-13th centuries (i.e. first decade of the Christian rule), several samples were selected from kiln 4 (U.S. [1576]) as well as ceramic material recovered in *silos* with the same chronology. After the Christian conquest of the town, ceramic diversity productions slightly decreased, although white painted ceramic is still very common and monochromatic glazed pottery is the only ceramic glazed ware registered.

In addition to previous ceramic samples, a partially complete CST ceramic bowl (Vala 37), with a chronology centred in the 11th-12th centuries, was selected on a different archaeological intervention, carried out in 2004 at *Rua João Afonso* archaeological site (RJA). It was discovered in a context with different materials related to pottery making activities, like wasters and kiln furniture such as stilts and kiln bars (Kiln 3-U.S. [11]).

Finally, from the RCO site have also been considered two ceramic fragments with a very specific production technique, consisting in the reappearance of white painted wares during the late medieval period, 15th-16th centuries, but with the application of *mudejar* motifs above a very strong reddish slip (Liberato, 2016; Liberato et al., 2019). The first fragment was recovered during the surface cleaning of the RCO site, while the second one comes from a metallurgical activity-related disposal deposit.

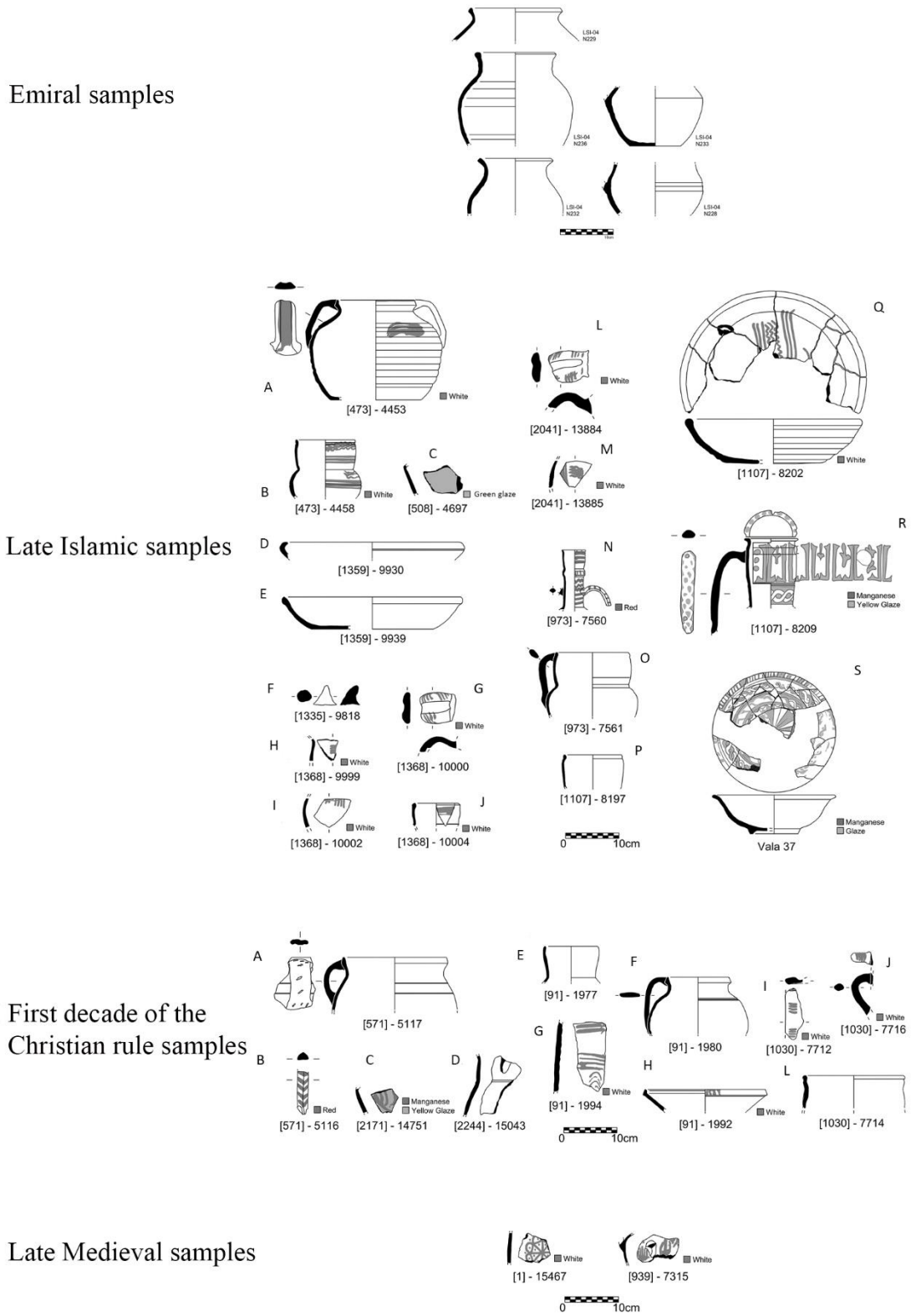

Figure 44 Image of the ceramic samples analysed in this section. From the top: Emiral sample, 8th to 9th centuries from Santa Iria Church, Ribeira of Santarém (SICh); Late Islamic Pottery, 11th to the first half of 12th century from Avenida 5 de Outubro (RCO) : A-B, context [470], C, context [520], D-E, context [1378], F-J, context [1720], L-M, context [2046], N-R context [2467]; Rua João Afonso (RJA): S, context Vala 37; First decades of Christian rule pottery, 12th to 13th centuries from Avenida Cinco de Outubro (RCO): A-B, context [476], C-D, context [2172], E-H, context [2466], I-L, context [1576]; Late Medieval White Painted\Reddish Slip Ware pottery, late 15th to 16th century from Rua 5 de Outubro (RCO).

Table 8 Samples list with archaeological reference, the recovering context (stratigraphic unit, [U.S.]), chronology, typology, decoration and the archaeological site. SICh, RCO and RJA.

Sample reference [U.S.-n°]	Archaeological context -[U.S.]	Chronology - century	Typology	Function	Decoration	Arch. site
LSI04-228	*Silo*	*8th-9th*	*Pot*	*Fire ceramic*	*Unpainted*	*SICh*
LSI04-229	*Silo*	*8th-9th*	*Pot*	*Fire ceramic*	*Unpainted*	*SICh*
LSI04-232	*Silo*	*8th-9th*	*Pot*	*Fire ceramic*	*Unpainted*	*SICh*
LSI04-233	*Silo*	*8th-9th*	*Pot*	*Fire ceramic*	*Unpainted*	*SICh*
LSI04-236	*Silo*	*8th-9th*	*Pot*	*Fire ceramic*	*Unpainted*	*SICh*
[1368]-10000	*Kiln 1-[1720]*	*11th-12th*	*Unclassified ceramic samples*	-	*White painted*	*RCO*
[1368-10002	*Kiln 1-[1720]*	*11th-12th*	*Unclassified ceramic samples*	-	*White painted*	*RCO*
[1368]-10004	*Kiln 1-[1720]*	*11th-12th*	*Unclassified ceramic samples*	-	*White painted*	*RCO*
[1368]-9999	*Kiln 1-[1720]*	*11th-12th*	*Unclassified ceramic samples*	-	*White painted*	*RCO*
[1335]-9818	*Kiln 1-[1720]*	*11th-12th*	*Unclassified ceramic samples*	-	*Unpainted*	*RCO*
[2041]-13884	*Kiln 2-[2046]*	*11th-12th*	*Unclassified ceramic samples*	-	*White painted*	*RCO*
[2041]-13885	*Kiln 2-[2046]*	*11th-12th*	*Unclassified ceramic samples*	-	*White painted*	*RCO*
[1107]-8202	*Silo-[2467]*	*11th-12th*	*Bowl*	*Kitchen ceramic*	*White painted*	*RCO*
[1107]-8209	*Silo-[2467]*	*11th-12th*	*Jug*	*Liquid container*	*CSP*	*RCO*
[1107]-8197	*Silo-[2467]*	*11th-12th*	*Jug*	*Liquid container*	*Unpainted*	*RCO*
[973]-7561	*Silo-[2467]*	*11th-12th*	*Jug*	*Liquid container*	*Unpainted*	*RCO*
[1359]-9939	*Silo-[1378]*	*11th-12th*	*Bowl*	*Kitchen ceramic*	*Unpainted*	*RCO*
[1359]-9930	*Silo-[1378]*	*11th-12th*	*Pan*	*Fire ceramic*	*Unpainted*	*RCO*
[473]-4458	*Silo-[470]*	*11th-12th*	*Jug*	*Liquid container*	*White painted*	*RCO*
[473]-4453	*Silo-[470]*	*11th-12th*	*Pot*	*Fire ceramic*	*White painted*	*RCO*
[1030]-7712	*Kiln 4-[1576]*	*12th-13th*	*Unclassified ceramic samples*	-	*White painted*	*RCO*
[1030]-7716	*Kiln 4-[1576]*	*12th-13th*	*Unclassified ceramic samples*	-	*White painted*	*RCO*
[1030]-7714	*Kiln 4-[1576]*	*12th-13th*	*Unclassified ceramic samples*	-	*Unpainted*	*RCO*
[91]-1977	*Silo-[2466]*	*13th*	*Jug*	*Liquid container*	*Unpainted*	*RCO*
[91]-1980	*Silo-[2466]*	*13th*	*Pot*	*Fire ceramic*	*Unpainted*	*RCO*
[91]-1992	*Silo-[2466]*	*13th*	*Cover*	*Fire ceramic*	*White painted*	*RCO*
[91]-1994	*Silo-[2466]*	*13th*	*Cooker*	*Fire ceramic*	*White painted*	*RCO*
[973]-7560	*Silo-[2467]*	*11th-12th*	*Jug*	*Liquid container*	*Red painted*	*RCO*
[508]-4967	*Silo-[520]*	*11th-12th*	*Bowl*	*Kitchen ceramic*	*Mon. Glaze*	*RCO*
[2244]-15043	*Silo-[2171]*	*13th*	*Jug*	*Liquid container*	*Unpainted*	*RCO*
[2171]-14751	*Silo-[2171]*	*13th*	*Bowl*	*Kitchen ceramic*	*Honey and black*	*RCO*
[571]-5517	*Silo-[476]*	*12th-13th*	*Pot*	*Fire ceramic*	*Unpainted*	*RCO*
[571]-5516	*Silo-[476]*	*12th-13th*	*Jug*	*Liquid container*	*Red painted*	*RCO*
[1]-15467	*Surface cleaning-[1]*	*15th-16th*	*Undetermined*	-	*White painted*	*RCO*
[939]-7351	*Metal. Activity-[939]*	*15th*	*Jug*	*Liquid container*	*White painted*	*RCO*

Sample reference [U.S.-n°]	Archaeological context -[U.S.]	Chronology - century	Typology	Function	Decoration	Arch. site
Vala37	*Kiln 3-[11]*	*XI-XII*	*Bowl*	*Kitchen ceramic*	*CST*	*RJA*

5.2.3 Analytical methods employed in this section

This section lists, with the aid of a small table (Table 9), the analytical methods employed in this section. For a detailed description of each technique and regarding instrumental conditions, all information can be found on chapter 4. Several tables have been prepared from data collection. Considering tables size, they were too big to be inserted in the text. So, they were included in the thesis as annexe 2 at the end of the dissertation.

Table 9 List of the analytical methods employed in this section.

Method		Samples analysed	Data table added as annex
Microscopy	*PLM*	All	Ceramic paste and temper
	SEM-EDS	All samples and on decorations	
Mineralogy	*XRPD*	All	
	μXRD	On a selection of samples	
	FT-IR ATR	On a selection of samples	
	μRaman	On a selection of samples	
Chemistry	*XRF*	All	Major oxides
	ICP-MS	All	Trace elements

5.2.4 Results

5.2.4.1 Microscopy: PLM on ceramic thin sections

A detailed description of the ceramic paste, porosity and of the temper of each sample is summarized at the end of the dissertation in annex 2 (Table 2 to 5).

PLM observations established that the ceramic assemblage is quite uniform in terms of mineralogical composition. Samples are mainly composed by quartz, potassium rich feldspars, plagioclase (mainly sodium rich), muscovite, biotite, secondary calcite, green-brown tourmaline (Fig. 45M/N). Sporadically, rock fragment inclusions (mainly granite, limestone, sandstone and in some cases slate) as well as calcretes were observed. Amongst limestone rock fragments, bio-sparites and intra-sparites were also identified (R.L. Folk, 1959), as well as isolated bioclasts as bivalves.

Bio-sparites consist of secondary precipitation carbonate cement and bioclasts as bivalves and calcareous algae, while intra-sparites mainly consist in secondary precipitated carbonate cement with quartz and feldspars intraclast. The identification of secondary calcite on several samples indicates that ceramics were probably fired at a temperature above 700-750 °C in an oxidized atmosphere (Cultrone et al., 2001).

Grain size distribution is generally unimodal for all samples. The silty fraction is the most abundant, indicating that the raw material was previously decanted to get rid of the coarser sandy fraction. Afterwards temper could be added according to the characteristics of the artefact to be prepared. The identification of bioclasts, of calcareous algae and other lithic fragments, both in a productive environment (kiln 1-2-3-4) and in *silos*, suggests a similar source for the raw material. Actually, our findings are compatible with the geological background of the Santarém area (Zbyszewsky, 1953). Moreover, thin-section analyses enable to sub-divide the samples into two different fabrics (Fig. 45).

Fabric 1 is characterized by an iron-rich ceramic matrix with inclusions size up to 2.4 mm (Fig. 45D/E/F). Fabric 2 is enriched in calcretes and/or sporadic limestone fragments, and it usually presents smaller inclusions (Fig. 45G/H/I), up to 1.4 mm in diameter. Limestone fragments were generally partially altered by the firing process and absorbed in the ceramic paste, leaving a characteristic “brown-grey rim” with secondary calcite on the inside (Fig. 45L).

Nevertheless, one sample ([1335]-9818), due to the elevated concentration of limestone fragments and shells, has not been inserted in any of the previous groups. The ceramic paste of this sample is quite heterogeneous (Fig. 45A/B). The reasons can be different. It could be the

result of raw material heterogeneity, incomplete mixing of different raw materials or incomplete firing in some areas.

Fabrics 1 and 2 presents internal variability in the amount and size of the inclusions, temper and sorting, leading to the formation of subgroups. Fabric 1 subgroups (A-B-C) are characterized by a progressive increase in the abundance of the inclusions. The size of the inclusions is smaller in subgroup A and larger in B. Subgroup C is generally used in thinner walls ceramic artefacts.

The characteristics of the ceramic paste marked the fabric 2 subgroups (A-B-C) differences, generally light brown in the case of subgroup A, a dark ceramic paste in the case of subgroup B and, in the case of subgroup C, by a clear distinction between the core and the border of the samples that is the result of the application of a thick iron rich slip.

The results obtained by PLM indicate a distinction in the ceramic paste preparation according to the object's functions but not only. It also evidenced, along time, the utilization of similar raw materials and recipes. Fabric 1 was mainly utilized for the production of pots and jugs in different periods. This is especially evident for samples recovered in the *SICh* and *RCO* archaeological sites.

In particular, jugs chronology spans from the 11th-12th centuries to the 15th century indicating that a certain degree of specialization in preparing these particular objects was preserved along the Islamic-Reconquista-Christian periods. On the contrary, in pots, samples chronology mainly focuses on the 8th-9th centuries with just one sample from the 12th-13th centuries.

Fabric 2 was generally utilized to produce glazed or red painted ceramics from both the 11th-12th and the 12th-13th centuries. It was also utilized for the production of one sample of red slipped white painted pottery with mudejar motifs ([1]-15467). The only exception was the sample of CST recovered from the *RJA* archaeological site, which was produced using fabric 1.

Moreover, fabric 2 was also used to produce fire ceramics, like pots and pans, after the 11th-12th centuries. This suggests an evolution in the productions of these objects. Regarding kitchen ceramics (i.e bowls), unpainted and white painted, they were indistinctivelly produced using both fabrics.

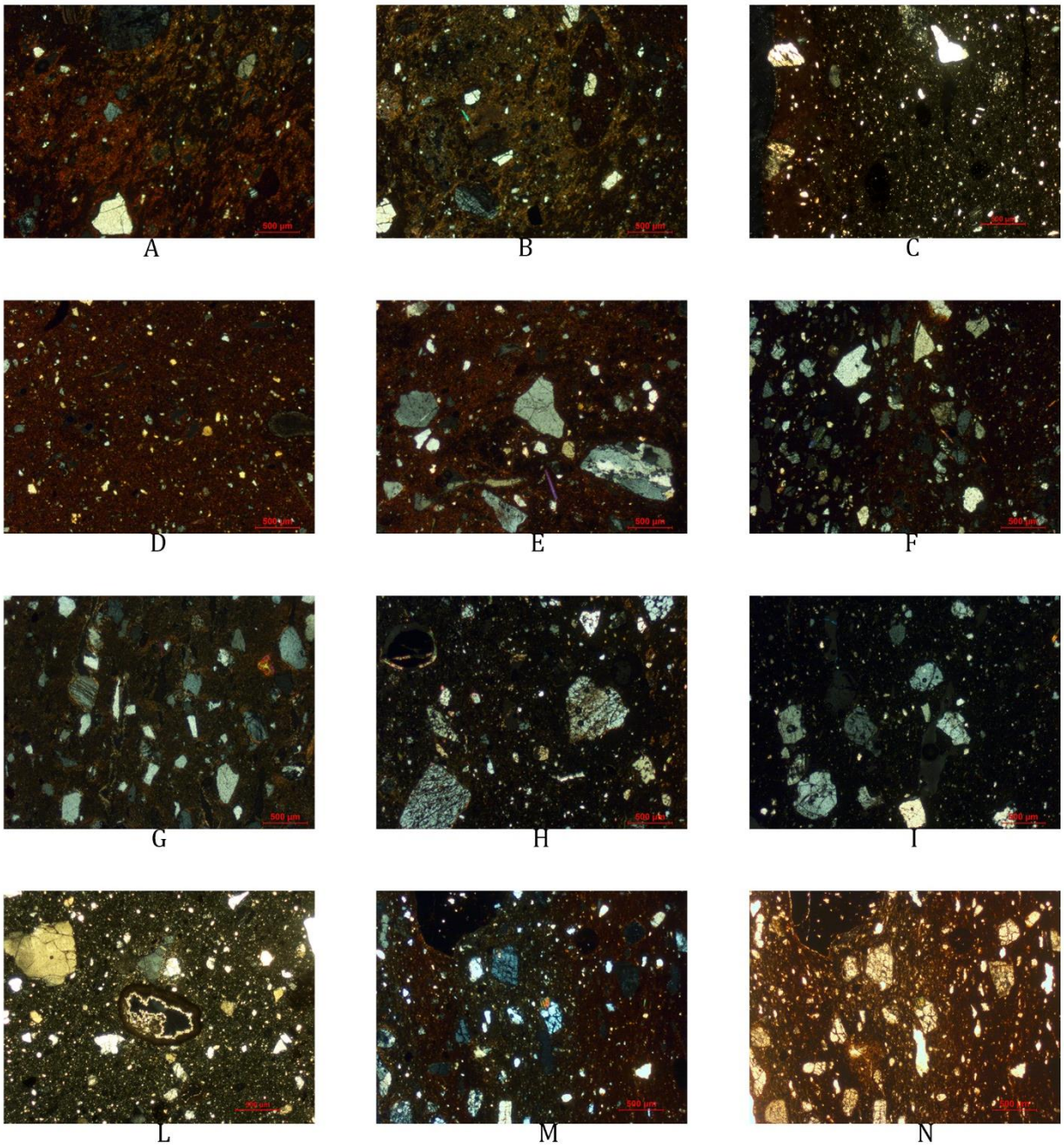

Figure 45 Images collected during PLM analysis of the different groups/sub-groups. A,B) images of the samples [1335]-9818 where two different raw material are visible in thin-section as well as a fragment of grog; C) sample [1]-15467 particular of the slip applied on the reddish slipped ware pottery; D,E,F) ceramic samples included in the iron rich ceramic fabric, group 1, (from the left) subgroup A (sample [973]-7560), B (sample LSI04 229), C (sample [973]-7561) respectively; G, H, I) ceramic samples included in the slightly calcareous ceramic fabric, group 2, (from the left) subgroup A (sample [1]-15467), B (sample [2041]-13885), C (sample [91]-1994) respectively; L) particular of a partially absorbed fragment of limestone with secondary calcite on sample [1030]-7716; M, N) XPL and PPL images of sample [91]-1980 with a small fragment of granitic rock (in the centre of the pictures) composed by quartz and green/brown tourmaline.

5.2.4.2 Mineralogical composition: XRPD of ceramic bodies and μXRD of the decorations

The results obtained by XRPD are presented in Table 10, and they are very similar to those obtained in section 5.1. Samples mineralogical composition is homogeneous, including the ceramic fragments recovered in kiln 1-2-3-4. Quartz is the main mineralogical phase. Feldspars were present in variable concentrations, being potassium rich feldspars the most common, while plagioclase feldspars (mostly sodium rich) were less represented. Illite-muscovite peaks were generally detected in most samples (abundant to traces). Just on samples [1030]-7714 and [1030]-7716 it was not identified. Hematite, calcite, mullite, leucite and biotite were also identified.

As explained in the petrographic section, the presence of secondary calcite indicates that samples were probably fired at a temperature above 700-750 ºC. Moreover, the presence of residual illite-muscovite peaks, which usually disappears above 950 °C (Nodari et al., 2007; Maritan et al., 2006), suggest that the ceramic kilns of the town of Santarém worked in a temperature range $>$ 700 ºC and $<$ 950 ºC. Just on two samples recovered on kiln 3 the formation of mullite, after phyllosilicates dehydroxylation and partial melting, suggest higher temperature of firing, above 900-950 °C (Cultrone et al., 2001; Rodriguez-Navarro et al., 2003). Nevertheless, considering the archaeological context of these two samples, recovered inside the kiln tunnel, they probably suffered several firing cycles thus favouring the formation of high temperature mineralogical phases.

μXRD analyses (Table 11) have been carried out on several samples to characterize the ceramic surface (slipped or not) and the decorative layers (painted or glazed). Quartz, K-feldspars, plagioclase, and illite-muscovite peaks were identified in all samples. Differences have been noted in the relative amounts of calcite, hematite and in one case, by the identification of gehlenite, a high temperature mineralogical phase.

Regarding white painted samples, the decoration was achieved using calcite or a lime-based pigment, while red paint was obtained using an iron oxides-based pigment considering the amount of hematite when compared to the ceramic paste.

Red slipped white painted pottery with mudejar motifs were also analysed (2 samples). They are both characterized by a deeply red slip enriched in hematite, while the white painted decoration is mainly composed of calcite. In particular, on sample [1]-15467 (Fig. 46), besides calcite, diopside and gehlenite were also identified, suggesting higher firing temperature for this piece. For the honey and black sample [2171]-14751 the decoration was obtained with an iron rich pigment as suggested by the identification of hematite and magnetite (Di Febo et al., 2017a).

Table 10 Mineralogical species identified by XRPD diffraction. Q, Quartz; Kf, Potassium-rich Feldspar; Pla, Plagioclase Feldspar; Bio, Biotite; Mus-Ill, Muscovite-Illte; Cal, Calcite; Hem, Hematite; Leu, leucite; Mu, Mullite. XXXX, very abundant; XXX, abundant; XX, moderate; X, scarce; Tr, traces

Sample	Typology	Site	Decoration	Chronology	Q	Kf	Pla	Bio	Mus-Ill	Cal	Hem	Leu	Mul
LSI04-228	*Pot*	*SICh*	*Unpainted*	*VIII-IX*	*XXXX*	*XXX*	*X*		*XX*	*X*			
LIS04-229	*Pot*	*SICh*	*Unpainted*	*VIII-IX*	*XXX*	*XXX*	*X*		*XX*	*TR*			
LSI04-232	*Pot*	*SICh*	*Unpainted*	*VIII-IX*	*XXXX*	*XX*	*X*		*X*				
LIS04-233	*Pot*	*SICh*	*Unpainted*	*VIII-IX*	*XXXX*	*XX*	*TR*		*XX*	*TR*	*TR*		
LIS04-236	*Pot*	*SICh*	*Unpainted*	*VIII-IX*	*XXXX*	*XXX*	*X*		*XX*	*TR*	*TR*		
[1368]-10000	*Waste*	*RCO*	*White paint*	*XI-XII*	*XXXX*	*XXX*	*X*		*XX*		*TR*		
[1368]-10002	*Waste*	*RCO*	*White paint*	*XI-XII*	*XXXX*	*XXX*			*XX*	*TR*	*TR*		
[1368]-10004	*Waste*	*RCO*	*White paint*	*XI-XII*	*XXXX*	*XX*	*X*		*X*	*TR*			
[1368]-9999	*Waste*	*RCO*	*White paint*	*XI-XII*	*XXXX*	*XX*	*XX*		*XX*	*TR*			
[1335]-9818	*Waste*	*RCO*	*Unpainted*	*XI-XII*	*XXXX*	*XX*	*X*		*XX*	*X*	*TR*		
[2041]-13884	*Waste*	*RCO*	*White paint*	*XI-XII*	*XXXX*	*XXX*	*X*		*XX*	*TR*	*TR*		
[2041]-13885	*Waste*	*RCO*	*White paint*	*XI-XII*	*XXXX*	*XXX*			*X*				
[1107]-8202	*Bowl*	*RCO*	*White paint*	*XI-XII*	*XXXX*	*XX*	*X*		*XXX*	*X*			
[1107]-8197	*Jug*	*RCO*	*Unpainted*	*XI-XII*	*XXX*	*XXX*	*X*		*XXX*	*TR*	*TR*		
[973]-7561	*Jug*	*RCO*	*Unpainted*	*XI-XII*	*XXX*	*XXX*	*XXX*		*X*		*TR*		
[1359]-9939	*Bowl*	*RCO*	*Unpainted*	*XI-XII*	*XXXX*	*X*	*X*		*XX*	*TR*			
[1359]-9930	*Pan*	*RCO*	*Unpainted*	*XI-XII*	*XXXX*	*XXX*	*X*		*XX*	*TR*			
[473]-4458	*Jug*	*RCO*	*White paint*	*XI-XII*	*XXXX*	*XXX*	*TR*		*X*	*TR*	*TR*		
[473]-4453	*Pot*	*RCO*	*White paint*	*XI-XII*	*XXXX*	*XXX*	*X*			*TR*	*TR*	*X*	
[1030]-7712	*Waste*	*RCO*	*White paint*	*XII-XIII*	*XXXX*	*XXX*			*TR*		*X*	*TR*	*X*
[1030]-7714	*Waste*	*RCO*	*Unpainted*	*XII-XIII*	*XXXX*	*XXX*	*X*		*TR*		*TR*		*X*
[1030]-7716	*Waste*	*RCO*	*White paint*	*XII-XIII*	*XXXX*	*XXX*							*X*
[91]-1977	*Jug*	*RCO*	*Unpainted*	*XIII*	*XXXX*	*XXX*	*TR*		*XX*		*TR*		
[91]-1980	*Pot*	*RCO*	*Unpainted*	*XIII*	*XXXX*	*XX*	*TR*		*XX*	*TR*			
[91]-1992	*Cover*	*RCO*	*White paint*	*XIII*	*XXXX*	*XXX*			*X*	*TR*	*TR*		
[91]-1994	*Cooker*	*RCO*	*White paint*	*XIII*	*XXX*	*XX*	*XXX*		*XX*		*TR*		
[1107]-8209	*Jug*	*RCO*	*CSP*	*XI-XII*	*XXX*	*XX*	*X*		*XXX*	*X*			
[973]-7560	*Jug*	*RCO*	*Red paint*	*XI-XII*	*XXXX*	*XX*	*X*		*XXX*		*TR*		
[508]-4697	*Bowl*	*RCO*	*Green Glaze*	*XI-XII*	*XXXX*	*XXX*	*X*		*XX*		*TR*		
[2244]-15043	*Jug*	*RCO*	*Unpainted*	*XIII*	*XXXX*	*XX*	*X*		*XXX*	*TR*			
[2171]-14751	*Bowl*	*RCO*	*Honey and black*	*XIII*	*XXXX*	*XXX*	*X*		*XX*	*TR*	*TR*		
[571]-5117	*Pot*	*RCO*	*Unpainted*	*XII-XIII*	*XXXX*	*XX*	*X*		*XX*				
[571]-5116	*Jug*	*RCO*	*Red paint*	*XII-XIII*	*XXXX*	*XX*	*X*		*XX*	*TR*			
[1]-15467	*Undetermined*	*RCO*	*White paint*	*XV-XVI*	*XXXX*	*XX*	*X*	*X*	*XX*	*TR*			
[939]-7351	*Jug*	*RCO*	*White paint*	*XV*	*XXX*	*XXX*	*X*		*XX*		*TR*		

Sample	Typology	Site	Decoration	Chronology	Q	Kf	Pla	Bio	Mus-Ill	Cal	Hem	Leu	Mul
Vala 37	*Bowl*	*RJA*	*CST*	*XI-XII*	*XXX*	*XX*	*TR*	*X*	*XXX*	*TR*		*TR*	

Table 11 Mineralogical species identified by µXRD diffraction. Q, Quartz; Kf, Potassium-rich Feldspar; Pla, Plagioclase Feldspar; Dio, Diopside; Ake, Akermanite; Mus-Ill, Muscovite-Illte; Cal, Calcite; Hem, Hematite; RL, Read Lead; Mag, Magnetite. XXXX, very abundant; XXX, abundant; XX, moderate; X, scarse; Tr, traces

Sample	Chronology	Point	Q	Kf	Pla	Dio	Ghe	Mus-Ill	Cal	Hem	RL	Mag
[1368]-9999	*XIth-XIIth*	*White paint*	*XXX*						*XXXX*			
		Cer. paste	*XXXX*	*X*	*TR*			*X*		*XX*		
[973]-7560	*XIth-XIIth*	*Red paint*	*XXXX*					*X*	*X*	*XX*		
		Cer. paste	*XXXX*	*X*	*X*			*X*	*X*			
[2171]-14751	*XIIIth*	*Black glaze*	*XX*						*TR*	*XX*	*XXX*	*X*
[571]-5116	*XIIth-XIIIth*	*Red paint*	*XXXX*	*TR*	*X*			*TR*	*TR*	*X*		
		Cer. paste	*XXX*	*X*	*X*			*X*		*TR*		
[1]-15467	*XVth-XVIth*	*White paint*	*XXXX*	*X*	*X*	*XX*	*XXX*	*X*	*X*			
		Slip	*XXXX*	*XX*	*XXX*			*X*	*XX*	*XX*		
[939]-7351	*XVth-XVIth*	*White paint*	*XXX*	*XX*	*X*	*XX*		*XX*	*XX*	*TR*		
		Slip	*XXXX*	*XX*	*X*			*X*	*X*	*XX*		

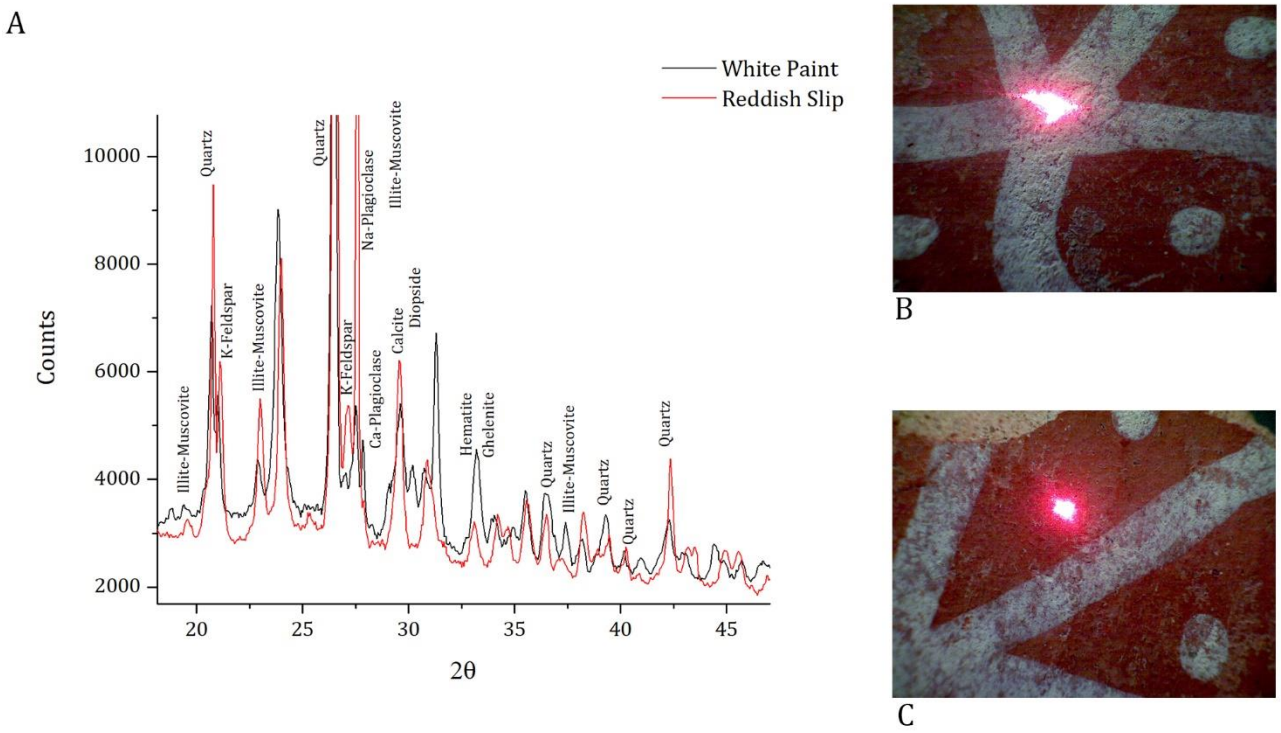

Figure 46 µXRD performed on the sample [1]-15467. A) Difractogram of the white paint (black) and of reddish slip (red); B) Point analysed of the white-painted decoration; C) Point analysed of the reddish slip.

5.2.4.3 Mineralogical composition: FT-IR ATR and µRaman spectroscopies

FT-IR ATR and µRAMAN analyses were developed on green/brown tourmaline grains, to corroborate PLM observation. The analyses were performed on sixteen ceramic samples (Table 12). For example, the FT-IR and RAMAN spectra of the glazed sample [508]-4967 are presented in figure 47.

Results confirmed PLM interpretation. Specifically analysed crystals can be classified as Schorlitic iron-rich tourmaline grains (Henry et al., 2011). Inclusions were identified based on the observation of specific Raman bands (cm^{-1}) 151, 238, 276, 371, 405, 445, 511, 536, 637, 710, 747 (A_1 active Raman species modes) and 837, 1066 (E active Raman species modes) (Alvarez and Coy-Yll, 1978; McKeown, 2008).

In the case of FT-IR ATR spectroscopy bands 3445, 1318, 1260, 1102, 1013, 962, 777, 705 cm^{-1} were observed. The best match was found with the reference sample R050304.2 from RRUFF database (Lafuente et al., 2016).

Tourmaline usually appears as accessory minerals in igneous and metamorphic rock. Very commonly is associated with pegmatite minerals like microcline, albite, quartz and muscovite. At the same time, it is very resistant to weathering, both from the mechanical and the chemical point of view (Krynine, 1946). Consequently, the identification of this specific mineral on stream sediments is quite common. Considering the typological variety (shape and decoration) of the ceramics, the identification of the same kind of tourmaline mineral indicates the exploitation of sediments with similar mineralogical inclusion for ceramic production, probably formed from the weathering of the same parent rock.

Table 12 List of the ceramic samples analysed by RAMAN and FT-IR spectroscopies with the indication of the sample reference, the recovering context, the chronology, the typology, the decoration and the archaeological site.

Sample reference [n°-US]	Ceramic Fabric	Chronology – century	Typology	Decoration	Arch site
LSI04-228	*1*	*8th-9th*	*Pot*	*Unpainted*	*SICh*
LSI04-229	*1*	*8th-9th*	*Pot*	*Unpainted*	*SICh*
LSI04-233	*1*	*8th-9th*	*Pot*	*Unpainted*	*SICh*
[1335]-9818	*-*	*11th-12th*	*Waste*	*Unpainted*	*RCO*
[1107]-8209	*2*	*11th-12th*	*Jug*	*CSP*	*RCO*
[1107]-8197	*1*	*11th-12th*	*Jug*	*Unpainted*	*RCO*
[973]-7561	*1*	*11th-12th*	*Jug*	*Unpainted*	*RCO*
[1359]-9930	*2*	*11th-12th*	*Pan*	*Unpainted*	*RCO*
[473]-4458	*1*	*11th-12th*	*Jug*	*Withe painted*	*RCO*
[91]-1980	*2*	*13th*	*Pot*	*Unpainted*	*RCO*
[508]-4967	*2*	*11th-12th*	*Bowl*	*Mon. Glaze*	*RCO*
[2244]-15043	*1*	*13th*	*Jug*	*Unpainted*	*RCO*
[571]-5517	*1*	*12th-13th*	*Pot*	*Unpainted*	*RCO*
[571]-5516	*2*	*12th-13th*	*Jug*	*Red painted*	*RCO*
Vala37	*1*	*11th-12th*	*Bowl*	*CST*	*RJA*
[1]-15467	*2*	*15th-16th*	*Undetermined*	*With painted*	*RCO*

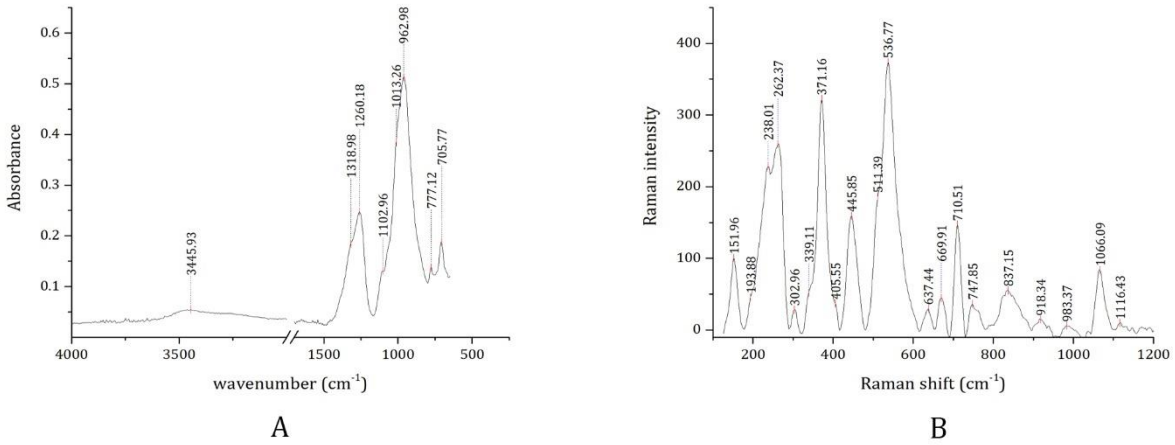

Figure 47 FT-IR-ATR (A) and µRAMAN (B) spectra of the sample [508]-4967 ceramic sample recovered in the RC0 archaeological site. Baseline corrections have been applied to each spectrum.

5.2.4.4 Chemical composition: XRF and ICP-MS analysis of ceramics

XRF and ICP-MS results are included in annex 2 (Table 6 to 11). Major oxides results show that in all cases, ceramic samples, including those fragments recovered in production contexts (kilns 1-2-3-4) and in *silos*, lie in the triangle formed by quartz, anorthite and mullite. This indicates that, without any distinction, ceramics were produced using a calcium poor raw material (Fig. 48A). Similar results were obtained in section 5.1.

Generally, ceramic samples do not contain more than 1.95 wt% of CaO (sample [1335]-9818) and they can not be considered lime-rich. The results obtained from the analysis are consistent with the geology of the area. Although close to Santarém, as evidence in section 5.1, calcium-rich clayey raw material could be available, it was not selected and exploited for ceramic production. Our results are consistent with the bibliography (Dias et al., 2001; Déléry, 2006; Prudêncio et al., 2006; Dias et al., 2008), and similar raw materials were also exploited in the Lisbon area pointing to the utilization of similar technology on both places.

This pattern of raw material exploitation continued during Islamic time, the *Reconquista* and during the Christian period. The same results were obtained in the case of CST and CSP decorated samples. Ceramic paste composition indicates that a silica rich raw material was exploited if compared to "*corda seca*" ceramic samples from different locations within the Iberian Peninsula (Peréz-Arantegui et al., 1999; Déléry, 2006).

This support the hypothesis that (I. C. Fernandes et al., 2015), in addition to the results already obtained for the Lisbon area (Dias et al., 2001; Dias et al., 2008), since the end of the 11th century – beginning of the 12th (*Taifa* – Almoravid period), *corda seca* staly ceramics were also produced at Santarém. Moreover, red painted, glazed and one sample of red slipped/white painted ceramics from the RCO archaeological site ([1107]-8109, [973]-7560, [508]-4967,

[2171]-14751, [571]-5116, [1]-15467) were depleted in Fe_2O_3 and enriched in Al_2O_3 (Fig. 48B). Considering the same chemical elements, the CST ceramic fragment Vala 37 (RJA site), and the fragments of red/slipped white painted pottery with mudejar motifs [939]-7351 (RCO site) are compatible with the majority of the samples from the RCO and from the SICh archaeological sites (i.e. enriched in Fe_2O_3). So, these results corroborate PLM classification.

The same division was noted plotting Fe_2O_3 *vs* TiO_2 and Fe_2O_3 *vs* Sc. These results are very similar to those obtained in section 5.1, indicating analogous raw material exploitation patterns.

In the case of the decorated ceramic (i.e. Fe_2O_3 poor), Fe_2O_3 and TiO_2 did not showed a linear correlation, suggesting that Ti rich mineralogical phases like anatase or rutile (TiO_2) were present in the ceramic paste. Nevertheless, these materials are slightly more enriched in Fe_2O_3 if compared to samples included in fabric/group 2 and raw material Ca1 on section 5.1, suggesting raw material mixing (Fig. 48C).

In the case of Fe_2O_3 rich ceramics, a linear correlation was observed both with TiO_2 and Sc, suggesting that ilmenite might be an important mineralogical phase. Identical results were obtained on section 5.1 in the case of fabric/group 1. In particular, Sc is a lithophile and immobile chemical element (Shotyk et al., 2001) and it can replace, considering the similarity of the ionic radii, for Fe^{2+} both in ilmenite and in different silicate ferromagnesian minerals (Stueber and Goles, 1967; Shimizu and Kuroda, 1969). So, the straight correlation observed between Fe_2O_3 and Sc gives valuable information on the characteristics of the raw material (Dias and Prudêncio, 2008). In our case, the observation carried out in thin section did not detect any ferromagnesian silicate minerals, so Sc is hosted by ilmenite crystals.

These results indicate that two different raw materials, enriched in anatase/rutile and ilmenite, were in most cases exploited and mixed for the production of undecorated - white painted ceramics and for decorated ceramics (red painted or glazed). A similar specialized pattern of raw material exploitation and ceramic production was already detected in the Lisbon area (Bugalhão et al., 2008a) during the Islamic period. Also, in this case, two different ceramic pastes were utilized to produce undecorated / white painted and glazed / red painted ceramics respectively.

Regarding trace elements results showed that Zr, Hf, Y and U, Th are positively correlated, and they are all included in zircon minerals ($ZrSiO_4$). Specifically, chemical elements like Hf, Y, U or Th may substitute Zr in its crystal structure. The zircon crystals that coexist in the same rock and crystallized in the same geochemical conditions must have the same chemical composition (Murad, 1978; Fedo et al., 2003). Therefore, the ratios between the

different elements in the zircon mineral can be used to identify different sources of raw materials in addition to Al_2O_3, Fe_2O_3, TiO_2 and Sc. Two of the most significant pair are Zr *vs* Hf (Fig. 48D) and Y *vs* Hf binary plot (Fig. 48E) which distinguish the samples in two different populations. This indicate that two different raw materials were employed for ceramic production in different kilns and *silos* during different periods.

Moreover, Zircon crystals, due to the relatively small coordination polyhedra, favours the inclusion of heavy rare earth (HREE) chemical elements (Henderson, 1984) if compared for example to monazite, allanite, apatite and sphene crystals. So, also differences in the concentration of HREE elements can give indications on the characteristics of the raw material (Hoskin and Ireland, 2000).

Considering ceramic samples REE_{CN} (McDonough and Sun, 1995), 3 different patterns were observed by the analysis of waste ceramics/from kiln 1-2-3-4 (Fig. 48F). On pattern 1 the abundance of $\sum LREE_{CN}$ and of $\sum HREE_{CN}$ tends to be lower; in pattern number 2 and 3 $\sum LREE_{CN}$ abundance tends to be the same, there is an enrichment of $\sum HREE_{CN}$ if compared to pattern 1, but pattern 2 is depleted in Er_{CN}, Yb_{CN} and Lu_{CN}.

Considering the correlation Zr *vs* Hf, ceramic samples with Zr/Hf ratio equal to 43-54 are represented by REE_{CN} pattern 2, while for Zr/Hf ratio equal 34-43 ceramic samples are represented by REE_{CN} pattern 1 and 3. These results point that $HREE_{CN}$ are hosted by 2 different populations of zircon minerals.

To conclude, the results obtained by the chemical analyses of the ceramic samples indicates that at least 3 different raw material were exploited and mixed in different proportion for ceramic production namely:

- One raw material enriched in Al_2O_3 and in anatase/rutile, mainly utilized for the production of decorated (i.e. from fabric 2) ceramic samples from the RCO archaeological site;
- Two raw materials, enriched in Fe_2O_3, ilmenite, with 2 different populations of zircon minerals for the production of unpainted/undecorated and white painted ceramic samples (i.e. from fabric 1).

Moreover, the results also indicate that these three different raw materials were employed or mixed during all the transition Islamic-Reconquista-Christian for ceramic production in Santarém.

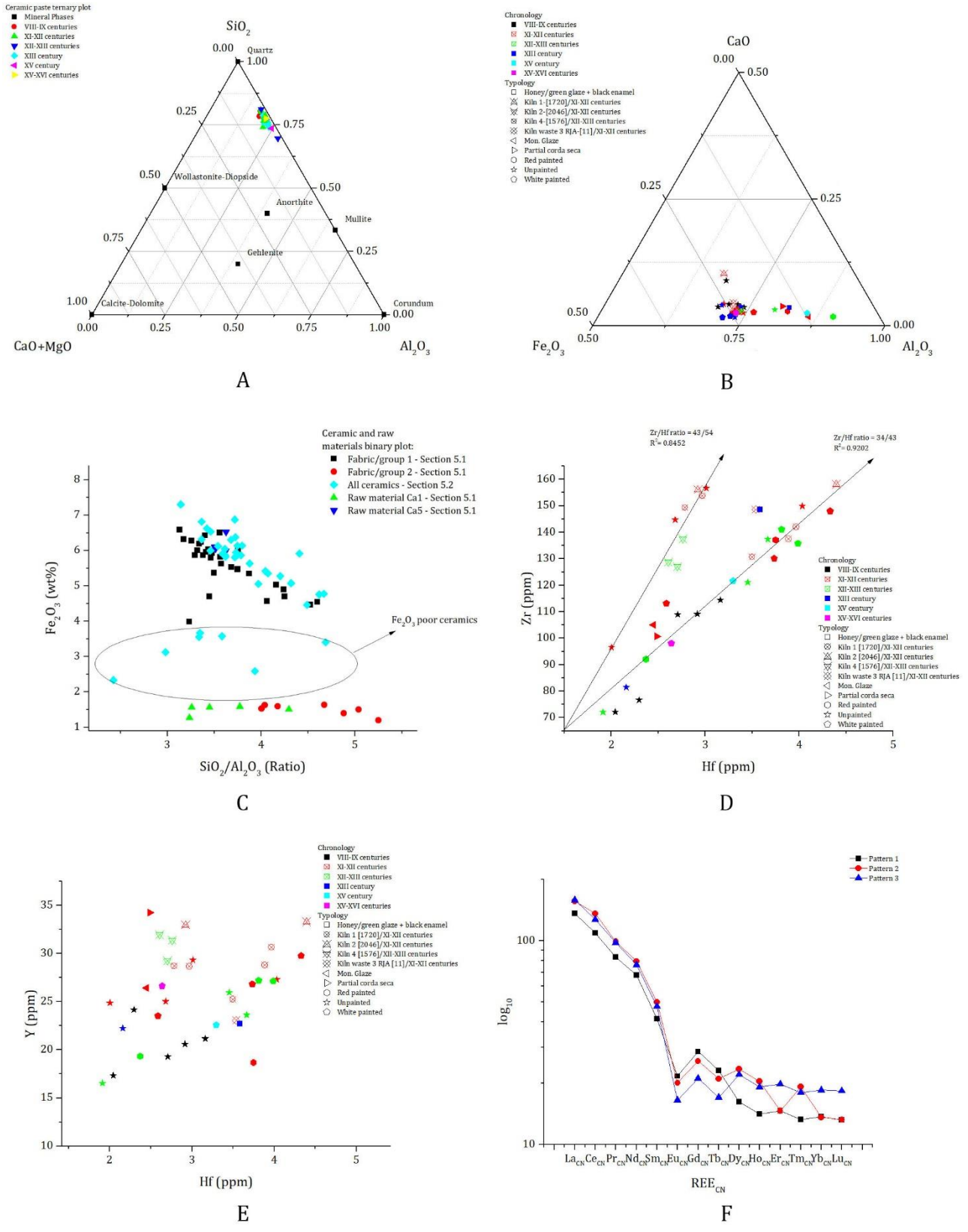

Figure 48 A)Ternary diagram of the ceramic samples after Heimann and Maggetti, 2014, 2016; B) Ternary diagram of the ceramic samples with Fe_2O_3, CaO and Al_2O_3; C) Comparative binary plot Fe_2O_3 vs SiO_2/Al_2O_3 of the ceramics and raw materials included in sections 5.1 and 5.2; D) Bynary plot of Zr/Hf; E) Binary plot Y/Hf; F) Distribution pattern of REE of the ceramic samples recovered in kiln 1-2-3-4. Pattern 1 include the sample Vala 37; Pattern 2 include samples [1335]-9818, [1368]-9999, [2041]-13884, [1030]-7712, [1030]-7714, [1030]-7716; Pattern 3 include samples [1368]-10000, [1368]-10002, [1368]-10004, [2041]-13885.

5.2.4.5 Microscopy: SEM-EDS micro-analysis of the ceramic paste, slip and painted decorations

SEM-EDS was utilized to corroborate petrographic observation and to estimate chemical elements distribution both in the ceramic matrix and temper. In particular, calcium distribution on the ceramic paste of fabric 2 (i.e. utilized in the production of glazed ceramics)

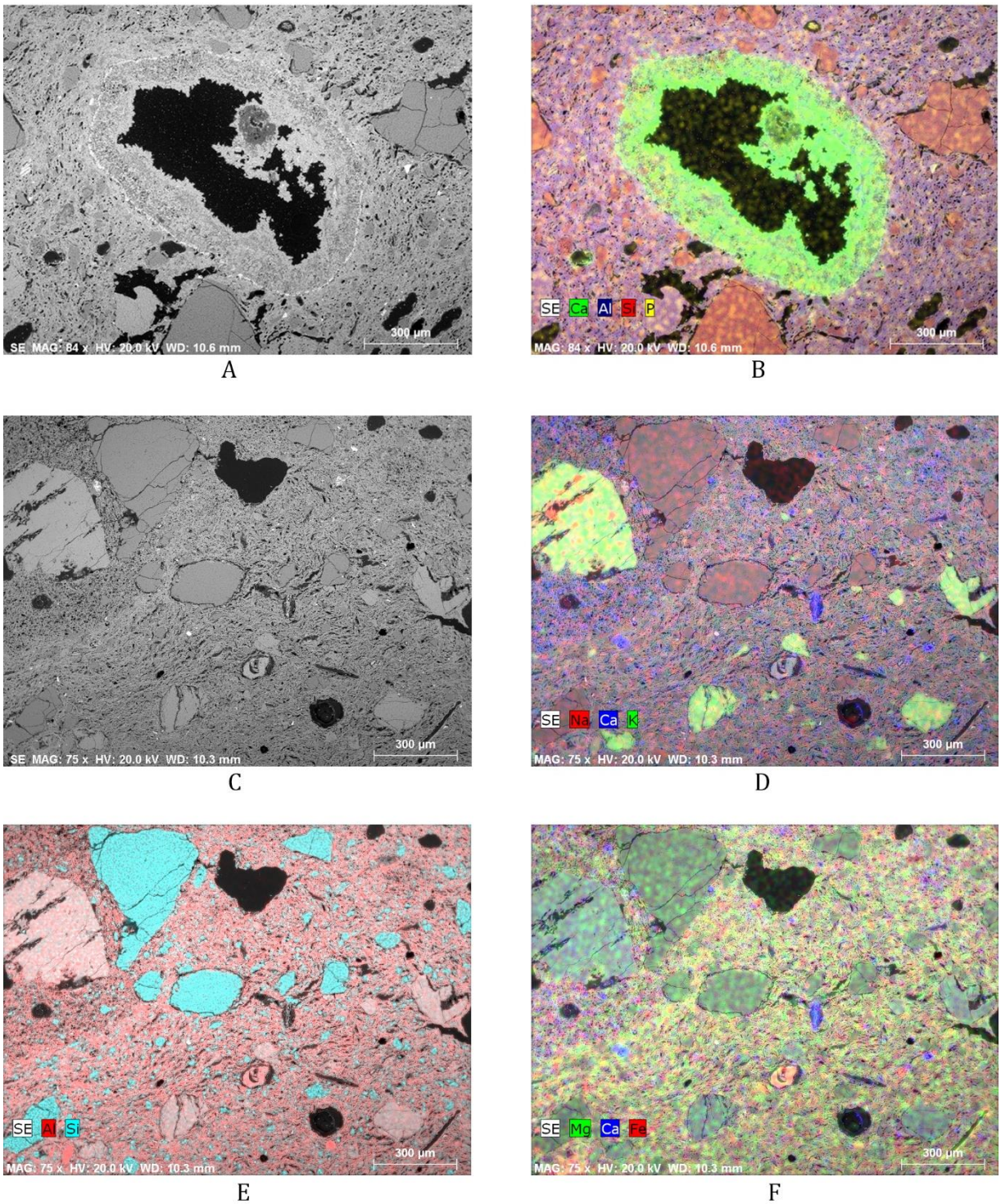

Figure 49 BSE images of the sample [1030]-7712 with elemental mapping distribution. Images A and B represent a partly absorbed fragment of limestone or a shell enriched in calcium and phosphorous. Images D, E, F,G represent the chemical distribution of elements in another portion of the thin-section, it is stressed the distribution of potassium, sodium and calcium to understand feldspars characteristics and of magnesium, iron and calcium to understand the characteristics of the ceramic paste.

was investigated (Fig. 49). Elemental mapping distribution analysis developed on sample [1030]-7712 (PLM figure 45L) showed that calcium is generally concentrated on isolated inclusions of thermally altered limestone fragments with variable size.

The ceramic matrix is enriched in iron, aluminium, magnesium and sodium while calcium appears as a minor chemical element. This also suggests that the amount of lime rich in- clusion, like calcretes, fragments of limestone or shells, does not influence significantly the bulk chemical composition of the ceramic fragments.

The study of temper by microanalysis also established feldspars composition. Temper grains are mainly composed by potassium rich feldspars and sodium rich plagioclase (Fig. 50), suggesting they proceed by the alteration of a felsic rock. On thin-sections, the former is represented by medium to very coarse sandy grains while the latter by silty to very fine sandy grains. Sporadically, the anorthitic component on Na-rich plagioclases has a concentration higher than the 25%.

Regarding micro-sized inclusion, these are generally composed by subrounded very fine sand / very fine silt grains of ilmenite (sometimes enriched in Mn), titanium oxides, iron oxides, barite, monazite and zircon. Tourmaline crystals were also analysed, and iron, magnesium and alkalis concentration confirmed its previous classification as schorlitic tourmaline (Henry et al., 2011).

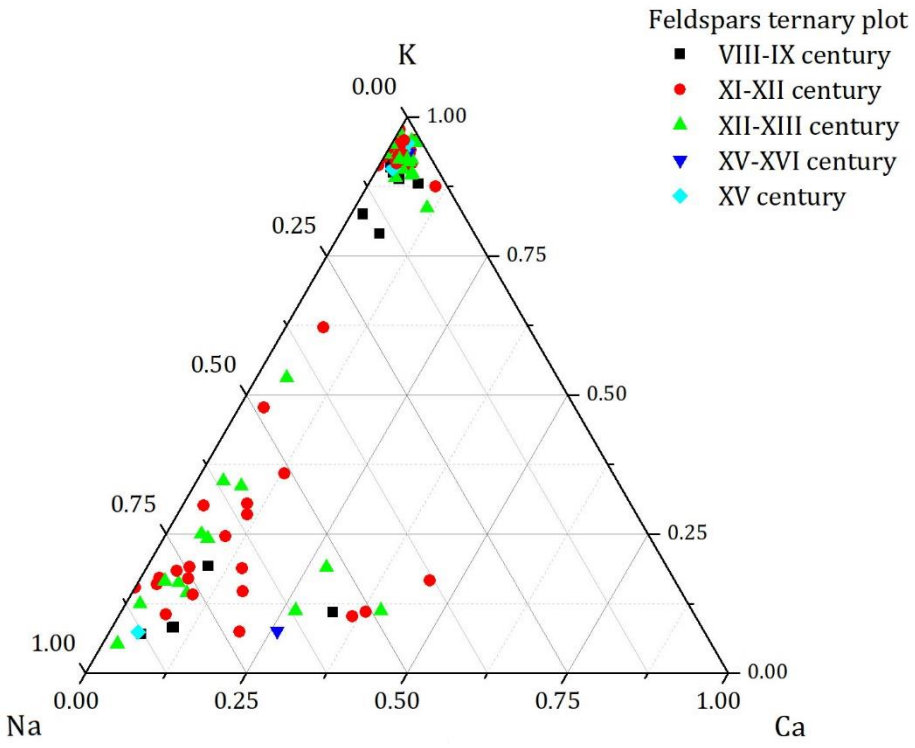

Figure 50 Feldspars ternary plot of the ceramic samples.

The analysis of the ceramic fragments by SEM-EDS indicate that, as expected after XRPD and XRF results, the ceramic paste was prepared using a calcium poor raw material.

Regarding white and red painted decoration, SEM-EDS results (Table 13) confirmed μXRD data. If compared with the ceramic paste, red paints are always enriched in FeO, while the white painted are enriched in CaO. Therefore, white painted ceramic was decorated using a calcium rich pigment (i.e. calcite or lime), while an iron rich pigment (i.e. hematite) and/or an iron rich clay were utilized for red paint application.

In the case of late medieval samples with white painted mudejar motifs (samples [939]-7315 and [1]-15467), slip chemical composition is different, if compared with the chemical composition with the ceramic paste. The sample [1]-15467 is enriched in alkalis ($Na_2O + K_2O$), indicating that different slips were used.

Table 13 *Chemical composition of the ceramic paste, slip, and white-red painted decorations. Results were normalized to 100% and uncertainty is 1σ.*

Sample	Point analyzed	Na_2O	MgO	Al_2O_3	SiO_2	P_2O_5	K_2O	CaO	TiO_2	FeO
[1368]-9999	*Ceramic paste*	*0.5*	*1.1*	*23.3*	*62.9*		*3.7*	*1.3*	*0.9*	*6.2*
	White paint	*2.2*	*2.7*	*17.5*	*47.4*		*4.8*	*19.8*	*0.8*	*4.7*
[571]-5116	*Ceramic paste*	*0.3*	*1.0*	*33.7*	*57.9*		*2.5*	*0.8*	*0.8*	*3.0*
	Red paint	*1.0*	*1.2*	*29.0*	*48.5*		*4.0*	*0.9*	*1.2*	*14.2*
[973]-7560	*Ceramic paste*	*0.9*	*1.4*	*23.1*	*63.9*		*4.5*	*1.0*	*1.2*	*3.9*
	Red paint	*1.6*	*1.2*	*23.6*	*46.8*	*0.4*	*8.2*	*6.3*	*1.3*	*10.5*
[939]-7315	*Ceramic paste*	*0.8*	*1.1*	*30.9*	*55.6*		*5.2*	*0.7*	*0.8*	*4.9*
	Slip	*0.9*	*1.9*	*19.4*	*55.1*		*6.6*	*1.0*	*0.8*	*14.4*
	White paint	*2.2*	*2.1*	*16.6*	*50.4*	*2.7*	*3.6*	*15.8*	*2.6*	*4.1*
[1]-15467	*Ceramic paste*	*0.6*	*1.2*	*29.5*	*58.6*	*0.3*	*4.0*	*1.1*	*0.7*	*4.0*
	Slip	*3.9*	*1.2*	*30.6*	*52.1*	*0.2*	*6.7*	*0.9*	*1.3*	*3.1*
	White paint	*3.1*	*1.7*	*16.7*	*52.9*	*0.5*	*1.9*	*16.1*	*0.9*	*6.2*

5.2.4.6 Microscopy: SEM-EDS micro-analysis of glazed decorations

Glazed decorations have been studied on 4 samples (Table 14). Three of them were recovered in the *RCO* archaeological site, while the last was recovered in the RJA archaeological site. The chronology is also different, especially in the RCO site, being one sample from the 13th century. Regarding monochromatic and honey and black glazed ceramics, the frontal and the back-side of the fragments were studied.

Table 14 Main characteristics registered on glazed ceramic samples from the RCO *and the* RJA archaeological site.

Sample	[1107]-8209	[508]-4967	[2171]-14751	Vala 37
Arch. site	RCO	RCO	RCO	RJA
Typology	Jug	Bowl	Bowl	Bowl
Chronology	*11th-12th*	*11th-12th*	*13th*	*11th-12th*
Decoration	CSP	Monochromatic	dichromatic	CST
Chromophores agent	CuO	CuO and FeO	FeO and MnO	FeO/Clay
Glazing technique	Frit	Frit	Frit	Frit
Firing technique	Single firing	Single firing	Single firing	Double firing
Opacification technique	SnO_2	None	None	SiO_2 crystals
Morphology	Heterogeneous	Homogeneous	Homogeneous	Heterogeneous

The goal was to understand the difference, if any, in the glazing technique between samples with Islamic and post Islamic chronology and to assess any similarity in glaze technology of *corda seca* glazed ceramic from the RCO and RJA archaeological site. To do so, the chromophore agents, the glazing technique, the firing technique, and the opacification method were investigated.

These characteristics were evaluated considering previous publications on Islamic-*Mudejar* glazed ceramics (Molera et al., 1996; Molera et al., 1997; Molera et al., 1999; Vendrell-Saz et al., 2006; Déléry, 2006; Chapoulie et al., 2005), the interaction between the lead glaze ad the ceramic paste (Molera et al., 2001a; Chapoulie et al., 2005; Molera et al., 1993) and the glazing technique (Tite et al., 1998; Walton and Tite, 2010). In the case of the ceramic sample from the *RCO* archaeological site (Fig. 51A/B/C/G/H/I/L), decorations are very similar:

- In all cases glazes are of the high lead type, and PbO/SiO_2 ratio is high (Fig. 52C, Table 15);
- Glazes have been applied using a lead silica frit. Besides, the chemical concentration of the major oxides of the glaze (excluding lead) does not match those of the ceramic paste (Fig. 52 A/B);
- Considering the diffusion of lead in the ceramic paste and the formation of potassium and potassium-sodium lead silicate at the interface between the glaze and the ceramic paste, the samples were single fired (Fig. 51C/H/L);

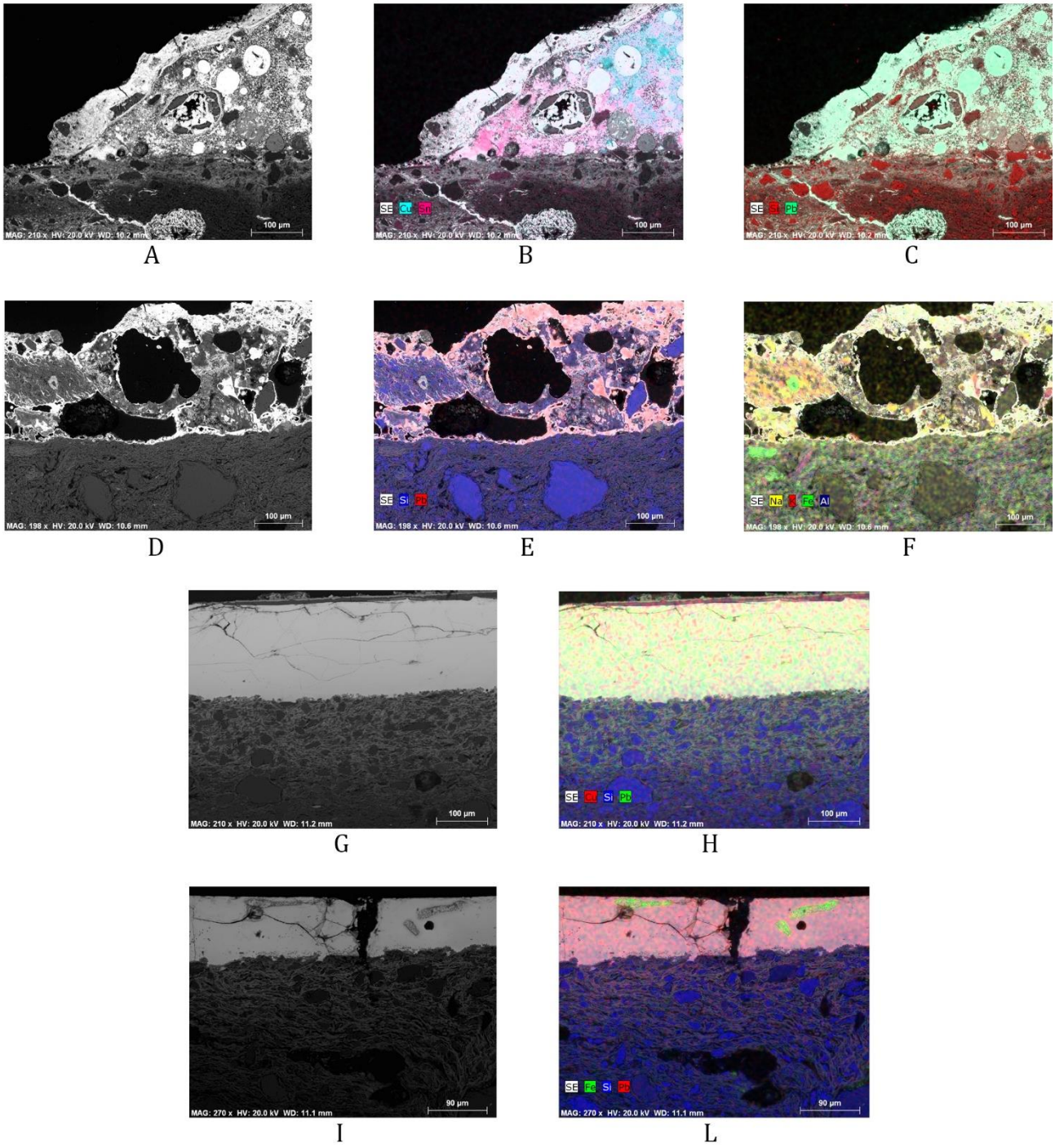

Figure 51 BSE images of samples [1107]-8109 (A), Vala 37 (D), [508]-4967 (G), [2171]-14751 (I). On samples from the RCO archaeological site the elemental mapping distribution show the diffusion of lead inside the ceramic paste for 100 µm roughly. Images B and C show the elemental mapping distribution of Cu-Sn and of Si-Pb in the sample [1107]-8197. Images E and F show the elemental mapping distribution of Si-Pb and of Na-K-Fe-Al on sample Vala 37. Image H shows the elemental mapping distribution of Cu-Si-Pb on sample [508]-4967. Image L shows the elemental mapping distribution of Fe-Si-Pb in the sample [2171]-14751.

- A Na_2O rich slip has been applied before glaze application (Table 15).

Glazed ceramics from the RCO site also present some specific characteristics that distinguish them:

- The sample [1107]-8209 with CSP decoration has a heterogeneous turquoise glaze delimited by a black line, the *corda* (Fig. 51B/C). The main chromatic agents were CuO for the glaze and MnO plus FeO in the case of the *corda.* The glaze also shows bubbles of metallic lead. This suggests that the silica lead frit was partially reduced during firing, suggesting a lack of oxygen in the kiln chamber (Comodi et al., 2004; Maltoni et al., 2012). Opacification was obtained by acicular SnO_2 crystals (Molera et al., 1999b);
- The sample [508]-4967 has a green glaze in the frontal side and a honey glaze in the back side (Fig. 51G-H). Glazes are very homogeneous. The main chromatic agents are CuO and FeO. On the back glaze, considering the elevated concentration of oxides of iron (2.14 wt%) which exceed the upper limit usually recovered on white glaze (Molera et al., 2001c), some clay was probably added to the lead silica frit;
- The sample [2171]-14751 has a honey/green and homogeneous glaze both on the frontal and on the back side with black enamel on the frontal side (Fig. 51I-L). The main chromatic agent was FeO. The black decoration was also enriched FeO, supporting the identification of hematite (Fe_2O_3) and magnetite (Fe_3O_4) by µXRD.

On the CST sample Vala 37 from *RJA* archaeological site the glaze is very weathered (Fig. 51D). In any case, small unaltered glaze portions could be analysed. If compared with CSP sample from the RCO archaeological site:

- The glaze is of the lead-alkali type, and PbO/SiO_2 ratio is low (Table 15, Fig. 52C);
- The artifact was doubled fired and was decorated using a frit (Fig. 52A/B);
- The main chromatic agent is FeO, and some clay was probably added to the glaze mixture as evidenced by the identification of a clay nodule inside the glaze by SEM-EDS (Fig. 51 E-F). In this case, the colour of the glaze could be yellow or green;
- The glaze was opacified with crystals of quartz.

Considering the results obtained by the analyses of the glazed decoration, results suggest that the glazing technique in the RCO archaeological site was uniform. Results are very similar to fabric/group 2 monochromatic glazed ceramics analysed in section 5.1 (fabric/group 1, 2), but a slip was not applied in the case of the *Alcaçova* of Santarém ceramics. Thus, in the timeframe comprised between 11th-12th and the 13th century the glazing technique was similar,

and it seems that the Christian conquest did not significantly change glaze technology.Our results are comparable to those obtained on Hispano-Moresque ceramics from Spain (Molera et al., 1997; Molera et al., 1999).

Several differences have been evidenced on *corda seca* glazed ceramic from RCO and RJA archaeological sites. Alkalis concentration, the PbO/SiO_2 ratio, the opacification and firing technique are the most important. These results show that two different contemporaneous workshops were using different glazing techniques. In particular, as showed in previous work on *corda seca* style ceramics (Chapoulie et al., 2005), the concentration of the two main oxides (i.e. SiO_2 and PbO) may vary, but the general tendency is that the concentration PbO usually decrease with time, especially on *corda seca* ceramic of the 12th century.

Nevertheless, the analyses of partial and total *corda seca* ceramic from the 11th-12th centuries recovered in Zaragoza (Peréz-Arantegui et al., 1999b) and Lisbon (Déléry, 2006a)

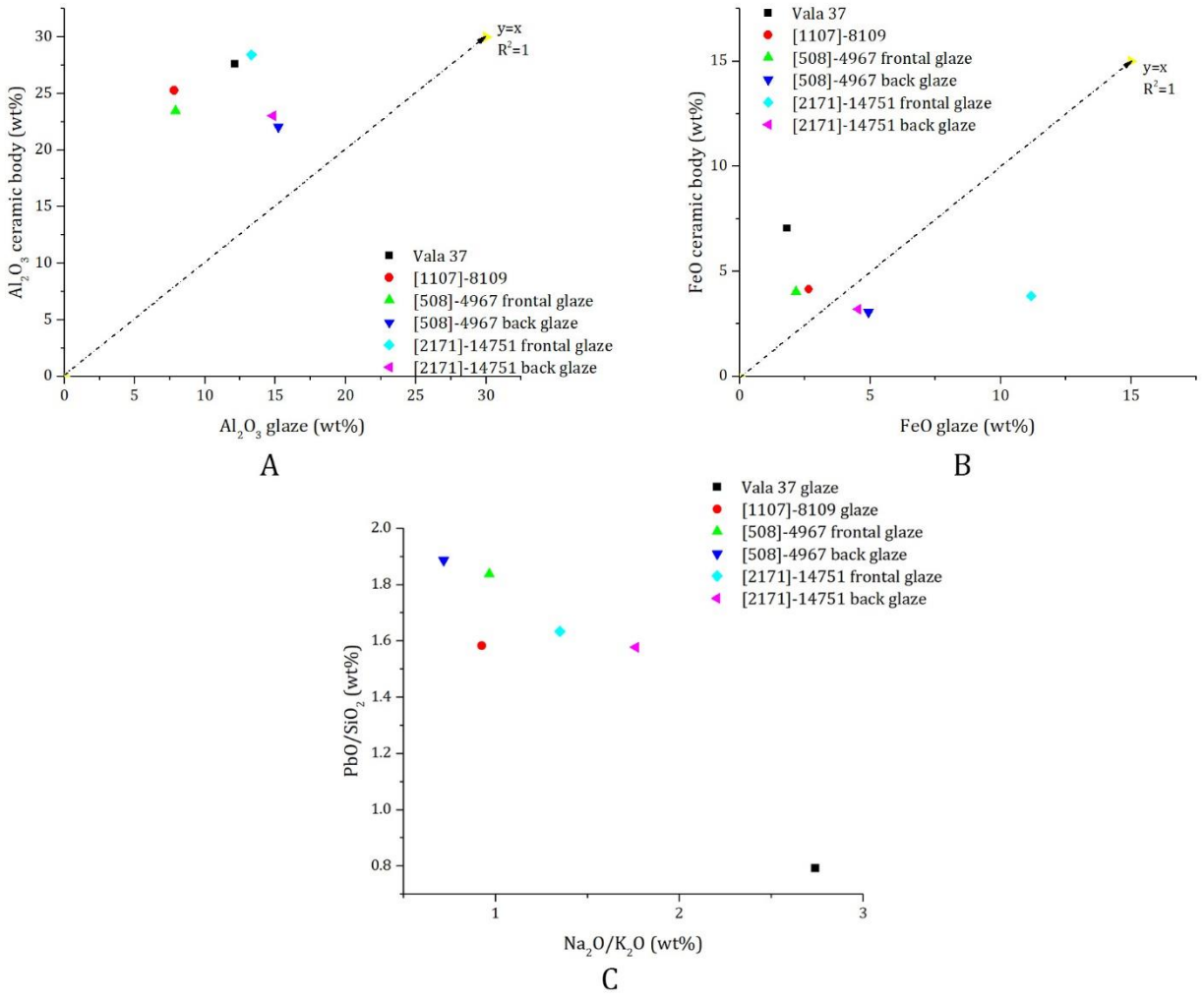

Figure 52 A-B) Binary plots. The graphs present the correlation of Al_2O_3 and FeO wt% measured in the ceramic body and on the glaze, respectively. C) Binary plot of the PbO/SiO_2 and Na_2O/K_2O ratios.

may also show a high concentration of PbO, indicating that different technical solutions could be employed.

Regarding the opacification method, the two techniques, oxide of tin *vs* crystals of quartz, together in the same artefact or alone, are well documented in the Iberian Peninsula during and after the Islamic domination (Coll Conesa et al., 1999; Peréz-Arantegui et al., 1999a; Molera et al., 2001b). In any case, the quartz opacification technique is related to an older ceramic tradition.

Firing cycles are also different. The bibliography showed (Chapoulie et al., 2005) that CSP ceramics could be single fired in the *al-Andalus* (i.e. as CSP ceramic from the *RCO* site). Still, CST ceramics were always double fired to favour the oxidation of the ceramic paste (Chapoulie et al., 2005). This process was essential to obtain the desired glaze colour.

The glazing technique of sample Vala 37 is also different from the CST ceramic samples from fabric/group 3 analysed in section 5.1. Glazes of these samples were homogeneous, opacified using SnO_2 crystals, and CaO concentration is higher. Conversely, sample Vale 37 showed opposite characteristics.

These shows that the technological transfer between different places of the *al-Andalus* was not linear and, probably, ceramists adapted the production cycle to the raw materials available.

Table 15 Chemical composition of the glaze and of the features/inclusions observed in the analyses of the glazed decorations. For corda seca *samples, just the decorated side has been analysed. For sample [508]-4967 and sample [2171]-14751, the frontal and the back side were analysed. Results were normalized to 100% and uncertainty is 1σ.*

Sample	Point analysed	Na_2O	MgO	Al_2O_3	SiO_2	P_2O_5	K_2O	CaO	TiO_2	MnO	FeO	CuO	SnO_2	BaO	PbO	PbO/SiO_2
Vala 37	*Glaze*	*5.4*	*0.3*	*7.8*	*45.3*	*0.7*	*2.0*	*1.7*			*1.2*				*35.8*	*0.79*
	Clay inclusion	*4.0*	*0.6*	*21.3*	*55.2*	*1.1*	*6.1*	*1.3*	*1.6*		*3.4*				*5.3*	
	Ceramic paste	*1.0*	*1.5*	*26.0*	*50.0*	*0.9*	*4.7*	*2.7*	*1.0*		*6.7*				*5.8*	
[1107]-8109	*Glaze*	*0.5*	*0.8*	*3.1*	*32.0*	*0.1*	*0.6*	*1.5*			*1.1*	*5.3*	*4.6*		*50.6*	*1.58*
	Corda, black	*0.6*	*0.5*	*4.4*	*24.5*	*1.4*	*1.3*	*1.9*	*0.6*	*3.9*	*13.3*	*1.6*	*1.1*		*44.9*	
	Lead inclusion	*0.2*	*0.4*	*1.9*	*9.0*	*0.2*	*0.4*	*1.0*			*0.7*	*1.6*	*1.0*	*1.8*	*82.0*	
	Slip	*2.0*	*1.3*	*18.4*	*45.3*	*1.6*	*3.8*	*2.1*	*1.4*		*4.5*	*1.4*			*18.0*	
	Ceramic paste	*1.7*	*1.4*	*24.5*	*57.5*	*1.2*	*3.7*	*1.6*	*1.3*		*4.0*				*3.3*	
[508]-4967 Frontal glaze	*Glaze*	*0.6*	*0.3*	*3.0*	*31.4*	*0.1*	*0.6*	*0.8*	*0.7*		*0.8*	*4.0*			*57.6*	*1.83*
	Interface crystals	*0.8*	*0.2*	*15.7*	*46.8*		*6.4*	*0.4*	*1.1*		*0.4*	*1.4*			*26.9*	
	Slip	*1.2*	*0.7*	*19.5*	*52.1*	*0.1*	*4.3*	*0.8*	*0.6*		*2.2*	*0.6*			*18.0*	
	Ceramic paste	*0.7*	*1.0*	*22.4*	*61.9*		*3.5*	*0.8*	*1.1*		*3.8*				*4.8*	
[508]-4967 back glaze	*Glaze*	*0.7*	*0.6*	*6.6*	*30.1*		*0.9*	*1.3*	*1.1*		*2.1*				*56.7*	*1.88*
	Interface crystals	*0.5*	*0.4*	*12.3*	*41.2*		*4.2*	*0.4*	*1.5*		*1.8*				*37.8*	
	Slip	*0.9*	*1.1*	*18.7*	*51.7*		*3.7*	*0.5*	*0.8*		*5.5*				*17.1*	
	Ceramic paste	*1.0*	*0.8*	*21.8*	*67.1*		*2.9*	*0.6*	*1.5*		*3.0*				*1.3*	
[2171]-14751 frontal glaze	*Black pigment*	*0.6*	*0.7*	*2.8*	*10.3*		*0.7*	*1.0*	*0.6*		*69.7*				*13.7*	
	Glaze	*2.1*	*0.6*	*6.6*	*30.8*		*1.5*	*2.5*			*5.6*				*50.3*	*1.63*
	Circular interface crystal	*5.9*	*0.4*	*14.3*	*33.9*		*1.3*	*4.0*			*3.3*				*37.0*	
	Interface crystals	*4.6*	*1.7*	*22.0*	*44.9*		*3.7*	*0.9*	*0.7*		*4.0*				*17.6*	
	Slip	*3.7*	*1.6*	*21.3*	*46.2*		*3.5*	*0.9*	*1.1*		*4.3*				*17.4*	
	Ceramic paste	*1.2*	*1.4*	*27.0*	*54.8*		*4.7*	*0.7*	*1.5*		*3.6*				*5.1*	
[2171]-14751 back glaze	*Glaze*	*1.9*	*0.9*	*7.4*	*31.9*	*0.4*	*1.1*	*3.2*	*0.8*		*2.3*				*50.3*	*1.57*
	Circular interface crystal	*6.7*	*0.4*	*14.3*	*34.0*		*1.5*	*4.2*	*1.2*		*0.5*				*37.2*	
	Interface crystal	*3.7*	*0.6*	*30.1*	*43.3*		*6.8*	*1.2*	*0.9*		*1.0*				*12.4*	
	Slip	*3.4*	*1.3*	*20.6*	*51.3*		*4.2*	*1.1*	*1.5*		*2.9*				*13.8*	
	Ceramic paste	*1.4*	*1.2*	*22.3*	*63.0*	*0.3*	*3.6*	*0.9*	*1.0*		*3.1*				*3.2*	

5.2.5 Final remarks of the section

On the basis of the results obtained by PLM analysis the presence, or not, of lime concretion (i.e. calcretes) and/or limestone fragments established that two different ceramic fabrics were identified. Just sample [1335]-9818 was not assigned to any of these two fabrics.

Liquid containers and fire ceramic were also produced with a certain degree of specialization, both during the Islamic period and the Christian Reconquista.

Decorated ceramic (i.e. glazed, red painted and white painted with mudejar motifs) were indifferently produced also using both fabrics, during the Islamic-Reconquista-Christian periods. Moreover, the homogeneity of the mineralogical composition of both ceramic samples recovered in production environment and in silos also suggest the exploitation of similar raw material/sediment deposits.

These observations have been further confirmed by μXRD, FT-IR ATR and μRaman, which confirmed similarities in temper characteristics in addition to similar firing technology. μXRD analysis of the decorations determined the characteristics of the white painted decoration (i.e. calcite), red painted decoration (i.e. hematite), of the reddish slip of mudejar ceramic (i.e. hematite) and of the black enamel on the glazed sample [2171]-14751 (i.e. magnetite and hematite).

Microanalyses by SEM-EDS confirmed that calcium contribution on the bulk chemical composition of the ceramic fragments is not significant, being included in calcretes and on thermally altered limestone fragments. Also, feldspars analysis corroborates the hypothesis of similar ceramic provenance because temper originated from the desegregation of felsic rocks. These results are compatibles with the identification of tourmaline (by FT-IR ATR and μRaman), indicating one more time, the utilization of the same raw materials.

Regarding raw material selection for ceramic production, they were chosen considering the object to be prepared. Al_2O_3 concentration on decorated samples from the *RCO* archaeological site (i.e. glazed samples and red painted samples) is higher if compared to unpainted, white painted and from the ceramic recovered in production environment. Moreover, trace elements analyses showed that the raw materials exploited were three, with different Zr/Hf and Y/Hf ratios and REE patterns. The same raw materials were exploited during all the Islamic-Reconquista-Christian transition periods.

The combination of archaeological and archaeometric data, clearly indicate that two different workshops were active and produced *corda seca* glazed ceramic at Santarém during Islamic time. In addition, glaze analysis evidenced they were significantly different in chemical

composition, firing technique and opacification method. Moreover, the production of glazed ceramic in the RCO archaeological site was very standardized along time, preserving the same glaze technique also after the Christian *Reconquista*. Nevertheless, more samples need to be analysed to confirm this hypothesis.

To summarize the archaeometrical study carried out on the ceramic samples demonstrate that in the town of Santarém, between the 11th and 13th century, two different workshops were active, with four different kilns. On the RCO archaeological site, the ceramic production continued without interruption, while on the RJA site, there are no evidence of ceramic production after the Christian Reconquista of the town. Moreover, the exploitation of similar raw material from the 8th-9th to the 15th-16th century was assessed.

In particular, the identification of *corda seca* style ceramics, CST (*RJA* archaeological site) and CSP (*RCO* archaeological site), production in two different workshops is a new archaeometric evidence by now just assessed in Lisbon in the Portuguese territory. Thus, the Tagus valley was, by now, one of the most important and active areas in the production of decorated ceramics, at least on Western Iberia.

To conclude, it is important to stress the continuity in raw material exploitation, in ceramic technology and in glaze manufacture also after the Reconquista when the power changes from Muslins to Christians. This means that the production of ceramic in the town of Santarém was autonomous from the prevailing power-ruling of the region.

5.3 Comparative pottery technology between the Middle Ages and Modern times in the Santarém area

The results in this section have been published in the *Journal of Archaeological and Anthropological Sciences* edited by Springer Nature. It presents the study results carried out on two different ceramic assemblages from the Santarém district, traditional and archaeological, through the combination of historical, archaeological, archaeometric and experimental archaeological data.

The principal aim is to understand ancient pottery technology and to evaluate whether ceramic production followed similar principles in the Middle Ages (from the Islamic to the Christian domination) and Modern times. Moreover, traditional ceramics, knowing the productive process, have been used as a tool to interpret ancient pottery technology. We considered different utilitarian ceramic groups, namely fire, table and food-liquid container wares.

Through the combination of polarized light microscopy (PLM), X-Ray powder diffraction (XRPD), X-ray fluorescence spectroscopy (XRF) with physical and mechanical tests, it has been possible to collect valuable information regarding pottery manufacturing, considering the chronology and the object function. Moreover, it is also considered the effect of raw materials mixing and ceramic paste preparation on ceramics final characteristics.

The results of this section indicate that both during the Middle Ages and in modern times, technical expertise played, and still play, a fundamental role in the creation of a specific object. In this specific case, behavioural and socio-cultural factors drove ceramists' decisions when selecting between different technological solutions, and every decision or technical choice is/was taken depending on the functional and performance characteristics desired for a specific artefact. This happened during the Middle Ages and is still happening nowadays to produce traditional ceramics in the district of Santarém, Portugal.

5.3.1 Introduction and goals of the section

In every historical period, pottery has always been considered an utilitarian or a symbolic-votive artefact. Its role in the construction and reproduction of social relations and cultural values is widely recognized also by social sciences (Sillar and Tite 2000).

Moreover, since the Neolithic, clay-made objects represent a conspicuous part of the archaeological findings, mainly due to their good resistance to weathering. This is why ceramic is one of the most studied archaeological evidence.

Nowadays, various disciplines, such as anthropology, archaeology and archaeometry, study this material. Also, history and ethnography, depending on the chronology, give a fundamental contribution to the understanding of ancient ceramic, especially through the analyses of historical resources and the study of rural, traditional and indigenous communities (Lindahl and Pikirayi 2010; Roux 2019; Arnold 2000).

However, what can affect pottery technology and-or artisan choices in the whole cycle of ceramic production? Many *variables* can influence it. Among them, we can mention environmental restrictions, access to raw material sources (fuel, water, clay, temper) and economic or political changes.

Several authors suggest that, considering all the possible *variables*, technology can also be affected by behavioural or socio-cultural factors, such as, for example, tradition, ideology, religion or ethnicity. In this case, the ceramist is the major player, and every decision or technical choice is taken depending on the functional and performance characteristics desired for a specific artefact (Schiffer and Skibo 1997; Schiffer and Skibo 1987). Technical expertise also plays a fundamental role in the creation of a specific object and, in this case, socio-cultural factors drive potter decisions when selecting between different technological options (Sillar 2000; Lemonier 1993; Lindahl and Pikirayi 2010).

A different point of view stressed the importance of looking at the various steps of the productive cycle as being part of an interdependent system. In this case, the previous *variables* (e.g. raw materials sources) and behavioural and socio-cultural factors have the same impact on pottery technology (Sillar and Tite 2000; Gosselain 2012). In this framework, the concept of "*chaîne opératoire*", firstly coined by Lehroi-Gourhan (1964), gives a systematic description of all the steps of the productive cycle, taking under consideration the whole interdependent system to understand what really influences ceramic technology.

Therefore, material science disciplines such as archaeometry can give a valuable contribution to the analysis of the "*chaîne opératoire*" and to evaluate ceramic technology. In

Table 16 DMS Geographical coordinates of Rua 5 de Outubro archaeological site (Santarém) and of Mr. Domingos' workshop (Muge). Data have been obtained using Google Earth Pro. Data degree of reliability extracted using Google Earth Pro, such as elevation and horizontal accuracy, are discussed in specialized bibliography (Goudarzi and Landry 2017; Pulighe et al. 2016; Wang et al. 2017).

Site	Geographical Coordinates (DMS)					Data source
	Degree	Minutes	Seconds	Orientation	Elevation	
Rua 5 de Outubro, archaeological site	39	14	7.49	N	106	Google earth
	8	40	45.9	W	106	
Muge, Traditional ceramic Workshop	39	6	17.4	N	10	
	8	42	57.06	W	10	

recent years, it has also been devised the term ethno-archaeometry (Gosselain, 1992). In this specific case, the different steps of the productive cycle were studied both for the analyses of contemporary pottery-making communities (Cantin and Mayor 2018; Cau Ontiveros et al.

2015; Buxeda I Garrigós et al. 2003) and/or to compare contemporary ceramics with archaeological finds (D'Ercole et al. 2017; Lindahl and Pikirayi 2010).

This approach has several advantages. In fact, the interpretation of traditional ceramic, knowing all the steps of the productive cycle and the technology, can help in the understanding of archaeological ceramics. Moreover, it is also possible to verify results, interpretations and the methodology, and the assumptions used in the technological characterization of pottery (Buxeda I Garrigós et al., 2003).

The main focus of this work is the study of contemporary/traditional and Medieval ceramics, Islamic to Post Islamic-Christians (11th to 16th century), from the village of Muge (Municipality of Salvaterra de Magos) and the city of Santarém, district of Santarém, Portugal (Table 16).

Precisely, we are going to compare the characteristics of traditional and archaeological ceramics considering different utilitarian artefacts with a specific function, such as table, fire (cooking pots) and storage (container) wares. Table ceramics were mainly utilized to serve and consume different types of dishes; fire ceramics were utilized for cooking, and consequently, they were exposed to a heat source; storage ceramics were adopted to store liquid and/or food.

Traditional ceramics are still produced nowadays in Muge in three different workshops. The owner of one of these workshops (Mr. Domingos) learned to do pottery when he was a young boy in the same village. The most ancient evidence of traditional ceramic production goes back to the end of the 19th century (Lepierre 1899; Santos Júnior 1932).

The area was already inhabited since the Iron Age, and there is evidence of pottery making since the Roman period, as evidenced by the recent archaeological excavation of the river harbour (Arruda et al., 2016). Islamic Medieval ceramics were also recovered (Lopes,

2015). Archaeological medieval ceramics have been recovered inside the old city of Santarém, located at 15-20 km from Muge, during the archaeological excavation of the site *"Rua 5 de Outubro"* (RCO). Ceramics from the same archaeological site have been studied on section 5.2, but with a different goal.

Our aims is to understand pottery production technology and function in the district of Santarém between the Middle Ages and Modern times. The study will be useful to understand whether or not there was continuity or change in ceramic characteristics during the Middle Ages (i.e., from the Islamic to the Christian period) and the difference, if any, with Modern ceramics[82].

Conscious of the fact that archaeological and traditional ceramics were not produced in the same workshop, we consider the analyses of Modern ceramics an interesting ethnographic approach for the understanding of ancient pottery technology. Moreover, every year, fewer people make traditional ceramic in the area. The study of this activity also pretend to preserve and strengthen the memory of the territory and its traditions. The different *variables* (environmental restrictions, access to raw material sources such as fuel, water, clay, temper, economic or political changes), and behavioural and socio-cultural factors (tradition, ideology, religious or ethnicity) that might have affected ceramic technology in the Middle Ages will be considered in this work.

A multi-analytical protocol has been developed, including an experimental archaeological firing test on sediments and physical and mechanical tests on ceramics (i.e., density, porosity, vapour permeability, Point Load Test strength index-PLT).In particular, the application of physical and mechanical tests to traditional and archaeological ceramics, according to methods well established in the literature (Columbu et al. 2014b; Columbu et al. 2014a; Columbu et al. 2015b; Columbu et al. 2015a), is rarely used in archaeometry.

Few authors utilized this approach in the past (De Bonis et al. 2014; Kilikoglou et al. 1998; Müller et al. 2010) mainly for the study of traditional or archaeological ceramics, but never to directly compare ceramics characteristics in the same work. The combination of physical and mechanical data obtained by PLM, XRPD and XRF can be very useful in the understanding of the production technologies related to the objects function.

[82] A brief socio-historical background of the city during the middle ages as well as the main historical events have been already introduced on paragraph 2.1.2.1 of chapter 2. Paragraph 5.2 has previously discussed and proved the continuity in raw material exploitation during the Middle Ages.

5.3.2 Ceramics sampling

5.3.2.1 Traditional ceramic from Muge

The first work that summarized the production of ceramic materials in Portugal go back to the 19th century (Lepierre, 1899). This book briefly described the regional distribution, location, the production typology (industrial or not) and the raw materials exploited for traditional Portuguese ceramics, also mentioning several workshops located at Muge. The production cycle of traditional ceramic in Muge, using the local red clay, was described by Santos Júnior (1932) while ethnographic issues were discussed by Gomes Pinto (2012).

Workshops have never changed their traditions, and the production of utilitarian ceramics is still the main activity. Nowadays, the ceramic production of Mr. Domingos at Muge (Fig. 53) is small and mainly for the local markets. The workshop is also small. We can identify four different individual spaces.

In the first room, the ceramist shapes the ceramics. Afterwards, we can find a storage room to store and dry its ceramics. Backyard, we find the kiln area and a big yard where the ceramist stores, treats and decants the raw clay. Basing on the description of Mr. Domingos the productive cycle can be summarized in three different phases: (1) extraction and preparation of the raw materials, (2) shaping and decoration and (3) firing.

Figure 53 Picture of Mr. Domingos (left) on its atelier in Muge

Table 17 DMS Geographical coordinates of weak *and* strong *clay mined by Mr. Domingos for the production of traditional ceramics. Data have been obtained using Google Earth Pro. Data degree of reliability extracted using Google Earth Pro, such as elevation and horizontal accuracy, are discussed in specialized bibliography (Goudarzi and Landry 2017; Pulighe et al. 2016; Wang et al. 2017).*

Site	Geographical Coordinates (DMS)					Data source
	Degree	Minutes	Seconds	Orientation	Elevation	
Weak clay	39	6	11.51	N	11	Google Earth Pro
	8	40	39.66	W	11	
Strong clay	39	4	17.45	N	24	
	8	40	56.34	W	24	

The ceramist uses two different raw materials: the “strong (or fat)" and the "weak (or light/slim)" clay (Fig. 54, 55). The raw materials are extracted near the village, in a private property, with the consent of the owner. Both are located in the geological layer Q3, which correspond to Pleistocene fluvial terraces (Table 17).

The *strong (fat) clay* is more plastic and stickier when water is added. So, we might infer that the adjective *fat* refers to the stickiness character of the clay, and the adjective *strong* probably describes the ability of the wet clay to retain the stress without breaking while the artefact is shaped. On *weak (light/slim) clay,* for the ceramist, the amount of inclusions is slightly higher.

These observations will be discussed in the next sections with the aid of granulometric, mineralogical and chemical analysis. The two raw materials are generally empirically mixed by the ceramist, but the proportion change depending on the artefact to be done. On fire ceramic and smaller object, the proportion of *weak clay* is higher if compare to table and food-liquid

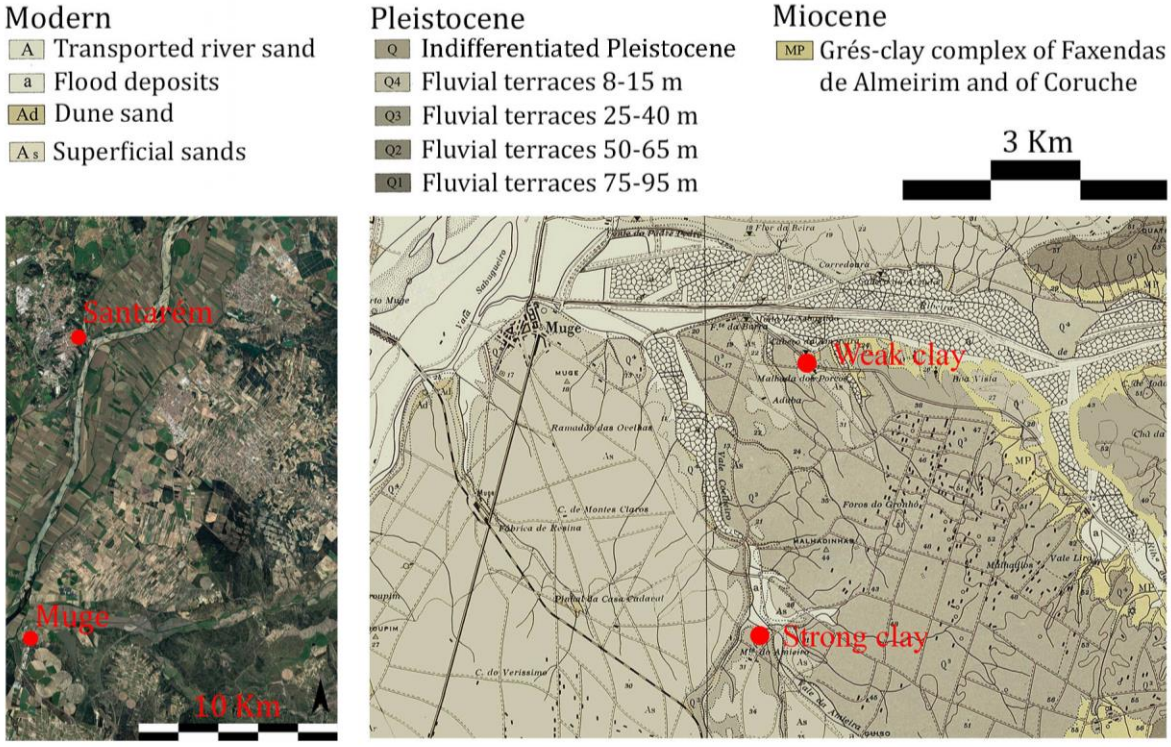

Figure 54 Adapted extract (Zbyszewsky and Da Viega Ferreira, 1968) of the geological maps (1:50000) of Muge with the indication of the raw material extraction sites.

containers. So, probably, we suppose that *weak clay* expands less, and it has better thermal characteristics when exposed to a heat source. Nevertheless, clay selection can also be related to other social and cultural phenomena (Livingstone Smith, 2000) but, based on the ceramist information, it looked like a volunteer technical choice.

To prepare the ceramic paste, Mr. Domingo firstly decides the proportion of the two clays and he roughly powdered them manually using a hammer or a sledgehammer. Afterwards, the mixture is introduced in a big tank, mixed with water and decanted for one-two days. Once most of the sand is extracted, to conclude the preparation process, the finest part of the mixture is then removed from the tank and inserted into an extrusion machine to produce cylinders of homogenized pressed clay.

Cylinders are then covered by a plastic thin film, in order to keep the humidity, and stored. The ceramic artefacts are usually shaped using a vertical potter wheel moved by a simple mechanical engine. Nowadays, Mr. Domingos uses it to add temper when needed (fine

Figure 55 Images of the weak *(B, D) and* strong *(A, C) clay utilized in the workshop of Mr. Domingos.*

industrial milled sand). The reason why the ceramist uses fine industrial milled sand is simple. He does not want to cut his finger during shaping.

Shaped objects are dried in a storage room, slightly ventilated and far from the sunlight in order to allow slow evaporation of the absorbed water. The drying time varies, depending on the season, being shorter during warmer months. Ceramic is fired in a two chambers kiln. The firing chamber is roughly 2x3 m and 2 m in height, and it is separated from the combustion chamber by a perforated bricks floor. Mr. Domingo knows that the temperature inside the firing chamber is not homogeneous. He usually controlled the temperature empirically, by looking at the colour of the flame, and he does not really know the real maximum temperature that the kiln can reach. He supposes the kiln can reach more than 900 °C. The whole process of firing may take 12 hours.

The kiln is heated gradually to the maximum temperature. In the meantime, the entrance of the kiln is closed with bricks and then is left to cool down gradually. Usually, unglazed ceramic undergoes a single firing process, while glazed ceramic is doubled fired. To apply the glaze, the ceramist utilizes synthetic powdered glass products that follow the National and European regulations (National regulations: Decreto-Lei nº 190/2007).

After our visit to the workshop of Mr. Domingo, we selected 14 different utilitarian ceramics (Fig. 56; Table 18). In total, we selected 5 fire ceramics with 2 lids, 5 table ceramics and 4 liquid-food containers (liquid) with 2 lids. Most of the fire and table ceramics were partially covered by glaze. Usually, just the surfaces in contact with the food or liquid were covered by glaze. On the contrary liquid-food containers were not glazed at all.

Figure 56 Traditional ceramic samples analysed in this section from Mr. Domingos's workshop.

Table 18 Samples list of traditional ceramics, from Muge (MG), analysed in this section.

[S.U]-Ref.	*Arc. Context/S.U.*	*Chronology - century*	*Typology*	*Function*	*Decoration*	*Arch. Site-Site*
Trd-1	Atelier	Contemporary	Pot Lid	Fire ceramics	Unglazed	MG
Trd-2	Atelier	Contemporary	Pot	Fire ceramics	Glazed	MG
Trd-3	Atelier	Contemporary	Chestnut roaster	Fire ceramics	Unglazed	MG
Trd-4	Atelier	Contemporary	*Tacho*	Fire ceramics	Glazed	MG
Trd-5	Atelier	Contemporary	*Tacho* Lid	Fire ceramics	Glazed	MG
Trd-6	Atelier	Contemporary	Jug	Food, liquid containers	Unglazed	MG
Trd-7	Atelier	Contemporary	Jug lid	Food, liquid containers	Unglazed	MG
Trd-8	Atelier	Contemporary	Water costrel	Food, liquid containers	Unglazed	MG
Trd-9	Atelier	Contemporary	Water costrel Lid	Food, liquid containers	Unglazed	MG
Trd-10	Atelier	Contemporary	Glazed plate	Table ceramics	Glazed	MG
Trd-11	Atelier	Contemporary	Painted plate	Table ceramics	Unglazed	MG
Trd-12	Atelier	Contemporary	Green bowl	Table ceramics	Glazed	MG
Trd-13	Atelier	Contemporary	Bowl	Table ceramics	Glazed	MG
Trd-14	Atelier	Contemporary	Yellow bowl	Table ceramics	Glazed	MG

5.3.2.2 Archaeological ceramics from Santarém

Archaeological ceramics, as in section 5.2, were recovered in the archaeological excavation of *Rua 5 de Outubro*, no. 2 to 8, in the city of Santarém. In total, 27 samples were selected (Fig. 57; Table 20). The chronology is comprised between the 11th and the 16th centuries. Fire ceramics, table ceramics and food and liquid containers were included in the collection.

With the exception of the stratigraphic unit [520], apparently related to metallurgical activity disposal, all the other archaeological contexts correspond to *silos*, as in sections 5.1 and 5.2. Also, in these cases, they were probably filled in a short period, and they constitute very reliable groups of samples from a chronological point of view.

The archaeological contexts [520] [583] and [1667] correspond to the period between the 11th century and the first half of the 12th century. Typical late Islamic materials were recovered. In the case of the archaeological context [476], the presence of northern ornamental solutions, such as cooking pots with punctured handles, in combination with southern pottery, appears to testify a chronology of deposition close to the integration of the city in the Portuguese kingdom, in 1147 AD.

The fillings of the contexts [2466] and [2172] probably formed during the end of the 12th century – beginning of the 13th century considering the recovery of first Dinasty's coins. From the transition between the 13th and the 14th centuries, just the context [828] was studied. The materials are dominated by coarse wares with some fragments of green-glazed pottery, traditionally associated with the workshop of Paris-Rouen, France (Liberato, 2012a).

The chronology of the context [2059] was established thanks to the recovery of some Mudejar fragments, probably from the Valencia and/or Seville regions, which appear most frequently in the territory of nowadays Portugal, from the 15th century onwards. Two of these samples have been studied in section 5.2, and they were both locally produced.

Regarding the archaeological ceramics shaping method, the objects could be shaped manually as in the case of artefacts with thicker walls (big earthen pots) or using the ceramist wheel (jugs, bowls, lids, pots, pans).

Objects surfaces could be treated, especially bowls and pans, with the application of a slip or by surface polishing. As already explained in section 5.2 on the archaeological excavation in *Rua 5 de Outubro,* several kilns were also identified, which date back to the last moments of the Islamic period and just after the Reconquista of the city, 12th – 13th century.

During the 15th century, the archaeological site became a residential area and all the productive activities were probably moved in the neighbourhood of the city. Kiln typology is

very similar to that excavated in Lisbon (Bugalhão and Folgado, 2001) and also comparable to several other structures discovered in the Iberian peninsula during the Islamic-Post Islamic period (Coll Conesa and García Porras, 2010). The kilns of Santarém (*fornos a grelha*) were circular in shape and mainly composed by two different compartments with a separated access, the fuel combustion corridor with a circular end, and the firing compartment for the ceramic, with an apse circular shape (Liberato, 2012a).

The compartments were separated by a perforated floor supported by several pillars. From the technological point of view, in section 5.2 several ceramic fragments recovered inside the kiln tunnel of different kilns were analysed. Results determined that ceramics were fired in a temperature range between 750 °C and 1000 °C.

Table 19 Samples list of archaeological, from Rua 5 de Outubro *archaeological site (RCO), and traditional ceramics, from Muge (MG), analysed in this section. In the column "Arch. Context/S.U." the stratigraphic unit of discovery is reported on square brackets.*

[S.U]-Ref.	*Arc. Context/S.U.*	*Chronology - century*	*Typology*	*Function*	*Decoration*	*Arch. Site-Site*
[509]-4724	[583]	*11th-12th*	Pot	Fire ceramics	White Painted	RCO
[504]-4665	[520]	*11th-12th*	Pan	Fire ceramics	Unpainted	RCO
[1666]-12037	[1667]	*11th-12th*	Lid	Fire ceramics	White Painted	RCO
[504]-4660	[520]	*11th-12th*	Big Jug	Food, liquid containers	White Painted	RCO
[504]-4666	[520]	*11th-12th*	Jug	Food, liquid containers	White Painted	RCO
[475]-4467	[476]	*11th-12th*	Big earthen pot	Food, liquid containers	Unpainted	RCO
[504]-4663	[520]	*11th-12th*	Bowl	Table ceramics	White Painted	RCO
[504]-4664	[520]	*11th-12th*	Bowl	Table ceramics	White Painted	RCO
[91]-1978	[2466]	*12th-13th*	Pot	Fire ceramics	Unpainted	RCO
[2244]-15045	[2172]	*12th-13th*	Pan	Fire ceramics	Unpainted	RCO
[91]-1983	[2466]	*12th-13th*	Lid	Fire ceramics	Unpainted	RCO
[2244]-15029	[2172]	*12th-13th*	Big Jug	Food, liquid containers	White Painted	RCO
[91]-1981	[2466]	*12th-13th*	Jug	Food, liquid containers	Unpainted	RCO
[91]-1979	[2466]	*12th-13th*	Big earthen pot	Food, liquid containers	Unpainted	RCO
[91]-1985	[2466]	*12th-13th*	Bowl	Table ceramics	Unpainted	RCO
[829]-6952	[828]	*13th-14th*	Pot	Fire ceramics	Unpainted	RCO
[829]-6953	[828]	*13th-14th*	Pan	Fire ceramics	Unpainted	RCO
[829]-6950	[828]	*13th-14th*	Lid	Fire ceramics	Unpainted	RCO
[829]-6966	[828]	*13th-14th*	Jug	Food, liquid containers	White Painted	RCO
[829]-6947	[828]	*13th-14th*	Bowl	Table ceramics	Unpainted	RCO
[829]-6962	[828]	*13th-14th*	Bowl	Table ceramics	Unpainted	RCO
[2058]-14121	[2059]	*15th-16th*	Pot	Fire ceramics	Unpainted	RCO
[2096]-14392	[2059]	*15th-16th*	Pan	Fire ceramics	Unpainted	RCO
[2058]-14124	[2059]	*15th-16th*	Lid	Fire ceramics	Unpainted	RCO
[2096]-14374	[2059]	*15th-16th*	Big earthen pot	Food, liquid containers	Unpainted	RCO
[2096]-14381	[2059]	*15th-16th*	Bowl	Table ceramics	Unpainted	RCO
[2058]-14122	[2059]	*15th-16th*	Bowl	Table ceramics	Unpainted	RCO

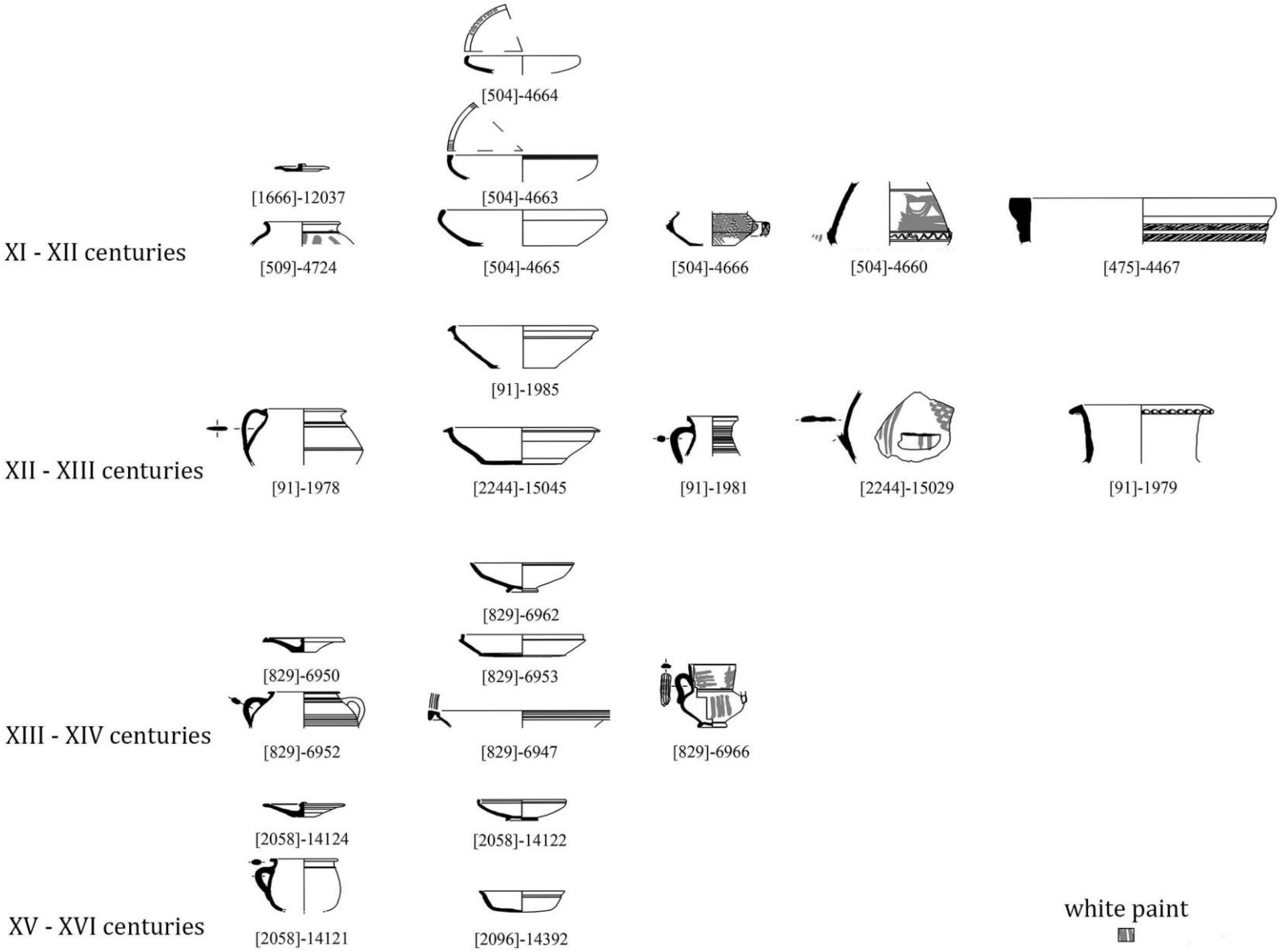

Figure 57 Archaeological materials from Rua 5 de Outubro *archaeological site analysed in this section.*

5.3.3 Analytical methods and procedures employed in this section

This section has been developed with a slightly different experimental protocol if compared to sections 5.1 and 5.2. Different firing tests were also performed both on traditional ceramic samples as well as on raw materials employed by Mr. Domingos on its atelier.

All ceramics have been first characterized by PLM, XRPD and XRF. HeP and PLT properties were determined on archaeological and traditional ceramic samples (untreated samples) following the methodology described in chapter 4, sections 4.6.1 and 4.6.2. On traditional ceramics, when glaze was present, two different samples were prepared (i.e. with and without glaze).

Due to sampling restrictions, it was not possible to perform PRM tests (procedure included in section 4.6.3) in all archaeological samples. Nevertheless, it was possible to analyse 4 tables, 2 liquid/food containers and 7 fire ceramics. On traditional ceramic it was possible to perform analyses in most samples.

Firing experiments were performed just on traditional ceramics, following the procedure described in section 4.7. This test was performed on different sub-samples to ascertain the real firing temperature in Mr. Domingos's workshop. HeP and PLT characteristics were determined first and XRPD analyses were performed in a second moment.

This section also includes the granulometric analysis of the raw clay materials utilized by Mr. Domingo: the *strong* and the *weak* clay. Grain size distribution was performed to evaluate sand and silt plus clay content, and to understand the perception of the raw materials by the ceramist basing on his description (procedure on section 4.2).

Clay minerals were identified by XRD, preparing oriented aggregate mounts (procedure on section 4.4.1). Moreover, XRPD were performed on raw clay samples and on the < 63 μm fractions. Firing tests on the <63 μm fractions were afterwards performed following the procedure described in section 4.7. XRPD Analyses were done after each firing step.

This experiment was developed to evaluate the mineralogical modification during firing on raw clay materials and to support experimental firing tests developed on traditional ceramics described in the previous paragraph.

Considering that the firing behaviour of clays is closely related with the original raw materials (clays) and the forming and firing process, chemical analyses by XRF spectroscopy were also developed, in particular on raw clay samples and on the < 63 μm fractions. The following table (Table 20) summarizes the materials and the methods utilized and the data tables included in the annex number 3.

Table 20 List of the analytical methods employed in this section.

Method		Samples analysed	Data tables added as annex
Granulometry		Sediments	
Microscopy	PLM	Ceramics (all)	Ceramic paste and temper
Mineralogy	XRPD	Ceramics (all) and sediments	
	Oriented aggregate mounts	Sediments	
Chemistry	XRF	Ceramics (all) and sediments	Major oxides
Experimental firing tests	Muffle furnace	Traditional ceramics and sediments	
Physical, mechanical and permeability tests	Hep	Ceramics (all) + fired traditional ceramics	Singular samples values
	PL	Ceramics (all) + fired traditional ceramics	Singular samples values
	PRM	Selection of traditional and archaeological ceramics	

5.3.4 Results

5.3.4.1 Microscopy: PLM on ceramic thin sections

Archaeological and traditional ceramics are similar in temper mineralogical composition. The single characteristic of each sample is reported at the end of this dissertation in annexe 3 (Table 3 to 6).

Inclusions are mainly composed by quartz, K-feldspar, rare plagioclase, muscovite, rare biotite, green - brown tourmaline, secondary and post-depositional calcite. Amongst rock fragments were identified quartzite, sandstone, granitoids and, in some cases, relics of thermally altered micritic limestone. Sometimes biomicrite and intramicrite fragments were also identified (Robert L. Folk, 1959). Intramicrite consists of microcrystalline carbonate matrix with quartz and feldspar intraclasts, while biomicrite consists of microcrystalline carbonate matrix with bioclasts as foraminifera (Fig. 58F).

Dispersed in the ceramic paste there were also unmixed clay pellets (Fig. 58G). Secondary calcite, in the form of a reaction rim, usually surrounds thermally altered or almost completely absorbed limestone fragments. In other cases, post-depositional calcite was dispersed in the ceramic paste or inside pores suggesting contamination from the soils.

The identification of thermally altered limestone fragments suggests a firing temperature, at least, comprised between 750 and 800 °C (Fig. 58C/D) or short firing time at higher temperature (Fabbri et al., 2014). Conversely, some pieces of traditional ceramic are not completely oxidized, suggesting incomplete firing (Fig. 58H).

It is important to notice that secondary calcite, thermally altered micritic limestone fragments, biomicrite, intramicrite and clay pellets were never observed in traditional ceramics. These first observations indicate that the raw materials exploited were different, and they were treated differently. Traditional ceramics show a more accurate homogenization of the clay. Porosity further differentiates the two assemblages, being smaller and highly aligned to the vessel wall in the case of traditional ceramics. This was probably the result of the throwing shaping method adopted by Mr. Domingo, and a different pressure applied to the object during shaping.

Grain size distribution is generally unimodal in all cases. Grain shape varies from angular to sub-rounded. The most rounded and abundant fraction is mainly concentrated in the silty fraction, suggesting transportation. The only exception is represented by silty sized micas crystals, generally angular and elongated. Bigger inclusions are generally sub-angular/angular

in shape, indicating that temper was added to the ceramic paste depending on the object to be prepared.

This is especially evident for a specific category of archaeological artefacts, like liquid and food containers with thicker walls (big jug-big earthen pot), such as samples [504]-4660, [475]-4467, [91]-1979, [2096]-14374. In these cases, more temper was added if compared to jugs with thinner walls. So, temper could be added depending on the thickness of the object wall to mitigate volume loss when the piece was dried and fired.

The effect of tempering is also visible on traditional ceramics, and it was also described by Mr. Domingos. The ceramist used to add commercial milled sand to the ceramic paste. Nevertheless, if compared to archaeological ceramics temper characteristics on traditional ceramic samples is uniform and sorting is very similar between different functional classes.

PLM allowed the subdivision of the shards into three different fabrics-groups (Fig. 58A/B/C/D/E). Fabric 1 and 2 from the archaeological assemblage, and fabric 3 from the traditional ceramic assemblage. In the case of fabric 3 there are not differences between objects with a different function, and the effect of mixing different clays adopted by the ceramist (i.e., *strong* and *weak* clays) is not visible.

Fabric 1 is characterized by an iron-rich ceramic matrix, with inclusion size up to 2.3 mm. The bigger inclusions were mainly observed on food-liquid containers such as big jug and on big earthen pots. The ceramic paste of fabric 2 is enriched in thermally altered or almost completely absorbed limestone fragments and inclusions up to 0.9 mm. Fabric 3 has an iron-rich ceramic paste with inclusion up to 1.3 mm.

Fabrics 1 and 2 present an internal variability, especially in the colour of the ceramic paste and the amount of inclusion. Sub-fabric 1A has a red ceramic paste with inclusion concentration ranging from 4.7 to 20.25 %. On sub-fabric 1A are also included big food-liquid containers (big jug-big earthen pot). In sub-fabric 1B the ceramic paste is red-brown and inclusion concentration range from 8.72 to 16.87 %.

Regarding sub-fabrics of fabric 2, A and B, the ceramic paste is light brown\grey-brown and inclusion concentration decrease progressively from A (14.66 to 20.60 %) to B (9.46 %) sub-fabric. In traditional ceramic samples, fabric 3, the ceramic paste is red and inclusion concentration range between 6.54 and 14.02 %.

Results indicate that fabric 1 was widely utilized for the production of archaeological ceramics in all periods. In particular, sub-fabric 1A was utilized for the production of table and food-liquid container ceramics (in two cases for fire ceramics also), while sub-fabric 1B was exclusively utilized for the production of fire ceramic. Fabric 2 appears sporadically in the

archaeological assemblage being utilized to create fire (2), table (1) and container (1) ceramics. Considering the ceramics characteristics, especially ceramic paste and temper, and after a comparison with ceramic samples analysed on section 5.1 and 5.2, the results of PLM analysis clearly suggest that the raw material was probably extracted in the vicinity of the archaeological site. The clayey raw material was roughly purified, and temper could be added in a second moment.

Moreover, also the identification of unmixed clay pellets is another clue, suggesting that the preparation and homogenization of the clay was not that accurate. The technology of production is very similar between the 11th and the 16th centuries. Even if the kilns in the archaeological site ceased to work before the 15th century (the site became a residential area), the processes of making pottery (for each functional class) seems very similar on different chronological periods, indicating specialization in ceramic production (Arnold, 2000). Our observations suggest that ceramics were not imported, and the same natural resources were widely available in different chronological periods without any restriction.

Conversely, the production of traditional ceramics, fabric 3, is quite similar in all cases, as evidenced by ceramic paste and temper characteristics (Annexe 3, Table 3 to 6). There is not a clear distinction between objects with different functions (fire, table and container ceramics). At this stage, the effect of mixing different clays (*strong* and *weak* clay) adopted by Mr. Domingos is not significant. It is also not possible to appreciate specialization in traditional ceramic production because more workshops should be considered.

Comparing archaeological samples and traditional ceramics as two distinct homogeneous groups, there is a clear difference in the ceramic paste and inclusions characteristics as well as in porosity size and alignment. The ceramic paste of traditional ceramics is highly homogenous, clay pellets are almost absent, inclusions are well sorted, temper concentration is very similar between different artefacts and porosity is usually smaller and parallel to the vessel wall. We can say that the production cycle of traditional ceramic is very similar in all cases, without significant differences between objects with different function.

On the contrary, on archaeological samples it is not, and it is specialized along time. If compared to nowadays traditional ceramics objects with different function were prepared in different way, like food-liquid containers (i.e., jugs-big jugs-big earthen pots) and fire ceramics (pots, lids, pans). All of these factors indicate a clear difference in ceramic productive cycle.

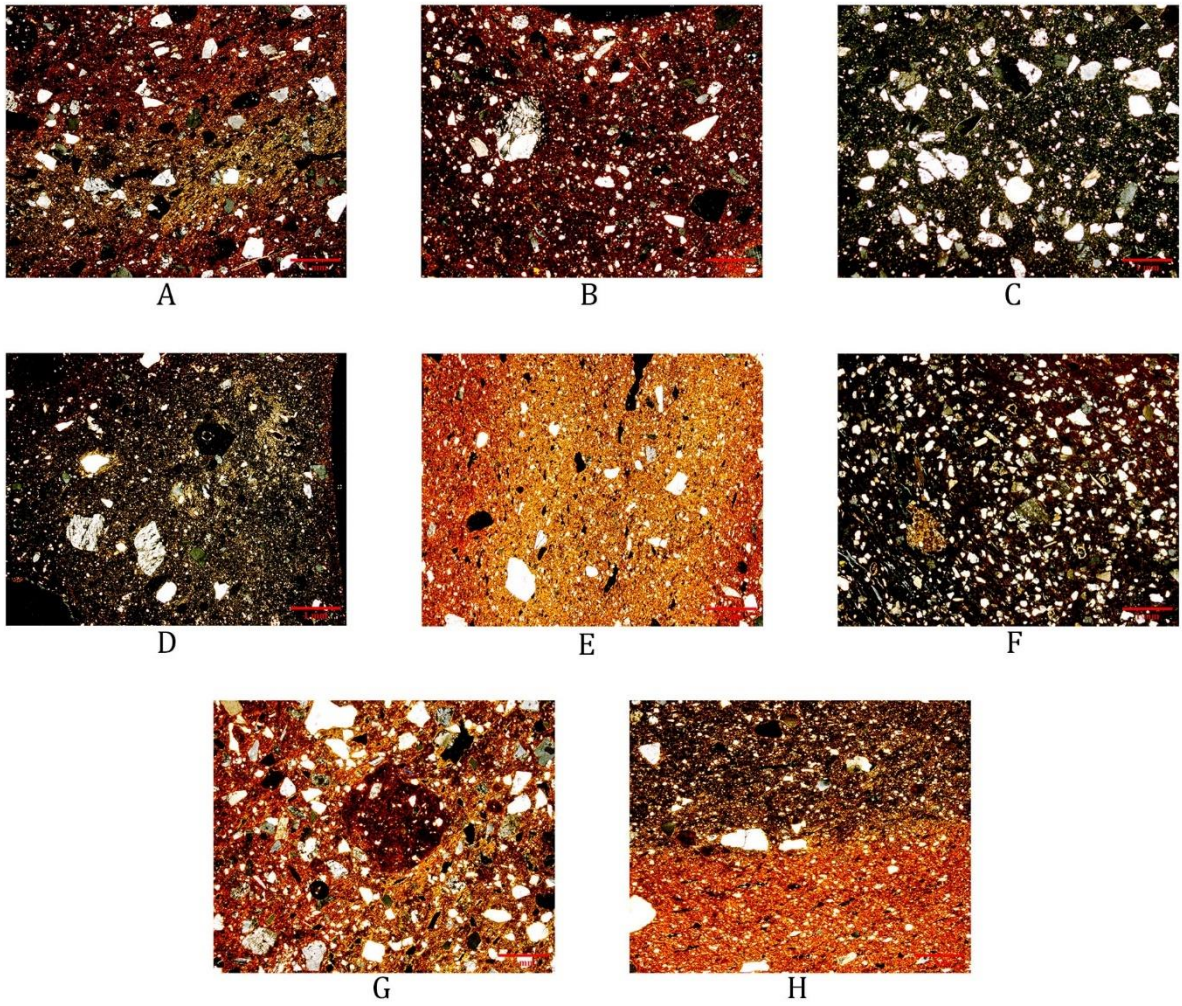

Figure 58 Immages collected during PLM analysis. (A) [91]-1979 group 1/subgroup A, (B) [2058]-14121 group 1/subgroup B, (C) [504]-4660 group 2/subgroup A, (D) [829]-6952 group 2/subgroup A, (E) Trd-6 (Jug) group 3, (F) [829]-6947 group 2/subgroup A with fragment of limestone, (G) [2096]-14374 group 1/subgroup A with clay pellets, (H) Trd-3 (Chestnust roaster) group 3 incomplete firing of the peace.

5.3.4.2 Mineralogical composition: XRPD of ceramic samples

In this section XRPD results of archaeological and traditional ceramic bodies as well as of the experimental firing test carried out on traditional ceramics are presented and discussed (Tables 21, 22, 23, 24; Fig. 59).

5.3.4.2.1 Archaeological and traditional ceramics

On archaeological and traditional ceramics, quartz is confirmed as the main mineralogical phase (Table 21, 22). Potassium rich feldspars and illite-muscovite are the second most abundant mineralogical phases identified, while sodium rich plagioclases are less represented. Hematite was identified almost in all samples. Its formation usually starts approximately at 750 °C (Maniatis et al. 1981; Nodari et al. 2007; Cultrone et al. 2004) under oxidizing conditions.

*Table 21 Semi-quantitative **XRPD** results, expressed in percentage (%), of archaeological ceramics from Rua 5 de Outubro archaeological site. Q, Quartz – Kf, Potassium-rich feldspars – Pla, Plagioclase feldspars – Mus/Ill, Muscovite-illite – Kao, Kaolinite –- Hem, Hematite – Cal, Calcite - Mu, Mullite – Tr, Traces*

Century	Function	Typology	[S.U.]-Ref.	Q	Kf	Na-Pla	Mus/Ill	Hem	Cal	Mu
11th–12th	Fire ceramics	Pot	[509]-4724	72	7	3	17	1		
		Pan	[504]-4665	62	17	6	15	1		
		Lid	[1666]-12037	59	18	4	18	1		
	Food, liquid containers	Big jug	[504]-4660	74	19	2		1		4
		Jug	[504]-4666	68	26	2		1		2
		Big earthen pot	[475]-4467	68	17	7	8	1		
	Table ceramics	Bowl	[504]-4663	56	15	8	20	1		
		Bowl	[504]-4664	54	22	5	18	1		
12th–13th	Fire ceramics	Pot	[91]-1978	56	9	5	30	1		
		Pan	[2244]-15045	61	17	6	15	1		
		Lid	[91]-1983	65	27	4	Tr	1		4
	Food, liquid containers	Big jug	[2244]-15029	55	21	10	13	1		
		Jug	[91]-1981	53	16	6	24	1		
		Big earthen pot	91-1979	50	26	6	16	1	1	
	Table ceramics	Bowl	[91]-1985	58	11	5	25	1		
13th–14th	Fire ceramics	Pot	[829]-6952	63	20	4	11	1	1	
		Pan	[829]-6953	59	25	3	11	1	1	
		Lid	[829]-6950	61	16	6	16	1		
	Food, liquid containers	Jug	[829]-6966	60	17	5	17	1		
	Table ceramics	Bowl	[829]-6947	44	26	15	14	1	1	
		Bowl	[829]-6962	63	20	6	10	1		
15th–16th	Fire ceramics	Pot	[2058]-14121	54	25	4	17	1		
		Pan	[2096]-14392	58	21	4	14	1	2	
		Lid	[2058]-14124	58	25	4	9	1	3	
	Food, liquid containers	Big earthen pot	[2096]-14374	50	23	7	18	1		
	Table ceramics	Bowl	[2096]-14381	69	13	4	13	1		
		Bowl	[2058]-14122	61	17	5	17	1		

Calcite was frequently identified on XRPD patterns, mainly on archaeological ceramics, and few times on traditional ceramics. On archaeological ceramics, after PLM analysis, it was generally related to thermally altered limestone fragments with secondary calcite in the border or, in other cases, to post-depositional contamination identified inside pores. On traditional ceramics, calcite was not detected by PLM. Its identification in very low amount in some XRPD patterns (Trd-3, Trd-4, Trd-6) can be associated to carbonation of some free lime_after thermal decomposition of calcium carbonate present in the raw material.

To evaluate firing temperature, the formation or the decomposition of several mineralogical phases have been considered. Hematite usually forms around 750 °C. Calcite normally decomposes between 750 and 800 °C (Fabbri et al., 2014). Illite-muscovite peaks are always present. Usually, it is supposed to disappear at a temperature higher than 950-1000 °C (Cultrone et al. 2001; Rodriguez-Navarro et al. 2003; Cultrone et al. 2004; Maritan et al. 2006). On three archaeological samples from the 11th – 12th and 12th – 13th centuries ([504]-4660, [504]-4666, [91]-1983) mullite formed at the expense of illite-muscovite (Cultrone et al. 2004; Rodriguez-Navarro et al. 2003; Riccardi et al. 1999; Jordán et al. 1999), suggesting higher firing temperature (about 1000 °C).

XRPD results of archaeological ceramics are quite uniform, suggesting the exploitation of the same sedimentary deposit and, with some exception, most of the archaeological samples were fired at a temperature below 1000 °C.

On traditional ceramics, in some cases, goethite and vermiculite were identified. In other cases, hematite was not identified. So, traditional ceramics were probably fired at lower temperature, maximum 750 °C, if compared to the archaeological ones. We can also extract one important methodological consideration. In both cases, XRPD patterns are not able to distinguish ceramic samples basing on their function. This result stresses the importance of PLM observations in ceramic studies.

5.3.4.2.2 Firing experiments on traditional ceramics

The firing experiments were carried out on different sub-samples of traditional ceramics (Table 22, 23, 24; Fig. 60), using two different firing steps (i.e. 750, 1000 °C). Results showed that illite-muscovite peaks disappeared progressively increasing the firing temperature, and hematite appeared and/or increased its intensity. Mullite, and in some cases (samples Trd-1, Trd-4 and Trd-6) portlandite normally appeared at 1000 °C .

Portlandite forms through the reaction between the free lime and the environmental humidity (Cultrone et al., 2001) and, usually, it transforms to calcite due to carbonation. In fact,

small amounts of calcite were detected on some untreated traditional ceramic samples, namely Trd-4 and Trd-6. In general, hematite is the most important mineralogical phase to infer the firing temperature in Mr. Domingos's workshop. In 8 cases out of 14, hematite was not identified on the untreated samples, but it was clearly identified on sub-samples fired at 750 °C. This indicates a firing temperature lower than 750 °C in many cases. So, the firing test further confirmed that the maximum firing temperature in Mr. Domingos's workshop is actually lower if compared to archaeological ceramics.

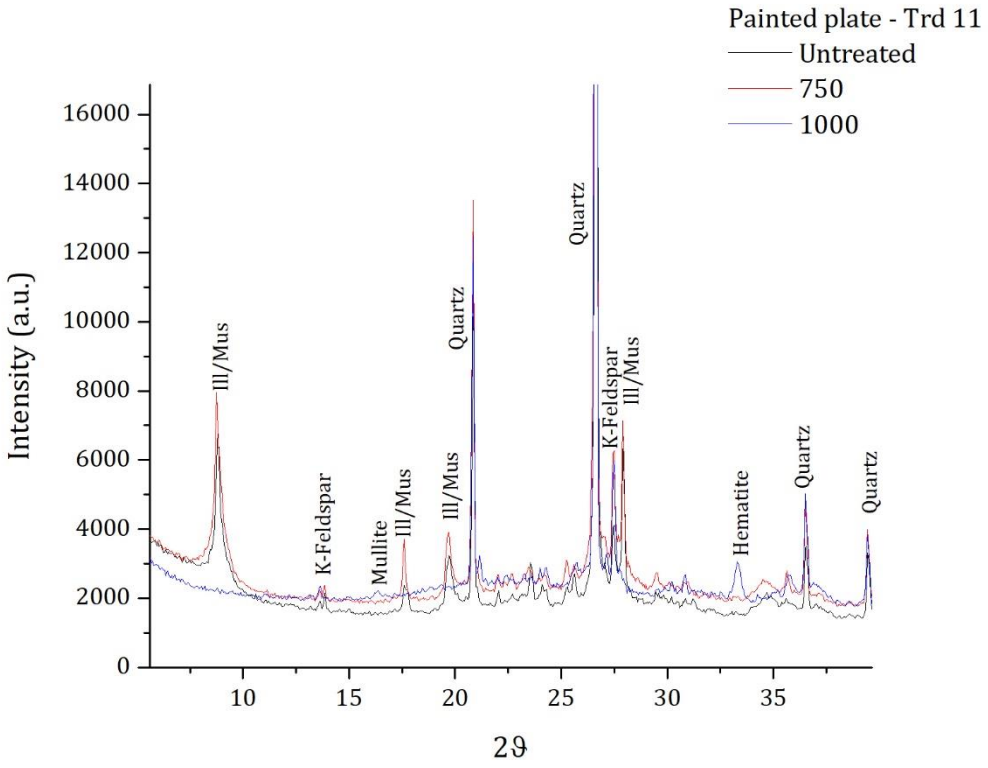

Figure 59 XRPD diffratograms of the painted plate (Trd-11), in black is presented the untreated sample , in red the sub-sample fired at 750 °C and in blue the sub sample fired at 1000 °C

Table 22 Semi-quantitative XRPD results, expressed in percentage (%), of traditional fire ceramic samples (Untreated sample, fired at 750 °C and 1000 °C). Q, Quartz – Kf, Potassium-rich feldspars – Pla, Plagioclase feldspars – Mus/Ill, Muscovite-illite – Kao, Kaolinite –- Hem, Hematite – Cal, Calcite – Ver, Vermiculite – Leu, Leucite - Mu, Mullite – Rut, Rutile – Por, Portlandite – Goe, Goethite - Tr = Traces

Function	Sample/Typology	TEMP (°C)	Q	Kf	Na-Pla	Mus/Ill	Hem	Cal	Ver	Leu	Mu	Rut	Por	Goe
Fire ceramics	**Trd-1/Pot**	**Un.Sample**	61	10	8	19	1					1		
		750	57	19	5	18	1							
		1000	71	22	3		1				2	1	1	
	Trd-1a/Pot bottom	**Un.Sample**	61	10	6	22	1							
		750	56	19	5	19	1					1		
		1000	72	18	5	Tr	1				3			
	Trd-2/Pot lid	**Un.Sample**	58	19	10	13								1
		750	55	19	8	19	Tr							
		1000	74	19	2		1				3	1		
	Trd-3/Chesnut roaster	**Un.Sample**	53	13	10	22		1				1		
		750	51	19	6	22	1							
		1000	70	20	6	1					3			
	Trd-4/*Tacho*	**Un.Sample**	64	14	4	15	1	1				1		
		750	60	18	5	16	1							
		1000	70	18	6	Tr	1				3	1	1	
	Trd-5/*Tacho lid*	**Un.Sample**	63	18	5	14								
		750	63	16	4	16	1							
		1000	72	18	5		1				3	1		

Table 23 Semi-quantitative XRPD results, expressed in percentage (%), of traditional food-liquid container ceramic samples (Untreated sample, fired at 750 °C and 1000 °C). Q, Quartz – Kf, Potassium-rich feldspars – Pla, Plagioclase feldspars – Mus/Ill, Muscovite-illite – Kao, Kaolinite –- Hem, Hematite – Cal, Calcite – Ver, Vermiculite – Leu, Leucite - Mu, Mullite – Rut, Rutile – Por, Portlandite - Tr = Traces

Function	Sample/Typology	TEMP (°C)	Q	Kf	Na-Pla	Mus/Ill	Hem	Cal	Ver	Leu	Mu	Rut	Por
Food, liquid containers	Trd-6/Jug wall	Un.Sample	54	10	15	20		1					
		750	56	18	5	19	1					1	
		1000	73	17	4		1			2	3		
	Trd-6a/Jug, bottom	Un.Sample	58	19	6	19							
		750	59	18	4	19	Tr						
		1000	71	18	5		1				3	1	1
	Trd-7/Jug lid	Un.Sample	62	10	7	21							
		750	56	16	6	20	1					1	
		1000	71	20	3		1			2	3		
	Trd-8/Water costrel wall	Un.Sample	64	10	8	15	1					1	
		750	60	19	4	16	1						
		1000	69	22	3		1			2	3		
	Trd-8a/Water costrel bottom	Un.Sample	56	19	7	17	1					1	
		750	62	17	4	17	1						
		1000	75	18	4		1				2		
	Trd-9/Water costrel lid	Un.Sample	60	12	7	21							
		750	57	18	6	18	1					1	
		1000	75	17	4		1				2		

Table 24 Semi-quantitative XRPD results, expressed in percentage (%), of traditional table ceramic samples (Untreated sample, fired at 750 °C and 1000 °C). Q, Quartz – Kf, Potassium-rich feldspars – Pla, Plagioclase feldspars – Mus/Ill, Muscovite-illite – Kao, Kaolinite –- Hem, Hematite – Cal, Calcite – Ver, Vermiculite – Leu, Leucite - Mu, Mullite – Rut, Rutile – Por, Portlandite - Tr = Traces

Function	Sample/Typology	TEMP (°C)	Q	Kf	Na-Pla	Mus/Ill	Hem	Cal	Ver	Leu	Mu	Rut	Por
Table ceramics	Trd-10/Glazed plate	Un.Sample	48	30	4	18	1						
		750	56	20	4	19	1						
		1000	73	19	4		1				3		
	Trd-11/Painted plate	Un.Sample	58	10	12	21							
		750	55	19	7	17	1					1	
		1000	71	17	8		1				3		
	Trd-12/Green bowl	Un.Sample	76	14	5	10	1						
		750	63	18	4	13	1					1	
		1000	70	18	6		1				3	1	
	Trd-13/Bowl	Un.Sample	58	15	4	22	1		Tr				
		750	66	11	5	17	1						
		1000	71	18	4		1			2	3		
	Trd-14/Yellow bowl	Un.Sample	59	14	10	16	1						
		750	59	19	4	17	1						
		1000	71	22	4	Tr	1				2		

5.3.4.3 Granulometry and mineralogical composition: Grain size distribution, XRD, and firing tests on raw materials

In this section, the results of raw materials granulometric analysis, XRPD on raw materials, oriented aggregate mounts XRD identification, and XRPD results of firing test carried out on raw materials (fraction <63 μm) are presented and discussed (Table 25, 26, 27).

5.3.4.3.1 Raw materials grain size distribution

Raw materials granulometric analysis of *strong* and *weak* clays evidenced that sand content is higher than silt and clay (Table 25). So, in both cases, after the decantation process, the ceramist extracts less than the 20 % of clay. Basing on the ceramist description of the raw materials, *weak* clay was supposed to be more enriched in sand content.

Results show that the *strong* clay is actually more enriched in sand (considering the different granulometric classes) if compared to the *weak* clay (82.03% against 78.51%). Nevertheless, *weak* clay is more enriched of very coarse sand (12.64%), in very fine sand (11.51%) and in silt plus clay (20.92%).

So, the enrichment in sand content described by Mr. Domingos regarding *weak* clay can be the result of two different factors. In the first case, when clays are mined, for Mr. Domingos *weak* clay might look rougher and consequently more enriched in sand.

In the second case, as evidenced by the ceramist, the raw materials were treated first to get rid of the bigger inclusions. Only in a second moment, industrial milled sand was added. Thus, the ceramist probably referred to the enrichment of very fine sand/ silt particles on treated *weak* clay if compared to *strong* clay.

Table 25 Granulometric analysis of strong and weak clays. Results expressed in weight percentage (w%). VCS, very coarse sand; CS, coarse sand; MS, medium sand; FS, fine sand; VFS, very fine sand; SC, silt plus clay

Sample/granulometry	VSC	CS	MS	FS	VFS	SC
***Strong* clay**	9.31	27.59	22.89	13.97	8.27	17.33
***Weak* clay**	12.64	24.33	18.44	11.58	11.51	20.92

5.3.4.3.2 Raw materials XRPD and oriented aggregate mounts analysis

Strong and *weak* clays are very similar in mineralogical composition. Nevertheless, some differences were observed (Table 26). In both cases, quartz, potassium-rich feldspars, sodium-rich plagioclase and rutile were identified. *Strong* clay is generally more enriched in quartz, while *weak* clay is more enriched in feldspars.

If tectosilicates and oxides (i.e. rutile) are considered, in *weak* clay, they represent the 65% on the raw sample and the 64% on the < 63 μm fraction. While in the case of *strong* clay,

they represent the 64% in the raw sample and the 57% of the < 63 μm fraction. Amongst clay minerals on *strong* clay muscovite-illite, kaolinite and smectite were identified, while on *weak* clay muscovite-illite, vermiculite, kaolinite and traces of smectites were detected. Illite-muscovite is the most represented among phyllosilicate on both raw materials, being more abundant in the *strong* clay. Smectite, vermiculite and kaolinite are less abundant. Smectite was identified by the 001 diffraction line positioned at 15.2 Å (very broad peak), while vermiculite by the 001 peak at 14.3 Å.

Table 26 Semi-quantitative XRPD results, expressed in percentage (%), of strong and weak clays: raw and < 63 μm fractions. Q, Quartz – Kf, Potassium-rich feldspars – Pla, Plagioclase feldspars – Mus/Ill, Muscovite-illite – Kao, Kaolinite – Rut, Rutile – Smc, Smectite – Ver, Vermiculite – Tr, Traces

Function	Typology	Fraction	Q	Kf	Pla	Mus/Ill	Kao	Rut	Smc	Ver
Raw clay materials	Strong clay	Raw	37	24	2	28	2	1	6	
		< 63 μm	36	16	4	33	4	1	6	
	Weak clay	Raw	27	29	8	25	3	1	Tr	7
		< 63 μm	31	25	7	27	3	1	Tr	5

The analysis of the oriented aggregate mounts on *strong* clay revealed that the peak at 15.4 Å moved to 17.6 Å after solvation with ethylene glycol. This confirms the presence of smectite minerals (Moore and Reynolds, 1997). In addition, when fired at 400 and 550 °C for 30 minutes, the smectite peak collapses close to 10 Å. In this case, we also recognized two peaks at 12.04 Å and 11.3 Å, respectively, indicating that dioctahedral vermiculite was present (Douglass 1989). *Weak* clay main peak was identified at 14.3 Å, and it did not expand after solvation with ethylene glycol, but, in addition, a peak appeared at 17.4 Å. So, smectite was also present in small amounts if compared to vermiculite.

The 060 diffraction lines of both *weak* and *strong* clays further confirmed the identification of dioctahedral vermiculite and that the smectite clay mineral is montmorillonite. In both cases, illite-muscovite and kaolinite were identified. Therefore, the plastic and sticky behaviour of *strong* clay when water is added can be explained by the clay mineralogy and the enrichment in smectite.

5.3.4.3.3 Raw materials: XRPD results of firing experiments on the < 63 μm fractions

Firing experiments on < 63 μm of *weak* and *strong* raw material fractions were performed to evaluate phase development during firing (Table 27). On both cases, the lack of calcium favoured the formation of hematite and mullite (Noll and Heimann, 2016; Heimann and Maggetti, 2019).

It is well known that calcareous raw material prevents the formation of high-temperature silica rich mineralogical phases and it favours the formation of high-temperature calcium rich ones (El Ouahabi et al. 2015; Trindade et al. 2009). Moreover, it improves the vitrification process of the ceramic paste (Maniatis et al., 1981). In this case, hematite, illite-muscovite and mullite peaks can be used to understand the thermometry of the firing process.

Illite-muscovite usually decomposes at 950-1050 °C, while mullite and hematite appear at 1000 °C and 750 °C, respectively (Trindade et al. 2009; Rodriguez-Navarro et al. 2009; Maritan et al. 2006; Nodari et al. 2007). On our samples, montmorillonite and vermiculite 15.2 and 14.4 Å peaks disappear after the first firing cycle at 400 °C. Several scholars (Kresten and Berggren 1978; McConville and Lee 2005; El Ouahabi et al. 2015) stated that montmorillonite and vermiculite might also be present at higher temperatures.

Table 27 Semi-quantitative XRPD results, expressed in percentage (%), of the mineralogical phase evolution during firing of strong and weak clays (with grain size < 63 µm fraction). Q, Quartz – Kf, Potassium-rich feldspars – Pla, Plagioclase feldspars – Mus/Ill, Muscovite-illite – Kao, Kaolinite – Rut, Rutile – Smc, Smectite – Ver, Vermiculite – Hem, Hematite – Mul, Mullite – Tr, Traces

Clay	Fraction	Firing T.	Q	Kf	Pla	Mus/Ill	Kao	Rut	Smc	Ver	Hem	Mul
Strong	< 63 µm	0	32	17	4	33	7	1	6			
		400	35	18	4	37	6	1	Tr			
		500	41	15	4	39	Tr	1	Tr			
		600	42	17	4	37		1				
		700	43	17	3	36		1				
		800	39	17	5	38		1			1	
		900	55	17	5	21		1			1	
		1000	74	17	2	Tr		1			2	3
Weak		0	32	22	6	28	5	2	Tr	5		
		400	35	20	6	32	6	2		Tr		
		500	38	17	8	36	Tr	1		Tr		
		600	42	16	6	35		1		Tr		
		700	43	11	6	37		2		?		
		800	38	17	11	32		2			1	
		900	60	17	5	15		1			1	
		1000	77	14	2			1			2	2

In our case, after the loss of interlayer water, montmorillonite shows a diffraction line close to 9.6 Å, while vermiculite at 11.6-11.3 Å. Above 500-600 °C vermiculite and montmorillonite diffraction lines disappeared, because resulted peaks were completely superimposed to illite-muscovite diffraction lines. Kaolinite disappears at 500-600 °C. Hematite was never detected at 700 °C, but it was present at 800 °C. This confirms that traditional ceramics were generally fired at lower temperature if compared to archaeological ceramics.

Raw material sintering and vitrification are consistent with the complete dehydroxylation of phyllosilicates and the formation of mullite at 1000 °C. It is important to notice that neither in *weak* nor in *strong* clay calcite and portlandite has been identified if compared to untreated and fired traditional ceramic samples. In our case, fired clays were analysed just after every firing cycle and they did not have time to crystallize.

5.3.4.4 Chemical composition: Ceramics and raw materials XRF analysis

XRF chemical analyses of *strong* and *weak* clays (raw and < 63 μm fractions) and of archaeological and traditional ceramics are presented in separate supplementary data tables in annex 3 (Table 7 to 10).

Basing on the classification proposed in section 4.5.1 (Heimann and Maggetti 2014; Heimann and Maggetti, 2019) *strong* and *weak* clays (raw and < 63 μm fractions) and all ceramic samples (archaeological and traditional) lie in the triangle comprised between quartz, Ca-plagioclase (anorthite) and mullite thus, without any distinction, the carbonate component is very low (Fig. 60A/B). In this case, as evidenced in sections 5.3.4.2 and 5.3.4.3, high temperature calcium rich mineralogical phases did not form.

The concentration of Al_2O_3 and of SiO_2 is very similar for all samples. The first ranges between 16.6 and 22.9 wt%, and the second between 65.20 and 73.20 wt%. Nevertheless, some differences were evident. On archaeological samples, CaO concentration is comprised between 0.51 and 3.57 wt%, while traditional ceramics do not contain more than 0.5 wt% of CaO.

The MgO/Fe_2O_3 ratio is also different, being generally lower on archaeological ceramics ($MgO/Fe_2O_3 < 0.2$). The only exception is represented by sample [829]-6947 ($MgO/Fe_2O_3 = 0.31$). In addition, the absolute concentration of MgO and Na_2O (Fig. 60C) is higher on traditional ceramics, but some archaeological ceramics from the 13^{th} – 14^{th} and 15^{th} – 16^{th} centuries are slightly enriched in Na_2O ([829]-6952, [829]-6962, [2058]-14124), and they partly overlap the traditional ceramic group. Excluding the sample [829]-6962, they are included on fabric 2 and they pertain to fire and table ceramics.

Differently from XRPD, XRF is able to differentiate different fabrics, but not ceramics with a different function. In any case, the results collected for archaeological ceramics point to the exploitation of the same raw material along time as suggested by XRPD and PLM results, and a small difference in chemical composition can be the result of the heterogeneity of the sedimentary deposits of the town of Santarém as evidenced on section 3.1.1.

Chemical analyses, even if small differences are evident between traditional and archaeological ceramics, show that the overall chemical composition is very similar. Actually, raw materials were extracted in different places, but they pertain to the same sedimentary basin. So, these results further support XRPD results and the identification of similar mineralogical phases in archaeological and traditional (i.e. untreated samples, fired at 750 and 1000 °C) is justified.

In the case of *strong* and *weak* clay (raw and < 63 μm fractions), they generally follow the same patterns identified for traditional ceramics. The main differences reside in the SiO_2

and Al_2O_3 content. In the *strong* clay, SiO_2 concentration drops from 65.9 to 56.6 wt% and, at the same time, Al_2O_3 concentration increase from 15.2 to 19.9 wt% in the < 63 µm fraction. Also, MgO, Fe_2O_3 and K_2O concentration increase. These results point to a strong increase in clay content in the finer fraction of the sediment. Similar results were obtained in section 5.1 during the analysis of the raw materials collect close to the city of Santarém.

On the contrary, on *weak* clay, SiO_2 concentration increases from 60.5 to 61.6 wt% while Al_2O_3 remain quite stable, being 17.2 in the raw sample and 17.1 wt% in the < 63µm fraction. Thus, the ratio between sand and clay seems to remain stable.

These results further support granulometric and XRPD analysis carried out on *strong* and *weak* clays suggesting that, in the finer fraction, the content of silty sized grains is higher on the *weak* clay.

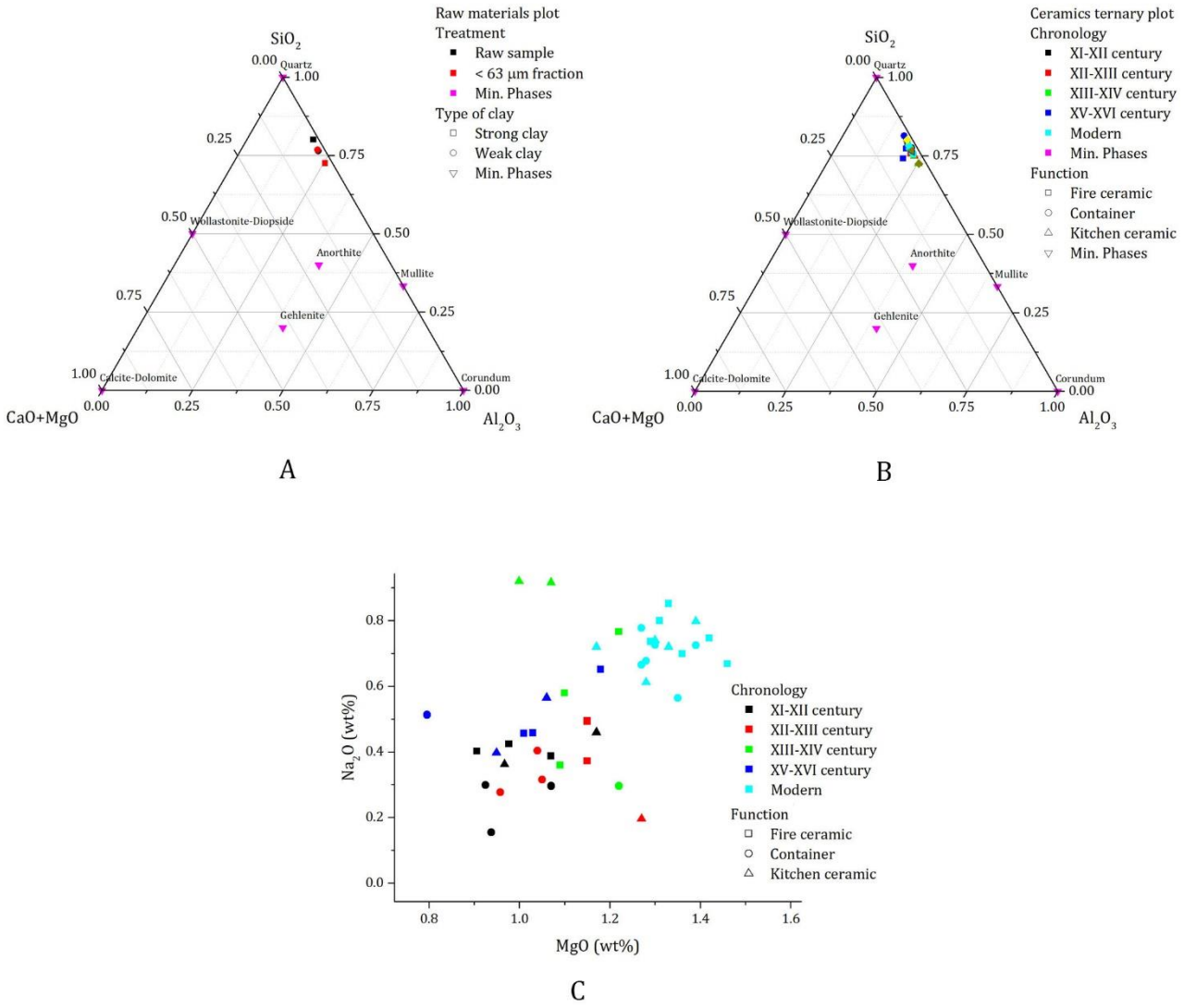

Figure 60 A,B SiO_2, Al_2O_3, [CaO+MgO] ternary plot of the strong and weak clay (raw and < 63 µm fractions) and of the ceramic samples (i.e. archaeological and traditional) after Heimann and Maggetti (2014; 2019); C, Binary plot of MgO and Na_2O of archaeological and traditional ceramic samples

5.3.4.5 Physical, mechanical and permeability properties

Physical (i.e., density, porosity, permeability) and mechanical (i.e., PLT strength index) ceramic characteristics are quite heterogeneous, especially between different functional classes. Considering ceramic samples like two different homogeneous groups (i.e., archaeological and modern), total porosity (Φ_T) made the first difference.

Mean values (Table 28, Fig. 61A) of all functional classes from different periods showed that traditional ceramics are more porous than archaeological ceramics. Normally, ceramic porosity is influenced by temper amount and size, by the firing temperature and, also by the pressure made by the potter when modelling the pot and kneading the paste.

One would expect higher porosity on ceramic with bigger inclusion and more temper (archaeological ceramics), because of structural discontinuities between temper and the ceramic paste (Allegretta et al. 2014; De Bonis et al. 2014; Müller et al. 2010). In any case, after PLM observation, a clear difference in porosity size and alignment was evident, but it was not possible to establish the exact amount on traditional and archaeological ceramics.

The effect of the firing temperature is widely discussed in the bibliography, and when firing temperature increases, porosity decreases consistently due to the vitrification of the ceramic paste (Kam et al. 2009; De Bonis et al. 2014; De Bonis et al. 2014).

Ceramics with similar mineralogical and chemical compositions, should follow the same transformation during firing. In this case, considering XRPD results, physical and mechanical characteristics suggest that ancient Middle Ages kilns in Santarém worked at higher temperature if compared to Mr. Domingos's kiln. Nevertheless, even if traditional and archaeological ceramics were fired at a different temperature, in both cases, specific criteria were adopted for the production of fire(i.e. cooking pots), food-liquid containers and table ceramics.

All singular sample values, medium values for functional class and chronological period of physical and mechanical properties can be found at the end of the dissertation on different data tables included in annexe 3 (Table 11 to 16).

Table 28 Mean values for physical and mechanical properties of archaeological ceramics (from 11th-16th century range), traditional-modern ceramics (UN, untreated samples) and traditional-modern ceramic sub-samples fired at 750 °C and 1000 °C

Century		Apparent density	Real density	Solid density	Total porosity	Open porosity to water	Open porosity to helium	Closed porosity to He	Weight imbibition coefficient	Saturation index	PLT Strength index
		g/cm³	*g/cm³*	*g/cm³*	*%*	*%*	*%*	*%*	*%*	*%*	*(MPa)*
		ρ_B	ρ_R	ρ_S	Φ_T	$\Phi_o H_2O$	$\Phi_o He$	$\Phi_c He$	ICw	SI	$Is_{(50)}$
11th-12th	**Average**	1.93	2.61	2.72	30.0	22.8	26.0	4.0	11.9	87.6	2.47
	St.dev.	0.05	0.05	0.09	2.8	2.9	2.5	3.0	1.9	7.1	0.78
12th-13th	**Average**	1.91	2.61	2.71	30.4	24.0	26.8	3.6	12.6	89.7	4.07
	St.dev.	0.04	0.04	0.06	3.4	1.8	2.2	2.3	1.2	5.4	1.42
13th-14th	**Average**	1.91	2.59	2.72	31.0	22.5	26.1	4.9	11.8	86.9	3.57
	St.dev.	0.04	0.11	0.05	2.3	3.1	3.9	3.0	1.8	5.5	1.25
15th-16th	**Average**	1.93	2.64	2.69	29.0	24.4	27.0	2.0	12.8	90.3	2.71
	St.dev.	0.06	0.05	0.03	2.4	2.9	2.6	1.3	1.6	5.9	0.93
Modern, UN	**Average**	1.85	2.64	2.73	33.3	26.9	29.9	3.4	14.5	90.1	2.48
	St.dev.	0.02	0.06	0.06	1.9	1.1	1.4	1.8	0.6	5.0	0.76
Modern 750 °C	**Average**	1.87	2.68	2.76	32.9	26.1	29.9	3.0	13.9	87.6	2.66
	St.dev.	0.04	0.07	0.07	2.6	1.3	2.3	1.8	0.8	6.3	1.01
Modern, 1000 °C	**Average**	1.94	2.61	2.74	30.3	21.3	25.7	4.7	11.0	83.5	3.95
	St.dev.	0.03	0.05	0.08	2.4	1.1	1.5	2.3	0.7	6.4	2.25

5.3.4.5.1 Traditional ceramics

The results obtained by PLM, XRPD and XRF analyses showed that traditional ceramics apparently represent a homogeneous group. The difference between different functional classes (fire ceramics, food/liquid containers, and table ceramics) resided in the clay mixture prepared by the ceramist (i.e., *strong*/*weak* clays ratio) and it is not appreciable by PLM, XRPD and XRF analyses. On the contrary, ceramics physical and mechanical property comparison show specific characteristics depending on the sample.

Considering mean values for each functional class (Table 29) the results evidence that: i) table ceramics have an intermediate value of total porosity (Φ_T), 34.1%, the highest values of closed helium porosity (Φ_cHe), 3.1%, and weight imbibition coefficient (IC_w), 14.6%; ii) fire ceramics have the lowest values of total porosity (Φ_T), 32.3%, the highest values of strength index ($Is_{(50)}$), 2.98 MPa, and the lowest weight imbibition coefficient (ICw), 14.1%; iii) food and liquid containers have the highest total porosity (Φ_T), 34.1%, open porosity (Φ_OHe), 31%, and the lowest mechanical strength ($Is_{(50)}$), 2.06 MPa.

Table ceramics are generally temporarily used to consume food, so no specific properties are required. In all table ceramics, Mr. Domingos prepare a clay mixture enriched in *strong* clay, and a glaze cover is added to the surface of the objects. Just in one case (painted plate), it was not added.

In order to understand the technological choice of Mr. Domingos (glaze application) we evaluated the effect of glaze on physical properties. The physical analyses (Fig. 61B) carried out on different sub-samples of table ceramics without and with glaze (also in this case we considered mean values for table ceramic with glaze and without glaze) show that the total porosity (Φ_T), the closed porosity to helium (Φ_cHe) and the open porosity to helium (Φ_OHe) are lower on sub-samples with glaze. Moreover, also weight imbibition coefficient (ICw) is lower on the glazed sub-samples.

If thickness normalized water vapour permeability values are considered (Table 30), it is lower on sub-samples with glaze if compared to the only unglazed sub-samples. So, glaze application decreases the porosity and consequently the absorbed water. Thus, for the ceramist, it is not important the porosity. The ceramic paste can be more or less porous because the surface of the object is sealed and impermeabilized by glaze application.

Fire ceramics are normally used for cooking or heating food (they are exposed to fire or to a heat source), and for this reason Mr. Domingos used a different clay mixture, more enriched in weak clay for their production. As a result, fire ceramics have the lowest total porosity (Φ_T), weight imbibition coefficient (ICw) and the highest PLT strength index if compared to food and

Table 29 Mean values with standard deviation for physical and mechanical properties of untreated modern ceramic samples (without glaze when present), and traditional-modern ceramic sub-samples fired at 750 °C and 1000 °C) from different functional classes

Function	Firing temperature		Apparent density	Real density	Solid density	Total Porosity	Open porosity to water	Open porosity to helium	Closed porosity to He	Weight imbibition coefficient	Saturation index	PLT strength index
			g/cm³	g/cm³	g/cm³	%	%	%	%	%	%	(MPa)
			ρB	ρR	ρS	Φ_T	Φ_o H_2O	Φ_oHe	Φ_cHe	ICw	SI	$Is_{(50)}$
Fire ceramics	UN	*Average*	1.85	2.62	2.70	32.3	26.1	29.2	3.1	14.1	89.5	2.98
		St. dev.	0.01	0.06	0.04	1.5	1.5	1.4	1.7	0.9	6.9	0.93
Food, liquid containers	UN	*Average*	1.84	2.66	2.75	34.1	27.0	31.0	3.1	14.6	87.0	2.06
		St. dev.	0.03	0.06	0.08	2.1	1.2	1.7	1.6	0.7	4.6	0.58
Table ceramics	UN	*Average*	1.86	2.64	2.74	33.5	27.7	29.5	4	14.9	93.9	2.4
		St. dev.	0.02	0.06	0.07	2	0.5	1.2	2.1	0.4	3.5	0.77
Fire ceramics	750 °C	*Average*	1.87	2.64	2.72	32.0	25.8	29.1	2.9	13.7	89.0	3.01
		St. dev.	0.05	0.07	0.07	2.8	1.1	2.0	2.4	0.7	5.6	0.90
Food, liquid containers	750 °C	*Average*	1.90	2.65	2.75	32.0	25.6	28.3	3.7	13.5	91.0	2.97
		St. dev.	0.05	0.07	0.05	1.3	1.2	1.5	1.1	0.7	7.5	0.68
Table ceramics	750 °C	*Average*	1.85	2.73	2.80	34.6	26.8	32.1	2.5	14.4	83.5	2.05
		St. dev.	0.02	0.04	0.06	2.1	1.2	1.4	1.2	0.8	2.8	1.05
Fire ceramics	1000 °C	*Average*	1.93	2.59	2.71	30.0	21.3	25.3	4.7	11.0	84.5	4.74
		St. dev.	0.02	0.05	0.08	2.7	1.5	1.3	2.4	0.9	8.1	3.31
Food, liquid containers	1000 °C	*Average*	1.97	2.62	2.75	30.0	21.6	24.8	5.2	10.9	87.0	3.37
		St. dev.	0.03	0.04	0.09	2.8	0.8	0.9	2.7	0.4	3.8	0.69
Table ceramics	1000 °C	*Average*	1.93	2.64	2.75	30.8	21.2	26.7	4.1	10.9	79.5	3.66
		St. dev.	0.04	0.03	0.04	1.6	0.7	1.4	1.7	0.6	3.2	1.41

liquid containers and table ceramics. If the specific function of these objects is considered (i.e. cooking food), the thermal conductivity must be as high as possible to transmit heat.

As explained on different experimental test (Hein et al. 2008; Allegretta et al. 2014; Allegretta et al. 2017), total porosity (Φ_T) has a negative correlation with this property. Thus fire ceramics must have low porosity to increase heat transfer (Roux, 2019). If open porosity (Φ_OHe) and closed porosity (Φ_CHe) to helium are considered separately, they also behave differently to heat transfer. The first one reduces heat transfer. Otherwise, a certain degree of closed porosity favours heat transfer because it usually forms as a consequence of the densification of the ceramic paste, increasing thermal conductivity.

In addition, ceramic with (pot, tacho) and without glaze (pot lid, chestnut roaster) have similar thickness normalized permeability (Table 30), much lower than table and food liquid container ceramics, suggesting that glaze application does not influence this property significantly. This result indicates that the clay mix enriched in *weak* clay is definitely more suitable for the manufacture of fire ceramics and, in this particular case, vermiculite clay mineral (i.e. identified in section 5.3.4.3) favour the densification of the ceramic paste and the development of these specific characteristics (Sutcu, 2015).

Food-liquid containers are normally used to store food and liquids and Mr. Domingos used a clay mixture, more enriched in strong clay for their production. As a consequence, like on table ceramics, food-liquid containers have the highest total (Φ_T) and open porosity (Φ_OHe, $\Phi_O H_2O$) and the lowest mechanical strength ($Is_{(50)}$). Permeability is also very high for this functional class (Table 30). This reflects the production of the so-called hydro-ceramics, which are prepared in order to favour high porosity (in particular open porosity) and permeability.

In fact, the ceramic paste must allow a thermal exchange (favoured by open porosity) by phase changing in order to ensure continuous condensation in the outer surface of the ceramic artefact (Roux, 2019). It is important to note that food-liquid containers were not covered by glaze.

Due to different porosities, and consequently also to the apparent density, the PLT strength index shows a different behaviour of the three functional subgroups, showing higher values on fire ceramics (Table 29). A different trend of fire ceramics was also observed in lower real density and solid density values if compared to other functional subgroups.

The firing tests (Table 29, Fig. 61A) carried out on different sub-samples of traditional ceramics (at 750 and 1000 °C) showed that physical and mechanical characteristics changed. In particular total porosity (Φ_T), open porosity to helium (Φ_OHe), open porosity to water ($\Phi_O H_2O$), saturation index (SI) and weight imbibition coefficient (IC_w) (Fig. 61C) decrease,

while closed porosity to helium (Φ_CHe) and PLT strength index ($Is_{(50)}$) increase. Moreover, from the results of the firing tests, an important general consideration can be done. In ceramics with similar mineralogical and chemical composition, when the firing temperature of the ceramic product increases (see results in Tables 28, 29) the original matrix porosity constantly decreases. This leads to a direct and constant negative correlation between the total porosity values (Φ_T) and the firing temperature. Thus, the apparent density, ρB, inversely correlated to the total porosity, shows a clear positive correlation with the firing temperature of the ceramic product.

From this evidence, in the case of the untreated modern ceramics (Table 28), the total porosity (Φ_T) values of 33.3% indicate a firing temperature probably lower than 750 °C. A porosity reduction is observed starting from the first firing step at 750 °C (32.9%), with a further reduction at 1000 °C (30.3%). Therefore, open porosity to helium (Φ_OHe) and water ($\Phi_O H_2O$), as well as the hydraulic properties (weight imbibition coefficients, IC_w, saturation index, SI) show a negative correlation with the firing temperature (similar to the total porosity, Φ_T).

This is generally followed by a positive correlation with the firing temperature of the closed porosity to helium, Φ_CHe, which after firing at 1000 °C reaches values between 4.1 and 5.2% (Table 29). This is the result of the progressive increase in shrinkage and compactness of the ceramic paste due to the thermal dehydroxylation of the clay minerals and the progressive vitrification of the ceramic paste, as evidenced by the identification of mullite on XRPD patterns.

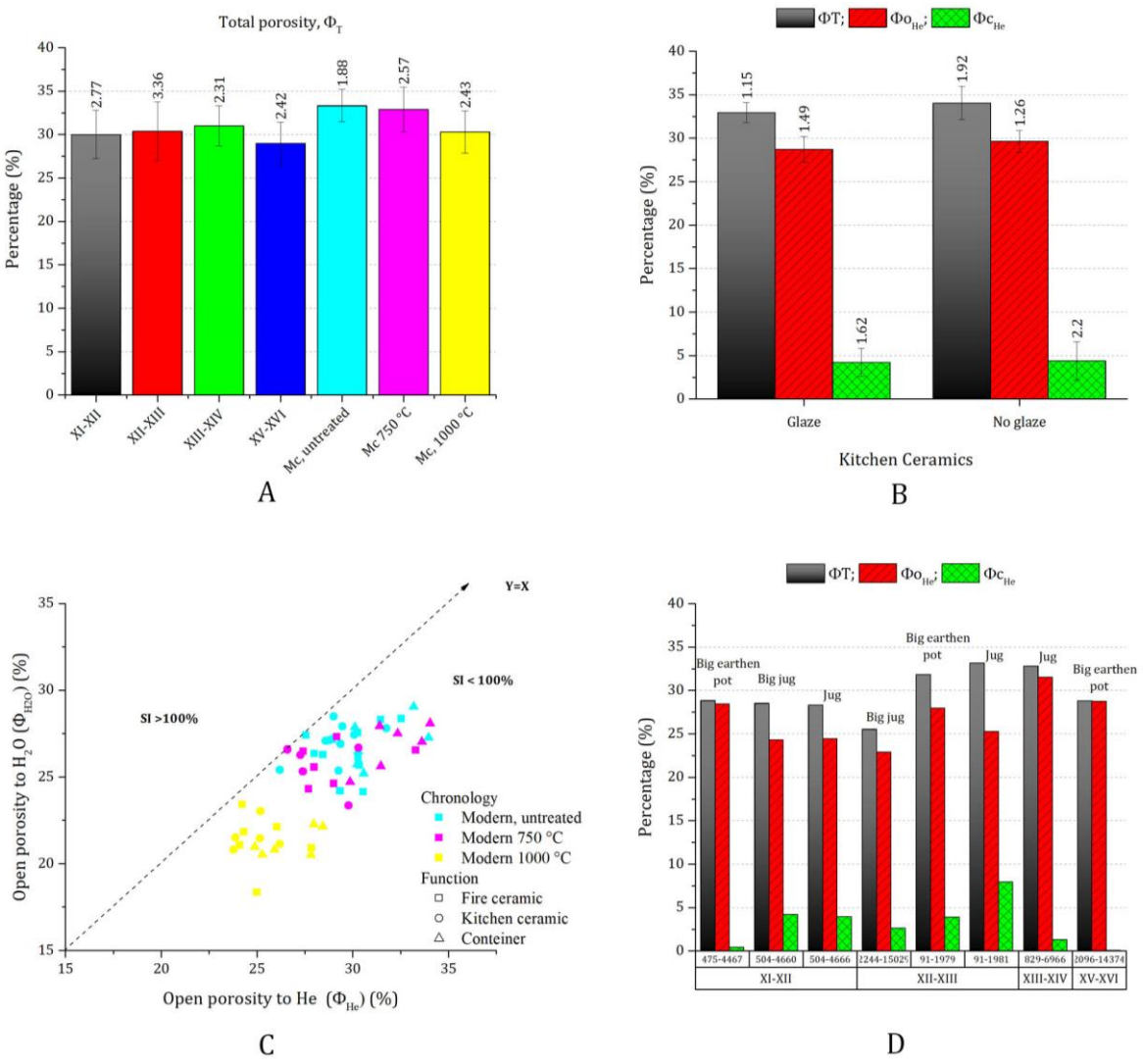

*Figure 61 Physical properties of archaeological and traditional ceramic samples: **A**, Φ_T medium values with standard deviation of archaeological, traditional and firing experiment on traditional ceramic samples; **B**, Φ_T, Φ_OHe and Φ_CHe medium values of traditional table ceramic samples with glaze and without glaze; **C**, Φ_OHe, $\Phi_O H_2O$ and S.I. values of raw traditional ceramic samples, fired at 750 °C and fired at 1000 °C; **D**, Φ_T, Φ_OHe and Φ_CHe of archaeological food-liquid container ceramic samples.*

Table 30 Permeability to water vapour results obtained for archaeological and traditional samples which pertain to different functional classes

Sample	Century	Typology	Function	Decoration	Permeability (g/m^2 x 24h)	Sample thickness (mm)	Thickness normalized permeability (g/m^2 x 24h)/ mm
[504]-4465	*11th-12th*	Pan	Fire ceramic	Unpainted	80.79	6.26	12,91
[504]-4660	*11th-12th*	Big jug	Food-liquid container	White painted	43.35	8.15	5,32
[504]-4464	*11th-12th*	Bowl	Table ceramic	White painted	115.36	7.8	14,79
[91]-1983	*12th-13th*	Lid	Fire ceramic	Unpainted	62.49	7.13	8,76
[2244]-15045	*12th-13th*	Pan	Fire ceramic	Unpainted	51.87	9.26	5,60
[91]-1978	*12th-13th*	Pot	Fire ceramic	Unpainted	48.63	4.73	10,28
[2244]-15029	*12th-13th*	Big jug	Food-liquid container	White painted	87.28	6.06	14,40
[91]-1985	*12th-13th*	Bowl	Table ceramic	Unpainted	61.85	5.56	11,12
[829]-6950	*13th-14th*	Lid	Fire ceramic	Unpainted	47.82	5.93	8,06
[829]-6953	*13th-14th*	Pan	Fire ceramic	Unpainted	51.02	6.63	7,70
[829]-6962	*13th-14th*	Bowl	Table ceramic	Unpainted	52.75	6.2	8,51
[2096]-14392	*15th-16th*	Pan	Fire ceramic	Unpainted	88.20	6.5	13,57
[2058]-14122	*15th-16th*	Bowl	Table ceramic	Unpainted	137.45	5.23	26,28
Pot lid	*Modern*	Pot lid	Fire ceramic	Unglazed	84.44	6.46	13,07
Pot	*Modern*	Pot	Fire ceramic	Glazed	90.42	6.43	14,06
Tacho	*Modern*	Tacho	Fire ceramic	Glazed	69.47	6.33	10,97
Chestnut roaster	*Modern*	Chestnut roaster	Fire ceramic	Unglazed	80.64	6.36	12,68
Jug	*Modern*	Jug	Food, liquid container	Unglazed	177.49	7.63	23,26
Water costrel	*Modern*	Water costrel	Food, liquid container	Unglazed	136.25	5.6	24,33
Jug lid	*Modern*	Jug lid	Food, liquid container	Unglazed	175.61	7.93	22,15
Yellow bowl	*Modern*	Yellow bowl	Table ceramic	Glazed	107.81	8.4	12,83
Bowl	*Modern*	Bowl	Table ceramic	Glazed	84.68	9	9,41
Green bowl	*Modern*	Green bowl	Table ceramic	Glazed	84.29	6.17	13,66
Glazed plate	*Modern*	Glazed plate	Table ceramic	Glazed	77.59	9.4	8,25
Painted plate	*Modern*	Painted plate	Table ceramic	Unglazed	167.41	6.73	24,88

5.3.4.5.1 Archaeological ceramics

In the case of archaeological samples, the results obtained after XRPD and XRF analyses showed that ceramics are quite homogeneous in mineralogical and chemical composition. Conversely, PLM observations showed that, depending on the functional class, ceramics were manufactured in a different way. In particular (see also sections 5.1, 5.2), table and food liquid containers were mainly produced using fabric 1 – sub-fabric 1A, while in the case of fire ceramics fabric 1 – sub-fabric 1B was utilized.

These observations have been further supported by physical and mechanical properties. Actually, physical and mechanical properties are quite heterogeneous but, considering mean values for different chronological period (Table 31), each functional class have specific characteristics, similar to that observed for traditional ceramics such as: i) table ceramics from each period have highest total (Φ_T), 30.2-35.2%, and closed porosities to helium (Φ_CHe), 2.9-8.1%; ii) fire ceramics have the lowest total porosity (Φ_T), 26.7-29.4%, in every chronological period; iii) food and liquid container gave heterogeneous results, which will be discussed in detail.

This suggests that ancient ceramists used a specific ceramic paste to obtain specific technological characteristics along time. In any case, it is not possible to understand whether different raw materials (i.e. temper and/or clay) were mixed.

Regarding table ceramics, the high total (Φ_T) and closed porosity to helium (Φ_CHe) is the result of a specific technological choice. Considering that firing temperature and total porosity are inversely correlated (Kam et al. 2009; De Bonis et al. 2014; Cultrone et al. 2004), the identification of illite/muscovite, but not mullite (Table 21), suggests a low degree of vitrification of the ceramic paste. At the same time firing temperature and closed porosity to helium (Φ_CHe) are linearly correlated. This correlation was also evident during the firing test carried out on traditional ceramics.

In the case of archaeological table ceramics, it was the result of a slip application, as highlighted during PLM observations. Slip is usually applied to increase waterproof characteristics of the outer ceramic surface (Roux, 2019) before firing. This hypothesis was tested by permeability tests (Table 30).

Results for table ceramics, especially thickness normalized permeability values, apparently show heterogeneous results. This can be the consequence of several factors such as ceramist expertise, shaping technique, surface treatments (slip, glaze layer) and chemical-physical alteration degree of the artefact surface. Consequently, in some cases, permeability is low (8.51, 11.12 g/m^2 x 24h /mm), similar to those observed on modern traditional ceramics

Table 31 Medium values with standard deviation of physical and mechanical properties of archaeological ceramic samples of different functional classes and chronology. When standard deviation is not reported, just one sample was analysed

Century	Function		Apparent density	Real density	Solid density	Total Porosity	Open porosity to water	Open porosity to helium	Closed porosity to helium	Weight imbibition coefficient	Saturation index	PLT strenght index
			g/cm³	*g/cm³*	*g/cm³*	*%*	*%*	*%*	*%*	*%*	*%*	*(MPa)*
			ρ_B	ρ_R	ρ_S	Φ_T	ΦoH_2O	ΦoHe	ΦcHe	ICw	S.I.	$Is_{(50)}$
11th-12th	**Fire ceramics**	Average	1.94	2.56	2.62	26.7	21.9	24.2	2.5	11.3	90.8	2.14
		St.dev.	0.04	0.00	0.02	0.8	0.4	1.6	0.8	0.4	4.9	0.66
	Food, liquid containers	Average	1.95	2.62	2.70	28.6	21.6	25.7	2.8	11.2	83.6	2.35
		St.dev.	0.07	0.02	0.07	0.2	3.7	1.9	1.7	2.3	9.0	0.83
	Table ceramics	Average	1.89	2.67	2.79	33.5	26.0	29.3	4.2	13.9	89.0	3.13
		St.dev.	0.01	0.01	0.02	1.0	0.4	0.0	1.1	0.3	1.2	0.39
12th-13th	**Fire ceramics**	Average	1.92	2.64	2.68	29.0	23.9	27.3	1.7	12.5	87.6	4.77
		St.dev.	0.03	0.03	0.05	2.3	2.2	1.3	1.0	1.4	5.2	1.79
	Food, liquid containers	Average	1.93	2.59	2.71	30.2	23.3	25.4	4.8	12.3	92.2	3.23
		St.dev.	0.03	0.04	0.05	3.3	0.9	2.1	2.3	0.8	5.5	0.51
	Table ceramics	Average	1.85	2.63	2.77	35.2	26.3	29.6	5.6	14.2	88.8	4.50
		St.dev.										
13th-14th	**Fire ceramics**	Average	1.95	2.61	2.72	29.4	21.8	25.4	4.0	11.2	86.4	4.07
		St.dev.	0.01	0.07	0.03	0.4	0.8	1.9	1.9	0.4	3.6	0.96
	Food, liquid containers	Average	1.87	2.73	2.77	32.8	28.7	31.5	1.3	15.3	91.2	4.17
		St.dev.										
	Table ceramics	Average	1.88	2.50	2.70	32.5	20.5	24.4	8.1	11.0	85.5	2.54
		St.dev.	0.04	0.10	0.06	2.8	2.1	4.6	1.8	1.2	7.7	1.29
15th-16th	**Fire ceramics**	Average	1.95	2.64	2.70	28.3	23.9	26.3	2.0	13.3	91.2	3.31
		St.dev.	0.07	0.01	0.02	3.0	2.1	2.8	0.9	0.4	6.2	0.67
	Food, liquid containers	Average	1.91	2.68	2.68	28.8	26.3	28.8	0.0	13.8	91.6	1.08
		St.dev.										
	Table ceramics	Average	1.90	2.62	2.70	30.2	24.2	27.3	2.9	12.8	88.2	2.63
		St.dev.	0.01	0.07	0.04	1.3	4.0	2.5	1.2	2.0	6.5	0.16

covered by glaze (8.25, 9.41 g/m^2 x 24h /mm). Just in one case (sample [2058]-14122 from the 15th – 16th century), permeability was very high (26.28 41 g/m^2 x 24h /mm), suggesting, in this case, surface alteration and-or a bad surface treatment. From these observations, archaeological table ceramics could also be more or less porous and surface treatments (i.e. slip application) were supposed to impermeabilize the object surface.

Fire ceramics have the lowest total porosity (Φ_T). Also, thickness normalized permeability is low, similar and even smaller to that obtained for traditional ceramics. These results are significant to understand the manufacturing technologies, indicating that similar criteria were adopted for the production of fire ceramics both in ancient times and in modern traditional ceramics.

Regarding archaeological food and liquid containers (Table 32), they have a slightly different function, namely to store liquid (jug, big jug) and food (big earthen pot). Usually, total porosity (Φ_T), open porosity to helium (Φ_OHe) and open porosity to water ($\Phi_O H_2O$) are higher on big earthen pots, while closed porosity to helium (Φ_CHe) is higher on jug and big jugs (Fig. 63D). The only exception is the jug [829]-6966 from the 13th – 14th century (Table 32), which is similar to big earthen pots. This difference is also shown by PLM, especially in the amount of temper, grain size and porosity, higher on big earthen pots.

Regarding permeability it was possible to perform analyses just on two samples of big jugs from the 11th – 12th and 12th – 13th centuries (samples [504]-4660, [2244]-15029). Normalized permeability results (Table 30) show medium-low values, especially if compared to modern traditional ceramics with the same function (jug and water costrel). So, if we consider that a good liquid container needs high total porosity (Φ_T), open porosity to helium (Φ_OHe) and water ($\Phi_O H_2O$) in order to favour liquid coolness (Roux, 2019), archaeological ceramics were less efficient than traditional ones. In the case of big earthen pots and jug [829]-6966, porosity was probably important, because it could act as an insulating barrier against the external environment.

In the case of PLT strength index ($Is_{(50)}$) it was not possible to establish a correlation with the firing temperature, as established for modern traditional ceramics, due to sampling restriction. Generally, in the case of archaeological ceramics of all periods, $Is_{(50)}$ decrease when the amount of temper increases and when temper grain size is bigger. Similar results were obtained and discussed by De Bonis et al. (2014) and Müller et al. (2010).

By comparing mean physical data (Table 28) between archaeological and traditional ceramics, some general considerations can be made, especially about the relationship between firing temperature and physical properties on archaeological ceramics. As explained above,

total porosity (Φ_T) varies according to the firing temperature (Kam et al., 2009) and, a significant porosity decreases usually happens above 900-950 °C accompanied by the complete dehydroxylation of clay minerals and the formation of high temperature mineralogical phases (De Bonis et al. 2014; Cultrone et al. 2004). These results were also highlighted on experimentally fired traditional ceramics sub-samples.

Considering that archaeological ceramics have values of total porosity, (Φ_T), between 29 and 31% vol., therefore similar to the modern ceramics fired at 1000 °C (which have values of the same property around 30%), it is probable that the firing temperature of archaeological ceramics varies between 800 and 1000 °C. Those belonging to the 11th – 12th and 15th – 16th centuries were probably fired around 950 °C, while those of the 12th – 13th and 13th – 14th centuries were fired at lower temperatures, probably around 800-850 °C. These observations are in agreement with XRPD data.

Table 32 *Physical and mechanical properties of archaeological food and liquid containers from all periods*

Century	Function	Samples	Typology	Apparent density	Real density	Solid density	Total porosity	Open porosity to water	Open porosity to helium	Closed porosity to He	Weight imbibition coefficient	Saturation index	PLT strength index
				g/cm³	*g/cm³*	*g/cm³*	*%*	*%*	*%*	*%*	*%*	*%*	*(MPa)*
				ρ_B	ρ_R	ρ_S	Φ_T	ΦoH_2O	ΦoHe	ΦcHe	ICw	S.I.	$Is_{(50)}$
11th-12th	Food, liquid containers	[504]-4660	Big jug	2.00	2.64	2.75	28.5	17.3	24.3	4.2	8.7	71.3	2.13
		[504]-4666	Jug	1.99	2.64	2.74	28.3	21.2	24.4	3.9	10.6	86.8	3.46
		[475]-4467	Big earthen pot	1.85	2.59	2.60	28.8	26.3	28.4	0.4	14.2	92.6	1.48
12th-13th	Food, liquid containers	[2244]-15029	Big jug	1.98	2.57	2.63	25.5	22.1	22.9	2.6	11.1	96.4	3.67
		[91]-1981	Jug	1.91	2.55	2.76	33.2	24.2	25.3	7.9	13.2	95.6	2.51
		[91]-1979	Big earthen pot	1.90	2.64	2.74	31.8	23.6	28.0	3.9	12.4	84.5	3.50
13th-14th	Food, liquid containers	[829]-6966	Jug	1.87	2.73	2.77	32.8	28.7	31.5	1.3	15.3	91.2	4.16
15th-16th	Food, liquid containers	[2096]-14374	Big earthen pot	1.91	2.68	2.68	28.8	26.3	28.8	0.0	13.8	91.6	1.07

5.3.5 Final remarks of the section

In this section, two different groups of artefacts, archaeological and traditional ceramics, with different functions and chronology, have been analysed. Our results showed that the methodology applied was effective to compare pottery technology between the Middle Ages and Modern times.

Moreover, it was also possible to get some important methodological considerations. Both ceramic groups were produced with local raw materials, extracted in different areas, in Santarém and Muge, respectively, but geologically similar. Physical and mechanical tests were essential in order to establish the characteristics of different functional objects.

In fact, archaeological and traditional ceramics were produced following specific technological criteria, mainly linked to the final object function and ceramic behaviour. However, this goal was achieved by two different approaches, which differs in the preparation of the ceramic paste and on the firing temperature:

- For archaeological samples, the ceramic paste was prepared differently for different functions of the objects. Actually, as evidenced by PLM, kitchen and food/liquid container ceramics are different from fire ceramics. These differences mainly reside on temper characteristics and they were not evident neither after XRPD nor XRF. Only PLM shows significant differences. At this stage it is not possible to assess if distinct clays were mixed. The ceramic production is specialized along the time;
- In traditional samples, the ceramic paste was prepared similarly in every case, with similar amount and temper characteristics, changing the proportion of *strong* and *weak* clay. Nevertheless, the effect of mixing different raw materials (clay) is not identifiable neither by PLM, XRF and XRPD analyses;
- Regarding firing temperature, archaeological ceramics were fired at a higher temperature if compared to traditional ones. This was evidenced by the linear correlation between firing temperature and total porosity established by different firing tests on traditional ceramics.

Considering PLM, XRPD and XRF results, archaeological ceramics raw material sources, particularly clay and temper, were widely available in every chronological period indicating ceramic production continuity using the sedimentary deposits close to the city of Santarém. Consequently, we suppose that fuel and water were also easily available for ceramic production in the Middle Ages.

Regarding ceramic with the same function, results did not detect any significant difference in pottery characteristics. Also, historical sources and archaeological data attest to

pottery production continuity in the town along the time. These observations suggest that the ceramic cycle and technology of production were not affected by the political and economic changes, occurred between the 11th and 16th centuries.

Moreover, as discussed, ceramic production during the Middle Ages was quite specialized, suggesting expertise continuity. In both Middle Ages ceramics from Santarém and traitional ceramics from Muge, we can also sustain that local socio-cultural factors mainly determined the ceramic characteristics and technology.

Basing on this research, we do not have data to state that religion, ideology and ethnicity have never played a role in the productive ceramic cycle. Actually, the archaeological record of the city evidenced the conservation of the Islamic ceramic characteristics during the Middle Ages. As evidenced by historical sources, Christians, Muslims and Jewish lived together (see section 3.1.2) in the same town in the timeframe considered.

Actually, during history, a modification of the ruling power does not usually correspond to a radical substitution of the local population. So, the technical expertise is more probably the result of a local tradition started during the Islamic period.

In any case, our data show that every decision or technical choice was taken depending on the functional and performance characteristics desired for a specific artefact. In this case, ceramists' technical expertise was the main factor that could influence pottery technology in the creation of a specific object. So, since the Middle Ages, ceramics were produced following specific criteria, and ancient technical expertise is still valid nowadays.

5.4 Islamic glazed ceramics from Mértola, Southern Portugal: provenance and technology

The results of this section were only parlty presented in a national congress *"Terra pedras, e cacos do Garb al-Andalus"*, held in Palmela in Jenuary 2020, but most of them are unpublished. Articles are under preparation.

The principal aim of this section is to determine Islamic glazed ceramics characteristics (ceramic paste and glaze) in the town of Mértola during the Islamic domination, from the Caliphal to the Almohad period.

Ceramics decorated using different styles like green and brown, partial *corda seca*, and honey and black glazed ceramics were considered for analysis. In addition several kiln rods and one sample of white painted ceramic, recovered in different productive contexts of the town, were included in the study as standard of local prodiction.

Ceramics were analysed using different analytical techniques such as OM, XRPD, XRF, ICP-MS, SEM-EDS and μRaman spectroscopy.

The analysis of the ceramic paste evidenced that most ceramics were locally produced using a raw material exploited in *Baixo Alentejo* Flysch geological unit (i.e. Mértola Formation). Other ceramic samples were imported in the town from the North of Africa (i.e. *Ifrīqiya*) and probably from the area of Malaga. In addition, the local raw material was adapted for the production glazed ceramics with addition of limestone, bone (or bone ash) and glass fragments. Similar characteristics were also observed in some imported ceramics, suggesting technological transfer between different places. This kind of ceramic supports are normally referred as proto-stone-paste ceramic bodies in the Middle East.

The analysis of the glazed ceramic decorations evidenced that different glaze types were used (i.e. high-lead or lead-alkaly types) and there is not a correleation between chronology and glazes chemical composition. Only in the case of partial *corad seca* glazed ceramics a higher content of silica was preferred. CuO (green/turquoise), MnO (black), FeO (honey, black) and Sb_2O_3 (yellow) were the main coloring agents. SnO_2, unmelted quartz grains and bones (or bone ash) were used to increase glaze opacity, alone or together. The introduction of bone (or bone ash) in the glaze mixture is a new technological solution, and it was never documented in Islamic Iberia.

5.4.1 Introduction and goals of this section

Whit the beginning of Islamic domination (8th century) artisans reached the *al-Andalus* from the Near East, and different kind of glazed ware began to be produced adopting, and spreading typical technological solutions of Eastern Islamic territories.

The most significant is the extensive use of lead glazes due to their technical advantages (Tite et al., 1998) and the aesthetic solutions allowed. The Iberian pyrite belt (Almodóvar et al., 2019), located on south-western Iberian is a possible source of lead ores.

Lead ores exploitation and use in the ceramic industry was not an Islamic innovation but a re-adoption of ancient expertise. The same technology was already employed during the Hellenistic period in Asia Minor, by Romans and throughout the Byzantine Empire. Afterwards, it has been adopted in the Islamic world, and its use also spread widelly in medieval Europe on several kinds of ceramic, including glazed tiles in Portugal and Spain (Peréz-Arantegui et al., 1995; Peréz-Arantegui et al., 1996; Tite et al., 1998; Ricci et al., 2005; Fortina et al., 2005; Greene, 2007; Marzo et al., 2009; Walton and Tite, 2010; Waksman et al., 2008; Métreau and Rosen, 2014; Palamara et al., 2016; Coentro et al., 2017).

In the Iberian Peninsula, the most ancient evidence of Islamic lead exploitation goes back to the middle of the 8th – beginning of the 9th around Córdova. In this case, lead slags from silver and lead mining were utilized to produce high lead and soda ash lead glasses (Schibille et al., 2020). In the second half of the 9th century, during the Emiral period, high lead-glazed ceramics began to be produced at Pechina (Almeria) and Malaga (Salinas and Zozaya, 2015; Salinas et al., 2019), and they were normally applied on calcareous ceramic bodies, although silica rich bodies could also be employed (Walton and Tite, 2010).

But undoubtedly, the most important innovation by the end of the 9th century and the beginning of the 10th century (Salinas and Pradell, 2018; Molera et al., 2018) was the introduction of white tin opacified lead-alkali glazes. This technique takes advantage of tin oxide particles precipitation in the glaze to make it opaque (Vendrell-Saz et al., 2000; Molera et al., 1999; Matin et al., 2018).

At present, it is clear how tin glazes arrived in the *al-Andalus.* Technical similarities and a later chronology of the Iberian glazed ceramics, if compared to the most ancient Islamic prototypes (Mason and Tite, 1997; Tite et al., 2015; Matin et al., 2018), support the accepted theory of the introduction from the Middle East (Salinas and Pradell, 2018; Salinas and Pradell, 2020).

Usually, tin opacified lead-alkali glazes were applied in a ceramic body made from a calcareous clay or in a stonepaste support (Mason and Tite, 1994; Tite et al., 2011). Calcareous clay materials promote glaze adhesion thanks to a higher thermal expansion coefficient if compared to no-calcareous clay bodies (Tite et al., 1998).

In the *al-Andalus*, tin has been utilized to produce three different decorated glazed wares. Initially, it was utilized on green and brown glazed ceramics production (Molera et al., 2001b; Molera et al., 1999a; Coll Conesa et al., 1999; Peréz-Arantegui et al., 1999; Salinas and Pradell, 2020; Molera et al., 2018; Salinas and Pradell, 2018). Afterwards, it was utilized on partial/total *corda seca* (Déléry, 2006; Chapoulie et al., 2005; Peréz-Arantegui et al., 1999b) and on metallic lustre glazed ceramics (Picon and Navarro Palazon, 1986; Garofano et al., 2015; Molera et al., 2001a; Chabanne et al., 2011; Barceló and Heidenreich, 2020).

In the case of *corda seca* ceramics, different coloured glazed preparations could be applied in the same piece (Chapoulie et al., 2005), with the application of both opacified and not opacified glazes.

In the present section, several Islamic glazed ceramics from Mértola, *Garb al-Andalus* (Southern Portugal-western Iberia during Islamic time), have been selected for analysis. The town-port of Mértola was closely linked to the capital of the *Kura* Beja during the Middle Ages, and acquired a prominent role from the 10th century, reaching the capital status of independent *"Taifa"* with *Ibn Ṭayfūr,* at the beginning of the 11th century with the fall of the Caliphate of Córdova.

The city became part of the *Kingdom* of Seville in the middle of the same century. With the end of the *Taifa* kingdoms, the *Almoravid* (end of the 9th century) and the *Almohad* (12th century) dynasties controlled the town. In the middle of the 13th century, Mértola was included in the Portuguese Kingdom.

The economic importance of the area comes from its geographic position. The town is located on the northernmost navigable limit of the River Guadiana. It is considered the regional intersection between the inland regional commercial network and long distance trade within the Mediterranean Sea and the Atlantic facade (Gómez Martínez, 2009b). Moreover, the area of Mértola lies on the Iberian Pyrite Belt, and different kinds of metal ores enriched in Mn, Fe, Zn, Cu, Pb, Au and Ag could be found in the nearby mining area of S. Domingo and close to the town (Matos et al., 2012; Oliveira and Silva, 2007; Mateus et al., 2011).

The local production of lustre and green and brown ceramics was already suggested (Zozaya and Aparicio Yague, 2003) at least since the *Taifa* kingdom period, 11th century. Still, no further research has been developed to confirm ceramic provenance and to evaluate ceramic

technology. Based on stylistic and typological considerations, archaeologists raised doubts (Gómez Martínez, 2003), suggesting that green and brown and corda seca ceramics were imported from different unidentified workshops probably located in southern *al-Andalus*. On the contrary, lustre metallic ceramics was probably produced in the town since the *Almohad* domination.

From the technological point of view, the lack of typic calcareous clay raw materials (i.e. derived from limestone or dolostone alteration) make difficult the production of tin opacified lead alkali glazed ceramics. Moreover, stonepaste technology had never been documented in the *al-Andalus* to produce decorated glazed wares, and just in the case of the Islamic ceramics from la Vega de Granada it has been suggested (Molera et al., 2018).

Considering the remarkable glazed ceramic diversification (Gómez Martínez, 2014), the chronology (which cover the whole Islamic occupation) and the availability of raw materials for glaze production in the area of Mértola, a set of green and brown, partial *corda seca* and honey and black glazed ceramics were selected for an archaeometric study and compared to kiln wastes and kiln rods locally recovered.

The goal is to assess ceramic provenance, glaze characteristics, manufacturing diversification and the applied ceramic and glaze technology during the Islamic occupation of the town. It will be considered if the lack of specific raw material (i.e. calcareous clay) for glazed ceramic production imposes a specific productive cycle in glazed ceramic manufacturing. Results will be compared with the existing bibliography to understand technological similarities and differences within the *al-Andalus* and within the Islamic world.

5.4.2 Geological setting

Mértola is located in the southwestern section of the Iberian Peninsula. From the geological point of view (Fig. 62), it is in the Iberian Pyrite Belt (IPB), included in the so-called Southern Portuguese Zone (SPZ), the southernmost segment of the Iberian Variscan Massif. The stratigraphic succession of the IPB is subdivided into three major Upper Palaeozoic (Givetian-Visean) sedimentary and igneous rocks lithostratigraphic units (Schermerhorn, 1971; Oliveira and Silva, 2007). They are the Phyllite/Slate–Quartzite Group (PQ Group), the Volcano–Sedimentary Complex (VSC) and a thick post-volcanic turbiditic succession called Baixo Alentejo Flysch group. The stratigraphic limits of each unit are depositional. The rocks were affected by hydrothermal (PQ group and VSC) and low-grade regional metamorphism (the three major lithostratigraphic units).

The PQ group is dominated by slate interlayered by fine-grained quartzite and siltstones. Slate and siltstone sequences might also be interposed by rare carbonate-rich lens/nodules with variable sizes. Quartz-rich greywackes, rare conglomerates, and jaspers lens can also be found. The *Barranco do Homem* (BH) sedimentary formation (Faria et al., 2015), the older unit of the PQ group, is visible in Mértola region. It is composed of quartz-rich greywackes interlayered by clay-rich slate and finely grained quartzite.

The VCS complex is represented by clay-rich and quartz-rich slates, siltstone, jaspers and cherts, mafic and felsic igneous rocks (mostly volcanic) and tuffs with nodules of manganese and iron oxides. In the same lithostratigraphic unit, diabase plutonic rocks, volcanogenic sediment, acid tuff, whitish felsite, and exotic slates (as *Borra de Vinho* Slate) can also be found. The different lithologies appear as lenticular outcrops with variable extension. In the region, the last member of the VSC complex is the *Freixial* formation (Fr). It is characterized by a flysch sequence composed of finely grained greywacke, siltstone, and calcarenite interposed clay-rich slates.

The *Baixo Alentejo* Flysch in this region is known as Mertola Formation. It is a turbiditic succession of pelitic deposits (i.e. slates) and bedded turbidites (i.e. greywackes). Some occurrences of carbonate-rich nodules can be observed.

In the region, galena (sometimes enriched in silver), pyrite, barite, sphalerite, cerussite, malachite and stibnite (Oliveira and Silva, 2007) have been exploited on different veins with NE-SW orientation. But the massive volcanogenic sulphide ore deposits (Almodóvar et al., 2019; Matos et al., 2012; Leistel et al., 1997; Barriga, 1990), as the São Domingos mine, are the distinctive ore deposits in the region. These giant deposits, with several million tonnes, are the

result of intense hydrothermal processes in an ancient seafloor that results in the accumulation of iron (pyrite), copper (chalcopyrite), lead (galena) and zinc (sphalerite) sulphides with some gold and silver.

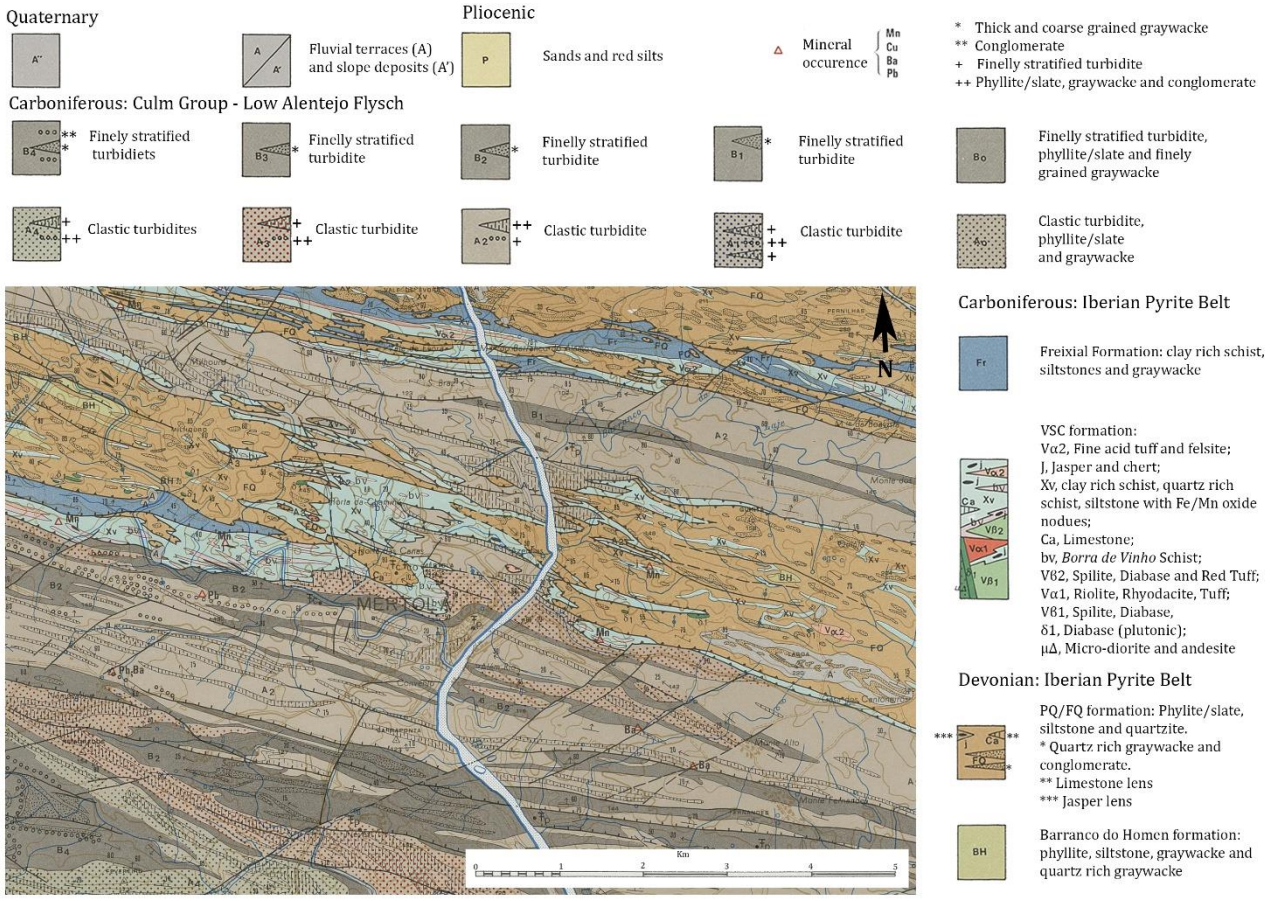

Figure 62 Geological setting of the area of Mértola, adapted after Oliveira and Silva (2007)

5.4.3 Islamic ceramics from Mértola

Samples ceramic chronology cover the Islamic occupation of the town, 10th - 13th century. In total 8 kiln bars, 1 white painted ceramic fragment, 16 green and brown, 6 partial corda seca and 1 honey and black glazed ceramics were selected (Table 33, Fig. 63, 64).

Kiln bars and the white painted ceramic fragments were recovered into two different productive contexts from the Almohad period (Gómez Martínez, 2016; Gómez Martínez, 2006). They will be utilized as a "standard" local raw material. One kiln bar is also partially covered by a green glaze.

The green and brown ceramic collection is notable, and mainly bowls were decorated using this technique (Gómez Martínez, 2014). Stylistically, Caliphal samples are comparable to *Madinat al-Zahara* ceramics from Córdova. The ornamental style and the iconographic meaning spread the political messages of the Umayyad dynasty (Barceló, 1993; Rosselló-Bordoy, 1987), so perhaps they were imported into the town. Samples from the *Taifa* Kingdom period represent the diversification of green and brown production in different Taifa kingdoms, with the introduction of the honey-coloured glaze in the decoration (CRVM-1668, CRVM-1671).

Sample CRVM-1097 is also different, having a green glaze on the outer surface of the piece. Almoravid ceramic samples are stylistically similar to North of African ceramics from (Gómez Martínez, forthcoming; Gómez Martínez et al., 2018) *Ifrīqiya*, widely recovered in the most important harbours of the Mediterranean Sea and of the Atlantic façade including Portugal, Spain and Italy. The decorative style is completely different from previous periods, and it is defined as "geometric" by archaeologists.

Information about Almohad samples is scarse, but the iconography recalls decorative solutions employed during the Caliphal period. At the present, the only attested workshop has been identified at *Calatrava la Vieja* and *Alarcos* (Retuerce Velasco and De Juan García, 1998).

The honey and black ceramic sample is also associated to the Almohad period, and it was probably locally produced.

Regarding partial *corda seca* ceramics, mainly jugs received this decoration. Mono and multi-coloured Almoravid and Almohad ceramic samples were selected. The typological and stylistic characteristics point to importation from southern Iberia, perhaps *Almeria* (Fernandes et al., 2015).

Table 33 Ceramic samples included in this section. The table reports samples archaeological reference, typology, decoration pattern, chronology, period, and the name of the archaeological site where the samples have been discovered at Mértola. GB = green and brown – CSP = Partial corda seca – HB = honey and black

Sample Ref.	Typology-dec.	Iconography	Century	Period	Arch. Site
RDC-108-2014-0001	Kiln rod with green glaze	None	2nd half 12th	Almohad	Rua Dr. Afonso Costa
RDC-108-2014-0002	Kiln rod	None	2nd half 12th	Almohad	Rua Dr. Afonso Costa
RDC-108-2014-0003	Kiln rod	None	2nd half 12th	Almohad	Rua Dr. Afonso Costa
RDC-108-2014-0004	Kiln rod	None	2nd half 12th	Almohad	Rua Dr. Afonso Costa
RDC-108-2014-0005	Kiln rod	None	2nd half 12th	Almohad	Rua Dr. Afonso Costa
RDC-108-2014-0006	Kiln rod	None	2nd half 12th	Almohad	Rua Dr. Afonso Costa
RDC-108-2014-0007	Kiln rod	None	2nd half 12th	Almohad	Rua Dr. Afonso Costa
RDC-108-2014-0008	Kiln rod	None	2nd half 12th	Almohad	Rua Dr. Afonso Costa
R25A-02-SXV-94	Kiln waste, Jar	White painted	1st half 13th	Almohad	Rua 25 de Abril
CRVM-0357	Bowl, GB	Eternal knot	2nd half 10th - early 11th	Caliphal	*Alcaçova*, Cryptoporticus A
CRVM-623	Bowl, GB	Geometric	2nd half 10th	Caliphal	*Alcaçova*
CRVM-666	Bowl, GB	Vegetal-lotus flower	2nd half 10th	Caliphal	*Alcaçova*
CRVM-642	Bowl, GB	Epigraphic	11th	Taifa	Castle hillside
CRVM-1097	Bowl, GB	Vegetalist	11th	Taifa	*Alcaçova*, Cryptoporticus A
CRVM-1659	Bowl, GB	Geometric	11th	Taifa	*Alcaçova*, Cryptoporticus A
CRVM-1668	Bowl, GB	Bands and points	11th	Taifa	*Alcaçova*
CRVM-1671	Bowl, GB	Phytomorphic	11th	Taifa	*Alcaçova*
LVG-02-SXVIII-187	Bowl, GB	Zoomorphic	11th	Taifa	Largo Vasco da Gama
CRVM-1665	Bowl, GB	Zoomorphic	1st half 12th	Almoravid	Castle
CRVM-1666	Bowl, GB	Zoomorphic	1st half 12th	Almoravid	Castle
CRVM-1670	Bowl, GB	Zoomorphic	1st half 12th	Almoravid	Castle hillside
CRVM-1667	Bowl, GB	Not determined	2nd half 12th	Almohad	Castle
CRVM-1669	Bowl, GB	Epigraphic	2nd half 12th	Almohad	Castle hillside
CRVM-223	Bowl, GB	Zoomorphic	2nd half 12th	Almohad	Castle hillside
CRVM-0670	Bowl, GB	Phytomorphic	2nd half 12th – early 13th	Almohad	Castle hillside
CRCSP-0030	Jug, CSP	Epigraphic	1st half 12th	Almoravid	Indeterminate
CRCSP-0031	Jug, CSP	Phytomorphic	12th	Almoravid	Indeterminate
CRCSP-0028	Jug, CSP	Geometric	1st half 12th	Almoravid	*Alcaçova*, Cryptoporticus A
CRCSP-0027	Jug, CSP	Phytomorphic	1st half 12th	Almoravid	*Alcaçova*, Cryptoporticus A
CRCSP-0021	Jug, CSP	Phytomorphic	12th	Almoravid	*Alcaçova*, Cryptoporticus A
CRCSP-0029	Jug, CSP	Phytomorphic	12th	Almohad	Indeterminate
CRVF-0003	Lid-HB	Phytomorphic	End 12th – beginning 13th	Almohad	*Alcaçova*, Cryptoporticus A

Figure 63 Picture of kiln rods, of the white-painted fragment and of green and brown ceramics from Mértola.

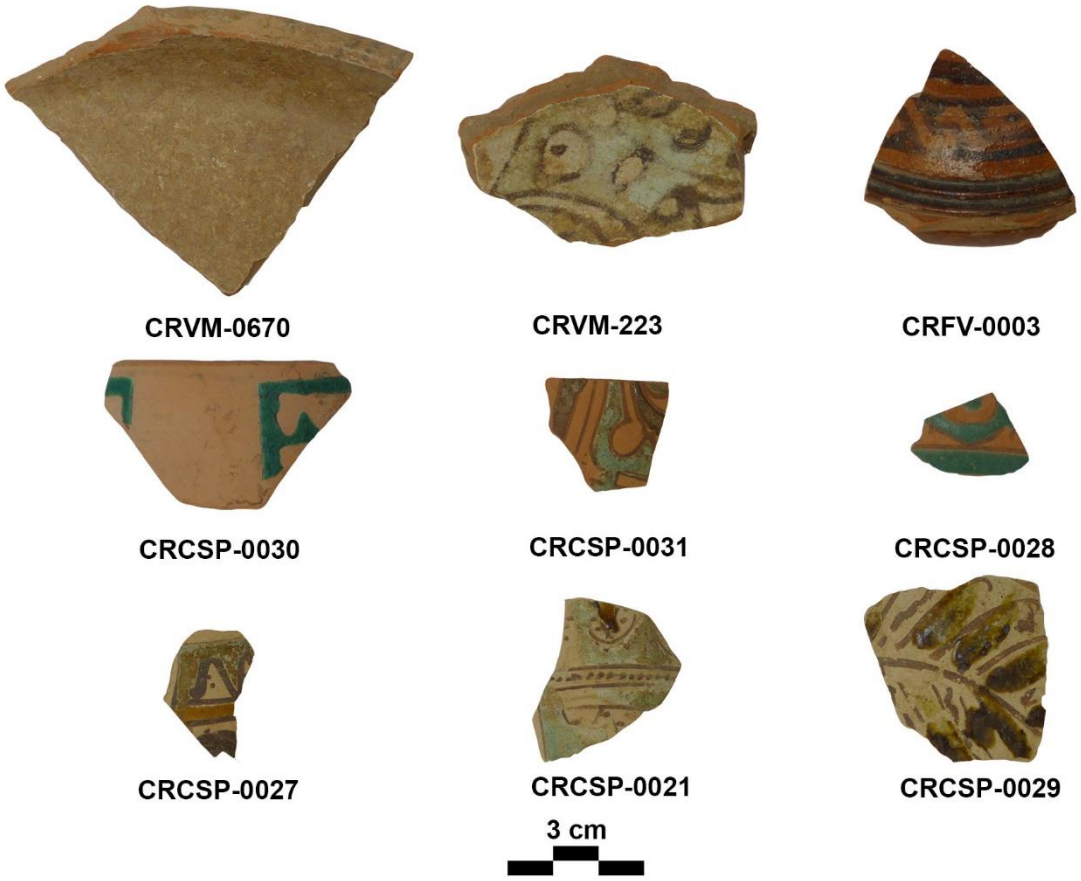

Figure 64 Picture of green and brown, honey and black and of partial corad seca ceramics from Mértola.

5.4.4 Analytical methods employed in this section

The analytical methods employed in this section are listed in Table 34. For a complete description of each technique and regarding instrumental conditions, detailed information can be found in chapter 4. Results not included in the section can be found in annexe 4 (Table 1 to 15, Image 1 to 13).

Table 34 List of the analytical methods employed in this section

Method		Samples analysed	Data table added as annex
Microscopy	*PLM*	All samples	Ceramic paste
	OM	Glazed samples	
	SEM-EDS	All samples and ceramic paste and glaze	Ceramic paste
Mineralogy	*XRPD*	All samples	
	µRaman	On a selection of samples	
Chemistry	*XRF*	All samples	Major oxides
	ICP-MS	All samples	Trace elements and REE

5.4.5 Results

5.4.5.1 Microscopy: PLM on ceramic thin sections

Ceramic paste characteristics are presented in annexe 4 (Table 2 to 4), while temper identification is presented in table 35.

Temper, porosity, and matrix evaluation evidenced two different clusters in the ternary plots presented in figure 65A/B. Kiln bars, the white-painted fragment and three samples of green and brown ceramics (CRVM-1659; CRVM-0670; CRVM-223) are more porous (6.11 to 13.78 %) and have more temper (11.97 to 21.65 %) if compared to the remanent decorated glazed ceramics (porosity 0.25 to 6.59 %, temper 1.53 to 14.12 %).

This preliminary classification evidenced a technological difference in the manufacturing of glazed ceramics. Different amounts of temper are used, depending on the characteristics of the clay raw material, to mitigate the ceramic body volume loss during firing. Thus, more temper was needed in the case of samples CRVM-1659/0670/223, probably due to specific characteristics of the clay.

If temper size and morphology are considered, a general trend can also be recognized on glazed ceramics compared to kiln rods and the white-painted sample. Temper is generally composed of silty grains with minor amounts of sandy ones.

Grain shape is variable, but in decorated samples, angular grains are less frequent. Moreover, in glazed samples, the maximum grain size is generally smaller (max 1100µm) if compared to kiln rods and the white-painted samples (max 5000µm).

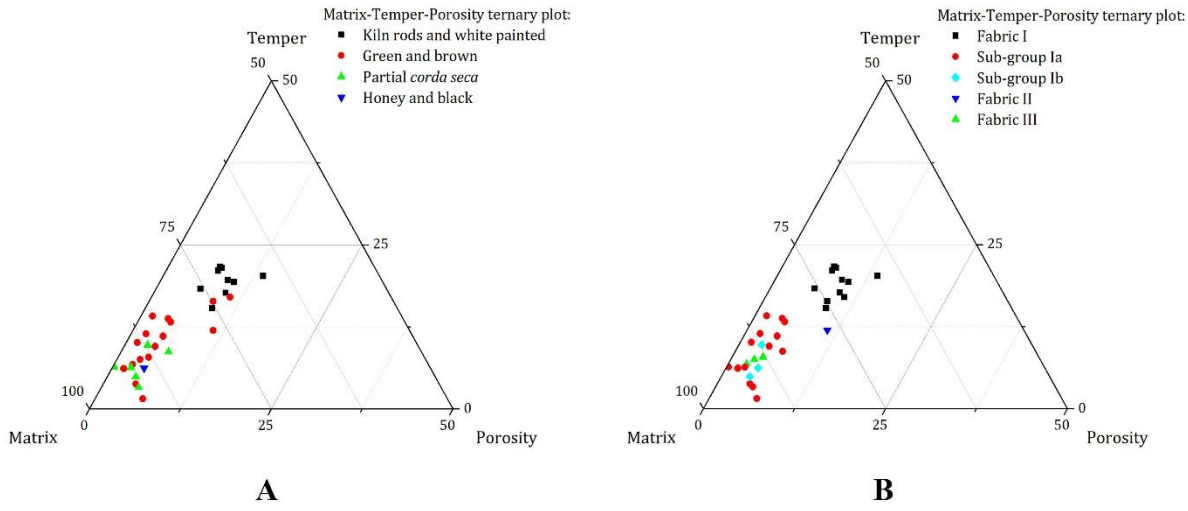

Figure 65 Ceramic paste ternary plot. Samples are classified by decorative style (A) and fabric (B). Temper and porosity percentage were evaluated by image analysis. Matrix percentage was calculated as the difference to 100% of temper plus porosity.

Grain size distribution is generally bimodal (Annex 4 - Table 2 to 4). Still, unimodal distribution has also been observed, especially on some green and brown and partial *corda seca* glazed samples from the Caliphal and Almohad periods. The colour of the ceramic paste is variable. Iron-rich ceramic pastes are generally red, while calcium-rich are generally buffy. Many ceramic pastes are also buffy-red.

These preliminary observations do not completely reveal samples variability, and basing on ceramic pastes characteristics and temper mineralogy, three different fabrics (I, II, III) and two subgroups (Ia, Ib) were identified by PLM. Fabric I and sub-groups Ia and Ib show identical temper characteristics, and the same minerals and rock fragments (i.e. quartize, slate, chert, graywake) were identified. Thus, sub-groups Ia and Ib are not new fabrics and they are included in fabric I, but they are slightly different in what texture concerns.

Fabric I (Fig. 66A) include eight kiln rods, the white-painted fragment and two green and brown samples (CRVM-223/0670). Ceramic pastes are red, moderately homogeneous, with abundant temper in all cases. The temper grain size distribution is generally bimodal, but on green and brown decorated samples is unimodal. Silicate minerals include quartz, muscovite, K-feldspar, plagioclase and rare green amphiboles. Amongst rock fragments, chert, slate, quartzite, and greywacke were identified. Lime-rich inclusions were also observed. They could appear as buffy inclusions (Type A) with thin and/or elongated or sub-rounded mineral inclusion. Alternatively, they could be present as isolated sub/well rounded brown nodules (Type B) suggesting limestone tempering. Secondary calcite might also be observed associated with lime-rich inclusion in both cases.

Sub-group Ia includes ten green and brown samples and three partial *corda seca* samples. Ceramic pastes are buffy-red or red, and one sample (CRVM-0357) has a slip below the glazed decoration (also identified by the observation of the polished cross section). The ceramic paste is more heterogeneous and enriched in small muscovite crystals. Sorting varies from moderate to well. Grog, glass fragments and lime-rich inclusions were also identified. Glass fragments appeared as greyish semi-transparent inclusions, sometimes with a bubble or a group of bubbles in the centre (Fig. 66C/F). Type A and B (Fig. 66B/D) lime-rich inclusions were identified, and the concentration of type B inclusions is higher on samples CRVM-1669/1671 suggesting lime tempering. Moreover, cloudy-grey sub-rounded/oval lime-rich inclusions (Type C) were also identified in samples CRVM-1666/1668 (Fig. 66E). On sample CRVM-1667, a marine green alga from the *dasicladaceans* family was also recognized. Secondary calcite could be observed associated with lime-rich inclusions.

Sub-group Ib includes the honey and black (CRVF-0003) sample and two partial *corda seca* style samples (CRCSP-0028/0031). Also, in this case, the ceramic paste is enriched in small muscovite crystals but, differently from sub-group Ia, ceramic pastes are red, moderately homogeneous, sorting is poor, and temper is generally more rounded. Glass fragments and type C–lime-rich inclusions (Fig. 66I) were identified. Moreover, a different kind of inclusion was observed in samples CRCSP-0031 and CRVF-0003, but it was not possible to establish its origin. These inclusion are generally anhedral, greyish/yellowsh in PPL and whitish in XPL (Fig. 66G/H).

Fabric II comprised only one green and brown sample CRVM-1659. The ceramic paste is buffy, enriched in lime, moderately homogeneous, and sorting is poor. The sample has a slip below the glazed decoration on both sides (also identified by the observation of polished cross-section). Inclusions are well rounded, especially quartz and feldspars, similar to what is expected for coastal sediment or aeolian sand. Silicate minerals comprise mainly quartz, rare muscovite, K-feldspar, plagioclase, and a crystal of clinopyroxene. Secondary calcite was observed within the porosity. Quartzite rock fragments were detected. A big glassy inclusion (Fig. 66L) and a big grog fragment were also identified.

Fabric III embrace three samples of green and brown ceramics and one sample of partial *corda seca* ceramic. The ceramic paste is buffy or buffy-grey (CRVM-1670), enriched in lime and homogeneous. In sample CRVM-1670, the colour of the ceramic paste suggests that it is not completely oxidized. Temper is moderately sorted and mainly includes quartz, K-feldspars, plagioclase, muscovite, biotite, amphibole (CRVM-1665), and secondary calcite within the ceramic matrix and in the pores. Amongst rock fragments (Fig. 66N), quartzite and muscovite/biotite-slates were identified. Grog and glass fragments (Fig. 66M) have also been observed.

Basing on the geological characteristic of the Mértola area, PLM analysis indicate that ceramics of fabric I and sub-fabric Ia and Ib were locally produced. The identification of similar rock fragments within the ceramic pastes (i.e. slate, quartzite, chert and greywacke) is compatible with the local geology, suggesting that similar raw materials were exploited to produce different ceramics during the Islamic period. Raw clay material was probably extracted in deposits associated with the *Baixo Alentejo Flysch* geological unit.

These observations confirm previously published data (Zozaya and Aparicio Yague, 2003). Different components were also added to the ceramic paste to produce glazed ceramics. This is testified by the heterogeneity of the ceramic matrix, with the identification of different

inclusions (i.e. lime rich and greyish/yellowish anhedral inclusion) and glass fragments, in two samples of fabric I (CRVM-223/0670) and sub-groups Ia and Ib.

Moreover, considering temper maximum grain size, sorting and the enrichment in small muscovite crystals, raw materials of sub-group Ia and Ib was more accurately decanted if compared to the fabric I. Besides, this effect is weak on green and brown samples CRVM-223/0670.

Fabric II and III are completely different, and they were probably imported to the town. In the case of fabric II temper morphology and mineralogy is similar to North African production from the area of Tunez (*Ifrīqiya*) (Capelli et al., 2011; Berti et al., 2009; Bonifay et al., 2002), suggesting that a typical coastal or aeolian sediment was added to the ceramic paste.

In the case of fabric III, ceramics provenance is doubtful. Nevertheless, ceramic paste and temper similarities have been observed in 14th to 16th century wall tiles produced in Malaga (Capelli et al., 2005), and in an Islamic lustre metallic ceramic sample from Pisa (Capelli et al., 2005), ascribed to the same area.

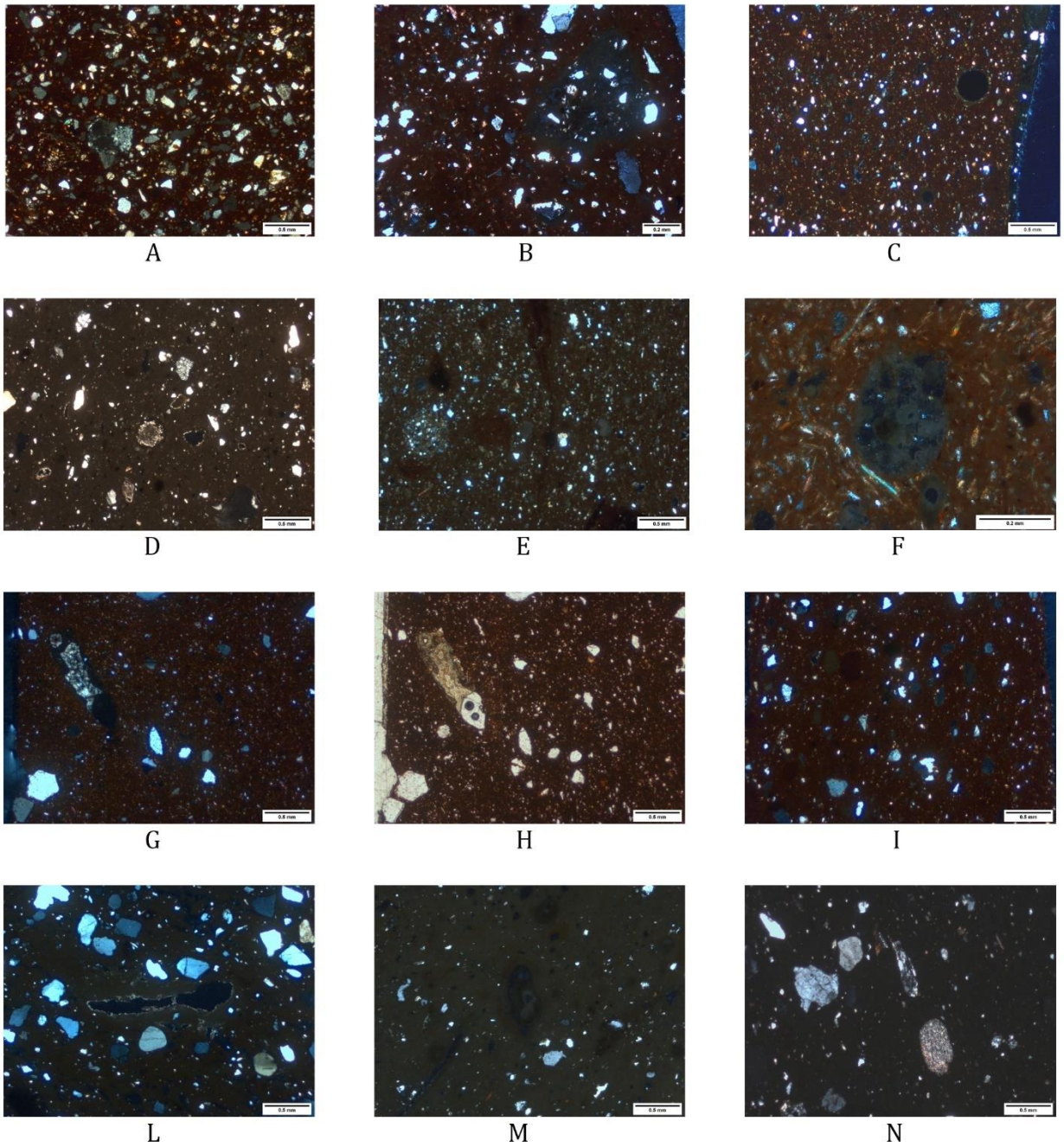

Figure 66 Picture of the ceramic samples collected at crossed nicols during PLM analysis. A) sample RDC-108-2014-0001 from fabric I; B) sample CRVM-642 from sub-group Ia with type A lime rich inclusion on the right side of the image; C) sample CRVM-0357 from sub-group Ia with some glass fragments on the right side of the image; D) sample CRVM-1671 from sub-group Ia with several type B lime rich inclusion (rounded and brown in color); E) sample CRVM-1668 from sub-group Ia with several type C lime rich inclusion (oval/sub-rounded greyish inclusion); F) sample CRCSP-0030 from sub-group Ia with several glassy inclusion with bobbles; G) sample CRVF-0003 from sub-group Ib with a big greyish/yellowish anhedral inclusion; H) sample CRVF-0003 from sub-group Ib, image of the big greyish/yellowish anhedral inclusion taken at parallel nicols; I) sample CRCSP-0028 from sub-group Ib with type C lime rich inclusions; L) sample CRVM-1659 from fabric II with a glassy inclusion at the center of the image; M) sample CRVM-1097 from fabric III with a glassy inclusion in the center of the image; N) sample CRVM-1665 from fabric III with a fragment of slate and quartzite in the center of the image.

Table 35 Ceramic samples Temper characteristics. Temper components: plagioclase (Pla), quartz (Q), potassium feldspar (Kf), biotite (Bio), muscovite (Mu), Calcite (Cal), oxides (Ox).

Samples	Fabric	Mineralogy	Rock fragments	Observations
RDC-108-2014-0001	I	Q, Kf, Pla, Mu, Amp, Sec. Cal	Slate Quartzite, Chert, Schist	Lime rich inclusions (Type B)
RDC-108-2014-0002	I	Q, Kf, Pla, Mu, Amp	Quartzite, Chert, Schist, Slate, Greywacke	
RDC-108-2014-0003	I	Q, Kf, Pla, Mu	Quartzite, Slate, Greywacke	Lime rich inclusions (Type B)
RDC-108-2014-0004	I	Q, Kf, Pla, Mu	Quartzite,Slate, Greywacke	
RDC-108-2014-0005	I	Q, Kf, Pla, Mu, Sec. Cal, Amp	Quartzite, Slate, Greywacke	Lime rich inclusion (Type B)
RDC-108-2014-0006	I	Q, Kf, Pla, Mu, Sec. Cal	Quartzite, Chert, Slate	
RDC-108-2014-0007	I	Q, Kf, Pla, Um, Amp	Quartzite, Chert, Slate, Greywacke	
RDC-108-2014-0008	I	Q, Kf, Pla, Mu, Amp, Sec. Cal	Quartzite, Chert, Slate, Greywacke	
R25A-02-SXV-94	I	Q, Kf, Pla, Mu	Slate, Quartzite, Greywacke	Lime rich inclusions (Type B)
CRVM-0357	Ia	Q, Pla, Mu, Ox	Quartzite, Chert	Clay paste rich in muscovite, Glass fragments, Slip below the glazed decoration
CRVM-623	Ia	Q, Pla, Mu, Ox, Sec. Calcite	Quartzite, Slate, Greywacke	Clay paste rich in muscovite, Glass fragments
CRVM-642	Ia	Q, Kf, Pla, Mu, Amp, Sec. Calcite	Quartzite, Greywacke	Clay paste rich in muscovite, Grog, Glass fragments, Lime rich inclusions (Type A)
CRVM-666	Ia	Q, Kf, Pla, Mu, Sec. Calcite	Quartzite, Chert, Slate, Greywacke	Clay paste rich in muscovite, Glass fragments
CRVM-1097	III	Q, Kf, Pla, Mu, Ox, Bio, Zircon	Quartzite, Muscovite/biotite Schist	Grog, Glass fragments
CRVM-1659	II	Q, Kf, Pl, Mu, Clino-prx, Sec. Cal	Quatzite	Grog, Glass fragments?, Slip below the glazed decoration
CRVM-1668	Ia	Q, Kf, Pla, Mu, Amp, Sec. Cal	Quartzite, Slate, Schist, Greywacke	Clay paste rich in muscovite, Lime rich inclusions (Type C), Grog
CRVM-1671	Ia	Q, Kf, Pla, Mu, Sec. Cal, Amp	Quartzite, Schist, Limestone, Chert, Greywacke	Clay paste rich in muscovite, Lime rich inclusions (Type B)
LVG-02-SXVIII-187	Ia	Q, Kf, Pla, Mu, Ox	Quartzite, Chert, Schist , Greywacke	Clay paste rich in muscovite, Glass fragments
CRVM-1665	III	Q, Kf, Pla, Ox, Mu, Bio, Amp	Quartzite, Muscovite/Biotite Schist	

Samples	Fabric	Mineralogy	Rock fragments	Observations
CRVM-1666	Ia	Q, Kf, Pla, Mu, Ox, Sec. Cal, Amp	Quartzite, Chert, Slate, Greywacke	Clay paste rich in muscovite, Lime rich inclusions (Type C)
CRVM-1670	III	Q, Kf, Pla, Ox, Mu, Bio	Quartzite, Muscovite/Biotite Schist	Glass fragment
CRVM-1667	Ia	Q, Kf, Pla, Mu, Sec. Calcite, Amp	Quartzite, Slate Schist, Greywacke	Clay paste rich in muscovite, Lime rich inclusions (Type A), Green *algae* (Dasycladaceans)
CRVM-1669	Ia	Q, Kf, Pla, Mu, Sec. Calcite, Amp	Quartzite, Schist, Slate	Clay paste rich in muscovite, Lime rich inclusions (Type B)
CRVM- 223	I	Q, Kf, Pla, Mu, Amp	Schist, Chert, Quartzite, Slate, Greywacke	Lime rich inclusions (Type A)
CRVM- 0670	I	Q, Kf, Pla, Mu	Quartzite, Schist, Chert, Greywacke, Slate	Lime rich inclusions (Type A), Grog, Glass Fragments
CRVF-0003	Ib	Q, Kf, Pla, Mu	Quartzite, Greywacke	Clay paste rich in muscovite, greyish/yellowish anhedral inclusion
CSP-0021	Ia	Q, Kf, Pla, Mu	Quartzite, Schist	Clay past rich in muscovite, Glass Fragments
CSP0027	Ia	Q, Kf, Pla, Mu	Quartzite	Clay paste rich in muscovite, Glass fragments
CSP0028	Ib	Q, Kf, Pla, Mu	Slate, Quartzite, Greywacke	Clay paste rich in muscovite, Lime rich inclusion (Type C)
CSP0029	III	Q, Kf, Pla, Mu, Bio, Sec. Cal.	Muscovite/Biotite Schist, Quartzite	Grog
CSP0030	Ia	Q, Kf, Pla, Mu	Quartzite, Greywacke	Clay paste rich in muscovite, Grog, Glass Fragments
CSP0031	Ib	Q, Kf, Pla, Mu	Quartzite, Slate	Clay paste rich in muscovite, Greyish/yellowish anhedral inclusion

5.4.5.2 Mineralogical composition: XRPD of ceramic samples

The results of XRPD analysis (Table 36) identified two different mineralogical groups (group 1 and 2). Samples of fabric I, including Ia and Ib sub-groups ceramics, can be in XRPD groups 1 or 2, but all samples from fabric II and III are in the XRPD group 2. In all cases, quartz is confirmed as the main mineralogical phase, with a variable concentration of feldspars (K-feldspars and plagioclases feldspars) and a minor amount of hematite. Muscovite/illite is almost always present. Amphibole was identified in some samples of groups 1 and 2.

Group 1 includes all kiln rods and the white-painted fragment from fabric I, the sample CSP-0030 from sub-group Ia, and samples CSP-0028 and CRVF-0003 from sub-group Ib. The group has consistent mineralogy with calcium-poor raw materials and quartz, feldspars, and hematite (probably formed during firing) were identified. On kiln rods and the white-painted fragment, the contribution of type B lime-rich inclusion to sample mineralogy is not significant, and calcite was never identified. Illite/Muscovite peaks were also detected, with some exception in the case of kiln rods. On samples, CSP-0030/0028 and CRVF-0003 hydroxyapatite (HAp) - $Ca_5(PO_4)_3(OH)$ and β-tricalciumphosphate (βTCP) - β-$Ca_3(PO_4)_2$ were also identified.

Most glazed samples were inserted in group 2, including two samples of green and brown ceramics from fabric I (CRVM-223/0670) and one sample of partial *corda seca* ceramics from subgroup Ib (CRCSP-0028). The mineralogical associations can be different, but Ca-rich mineralogical phases such as calcite, diopside, anorthite and gehlenite were always detected, accompanied by minor amounts of analcime and hematite. Diopside, gehlenite and Ca-rich plagioclases were newly formed high-temperature mineralogical phases included within the ceramic paste. Thus, in this group, a calcium-rich raw material has been chosen. As in group 1, HAp was identified on different samples (CRVM-0357/623/1659/1666 and LVG-02-SXVIII-187). But βTCP was not identified. Lead oxide was also identified on sample CRCSP-0027.

Considering that "geologic" apatite normally appears only as a minor phase in different rock (igneous/metamorphic/sedimentary), these results suggest that bone fragments and/or bone ash (i.e. organic apatite - HAp) was added to the ceramic paste, both on the group 1 and 2.

With regard to firing temperature, on group 1, the absence of mullite (Cultrone et al., 2014) and the presence of residual illite/muscovite peaks on XRPD patterns, which normally disappear at roughly 950 °C (Nodari et al., 2007; Maritan et al., 2006), suggest a firing temperature interval between 850 and 1000 ºC. In the case of group 2, illite/muscovite was identified, except for samples CRVM-1659, 1097 and CSP-0029. Diopside, anorthite, gehlenite normally appear from 800 °C onward (Jordán et al., 1999; Trindade et al., 2009; Heimann and

Maggetti, 2019). Thus, group 2 was probably fired in a temperature interval similar or slightly higher to group 1.

The identification of HAp and βTCP do not change firing temperature interpretation in both cases. When HAp is calcinated alone, it starts to dehydroxylate depending on the Ca/P ratio approximately from 750-900 °C (Tõnsuaadu et al., 2012), and it normally retains some hydroxyl group up to 1400 °C. This process leads to the formation of β-tricalciumphosphate – β-TCP/β-$Ca_3(PO_4)_2$ – lime and water. Nevertheless, when mixed with clay, HAp decomposition starts at 775 °C (Iqbal et al., 2000a; Iqbal et al., 2000b). At 900 °C, lime from HAp decomposition reacts with clay decomposition products and anorthite begins to crystalize. Normally, all HAp is totally decomposed for a temperature higher than 1200 °C, and only β-TCP is identified by XRPD .

Table 36 XRPD results table. Q, Quartz; H, Hematite; Dio, Diopside; Kf, Potassium-rich-feldspar; Pla, Plagioclase feldspars; Amp, Amphibole; Mu/Ill, Muscovite-illite; Ana, Analcime; Ca, Calcite; G, Gehlenite; Rut, Rutile; HAp, Hydroxyapatite; βTCP, β-Tricalciumphosphate. XXXX, very abundant; XXX, abundant; XX, moderate; X, scarce; Tr, traces.

Sample ref.	*Group*	*Fabric/subfabric*	*Chronology - century*	*Q*	*H*	*Dio*	*Kf*	*Pl*	*Ill/Mu*	*Amp*	*Ana*	*Ca*	*G*	*PbO*	*Rut*	*HAp*	*βTCP*
RDC-108-2014-0001	1	I	*11th-12th*	xxxx	Tr		x	xx	x								
RDC-108-2014-0002	1	I	*11th-12th*	xxxx	x		x	xx	x								
RDC-108-2014-0003	1	I	*11th-12th*	xxxx	x		x	xx	x	x							
RDC-108-2014-0004	1	I	*11th-12th*	xxxx	x		x	xx	x								
RDC-108-2014-0005	1	I	*11th-12th*	xxxx	x		xx	x	x								
RDC-108-2014-0006	1	I	*11th-12th*	xxxx	x		x	x	Tr								
RDC-108-2014-0007	1	I	*11th-12th*	xxxx	x		x	xx	xx	x							
RDC-108-2014-0008	1	I	*11th-12th*	xxxx	x		x	xx	Tr	Tr							
R25A-02-SXV-94	1	I	*1st half 13th*	xxxx	x		x	x									
CRVM-0357	2	Ia	*2nd half 10th - early 11th*	xxxx	x	xx	xx	xx	xx			x	x			Tr	
CRVM-623	2	Ia	*2nd half 10th*	xxxx	x	xxx	x	xx	x		x		xx			x	
CRVM-642	2	Ia	*11th*	xxxx	x	xx	x	xx	x				x				
CRVM-666	2	Ia	*2nd half 10th*	xxxx	x	xx	x	xx	x				xx				
CRVM-1097	2	III	*11th*	xxxx	x	xxx	x	xx	Tr		xx		x				
CRVM-1659	2	II	*11th*	xxxx	xx	xx	xx	xx					xx			x	
CRVM-1668	2	Ia	*11th*	xxxx	x	xx	x	xx	xx			xx	xx				
CRVM-1671	2	Ia	*11th*	xxxx	x	xx	x	xx	x			xx	xx				
LVG-02-SXVIII-187	2	Ia	*11th*	xxxx	x	xx	x	x	x				xx			x	
CRVM-1665	2	III	*1st half 12th*	xxxx	x	xx	x	xxx	x		x		tr				
CRVM-1666	2	Ia	*1st half 12th*	xxxx	x	xx	xx	xx	x				xx			x	
CRVM-1670	2	III	*1st half 12th*	xxxx	x	xx	xx	xx	x				tr				
CRVM-1667	2	Ia	*2nd half 12th*	xxxx	x	xx	xx	xx	x				xx				
CRVM-1669	2	Ia	*2nd half 12th*	xxxx	x	x	x	x	xx			xx	x				
GRVM-0670	2	I	*1st half 12th*	xxxx	x	x	xx	x	xx			x	x				

Sample ref.	*Group*	*Fabric/subfabric*	*Chronology - century*	*Q*	*H*	*Dio*	*Kf*	*Pl*	*Ill/Mu*	*Amp*	*Ana*	*Ca*	*G*	*PbO*	*Rut*	*HAp*	*βTCP*
CRVM-223	2	I	*2nd half 12th*	xxxx	x	x	xx	x	x			x	x				
CRCSP-0030	1	Ia	*12th*	xxxx	x		x	xx	xx							x	x
CRCSP-0031	2	Ib	*12th*	xxxx		x	x	xx	x	x	x				x		
CRCSP-0028	1	Ib	*12th*	xxxx	x		x	x	x		x				x	Tr	Tr
CRCSP-0027	2	Ia	*12th*	xxxx	x	xx	tr	xx	x			x	xx	x			
CRCSP-0021	2	Ia	*12th*	xxxx	x	xx	x	xx	x			tr	xx			x	
CRCSP-0029	2	III	*12th*	xxxx	x	xx	tr	xx		x	x	x	xxx				
CRVF-0003	1	Ib	*End 12th – beginning 13th*	xxxx	x		xx	xx	xx							Tr	Tr

5.4.5.3 Chemical composition: XRF and ICP-MS results

XRF and ICP-MS results are presented in annexe 4 (Table 5 to 13). According to the classification proposed by Heimann and Maggetti (2019), the ceramic sample compositions were plotted in the SiO_2, Al_2O_3 and CaO+MgO triangular space (Fig. 67A/B). The triangular space is a "forecast" of the mineralogical assemblage, which can appear after the firing process at 950 °C, considering the chemical composition of the samples. As expected after XRPD analysis, all glazed samples included in group 2 are comprised in the lime-rich area (Quartz-Anorthite-Diopside/Wollastonite). On the contrary, samples from group 1 are plotted in the lime-poor area (Quartz-Anorthite-Mullite).

This difference is diagnostic because the concentration of CaO in the ceramic paste determines the formation of new Ca-rich mineralogical phases during the firing process, completely lacking in the lime-poor samples (see XRPD section, 5.4.5.2).

It is evident a specific technological choice to produce green and brown, and some of the partial *corda seca* glazed ceramics using a CaO rich raw material. This predisposition has been already documented in Islamic Iberia (Molera et al., 2001; Peréz-Arantegui et al., 1999; Déléry, 2006; Chapoulie et al., 2005) and more generally in the Islamic world (Tite et al., 1998).

The formation of lime (i.e. CaO) is normally due to the decomposition of calcite, which acts as a fluxing agent, and it favours the ceramic body sintering (Noll and Heimann, 2016) improving the ceramic paste mechanical properties (Nodari et al., 2007). Moreover, a high concentration of lime in the ceramic paste produces a lighter ceramic body (Molera et al., 1998).

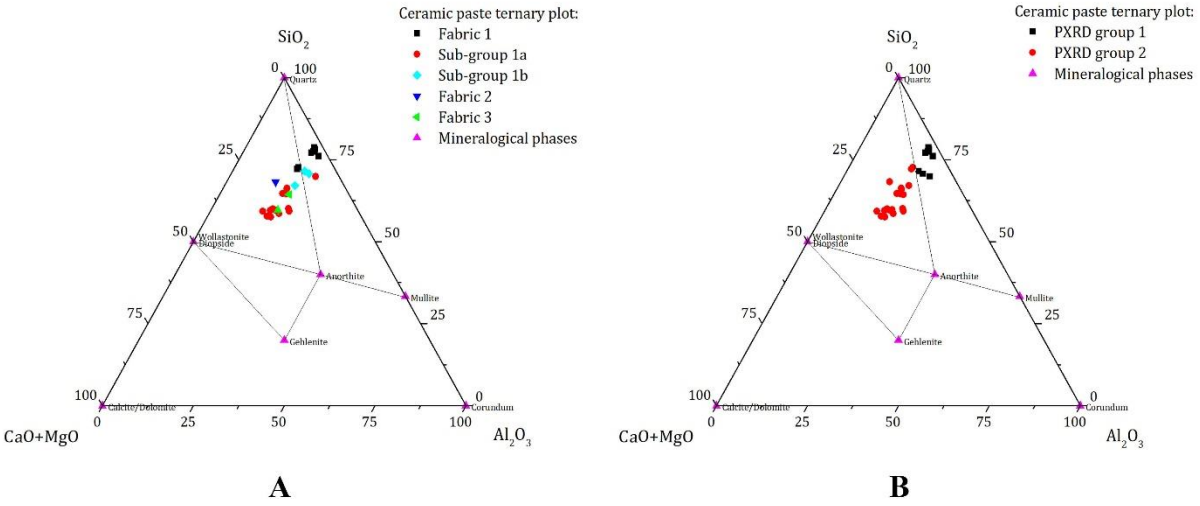

Figure 67 *Ternary phase diagram SiO2, Al2O3 and CaO+MgO. The area between Quartz-Anorthite-Mullite positions is considered lime poor/non calcareous. The area comprised between Quartz-Anorthite-Diopside/Wollastonite is considered lime rich/calcareous; the area comprised between Diopside/Wollastonite-Anorthite-Gehlenite is considered very lime rich. Samples are classified basing on fabrics/sub-groups (A) and by XRPD groups (B).*

The presence of lime also reduces the risk of crazing especially when used in combination with tin opacified lead-alkali glazes (Tite et al., 1998). Nevertheless, some of the samples of sub-group Ia, even with a significant concentration of CaO, present a red or buffy-red ceramic paste.

On kiln rods and the white-painted sample, P_2O_5 concentration is generally lower than 0.38 wt% (RDC-108-2014-0001). On the contrary, on glazed samples, it varies between 0.29 wt% (CRVM-0670) and 11.40 wt% (CRCSP-0030), and 9 out of 23 samples from different fabrics and sub-groups have a concentration higher than the 1.84 wt% (Annexe 4, Table 5, 6, 7). A low concentration of P_2O_5 would suggest environmental sample contamination during burial (Molera et al., 2001c). Besides, in several cases, chemical analyses may support the identification of HAp and βTCP by XRPD (Table 36) in several samples, pointing to the addition of bones (or bone ashes) to the ceramic paste.

Thus, XRPD and XRF results suggest that glazed sample ceramic pastes could also be tempered using bones in addition to limestone (i.e. suggested during PLM analysis). They can contribute to CaO (limestone, bones) and P_2O_5 (bones) concentration of sample ceramic pastes. The mixing proportion of these two components is not clear, but the binary plot CaO *vs* P_2O_5 (Fig. 68A) seems to indicate that they could be mixed together and added or included alone. Microanalysis will be important to clarify this technological aspect.

In the case of PbO, the maximum concentration on kiln rods and the white-painted fragment was 0.144 wt% (RDC-108-2014-0007). In glazed decorated ceramics, PbO concentration varies between 0.127 wt% (CSP-0030) and 1.161 wt% (CRVM-623/1665). Even if the glazed decoration was accurately removed using an automatic straight grinder with a diamond tip, PbO was detected in many glazed samples. When PbO concentration is low, it can be the result of incomplete removal of the glaze during sample preparation.

On the contrary, if PbO concentration is higher, it might support PLM observation (i.e. glass fragments identification), pointing to a volunteer addition of PbO rich component (i.e. probably a lead rich frit/glass) to the ceramic paste. If it is the case, considering the PbO contribution to samples chemical composition, ceramic bodies could be classified as proto-stone-paste (Mason and Tite, 1994). Moreover, the binary plot presented in figure 68B suggests that bones (or bone ashes) could also be mixed with glass/frit.

The binary plot presented in figure 68C (K_2O *vs* Na_2O) evidence that ceramic samples from fabric II and III are depleted in K_2O (below 1.72 wt%) and enriched in Na_2O (above 0.85 wt%). So, in the case of fabric II and III K_2O/Na_2O ratio is significantly smaller (< 1.3) than in fabric I including sub-group Ia and Ib (>1.7). This indicates that in samples of fabric I and sub-group Ia and Ib, the amount of K bearing mineralogical phases (i.e. Muscovite/Illite/K-

Feldspar) is higher, indicating the use of different raw materials if compared to fabric II and III. This is also testified by the linear correlation between K_2O and Th, Rb, Cs, which may substitute K^+ ions within the same mineralogical phases.

K_2O wt% difference between samples of fabric I and sub-group Ia and Ib is probably the result of different raw material treatment and the consequent modification of clay/temper ratio. This tendency was also evidenced during PLM analysis, and smaller temper grain sizes characterized glazed samples (mainly with Ia and Ib sub-groups). The evaluation of Na_2O *vs* Fe_2O_3 (Fig. 68D) and Na_2O *vs* Al_2O_3 binary plots also point to the exploitation of different clay raw-materials enriched in Na_2O in the case of fabric II and III.

Moreover, samples are also sensitive to CaO/MgO ratio (Fig. 68E). Basing on K_2O concentration and CaO/MgO ratio, the plot clearly distinguishes all fabrics and sub-groups. The only ceramic samples which plot in a different field (i.e. on Ia sub-group filed) are the green and brown samples CRVM-223/0670 from fabric I because of the slightly higher CaO concentration. The modification of the CaO/MgO ratio in samples included in fabric I, sub-groups Ia and Ib is coherent with the addition of a CaO-rich component as suggested in the PLM section.

These results indicate that three different components could be added to samples ceramic paste, including bones (or bone ashes), glass/frit fragments and limestone. This technological solution is particularly evident in fabric I samples and in sub-group Ia and Ib samples. Besides, considering that the *Baixo Alentejo Flysch* geological unit is generally poor in CaO, Islamic ceramists from Mértola dopped the local raw material because it was probably not suitable to produce green and brown and partial *corda seca* glazed ceramics. Nonetheless, some samples included in fabric II and III show similar charcatristic, suggesting a technological transfere between different places.

For what concern REE (Rare Earth Chemical Elements), all samples present a negative Eu_{CN} anomaly suggesting Eu fractionation at the source in each case. Ce_{CN} anomaly is small and/or absent. The plot presented in figure 68F shows the mean REE_{CN} profile of each fabric/sub-group. The mean profiles of fabric I and sub-group Ia and Ib are generally more abundant in REE_{CN}. As soon the CaO concentration increase, REE_{CN} concentration decrease as evidenced on fabric II and III patterns.

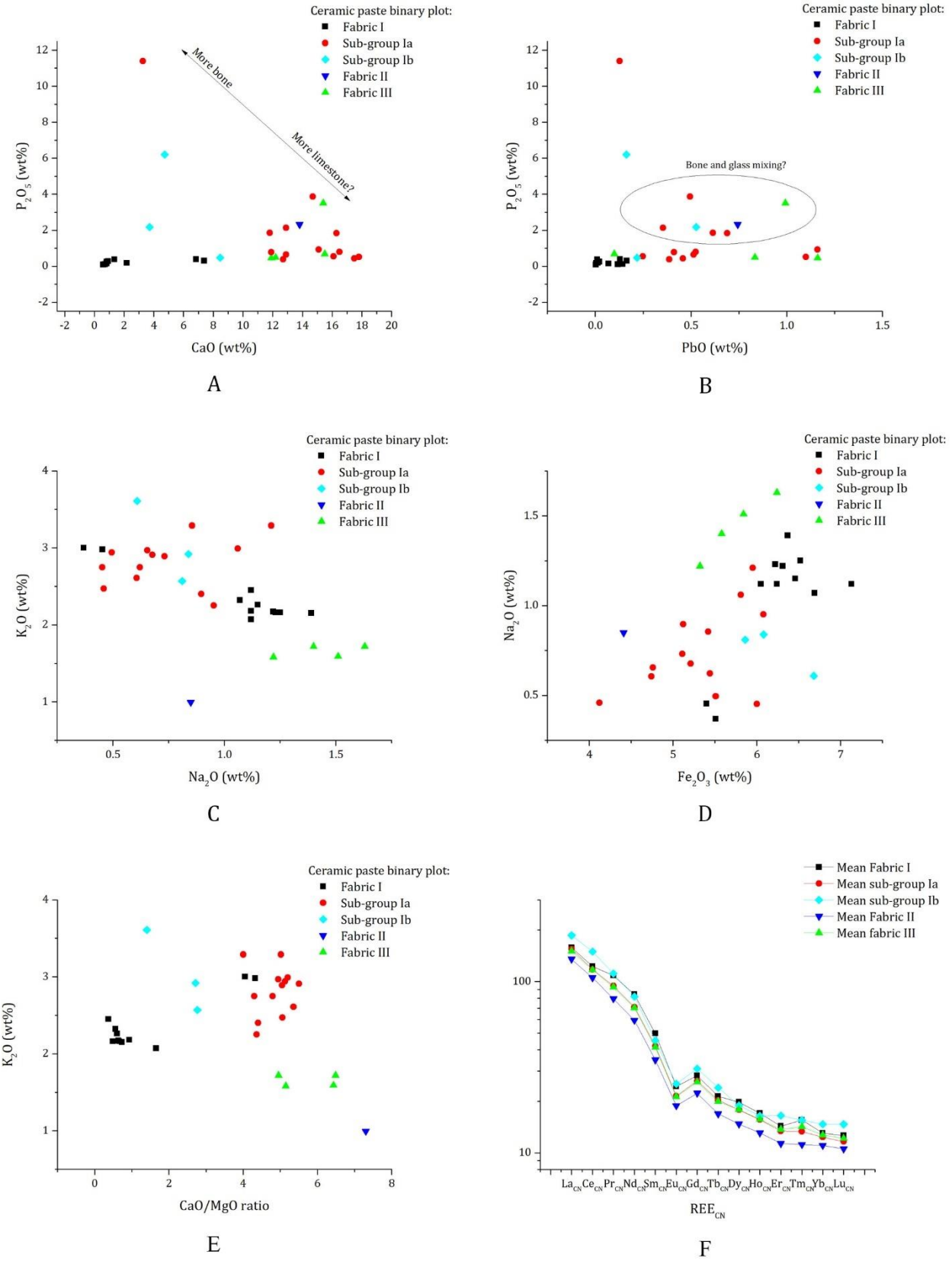

Figure 68 A) Binary plot P_2O_5 vs CaO, B) binary plot P_2O_5 vs PbO, C) binary plot Na_2O vs K_2O, D) binary plot Na2O vs Fe_2O_3, E), K_2O vs CaO/MgO binary plots and F) REE_{CN} mean pattern of the ceramic samples. Samples are divided by fabrics and sub-groups identified during PLM analysis

5.4.5.4 Microscopy and mineralogical analysis: SEM-EDS and µRaman spectroscopy

SEM-EDS and Raman spectroscopy analysis have been developed to complement PLM observations and to determine temper, clay matrix, slip, glass/frit fragments and lime-rich inclusion characteristics. After XRPD and XRF analysis, special attention had been paid to the distribution of CaO, PbO and P_2O_5 in samples ceramic pastes. Much of the features reported were previously observed by PLM, and table 37 is the final result of PLM plus SEM-EDS observations. Some of the features were classified as glass fragments (i.e. all kinds of glass – frit fragments, vitrified) or lime-rich inclusions during PLM analysis. SEM-EDS analysis reveals new chemical and morphological characteristics, unvisibles during PLM.

For example, the cloudy, semi-transparent and/or greyish glass fragments could be enriched PbO, composed by CaO and P_2O_5, or enriched in all these oxides.

Moreover, in the case of CaO and P_2O_5 areas, a distinction has been made based on size and position in the ceramic matrix. Consequently, some areas were classified "wide" when CaO and P_2O_5 were included in extended portions of the ceramic paste; "delimited" when oxides were concentrated in smaller and restricted areas (i.e. isolated inclusion); or "lisp" when it was located in between the ceramic paste and the glaze.

Part of the results obtained by SEM-EDS analyses of the ceramic paste are presented within this section (Fig. 71 to 75; Table 38 to 41). Data not presented in this section are summarized in the annex number 4 (Table 14, Image 1 to 13). Annexed files present the micro-structural and chemical analysis results of different features and PLM classification. Table 14 of annex 4 also specifies when PLM classification was confirmed or not by micro-analysis. SEM-EDS was also utilized to study glazed decorations. In this case, chemical data are presented in this section. µRaman spectroscopy was applied when possible for the identification of specific inclusion both in the ceramic paste and on glazed decorations.

Table 37 Summary table of the features analysed, and final classification resulted following SEM-EDS micro-analysis. Some of them are presented within the text and they are underlined. Those features identified during PLM analysis are reported in italic and bold. Greysih/yellowish anhedral inclusions are represented by GYA in the table.

Sample	Fabric/ Sub-group	XRPD group	Grog	Frit fragments	Alkaline glass	Partially digested glass	$PbO-SiO_2$ glass	$PbO-SiO_2-SnO_2$ glass	CaO and P_2O_5 rich areas: Wide/delimited	Vitrified, or not, bone fragment	Lime-rich Inclusion Type
CRVM-0357	Ia	2				1 $PbO-SiO_2$; 1 $PbO-SiO_2-SnO_2$	3 (1 with bone)	***1***	***Slip***	***Vitrified***	
CRVM-623	Ia	2				***2 ($PbO-SiO_2$)***			Wide - delimited		
CRVM-642	Ia	2				1 $PbO-SiO_2-SnO_2$			Wide		***Type A***
CRVM-666	Ia	2							***Delimited***		
CRVM-1097	III	2		1 (alkali)		2 $PbO-SiO_2$			***Delimited***		
CRVM-1659	II	*2*	***X***						***Wide – delimited - slip***		
CRVM-1665	III	2			1 Silica-alkali						
CRVM-1666	Ia	2						***1 (whit bone)***	Delimited	Bone fragment	***Type C***
CRVM-1667	Ia	2	X				1	1			***Type A***
CRVM-1668	Ia	2				1 $PbO-SiO_2$; 1 $PbO-SiO_2-SnO_2$			Delimited	***Vitrified***	***Type B, Type C***
CRVM-1669	Ia	2									***Type B***
CRVM-1670	III	2			2 lime rich ***(1)***						
CRVM-1671	Ia	2				2 $PbO-SiO_2$		1			***Type B***
LVG-02-SXVIII-187	Ia	2					2 with bone ***(1)***	***1***	Wide	Bone fragment	
CRVM-0670	I	2					1	1 (with bone)			***Type A***
CRVM-223	I	2				1 $PbO-SiO_2$	2			Bone fragment	***Type A***
CRCSP-0021	Ia	2				1 $PbO-SiO_2$; 2 $PbO-SiO_2-SnO_2$			Wide, ***delimited***		
CRCSP-0027	Ia	2								2 Vitrified ***(1)***	
CRCSP-0028	Ib	1								2 Vitrified	***Type C***
CRCSP-0030	Ia	1							Wide	***Vitrified***	***Type C***
CRCSP-0031	Ib	2				1 $PbO-SiO_2$	2 (1 with bone)				***GYA***
CRVF-0003	Ib	1							***Wide***		***GYA***

5.4.5.4.1 Ceramic paste

As temper grains, mainly sand and silt, it was possible to identify muscovite, biotite, rare amphibole (Fe and Ca-rich), quartz, potassium-rich feldspars, sodium-rich plagioclase, and less frequently calcium-rich plagioclase (Fig. 69). Feldspars compostion is compatible with felsic or intermediate rocks. Among micro-sized silty inclusions, ilmenite, titanium oxides, iron oxides, barite, monazite, and zircon were observed. On fabric I and sub-groups Ia and Ib, ilmenite crystals are frequently enriched in manganese.

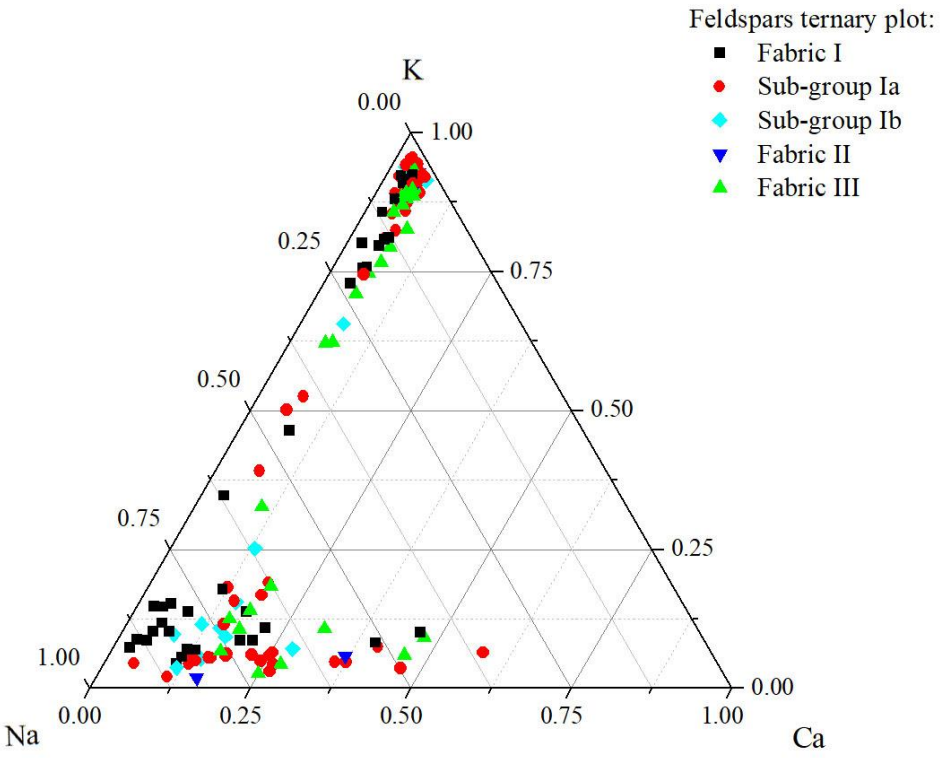

Figure 69 Feldspars ternary plot, results obtained by SEM-EDS.

Elemental mapping evidenced differences in ceramic paste characteristics on fabrics and sub-groups. Similar features were observed on ceramic samples of fabric I, including sub-group Ia and Ib. On the contrary, samples of fabric II and III are different, supporting the hypothesis they have a different origin (i.e. imported to Mértola).

Fabric I

On samples included in fabric I, Fe_2O_3 is evenly distributed in the clay matrix and usually associated with MgO, K_2O and Al_2O_3. The only exceptions are the green and brown samples CRVM-223/0670. These samples have lower Fe_2O_3 and higher CaO concentrations than kiln rods and the white-painted fragment of the same fabric, as evidenced by XRF spectroscopy. Nonetheless, SEM-EDS evidenced that CaO is partially included in the ceramic matrix and in

type A lime-rich inclusion. They appear as unmixed clay nodules with temper, and CaO concentration may be as high as 21.54 wt% (Annexe 4, Image 12D, 13B and Table 14).

Moreover, on sample CRVM-223, CaO is also hosted by several small and spongy inclusions, where it is associated with P_2O_5 (Fig. 70A, Table 38). Based on morphology and chemical composition, they were classified as bone fragments. This technological option is new in Islamic Iberia, and the introduction of bones (or bone ashes) fragments in the ceramic paste is not common in the Islamic world. At the moment, in Europe, it is just documentd for the production of 18th century bone-ash/bone china ceramic (Tite and Bimson, 1991).

Glass fragments were also identified in the ceramic paste. They could be almost intact and with slightly straight edges, or partly digested and absorbed in the ceramic body during the firing process. The analysis of a digested glass fragment of sample CRVM-223 evidenced that PbO and SiO_2 were the main components of the glass, and a significant concentration of Al_2O_3 and CaO was detected. In addition, the clay matrix that surrounds the relic glass generally shows continuous vitrification due to the interaction with the glass, and it has lighter colour on BSE images indicating that some PbO diffused in the ceramic body (Fig. 70B, Table 38).

The presence of SnO_2 distinguishes some unaltered glass fragments. If SnO_2 is not present, PbO and SiO_2 are the main components, and a significant concentration of CaO can be present (Annexe 4, Image 12E, 13C and Table 14). On sample CRVM-0670, a Pb-SiO_2-SnO_2 glass fragment was identified below the ceramic-glaze interface, with a bone fragment inside (Annex 4, Image 12F and Table 14).

These observations clearly point to different raw material mixing in the green and brown samples included in fabric I. Moreover, the identification of a bone fragment inside a glass fragment indicates te that bones were also utilized in some stage of the glaze fritting process of tin opacified glazes. In any case, there are no doubts that elements from glaze/making were included in the paste, but they were in a minor amount if compared to temper and clay. Thus ceramic bodies of samples CRVM223/0670 has very similar characteristics to typical proto-stone-paste ceramic bodies produced in the Middle East (Mason and Tite, 1994). These observations indicate that local raw materials were not suitable to produce decorated glazed ceramics. So, the local ceramist adapted to the availability of the raw materials.

Sub-group Ia

On ceramic samples included in sub-group Ia CaO concentration is higher, as evidenced by XRF results, but it is not evenly distributed in the paste and it can be associated with P_2O_5

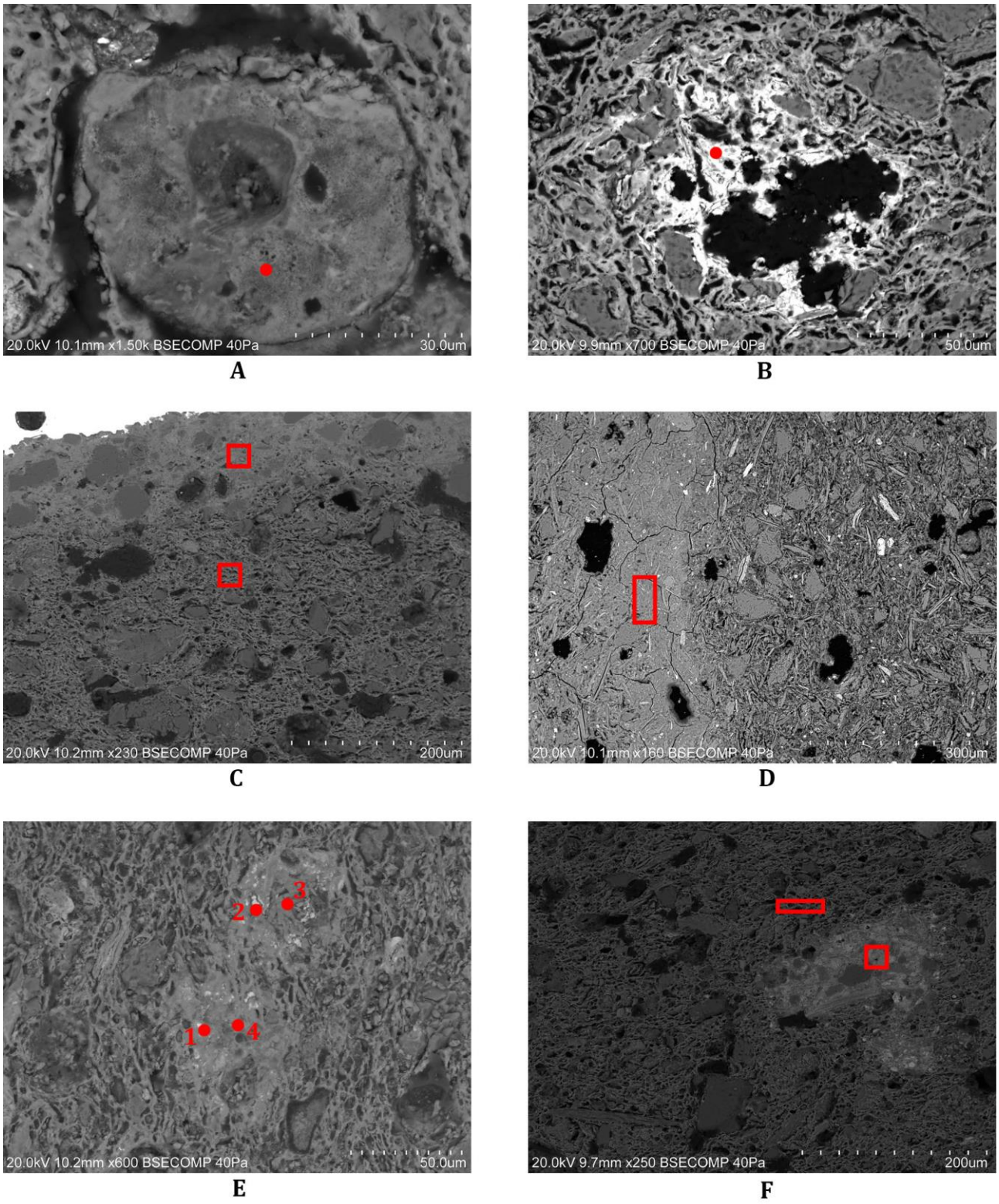

Figure 70 Backscattered images of the analyzed samples. Spot and area analysis are evidenced by red spots or squares, respectivelly. A) Bone inclusion in the ceramic matrix of sample CRVM-223; B) Partly melted and digested glass fragment in the ceramic matrix of sample CRVM-223; C) Slip layer identified on sample CRVM-0357; D) Vitrified ceramic matrix observed in the sample CRCSP-0030; E) Relics of a melted and digested inclusion on sample CRVM-666; F) Raw material with different characteristics identified on sample CRVM-623.

Table 38 Chemical data obtained by SEM-EDS of spots and areas analyses of figure 70. Results normalized to 100%, uncertainty 1σ.

Sample	PLM classification	Figure	Feature	Spot/area analysed	Na_2O	MgO	Al_2O_3	SiO_2	P_2O_5	K_2O	CaO	TiO_2	MnO	FeO	CuO	PbO
CRVM-223		71A	Bone fragment	Centre of the particle	0.16	6.91	17.57	24.21	14.72	1.56	25.13	1.26		8.49		
CRVM-223		71B	Partially absorbed glass fragment, fr. 16	Residual glass	0.95	1.47	14.72	47.37	0.17	2.17	7.28	1.07		3.91		20.89
CRVM-0357	Slip	71C	Slip	Slip layer	1.54	2.15	14.59	34.81	7.54	2.37	22.92	0.55	0.62	5.59	0.79	6.53
CRVM-0357		71C	Slip	Ceramic matrix	1.99	2.81	18.39	49.50	0.54	3.46	12.48	0.91		6.51		3.40
CRCSP-0030		71D	CaO and P_2O_5 rich area - wide, n. 17	CaO and P_2O_5 rich area	1.05	0.39	20.35	40.11	22.01	3.10	7.06	1.00		4.93		
CRVM-666	Glass	71E	CaO and P_2O_5 rich area - delimited, n. 6	Spot 1	0.92	2.94	6.31	32.98	10.54	1.87	22.71	0.81		1.73		19.20
CRVM-666		71E	CaO and P_2O_5 rich area - delimited, n. 6	Spot 2	1.25	2.51	2.57	12.66	17.99	3.41	36.51	0.80		1.78		20.52
CRVM-666		71E	CaO and P_2O_5 rich area - delimited, n. 6	Spot 3	0.00	2.31	3.19	9.41	0.64		82.44			2.01		
CRVM-666		71E	CaO and P_2O_5 rich area - delimited, n. 6	Spot 4	0.31	5.96	11.56	47.20	0.60	4.67	18.88	2.43		2.70		5.69
CRVM-623		71F	CaO and P_2O_5 rich area - delimited, n. 3	Ceramic matrix	1.39	3.30	17.71	46.06	0.21	2.07	18.43	1.18	0.26	6.79		2.60
CRVM-623		71F	CaO and P_2O_5 rich area - delimited, n. 3	CaO and P_2O_5 rich area	0.67	1.47	7.56	16.02	19.74	0.84	39.76	0.42	0.86	3.02		9.65

and/or PbO (Table 37), showing different characteristics. On sample CRVM-0357, a 170 µm thick slip layer, very rich in CaO and P_2O_5, was identified on the decorated side of the fragment (Fig. 70C, Table 38) associated with SiO_2 and Al_2O_3. Thus, a CaO and P_2O_5 rich raw material was mixed with some clay and applied on the ceramic surface before glaze application.

CaO and P_2O_5 rich areas were identified in 10 out of 13 ceramic samples included in the sub-group. They could be homogeneously distributed in wide portions of the matrix (5 cases, Table 37), and the ceramic body could also be completely vitrified by the firing process (Fig. 70D, Table 38). This suggests the use of a different raw materials. Moreover, CaO and P_2O_5 rich areas were also observed in delimited portion of the ceramic paste (5 cases, Table 37). They could have diffeuse limits and be vetrified around (Fig. 70E, Table 38), suggesting that the original particles were almost totally digested. Sometime, delimited CaO and P_2O_5 rich domains are complex and associated with temper and clay (Fig. 70F, 71A– Table 38, 39), or just with temper (Fig. 71B– Table 39), or they were concentrated in specific isolated inclusions (Fig. 71C, Table 39). From the morphological point of view, the inclusion (Fig. 71C, Table 39) does not show any porosity, and it looks completely vitreous with a series of concentric bands[83].

CaO concentration is also significant in lime-rich inclusion (Type A, B, C – Table 37). On a type A lime rich inclusion identified on sample CRVM-642 (Fig. 66B), SEM-EDS identified a vitrified inclusion identical to that described in figure 71C, and invisible during PLM observations (Fig. 71D). Inclusion spot analysis (Table 39) revealed that the concentration of CaO and P_2O_5 is very high. In addition, µRaman spectroscopy identified the *v1* $(PO_4)^{-2}$ vibrational mode at 961 cm^{-1}, typic of organic apatite (Penel et al., 1998). Thus, all particles with similar characteristics can be classified as bone relics[84].

Type B lime-rich inclusions were abundant on sample CRVM-1669/1671 after PLM observations. The elevated CaO concentration (as high as 79 wt%, Annexe 4 Table 14) supports the hypothesis of limestone tempering advanced during PLM observations (Fig. 66D).

Type C lime-rich inclusions (Fig. 66E) were heterogeneous, enriched in P_2O_5 and bone fragments could be found inside (Fig. 71E/F, Table 39). Bone fragment morphology (i.e. spongy) is very similar to those observed on sample CRVM-223 from fabric I (Fig. 70A), and similar particles were also identified dispersed in the ceramic paste of different green and brown and partial *corda seca* decorated samples (Annex 4, Image 6, 9C/D/E/F, 10F, Table 14).

[83] Similar inclusions were also observed during SEM-EDS analysis on samples CRVM-0357 and CRCSP-0021/0027/0028 (Annexe 4, Image 1D, 10A/F, 11A/B, Table 14).

[84] The vitreous inclusion observed in sample CRVM-642 has identical characteristics to the inclusions identified during SEM-EDS analysis in different samples listed in the footnote number 83.

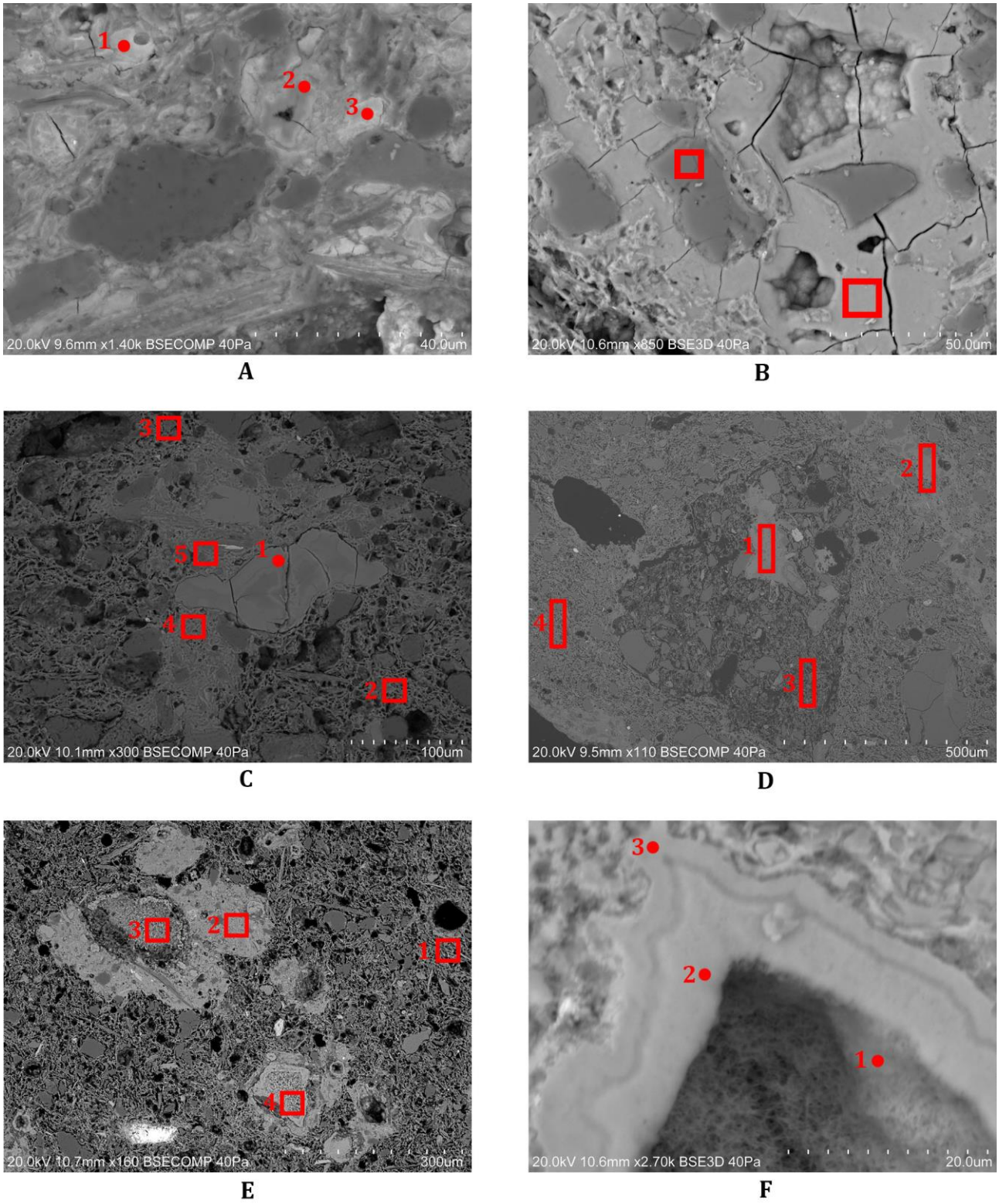

Figure 71 Backscattered images of the analyzed samples. Spot and area analysis are evidenced by red spots or squares, respectivelly. A) Magnified area of the image 8A of sample CRVM-623; B) Vitrified CaO and P_2O_5 rich area identified on sample CRVM-1666; C) CaO and P_2O_5 rich area identified on sample CRVM-1668 with a vitrified inclusion in the center of the image; D) Type A lime rich inclusion on sample CRVM-642 (Fig. 67B), a vitrified triangular particle is visible in the upper part of the inclusion; E) Type C lime rich inclusion on sample CRVM-1666, different spongy particles can be seen in the upper and bottom part of the image; F) Magnified image of a spongy particle (i.e. bone) observed in the bottom part of image E, sample CRVM-1666.

Table 39 Chemical data obtained by SEM-EDS of spots and areas analyses of figure 71. Results normalized to 100%, uncertainty 1σ.

Sample	PLM classification	Figure	Feature analysed	Spot/area analysed	Na_2O	MgO	Al_2O_3	SiO_2	P_2O_5	K_2O	CaO	TiO_2	MnO	FeO	PbO
CRVM-623		72A	CaO and P_2O_5 rich area - delimited, n. 3	Spot 1	0.56	1.15	5.74	13.40	23.22	1.10	34.09	0.56		1.56	18.63
CRVM-623		72A	CaO and P_2O_5 rich area - delimited, n. 3	Spot 2	0.67	0.92	3.99	9.94	28.76	1.13	42.97	0.93		1.83	8.87
CRVM-623		72A	CaO and P_2O_5 rich area - delimited, n. 3	Spot 3	0.94	1.41	5.63	12.04	22.86	1.09	33.47	0.67		2.08	19.81
CRVM-1666		72B	CaO and P_2O_5 rich area - delimited, n. 12	Vitrified area	0.92	0.99	1.95	6.41	37.11	0.57	48.12		1.57	1.45	0.90
CRVM-1666		72B	CaO and P_2O_5 rich area - delimited, n. 12	Quartz grain	0.33	0.25	2.13	89.30	1.90	0.69	3.89			1.53	
CRVM-1668		72C	CaO and P_2O_5 rich area - delimited, n. 13	Spot 1	0.33	0.79	3.14	9.01	33.57	1.01	50.42	0.39		1.33	
CRVM-1668		72C	CaO and P_2O_5 rich area - delimited, n. 13	Ceramic matrix, area 2	1.06	2.71	15.86	46.20	0.93	3.05	20.87	1.31		8.00	
CRVM-1668		72C	CaO and P_2O_5 rich area - delimited, n. 13	Ceramic matrix, area 3	0.83	2.84	17.99	45.30	1.04	3.16	19.00	1.17		8.69	
CRVM-1668		72C	CaO and P_2O_5 rich area - delimited, n. 13	CaO and P_2O_5 rich matrix, area 4	0.79	1.90	12.87	35.39	10.54	2.82	28.67	0.62	0.70	5.12	0.59
CRVM-1668		72C	CaO and P_2O_5 rich area - delimited, n. 13	CaO and P_2O_5 rich matrix, area 5	0.67	2.35	13.26	40.30	10.24	3.64	24.31	0.93		4.30	
CRVM-642	Type A lime rich inclusion	72D	Type A lime rich inclusion	Vitrified bone, area 1	0.42	0.99	5.10	16.90	28.92	1.16	41.65	0.81	1.65	2.40	
CRVM-642		72D	Type A lime rich inclusion	Ceramic matrix, area 2	0.78	2.92	16.18	48.15	5.78	3.98	16.03	1.03		5.16	
CRVM-642		72D	Type A lime rich inclusion	Inclusion matrix, area 3	1.14	3.55	14.41	55.42	2.19	1.85	16.61	1.17		3.65	
CRVM-642		72D	Type A lime rich inclusion	Ceramic matrix, area 4	1.02	2.31	16.71	57.17	0.55	3.49	11.91	0.75		6.10	
CRVM-1666	Type C lime rich inclusion	72E	Type C lime rich inclusion	Ceramic matrix, area 1	1.09	2.75	17.20	45.64	1.37	3.27	19.39	2.16		7.13	
CRVM-1666		72E	Type C lime rich inclusion	CaO and P_2O_5 rich matrix, area 2	0.73	2.01	10.94	34.19	15.81	2.53	28.14	0.60	0.95	4.10	
CRVM-1666		72E	Type C lime rich inclusion	Bone fragment, area 3	1.01	1.13	2.67	6.43	36.81	0.97	48.21	0.35	0.89	1.53	
CRVM-1666		72E	Type C lime rich inclusion	Bone fragment, area 4	0.73	1.49	4.39	10.27	35.80	0.84	43.91	0.98	0.21	1.38	
CRVM-1666		72F	Bone fragment	Spot 1	0.48	1.01	4.53	13.46	17.66	1.63	58.89			2.35	
CRVM-1666		72F	Bone fragment	Spot 2	0.68	1.19	2.12	5.91	38.05	0.54	49.94	0.68		0.90	
CRVM-1666		72F	Bone fragment	Spot 3	0.89	1.08	3.73	8.70	34.60	0.89	46.51		0.70	1.52	1.38

Therefore, a double source of CaO has been confirmed with the simultaneous addition of bone fragments (or bone ashes) and limestone to ceramic pastes, as suggested by XRF analysis. Indeed, bone fragments were clearly identified but, in other cases, CaO and P_2O_5 are dispersed in the ceramic paste suggesting very small particles grain size or complete absorption of the bone fragments. The addition of bone fragments promotes ceramic body vitrification (Gouvêa et al., 2015). So, the use of a similar technology on sampes included in fabric I and sub-group Ia is evident.

Glass fragments were detected in 10 out of 13 samples in sub-group Ia. As on fabric I samples, they could be partially melted and assimiltaed in the ceramic matrix as a consequence of the firing process, or mostly unaltered, with straight edges and without a significant reaction with the clay matrix. In some cases, digested and unaltered glass fragments could coexist in the same sample (Table 37).

Partially melted and digested glass fragments (Fig. 72A, B, Table 40) have been analysed in 6 out of 13 samples (Table 37, Annex 4 – Table 14). The chemical composition is highly variable, but SEM-EDS analysis established that in all cases, they contain PbO and SiO_2. SnO_2 could also be present. Because of the interaction with the ceramic matrix, alkalis (Na_2O+K_2O), Al_2O_3 and FeO content could be high, but in all cases, CaO and P_2O_5 concentration were the most significant.

Unaltered glass fragments were identified in 5 out of 13 samples (Table 37), and they were classified based on the identification of SnO_2. Bone fragments (Fig. 72C/D, Table 40, Annex 4 – Image 9D/E, Table 14) were identified in both cases in the middle of the glass. Also, in this case, the introduction of material from glaze-making is confirmed, and bones were included in the original glaze mixture, which probably was quite heterogeneous. The ceramic bodies have also similar characteristics to proto-stone paste ceramic bodies (Mason and Tite, 1994).

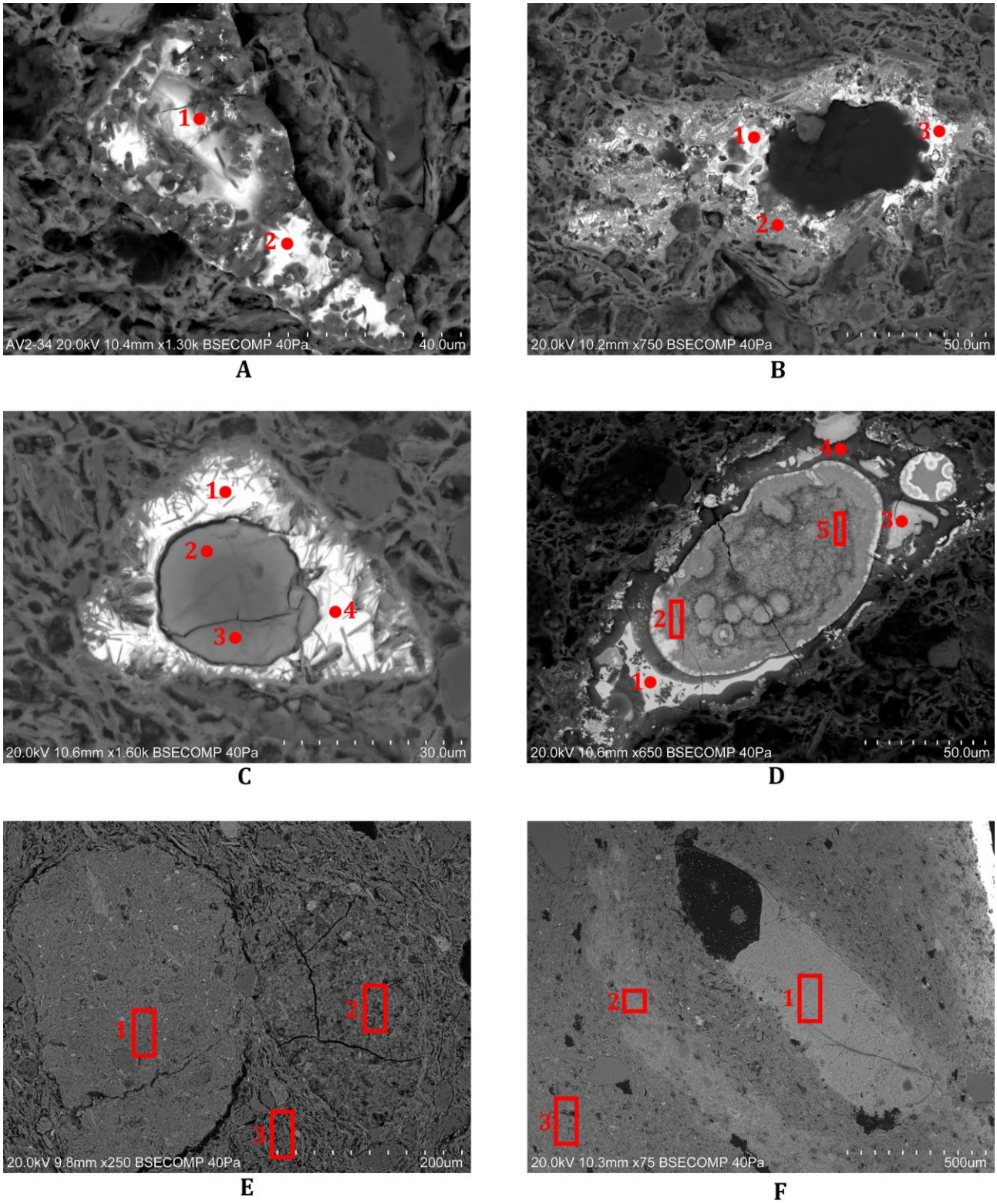

Figure 72 Backscattered images of the analyzed samples. Spot and area analysis are evidenced by red spots or squares, respectivelly. A) Partially digested glass fragment on sample CRVM-0357; B) Partially digested glass fragment on sample CRVM-1668; C) SiO_2 and PbO glass with a fragment of bone on sample CRVM-0357; D) SiO_2, PbO and SnO_2 glass with a fragment of bone on sample CRVM-1666; E) Type C lime rich inclusion, oval nodule on the right side of the picture, on sample CRCSP-0028; F) Yellowish/grayish anhedral inclusion on sample CRVF-0003 (Fig. 67G/H).

Table 40 Chemical data obtained by SEM-EDS of spots and areas analyses of figure 72. Results normalized to 100%, uncertainty 1σ.

Sample	PLM classification	Figure	Feature analysed	Specific spot/area analysed	Na_2O	MgO	Al_2O_3	SiO_2	P_2O_5	K_2O	CaO	TiO_2	MnO	FeO	SnO_2	PbO
CRVM-0357		74A	Partially absorbed glass fragment, fr. 2	Residual glass, Spot 1	0.48	0.79	4.59	42.13	5.57	1.69	11.57	0.66	2.58	0.00	14.70	16.24
CRVM-0357		74A	Partially absorbed glass fragment, fr. 2	Residual glass, Spot 2	0.67	0.93	3.48	23.88	14.11	0.98	14.70	0.71	0.28	1.84	1.44	37.00
CRVM-1668		74B	Partially absorbed glass fragment, fr. 8	Residual glass, Spot 1	0.42	1.60	5.25	29.80		1.27	6.17	1.09		4.28	13.67	36.45
CRVM-1668		74B	Partially absorbed glass fragment, fr. 8	Acicular crystals, Spot 2	1.39	2.04	17.79	46.49		3.96	9.49	0.56		4.08		14.20
CRVM-1668		74B	Partially absorbed glass fragment, fr. 8	Residual glass, Spot 3	0.45	1.11	5.47	33.21		1.07	5.01	0.78		3.73	0.48	48.70
CRVM-0357		74C	Glass fragment Si and Pb, fr. 1	Glass, Spot 1	1.02	0.61	7.66	32.00	0.52	1.66	5.56	0.94		2.67		47.36
CRVM-0357		74C	Glass fragment Si and Pb, fr. 1	Bone fragment, Spot 2	0.71	1.58	2.84	8.47	30.70	0.98	45.04			1.06		8.61
CRVM-0357		74C	Glass fragment Si and Pb, fr. 1	Bone fragment, Spot 3	0.84	1.27	2.90	9.52	30.83	1.07	42.26	0.83		1.09		9.37
CRVM-0357		74C	Glass fragment Si and Pb, fr. 1	Glass, Spot 4	1.28	0.66	6.96	29.07	4.58	1.61	11.56	0.79		2.59		40.89
CRVM-1666	Glass	74D	Glass fragment Si, Pb and Sn, fr 2	Glass, Spot 1	0.63	0.69	4.11	37.36	0.99	4.24	4.99	0.69		3.90		42.41
CRVM-1666		74D	Glass fragment Si, Pb and Sn, fr 2	Bone inclusion, area 2	0.39	1.04	5.15	6.69	22.15	0.69	30.28	1.43	0.77	1.81		29.60
CRVM-1666		74D	Glass fragment Si, Pb and Sn, fr 2	Glass, Spot 3	0.41	0.49	4.60	31.99	9.33	1.07	7.39	0.77	3.06	0.00	6.46	34.44
CRVM-1666		74D	Glass fragment Si, Pb and Sn, fr 2	Glass, Spot 4	0.34	1.04	6.25	62.29	2.38	1.93	4.11	0.78		3.41	1.18	16.31
CRVM-1666		74D	Glass fragment Si, Pb and Sn, fr 2	Bone inclusion, area 5	0.47	0.89	14.68	7.59	25.06	0.59	18.50	0.55		2.03		29.63
CSP-0028	Type C lime rich inclusion	74E	Type C lime rich inclusion	Left side nodule, area 1	1.62	2.83	22.47	56.06	2.44	3.79	2.71	1.15		6.91		
CSP-0028		74E	Type C lime rich inclusion	Right side (CaO, P_2O_5 rich), area 2	0.66	1.22	15.72	50.63	11.47	2.63	11.60	1.01		6.06		
CSP-0028		74E	Type C lime rich inclusion	Clay matrix, area 3	1.19	1.93	21.06	53.44	5.08	3.92	5.77	0.94		6.67		
CRVF-0003	Grey-yellow anhedral inclusion	74F	Grey-yellow anhedral inclusion	Vetrified bone, area 1	0.90	0.80	1.35	7.64	37.03		51.05	0.00	1.22	0.00		
CRVF-0003		74F	Grey-yellow anhedral inclusion	Clay matrix, area 2	0.89	1.73	16.43	48.78	7.98	6.98	12.33	1.34		3.56		
CRVF-0003		74F	Grey-yellow anhedral inclusion	Clay matrix, area 3	1.51	2.73	18.54	62.37	1.30	5.72	3.46	0.93		3.44		

Sub-group Ib

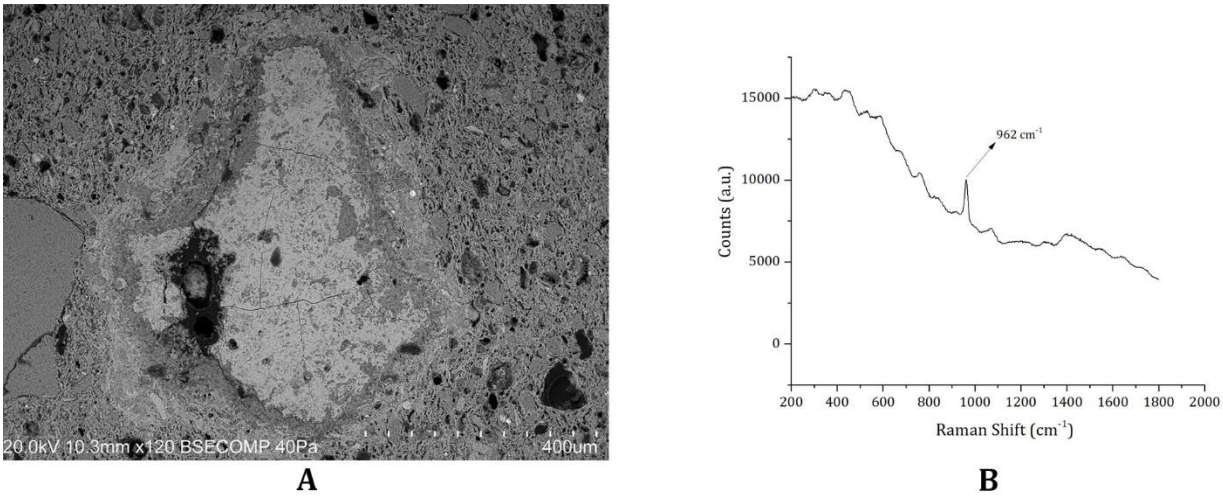

Figure 73 BSE image of a greyish/yellowish anhedral inclusions (GYA) on sample CRCSP-0031, and the µRaman spectrum obtained by the analysis

On samples included in sub-group Ib the Fe_2O_3, K_2O, MgO and Al_2O_3 are uniformly distributed on the ceramic matrix. CaO was identified in delimited areas and always associated with P_2O_5 (Table 37). Moreover, CaO and P_2O_5 concentrations are always tightly related in type C lime-rich inclusions, and in grey/yellow anhedral (GYA) inclusions (Fig. 73A, 72E/F, Table 40, Annex 4 – Table 14). Type C lime-rich inclusions (Fig. 72E, Table 41) could present a significant concentration of Al_2O_3 and SiO_2 in addition to CaO and P_2O_5 suggesting a raw material mixing.

On samples, CRVF-0003 and CRCSP-0031 CaO and P_2O_5 are concentrated in GYA inclusions (Fig. 74A, 73F). The analysis of the inclusions by µRaman spectroscopy identified the organic apatite *v1* $(PO_4)^{-2}$ vibrational mode (Penel et al., 1998) positioned at 963 and 962 cm^{-1}, respectively (Fig. 73B). Similar observations were done for different samples included in sub-group Ia.

Thus, also in this case bones were mixed in the ceramic paste and a similar technology adopted in different samples from fabric I (i.e. green and brown samples) and sub-group Ib has been observed.

Fabric II and III

On samples included in fabric II and III, CaO is evenly distributed in the ceramic matrix associated with MgO, Al_2O_3 and Fe_2O_3, pointing to the exploitation of a homogeneous raw material as evidenced during PLM analyses. In these cases, the raw material probably formed from the alteration of a carbonate rock (i.e. limestone or dolostone).

On sample CRVM-1659 (fabric II), a CaO and P_2O_5 rich slip was observed below the glazed on both sides (Annex 4 - Image 3C, Table 14). In addition, a considerable enrichment of CaO and P_2O_5 was also observed on different areas of the ceramic paste, inside glassy oval inclusion (Annex 4 – Image 9E, 4, Table 14)or on glassy areas around pores.

The analysis of the glassy area around the big pore (Fig. 66L, 74A/B – Table 41) evidenced an elevated concentration of CaO and P_2O_5, in addition to several small fragments of vitrified bone and PbO rich particles with high contrast on BSE images. As already evidenced on ceramic samples included in the fabric I and sub-groups Ia and Ib, different raw materials were probably mixed and added separately to the ceramic paste. Similar technological options were adopted in Mértola as evidenced on samples included in fabric I and sub-groups Ia and Ib, indicating technological transfer.

On samples included in fabric III both glass (partially digested and unaltered) and frit, fragments were identified in 3 of the 4 samples (Table 37). Nevertheless, few observations were carried out because glass and frit fragments were not very common.

When present, they are enriched in alkalis (Na_2O+K_2O). The analysis (Table 41) of a partially digested glass fragment on sample CRVM-1097 (Fig. 75C) showed that PbO and SiO_2 are the main glass components, and alkalis concentration could be up to 6.64 wt%. Moreover, a fragment of frit was also identified (Fig. 74D). It is highly heterogeneous, containing big grains of unmelted quartz crystals with rounded edges. SiO_2 is more abundant than PbO, and alkalis content could be high. P_2O_5 concentration was high on XRF results, but no bone fragments were observed in the ceramic paste. In this case, if bones were introduced, theye were totally absorbed into the ceramic paste.

On samples CRVM-1665/1670 (Fig. 74E/F, Table 41), PbO concentration is very low on glass fragments (maximum 1.37 wt%), and the main components were SiO_2 and alkalis (Na_2O + K_2O). Thus, a different technology was used if compared to fabric I and II ceramics.

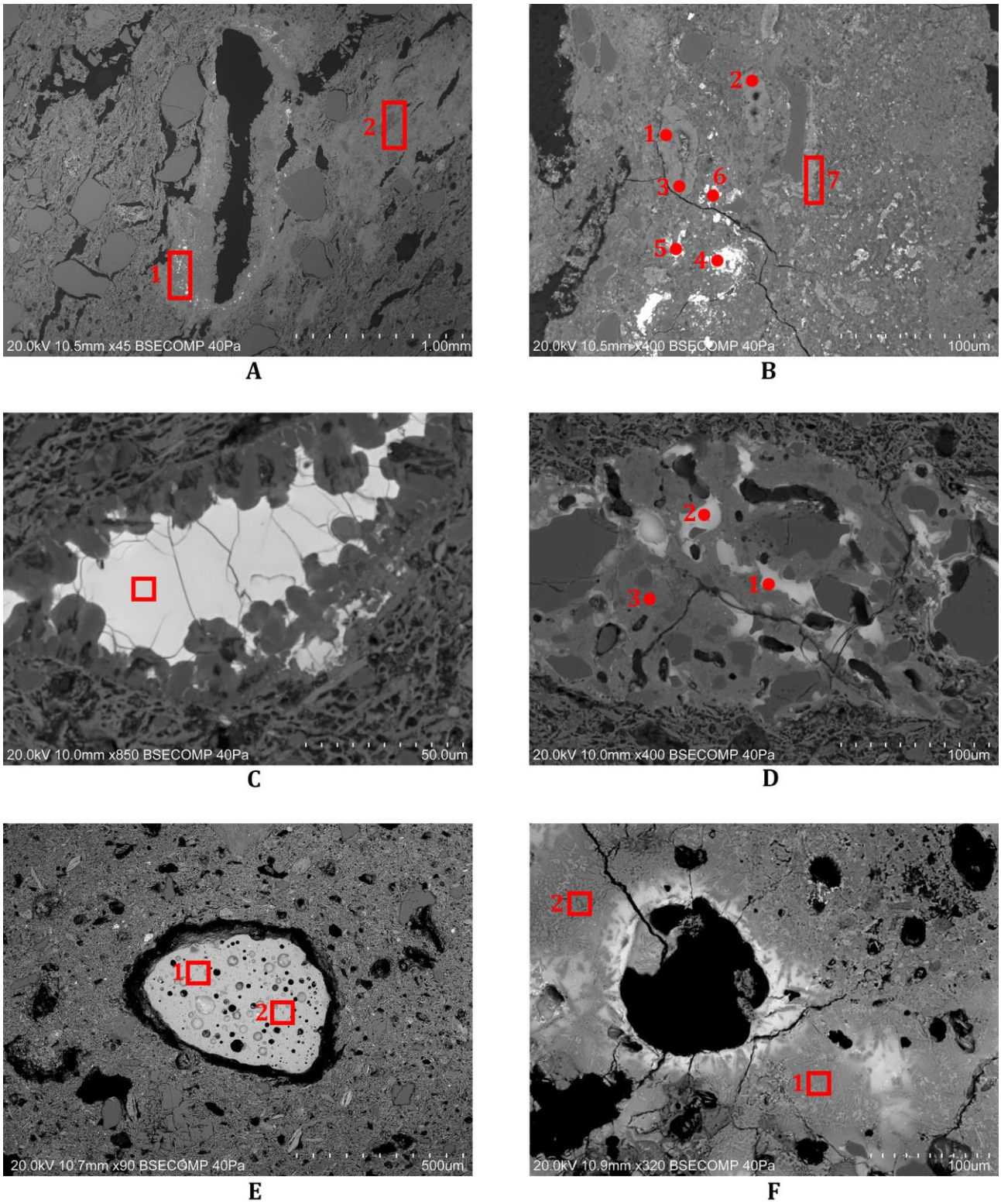

Figure 74 Backscattered images of the analyzed samples. Spot and area analysis are evidenced by red spots or squares, respectively. A) Glassy area around a big pore on sample CRVM-1659 (Fig. 67B); B) Magnified area (bottom left side of the pore) of image A in sample CRVM-1659; C) Partially digested glass fragment on sample CRVM-1097; D) Frit fragment identified on sample CRVM-1097; E) Glass fragment identified on sample CRVM-1665; F) Glass fragment identified on sample CRVM-1670.

Table 41 Chemical data obtained by SEM-EDS of spots and areas analyses of figure 74. Results normalized to 100%, uncertainty 1σ.

Sample	PLM classification	Figure	Feature analysed	Specific spot/area of the feature analysed	Na_2O	MgO	Al_2O_3	SiO_2	P_2O_5	K_2O	CaO	TiO_2	MnO	FeO	CuO	PbO
CRVM-1659	Glass	11A	CaO and P_2O_5 rich area - wide, n. 8	Clay matrix (P_2O_5 rich), area 1	1.16	1.64	11.99	40.69	10.97	1.62	25.56	1.04	0.32	4.04		0.96
CRVM-1659		11A	CaO and P_2O_5 rich area - delimited, n. 8	Border of the pore, area 2 2	0.75	1.16	12.61	43.78	6.49	1.04	25.51	0.83		4.32		3.51
CRVM-1659		11B	CaO and P_2O_5 rich area - delimited, n. 8	Vitrified bone, Spot 1	0.73	0.77	3.70	16.42	28.34	0.74	46.04	0.30		1.80		1.16
CRVM-1659		11B	CaO and P_2O_5 rich area - delimited, n. 8	Vitrified bone, Spot 2	0.43	0.57	2.26	10.08	31.11	0.63	53.03			0.94		0.95
CRVM-1659		11B	CaO and P_2O_5 rich area - delimited, n. 8	Vitrified bone, Spot 3	0.62	0.81	2.91	11.97	32.75	0.41	48.47	0.38		1.20		0.48
CRVM-1659		11B	CaO and P_2O_5 rich area - delimited, n. 8	PbO rich point, Spot 4	0.89	0.68	3.61	15.71	15.18	0.20	14.06	0.63		2.26		46.77
CRVM-1659		11B	CaO and P_2O_5 rich area - delimited, n. 8	PbO rich, Spot 5	0.46	0.92	9.01	26.32	12.42	0.58	17.72	0.95		3.68		27.92
CRVM-1659		11B	CaO and P_2O_5 rich area - delimited, n. 8	PbO rich, Spot 6	0.70	1.49	10.75	27.36	11.74	0.63	23.76	0.73		3.07		19.78
CRVM-1659		11B	CaO and P_2O_5 rich area - delimited, n. 8	CaO, P_2O_5 rich, area 7	0.21	0.61	5.11	35.08	21.44	0.72	31.69	0.54		1.91		2.68
CRVM-1097		11C	Partially absorbed glass fragment, fr 7	Residual glass	2.63	1.10	7.48	41.27	0.43	3.46	4.83	1.42		5.05		32.33
CRVM-1097		11D	Silica-lead-alkali frit, fr. 1	Spot 1	2.93	1.48	8.52	55.55		6.51	2.50	0.47		3.47		18.57
CRVM-1097		11D	Silica-lead-alkali frit, fr. 1	Spot 2	3.17	1.20	6.16	52.60		4.59	2.49	0.71		3.49	1.62	23.95
CRVM-1097		11D	Silica-lead-alkali frit, fr. 1	Spot 3	1.10	2.28	20.11	52.18	0.24	12.32	1.98	0.54		7.69		1.56
CRVM-1665		11E	Silica-alkali glass, fr. 1	Area 1	2.66	3.45	8.27	54.16		6.57	1.67	0.73		21.96		0.54
CRVM-1665		11E	Silica-alkali glass, fr. 1	Area 2	2.44	3.91	8.30	54.93		6.04	2.70	0.51		21.18		
CRVM-1670	Glass	11F	Silica-alkali-lime glass, fr.1	Area 1	3.35	6.56	4.31	58.90	4.81	4.64	14.01	0.53	0.16	1.36		1.37
CRVM-1670		11F	Silica-alkali-lime glass, fr.1	Area 2	2.17	9.25	3.72	58.59	3.83	3.37	15.89	0.62		1.24		1.33

5.4.5.4.2 Glazed decorations

The analyses of the glazed decorations were performed in all glazed samples, including in the kiln bar RDC-108-2014-0001, where vestiges of green glaze were observed. Regarding decorated ceramics, 16 samples of green and brown, 6 samples of partial *corda seca* and 1 sample of honey and black glazed ceramics were analysed. As already stated in section 5.4.3, glazed ceramics have different chronologies and were decorated using different styles.

On green and brown ceramics, decorations (i.e. coloured glazes) are always applied over a white lead-alkali glaze background (the decorated side), obtained by SnO_2 opacification (Vendrell-Saz et al., 2000; Molera et al., 2001c). The reverse side is usually covered by a glaze with similar characteristics.

Nevertheless, during the *Taifa* period exceptions to this rule are documented, and the colour of the background and/or the reverse glaze side can be honey, green (Gómez Martínez, 2014) or black/brown (Beltrame et al., 2015).

Honey and black ceramics are normally covered by a transparent high-lead glaze on both sides, and the decorative pattern is normally developed using a black pigment.

Tipically, partial *corda seca* style ceramics are not completely covered by glaze. The decoration is outlined using a black pigment (the *corda line*), normally enriched in MnO and/or FeO and mixed with a fatty substance that enables the application and prevents the raw glazing materials from mixing (Peréz-Arantegui et al., 1999b). Afterwards, the motif is filled using different coloured glazes and can be (or not) opacified using SnO_2 (Chapoulie et al., 2005; Déléry, 2006a).

Moreover, different technical processes are also involved in the manufacture (Pradell and Molera, 2020). On green and brown ceramics, decorations were mostly applied overglaze (Molera et al., 2001c). On honey and black ceramics, overglaze and underglaze pigment application were possible. Conversely, on *corda seca* glazed ceramics, different coloured glazes could be applied side by side (Chapoulie et al., 2005) and split just by the *corda* line. Thus, glazes with different chemical compositions and characteristics could be utilized by the ceramist. For these reasons, glazes characteristics will be described in different sections, depending of the sample decorative style. At first, some common technical characteristics will be evaluated and discussed.

The results obtained in sections 5.4.5.1, 5.4.5.2, 5.4.5.3 and 5.4.5.4.1 will also be kept under consideration to identify specific technological patterns within different fabrics and sub-groups.

5.4.5.4.2.1 Application technique, fire technology and interface characteristics

The main components of studied glazes are PbO and SiO_2 in different proportions. SnO_2 can also be present as an opacifier. Even if ceramics differ in decorative style and chronology, most of them show similar glaze application techniques (Walton and Tite, 2010) and firing technology (Molera et al., 2001b).

In the present samples, considering the model developed by Walton and Tite (2010), glazes were applied using frits. To compare different glazes, colourants, opacifier agent and lead oxide content were subtracted from glazes chemical composition, and resulted values were recasted to 100% (Annexe 4, Table 15). A similar operation is also performed on the chemical composition of the ceramic paste if some PbO is present (Annexe 4, Table 16). In this manner, glazes and ceramic pastes, can be compared. Some scholars also suggest the use of this model to evaluate the addition of different components to the glaze mixture (Salinas and Pradell, 2018; Molera et al., 2018). The resulted glaze chemical composition should be equal or very similar to the chemical composition of the ceramic paste only when the lead is applied without silica. This never happens on our ceramic samples, clearly pointing to the use of frits.

Regarding firing technology, all ceramics were doubled fired, and glazed decorations were applied over biscuit fired ceramic bodies. Just in one case of sample CRVM-1670 (fabric III) this interpretation is doubtful. The ceramic paste of this sample is buffy-grey in colour, indicating that it was not completely oxidized during firing (Fig. 77A).

Even in double firing ceramics, the glazing process involves glaze adhesion and chemical reactions between the ceramic body and the glaze. This determines ceramic/glaze interface formation where new crystallites nucleate (Molera et al., 2001b). Firing temperature, duration of the firing cycle, cooling rate and the chemical composition of the ceramic paste influence this process. Nevertheless, the formation of new crystallites in the ceramic/glaze interface and the diffusion of chemical elements in both directions (i.e. PbO to the ceramic paste – Al, Ca, Mg, K, Na, Fe to the glaze) is more intense in unfired ceramic bodies.

In our samples, ceramic-glaze interface thickness is slightly variable, ranging between 2 and 50 μm. Smaller (< 5 μm) and higher (> 25 μm) values are associated with partial *corda seca* ceramics, while green and brown and the honey and black sample have intermediate/smaller values (< 25 μm). In all cases (Fig. 75A/D), interfaces are composed of a net of acicular K-Pb feldspars (Molera et al., 1993), and the diffusion of lead into the ceramic paste is rather low. Ca, Mg, Fe rich pyroxenes could also be present dispersed in the glaze.

Moreover, Ca and P-rich particles were observed just above the interface (sample CRVM-1659, in all glazes colours), mixed within it (Fig. 75E/F CRCSP-0027 - in all glazes colours,

CRCSP-0021 – honey glaze) or just below it (CRVM-0670, decorated side – CRVM-623, black and green glaze – CRVM-1669 green glaze).

They appear as small (2-10 μm in size) sub-rounded whitish inclusion on BSE images. In any case, they are not contamination but the consequence of a volunteer addition. These observations suggest they were bones (i.e. bone ashes), voluntarily added before glaze application by the ceramist.

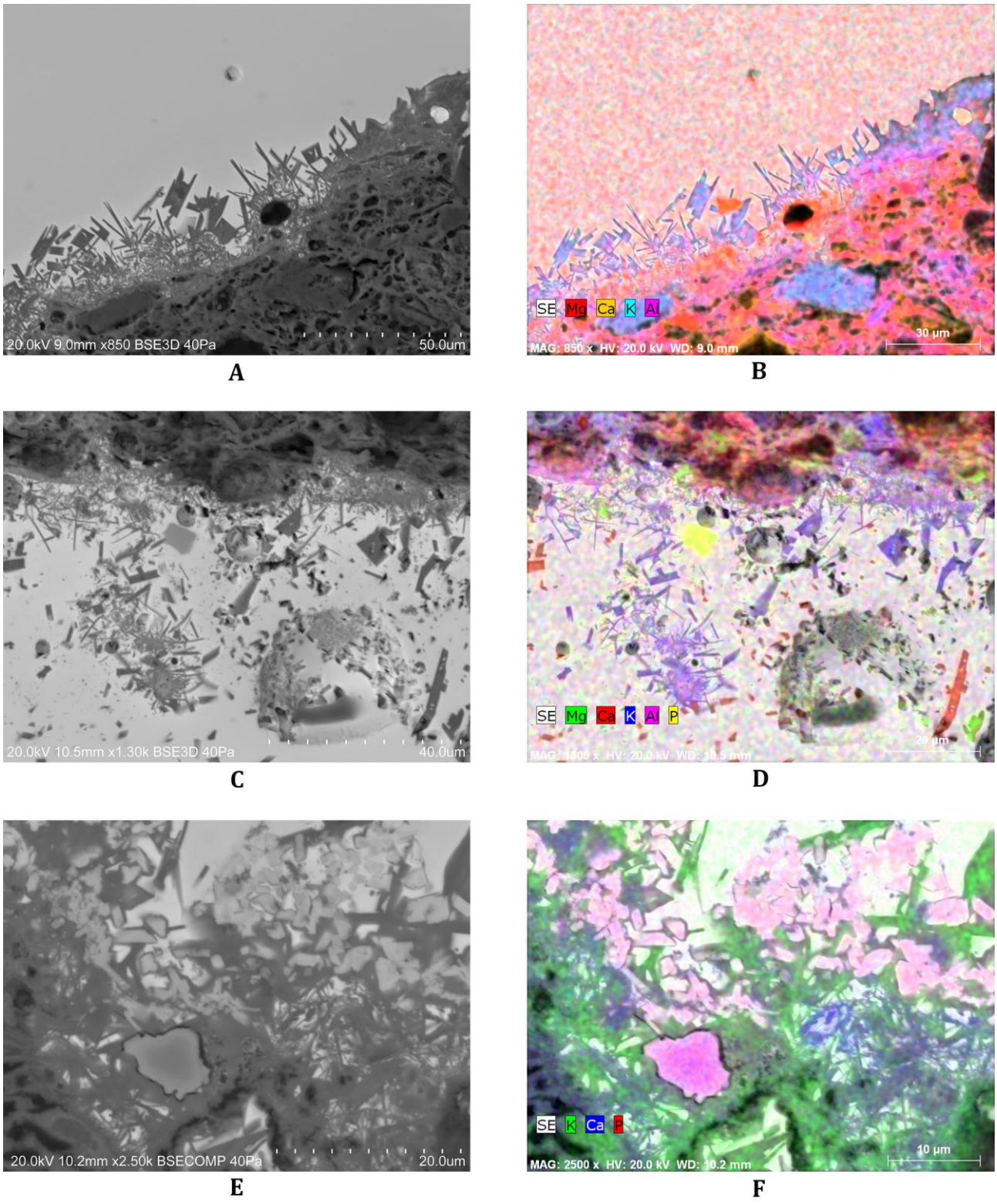

Figure 75 Backscattered images and elemental mapping distribution of the ceramic-glaze interface of samples CRVM-642 (A, B – background – decorated side), CRVM-1671 (C, D – reverse side) and sample CRCSP-0027 (E, F – honey glaze).

.

5.4.5.4.2.2 Glaze drops on the kiln bar

The green glaze drops on the kiln rod RDC-108-2014-0001 (Fig. 76A/B) can give important information about the raw materials available and glaze technologies used in Mértola, during the last period of the Islamic domination of the town (i.e. Almohad period). The analysis of the green glaze drops shows a high lead glaze, with a chemical composition (Table 42) close to the eutectic mixture (Di Febo et al., 2018).

The colour is due to the presence of FeO. Lead ores could be easily found in the area (see section 5.4.2), and considering the relatively low Al_2O_3 and FeO content, pure sand was used to prepare the glaze mixture. Besides, alkali (Na_2O+K_2O) and alkaline earth (CaO+MgO) concentrations are rather low. Glazes with similar chemical composition are very common on Islamic Iberia during a different chronological period (Salinas et al., 2019; Molera et al., 1999a).

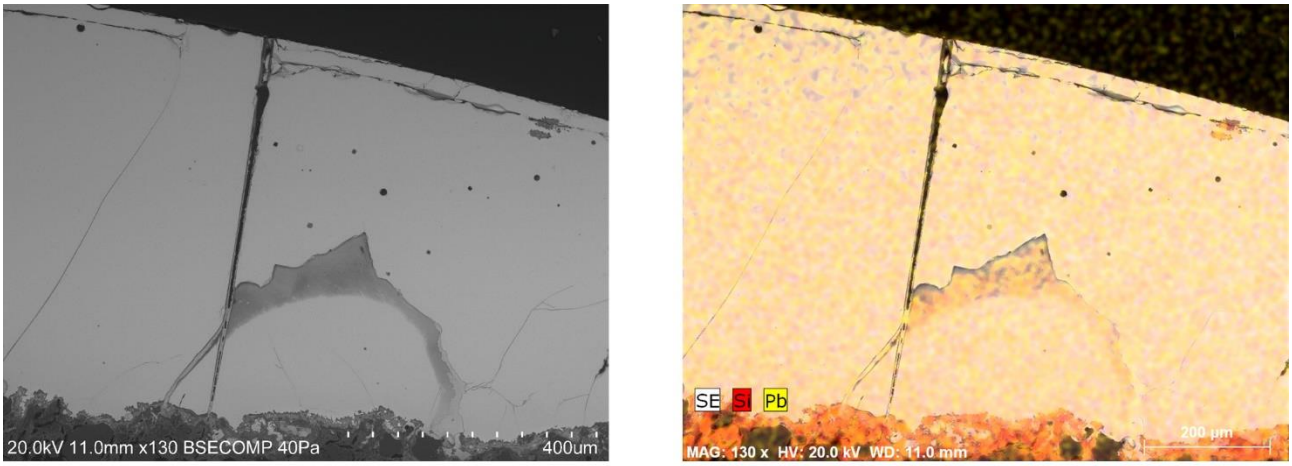

Figure 76 BSE image (A) of the glaze drop observed on sample RDC-108-2014-0001 and the associated elemental mapping distribution of Pb and Si (B).

Table 42 Chemical composition of the glaze drop observed on sample RDC-108-2014-0001. Results normalized to 100%, uncertainty 1σ.

Sample	Glaze Thickness (range), µm	Na_2O	MgO	Al_2O_3	SiO_2	K_2O	CaO	TiO_2	FeO	PbO	PbO/ SiO_2	Alkali + alkaline earth
RDC-108-2014-0001	810-760	0.54	0.49	3.70	29.31	1.31	0.83	0.36	1.33	62.12	2.12	3.17

5.4.5.4.2.3 Green and brown glazed ceramics

The results obtained from glazes analysis of green and brown ceramics are presented on tables 43 (glazes thickness), 44, 45, 46 and 47 (glazes chemical composition). Green and brown samples include ceramics from fabrics I, II, III and sub-group Ia. Glaze thickness is inconstant, but the glazes on the reverse side are generally thinner (Table 43).

On the decorated sides different coloured glazes were analysed, including green, black, turquoise, and yellow glazes. They have been mostly applied overglaze on a white-coloured (Fig. 77B) background. In one sample (CRVM-642), coloured glazes were applied over a honey-coloured background. Nevertheless, on samples CRVM-1669 and CRVM-223 the black pigment was applied underglaze (Fig. 77C).

The reverse side of the samples are mostly white, but honey or green (CRVM-1097) glazes were also observed. Just in the case of sample CRVM-1670, it was impossible to evaluate the characteristics of the background of the decorated side, and of the reverse glaze as they were too weathered (Fig. 77A). In any case, chemical data are reported as informative in tables 45, 46 and 47

Table 43 Glaze thickness and colour of green and brown glazed ceramics included in fabric I, II, III and sub-group Ia.

Glaze thickness (range), µm						
Sample	Decorated side					Reverse side
	Background	Coloured glazes				
		Black	Green	Turquoise	Yellow	
CRVM-0357	150 – 100 (white)	170 - 130	150 - 120		Traces	160 - 50 (white)
CRVM-623	320 – 220 (white)	350 - 340	480 - 380			80 - 70 (white)
CRVM-666	200 – 150 (white)	270 - 260	760 - 290			140 - 110 (white)
CRVM-642	80 - 60 (honey)	230 - 180	260 - 250			90 - 80 (honey)
CRVM-1097	140 – 110 (white)	380 - 250	220-180			180 - 130 (green)
CRVM-1659	160 – 130 (white)	320 - 300	250 - 210		170 - 120	140 - 90 (white)
CRVM-1668	130 – 120 (white)	310 - 250	250 - 220			130 - 110 (white)
CRVM-1671	130 – 120 (white)	130 - 110	230 - 170			260 - 230 (honey)
LVG-02-SXVIII-187	170 – 140 (white)	170 - 160	170-160			110 - 60 (white)
CRVM-1665	160 – 90 (white)	150 - 130		140 - 120		110 - 80 (honey)
CRVM-1666	160 – 130 (white)	320 - 310				90 - 50 (white)
CRVM-1670	180 – 170 (white?)	70 - 50		200 - 130		120 - 80 (white)
CRVM-1667	180 – 120 (white)	170 - 130				70 - 50 (honey)
CRVM-1669	100 – 90 (white)	160 - 140	160 - 150			130 - 120 (honey)
CRVM-223	120 – 110 (white)	200 - 180	190 - 160			80 (white)
CRVM-0670	160 – 110 (white)					130 - 110 (white)

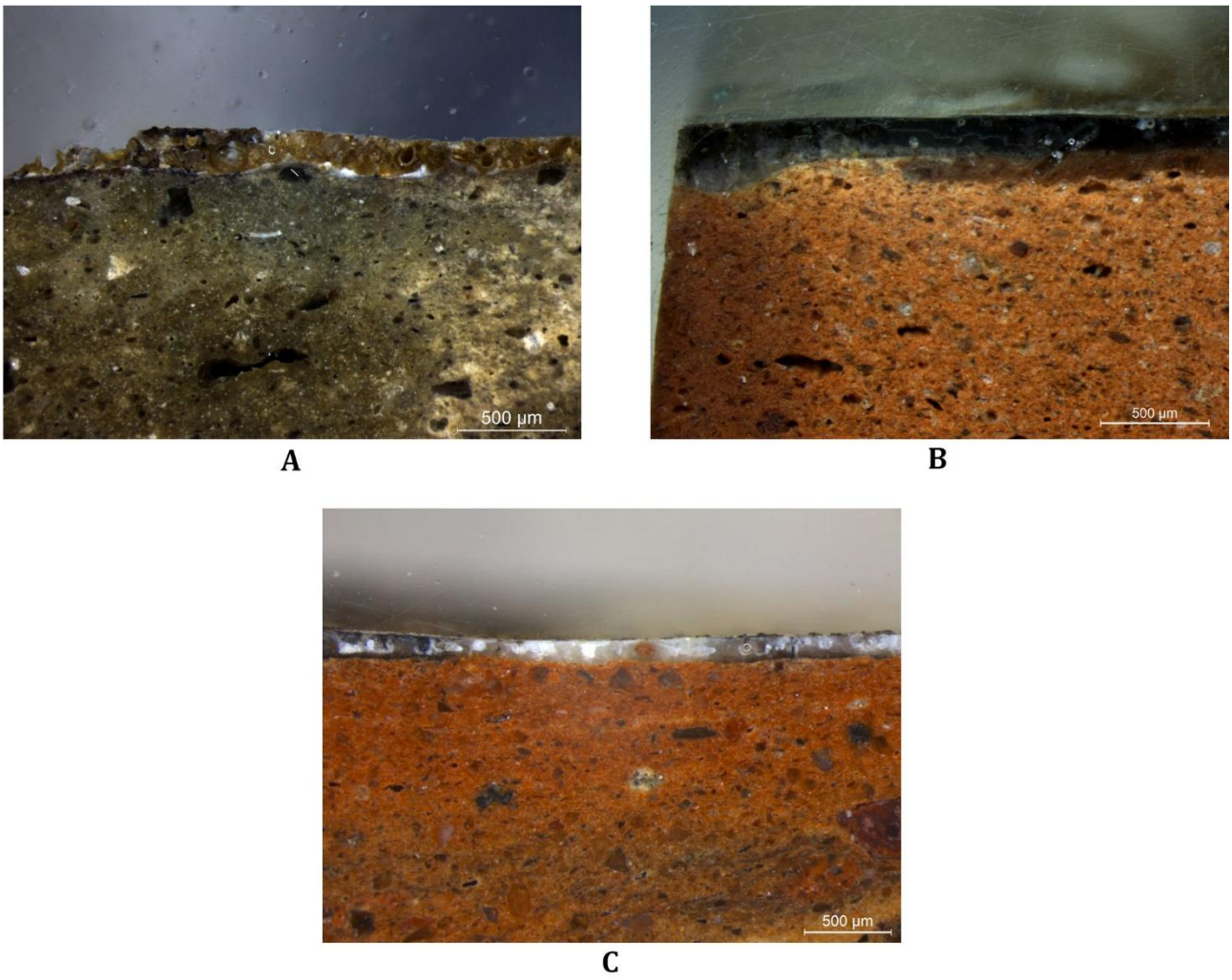

Figure 77 Pictures collected by optical microscopy. A, weathered glaze on sample CRVM-1670; B, overglaze application of the black decoration in sample CRVM-0357; C, underglaze application of the black decoration in sample CRVM-223.

Background glazes of the decorated side

The background glazes of the decorated side (Fig. 78A/C/E) are generally white, except for one sample where the background is honey (Table 43, 44). They could be totally/partly weathered or not affected by burial. In general, unaltered glazes look homogeneous or slightly heterogeneous, with some K-feldspars and/or Ca-Mg pyroxenes floating in them.

The white colour was obtained by opacification using SnO_2 (Vendrell-Saz et al., 2000). The concentration of tin oxides is variable but generally lower than similar ceramic samples from eastern Iberia (Molera et al., 2018; Molera et al., 2001c; Salinas and Pradell, 2018; Salinas and Pradell, 2020; Coll Conesa et al., 1999). Just three samples showed SnO_2 concentration higher than 5 wt%, including two samples from fabric III and one of subgroup Ia. Tin is mainly present as small cassiterite (SnO_2) acicular micro-crystals, heterogeneously distributed in the glaze and often showing crystals clusters. On the honey-coloured glaze, SnO_2 concentration was rather

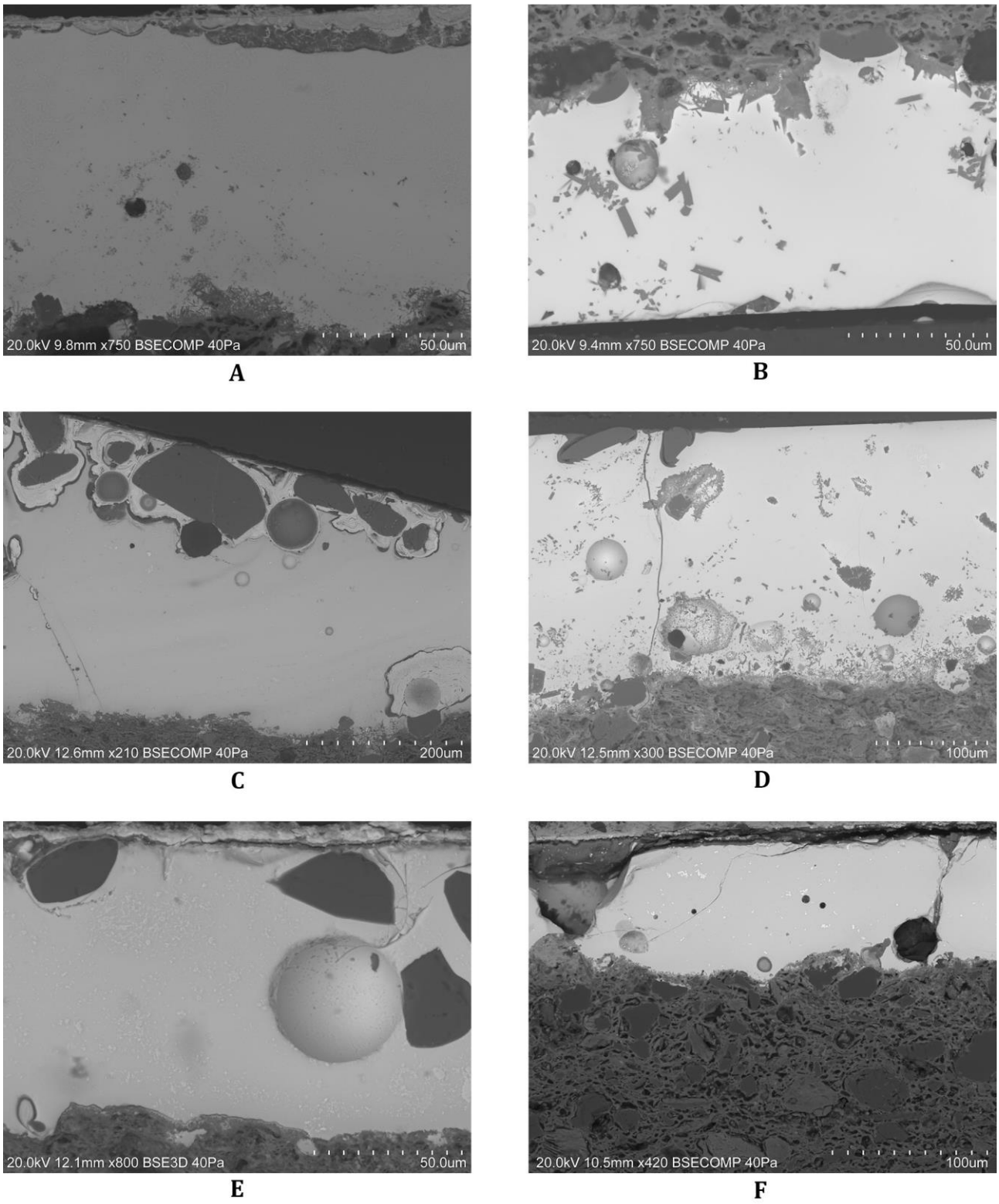

Figure 78 BSE-images of green and brown glaze samples. A, C, E) decorated side of samples CRVM-1671/1097/1665; B, D, F) reverse side of samples CRVM-642/1671/0670.

low and concentrated on scattered areas of the glaze. The concentration of Al_2O_3, K_2O and FeO (colouring agent) is high, pointing to the addition of some clay to the glaze mixture.

Close to the glaze surface, unmelted quartz grains were also observed in several samples (Table 44 - Fig. 78C/E). The presence of quartz can be associated with incomplete firing (i.e.

heterogeneous frits) or a voluntary addition by the ceramist. Nevertheless, the identification of partially absorbed glass fragments on ceramic sample pastes in fabric I and sub-group Ia/b suggest that glaze raw materials were accurately fritted and homogenized. Moreover, the identification of a frit fragment on sample CRVM-1097 (Fig. 74D) indicates that quartz was fritted in the presence of alkalis before application. So this process is coherent with the procedure described in the Persian treatise by Abu 'l-Qasim (Allan, 1973), and consequently, quartz grains were added intentionally to increase glaze opacity (Molera et al., 2001c; Pradell and Molera, 2020). In this case, less tin is needed to obtain a white glaze. This technique of opacification, usually referred to as double, have been already documented in the al-Andalus (Coll Conesa et al., 1999; Peréz-Arantegui et al., 1999a; Chapoulie et al., 2005), but it was initally documented in Middle East (Mason and Tite, 1997).

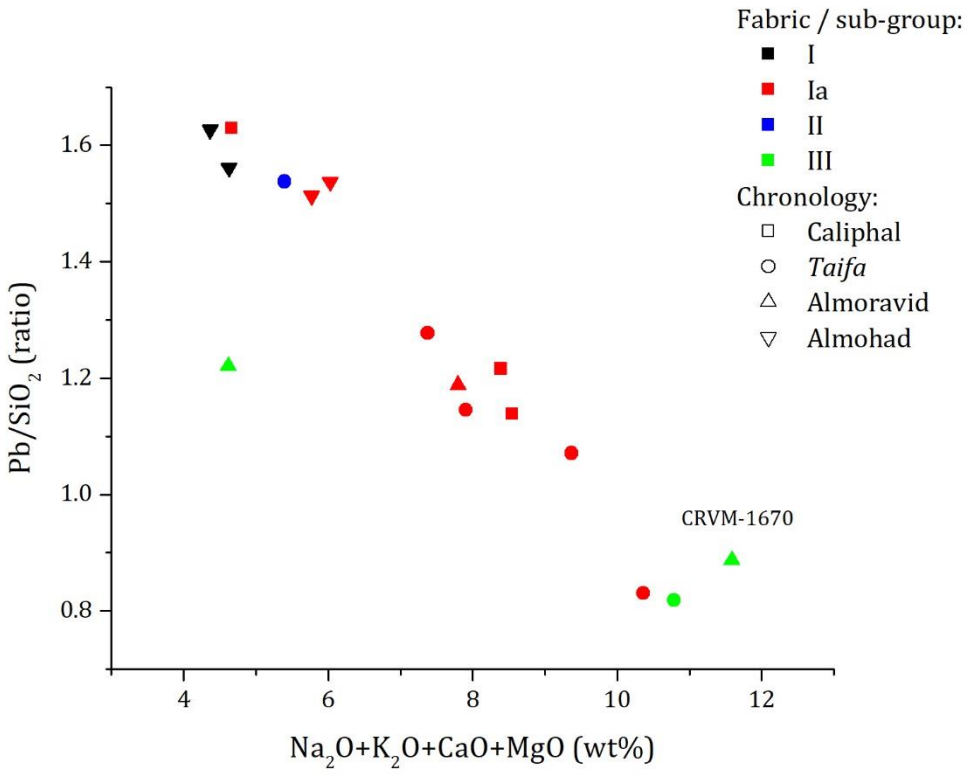

Figure 79 PbO/SiO_2 vs $Na_2O+K_2O+CaO+MgO$ binary plot of green and brown samples (decorated side).

Considering glaze chemical composition (Table 44), samples are divided basing on the PbO/SiO_2 ratio and the alkali (Na_2O+K_2O) plus alkaline earth ($CaO+MgO$) content (Fig. 79). They can be classified as high lead type ($PbO > 50$ wt% - low alkali+alkaline earth) or lead-alkali type ($PbO < 50$ wt% - high alkali+alkaline earth). In any case, there is not a correlation neither between glazes chemical composition and fabric (i.e. provenance), nor with sample chronology. This evidence that different glazes mixture could be adopted anytime, probably depending on the raw material available.

From the technological point of view, the previous model is coherent with the addition of a flux (alkali metals) and a stabilizer/property modifier (alkaline earth metals) to the glaze mixtures (Pradell and Molera, 2020). This effect is stronger on lead-alkali glazes and weak and/or absent on high lead glazes. Some researchers point to the addition of plant ash as a possible source of alkalis (Salinas and Pradell, 2018; Salinas and Pradell, 2020), and in this case, Na_2O concentration is an important issue.

Consequently, to evaluate the addition of a different component to the glaze mixture the chemical composition of glazes and ceramic pastes must be compared. To perform this operation data presented in annexe 4 (Table 15, 16) can be utilized (i.e. the same data utilized to evaluate glazes application technique)[85].

If Na_2O recasted concentrations of samples glazes and ceramic pastes are compared, resulted values are different, being higher in the case of glazes. This suggests that the contribution of the ceramic paste to the final Na_2O concentration is low, and that a flux was added to the glaze mixtures in most cases. In the case of K_2O, recasted values can be higher or smaller than the ceramic paste. Higher values are compatible with the addition of a different source of alkali. For smaller values, the contribution of the ceramic paste to the glazes chemical composition is low, and potassium is generally included on lead-potassium feldspars formed in the ceramic-glaze interface.

Among alkaline earth elements, MgO content is rather low and constant in all cases (Table 44). On the contrary, CaO concentration can be significant and it will be further discussed for each fabric and sub-group.

On samples included in fabric I and subgroup Ia both glaze types (i.e. high-lead and lead-alkali types) are present. CaO concentration can vary consistently, and considering the results obtained in sections 5.4.5.2, 5.4.5.3 and 5.4.5.4.1 (i.e. XRPD, XRF-ICP/MS and SEM -EDS ceramic paste sections), hydroxyapatite in bones was a possible source of CaO.

Nevertheless, particles/inclusion attributable to bone fragments were not identified on samples background glazes and P_2O_5 concentration (< 0.8 wt%) is normally rather low, pointing to other CaO sources. Al_2O_3 and FeO concentration suggest a contribution of the clay components to the chemical composition of the glaze and/or the use of slightly impure sand.

The only green and brown sample included in fabric II (Sample CRVM-1659 - *Taifa* period) has a high lead glaze. Alkali, alkaline earth and P_2O_5 concentration are low. From the

[85] The data utilized have been obtained following the model developed by Walton and Tite (2010). In this case these datasets are utilized to evaluate the contribution of the ceramic paste to the glazes chemical composition and to understand if a different component was added to the glaze mixture in addition to SiO_2 and PbO.

analysis of the ceramic paste, the analysis of the glassy area around a big pore (Fig. 74A/B, Table 41) enriched in CaO, PbO and P_2O_5 suggested that bones could have been used in the ceramic body. Nevertheless, traces of bones have not been identified in the glaze, and Ca and P rich particles were just observed close to the glaze/ceramic interface. In this case a Ca and P rich slip was observed. Thus, the presence of these particles can be linked to slip application. Al_2O_3 and FeO content suggest a low/not significant contribution of clay minerals to the final glaze composition and the utilization of pure sand.

Glazes of green and brown included in fabric III show heterogeneous characteristics, and one sample could not be evaluated (CRVM-1670, too weathered). Sample CRVM-1097 (*Taifa* period) is of the lead-alkali type, with elevated alkali – alkaline earth content and low in SnO_2 concentration if compared to sample CRVM-1665 (Almoravid period). Al_2O_3 and FeO content are low, suggesting the utilization of pure sand in both cases. Glass fragments with similar chemical composition to the glaze were identified in the ceramic paste of sample CRVM-1097 (Fig. 74C, Table 41).

Table 44 Chemical analysis results obtained by SEM-EDS analysis of the background glazes of samples decorated side. Results normalized to 100%, uncertainty 1σ. Qz, presence or absence of quartz grains in the glaze. Alt., glaze alteration; U, unaltered – P, partly altered – A, totally altered.

Sample	Chronology	Glaze colour	Fabric - subgroup	QZ	Alt.	Na_2O	MgO	Al_2O_3	SiO_2	P_2O_5	K_2O	CaO	TiO_2	FeO	CuO	SnO_2	PbO	PbO/ SiO_2	Alkali + alkaline earth
CRVM-0357	Caliphal	White	Ia		U	1.58	0.45	1.18	34.80	0.10	0.81	1.83	0.00	1.41		1.16	56.69	1.63	4.67
CRVM-623	Caliphal	White	Ia		P	1.91	0.86	3.39	38.36	0.20	2.51	3.11	1.20	1.10		0.70	46.65	1.22	8.39
CRVM-666	Caliphal	White	Ia		P	1.84	0.87	3.79	38.77	0.24	2.33	3.51	0.52	1.86		2.14	44.13	1.14	8.55
CRVM-642	*Taifa*	Honey	Ia		U	0.88	0.72	5.60	38.39	0.26	2.60	5.17	1.00	2.96	1.04	0.26	41.12	1.07	9.37
CRVM-1097	*Taifa*	White	III	X	U	2.61	1.05	1.20	46.21	0.77	2.61	4.52	0.77	1.04		1.38	37.84	0.82	10.79
CRVM-1659	*Taifa*	White	II	X	U	0.93	0.30	0.91	35.62	0.55	1.23	2.93	0.38	0.80		1.55	54.78	1.54	5.40
CRVM-1668	*Taifa*	White	Ia	X	P	2.59	0.61	2.93	38.03	0.23	0.95	3.22	0.31	1.48		1.06	48.57	1.28	7.38
CRVM-1671	*Taifa*	White	Ia	X	P	1.97	1.17	5.74	44.00	0.33	2.11	5.10	0.38	1.95		0.69	36.57	0.83	10.36
LVG-02-SXVIII-187	*Taifa*	White	Ia		U	2.23	0.61	1.45	41.02	0.34	1.60	3.45	0.22	0.72		1.38	46.97	1.15	7.90
CRVM-1665	Almoravid	White	III	X	U	1.30	0.26	1.47	37.91		1.52	1.53	0.27	1.17		8.29	46.28	1.22	4.62
CRVM-1666	Almoravid	White	Ia		U	2.29	0.50	1.26	40.00	0.80	2.07	2.94		1.07		1.56	47.53	1.19	7.80
CRVM-1670	Almoravid	White?	III	X	A	0.77	0.62	5.40	31.22	7.44	2.02	8.18		2.99		13.67	27.70	0.89	11.59
CRVM-1667	Almohad	White	Ia		U	1.28	0.83	2.18	33.15		0.89	2.78	0.85	1.68		6.22	50.15	1.51	5.77
CRVM-1669	Almohad	White	Ia		P	2.16	0.60	2.28	34.12	0.27	0.74	2.53		1.73		3.13	52.45	1.54	6.03
CRVM-223	Almohad	White	I		P	0.41	0.61	3.68	33.60		0.64	2.70	0.55	1.95		1.19	54.67	1.63	4.36
CRVM-0670	Almohad	White	I		U	1.84	0.56	1.62	34.39	0.32	0.65	1.57	0.88	1.31		3.18	53.68	1.56	4.63

Table 45 Chemical analysis results obtained by SEM-EDS analysis of the sample reverse glazes. Spot analysis developed on specific samples are reported in italic. Results normalized to 100%, uncertainty 1σ. Qz, presence or absence of quartz grains in the glaze. Alt., glaze alteration; U, unaltered – P, partly altered – A, totally altered.

Sample	Chronology	Glaze Colour/ Inclusion	Fabric -sub-group	Qz	Alt.	Na_2O	MgO	Al_2O_3	SiO_2	P_2O_5	K_2O	CaO	TiO_2	MnO	FeO	CuO	SnO_2	PbO	PbO/ SiO_2	Alkali + alkaline earth
CRVM-0357	Caliphal	White	Ia		U	1.49	0.56	1.63	33.55	0.76	1.56	3.08			1.23		1.46	54.68	1.63	6.69
CRVM-623	Caliphal	White	Ia		U	2.15	0.61	1.45	40.84	0.34	1.59	3.43	0.22		0.76	0.50	1.37	46.73	1.14	7.79
		CaO – MgO rich pyroxene		-	-	1.70	11.33	3.57	37.7	0.83	1.9	17.09	0.96		2.64			22.27		
		CaO – P_2O_5 rich particles		-	-	1.43	2.02	3.57	37.7	13.2	1.9	23.05			1.64			37.25		
CRVM-666	Caliphal	White	Ia		U	0.68	0.48	4.12	29.94		1.33	1.95	0.35		1.27		1.44	58.44	1.95	4.44
CRVM-642	*Taifa*	Honey	Ia		U	0.73	0.87	6.11	38.28	0.18	2.27	5.37	0.77		3.15	0.97		41.31	1.08	9.23
CRVM-1097	*Taifa*	Green	III		U	2.25	0.89	2.17	40.26	0.87	2.28	4.12	0.29		1.81	3.42	0.77	40.06	0.99	9.54
		CaO – MgO rich pyroxene		-	-	1.49	12.71	3.48	46.39	1.22	1.36	19.71			2.31	0.5	0.89	9.95		
		CaO – P_2O_5 rich particles		-	-	2.13	1.33	4.13	33.98	10.26	2.95	20.42			1.37	1.13	0.87	21.43		
CRVM-1659	*Taifa*	White	II	X	U	1.10	0.24	1.16	36.46	0.15	1.74	2.94	0.43		0.65		2.89	52.23	1.43	6.02
CRVM-1668	*Taifa*	White	Ia	X	P	2.50	0.67	2.80	38.08	0.42	0.91	3.03	1.32		1.85		1.01	47.40	1.24	7.11
CRVM-1671	*Taifa*	Honey	Ia	X	U	0.92	0.74	6.06	36.59	0.20	1.84	5.18	0.71		2.26		1.94	43.57	1.19	8.68
LVG-02-SXVIII-187	*Taifa*	White	Ia		U	2.16	0.61	1.46	41.06	0.34	1.60	3.46	0.23		0.56		1.38	47.14	1.15	7.84
CRVM-1665	Almoravid	Honey	III	X	U	1.75	0.57	3.39	34.69	0.74	1.45	3.43	0.41		1.51		0.33	51.74	1.49	7.20
CRVM-1666	Almoravid	White	Ia	X	U	2.34	0.76	3.23	38.86	0.58	2.14	3.65	0.54	0.69	1.87		0.91	44.44	1.14	8.88
CRVM-1670	Almoravid	White	III		A	0.85	0.89	6.68	40.60	3.36	2.35	5.38			3.16		9.08	27.65	0.68	9.47
CRVM-1667	Almohad	Honey	Ia		U	0.84	0.82	4.49	39.00		1.13	3.79	1.07		2.77		0.37	45.71	1.17	6.58
CRVM-1669	Almohad	Honey	Ia		P	0.48	0.81	4.79	20.77	0.32	0.72	3.47	0.70		1.47			66.47	3.20	5.49
CRVM-223	Almohad	White	I		P	1.81	0.63	1.8	35.54	0.22	0.66	1.54	0.60		1.59		2.37	53.24	1.50	4.64
CRVM-0670	Almohad	White	I		U	0.50	0.57	2.38	30.70	0.25	0.63	2.02	0.84		2.34		1.05	58.72	1.91	3.73

Reverse side glazes

Differently from background glazes, reverse glazes (Fig. 78B/D/F, Table 45) have more crystallites dispersed in them (i.e. K-feldspars and/or Ca-Mg pyroxenes). Most of the samples have a very similar chemical composition to the background side, and analogous technology was used. Nevertheless, in the same piece, some dissimilarities were registered with the background glaze of the decorated side due to a different PbO/SiO_2 ratio, alkali + alkaline earth content, as a consequence of the addition of a colouring agent (CuO, sample CRVM-1097), or because of a different FeO and SnO_2 concentrations. Consequently, also, in this case, do not exist a correlation between the glaze technology used, fabrics or with chronology. So different glaze recipes could be used anytime, and they could be different or not from the background glaze.

In any of these cases, the results obtained by the analysis of the background glaze of the decorated and of the reverse sides evidenced that ceramists could produce glaze mixture with different chemical composition but with slightly similar maturing temperature. Moreover,

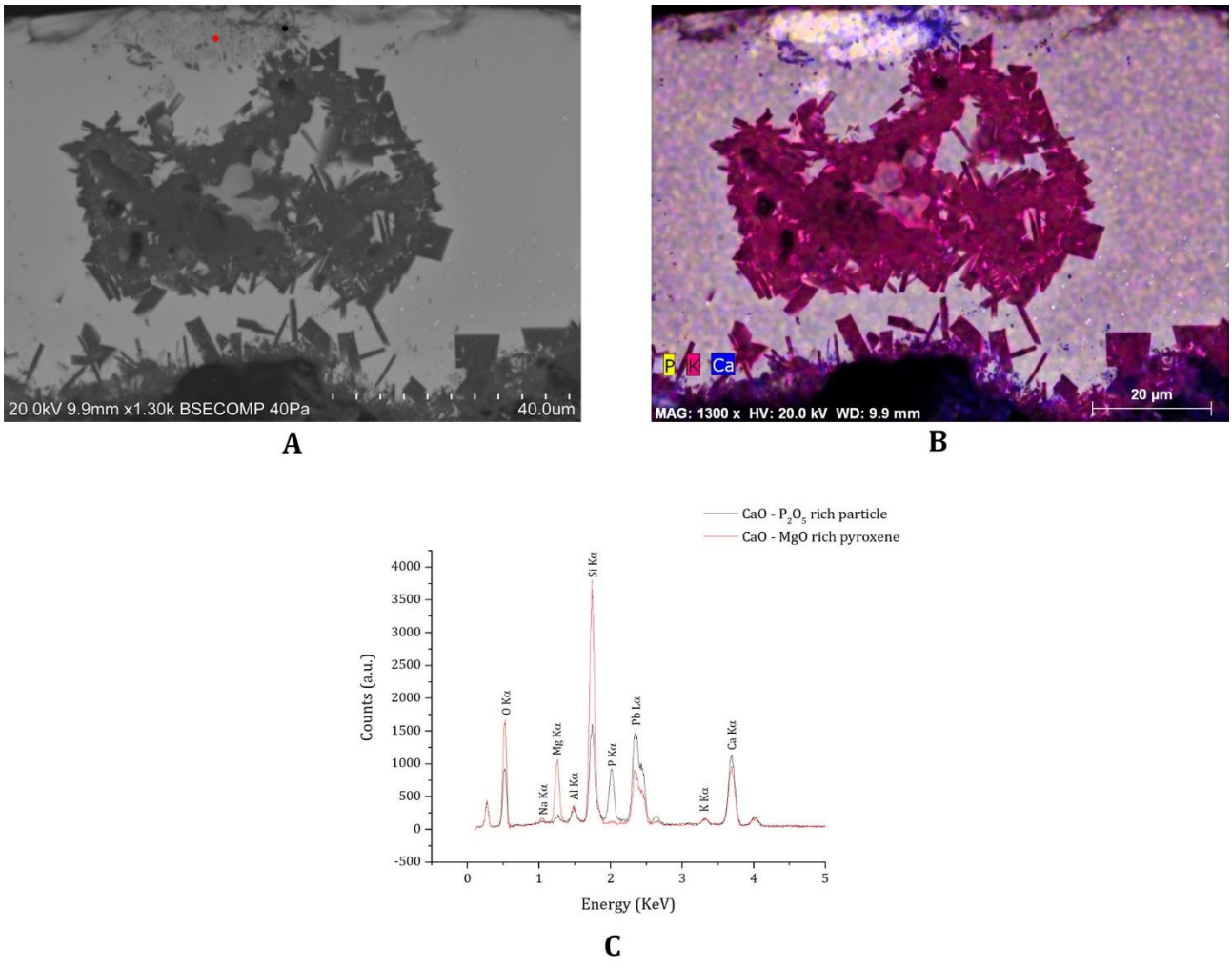

Figure 80 BSE image (A) of different inclusion observed in the reverse glaze of sample CRVM-623, and (B) the elemental mapping distribution of Ca, P and K. SEM-EDS micro-analysis spectras (C) obtained by the analysis of different rounded and acicular inclusions observed in the top part of picture A (red and black spots).

glazes also probably had similar contraction rate to the ceramic body, and the risk of glaze cracking, crazing, or shivering was reduced. We suppose that the difference between glazes result from the ceramicst choice or depend on raw material availability.

Moreover, CaO and P_2O_5 rich clusters of particles (1-2 μm in size) were observed inside the glaze of samples CRVM-623 (sub-group Ia) and CRVM-1097 (fabric III). Most of them did not react with the glaze, but some did, and probably acicular Ca-Mg rich pyroxene [86] (Table 45) crystalized (Fig. 80). The chemical composition of CaO and P_2O_5 rich particles (Table 45) suggest they were originally bone particles.

This result indicates that bone particles did not easily melt in a PbO and SiO_2 rich glaze at the estimated ceramic firing temperature (850-1000 °C), or the firing time was too short to allow it. Consequently, only a small amount of the particles agglomerate transformed in differents crystallites (probably a CaO – MgO rich pyroxene) depleted in P_2O_5. Only in this case, P_2O_5 and CaO rich crystallites could nucleate.

Similar results were obtained by different scholars (Silvestri et al., 2016; Silvestri et al., 2014; Neri et al., 2017) during the analysis of Byzantine mosaic tiles from different places. In these cases, bone ash was utilized as a primary opacifier.

Bones were also recovered at al-Raqqa (Syria), at an early Islamic glass workshop inside different furnaces, and also identified by SEM-EDS during the analysis of different glass scraps (Henderson, 1995; Henderson, 1999). The author suggests that calcined bones could be utilized as CaO source. Nevertheless, its identification clearly evidenced that bone did not melt, and they were probably utilized as opacificant in glass manufacturing as suggested by different scholars (Freestone and Stapleton, 1998).

The utilization of bones as opacificant on Islamic glazed ceramic have never been attested until now, and results show that bones were voluntary introduced in the glaze mixture by the ceramist as opacificant. At present , it is probable that bones were utilized as second opacificant solution to save raw material (i.e. SnO_2).

[86] In the present thesis electron probe microanalyses (i.e. EMPA) were not performed on crystallites dispersed in the glaze. So it was not possible a complete crystal chemistry evaluation of specific inclusion.

Coloured glaze: Black

On black glazes, thickness range from 50 to 350 µm (Table 43). The colour results from the application of a MnO rich mineral as colouring agent (Molera et al., 2013). MnO (Table 46) normally ranges between 1.03-3.58 wt%, and FeO and CuO could also be present. Moreover, on sample CRVM-1659, CuO was major colouring agent, with a concentration close to 10 wt%, and resulting in an extremely dark green coloured glaze. SnO_2 was also identified in most samples.

Unmelted quartz crystals could be present close to the glaze surface or in all the glaze thickness (Fig. 82A). Black decorations generally appear unaltered or slightly weathered. On sample CRVM-1670 it was not possible to reasonably evaluate the decoration composition (informative values reported) due to extreme alteration.

The pigment was usually applied overglaze, and it generally dissolved in the glaze, although in some samples, different crystallites enriched in MnO and FeO were observed (CRVM-0357/1665/1667/1669/223). In two cases (CRVM-1669/223), crystallites position inside the glaze suggest underglaze pigment application (Fig. 81).

Two different crystallite types usually appear with different contrast on BSE images. The darker ones are normally sub-rounded, while the lighter ones are acicular or rhombohedral in shape. SEM-EDS analysis indicates that they might be probably classified as braunite (Mn rich nesosilicate) and as kentrolite (Pb-Mn rich sorosilicate). Chemical analysis results by spot analysis are reported in table 46.

It is difficult to establish with certainty which pigment was utilized in the decoration, but pyrolusite (MnO_2) have been widely utilized during history on black decorations. During firing Mn is reduced from Mn^{4+} to $Mn^{2+,}$ and it can also convert into jacobsite ($MnFe_2O_4$) in the presence of iron (Crum et al., 2009). The further reaction of the pigment with a SiO_2 rich matrix

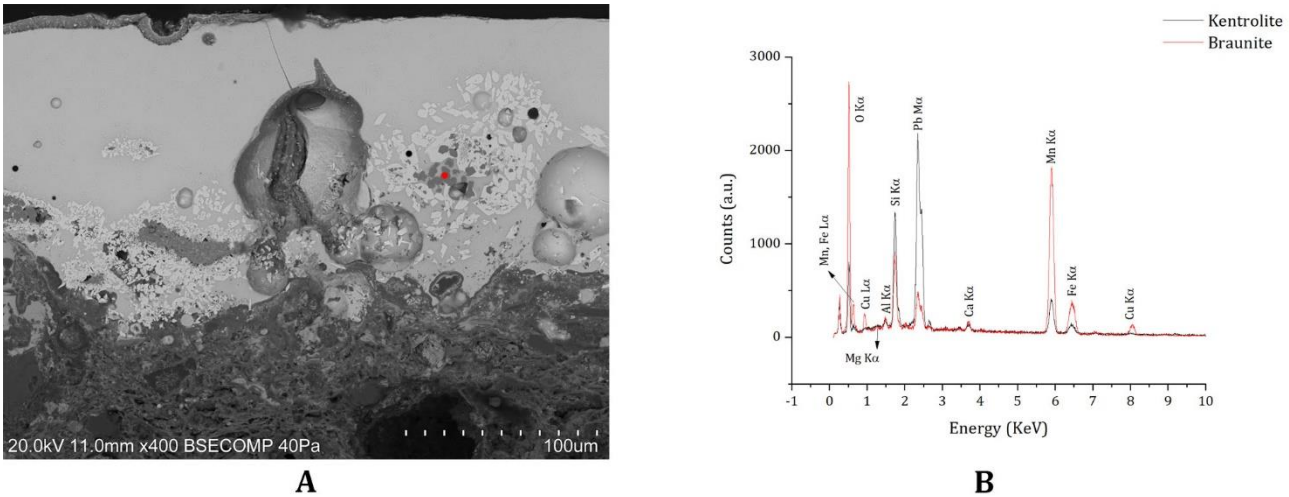

Figure 81 BSE image (A) of the black glaze analyzed on sample CRVM-1669, and EDS spectrum of two different spot (i.e. rea and black).

favours the crystallization of braunite (Mn_7SiO_{12}), which at higher temperature transform into kentrolite ($Pb_2MnSi_2O_9$) as a consequence of the reaction with the PbO included in the glaze melt (Molera et al., 2013).

P_2O_5 concentration is rather low (<0.87 wt%) or absent, similarly to the background and the reverse glaze. In any case, bone fragments were observed on samples CRVM-666/1668/ LVG-02-SXVIII-187. Bone particles inside glazes could appear as isolated (Fig. 82A/B/C) small clusters of particles (1668/ LVG-02-SXVIII-187), or the glaze can be enriched (CRVM-666) in numerous bone inclusions smaller than 1-2 µm.

SEM-EDS spot chemical analysis of particle inclusion and glaze are reported in table 46. The identification of hydroxyapatite was further confirmed by µRaman spectroscopy analysis (Fig. 83D), thanks to the identification of the *v1* $(PO_4)^{-2}$ vibrational mode positioned at 953 (CRVM-1668) and 955 (CRVM-666) cm^{-1}. Raman bands were slightly shifted to lower

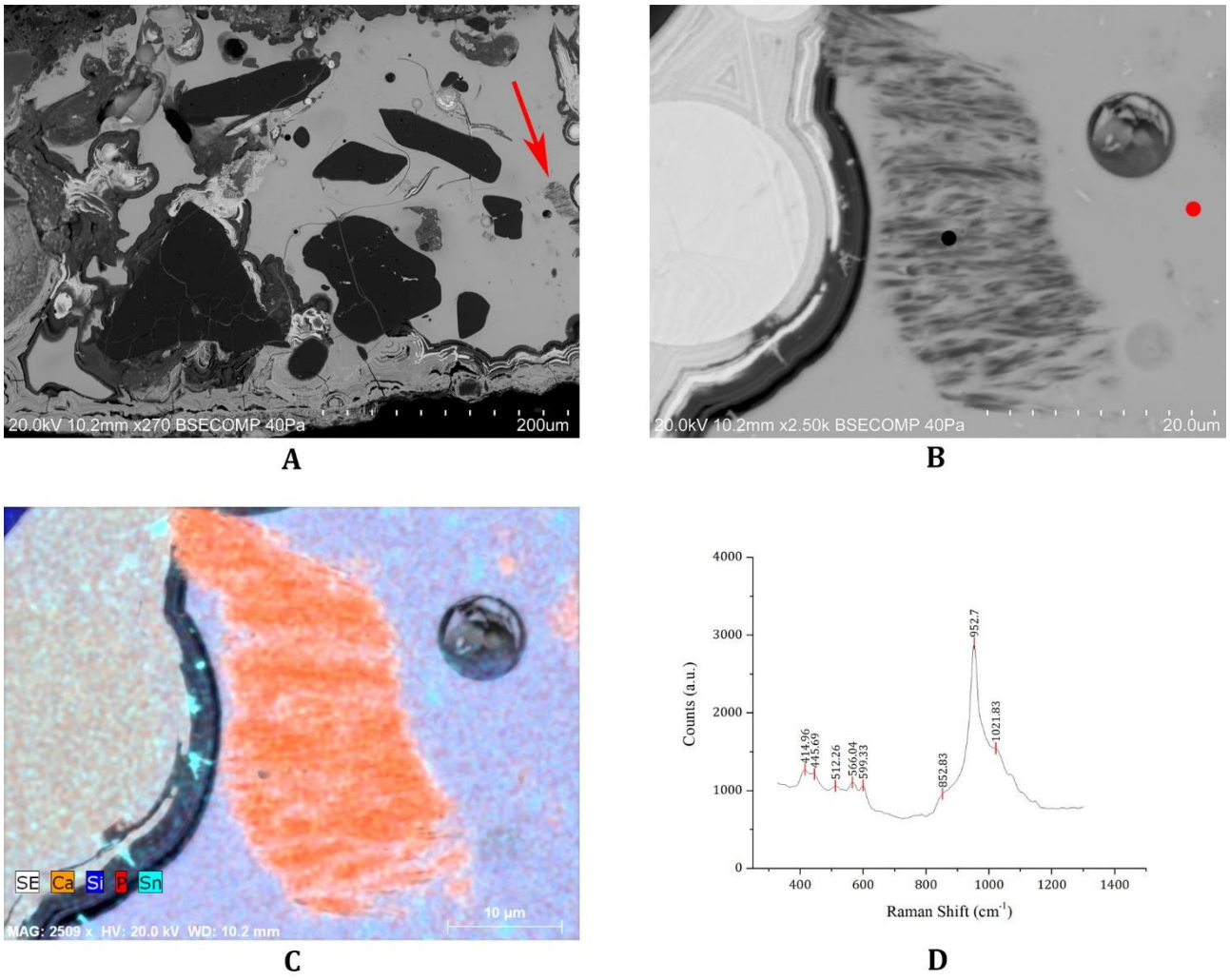

Figure 82 BSE image (A) of the black glaze observed on sample CRVM-1668 and of the magnification (B) of the bone inclusion. The glaze and the inclusion spot chemical analysis have been done, and they are marked by a red and a black spots, respectively. In figure C, elemental mapping distribution of Ca, P, Si and Sn is reported as well as the µRaman spectrum obtained by the analysis of the inclusion.

frequencies if compared to the values reported in the literature (Penel et al., 1998; Colomban et al., 2004).

The results show the voluntary addition of bones fragments in combination with the pigment to the glaze mixture. This component was added to opacify the glaze in addition to cassiterite and quartz crystals when present.

Table 46 Chemical analysis results obtained by SEM-EDS analysis of the sample black glazes. Spot analysis developed on specific samples are reported in italic. Results normalized to 100%, uncertainty 1σ. Qz, presence (X) or absence of quartz grains in the glaze. Alt., glaze alteration; U, unaltered – P, partly altered – A, totally altered.

Sample	Chronology	Glaze colour/ inclusion	Fabric-subgroup	Qz	Alt.	Na_2O	MgO	Al_2O_3	SiO_2	P_2O_5	K_2O	CaO	TiO_2	MnO	FeO	CuO	SnO_2	PbO
CRVM-0357	Caliphal	Black	Ia	X	U	1.95	0.29	1.15	34.94		0.45	1.12	0.81	1.03	0.64		1.04	56.57
CRVM-623	Caliphal	Black	Ia		U	1.98	0.61	1.87	42.07	0.17	2.50	3.11	0.43	1.88	1.97	1.05	1.48	40.89
CRVM-666	Caliphal	Black	Ia		U	1.72	0.71	2.73	35.25	0.87	1.68	4.84		0.73	0.95	0.74	1.89	47.88
		Bone inclusion				*1.01*	*0.4*	*1*	*14.16*	*21.5*	*0.78*	*34.34*		*1*				*25.85*
		Glaze				*2.33*	*1*	*1.69*	*29.29*	*1.84*	*1*	*6.41*		*2.79*		*1.62*	*1.44*	*50.59*
CRVM-642	*Taifa*	Black	Ia	X	U	0.86	0.52	5.31	38.06	0.19	2.08	4.88	0.99	2.50	2.66	2.00		39.94
CRVM-1097	*Taifa*	Dark-black-green	III		U	2.54	1.02	2.29	41.00	0.49	2.00	4.26		0.70	1.47	4.63	1.37	38.24
CRVM-1659	*Taifa*	Black	II		U	0.77	0.30	0.95	30.56		0.54	1.70				9.58	1.46	54.15
CRVM-1668	*Taifa*	Black	Ia	X	P	2.34	0.54	1.58	38.71	0.46	0.63	2.55		1.04	0.76	2.14	1.53	47.73
		Bone inclusion		-	-	0.76		0.60	15.89	23		33.92		1.02		0.77		23.04
		Glaze		-	-	3.35	0.71	2.01	41.92	0.79	0.92	3.40		1.57	0.7	1.59	1.65	41.40
CRVM-1671	*Taifa*	Black	Ia		P	2.27	0.67	4.19	42.45	0.34	1.68	3.87	0.34	2.60	2.29			39.30
LVG-02-SXVIII-187	*Taifa*	Black	Ia		U	2.06	0.60	1.59	39.33	0.58	1.31	3.29		1.05	1.18	1.32	1.49	46.19
		Bone inclusion				*0.93*		*0.44*	*11.41*	*19.7*	*0.5*	*33.94*						*33.03*
		Glaze				*2.91*	*0.9*	*1.4*	*39.59*	*0.7*	*1.86*	*4.06*		*0.45*	*0.57*		*1.66*	*45.9*
CRVM-1665	Almoravid	Black	III	X		1.45	0.35	2.42	37.50		1.51	1.72		3.58	2.20		2.83	46.44
CRVM-1666	Almoravid	Black	Ia		U	2.31	0.45	1.51	38.91	0.46	1.72	2.76		2.26	1.23	1.36	1.56	45.47
CRVM-1670	Almoravid	Black	III		A	2.81	0.43	3.35	42.11	0.51	2.70	2.28	0.43	2.00	1.99		6.18	35.21
CRVM-1667	Almohad	Black	Ia		U	2.10	1.04	1.66	33.26		0.77	2.47	0.00	1.97	1.72		3.67	51.33
CRVM-1669	Almohad	Black	Ia		U	1.89	0.51	1.33	31.42		0.46	2.07	0.28	2.90	1.75	2.79	3.36	51.24
		Braunite		-	-		*0.89*	*1.77*	*9.72*	*0.51*		*1.31*		*59.35*	*8.08*	*8.04*		*10.73*
		Kentrolite		-	-	*0.87*	*0.75*	*1.49*	*18.97*			*1.41*		*16.28*	*3.38*	*0.79*	*1.65*	*54.41*
CRVM-223	Almohad	Black	I	X	U	1.54	0.62	2.14	34.63		0.68	1.69	0.92	1.95	1.34	1.96	2.65	49.87

Coloured glaze: Green and turquoise

Green and turquoise coloured glazes were obtained by the application (overglaze) of a CuO-rich pigment, which is completely dissolved in the glaze. In all cases, cassiterite (SnO_2) dispersed crystals were also identified. CuO concentration (Table 47) ranges between 1.19 and 6.95 wt%, and turquoise glazes normally showed a higher concentration of both CuO and SnO_2. Small amounts of MnO were also identified.

Unmelted quartz crystals could also be present, and on sample CRVM-1097 they are positioned in the upper surface of the glaze, suggesting that they were appropriately added to increase the glaze opacity. On sample CRVM-642 several particles of clay were also observed. Besides, in this sample, Al_2O_3 and FeO are relatively high. Bubbles rarely appeared, with the exception of sample CRVM-666.

P_2O_5 concentration was usually low in most cases, but on sample CRVM-666, it was higher (4.13 wt%). Besides, hydroxyapatite inclusions were observed on samples CRVM-666/1668, and the identification was confirmed both by SEM-EDS (Table 47) and μRaman

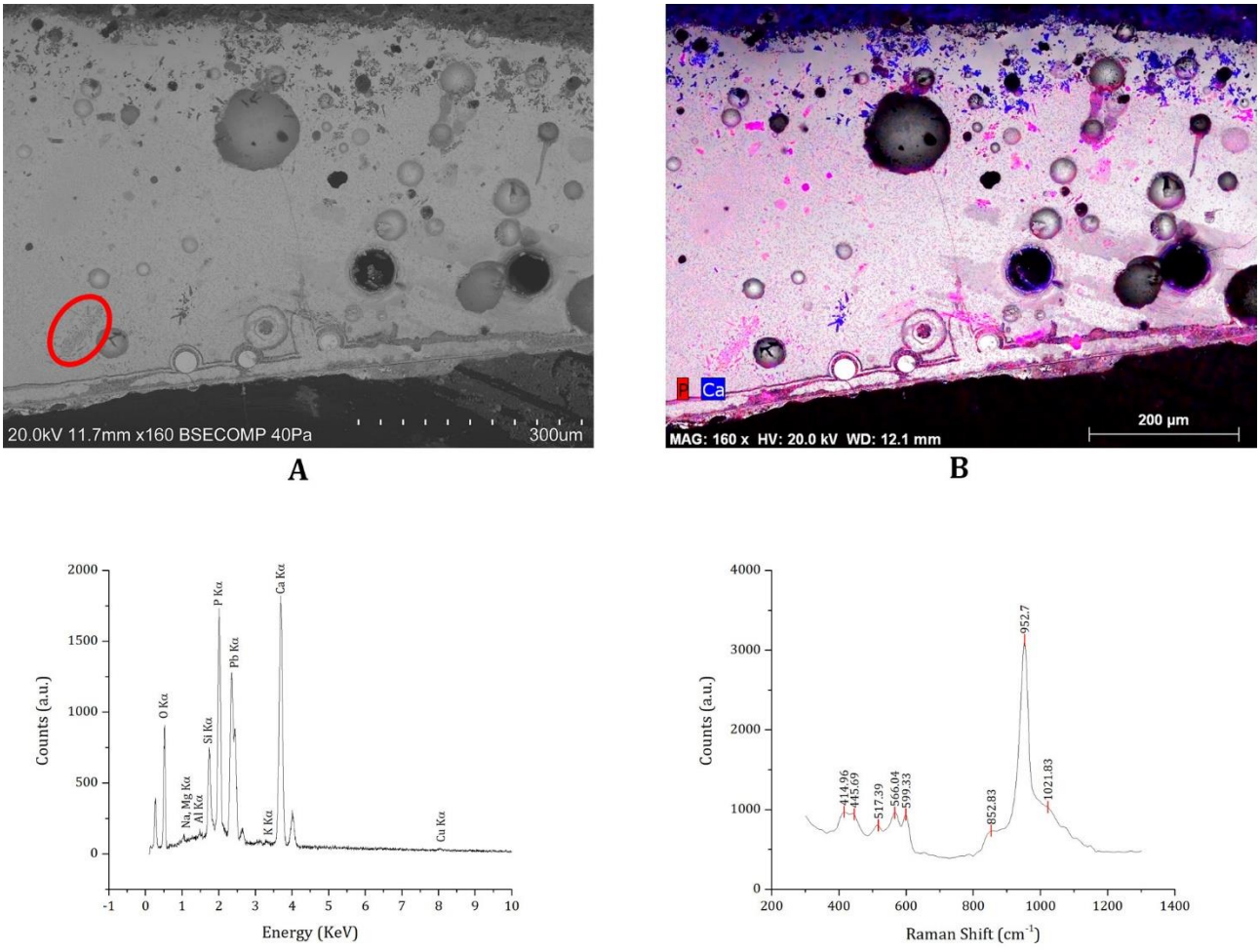

Figure 83 BSE image (A) of the green glaze of sample CRVM-666 and of the elemental mapping distribution of P and Ca within the glaze (B). Spot chemical analysis of the area evidenced by a circle in picture A, are presented in table 47. In figure C and D, the EDS and μRaman spectrum of grey particles evidenced by a red circle on figure A.

spectroscopy. In both cases, they are characterized by a high concentration of CaO and P_2O_5 and by the identification of the *v1* $(PO_4)^{-2}$ vibrational mode at 951 and 953 cm^{-1}, respectively (Fig.83C/D). Raman bands were slightly shifted to lower frequencies if compared to the values reported in the literature (Penel et al., 1998; Colomban et al., 2004), similarly to the black coloured glaze.

On samples CRVM-1668, a small aggregate of particles appears, while on sample CRVM-666, hydroxyapatite occurs as small inclusion (smaller than 1-2 μm) dispersed in the glaze (Fig. 83A). Moreover, elemental mapping distribution (Fig. 83B) evidenced the lack of hydroxyapatite particles close to the glaze-ceramic interface, suggest that hydroxyapatite was probably added overglaze in combination with the CuO rich pigment. Also, in these cases, hydroxyapatite identification clearly points to the addition of bone particles as opacificant.

Coloured glaze: Yellow

A yellow glazed (Fig. 84A) sample was analysed (CRVM-1659). Differently from the green and the black glaze on the same samples, many unmelted quartz crystals were observed (Fig. 84B). Moreover, the decoration was applied over the white tin opacified decoration. The decoration is characterized by a relatively high concentration of FeO and Sb_2O_3 (Table 48). The first one is homogeneously dispersed in the yellow glaze. On the contrary, microanalysis evidenced that antimony is generally hosted by numerous polyhedral lead antimoniate ($Pb_2Sb_2O_7$) inclusions, acting as an opacifier and as colouring agent.

The characteristics of the glaze, such as the chemical composition, the method of application and the utilization of antimony, show strong similarities with Fatimid glazed ceramic production from the North of Africa (i.e. *Ifrīqiya*) (Salinas et al., 2019a).

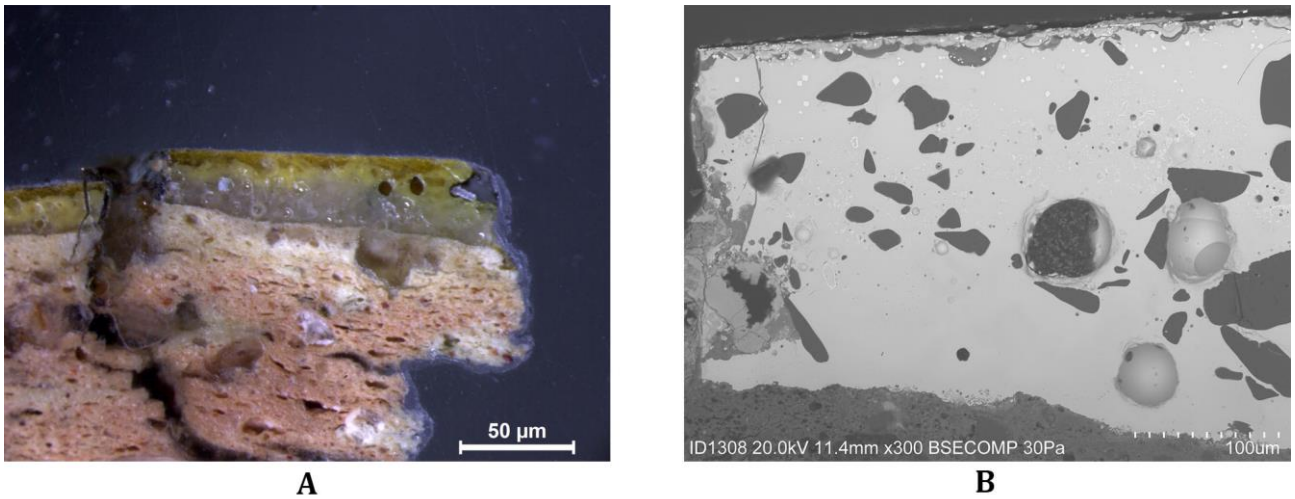

Figure 84 Image collected by optical microscopy (A) and BSE image (B) of the yellow glaze on sample CRVM-1659.

Table 47 Chemical analysis results obtained by SEM-EDS analysis of the sample green-turquoise glazes. Spot analysis developed on specific samples are reported in italic. Results normalized to 100%, uncertainty 1σ. Qz, presence (X) or absence of quartz grains in the glaze. Alt., glaze alteration; U, unaltered – P, partly altered – A, totally altered.

Sample	Chronology	Glaze colour /inclusion	Fabric-subgroup	Qz	Alt.	Na_2O	MgO	Al_2O_3	SiO_2	P_2O_5	K_2O	CaO	TiO_2	MnO	FeO	CuO	SnO_2	PbO
CRVM-357	Caliphal	Green	Ia		U	1.29	0.66	2.56	34.17		0.72	1.72			1.80	3.91	1.13	52.02
CRVM-623	Caliphal	Green	Ia		U	2.02	0.73	2.72	39.28	0.22	2.02	2.95		1.68	1.30	2.63	1.10	43.33
CRVM-666	Caliphal	Green	Ia		U	1.05	0.47	0.95	24.84	4.13	0.61	9.24			0.13	1.95	0.84	55.78
		Bone inclusion				*0.87*	*0.29*	*0.5*		*25.11*	*0.26*	*37.5*			*0.24*	*0.55*	*7.01*	*27.69*
		Glaze				*1.69*	*0.98*	*1.33*	*25.39*	*2.13*	*0.67*	*6.31*			*0.47*	*2.62*	*1.17*	*57.25*
CRVM-642	*Taifa*	Green	Ia	Q	U	0.68	0.69	5.17	39.87	0.42	2.58	4.53	0.78		2.58	2.06		40.62
CRVM-1097	*Taifa*	Green	III	Q	U	2.45	0.91	1.83	43.14	0.28	2.10	3.54		1.22	1.81	3.06	1.12	38.55
CRVM-1659	*Taifa*	Green	II		U	1.05	0.56	0.92	34.30		0.81	1.76			1.28	3.22	1.85	54.24
CRVM-1668	*Taifa*	Green	Ia		U	2.14	0.35	1.16	36.48	0.34	0.49	2.26		0.97	0.86	2.29	1.32	51.33
		Bone inclusion				*0.68*	*0.02*	*0.51*	*12.45*	*25.45*		*37.70*		*0.37*	*0.40*	*0.83*		*21.60*
		Glaze				*3.05*	*0.66*	*1.78*	*39.21*	*0.47*	*0.77*	*3.6*		*0.87*	*0.59*	*2.41*	*1.28*	*45.32*
CRVM-1671	*Taifa*	Green	Ia	Q	U	1.42	1.03	3.52	40.74	0.24	1.25	4.17	0.68		1.18	6.95	0.66	38.17
LVG-02-SXVIII-187	*Taifa*	Green	Ia	Q	P	1.92	0.65	1.19	39.62	0.65	1.40	3.91	0.67	0.37	0.92	1.19	1.26	46.25
CRVM-1665	Almoravid	Turquoise	III		U	1.17	0.32	1.79	36.40		1.33	2.37			1.21	3.06	4.97	47.39
CRVM-1670	Almoravid	Turquoise	III		P	1.80	0.45	1.69	35.97		1.57	3.00	1.94		1.53	5.09	2.86	44.10
CRVM-1669	Almohad	Turquoise	Ia		U	1.69	0.50	1.73	31.33	0.36	0.43	2.81			2.15	5.36	3.02	50.62
CRVM-223	Almohad	Green	I		U	1.59	0.66	1.48	35.31	0.08	0.71	1.39	0.90		1.36	1.72	3.11	51.69

Table 48 Chemical analysis results obtained by SEM-EDS analysis of the yellow glaze on sample CRVM-1659. Results normalized to 100%, uncertainty 1σ.

Sample	Chronology	Fabric-subgroup	Na_2O	MgO	Al_2O_3	SiO_2	K_2O	CaO	MnO	FeO	Sb_2O_3	PbO
CRVM-1659	Taifa	II	0.94	0.26	1.08	34.50	0.62	1.17	0.23	1.42	3.49	56.29

5.4.5.4.2.4 Partial *Corda Seca* glazed ceramic

The decoration of 6 samples of partial *corda seca* ceramics were analysed, and results are presented in tables 49 and 50.

Differently from green and brown glazed ceramics, samples are mostly from the Almoravid period, except for sample CRCSP-0029 that has a later chronology (i.e. Almohad).

Turquoise, honey and black glazes were observed and analysed (Fig. 85, Table 49). Fragments could be decorated just with one (samples CRCSP-0030-0028-0029), two (samples CRCSP-0031/0021) or three (samples CRCSP-0027) different coloured glazes. The results of the analysis of the corda line are also presented for some samples (CRCSP-0030/0031/0021/0029). Glaze thickness is variable, and it can be more than 300 µm thick in some samples (Table 49).

On *corda seca* style ceramics different frits can be prepared separately (Chapoulie et al., 2005), and they can be opacified or not. To obtain a good final result the ceramist must avoid glazes overlapping during firing.

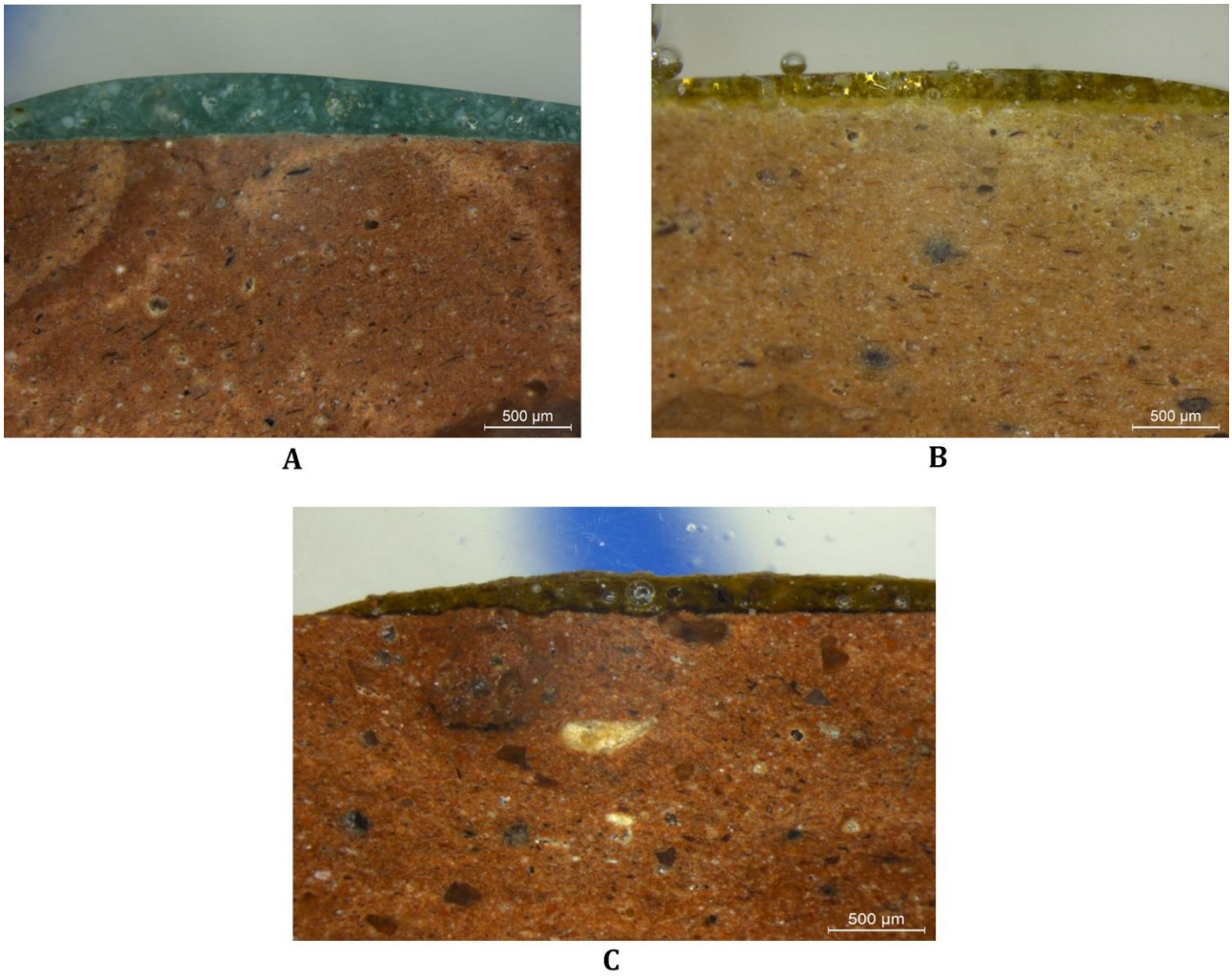

Figure 85 Pictures collected by optical microscopy. A) Sample CRCSP-0030 – Turquoise glaze; B) Sample CRCSP-0021 – honey glaze; C) CRCSP-0031 – black glaze.

Glazes characteristics will be described separately considering the different colours. A general classification will be made considering SiO_2, PbO, alkali and alkaline earth metals content, similarly to green and brown glazed ceramics. Samples are also included in different fabric sub-groups (Ia and Ib), and fabric (III, sample CRCSP-0029), and the results obtained on sections 5.4.5.1, 5.4.5.2, 5.4.5.3 and 5.4.5.4.1 (i.e. OM, XRPD, XRF-ICP/MS and SEM -EDS ceramic paste sections) will be considered to evaluate glaze technology.

Table 49 Sample glazes thickness analyzed for partial corda seca ceramics

Sample	Fabric/ Sub-group	Glaze thickness (range), mm			
		Black	Turquoise	Honey	*Corda line*
CRCSP-0030	Ia		370-240		20-10
CRCSP-0031	Ib	210 - 120	190-90		10
CRCSP-0028	Ib		160-100		
CRCSP-0027	Ia	160-110	180-160	200-160	
CRCSP-0021	Ia		170-150	180-140	80-20
CRCSP-0029	III			340-130	20

Glazes (Table 50) are mostly of the lead-alkali type (PbO $<$ 50 wt%. - high alkali+alkaline earth), and just in one case (CRCSP-0031 black) it was classified as high-lead (PbO $>$ 50 wt% - low alkali+alkaline earth). Nevertheless, there are two exceptions to this general classification. Samples CRCSP-0028/0031 glazes (i.e. turquoise glazes) have a PbO concentration lower than 50 wt% and low alkali plus alkaline earth content compared to high-lead and lead-alkali type glazes, respectively.

In any case, from the compositional point of view, PbO and SiO_2 content reflect the typical concentration identified by different researchers (Déléry, 2006a; Chapoulie et al., 2005) for *Taifa* and Almoravid *corda seca* glazed ceramics. The authors also reported an increase in SiO_2 concentration compared to the firsts prototypes of *corda seca* glazed ceramics. This, modification in glaze composition enhance glaze melt viscosity (Tite et al., 1998), and consequently, to decrease the risk of glaze overlapping. A similar PbO/SiO_2 ratio was reported in some green and brown ceramics presented in section 5.4.5.4.2.3.

Alkali and alkaline earth metals oxides were utilized as flux and/or stabilizer/modifier properties (Pradell and Molera, 2020).

Table 15 and 16 from annex 4 were used to estimate the introduction of different components to the glaze mixture in addition to SiO_2 and PbO. A similar operation was performed to evaluate the addition of different compontent to the glaze mixture of green and brown glazed secramics in section 5.4.5.4.2.3.

Several differences can be noted in the recasted chemical concentration of sample ceramic pastes and glazes. It suggests that distinct raw materials were used and the contribution of the ceramic paste to the final glaze composition is marginal.

Na_2O recasted concentration in the glaze is very high compared to the ceramic paste, suggesting the addition of flux, probably from plant ash (Pradell and Molera, 2020). This effect was weak or absent on samples CRCSP-0029 (honey glaze) and CRCSP-0031 (black glaze). In the case of K_2O, concentrations are slightly similar, and small variations can be associated with the addition of some clay to the glaze mixture. This is particularly evident in the case of honey and black glazes chemical compositions compared to the turquoise glaze in Table 50.

Among alkaline earth metal oxides, MgO content is rather low and similar in all cases, and just small differences have been noted. Glazes are also depleted in CaO if compared to ceramic paste. This suggests, in the case of MgO and CaO, low diffusion from the ceramic paste to the glaze.

Bone fragments (Table 50) were identified in the glaze of two different samples (CRCSP-0027, turquoise and honey / CRCSP-0030, turquoise) from sub-group Ia. They appear as isolated clusters of particles or, like on sample CRCSP-0027 (Fig. 86A), as a piece of bone inside the glaze. Thus, they were probably introduced as opacifier in the glaze, similarly to green and brown ceramics. Our observation also suggests that they were probably introduced during the fritting process. Nonetheless, P_2O_5 concentration is rather low or absent in all cases, and even on samples CRCSP-0027/0030 it marginally contributes to the final glaze composition.

Turquoise glazes

Turquoise glazes were identified on five samples included in sub-groups Ia and Ib (Fig. 86A, B - Table 49, 50). The principal colouring agent was CuO with variable amounts of FeO, and in all cases, it was opacified using SnO_2. It appears as small acicular/sub-rounded cassiterite inclusions dispersed in the glaze.

Unmelted crystals of quartz were also observed dispersed in the glaze on samples CRCSP-0028/0031 (sub-group Ib), and they contribute to the glaze opacity. So, glazes were opacified twice (Chapoulie et al., 2005) as observed for green and brown ceramics in section 5.4.5.4.2.3. These samples also have different glaze chemical compositions within the turquoise glaze group. These observations clearly suggest that various workshops existed in Mértola during the Almoravid period, and they produced the same glaze colour differently. Besides, ceramics are included in different sub-groups (Ia and Ib), and both were locally produced.

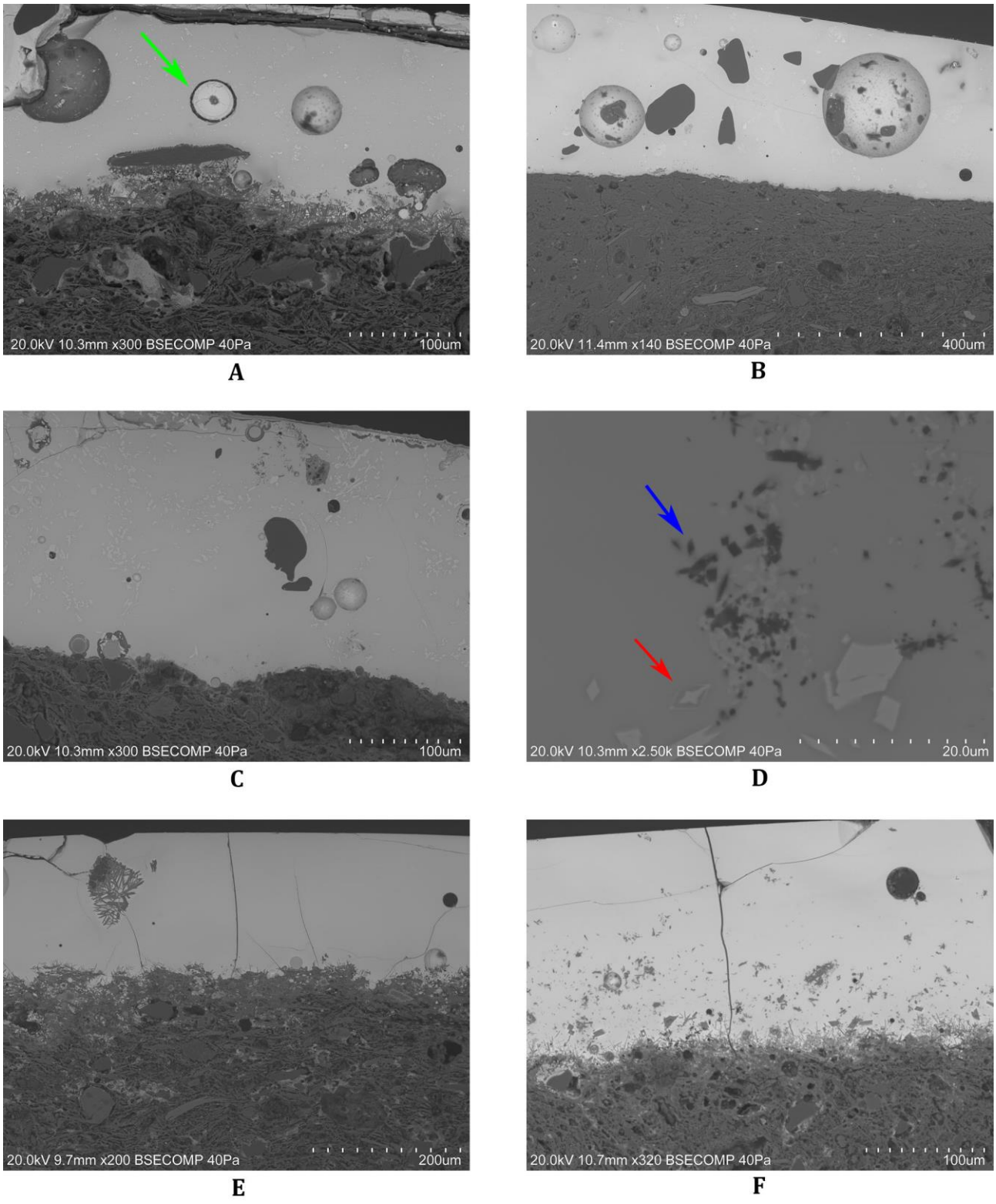

Figure 86 BSE images of the turquoise glazes on sample CRCSP-0027 (A), CRCSP-0030 (B); of the black glaze on sample CRCSP-0031 (C, D); of the honey glaze on samples CRCSP-0021 (E) and CRCSP-0029 (F). On figure A, a bone fragment is evidenced by a green arrow, while on figure D the blue and red arrows evidenced hematite and melanotekite crystals respectively.

Table 50 Chemical analysis results obtained by SEM-EDS analysis of partial corda seca glazed ceramics. Results normalized to 100%, uncertainty 1σ.

Sample	Chronology	Glaze colour / *corda*	Fabric - subgroup	Na_2O	MgO	Al_2O_3	SiO_2	P_2O_5	K_2O	CaO	TiO_2	MnO	FeO	CuO	ZnO	SnO_2	PbO	Alkali + alkaline earth
CRCSP-0030	Almoravid	Turquoise	Ia	3.53	0.75	1.40	42.94	0.39	2.12	2.17	0.44		1.22	3.34	0.73	2.38	38.58	8.57
		Bone inclusion		*1.08*	*0.44*	*0.94*	*13.22*	*25.74*	*0.55*	*33.16*			*1.20*	*1.34*		*1.16*	*21.16*	
		Glaze		*3.62*	*0.60*	*1.27*	*46.09*	*0.79*	*2.17*	*2.91*	*0.72*		*0.32*	*3.34*		*1.13*	*37.04*	
CRCSP-0030	Almoravid	*Corda*	Ia	2.89	1.58	2.34	46.65	1.14	3.32	4.27	0.80	1.42	11.91	1.89		3.08	18.70	12.07
CRCSP-0031	Almoravid	Turquoise	Ib	1.95	0.73	1.92	37.40	0.23	1.10	1.96	0.61		1.50	2.57		1.57	48.47	5.74
CRCSP-0031	Almoravid	Black	Ib	0.78	0.44	1.99	33.55		0.72	1.43	0.88		6.07				54.15	3.36
CRCSP-0031	Almoravid	*Corda*	Ib	2.12	2.32	19.08	48.23	0.25	3.46	5.35	1.02		6.25				11.91	13.25
CRCSP-0031	Almoravid	*Blue arrow*	Ib	0.78	8.81	1.95	42.93	0.91	0.69	12.43	0.5		5.76				25.22	22.71
CRCSP-0031	Almoravid	*Red arrow*	Ib	0.75	0.39	0.98	20.62	0.69	0.25	0.73	0.73		14.56				60.29	2.13
CRCSP-0028	Almoravid	Turquoise	Ib	2.71	0.65	1.60	37.58	0.44	0.98	1.59	1.43		0.83	3.38		2.68	46.13	5.93
CRCSP-0027	Almoravid	Turquoise	Ia	3.09	0.85	2.16	42.70	0.30	1.82	3.07	0.70		1.68	3.14		2.17	38.33	8.83
		Bone inclusion		*0.53*	*0.26*	*1*	*7.62*	*16.47*	*0.32*	*13.80*			*1.12*	*1.86*		*1.51*	*55.53*	
		Glaze		*2.63*	*0.91*	*2.01*	*43.78*	*0.17*	*2.06*	*2.96*	*1.02*		*0.69*	*3.46*		*1.19*	*39.11*	
CRCSP-0027	Almoravid	Honey	Ia	1.76	0.65	4.63	37.48	0.22	2.06	4.27	1.06	0.25	2.39				45.24	8.73
		Bone inclusion		*1.46*	*0.73*	*4.32*	*9.84*	*16.26*	*1.38*	*19.76*			*1.41*				*44.48*	
		Glaze		*2.05*	*0.92*	*3.84*	*42.63*		*2.11*	*3.43*	*0.34*		*2.38*	*1.71*		*1.36*	*39.55*	
CRCSP-0027	Almoravid	Black	Ia	1.98	0.74	5.53	40.83	0.36	2.85	4.47	0.81	1.34	3.81				37.28	10.04
CRCSP-0021	Almoravid	Turquoise	Ia	3.14	1.18	2.80	41.56	0.52	2.20	4.20	0.63		3.05	3.09		2.71	34.94	10.72
CRCSP-0021	Almoravid	Honey	Ia	1.81	0.67	4.86	36.47		2.42	5.33	0.94		3.69				43.82	10.23
CRCSP-0021	Almoravid	Black	Ia	1.85	1.00	4.54	33.84	0.23	2.18	6.91	0.99	1.79	20.86	1.30			24.51	11.94
CRCSP-0029	Almohad	Honey	III	0.87	0.77	5.91	38.50	0.15	1.94	5.07	0.78		4.13	0.92			40.96	8.65
CRCSP-0029	Almohad	*Corda*	III	1.10	1.89	3.41	19.13	0.48	0.58	4.94	0.26	1.27	66.95					

Black glaze

Black glaze (Table 50) were analysed on two different samples (CRCSP-0027/0031) included in sub-groups Ia and Ib. Nevertheless, they have different characteristics supporting the hypothesis they were manufactured in different workshops, as in the case of turquoise glazes.

On sample CRCSP-0027, the main colouring agents were FeO and MnO, and they were generally dissolved in the glaze. Nevertheless, some FeO and MnO rich particles were observed close to the interface, suggesting that the black pigment was applied under the glaze. Moreover, the observation of several Al_2O_3-K_2O rich inclusions identified in the middle of the glaze also points to the addition of some clay to the glaze mixture. SnO_2, in this case, was not detected.

Conversely, on sample CRCSP-0031, FeO was the only coloring agent. It was partly dissolved in the glaze or concentrate on numerous crystallites with high contrast on BSE image (Fig. 86C). Particles position and concentration in the top part of the glaze point to overglaze pigment application. On figure 86D is presented another BSE image, where crystallites with high and low contrast are clearly visible. Micro-chemical and morphological analysis suggest that high contrast crystallites might be classified as melanotekite ($Pb_2Fe_2Si_2O_9$) crystals (Di Febo et al., 2017a; Di Febo et al., 2017b), which crystallize above 900°C by the reaction of hematite (low contrast crystallites on BSE image) with the lead glaze.

Honey glazes

Honey glazes (Fig. 86E/F) were analysed in three different samples (CRCSP-0021/0027/0029), two from sub-group Ia and one sample from fabric III. The chronology is also different and two samples are from the Almoravid and one from the Almohad period. The colour is always due to the presence of FeO (Table 50) in the glaze and by the colour of the ceramic paste seen through the transparent glaze. Glazes chemical composition is also very similar (Table 50), but bone fragments were identified dispersed in the glaze (CRCSP-0027) or mixed in the ceramic paste/glaze interface (CRCSP-0021/0027, see section 5.4.5.4.2.1 and Fig. 76E/F) in samples included in sub-group Ia.

Corda seca line

The *corda seca* line (Table 50) was generally painted using MnO and/or FeO rich pigments. Some glaze was observed over the line on samples CRCSP-0021/0030/0031, and in one case, SnO_2 was identified as well. Thus, it is not clear whether some glaze involuntary overlapped the *corda seca* line or if it is a technological choice.

5.4.5.4.2.5 Honey and Black glazed ceramic

The honey and black ceramic was decorated by a high-lead glaze on both sides of the artefact. Alkali and alkaline earth metal oxides contents are very low. Globally, glazes have a very similar chemical composition to the glaze drop analysed on the kiln bar in section 5.4.5.4.2.2, and it has the same chronology. FeO is the colouring agent of the background of the decorated side and of the reverse side, and glazes are honey in colour.

The black glaze is very similar in chemical composition to the background and of the reverse side glazes. The black colour was obtained by the addition of a MnO and FeO rich pigment.

SEM-EDS analysis of the black glaze evidenced the abundance of MnO-FeO rich crystallites very close to the ceramic paste, suggesting that the pigment was applied underglaze (Fig. 87A/B). Micromorphological and chemical analyses by SEM-EDS (Fig. 87C/D) evidenced that crystallites with low contrast on BSE images are MnO rich, and they might be classified as braunite (Mn_7SiO_{12}). Crystallites with higher contrast that nucleate from braunite minerals can be classified as kentrolite ($Pb_2MnSi_2O_9$) (Molera et al., 2013).

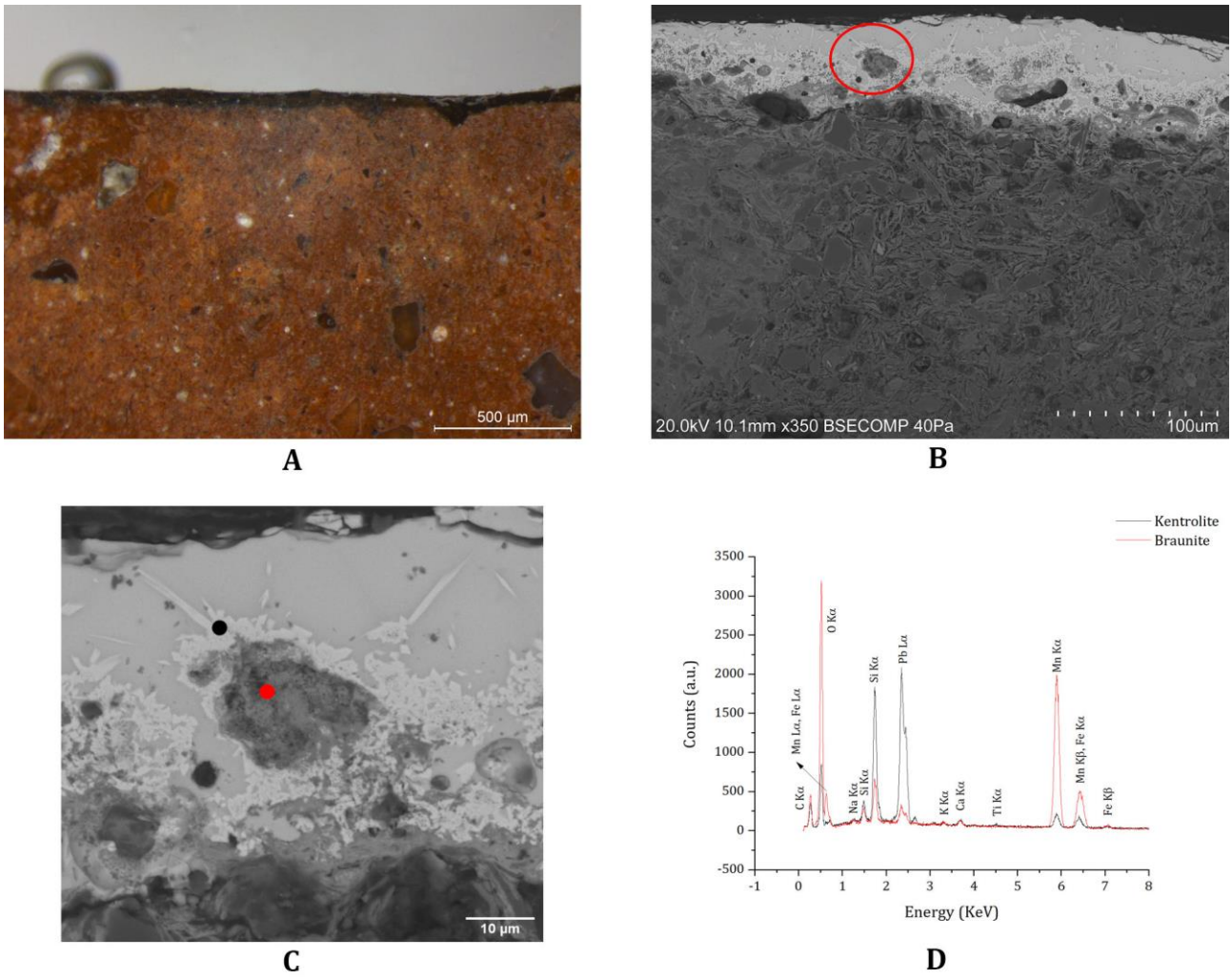

Figure 87 Pictures collected by optical microscopy (A) and on BSE mode of the black glaze on sample CRVF-0003. On figure C two different spots (red and black) were analyzed by micro-analysis and on figure D the spectrum are presented.

Table 51 Chemical analysis results obtained by SEM-EDS analysis of the honey and black sample. Results normalized to 100%, uncertainty 1σ.

Sample	Glaze side	Glaze colour	Thickness, µm	Na_2O	MgO	Al_2O_3	SiO_2	P_2O_5	K_2O	CaO	TiO_2	MnO	FeO	PbO	PbO/SiO_2	Alkali + alkaline earth
CRVF-0003	Decorated side / background	Honey	60-40	0.63	0.85	4.99	32.64		0.93	1.36	1.31		2.22	55.06	1.69	3.69
	Decorated side / coloured glaze	Black	60-50	0.40	0.64	4.76	32.80		0.88	1.76	0.93	2.25	1.94	53.64	1.64	3.68
		Black spot	n.a.	0.58	0.4	3.55	26.04	0.27	0.66	1.48	1.21	5.64	5.13	55.03		3.12
		Red spot	n.a.	0.66	0.67	3.03	9.24	0.44	0.36	0.98		63.61	14.75	6.27		2.66
	Reverse side	Honey	70-50	0.42	0.93	5.33	34.10		0.82	1.44	0.79		2.16	54.01	1.58	3.56

5.4.6 Final remarks of the section

The results obtained by the analysis of the ceramic samples from the town of Mértola evidenced that most decorated glazed ceramics included in fabric I and sub-group Ia and Ib were locally produced in different chronological periods. This is a new archaeometric contribution, only suggested in the past (Zozaya and Aparicio Yague, 2003).

Indeed, the minerals and rock fragments identified are compatible with the local geology, indicating that the raw material was exploited associated with the *Baixo Alentejo Flysch* geological unit. Moreover, the identification of different inclusion types (i.e. lime rich – yellowish/greys anhedral inclusions - glass fragments) on glazed ceramic pastes during PLM analyses, clearly indicates that a specific and different (i.e. from the white painted fragment and kiln rods) manufacturing process was employed, with the addition of different components to the ceramic pastes.

So, the ceramic paste texture could be dissimilar, and this is why different sub-groups (Ia, Ib) of fabric I have been created. The utilization of a specific preparation process is also testified by temper and porosity amount, when compared to the white painted fragment and to kiln rods. Besides, glazed ceramics are less porous and have less temper. Moreover, on glazed ceramic samples temper grain size was generally smaller, ans grains were also more rounded. Thus, raw materials was decanted to get rid of the bigger inclusions, and temper was added depending on the final characteristics of the ceramic paste.

Different artefacts included in fabric II and III were produced using a typical calcareous raw material, and they were imported to the town from the North of Africa (CRVM-1659) and, probably, from the area of Malaga (CRVM-1097-1659-1665-1670, CRCSP-0029). These include four green and brown and one partial *corda seca* decorated ceramics.

XRPD results, identified two different mineralogical groups related to a silica rich and a calcium rich clays, testifying the potter's choice to produce glazed ceramic using a calcium rich raw material. This technology is widely attested on Islamic Iberia (Tite et al., 1998; Molera et al., 2001; Salinas and Pradell, 2018; Salinas and Pradell, 2020; Chapoulie et al., 2005; Peréz-Arantegui et al., 1999) to produce glazed ceramics. Besides, a CaO rich ceramic paste favours glaze adhesion to the ceramic support.

On XRPD pattern hydroxyapatite (HAp - $Ca_5(PO_4)_3(OH)$) was also identified in many samples, indicating that bones (or bone ashes) were added to the ceramic pastes. As evidenced in the literature, HAp start to dehydroxylate only approximately from 750-900 °C depending on the Ca/P ratio (Tõnsuaadu et al., 2012), and it retains some hydroxyl groups up to 1400 °C. HAp high temperature decomposition product (β-tricalciumphosphate – βTCP (β-$Ca_3(PO_4)_2$)

were detected on XRPD pattern of three samples (CRCSP0028-0030, CRVF-0003), indicating that HAp was relatively stable at the estimated ceramic firing temperature (850-1000 °C). On these samples, pyroxene and gehlenite did not crystalized, and βTCP peaks could be identified. Moreover, in one sample, PbO was also observed, indicating that also glass fragments were added to the ceramic paste.

XRF and ICP-MS analysis clearly identified all fabrics and sub-groups, and locally produced ceramics and kiln rods (fabric I, sub-groups Ia, Ib) were generally enriched in K_2O and depleted in Na_2O if compared to imported ones (fabric II, III). Chemical analyses also justified the formation of specific high temperature calcium rich mineralogical phases identified on XRPD patterns, but CaO origin was an important issue. Chemical data clearly suggested that different sources of CaO were possible in fabric I (excluding kiln rods and the white painted fragment) and sub-groups Ia and Ib ceramics, including bones (or bone ashes) and/or limestone fragments. Nevertheless, limestone fragments were generally the major source of CaO.

PbO concentration was also significant in several samples, indicating that glass/frit fragments were also added. These effects could also be present also in some imported ceramics suggesting a technological transfer between different places. In addition PbO could also be associated to P_2O_5 suggesting they could be included or mixed with glass/fritt.

SEM-EDS and, when obtained, μRaman results put in evidence new features and characteristics of sample ceramic pastes which could not be detected by PLM. Analyses established the characteristics and origin of the different components added to samples ceramic pastes. In addition micro-analyses definitely supported PLM, chemical and mineralogical observations. In most glazed samples bones (or bone ashes), glass/frit and limestone fragments could be added, simultaneously or not, to produce glazed ceramics included in different fabrics and sub-groups, excluding kiln rods and the white painted fragment.

Thus, a ceramist from Mértola needed to modify the characteristics of the local raw material because it was not suitable to produce green and brown, partial *corda seca* and honey and black glazed ceramics. This is particularly evident on glazed samples produced at Mértola and included in fabric I and sub-groups Ia and Ib. Moreover, similar characteristics were also observed on some imported ceramics (CRVM-1659/1097).

From the technological point of view samples ceramic bodies show similar characteristics to proto-stone-paste ceramic bodies from the Middle East (Mason and Tite, 1994) but, in or cases, with the addition of bones (or bone ashes). These technological options

are mostly new in Islamic Iberia, and the introduction of glass/frit fragments clearly indicate a technological transfer from the Middle East.

Moreover, the identification of a CaO and P_2O_5 rich slip in between the glaze and the ceramic body of samples CRVM-0357 (sub-group Ia) and sample CRVM-1659 (fabric II) clearly indicate that bones (or bone ashes) were mixed with clay and applied to the object surface. In these cases, ceramists were surely aware of the final colour of the slip (i.e. whitish), so it was probably applied to mask the reddish colour of the ceramic body and to increase glaze opacity (Pradell and Molera, 2020; Mason and Tite, 1994).

Glazed decoration on green and brown ceramic samples analysis evidenced that different glaze types (i.e. high lead or lead-alkali glaze) could be applied in the same piece. Consequently, a connection between the glaze technology applied, fabric and samples chronology did not exist. Only during the Almohad period, results suggest that high lead glazes were preferred in the production of green and brown and honey and black ceramics.

Conversely, partial *corad seca* glazes were generally of the lead -alkali type, and results are compatible with the literature for Almoravid *corda seca* glaze ceramics (Chapoulie et al., 2005).

In any case, the data allow the identification of bones (or bone ashes) in different glazed samples with different chronology and decorative styles, including green and brown and partial *corda seca* ceramics. This shows a voluntary addition of this component by the ceramist in the glaze mixture. The identification of bones (or bone ashes) particles by SEM-EDS and μRaman spectroscopy showed that they did not melt in the glaze at the estimated working temperature of the kilns (850-1000 °C), and that they could not be considered a source of CaO. Therefore, bones (or bone ashes) particles were added to increase glaze opacify in some green and brown and partial *corda seca* glazed ceramics.

Bones (or bone ashes) were mostly utilized to opacify Byzantine mosaic tiles (Silvestri et al., 2014; Silvestri et al., 2016; Neri et al., 2017) and rarely Islamic glasses from the Middle East (Freestone and Stapleton, 1998). Consequently, also in this case a technological transfer from the Middle East is the most probable option.

The archaeometric study of the Islamic ceramics from Mértola evidenced that green and brown ceramics were mostly produced in the town since the Caliphal period, and only some of them were imported. The same considerations can be made in the case of partial *corda seca* and honey and black ceramics since the Almoravid period. Therefore, this is an important archaeometric contribution to archaeologist, and diffusion of Mértola ceramics has now to be established.

To conclude, if compared with the Islamic ceramic produced in the city of Santarém there is a clear difference. The result of this research established that at Santarém two different raw materials were utilized to produce unglazed and glazed ceramics. Differently at Mértola the same raw material was adapted to produce different unglazed and glazed ceramic artefacts.

This is also a new archaeometric contribution show how Islamic ceramist were able to produce similar object using different raw materials and technological solutions.

6 Conclusions

Caliph: Comprehensive archaeological and laboratory investigation of Islamic pottery in Portuguese History

The main goal of this PhD thesis is to contribute to the knowledge about ceramic production and the societies that manufacture and trade in the *Garb al-Andalus* (Western Iberia during the Islamic times).

Most of the archaeometric data published by previous authors were collected on ceramic samples recovered in Spanish territory. Therefore, "Portuguese" Islamic ceramics are almost unknown from an archaeometric point of view. Moreover, post-Islamic and traditional ceramic assemblages were studied to evaluate the permanency of the Islamic culture. The relation of the population with the environment, namely with the availability and selection of the raw materials, must also be considered.

The study used complementary archaeometric methods such as polarized light microscopy (PLM), X-Ray diffraction (XRD), μRaman spectroscopy, FT-IR spectroscopy, X-Ray fluorescence spectroscopy, inductively coupled plasma mass spectroscopy (ICP-MS) and scanning electron microscope coupled to an EDS spectrometer (SEM-EDS).

Time and space are two variables that were considered in the project development and ceramic samples selection:

- Time, because it was essential to evaluate and understand the characteristics and evolution of utilitarian and decorated ceramics during the Islamic period and the influence of the "Portuguese Reconquista" on ceramic craftsmanship techniques. The city of Santarém has been chosen as a starting point.
- Space, because it is also essential to evaluate Islamic ceramics in different cities, regarding ceramic technology, influences and provenance of the objects. So, the city of Mértola was selected to compare with Santarém.

The selection of the city of Santarém and Mértola was not casual, and they were chosen for several reasons:

- Both cities are positioned far away from the coastline but located on the riverbanks (of the rivers Tagus and Guadiana). Thus, they were indirectly connected to the Atlantic Ocean and open to long-distance trade with different territories located on the borders of the Mediterranean Sea.
- The city of Santarém offered the opportunity to evaluate archaeological sites and ceramic materials with a chronological continuity from the 8th - 9th century to the 15th - 16th century. Moreover, presently, several traditional ceramics artisans were active in the area. Thus, it was possible to sample Islamic-*Reconquista*-

Portuguese ceramics and study ceramic provenance, technology, and craftsmanship legacy.

- The investigation of two different cities is an opportunity to evaluate Islamic ceramic provenance and technology in the *Garb al-Andalus*.
- The Islamic ceramic collection of Mértola is one of the most important in Portugal, and ceramic with different decorative styles is present. Such variety is not available at Santarém, as it is typical of Southern Iberian cities. So, it was possible to evaluate the ceramic technology evolution since the very beginning of the Islamic domination.

Results evidenced that different kinds of ceramics wares were produced in Santarém during the Islamic domination, such as undecorated, painted (white and red painted) and glazed ceramics. In this category monochromatic, dichromatic (honey and black) and *corda seca* (partial and total) glazed ceramics were produced. Moreover, locally produced glazed ceramics could coexist with exogenous pieces, demonstrating that ceramics were also imported to the city from different unidentified places located in South/South-East Iberia.

Moreover, sediment – ceramics comparative analysis evidenced that two different raw materials were exploited and eventually mixed to produce undecorated/painted and glazed ceramics. In particular, red painted and glazed ceramics were produced using a kaolinite-rich raw material, which turned white after firing. Only in one case total *corda seca* style ceramic was produced using the same raw material usually exploited to produce undecorated and white painted wares.

This pattern of raw material exploitation continued during the Reconquista and after the integration of the city in the Portuguese Kingdom. Consequently, a complete change of the ruling power did not correspond to a substantial modification in ceramic technology.

Besides, ceramics were produced following specific technological criteria directly connected to the object function. These guidelines are still present nowadays in local traditional ceramics. The technological transfer was constant, and it continued without interruption, at least since the Islamic period. This also indicates that a community, independently from the historical period, is strictly connected to the raw materials available in the area where it lives.

Islamic and post-Islamic glazes were mainly produced using a high-lead or lead-alkali type mixture with a variable concentration of alkali and alkaline earth metals. Opacification was mainly obtained by the addition of quartz or SnO_2. Different colouring agents were also employed, such as CuO (green/turquoise), FeO (green/black) and MnO (black). The firing cycle

could be adapted to the different raw materials and objects, and single-fired and double fired ceramics were identified.

In the case of Mértola ceramics, the results were quite surprising, and it can modify the more recent interpretation models of the city. Most of the ceramics included in this PhD thesis were locally produced. The city surely was a producing center of fine ceramics, and not just an importer, as already suggested by different scholars.

The production was constant and continued without interruption since the Caliphal period, at least for green and brown ceramics. Partial *corda seca* and honey and back ceramics were also produced in the town. These ceramics productions also coexisted with imported pieces (green and brown – partial *corda seca*) from *Ifriqiya* (actual Tunisia) and from South/South-East Iberia, probably the area of Malaga. Moreover, ceramists adapted the productive ceramic cycle to the locally available raw materials.

More specifically, local ceramists transformed the local raw material with the addition of different components to the ceramic paste, such as glass/frit, bones (Hydroxyapatite - $Ca_5(PO4)_3(OH)$) or limestone fragments. So, it was easier to successfully apply high-lead and lead-alkali tin opacified glazes to the ceramic support. This kind of ceramic paste has similar characteristics to the most ancient Islamic proto-stone-paste ceramic bodies produced in the Middle East.

Similar characteristics were observed in two imported ceramic samples of green and brown ceramics, suggesting a common practice.

Bones (or bone ash) were also mixed with clay and applied as a slip to hide the reddish colour of the ceramic paste, or as opacifier (in addition to SnO_2 and quartz crystals). Moreover, as evidenced by the identification of different glass fragments in the ceramic paste, it could also be utilized in the fritting process of high-lead and lead-alkali frits.

Consequently, glazes could be enriched in alkaline earth metals, in particular CaO. This tendency was stronger in lead-alkali glazes and weaker in high-lead glazes, and bone (or bone ash) fragments could also be found in the glazed decorations. CuO (green, turquoise), MnO (black), FeO (honey, green, black) and Sb_2O_3 (yellow) were the main colouring agents identified on glazed samples.

Some important methodological considerations must be made to stress the importance of a specific technique for a specific thematic:

- In section 5.1, the combination of XRF and ICP-MS analysis on sediments and ceramics was essential to evaluate ceramic provenance and ceramist technological choices to produce different ceramic wares. Especially, it was

possible to determine that SiO_2 content has a dilution effect on trace elements and REE concentration. So, quartz tempering decreases trace elements and REE content.

- In section 5.2, the combination FT-IR, μRaman and ICP-MS analyses were essential to evaluate archaeological ceramic compatibility with kiln wastes and determine raw materials exploitation patterns over time. Thanks to FT-IR and μRaman spectroscopy, it was possible to identify identical mineralogical species in different ceramic fragments. At the same time, ICP-MS established a connection between kiln waste and ceramic samples thanks to the Zr, Y, Hf, U and Th concentrations.
- In section 5.3, physical and mechanical tests were essential to correlate the ceramic typology and the object function, both on archaeological and traditional ceramics. Besides, they were produced following specific technical criteria. These characteristics could not be determined by PLM, XRPD and XRF analysis.
- In section 5.4, microanalysis by SEM-EDS and μRaman spectroscopy allow the identification and analysis of glass/frit (in the ceramic paste), limestone (in the ceramic paste) and bone (or bone ash) fragments (in ceramic the paste and glaze). Thanks to the combination of these two analytical techniques, it was possible to determine the introduction of different technological solutions in Islamic Iberia. The first one is the adaptation of local clayey raw materials to produce glaze ceramics. In this case ceramic pastes have similar characteristics to the proto-stone-paste ceramic bodies produced in the Middle East. The second one is the utilization of bones (or bone ash) to increase glaze opacity.
- In every section, PLM analysis was the most useful and cheap method of study. All work was developed after a deep and complete study of ceramic thin sections.

To conclude, this Ph.D. is a contribution to the understanding of Islamic ceramic in the Portuguese territory. Complementary studies are needed for a complete evaluation of the material culture of this period. The future research lines should surely include the expansion of ceramic sampling to different cities and the use of other methodological approaches. In particular, pXRF (portable X-Ray Fluorescence) would allow the analysis of a large number of artefacts to establish compositional clusters in the Garb al-Andalus and lead isotope analysis by LA-ICP-MS on selected samples of glazed ceramics can help in establishing the circulations of lead ore for glaze production in the same territory.

Bibliography

Caliph: Comprehensive archaeological and laboratory investigation of Islamic pottery in Portuguese History

Abdel-Rehim, A.M., 2006. Thermal and XRD analysis of Egyptian galena. J. Therm. Anal. Calorim. 86, 393–401. https://doi.org/10.1007/s10973-005-6785-6

Acién Almansa, M.P., 1993. La cultura material de época emiral en el sur de al-Andalus. Nuevas perspectivas, in: Malpica Cuello, A. (Ed.), La Cerámica Altomedieval En El Sur de Al-Andalus : Primer Encuentro de Arqueología y Patrimonio. Universidade de Granada, Granada. España, pp. 153–172.

Acién Almansa, M.P., 1984. La formación y destrucción de Al-Andalus, in: Barceló Perelló, M. (Ed.), Tierras Fronterizas : Andalucía, Canarias. Editorial Argos Vergara, pp. 21–46.

Acién Almansa, M.P., Martínez Madrid, R., 1989. Cerámica islámica arcaica del sureste de al-andalus. Boletín Arqueol. Mediev. 3, 123–135.

Adams, E.A., Mackenzie, W.S., Guilford, C., 1984. Atlas of sedimentary rock under the microscopes, Longman Sc. ed. longman Group, Harlow.

Alba Calzado, M., Gutiérrez Lloret, S., 2008. Las produciones de transición al Mundo Islámico: el problema de la cerámica paleoandalusí (siglos VIII y IX), in: Bernal Casasola, D., Ribera i Lacomba, A. (Eds.), Cerámica Hispanorromanas. Un Estado de La Cuestión. Universidad de Cadiz, pp. 585–613.

Albero Santacreu, D.J., Mateu Vicens, G., Ramos Benito, A., Carvajal López, J.C., Georgakopoulou, M., 2019. Pottery in the backyard: Almohad ceramic distribution networks in rural areas (SW Mallorca, Spain). Archaeol. Anthropol. Sci. 11, 4769–4788. https://doi.org/10.1007/s12520-019-00814-7

Allan, J.W., 1973. Abū ' l-Qāsim ' s Treatise on Ceramics. Iran 11, 111–120.

Allegretta, I., Eramo, G., Pinto, D., Hein, A., 2017. The effect of mineralogy, microstructure and firing temperature on the effective thermal conductivity of traditional hot processing ceramics. Appl. Clay Sci. 135, 260–270. https://doi.org/10.1016/j.clay.2016.10.001

Allegretta, I., Eramo, G., Pinto, D., Hein, A., 2014. The effect of temper on the thermal conductivity of traditional ceramics: Nature, percentage and granulometry. Thermochim. Acta 581, 100–109. https://doi.org/10.1016/j.tca.2014.02.024

Almeida, M.J., 2002. O planalto de Marvilla e os núcleos Ribeirinhos, in: Arruda, A.M., Viegas, C., Almeida, M.J. (Eds.), De Scallabis a Santrém. Museo Nacioanal de Arqueologia, Lisbon, Portugal, pp. 83–93.

Almodóvar, G.R., Yesares, L., Sáez, R., Toscano, M., González, F., Pons, J.M., 2019. Massive sulfide

ores in the iberian pyrite belt: Mineralogical and textural evolution. Minerals 9. https://doi.org/10.3390/min9110653

Alvarez, M.A., Coy-Yll, R., 1978. Raman spectra of tourmaline. Spectrochim. Acta Part A Mol. Spectrosc. 34, 899–908. https://doi.org/10.1016/0584-8539(78)80010-5

Alves Conde, M.S., 2005. Fronteira, guerra e organização social do espaço: o Vale do Tejo entre muçulmanos e cristão, in: Barroca, M.J., Ferreira Fernandes, I.C. (Eds.), Muçulmanos e Cristão Entre o Tejo e o Douro (Sécs. VIII a XIII). Câmara Municipal de Palmela - Faculdade de Letras Universidade do Porto, Palmela, pp. 43–52.

Armstrong, P., Hatcher, H., Tite, M.S., 1997. Changes in Byzantine glazing technology from the ninth to thirteenth centuries, in: D'Archimbaud, G.D. (Ed.), La Céramique Médiévale En Méditerranée. Actes Du VI Congrés de l'AIECM2, Aix-En-Provence, 13-18 Novemvre 1995. Narration Édition, Aix-en-Provence, pp. 225–229.

Arnold, D.E., 2000. Does the Standardization of Ceramic Really Mean Specialization? J. Archaeol. Method Theory 7, 333–375. https://doi.org/10.1023/A:1026570906712

Arnold, D.E., Neff, H., Bishop, R.L., 1991. Compositional Analysis and "Sources" of Pottery: An Ethnoarcheological Approach. Am. Anthropol. 93, 70–90. https://doi.org/10.1525/aa.1991.93.1.02a00040

Arruda, A.M., 2002a. Los Fenicios en Portugal. Fenicios y mundo indígena en el centro y sur de Portugal (siglos VIII-VI a. C.). Cuad. Arqueol. Mediterránea 5–6.

Arruda, A.M., 2002b. A Alcáçova de Santarém e os Fenícios no Estuário do Tejo, in: Arruda, A.M., Viegas, C., Almeida, M.J. (Eds.), De Scallabis a Santrém. Museo Nacioanal de Arqueologia, Lisboa, Portugal, pp. 29–35.

Arruda, A.M., 1993. A ocupação da Idade do Ferro da Alcaçova de Santarém no contexto da expansão Fenícia na fachada Atlântica peninsular. Estud. Orientais 4, 193–214.

Arruda, A.M., Pereira, C., Pimenta, J., Sousa, E., Mendes, H., Soares, R., 2016. As contas de vidro do Porto do Sabugeiro (Muge, Salvaterra de Magos, Portugal) / Glass beads from Porto do Sabugeiro (Muge, Salvaterra dos Magos, Portugal). Cuad. Prehist. y Arqueol. 42, 79–101. https://doi.org/10.15366/cupauam2016.42.002

Arruda, A.M., Viegas, C., 1999. Cerâmicas islâmicas da Alcáçova de Santarém. Rev. Port. Arqueol. 2, 105–186.

ASTM International, 2021. ASTM D5731-16, Standard Test Method for Determination of the

Point Load Strength Index of Rock and Application to Rock Strenght Classifications. http://www.astm.org/cgi-bin/resolver.cgi?D5731.

Azevêdo, T.M., Nunes, E., Ramos, C., 2004. Some morphological aspects and hydrological characterization of the Tagus floods in the Santarém Region, Portugal. Nat. Hazards 31, 587–601. https://doi.org/10.1023/B:NHAZ.0000024892.61336.ec

Azuar López, R., 2010. De nuevo sobre el mercado de producciones ceramicas entre Al-Andaluz y las repúblicas de Génova y Pisa (Siglo XI d.C.). Arqueol. Mediev. 11, 61–68.

Azuar López, R., 2005. Una necesaria revisión de las cerámicas andalusíes halladas en Italia. Arqueol. y Territ. Mediev. 12, 175–199. https://doi.org/10.17561/aytm.v12i1.1724

Baldassarri, M., Berti, G., 2009. Nuovi dati sulle importazioni di ceramiche islamiche e bizantine a Pisa, in: Zozaya, J., Routerce, M., Hervás, M.Á., De Juan, A. (Eds.), Actas Del VIII Congreso Internacional de Cerámica Medieval En El Mediterráneo, Tomo I. Asociación Española de Arqueología Medieval, Cuidad Real - Almagro 2006, pp. 63–80.

Barbosa, B.P., 1995. Alostratigrafia e litostratigrafia das unidades continentais da Bacia terciária do baixo Tejo. Relações com o eustatismo e a tectónica. Universidade de Lisboa.

Barceló, C., Heidenreich, A., 2020. Lusterware Made in the Abbadid Taifa of Seville (Eleventh Century) and Its Early Production in the Mediterranean Region. Muqarnas 31, 277–306.

Barceló, M., 1993. Al-Mulk, el verde y el blanco. La vajilla califal omeya de Medinat al-Zahra, in: Malpica Cuello, A. (Ed.), La Cerámica Altomedieval En El Sur de Al-Andalus : Primer Encuentro de Arqueología y Patrimonio. Univ. de Granada, Granada, pp. 291–299.

Barriga, F.J.A.S., 1990. Metallogenesis in the Iberian Pyrite Belt, in: Pre-Mesozoic Geology of Iberia. Springer Berlin Heidelberg, Berlin, Heidelberg, pp. 369–379. https://doi.org/10.1007/978-3-642-83980-1_26

Barroca, M.J., 2003. Da Reconquista a D. Dinis, in: Mattoso, J. (Ed.), Nova História Militar de Portugal, Vol. I. Circulo de Leitores, Lisboa, pp. 20–161.

Batata, C., Barradas, E., Sousa, V., 2004. Novos vestígios da presença islâmica em Santarém, in: Amado, C., Mata, L. (Eds.), Santarém e o Magreb: Encontro Secular (970 - 1578): Catálogo Da Esposição. Museo municipal de Santarém - Câmara Municipal de Santarém, Santarém.

Bau, M., Schmidt, K., Pack, A., Bendel, V., Kraemer, D., 2018. The European Shale: An improved data set for normalisation of rare earth element and yttrium concentrations in environmental and biological samples from Europe. Appl. Geochemistry 90, 142–149.

https://doi.org/10.1016/j.apgeochem.2018.01.008

Bazzana, A., Lemoinne, C., Picon, M., 1986. Le problème de l'origine de la diffusion des céramiques dites califales, recherche préliminaire, in: Zozaya, J. (Ed.), Segundo Coloquio Internacional de Cerámica Medieval En El Mediterráneo Occidental. Toledo, 2-7 Noviembre 1981. Ministerio de Cultura - Direccíon Geral de Bellas Arte y Archivos, Madrid, pp. 33–38.

Bazzana, A., Picon, M., 1981. Ateliers producteurs et diffusion des céramiques "verde y morado" à l'époque du califat de Cordoue, in: Bazzana, A., Poisson, J.M. (Eds.), Cinq Ans de Recherches Dans Le Domaine Méditerranéen et La France Du Centre Est. Université Lyon 2. E.H.E.S.S, Lyon, pp. 197–206.

Beltrame, M., Santos, J.R., Gómez Martínez, S., Correia, F.B., Candeias, A., Mirão, J., Martínez, S.G., Correia, F.B., Candeias, A., Mirão, J., 2015. Nova variante de cerâmica decorada a "verde e manganês" em Évora. Conimbriga 54, 225–254. https://doi.org/10.14195/1647-8657_54_8

Beran, A., Voll, D., Schneider, H., 2004. IR Spectroscopy as a tool for the characterization of caramic percursor phases, in: Beran, A., Libowitzky, E. (Eds.), Spectroscopic Methods in Mineralogy - Emu Notes in Mineralogy Volume 6. Eötvös University, Budapest, pp. 189–226.

Berti, G., 2010. Pisa ed il mediterraneo nel Medio Evo: scambi internazionali di merci e di conoscenze. Arqueol. Mediev. 142–161.

Berti, G., Capelli, C., Cabella, R., 2009. Le importazioni dalla Penisola Iberica (Al-Andaluz) e dalle Isole Baleari tra i Bacini di Pisa (secoli X-XII), in: Zozaya, J., Routerce, M., Hervás, M.Á., De Juan, A. (Eds.), Actas Del VIII Congreso Internacional de Cerámica Medieval En El Mediterráneo. Asociación Española de Arqueología Medieval, Ciudad Real, pp. 81–89.

Berti, G., Mannoni, T., 1997. Céramique de l'Andalusie décorées en "verde y manganeso" parmi les "bacini" de Pise de la fin du Xe siècle, in: Demians D'Archimbaud, G. (Ed.), La Céramique Médiévale En Méditerranée. Actes Du VIe Congrès de l'AIECM2. Aix-En-Provence, 13-18 Novembre 1995. Narrations Ed., Aix-en-Provence, pp. 435–437.

Berti, G., Mannoni, T., 1995. Le ceramiche a « cuerda seca » utilizzate come « bacini » in Toscana ed in Corsica, in: El Hraîki, R., Erbati, E. (Eds.), Actes Du 5éme Colloque Sur La Céramique Médiévale, Rabat 11-17 Novembre 1991. Dar al Manahil (Ministère des Affaires Culturelles), Rabat, pp. 400–404.

Berti, G., Mannoni, T., 1991. Ceramiche medievali nel Mediterraneo Occidentale: considerazioni su alcune caratteristiche tecniche, in: A Cerâmica Medieval No Mediterrâneo Ocidental. Lisboa, 1987. Mértola, 1991. Campo Arqueológico de Mértola, Mértola, pp. 163–173.

Berti, G., Rosselló-Bordoy, G., Tongiorgi, E., 1986. Alcuni bacini ceramici di Pisa e la corrispondente produzione di maiorca nel secolo XI. Archeol. Mediev. Cult. Mater. insediamenti, Territ. XIII, 97–115. https://doi.org/10.1400/243888

Berti, G., Tongiori, L., 1985. Ceramiche importate dalla Spagna nell'area pisana dal XII al XV secolo. All'Insegna del Giglio, Firenze.

Berti, G., Tongiori, L., 1981. I bacini ceramici medievali delle chiese di Pisa, Quaderni d. ed. All'Insegna del Giglio, Roma.

Berti, G., Tongiori, L., 1980. Ceramiche decorate (XI-XIV secolo) di importazione da vari centri del Mediterraneo e di produzione locale sulla base della documentazione in Toscana, in: La Céramique Médiévale En Mediterranée Occidentale (X-Xv Siècles), 11-14 Septembre, Valbonne, France. C.N.R.S, Paris, pp. 83–91.

Bonifay, M., 2004. Etudes sur la céramique romaine tardive d'Afrique, BAR Intern. ed. Archaeopress, Oxford.

Bonifay, M., Capelli, C., Martin, T., Picon, M., Vallauri, L., 2002. Le littoral de la Tunisie, étude géoarchéologique et historique (1987-1997). La céramique. Antiq. africaines 38, 125–202. https://doi.org/10.3406/antaf.2002.1355

Branco, F., 2013. Fortificações de iniciativa omíada no Gharb al-Andalus nos séculos IX e X hipóteses em torno da chegada dos Majus (entre Tejo e Mondego), in: Fernandes, I.C. (Ed.), Fortificações e Territórios Na Peninsula Ibérica e No Magreb (Sésulos VI a XVI). Actas Do II Simpósio Internacional Sobre Castelos. Colibri, Lisbon, Portugal, pp. 73–84.

Branco, F., 2010. Fortificação, guerra e poderes no Gharb al-Andalus (dos inícios da islamização ao domínio norte-africano). University of Évora.

Bridgman, R., 2007. Re-examining Almohad economies in south-western Al-Andalus through Petrological analysis of archaeological ceramics. Mediev. Early Mod. Iber. World. https://doi.org/10.1163/ej.9789004162273.i-304.29

Bridgman, R., Torres, P.L., Reina, M.V., 2009. Crossing the Cultural Divide? Continuity in Ceramic Production and Consumption between the Almoravid and Mudéjar Periods in Seville. Al-Masaq Islam Mediev. Mediterr. 21, 13–29. https://doi.org/10.1080/09503110802704395

Bugalhão, J., Folgado, D., 2001. O arrabalde ocidental da Lisboa islâmica: urbanismo e produção oleira. Arqueol. Mediev. 7, 111–145.

Bugalhão, J., Gomes, S., Sousa, M.J., Folgado, D., Tinturé, A.G., Moreno-García, M., Dias, M.I., Prudêncio, M.I., 2008a. Produção e consumo de cerâmica islâmica em Lisboa: conclusões de um projecto de investigação. Arqueol. Mediev. 10, 113–134.

Bugalhão, J., Gomes, S., Sousa, M.J., Folgado, D., Tinturés, A.G., Moreno-García, M., Dias, M.I., Prudêncio, M.I., 2008b. Produção e consumo de cerâmica islâmica em Lisboa. Conclusóes de um projecto de investigação. Arqueol. Mediev. 113–134.

Buxeda I Garrigós, J., Cau Ontiveros, M.A., Kilikoglou, V., 2003. Chemical variability in clays and pottery from a traditional cooking pot production village: Testing assumptions in Pereruela. Archaeometry 45, 1–17. https://doi.org/10.1111/1475-4754.00093

Cameron, A., 2015. The mediterranean world in late antiquity 395-700 AD: Second edition, Routledge. ed, The Mediterranean World in Late Antiquity 395-700 AD: Second Edition. Routledge. https://doi.org/10.4324/9780203809082

Cantin, N., Mayor, A., 2018. Ethno-archaeometry in eastern Senegal: The connections between raw materials and finished ceramic products. J. Archaeol. Sci. Reports 21, 1181–1190. https://doi.org/10.1016/j.jasrep.2017.01.015

Capelli, C., Bonifay, M., 2014. Archéométrie et archéologie des céramiques africanes: une approche pluridisciplinaire, 2. Nouvelles donnees sur la ceramique culinaire et les amphores, in: Poulou-Papadimitriou, N., Nodarou, E., Kilikoglou, V. (Eds.), LRCW 4 Late Roman Coarse Wares , Cooking Wares and Amphorae in the Mediterranean Archaeology and Archaeometry. Archaeopress - British Archaeological Reports, Oxford, pp. 235–253.

Capelli, C., Bonifay, M., 2007. Archéométrie et archéologie des céramiques africaines: une approche pluridisciplinaire, in: Bonifay, M., Tréglia, J.-C. (Eds.), LRCW 2 Late Roman Coarse Wares , Cooking Wares and Amphorae in the Mediterranean Archaeology and Archaeometry - BAR International Series 1662 (II). Archaeopress - British Archaeological Reports, Oxford, pp. 551–568.

Capelli, C., Cabella, R., Piazza, M., 2007. The late Roman pottery production in Eastern Alpine area and Danubian provinces: archaeometric analysis on fabrics and glazes, in: Magrini, C., Sbarra, F. (Eds.), Atti Del I Incontro Internazionale de Archeologia a Carlino, 14-15 Dicembre 2007. La Ceramica Invetriata Tardoromana Nell'arco Alpino Orientale e Nelle Provincie Danubiane. Comune di Carlino, Carlino, pp. 71–109.

Capelli, C., García Porras, A., Ramagli, P., 2005. Análisis aarqueométrico y arqueológico integrado sobre azulejo vidriados haalldos en contextos des los siglos XIV al XVI en Liguria (Italia): las produciones de Málaga y Savona, in: Carta, A. (Ed.), Arqueometría y Arqueologia Medieval. Al-Baraka, Granada, pp. 117–169.

Capelli, C., Waksman, Y., Cabella, R., Gragueb, S., Treglia, J.-C., 2011. Il contributo delle analisi di laboratorio allo studio delle ceramiche nordafricane. L'esempio di Sabra al-MansuRiya (dati preliminari), in: Cressier, P., Fentress, E. (Eds.), La Céramique Maghrébine Du Haut Moyen Âge (VIII_X Siécle). État Des Recherches, Problémes et Perspectives. École Française de Rome, Rome, pp. 221–232.

Carvajal, J.C., Day, P.M., 2013. Cooking pots and islamicization in the early medieval vega of granada (Al-andalus, sixth to twelfth centuries). Oxford J. Archaeol. 32, 433–451. https://doi.org/10.1111/ojoa.12023

Carvajal López, J.C., 2008. La cerámica de Madinat Ilbira (Atarfe) y el poblamiento altomedieval en la Vega de Granada. Tharg, Granada.

Carvajal López, J.C., Day, P.M., 2015. The production and distribution of cooking pots in two towns of South East Spain in the 6th-11th centuries. J. Archaeol. Sci. Reports 2, 282–290. https://doi.org/10.1016/j.jasrep.2015.03.002

Carvajal López, J.C., Hein, A., Glascock, M.D., Day, P.M., 2018. Combined petrographic and chemical analysis of water containers and glazed wares in the Early Islamic Vega of Granada (southeast Spain, 6th to 12th centuries CE). J. Archaeol. Sci. Reports 21, 1130–1140. https://doi.org/10.1016/j.jasrep.2017.09.016

Casimiro, T.M., Boavida, C., Silva, T., 2018. Ceramics and cultural change in medieval (14th-15th century) Portugal The case of post-Reconquista Santarém. Mediev. Ceram. 37, 21–36.

Castillo Galdeano, F., Martínez Madrid, R., 1993. Producciones cerámicas en Baŷŷāna, in: Malpica Cuello, A. (Ed.), La Cerámica Altomedieval En El Sur de Al-Andalus : Primer Encuentro de Arqueología y Patrimonio. Universidade de Granada, Granada. España, pp. 68–116.

Catarino, H., 1999. O Garbe al-Andaluz: definição territorial e administrativa, in: Graça Maia Marques, M. (Ed.), O Algarve Da Antiguidade Ao Nossos Dias: Elementos Para a Sua Hístoria. Colibri, Lisboa, Portugal, pp. 69–74.

Catarino, H., 1995. A occupação Islamica, in: Medina, J. (Ed.), História de Portugal: Dos Tempos

Pré-Histórico Aos Nossos Dias. Vol 3: O Mundo Luso-Romano. Amadora Clube Internacional do Livro, Madrid, pp. 267–349.

Cau Ontiveros, M.A., Montana, G., Tsantini, E., Randazzo, L., 2015. Ceramic Ethnoarchaeometry in Western Sardinia: Production of Cooking Ware at Pabillonis. Archaeometry 57, 453–475. https://doi.org/10.1111/arcm.12100

Chabanne, D., Aucouturier, M., Bouquillon, A., Darque-Ceretti, E., Makariou, S., Dectot, X., Faÿ-Hallé, A., Miroudot, D., 2011. Ceramics with metallic lustre decoration. A detailed knowledge of Islamic productions from 9th century until Renaissance 1–23.

Chapoulie, R., Déléry, C., Daniel, F., Vendrell-Saz, M., 2005. Cuerda seca ceramics from Al-Andalus, Islamic Spain and Portugal (10th-12th centuries AD): Investigation with SEM-EDX and cathodoluminescence. Archaeometry 47, 519–534. https://doi.org/10.1111/j.1475-4754.2005.00217.x

Christine Henry, S.H., 2012. Sarah Hélène Cerâmica islâmica em corda seca de Mértola dos séculos X a XIII " Cuerda seca " Islamic ceramics from the X-XIIIth centuries of Mértola Sarah Hélène Christine Henry Cerâmica islâmica em corda seca de Mértola dos séculos X a XIII " Cuerda seca. University of Aveiro.

Chukanov, N. V., Chervonnyi, A.D., 2016. Infrared Spectroscopy of Minerals and Related Compounds. https://doi.org/10.1007/978-3-319-25349-7

Chukanov, N. V, 2014. Infrared spectra of minerals and reference samples data, Infrared spectra of mineral species: Extended library. https://doi.org/10.1007/978-94-007-7128-4

Coates, J., 2006. Interpretation of Infrared Spectra, A Practical Approach, in: Encyclopedia of Analytical Chemistry. John Wiley & Sons, Ltd, Chichester, UK, pp. 196–199. https://doi.org/10.1002/9780470027318.a5606

Coentro, S., Alves, L.C., Relvas, C., Ferreira, T., Mirão, J., Molera, J., Pradell, T., Trindade, R.A.A., Da Silva, R.C., Muralha, V.S.F., 2017. The Glaze Technology of Hispano-Moresque Ceramic Tiles: A Comparison Between Portuguese and Spanish Collections. Archaeometry 59, 667–684. https://doi.org/10.1111/arcm.12280

Coentro, S., Trindade, R.A.A., Mirão, J., Candeias, A., Alves, L.C., Silva, R.M.C., Muralha, V.S.F., 2014. Hispano-Moresque ceramic tiles from the Monastery of Santa Clara-a-Velha (Coimbra, Portugal). J. Archaeol. Sci. 41, 21–28. https://doi.org/10.1016/j.jas.2013.07.031

Coll Conesa, J., Botella, P., Larena, M.T., Doménech, M.T., Aura, E., 1999. Caracterización química

de cubiertas blancas opacas musulmanas de la Valencia medieval (ss. X-XI). Caesaraugusta 73, 44–49.

Coll Conesa, J., García Porras, A., 2010. Tipologia, cronologia e produzione dei forni per ceramica in al-Andalus, in: Fornaci. Tecnologie e Produzione Della Ceramica in Età Medievale e Moderna. Atti Del XLII Convegno Internazionale Della Ceramica, Savona 29-30 Maggio 2009. Centro Ligure per la Storia della Ceramica, Firenze, pp. 25–44.

Colomban, P., Milande, V., Lucas, H., 2004. On-site Raman analysis of Medici porcelain. J. Raman Spectrosc. 35, 68–72. https://doi.org/10.1002/jrs.1085

Columbu, S., Antonelli, F., Lezzerini, M., Miriello, D., Adembri, B., Blanco, A., 2014a. Provenance of marbles used in the Heliocaminus Baths of Hadrian's Villa (Tivoli, Italy). J. Archaeol. Sci. 49, 332–342. https://doi.org/10.1016/j.jas.2014.05.026

Columbu, S., Cruciani, G., Fancello, D., Franceschelli, M., Musumeci, G., 2015a. Petrophysical properties of a granite-protomylonite-ultramylonite sequence: insight from the Monte Grighini shear zone, central Sardinia, Italy. Eur. J. Mineral. 27, 471–486. https://doi.org/10.1127/ejm/2015/0027-2447

Columbu, S., Gioncada, A., Lezzerini, M., Marchi, M., 2014b. Hydric dilatation of ignimbritic stones used in the church of santa maria di otti (oschiri, northern sardinia, italy). Ital. J. Geosci. 133, 149–160. https://doi.org/10.3301/IJG.2013.20

Columbu, S., Lisci, C., Sitzia, F., Buccellato, G., 2017. Physical–mechanical consolidation and protection of Miocenic limestone used on Mediterranean historical monuments: the case study of Pietra Cantone (southern Sardinia, Italy). Environ. Earth Sci. 76. https://doi.org/10.1007/s12665-017-6455-6

Columbu, S., Sitzia, F., Verdiani, G., 2015b. Contribution of petrophysical analysis and 3D digital survey in the archaeometric investigations of the Emperor Hadrian's Baths (Tivoli, Italy). Rend. Lincei 26, 455–474. https://doi.org/10.1007/s12210-015-0469-3

Comodi, P., Bernardi, M., Bentivoglio, A., Gatta, G.D., Zanazzi, P.F., 2004. The production and technology of glazed ceramics from the Middle Ages, found in the Saepinum territory (Italy) : A multimethodic approach. Archaeometry 46, 405–419. https://doi.org/10.1111/j.1475-4754.2004.00165.x

Constable, O.R., 1996. Comercio y comerciantes en la España musulmana la reordenación comercial de la Península Ibérica del 900 al 1500. Omega, Barcelona.

Costa, P.P., 2005. As ordens militares no espaço entre o Douro e o Tejo (séculos XII-XIII), in: Barroca, M.J., Ferreira Fernandes, I.C. (Eds.), Muçulmanos e Cristão Entre o Tejo e o Douro (Sécs. VIII a XIII). Câmara Municipal de Palmela - Faculdade de Letras Universidade do Porto, Palmela, pp. 151–158.

Costança dos Santos, C., Coelho, C., Liberato, M., Gomes, A.S., Bugalhão, J., Catarino, H., Cavaco, S., Covaneiro, J., Fernandes, I.C., Gómez Martínez, S., Gonçalves, M.J., Inácio, I., 2016. Acerca de las cerámicas de almacenamiento: las tinajas (al-hawābī) en el Garb al-Andalus, in: Amouric, H., François, V., Valluri, L. (Eds.), Actes Du Ier Congrès International Thématique de l'AIECM3. Jarres et Grands Contenants Entre Moyen Âge et Époque Moderne. Lucie Édition, Aix-en-Provence, pp. 185–198.

Crum, J. V., Riley, B.J., Vienna, J.D., 2009. Binary phase diagram of the manganese oxide-iron oxide system. J. Am. Ceram. Soc. 92, 2378–2384. https://doi.org/10.1111/j.1551-2916.2009.03230.x

Cultrone, G., Molina, E., Arizzi, A., 2014. The combined use of petrographic, chemical and physical techniques to define the technological features of Iberian ceramics from the Canto Tortoso area (Granada, Spain). Ceram. Int. 40, 10803–10816. https://doi.org/10.1016/j.ceramint.2014.03.072

Cultrone, G., Rodriguez-Navarro, C., Sebastian, E., Cazalla, O., De La Torre, M.J., 2001. Carbonate and silicate phase reactions during ceramic firing. Eur. J. Mineral. 13, 621–634. https://doi.org/10.1127/0935-1221/2001/0013-0621

Cultrone, G., Sebastián, E., Elert, K., de la Torre, M.J., Cazalla, O., Rodriguez-Navarro, C., 2004. Influence of mineralogy and firing temperature on the porosity of bricks. J. Eur. Ceram. Soc. 24, 547–564. https://doi.org/10.1016/S0955-2219(03)00249-8

Cunha, P.P., 2019. Cenozoic Basins of Western Iberia: Mondego, Lower Tejo and Alvalade Basins. Springer International Publishing, pp. 105–130. https://doi.org/10.1007/978-3-030-11190-8_4

Cunha, P.P., Martins, A.A., Daveau, S., Friend, P.F., 2005. Tectonic control of the Tejo river fluvial incision during the late Cenozoic, in Ródão - Central Portugal (Atlantic Iberian border). Geomorphology 64, 271–298. https://doi.org/10.1016/j.geomorph.2004.07.004

Custodio, J., 2002. As fortificações de Santarém - século XII e XIII, in: Fernandes, I.C. (Ed.), Mil Anos de Fortifi Cações Na Península Ibérica e No Magreb (500-1500), Actas Do Simpósio Internacional Sobre Castelos. Colibri - Camera Municipal de Palmela, Palmela, pp. 405–422.

D'Ercole, G., Garcea, E.A.A., Eramo, G., Muntoni, I.M., 2017. Variability and continuity of ceramic manufacturing of prehistoric pottery from Upper Nubia, Sudan: An ethnographic comparison. J. Archaeol. Sci. Reports 16, 553–563. https://doi.org/10.1016/j.jasrep.2017.04.012

Daoulatli, A., 1979. Poteries et céramiques tunisiennes, Lumières s. ed. Institut national d'archéologie et d'art, Tunis.

De Bonis, A., Cultrone, G., Grifa, C., Langella, A., Morra, V., 2014. Clays from the Bay of Naples (Italy): New insight on ancient and traditional ceramics. J. Eur. Ceram. Soc. 34, 3229–3244. https://doi.org/10.1016/j.jeurceramsoc.2014.04.014

De Juan Ares, J., Schibille, N., 2017. Glass import and production in Hispania during the early medieval period: The glass from Ciudad de Vascos (Toledo). PLoS One 12, 1–19. https://doi.org/10.1371/journal.pone.0182129

De Juan Ares, J., Schibille, N., De Embún, T.X., 2018. The first glass of Al-Andalus: Analytical evidence from the early islamic site of Cabezo Pardo (Alicante). Lucentum 2018, 271–279. https://doi.org/10.14198/LVCENTVM2018.37.15

De Juan Ares, J., Vigil-Escalera Guirado, A., Cáceres Gutiérrez, Y., Schibille, N., 2019. Changes in the supply of eastern Mediterranean glasses to Visigothic Spain. J. Archaeol. Sci. 107, 23–31. https://doi.org/10.1016/j.jas.2019.04.006

Déléry, C., 2009. Using Cuerda Seca Ceramics as a Historical Source to Evaluate Trade and Cultural Relations between Christian Ruled Lands and Al-Andalus, from the Tenth to Thirteenth Centuries. Al-Masāq 21, 31–58. https://doi.org/10.1080/09503110802704411

Déléry, C., 2006a. Dynamiques économiques, sociales et culturelles d'al-Andalus à partir d'une étude de la céramique de cuerda seca (seconde moitié du Xe siècle-premièr moitié du XIIIe siècle). Université Toulouse II- Le Mirail.

Déléry, C., 2006b. Dynamiques économiques, sociales et culturelles d'al-Andalus à partir d'une étude de la céramique de cuerda seca (seconde moité du X siècle-première moité du XIII siècle). University of Toulouse II - Le Miral.

Déléry, C., Gómez Martínez, S., 2006. Algunas piezas orientales y el problema del origen de la técnica de cuerda seca, in: Gómez Martínez, S. (Ed.), Al-Ândalus : Espaço de Mudança : Balanço de 25 Anos de História e Arqueologia Medievais : Seminário Internacional,

Mértola, 16, 17 e 18 de Maio de 2005 : Homenagem a Juan Zozaya Stabel-Hansen. Campo Arqueológico de Mértola, Mértola, pp. 148–160.

Demians D'Archimbaud, G., Lemoinne, C., Picon, M., Valluri, L., 1986. Recherches de laboratoire sur les ateliers medievaux espagnols, in: Zozaya, J. (Ed.), Segundo Coloquio Internacional de Cerámica Medieval En El Mediterráneo Occidental. Toledo, 2-7 Noviembre 1981. Ministerio de Cultura - Direccíon Geral de Bellas Arte y Archivos, Madrid, pp. 43–45.

Di Febo, R., Molera, J., Pradell, T., Melgarejo, J.C., Madrenas, J., Vallcorba, O., 2018. The production of a lead glaze with galena: Thermal transformations in the PbS–SiO2 system. J. Am. Ceram. Soc. 101, 2119–2129. https://doi.org/10.1111/jace.15346

Di Febo, R., Molera, J., Pradell, T., Vallcorba, O., Capelli, C., 2017a. Technological implications of neo-formed hematite crystals in ceramic lead glazes. Sci. Technol. Archaeol. Res. 3, 366–375. https://doi.org/10.1080/20548923.2017.1419675

Di Febo, R., Molera, J., Pradell, T., Vallcorba, O., Melgarejo, J.C., Capelli, C., 2017b. Thin-section petrography and SR-μXRD for the identification of micro-crystallites in the brown decorations of ceramic lead glazes. Eur. J. Mineral. 29, 861–870. https://doi.org/10.1127/ejm/2017/0029-2638

Dias, M.I., Prudêncio, M.I., 2008. On the importance of using scandium to normalize geochemical data preceding multivariate analyses applied to archaeometric pottery studies. Microchem. J. 88, 136–141. https://doi.org/10.1016/j.microc.2007.11.009

Dias, M.I., Prudêncio, M.I., Bugalhão, J., Gomes, S., Sousa, M.J., Folgado, D., 2008. A produção de cerâmica no arrabalde ocidental da Lisboa Islâmica. Primeiros resultados arqueométricos, in: Bicho, N. (Ed.), Actas Do IV Congresso de Arqueologia Peninsular - A Ocupação Islâmica Da Península Iberica. Centro de Estudos de Patrimonio - Universidade do Algarve, Faro, pp. 157–167.

Dias, M.I., Prudêncio, M.I., Gouveia, M.A., 2001. Arqueomteria da cerâmica Islaâmica das regiões de Lisboa, Santarém e Alcaçer do Sal (Portugal): caracterização química e mineralogica, in: Garb: Sitio Islâmicos Do Sul Peninsular. IPPAR - Junta da Extremadura, Lisbon, pp. 257–282.

Dias, M.I., Prudêncio, M.I., Gouveia, M.A., Gomes, A., Gaspar, A., 2009. Tecnologias de produção de cerâmicas pintads dos séculos XI-XII do Castelo de S. Jorges (Lisboa, Portugal), in: Zozaya, J., Retuerce, M., Hervás, M.Á., De Juan, A. (Eds.), Actas Del VIII Congreso Internacional de Cerámica Medieval En El Mediterráneo, Tomo II. Asociación Española de

Arqueología Medieval, Cuidad Real - Almagro 2006, pp. 963–966.

Dondi, M., Principi, P., Raimondo, M., Zanarini, G., 2003. Water vapour permeability of clay bricks. Constr. Build. Mater. 17, 253–258. https://doi.org/10.1016/S0950-0618(02)00117-4

Douglass, L.A., 1989. Vermiculites, in: Dixon, J.B., Weed, S.B. (Eds.), Minerals in Soil Environments, 2nd Edition. Soil Science Society of America, Madison, pp. 625–674.

Duckworth, C.N., de la Llave, R.C., Faber, E.W., Edwards, D.J.G., Henderson, J., 2015. Electron Microprobe Analysis of 9th-12th Century Islamic Glass from Córdoba, Spain. Archaeometry 57, 27–50. https://doi.org/10.1111/arcm.12079

Eggins, S.M., Woodhead, J.D., Kinsley, L.P.J., Mortimer, G.E., Sylvester, P.J., McCulloch, M.T., Hergt, J.M., Handler, M.R., 1997. n ! Zi- internal standardisation. Chem. Geol. 1, 311–326. https://doi.org/http://dx.doi.org/10.1016/S0009-2541(96)00100-3

El Ouahabi, M., Daoudi, L., Hatert, F., Fagel, N., 2015. Modified mineral phases during clay ceramic firing. Clays Clay Miner. 63, 404–413. https://doi.org/10.1346/CCMN.2015.0630506

Fabbri, B., Gualtieri, S., Shoval, S., 2014. The presence of calcite in archeological ceramics. J. Eur. Ceram. Soc. 34, 1899–1911. https://doi.org/10.1016/j.jeurceramsoc.2014.01.007

Faria, R., Pereira, Z., Matos, J.X., Rosa, C., Caetano Alves, M.I., Oliveira, J.T., 2015. Estudo palinostratigráfico do setor Malhadinha, região NE Alvares, concelho de Mértola, Faixa Piritosa Ibérica. Comun. Geol. 102, 5–11.

Fedo, C.M., Sircombe, K.N., Rainbird, R.H., 2003. Detrital Zircon Analysis of the Sedimentary Record. Rev. Mineral. Geochemistry 53, 277–303. https://doi.org/10.2113/0530277

Fernandes, H., 2002. Em torno de Santarin: Posição e funções, in: Arruda, A.M., Viegas, C., Almeida, M.J. (Eds.), De Scallabis a Santrém. Museo Nacioanal de Arqueologia, Lisbon, Portugal, pp. 47–60.

Fernandes, I.C., Gómez Martínez, S., Gonçalves, M.J., Inácio, I., Santos, C. Dos, Bugalhão, J., Liberato, M., Gomes, A.S., Catarino, H., Cavaco, S., Covaneiro, J., 2015. O comércio da Corda Seca (Total e Parcial) no Gharb al-Ândalus. Actas do X Congresso de Cerâmica Medieval no Mediterrâneo, in: Gómez Martínez, S., Gonçalves, M.J. (Eds.), Actas Do X Congresso Iinternacional "A Cerâmica Medieval No Mediterrâneo". Silves-Mértola, 22 a 27 de Outubro de 2012. Campo Arqueológico de Mértola, Câmara Municipal de Silves, Loule, pp. 649–666.

Fernandes, L., Coroado, J., Calado, M., Costantino, C., 2015. Occupação medieval Islâmica no Museu de Lisboa - Teatro Romano de Lisboa: o caso do aproveitamento post scaenium no decurso do século XII, in: Gonçalves, M.J., Gómez Martínez, S. (Eds.), Actas Do X Congresso Iinternacional "A Cerâmica Medieval No Mediterrâneo". Silves-Mértola, 22 a 27 de Outubro de 2012. Campo Arqueológico de Mértola, Cârama Municipal de Silves, Silves-Mértola, pp. 509–518.

Fernández, A., Martín, M.A., Moreda Blanco, J., 1989. Excavaciones arqueológicas en el Monasterio de San Benito el Real de Valladolid. Un interessante fragmento de céramica con decoracíon esgrafiada y cuerda seca parcial. Boletín Arqueol. Mediev. 233–241.

Ferreira, L.F.V., Gomes, R.V., Pereira, M.F.C., Santos, L.F., Machado, I.F., 2016. Islamic ceramics in Portugal found at Silves Castle (8th to 13th c.): An archaeometric characterization. J. Archaeol. Sci. Reports 8, 434–443. https://doi.org/10.1016/j.jasrep.2016.06.051

Finlay, A.J., McComish, J.M., Ottley, C.J., Bates, C.R., Selby, D., 2012. Trace element fingerprinting of ceramic building material from Carpow and York Roman fortresses manufactured by the VI Legion. J. Archaeol. Sci. 39, 2385–2391. https://doi.org/10.1016/j.jas.2012.03.002

Flecker, M., 2001. A ninth-century AD arab or indian shipweck in indonesia: First evidence for direct trade with china. World Archaeol. 32, 335–354. https://doi.org/10.1080/00438240120048662

Flores Escobosa, I., Muñoz Martín, M. del M., Lirola Delgado, J., 1998. Las producciones de un alfar islámico en Almería. Arqueol. y Territ. Mediev. 6, 207–239. https://doi.org/10.17561/aytm.v6i0.1533

Folk, R.L., 1959. Practical petrographic classification of limestones. Am. Assoc. Pet. Geol. Bull. 43, 1–38.

Folk, Robert L., 1959. American Association of Petroleum Geologists Practical Petrographic Classification of Limestones'. Bull. Am. Assoc. Pet. Geol. 43. https://doi.org/10.1306/0BDA5C36-16BD-11D7-8645000102C1865D

Fortina, C., Santagostino Barbone, A., Turbanti Memmi, I., 2005. Sienese "archaic" majolica: A technological study of ceramic bodies and coatings. Archaeometry 47, 535–555. https://doi.org/10.1111/j.1475-4754.2005.00218.x

Franklin, J.A., 1985. Suggested method for determining point load strength. Int. J. Rock Mech. Min. Sci. Geomech. Abstr. 22, 51–60. https://doi.org/10.1016/0148-9062(85)92327-7

Freestone, I.C., Middleton, a. P., 1987. Mineralogical applications of the analytical SEM in archaeology. Mineral. Mag. 51, 21–31. https://doi.org/10.1180/minmag.1987.051.359.03

Freestone, I.C., Stapleton, C.P., 1998. Composition and Technology of Islamic Enamelled glass from the thirteenth and fourteenht centuries, in: Ward, R. (Ed.), Gilded and Enamelled Glass from the Middle East. British Museum press, London, pp. 122–127.

Frezzotti, M.L., Tecce, F., Casagli, A., 2012. Raman spectroscopy for fluid inclusion analysis. J. Geochemical Explor. 112, 1–20. https://doi.org/10.1016/j.gexplo.2011.09.009

Froh, J., 2004. Archaeological ceramics studies by scanning electron microscopy. Hyperfine Interact. 154, 159–176.

García Fitz, F., 2019. Crítica e hipercrítica en torno al concepto de reconquista. Una aproximación a la historiografía reciente, in: Ayala Martínez, C., Fernandes, I.C., Palacios Ontalva, S. (Eds.), La Reconquista: Ideología y Justificación de La Guerra Santa Peninsular. Ediciones de La Ergástula, S.L., Madrid, pp. 79–98.

García Fitz, F., 2009. La Reconquista: un estado de la cuestión. Clío Crímen Rev. del Cent. Hist. del Crim. Durango 6, 142–215.

García Porras, A., 2001. La distribución de productos cerámicos entre la época Almohade y la Nazarí. El caso de El Castillejo (Los Guájares, Granada). Arqueoweb Rev. sobre Arqueol. en Internet 9, 3.

García Sanjuán, A., 2019. Cómo desactivar una bomba historiográfica: la pervivencia actual del paradigma de la Reconquista, in: Ayala Martínez, C., Fernandes, I.C., Palacios Ontalva, S. (Eds.), La Reconquista: Ideología y Justificación de La Guerra Santa Peninsular. Ediciones de La Ergástula, S.L., Madrid, pp. 99–121.

Garcia y Garcia, A., 2007. La conquista de Santarém en el contexto de la cruzada Ibérica, in: Nelson Ferrão, H. (Ed.), Santarém Na Idade Média: Actas Do Colóquio 13-14 Março 1998. Câmara Municipal de Santarém, Santarém, pp. 101–106.

Garofano, I., Robador, M.D., Perez-Rodriguez, J.L., Castaing, J., Pacheco, C., Duran, A., 2015. Ceramics from the Alcazar Palace in Seville (Spain) dated between the 11th and 15th centuries: Compositions, technological features and degradation processes. J. Eur. Ceram. Soc. 35, 4307–4319. https://doi.org/10.1016/j.jeurceramsoc.2015.07.033

Georgiou, C.D., Sun, H.J., McKay, C.P., Grintzalis, K., Papapostolou, I., Zisimopoulos, D., Panagiotidis, K., Zhang, G., Koutsopoulou, E., Christidis, G.E., Margiolaki, I., 2015. Evidence

for photochemical production of reactive oxygen species in desert soils. Nat. Commun. 6, 7100. https://doi.org/10.1038/ncomms8100

Gisbert, J.A., 1990. Los hornos del alfar islámico de la Av. Montgó/Calle Teulada, casco urbano de Denia (Alicante), in: Bazzana, A., Amigues, F. (Eds.), Fours de Potiers et "Testares" Médiévaux En Méditerranée Occidentale. Casa de Velázquez, Madrid, pp. 75–91.

Gisbert, J.A., Azuar López, R., Burguera, V., 1992. La producción cerámica en Daniya. El alfar islámico de la Av. Montgó/Calle Teulada (Denia-Alicante), in: Alves da Silva, L., Mateus, R. (Eds.), Actas Del IV Congreso A Cerâmica Medeival Do Mediterráneo Occidental. Campo Arqueológico de Mértola, Mértola, pp. 247–262.

Goldstein, J., Newbury, D.E., Joy, D.C., Lyman, C.E., Echlin, P., Lifshin, E., Sawyer, L., Michael, J.R., 2003. Scanning Electron Microscopy and X-ray Microanalysis, Scanning Electron Microscopy and Xray Microanalysis. https://doi.org/10.1007/978-1-4615-0215-9

Gomes, A., Gaspar, A., Guerra, S., Valongo, A., Pimenta, J., Pinto, P., Mendes, H.C., Ribeiro, S., 2009. A cerâmica vidrada da Alcaçova do Castelo de S. Jorge, in: Hervás, M.Á., Retuerce Velasco, M., Juan Antonio, G., Zozaya, J. (Eds.), Actas Del VIII Congreso Internacional de Cerámica Medieval En El Mediterráneo, Tomo I. Asociación Española de Arqueología Medieval, Cuidad Real - Almagro 2006, pp. 399–404.

Gomes Pinto, C.G., 2012. Gestos, memórias e formas materiais legadas pelo barro. A produção olárica no Ribatejo na coleção de olaria traditional do Museu nacional de Etnologia. Universidade Nova de Lisboa.

Gómez Martínez, S., 2019. La cerámica en al-Andalus: producción y comercio, in: Delgado Pérez, M.M., Pérez-Aguilar, L.-G. (Eds.), Economía y Trabayo. Las Bases Materiales de La Vida En Al-Andalus. Alfar Universidad, Sevilla, pp. 199–234.

Gómez Martínez, S., 2016. El arrabal portuario de Mértola (Portugal): El registro cerámico Andalusí. Onoba 4, 181–196.

Gómez Martínez, S., 2014. Cerámica Islamica de Mértola. Campo Arqueológico de Mértola, Mértola.

Gómez Martínez, S., 2009a. El papel de Mértola (Portugal) en el commercio regional de céramica (siglo XI-XIII), in: Actas Del VII Congresso de Arqueologia Medieval En Al Mediterraneo. Asociación Española de Arqueología Medieval, Cuidad Real - Almagro 2006, pp. 23–37.

Gómez Martínez, S., 2009b. New Perspectives in the Study of Al-Andalus Ceramics, Mértola (Portugal) and the Mediterranean Maritime Routes in the Islamic Period. Al-Masaq 21, 59–82. https://doi.org/10.1080/09503110802704437

Gómez Martínez, S., 2006. Cerámica Islámica de Mértola: producción y comercio. Universidad Complutense de Madrid.

Gómez Martínez, S., 2003. Producciones cerámicas en la Mértola islâmica, in: Bakirtizis, C. (Ed.), VIIe Congrés International Sur La Céramique Médiévale En Méditerranée, Thessaloniki, 11-16 Octobre 1999. Édition de la Caisse des Recettes Archéologiques, Athènes, pp. 653–658.

Gómez Martínez, S., n.d. Le vert e brun au XIIème siècle. La diffusion du style de Ifriqiya à al-Andalus. Forthcoming, in: La Diffusion de La Céramique Islamique de Tunisie En Méditerranee. 4-5 Septembre 2019, Tunis.

Gómez Martínez, S., Bugalhão, J., Catarino, H., Cavaco, S., Coelho, C., Covaneiro, J., Fernandes, I.C., Gomes, A.S., Gonçalves, M.J., Inácio, I., Liberato, M., Dos Santos, C., 2018. El verde y morado en el extremo occidental de al-Andalus (Siglos X al XII), in: Karakaya, D., Little, T.G. (Eds.), Actas Do XI Congresso on Medieval and Modern Period Mediterranean Ceramics, 19-24 October 2015, Antalya, Turkey, Vol. 2. Koç University VEKAM, Ankara, pp. 21–30.

Gómez Martínez, S., Gonçalves, M.J., Inácio, I., Dos Santos, C., Coelho, C., Liberato, M., Gomes, A.S., Bugalhão, J., Catarino, H., Cavaco, S., Covaneiro, J., Fernandes, I.C., 2015. A cidade e o seu território no Garb al-Andaluz através da cerâmica, in: Gómez Martínez, S., Gonçalves, M.J. (Eds.), Actas Do X Congresso de Cerâmica Medieval No Mediterrâneo Ocidental, Silves 22-27 Outobro 2012. Campo Arqueológico de Mértola, Cârama Municipal de Silves, Silves-Mértola, pp. 19–50.

Gonçalves, M.J., 2012. Evidências do Comércio no Mediterrâneo Antigo. A cerâmica "verde e manganês" presente num arrabalde Islâmico de Silves (Portugal), in: Gelichi, S., Ferri, M., Sabbionesi, L. (Eds.), Atti Del IX Congresso Internazionale Sulla Ceramica Medievale Nel Mediterraneo, Venezia, Scuola Grande Dei Carmini Auditorium Santa Margherida 23-27 Novembre 2009. All'Insegna del Giglio, Venezia, pp. 179–181.

Gonçalves, M.J., 2010. Objectos de troca no Mediterrâneo Antigo: cerâmica "verde e manganês" de um arrabalde Islâmico de Silves. Arqueol. Mediev. 11, 25–41.

Gonçalves, M.J., Inácio, I., Guimarães dos Santos, C., Coelho, C., Liberato, M., Gomes, A.S., Bugalhão, J., Catarino, H., Cavaco, S., Covaneiro, J., Fernandes, I.C., Gómez Martínez, S., 2015.

Vinte anos de céramica islámica do Gharb al-Andalus. Ensaio crono-tipológico das formas abertas (I), in: Mediana Rosales, N. (Ed.), VII Encontro de Arqueologia Del Suroeste Peninsular. Aroche-Serpa, Novembro 2013. Ayuntamento de Aroche, Aroche (Huelva), pp. 1025–1041.

González-García, F., González-Rodríguez, M., Gonzalez Vilchez, C., Vallejo Triano, A., Escudero Aranda, J., 1999. Estudio arqueométrico de piezas cerámicas de Madīnat al-Zahrā. Cuad. Medinat al-Zahra 4, 11–38.

González García, F., Gonzales Rodriguesz, M., Gonzalez Vilchez, C., Vallejo Triano, A., 1992. Estudio arqueométrico de algunas cerámicas medievales de Madinat Al-Zahra (Córdoba) - CSIC. Boletín la Soc. Española Cerámica y Vidr. 31, 491–498.

Gosselain, O.P., 2012. Technology, Oxford Han. ed. Oxford University Press, Oxford. https://doi.org/10.1093/oxfordhb/9780199232444.013.0018

Gosselain, O.P., 1992. Bonfire of the enquiries. Pottery firing temperatures in archaeology: What for? J. Archaeol. Sci. 19, 243–259. https://doi.org/10.1016/0305-4403(92)90014-T

Goudarzi, M.A., Landry, R.J., 2017. Assessing horizontal positional accuracy of Google Earth imagery in the city of Montreal, Canada. Geod. Cartogr. 43, 56–65. https://doi.org/10.3846/20296991.2017.1330767

Gouvêa, D., Kaneko, T.T., Kahn, H., De Souza Conceição, E., Antoniassi, J.L., 2015. Using bone ash as an additive in porcelain sintering. Ceram. Int. 41, 487–496. https://doi.org/10.1016/j.ceramint.2014.08.096

Gragueb, S., Tréglia, J.-C., Capelli, C., Waksman, Y., 2011. Jarres et amphores de Sabra al-Mansuria (Kairouan, Tunisie), in: Cressier, P., Fentress, E. (Eds.), La Céramique Maghrébine Du Haut Moyen Âge (VIII_X Siécle). État Des Recherches, Problémes et Perspectives. École Française de Rome, Rome, pp. 197–220.

Greene, K., 2007. Late hellenistic and early Roman invention and innovation: The case of lead-glazed pottery. Am. J. Archaeol. 111, 653–671. https://doi.org/10.3764/aja.111.4.653

Gribble, C.D., Hall, A.J., 1985. A Practical Introduction to Optical Mineralogy. Springer Netherlands, Dordrecht. https://doi.org/10.1007/978-94-011-7804-4

Gutiérrez Lloret, S., 2015a. Early al-Andalus : an Archaeological Approach to the Process of Islamization in the Iberian Peninsula (7 th to 10 th centuries), in: Gelichi, S., Hodges, R. (Eds.), New Direction in Early Medieval European Archaeology: Spain and Italy Compared.

Berpols Publisher, Turnhot, pp. 43–85. https://doi.org/10.1484/M.HAMA-EB.5.108001

Gutiérrez Lloret, S., 2015b. Cerámica e Islamización: el origen de la tradición alfarera, in: Rodríguez Manzaneque, M.J. (Ed.), Origen y Evolución de La Alfarería de Agost y Comarcas Limítrofes. Asociación de Ceramología, Alicante, pp. 9–22.

Gutiérrez Lloret, S., 2011. Al-Andalus y el Magreb: la cerámica altomedieval en las dos orillas del mundo mediterráneo occidental., in: Cressier, P., Fentress, E. (Eds.), La Céramique Maghrébine Du Haut Moyen Âge (VIII_X Siécle). État Des Recherches, Problémes et Perspectives. École Française de Rome, Rome, pp. 253–266.

Gutiérrez Lloret, S., 2007. La islamización de Tudmīr: balance y perspectivas, in: Sénac, P. (Ed.), Villes et Campagnes de Tarraconaise et d'al-Andalus (VIe-XIe Siècles): La Transition. Centre National de la Recherche Scientifique | Université de Toulouse-Le Mirail, Paris, pp. 275–318.

Gutierrez, P.C., Pradell, T., Molera, J., Smith, A.D., Climent-Font, A., Tite, M.S., 2010. Color and golden shine of silver Islamic luster. J. Am. Ceram. Soc. 93, 2320–2328. https://doi.org/10.1111/j.1551-2916.2010.03741.x

Hallett, J., 2011. Pearl Cups Like the Moon: The Abbasid reception of Chinese ceramics, in: Kharl, R., Guy, J., Wilson, J.K., Raby, J. (Eds.), Shipwrecked: Tang Treasures and Monsoon Winds. Smithsonian Institution Press, Washington, EUA, pp. 75–81.

Hayes, J.W., 1972. Late Roman pottery: a Catalogue of Romn Fine Wares. British School at Rome, London.

Heimann, R.B., Maggetti, M., 2019. The struggle between thermodynamics and kinetics: Phase evolution of ancient and historical ceramics. Eur. Mineral. Union Notes Mineral. 20, 233–281. https://doi.org/10.1180/EMU-notes.20.6

Heimann, R.B., Maggetti, M., 2014. Ancient and Historical ceramics. Materials, Technology, Art and Culinary Tradition. Schweizerbart Science Pubblisher, Stuttgrat.

Hein, A., Müller, N.S., Day, P.M., Kilikoglou, V., 2008. Thermal conductivity of archaeological ceramics: The effect of inclusions, porosity and firing temperature. Thermochim. Acta 480, 35–42. https://doi.org/10.1016/j.tca.2008.09.012

Henderson, J., 1999. Archaeological and scientific evidence for the production of early Islamic glass in al-Raqqa, Syria. Levant 31, 225–241. https://doi.org/10.1179/lev.1999.31.1.225

Henderson, J., 1995. An Investigation of Early Islamic Glass Production at Raqqa, Syria. MRS

Proc. 352, 433. https://doi.org/10.1557/PROC-352-433

Henderson, P., 1984. General Geochemical Properties and Abundances of the Rare Earth Elements, in: Henderson, P. (Ed.), Rare Earth Element Geochemistry. Elsevier, Amsterdam-Oxford-New York-Tokyo, pp. 1–32. https://doi.org/10.1016/B978-0-444-42148-7.50006-X

Henry, D.J., Novák, M., Hawthorne, F.C., Ertl, A., Dutrow, B.L., Uher, P., Pezzotta, F., 2011. Nomenclature of the tourmaline-supergroup minerals. Am. Mineral. 96, 895–913. https://doi.org/10.2138/am.2011.3636

Hill, D. V., Speakman, R.J., Glascock, M.D., 2004. Chemical and mineralogical characterization of Sasanian and Early Islamic glazed ceramics from the Deh Luran Plain, southwestern Iran. Archaeometry 46, 585–605. https://doi.org/10.1111/j.1475-4754.2004.00175.x

Hoskin, P.W.O., Ireland, T.R., 2000. Rare earth element chemistry of zircon and its use as a provenance indicator. Geology 28, 627–630. https://doi.org/10.1130/0091-7613(2000)028<0627:REECOZ>2.3.CO;2

Idrisi, 1866. Description de l'Afrique et de l'Espagne : texte arabe publié pour la première fois d'après les manuscrits de Paris et d'Oxford avec une traduction, des notes et un glossaire par R. Dozy et M.J. de Goeje / par Edrîsî. Leiden Unversity, Leiden.

Iñiguez, C., Mayorga, J., 1993. Un alfar emiral em Málaga, in: Malpica Cuello, A. (Ed.), La Cerámica Altomedieval En El Sur de Al-Andalus : Primer Encuentro de Arqueología y Patrimonio. Universidade de Granada, Granada. España, pp. 117–138.

Iqbal, Y., Messer, P.F., Lee, W.E., 2000a. Microstructural evolution in bone china. Br. Ceram. Trans. 99, 193–199. https://doi.org/10.1179/096797800680938

Iqbal, Y., Messer, P.F., Lee, W.E., 2000b. Non-equilibrium microstructure of bone china. Br. Ceram. Trans. 99, 110–116. https://doi.org/10.1179/096797800680811

Jones, R.R., Hooper, D.C., Zhang, L., Wolverson, D., Valev, V.K., 2019. Raman Techniques: Fundamentals and Frontiers. Nanoscale Res. Lett. 14. https://doi.org/10.1186/s11671-019-3039-2

Jordán, M.M., Boix, A., Sanfeliu, T., De La Fuente, C., 1999. Firing transformations of cretaceous clays used in the manufacturing of ceramic tiles. Appl. Clay Sci. 14, 225–234. https://doi.org/10.1016/S0169-1317(98)00052-0

Kam, S., Zerbo, L., Bathiebo, J., Soro, J., Naba, S., Wenmenga, U., Traoré, K., Gomina, M., Blanchart,

P., 2009. Permeability to water of sintered clay ceramics. Appl. Clay Sci. 46, 351–357. https://doi.org/10.1016/j.clay.2009.09.005

Karagiannopoulou, M., 2017. Material Characterization of Almohad large Decorated Ceramic Vessels: XII-XIII centuries. University of Evora.

Kilikoglou, V., Vekinis, G., Maniatis, Y., Day, P.M., 1998. Mechanical Performance of Quartz-Tempered Ceramics: Part I, Strength and Toughness. Archaeometry 40, 261–279. https://doi.org/10.1111/j.1475-4754.1998.tb00837.x

Klein, C., 2002. Mineral Sciences, 22nd editi. ed. Jonh Wiley and Sons, INC, New York.

Kreimeyer, R., 1987. Some notes on the firing colour of clay bricks. Appl. Clay Sci. 2, 175–183. https://doi.org/10.1016/0169-1317(87)90007-X

Kresten, P., Berggren, G., 1978. The thermal decomposition of vermiculite. Thermochim. Acta 23, 171–182. https://doi.org/10.1016/0040-6031(78)85123-5

Krynine, P.D., 1946. The Tourmaline Group. J. Geol. 54, 65–87.

Lafuente, B., Downs, R.T., Yang, H., Stone, N., 2016. The power of databases: The RRUFF project, Highlights in Mineralogical Crystallography. https://doi.org/10.1515/9783110417104-003

Lafuente Ibáñez, P., 1994. Cerámica islámica en el área suroccidental de Andalucía estado de la cuestión, in: Campos Carrasco, J.M., Pérez Macías, J.A., Gómez Rui, F. (Eds.), Arqueología En El Entorno Del Bajo Guadiana Actas Del Encuentro Internacional de Arqueología Del Suroeste [(Celebrado En) Huelva y Niebla, 25 a 27 de Febrero de 1993. Universidad de Huelva, Huelva, pp. 565–584.

Lapuente, P., Peréz-Arantegui, J., 1999. Characterisation and technology from studies of clay bodies of local Islamic production in Zaragoza (Spain). J. Eur. Ceram. Soc. 19, 1835–1846. https://doi.org/10.1016/S0955-2219(98)00286-6

Lawrence, W.G., West, R.R., 1982. Ceramic science for the potter, Second edi. ed. Gentle Breeze Pubblication, Radnor, Pensilvenia.

Lehroi-Gourhan, A., 1964. Le geste et la Perole. Tome I Technique et linguage, A. Michel. ed. Paris.

Leistel, J.M., Marcoux, E., Thiéblemont, D., Quesada, C., Sánchez, A., Almodóvar, G.R., Pascual, E., Sáez, R., 1997. The volcanic-hosted massive sulphide deposits of the Iberian Pyrite Belt. Miner. Depos. 33, 2–30. https://doi.org/10.1007/s001260050130

Lemonier, P., 1993. Technological choises: transformation in material culture since the neolithic. Routledge, London and New York.

Lepierre, C., 1899. Estudo chimico e technologico sobre a ceramica portugueza moderna, Boletim do Trabalho Industrial. Imprensa Nacional, Lisboa.

Liberato, M., 2016. A pintura a branco na Santarém Medieval. Séculos XI-XVI, in: Gonçalves, M.J., Gómez-Martínez, S. (Eds.), Actas Do X Congresso de Cerâmica Medieval No Mediterrâneo Ocidental, Silves 22-27 Outobro 2012. Campo Arqueológico de Mértola, Câmara Municipal de Silves, Silves-Mértola, pp. 777–791.

Liberato, M., 2012a. A cerâmica pintada a branco na Santarém Medieval, Uma abordagem diacrónica: séculos XI a XVI. University of Lisbon.

Liberato, M., 2012b. Novos dados sobre a paisagem urbana da Santarém medieval (séculos V-XII): a necrópole visigoda e islâmica de Alporão. Mediev. online. https://doi.org/10.4000/medievalista.803

Liberato, M., Santos, H., 2018. Cerâmicas alto-medievais de Santarém, Portugal: aspectos formais e tecnológicos, in: Actas Do Congreso Internacional de Cerámicas Altomedievales En Hispania y Su Entorno. pp. 212–219.

Liberato, M., Santos, H., Santos, N., Beltrame, M., Mirão, J., 2019. Cerâmica pintada a branco sobre engobe vermelho: Uma produção tardo-medieval de difusão suprarregional. O Arqueólogo Port. 6–7, 265–282.

Lindahl, A., Pikirayi, I., 2010. Ceramics and change: An overview of pottery production techniques in northern South Africa and eastern Zimbabwe during the first and second millennium AD. Archaeol. Anthropol. Sci. 2, 133–149. https://doi.org/10.1007/s12520-010-0031-2

Livingstone Smith, A., 2000. Processing Clay for Pottery in Northern Cameroon: Social and Technical Requirements. Archaeometry 42, 21–42. https://doi.org/10.1111/j.1475-4754.2000.tb00864.x

Lopes, G., 2015. Materiais do povoado Islâmico do Serradinho (Muge, Salvaterra de Magos). Cira Arqueol. 4, 171–186.

Louhichi, A., Picon, M., 1983. Importation de matériel céramique ifriqiyen en Mauritanie. Rev. d'Archéométrie 7, 45–58. https://doi.org/10.3406/arsci.1983.1201

Lowell, S., Shields, J.E., Thomas, M.A., Thommes, M., 2004. Characterization of Porous Solids and

Powders: Surface Area, Pore Size and Density, Particle Technology Series. Springer Netherlands, Dordrecht. https://doi.org/10.1007/978-1-4020-2303-3

Maggetti, M., Galletti, G., 1982. Die Referenzgruppe(n) Lousanna - mineralogische und chemische Untersuchungen der keramischen Produktion der Topferwerkstatten Berna. Schweizerischen Gesellschaft fur Ur- und Furhgeschichte 109–132.

Maltoni, S., Silvestri, A., Maritan, L., Molin, G., 2012. The Medieval lead-glazed pottery from Nogara (north-east Italy): A multi-methodological study. J. Archaeol. Sci. 39, 2071–2078. https://doi.org/10.1016/j.jas.2012.03.016

Maniatis, Y., Simopoulos, A., Kostikas, A., 1981. Moessbauer Study of the Effect of Calcium Content on Iron Oxide Transformations in Fired Clays. J. Am. Ceram. Soc. 64, 263–269. https://doi.org/10.1111/j.1151-2916.1981.tb09599.x

Maniatis, Y., Tite, M.S., 1981. Technological examination of Neolithic-Bronze Age pottery from central and southeast Europe and from the Near East. J. Archaeol. Sci. 8, 59–76. https://doi.org/10.1016/0305-4403(81)90012-1

Mantas, V.G., 2002. A rede viária de Scallabis, in: Arruda, A.M., Viegas, C., Almeida, M.J. (Eds.), De Scallabis a Santrém. Museo Nacioanal de Arqueologia, Lisbon, Portugal, pp. 107–112.

Maritan, L., Nodari, L., Mazzoli, C., Milano, A., Russo, U., 2006. Influence of firing conditions on ceramic products: Experimental study on clay rich in organic matter. Appl. Clay Sci. 31, 1–15. https://doi.org/10.1016/j.clay.2005.08.007

Markovic, M., 2016. Technological characterization of molded Islamic pottery from Iberian Peninsula. University of Évora.

Marques Prazeres, C., 2011. Caracterização geoquímica , radiométrica e mineralógica de algumas mineralizações de urânio da região de Nisa. University of Lisbon.

Martín Patino, M.T., Garotte Martín, I., Fernández Galbaldón, S., 1987. Resultados de los análisis químicos y mineralógicos de las cerámicas almohades del yacimiento de la Encarnación (Jerez de la Frontera). Estud. Hist. y Arqueol. Mediev. 7–8, 197–208.

Marzo, P., Laborda, F., Peréz-Arantegui, J., 2009. Medieval and postmedieval Hispano-Moresque glazed ceramics: new possibilities of characterization by means of lead isotope ratio determination by Quadrupole ICP-MS, in: Degryse, P., Henderson, J., Hodgins, G. (Eds.), Isotopes in Vitreous Materials. Leuven University Press, pp. 131–144. https://doi.org/10.2307/j.ctt9qdx40.11

Mason, R.B., 1995. New Looks at Old Pots: Results of Recent Multidisciplinary Studies of Glazed Ceramics from the Islamic World. Muqarnas 12, 1. https://doi.org/10.2307/1523219

Mason, R.B., 1991. Petrology of Islamic ceramics, in: Middleton, A., Freestone, I.C. (Eds.), Recent Development in Ceramic Petrology. British Museum, London, pp. 185–210.

Mason, R.B., Keall, E.J., 1991. The 'Abbasid glazed wares of Siraf and the Basra connection: petrographic analysis. Iran J. Br. Inst. Persian Stud. 29, 55–66.

Mason, R.B., Tite, M.S., 1997. The beginnings of tin-opacification of pottery glazes. Archaeometry 39, 41–58. https://doi.org/10.1111/j.1475-4754.1997.tb00789.x

Mason, R.B., Tite, M.S., 1994. The beginnings of Islamic stonepaste technology. Archaeometry 36, 77–91. https://doi.org/10.1111/j.1475-4754.1994.tb01066.x

Mateus, A., Pinto, A., Alves, L.C., Matos, J.X., Figueiras, J., Neng, N.R., 2011. Roman and modern slag at S. Domingos mine (IPB, Portugal): Compositional features and implications for their long-term stability and potential reuse. Int. J. Environ. Waste Manag. 8, 133–159. https://doi.org/10.1504/IJEWM.2011.040971

Matin, M., 2019. Tin-based opacifiers in archaeological glass and ceramic glazes: a review and new perspectives. Archaeol. Anthropol. Sci. 11, 1155–1167. https://doi.org/10.1007/s12520-018-0735-2

Matin, M., Tite, M.S., Watson, O., 2018. On the origins of tin-opacified ceramic glazes: New evidence from early Islamic Egypt, the Levant, Mesopotamia, Iran, and Central Asia. J. Archaeol. Sci. 97, 42–66. https://doi.org/10.1016/j.jas.2018.06.011

Matos, J.X., Pereira, Z., Batista, M.J., Oliveira, D., 2012. São Domingos Mining Site - Iberian Pyrite Belt, in: Batista, M.J. (Ed.), 9th International Conference on Environmental Geochemistry (9th ISEG): Multidisciplinary Contribution for Environmental Characterization and Improvement at the S. Domingos Mining Site. Univrsity of Aveiro, Aveiro, pp. 7–12.

McConville, C.J., Lee, W.E., 2005. Microstructural development on firing illite and smectite clays compared with that in kaolinite. J. Am. Ceram. Soc. 88, 2267–2276. https://doi.org/10.1111/j.1551-2916.2005.00390.x

McDonough, W.F., Sun, S. -s., 1995. The composition of the Earth. Chem. Geol. 120, 223–253. https://doi.org/10.1016/0009-2541(94)00140-4

McKeown, D.A., 2008. Raman spectroscopy, vibrational analysis, and heating of buergerite tourmaline. Phys. Chem. Miner. 35, 259–270. https://doi.org/10.1007/s00269-008-0219-

5

Medeghini, L., De Vito, C., Coletti, F., Govi, A., Fabrizi, L., Di Fazio, M., Mignardi, S., 2018. Glazed roman ceramic: A multi-analytical approach. Period. di Mineral. 87, 229–244. https://doi.org/10.2451/2018PM781

Meo, A., 2018. L'ordinario e L'eccezione. Per un Aggiornamento Cronologico dell'introduzione dei Bacini Islamici a Pisa, in: Karakaya, D., Glenn Little, T. (Eds.), Actas Do XI Congresso on Medieval and Modern Period Mediterranean Ceramics, 19-24 October 2015, Antalya, Turkey, Vol. 1. Koç University VEKAM, Ankara, pp. 59–75.

Métreau, L., Rosen, J., 2014. Origin and Development of French Faience : The Contribution of Archaeology and the Physical Sciences. Tech. Breifs Hist. Archaeol. 8, 1–21.

Molera, J., Carvajal López, J.C., Molina, G., Pradell, T., 2018. Glazes, colourants and decorations in early Islamic glazed ceramics from the Vega of Granada (9th to 12th centuries CE). J. Archaeol. Sci. Reports 21, 1141–1151. https://doi.org/10.1016/j.jasrep.2017.05.017

Molera, J., Coll Conesa, J., Labrador, A., Pradell, T., 2013. Manganese brown decorations in 10th to 18th century Spanish tin glazed ceramics. Appl. Clay Sci. 82, 86–90. https://doi.org/10.1016/j.clay.2013.05.018

Molera, J., García-Vallés, M., Pradell, T., Vendrell-Saz, M., 1996. Hispano-Moresque pottery production of the 14th-century workshop of Testar del Molí (Paterna, Spain). Archaeometry 38, 67–80. https://doi.org/10.1111/j.1475-4754.1996.tb00761.x

Molera, J., Mesquida, M., Peréz-Arantegui, J., Pradell, T., Vendrell, M., 2001a. Lustre Recipes from A Medieval Workshop in Paterna. Archaeometry 43, 455–460. https://doi.org/10.1111/1475-4754.00028

Molera, J., Pradell, T., Martinez-Manent, S., Vendrell-Saz, M., 1993. The growth of sanidine crystals in the lead of glazes of Hispano-Moresque pottery. Appl. Clay Sci. 7, 483–491. https://doi.org/10.1016/0169-1317(93)90017-U

Molera, J., Pradell, T., Merino, L., García-Vallés, M., García-Orellana, J., Salvadó, N., Vendrell-Saz, M., 1999a. La tecnología de la cerámica islámica y mudéjar. Caesaraugusta 73, 15–42.

Molera, J., Pradell, T., Salvado, N., 2001b. Interactions between clay bodies and lead glazes. J. Am. Ceram. Soc. 84, 1120–1128. https://doi.org/10.1111/j.1151-2916.2001.tb00799.x

Molera, J., Pradell, T., Salvado, N., Vendrell-Saz, M., 1999b. Evidence of Tin Oxide Recrystallization in Opacified Lead Glazes. J. Am. Ceram. Soc. 82, 2871–2875.

https://doi.org/10.1111/j.1151-2916.1999.tb02170.x

Molera, J., Pradell, T., Salvadó, N., Vendrell-Saz, M., 2009. Lead Frits in Islamic and Hispano-moresque Glazed Production, in: From Mine to Microscope: Advances in the Study of Ancient Technology. Oxbow, Oxford, pp. 11–22. https://doi.org/10.1016/j.jas.2009.11.021

Molera, J., Pradell, T., Vendrell-Saz, M., 1998. The colours of Ca-rich ceramic pastes: Origin and characterization. Appl. Clay Sci. 13, 187–202. https://doi.org/10.1016/S0169-1317(98)00024-6

Molera, J., Vendrell-Saz, M., García-Vallés, M., Pradell, T., 1997. Technology and colour development of Hispano-Moresque lead-glazed pottery. Archaeometry 39, 23–39. https://doi.org/10.1111/j.1475-4754.1997.tb00788.x

Molera, J., Vendrell-Saz, M., Peréz-Arantegui, J., 2001c. Chemical and Textural Characterization of Tin Glazes in Islamic Ceramics from Eastern Spain. J. Archaeol. Sci. 28, 331–340. https://doi.org/10.1006/jasc.2000.0606

Moore, D.M., Reynolds, R.C., 1997. X-Ray Diffraction and the Identification and Analysis of Clay Minerals. Oxford University Press, Oxford.

Moretti, C., Hreglich, S., 1984. Opacification and colouring of glass by the use of “anime.” Glas. Technol. 25, 277–282.

Moussalli, A.S., Gordon, D.N., Moussalli, A., 2016. Muḥammad [WWW Document]. Oxford Encycl. Islam. World. Oxford Islam. Stud. Online. URL http://www.oxfordislamicstudies.com/article/opr/t236/e0550 (accessed 6.13.20).

Müller, N.S., Kilikoglou, V., Day, P.M., Vekinis, G., 2010. The influence of temper shape on the mechanical properties of archaeological ceramics. J. Eur. Ceram. Soc. 30, 2457–2465. https://doi.org/10.1016/j.jeurceramsoc.2010.04.039

Murad, E., 1978. Yttrium and Zirconium As Geochemical Guide Elements in Soil and Stream Sediment Sequences. J. Soil Sci. 29, 219–223. https://doi.org/10.1111/j.1365-2389.1978.tb02052.x

Nasdala, L., Smith, D.C., Kaindal, R., Ziemann, M.A., 2004. Raman spectroscopy in mineralogy research, in: Beran, A., Libowitzky, E. (Eds.), Spectroscopic Methods in Mineralogy - Emu Notes in Mineralogy Volume 6. Eötvös University, Budapest, pp. 281–343.

Navarro Palazon, J., 1986. La ceramica esgrafiada andalusi de Murcia. Casa de Velázquez,

Madrid.

Neff, H., 2017. Inductively Coupled Plasma-Mass Spectrometry (ICP-MS), in: Gilbert, A.S. (Ed.), Encyclopedia of Geoarchaeology. Springer, Dordrecht, pp. 433–441. https://doi.org/10.1007/978-1-4020-4409-0_19

Neiva, J.M.C., 2003. Portuguese uranium deposits and their genesis, in: A Geologia de Engenharia e Os Recursos Geológicos. Vol. I: Geologia de Engenharia. Imprensa da Universidade de Coimbra, Coimbra, pp. 15–76. https://doi.org/10.14195/978-989-26-0321-6_1

Neri, E., Jackson, M., O'Hea, M., Gregory, T., Blet-Lemarquand, M., Schibille, N., 2017. Analyses of glass tesserae from Kilise Tepe: New insights into an early Byzantine production technology. J. Archaeol. Sci. Reports 11, 600–612. https://doi.org/10.1016/j.jasrep.2016.12.036

Nodari, L., Marcuz, E., Maritan, L., Mazzoli, C., Russo, U., 2007. Hematite nucleation and growth in the firing of carbonate-rich clay for pottery production. J. Eur. Ceram. Soc. 27, 4665–4673. https://doi.org/10.1016/j.jeurceramsoc.2007.03.031

Noll, W., Heimann, R.B., 2016. Ancient Old World Pottery. Materials, Technology, and Decoration. E. Schweizerbart'Sche Varlagsbuchhandlung Pubblisher, Stuttgrat, Germany.

Normal, 1985. Normal - 21/85. Permeabilita al vapor d'acqua. 21/85.

Northedge, A., 2001. Thoughts on the introduction of polychrome glazed pottery in the Middle East, in: E. Villeneuve, Watson, P.M. (Eds.), La Céramique Byzantine et Proto-Islamique En Syrie-Jordanie (IVe-VIIIe Siècles Apr. J.-C.) : Amman Les 3, 4 et 5 Décembre 1994. Institut français d'archéologie du Proche-Orient, Beyrouth, pp. 207–214.

Oliveira, J.T., Silva, J.B., 2007. Geological Map of Portugal, scale 1:500000, with esplicative notes. Map 46-D / Mértola.

Ottley, C.J., Pearson, D.G., Irvine, G.J., 2003. A routine method for the dissolution of geological samples for the analysis of REE and trace elements via ICP-MS, in: Grenville, H., D. Tunner, S. (Eds.), The Proceedings of the Sth International Conference on Plasma Source Mass Spectrometry Held at the University of Durham on 8-13 September 2002. The Royal Society of Chemistry, Cambridge, pp. 221–230. https://doi.org/10.1039/9781847551689-00221

Pace, M., Prevot, B.A., Mirti, P., Ricciardi, R.V., 2008. The technology of production of sasanian

glazed pottery from veh ardašïr (Central Iraq). Archaeometry 50, 591–605. https://doi.org/10.1111/j.1475-4754.2007.00369.x

Pais, J., 2004. The Neogene of the Lower Tagus Basin (Portugal). Rev. Española Paleontol. 19, 229–242.

Pais, J., Cunha, P., Legoinha, P., Dias, R.P., Pereira, D., Ramos, A., 2013. Cenozóico das Bacias do Douro (sector ocidental), Mondego, Baixo Tejo e Alvalade, in: Dias, R., Araújo, A., Terrinha, P., Kullberg, J.C. (Eds.), Geologia de Portugal, Vol. II. Geologia Meso-Cenozóica de Portugal. Escolar Editora, Lisboa, Portugal, pp. 461–532.

Palamara, E., Zacharias, N., Xanthopoulou, M., Kasztovszky, Z., Kovács, I., Palles, D., Kamitsos, E.I., 2016. Technology issues of Byzantine glazed pottery from Corinth, Greece. Microchem. J. 129, 137–150. https://doi.org/10.1016/j.microc.2016.06.008

Paz Peralta, J.Á., 2008. La producción de céramica vidriada, in: Bernal Casasola, D., Ribera i Lacomba, A. (Eds.), Cerámica Hispanorromanas. Un Estado de La Cuestión. Universidad de Cadiz, Cadiz, pp. 489–496.

Peccerillo, A., Perugini, D., 2005. Introduzione alla petrografia ottica. Morlacchi editore, Perugia.

Penel, G., Leroy, G., Rey, C., Bres, E., 1998. MicroRaman spectral study of the PO4 and CO3 vibrational modes in synthetic and biological apatites. Calcif. Tissue Int. 63, 475–481. https://doi.org/10.1007/s002239900561

Peréz-Arantegui, J., Castillo, J.R., 2000. Characterization of red-coloured slips (almagra) on Islamic ceramics in Muslim Spain. Archaeometry 42, 119–128. https://doi.org/10.1111/j.1475-4754.2000.tb00870.x

Peréz-Arantegui, J., Garcia-Ruiz, E., Castillo, J.R., 1999a. La cerámica “verde y negro” de los talleres islámico de Zaragoza: características tecnológicas de sus recubrimentos. Caesaraugusta 73, 43–49.

Peréz-Arantegui, J., Lapuente, P., 2003. Las técnicas de prducciónes de cerámica en los talleres islámico de Zaragoza (España), in: Bakirtzis, C. (Ed.), VIIe Congrés International Sur La Céramique Médiévale En Méditerranée, Thessaloniki, 11-16 Octobre 1999. Caisse des Recettes Archéologiques, Athènes, pp. 375–380.

Peréz-Arantegui, J., Larrea, A., Molera, J., Pradell, T., Vendrell-Saz, M., 2004. Some aspects of the characterization of decorations on ceramic glazes. Appl. Phys. A Mater. Sci. Process. 79, 235–239. https://doi.org/10.1007/s00339-004-2508-2

Peréz-Arantegui, J., Soto, M., Castillo, J.R., 1999b. Examination of the 'Cuerda Seca' Decoration Technique on Islamic Ceramics from al-Andalus (Spain). J. Archaeol. Sci. 26, 935–941. https://doi.org/10.1006/jasc.1999.0400

Peréz-Arantegui, J., Uruñuela, M.I., Castillo, J.R., 1996. Roman glazed ceramics in the Western Mediterranean: Chemical characterization by inductively coupled plasma atomic emission spectrometry of ceramic bodies. J. Archaeol. Sci. 23, 903–914. https://doi.org/10.1006/jasc.1996.0085

Peréz-Arantegui, J., Uruñuela, M.I., Lapuente, P., Castillo, J.R., 1995. Study of Roman lead glazing technology between 1st and 2nd centuries ad by Scanning Electron Microscopy, in: Fabbri, B. (Ed.), 4th European Ceramic Society Conference: Cultural Ceramic Heritage/ 3rd European Meeting on Ancient Ceramics, Riccione, Italy. Faenza Gruppo Ed., Faenza.

Picon, M., Navarro Palazon, J., 1986. La loza dorada de la Provincie de Murcie: étude en laboratoire, in: La Ceramica Medievale Nel Mediterraneo Occidentale. Siena-Faenza, 8-13 Ottobre 1984. All'Insegna del Giglio, Firenze, pp. 144–146.

Pradell, T., Molera, J., 2020. Ceramic technology. How to characterise ceramic glazes. Archaeol. Anthropol. Sci. 12. https://doi.org/10.1007/s12520-020-01136-9

Pradell, T., Molera, J., Salvadó, N., Labrador, A., 2010. Synchrotron radiation micro-XRD in the study of glaze technology. Appl. Phys. A Mater. Sci. Process. https://doi.org/10.1007/s00339-010-5639-7

Pradell, T., Molera, J., Smith, A.D., Climent-Font, A., Tite, M.S., 2008a. Technology of Islamic lustre. J. Cult. Herit. 9, e123–e128. https://doi.org/10.1016/j.culher.2008.06.010

Pradell, T., Molera, J., Smith, A.D., Tite, M.S., 2008b. The invention of lustre: Iraq 9th and 10th centuries AD. J. Archaeol. Sci. 35, 1201–1215. https://doi.org/10.1016/j.jas.2007.08.016

Pradell, T., Molina, G., Molera, J., Marinetto Sánchez, P., 2012. Primeros resultados del estudio analítico de la cerámica vidriada decorada Nazarí : la cerámica palatina (ss . XIV-XV), in: Actas Del I Congreso Internacional Red Europea de Museos de Arte Islámico. pp. 397–418.

Pradell, T., Molina, G., Molera, J., Pla, J., Labrador, A., 2013. The use of micro-XRD for the study of glaze color decorations. Appl. Phys. A Mater. Sci. Process. https://doi.org/10.1007/s00339-012-7445-x

Pradell, T., Molina, G., Molera, J., Tite, M.S., 2016. Composition of the Lustre Pigment Used in the Production Of 13th Century AD Raqqa Lustreware from Syria. Archaeometry 58, 979–986.

https://doi.org/10.1111/arcm.12211

Prudêncio, M.I., Dias, M.I., Gouveia, M.A., Gomes, A.S., Gaspar, A., 2006. Evolução das tecnologias de produção cerâmica dos séculos XI a XVI na cidade de Lisboa, in: Zozaja, J., Retuerce, M., Hervas, M.A., De Juan, A. (Eds.), Actas Del VIII Congreso Internacional de Cerámica Medieval En El Mediterráneo. Asociación Española de Arqueología Medieval, Ciudad Real-Almagro, p. Tome 1, pg 509–514.

Pulighe, G., Baiocchi, V., Lupia, F., 2016. Horizontal accuracy assessment of very high resolution Google Earth images in the city of Rome, Italy. Int. J. Digit. Earth 9, 342–362. https://doi.org/10.1080/17538947.2015.1031716

Queiroz, P.F., 2001. Estudos de Arqueobotânica no Convento de S. Francisco de Santarém, in: Garb: Sitio Islâmicos Do Sul Peninsular. Ministério da Cultura, IPPAR, Junta da Extremadura, pp. 89–117.

Quinn, P.S., 2013. Ceramic Petrography. The interpretation of archaeological pottery & related artefacts in thin section. Archaeopress, Oxford.

Retuerce Velasco, M., De Juan García, A., 1998. La cerámica almohade en verde y manganeso de la meseta. Arqueol. y Territ. Mediev. 6, 241–260. https://doi.org/10.17561/aytm.v6i0.1534

Retuerce Velasco, M., Zozaya, J., 1991. Variantes y constantes en la cerámica andalusí, in: Alves da Silva, L., Mateus, R. (Eds.), A Cerámica Medieval No Mediterraneo Occidental. Lisboa 16-22 Nov. 1987. Campo Arqueológico de Mértola, pp. 315–326.

Retuerce Velasco, M., Zozaya, J., 1986. Variantes geográficas de la cerámica omeya andalusí: los temas decorativos, in: La Ceramica Medievale Nel Mediterraneo Occidentale. Siena-Faenza, 8-13 Ottobre 1984. All'Insegna del Giglio, Firenze, pp. 69–128.

Retuerce Velasco, Manuel, Hervás, M.Á., De Juan, A., 2009. La céramica islámica de Calatrava la Veja y Alarcos. Nuevos hallazgos, in: Zozaya Stabel-Hansen, J., Retuerce Velasco, Manue, Hervás Herrera, M.Á., De Juan García, A. (Eds.), VIIe Congreso International de Céramica Medieval En El Mediterráneo. Asociación Española de Arqueología Medieval, Cuidad Real - Almagro 2006, pp. 729–758.

Riccardi, M.P., Messiga, B., Duminuco, P., 1999. An approach to the dynamics of clay firing. Appl. Clay Sci. 15, 393–409. https://doi.org/10.1016/S0169-1317(99)00032-0

Ricci, C., Borgia, I., Brunetti, B.G., Sgamellotti, A., Fabbri, B., Burla, M.C., Polidori, G., 2005. A study

on late medieval transparent-glazed pottery and archaic majolica from Orvieto (Central Italy). Archaeometry 47, 557–570. https://doi.org/10.1111/j.1475-4754.2005.00219.x

Rodriguez-Navarro, C., Cultrone, G., Sanchez-Navas, A., Sebastian, E., 2003. TEM study of mullite growth after muscovite breakdown. Am. Mineral. 88, 713–724. https://doi.org/10.2138/am-2003-5-601

Rodriguez-Navarro, C., Ruiz-Agudo, E., Luque, A., Rodriguez-Navarro, A.B., Ortega-Huertas, M., 2009. Thermal decomposition of calcite: Mechanisms of formation and textural evolution of CaO nanocrystals. Am. Mineral. 94, 578–593. https://doi.org/10.2138/am.2009.3021

Rodríguez Aguilera, A., 1999. Estudio de las producciones postcalifales del alfar de la casa de los Tiros (Granada). Siglo XI-XII. Arqueol. Mediev. 6, 101–122.

Rodríguez Aguilera, A., 1997. Un centro productor urbano de cerámica postcalifal (SS.XI/XII) en Andalucía oriental. El alfar de la casa de los Tiros, in: Démians d'Archimbaud, G. (Ed.), La Céramique Médiévale En Méditerranée. Actes Du VIe Congrès de l'AIECM2. Aix-En-Provence, 13-18 Novembre 1995. Narration Édition, Aix-en-Provence, pp. 367–370.

Rodziewicz, M., 1983. Egyptian glazed pottery of the eighth to ninth centuries. Bull. la Société d'archéologie copte 25, 73–75.

Rodziewicz, M., 1976. Alexandrie I, La céramique romaine tardive d'Alexandrie. Éditions scientifiques de Pologne, Warsaw.

Rollinson, H., 1993. Using geochimical data: evaluation, presentation, interpretation. Routledge, New York.

Romão, J., Metodiev, D., Dias, R., Ribeiro, A., 2013. Evolução geodiâmica dos sectores meridionais da Zona Centro-Ibérica, in: Dias, R., Araújo, A., Terrinha, P., Kullberg, J.C. (Eds.), Geologia de Portugal, Vol. I. Geologia Pré-Mesozóica de Portugal. Escolar Editora, Lisboa, Portugal, pp. 205–258.

Roqué, J., Molera, J., Cepriá, G., Vendrell-Saz, M., Peréz-Arantegui, J., 2008. Analytical study of the behaviour of some ingredients used in lustre ceramic decorations following different recipes. Phase Transitions 81, 267–282. https://doi.org/10.1080/01411590701514441

Rosselló-Bordoy, G., 2002a. El ajuar de las casas andalusíes, Colección. ed. Sarría, Malaga.

Rosselló-Bordoy, G., 2002b. Cerámica califal, Cerámicas periféricas. Una aproximación a la cerámica andalusí de los siglos X-XI, in: Luis del Pino, J. (Ed.), Al-Andalus Omeya. Fundación PRASA, Córdoba, pp. 67–104.

Rosselló-Bordoy, G., 1991. El nombre de las cosas en al-Andalus, una propuesta de terminología cerámica. Museo de Mallorca, Palma De Mellorca.

Rosselló-Bordoy, G., 1987. Algunas observaciones sobre la decoracíon cerámica en verde y manganeso. Cuad. Medinat al-Zahra 1, 125–137.

Rosselló-Bordoy, G., 1985. Un ataifor norteafricano: un ensayo de interpretación. Sharq al-Andalus 2, 192–205.

Rosselló-Bordoy, G., 1978. Ensayo de sistematización de la cerámica árabe de Mellorca. Instituto de Estudios Balearicos, Palma De Mellorca.

Roux, V., 2019. Ceramics and Society A Technological Approach to Archaeological Assemblages. Springer Nature Switzerland.

Sader, J.A., Ryan, S., 2020. Advances in ICP-MS technology and the application of multi-element geochemistry to exploration. Geochemistry Explor. Environ. Anal. 20, 167–175. https://doi.org/10.1144/geochem2019-049

Salinas, E., 2013. Cerámica vidriada de época emiral en Córdoba. Arqueol. y Territ. Mediev. 20, 67–96. https://doi.org/10.17561/aytm.v20i0.1446

Salinas, E., Juan, J. De, Piñero, J.M., Casal, M.T., Schibille, N., Pradell, T., 2021. From Glass to Glaze in al-Andalus: Local Invention and Technological Transfer. Eur. J. Archaeol. 1–20. https://doi.org/10.1017/eaa.2021.23

Salinas, E., Pradell, T., 2020. Madīnat al-Zahrā' or Madīnat Qurtuba? First evidences of the Caliphate tin glaze production of 'verde y manganeso' ware. Archaeol. Anthropol. Sci. 12, 207. https://doi.org/10.1007/s12520-020-01170-7

Salinas, E., Pradell, T., 2018. The transition from lead transparent to tin-opacified glaze productions in the western Islamic lands: al-Andalus, c. 875–929 CE. J. Archaeol. Sci. 94, 1–11. https://doi.org/10.1016/j.jas.2018.03.010

Salinas, E., Pradell, T., Matin, M., Tite, M.S., 2019a. From tin- to antimony-based yellow opacifiers in the early Islamic Egyptian glazes: Regional influences and ruling dynasties. J. Archaeol. Sci. Reports 26. https://doi.org/10.1016/j.jasrep.2019.101923

Salinas, E., Pradell, T., Molera, J., 2019b. Glaze production at an early Islamic workshop in al-Andalus. Archaeol. Anthropol. Sci. 11, 2201–2213. https://doi.org/10.1007/s12520-018-0666-y

Salinas, E., Pradell, T., Tite, M.S., 2019c. Tracing the tin-opacified yellow glazed ceramics in the

western Islamic world: the findings at Madīnat al-Zahrā'. Archaeol. Anthropol. Sci. 11, 777–787. https://doi.org/10.1007/s12520-017-0562-x

Salinas, E., Zozaya, J., 2015. Pechina: el antecedente de las cerámicas vidriadas islámicas en al-Andalus, in: Gonçalves, M.J., Martínez, S.G. (Eds.), X Congresso Internacional Cerâmica Medieval No Mediterrâneo. Silves-Mértola, 2012. Câmara Municipal De Silves & Campo Arqueológico de Mértola, Silves, pp. 573–576.

Santos, F., 2011. O Médio Tejo dos meados do século IX à primeira metade do século XIII : Militarização e povoamento. University of Lisbon.

Santos, J.R., 2016. Conjunto de cerâmica omíada (séculos X-XI) do Colégio dos Meninos do Coro de Évora. Arqueol. Mediev. 13, 91–100.

Santos, J.R., 2015. Um olhar sobre o quotodiano de Évora no período medieval - islâmico. Séculos VIII a XI. University of Évora.

Santos Júnior, J., 1932. Olarias de muge: Notas Etnográficas. Trab. Antropol. e Etnol. 5, 217–226.

Schermerhorn, L.J.G., 1971. An outline stratigraphy of the Iberian Pyrite Belt. Bol. Geol. y Min. 82, 239–268.

Schibille, N., De Juan Ares, J., Casal García, M.T., Guerrot, C., 2020. Ex novo development of lead glassmaking in early Umayyad Spain. Proc. Natl. Acad. Sci. 202003440. https://doi.org/10.1073/pnas.2003440117

Schiffer, M.B., Skibo, J.M., 1997. The Explanation of Artifact Variability. Am. Antiq. 62, 27–50. https://doi.org/10.2307/282378

Schiffer, M.B., Skibo, J.M., 1987. Theory and Experiment in the Study of Technological Change. Curr. Anthropol. 28, 595–622. https://doi.org/10.1086/203601

Schreiner, M., Melcher, M., Uhlir, K., 2007. Scanning electron microscopy and energy dispersive analysis: Applications in the field of cultural heritage. Anal. Bioanal. Chem. 387, 737–747. https://doi.org/10.1007/s00216-006-0718-5

Shimizu, T., Kuroda, R., 1969. Abundance of scandium in igneous rocks of Japan. Geochim. Cosmochim. Acta 33, 290–292. https://doi.org/10.1016/0016-7037(69)90146-X

Shotyk, W., Weiss, D., Kramers, J.D., Frei, R., Cheburkin, A.K., Gloor, M., Reese, S., 2001. Geochemistry of the peat bog at Etang de la Gruère, Jura Mountains, Switzerland, and its record of atmospheric pb and lithogenic trace metals (Sc, Ti, Y, Zr, and REE) since 12,37014C yr bp. Geochim. Cosmochim. Acta 65, 2337–2360.

https://doi.org/10.1016/S0016-7037(01)00586-5

Sidarus, A.Y., 2007. Shantarîn/Santarém, fronteira ambivalente Islamo-Cristã, in: Nelson Ferrão, H. (Ed.), Santarém Na Idade Média: Actas Do Colóquio 13-14 Março 1998. Camara Municipale de Santarém, Santarém, pp. 319–336.

Sidarus, A.Y., 1996. Novas perspectivas sobre o Gharb Al-Ândalus no tempo de D. Afonso Henriques, in: Actas Do 2º Congresso Histórico de Guimaraes. Vol. 2: A Politíca Portuguesa e as Suas Relações Exteriores. Câmara Municipal de Guimaraes - Universidade do Minho, pp. 247–270.

Sillar, B., 2000. Dung By Preference: the Choice of Fuel As an Example of How Andean Pottery Production Is Embedded Within Wider Technical, Social, and Economic Practices. Archaeometry 42, 43–60. https://doi.org/10.1111/j.1475-4754.2000.tb00865.x

Silva, J., Brito, J. de, Veiga, R., 2009. Incorporation of fine ceramics in mortars. Constr. Build. Mater. 23, 556–564. https://doi.org/10.1016/j.conbuildmat.2007.10.014

Silvestri, A., Nestola, F., Peruzzo, L., 2016. Multi-methodological characterisation of calcium phosphate in late-Antique glass mosaic tesserae. Microchem. J. 124, 811–818. https://doi.org/10.1016/j.microc.2015.10.026

Silvestri, A., Tonietto, S., Molin, G., Guerriero, P., 2014. The palaeo-Christian glass mosaic of St. Prosdocimus (Padova, Italy): Archaeometric characterisation of tesserae with copper- or tin-based opacifiers. J. Archaeol. Sci. 42, 51–67. https://doi.org/10.1016/j.jas.2013.10.018

Sitzia, F., 2020. Monitoraggio del degrado e conservazione del Patrimonio monumentale della Regione Sardegna attraverso la caratterizazzione geochimica, petrofisica e micro-fotogrametricha di superfici lapidee. University of Cagliari.

Stueber, A.M., Goles, G.G., 1967. Abundances of Na, Mn, Cr, Sc and Co in ultramafic rocks. Geochim. Cosmochim. Acta 31, 75–93. https://doi.org/10.1016/0016-7037(67)90099-3

Sutcu, M., 2015. Influence of expanded vermiculite on physical properties and thermal conductivity of clay bricks. Ceram. Int. 41, 2819–2827. https://doi.org/10.1016/j.ceramint.2014.10.102

Tamari, S., 2004. Optimum design of the constant-volume gas pycnometer for determining the volume of solid particles. Meas. Sci. Technol. 15, 549–558. https://doi.org/10.1088/0957-0233/15/3/007

Tapia Garrido, J.A., 1981. Historia de Almeria y su provincia - Vol. 13. Cajal, Almeria.

Thomas, D.S.G., 1987. The roundness of aeolian quartz sand grains. Sediment. Geol. 52, 149–153. https://doi.org/10.1016/0037-0738(87)90020-0

Ting, C., Taxel, I., 2020. Indigeneity and innovation of early Islamic glaze technology: the case of the Coptic Glazed Ware. Archaeol. Anthropol. Sci. 12. https://doi.org/10.1007/s12520-019-01007-y

Tite, M.S., 1991. The Impact of Electron Microscopy on Ceramic Studies. Br. Acad. 77, 111–131.

Tite, M.S., Bimson, M., 1991. A technological study of English porcelains. Archaeometry 33, 3–27. https://doi.org/10.1111/j.1475-4754.1991.tb00682.x

Tite, M.S., Freestone, I.C., Mason, R.B., Molera, J., Vendrell-Saz, M., Wood, N., 1998. Lead Glazes in Antiquity—Methods of Production and Reasons for Use. Archaeometry 40, 241–260. https://doi.org/10.1111/j.1475-4754.1998.tb00836.x

Tite, M.S., Sillar, B., 2000. The challenge of "technological choices" for materials science approaches in archaeology. Archaeometry 42, 2–20.

Tite, M.S., Watson, O., Pradell, T., Matin, M., Molina, G., Domoney, K., Bouquillon, A., 2015. Revisiting the beginnings of tin-opacified Islamic glazes. J. Archaeol. Sci. 57, 80–91. https://doi.org/10.1016/j.jas.2015.02.005

Tite, M.S., Wolf, S., Mason, R.B., 2011. The technological development of stonepaste ceramics from the Islamic Middle East. J. Archaeol. Sci. 38, 570–580. https://doi.org/10.1016/j.jas.2010.10.011

Tõnsuaadu, K., Gross, K.A., Pluduma, L., Veiderma, M., 2012. A review on the thermal stability of calcium apatites. J. Therm. Anal. Calorim. 110, 647–659. https://doi.org/10.1007/s10973-011-1877-y

Trinidade, M.J., Dias, M.I., Coroado, J., Rocha, F., 2009. Mineralogical transformations of calcareous rich clays with firing: A comparative study between calcite and dolomite rich clays from Algarve, Portugal. Appl. Clay Sci. 42, 345–355. https://doi.org/10.1016/j.clay.2008.02.008

V. da Rocha Beirante, M.A., 1980. Santarém Medieval. Universidade Nova de Lisboa, Faculdade de Ciências Sociais e Humanas, Lisboa.

Valdés Fernandés, F., 1985. La Alcazaba de Badajoz (1977-1982) y testar de la puerta del Pilar, Excavacion. ed. Ministerio de Educación, Cultura y Deporte, Madrid.

Van Grieken, R.E., Markowicz, A.A., 2001. Handbook of X-Ray Spectroscopy, Second. ed. Mercel

Dekker, INC, New York - Basel.

Vendrell-Saz, M., Molera, J., Roqué, J., Peréz-Arantegui, J., 2006. Islamic and Hispano-Moresque (múdejar) lead glazes in Spain: a technical approach. Geol. Soc. London, Spec. Publ. 257, 163–173. https://doi.org/10.1144/GSL.SP.2006.257.01.13

Vendrell-Saz, M., Molera, J., Tite, M.S., 2000. Optical Properties of Tin-Opacified Glazes. Archaeometry 42, 325–340. https://doi.org/10.1111/j.1475-4754.2000.tb00885.x

Vera, J.A., 2004. Geología da España, Geología y. ed. Instituto Geológico y Minero de España, Madrid.

Viegas, C., 2003. A terra sigillata da Alcáçova de Santarém. Cerâmica, economia e comércio, Trabalhos. ed. Instituto Português de Arqueologia, Lisbon, Portugal.

Viegas, C., Arruda, A.M., Bargão, P., 2005. As ânforas da Bética costeira na Alcáçova de Santarém. Rev. Port. Arqueol. 8, 279–297.

Vitelli, G., 1981. Islamic Carthage: The archaeological, historical and ceramic evidence, CEDAC doss. ed. Centre d'études et de documentation archéologique de Carthage, Tunis.

Waksman, Y., Bouquillon, A., Cantin, N., Katona, I., 2008. Approche archéométrique des premières «Byzantine Glazed White Ware» et de productions glaçurées romaines et romaines tardives. Rei Cretariæ Rom. Acta 40, 531–536.

Waksman, Y., Bouquillon, A., Cantin, N., Katona, I., 2007. The first Byzantine "Glazed White Wares" in the early medieval technological context, in: Waksman, S.Y. (Ed.), Archaeometric and Archaeological Approaches to Ceramics : Papers Presented at EMAC '05, 8th European Meeting on Ancient Ceramics, Lyon 2005. Archaeopress - British Archaeological Reports, Oxford, pp. 129–135.

Walton, M.S., Tite, M.S., 2010. Production technology of roman lead-glazed pottery and its continuance into late antiquity. Archaeometry 52, 733–759. https://doi.org/10.1111/j.1475-4754.2009.00506.x

Wang, Yinsong, Zou, Y., Henrickson, K., Wang, Yinhai, Tang, J., Park, B.J., 2017. Google Earth elevation data extraction and accuracy assessment for transportation applications. PLoS One 12, 1–17. https://doi.org/10.1371/journal.pone.0175756

Watson, O., 2014. Revisiting Samarra: the Rise of Islamic Glazed Pottery, Beiträge Zur Islamischen Kunst Und Archäologie.

Watson, O., 2006. Ceramics from Islamic Lands, Sabah Collection series. Thames & Hudson,

London.

Watson, O., 1999. VIII. Report on the Glazed Ceramics, in: Miglus, P.A. (Ed.), Die Fruislamische Keramik Von Tall Aswad. Deutsches Archaologisches Institut, Mainz and Rhein, pp. 81–87.

Wickham, C., 2005. Framing the Early Middle Ages. Europe and Mediterranean, 400-800. Oxford University Press, Oxford. https://doi.org/10.1093/acprof:oso/9780199264490.001.0001

Wilschefski, S., Baxter, M., 2019. Inductively Coupled Plasma Mass Spectrometry: Introduction to Analytical Aspects. Clin. Biochem. Rev. 40, 115–133. https://doi.org/10.33176/aacb-19-00024

Wood, N., Tite, M.S., Doherty, C., Gilmore, B., 2007. A technological examination of ninth-tenth century AD Abbasid blue-and-white ware from Iraq, and its comparison with eighth century AD Chinese blue-and-white sancai ware. Archaeometry 49, 665–684. https://doi.org/10.1111/j.1475-4754.2007.00327.x

Zbyszewsky, G., 1953. Geological Map of Portugal, scale 1:50000, with esplicative notes. Map 31-A, Santarém.

Zbyszewsky, G., Da Viega Ferreira, O., 1968. Geological Map of Portugal, scale 1:50000, with esplicative notes. Map 31-C, Coruche.

Zozaya, J., 1993. Importaciones casuales en Al-Andalus: las vías de comercio, in: Salvaterra Cuenca, V. (Ed.), IV Congreso de Arqueología Medieval Española. Sociedades En Transición: Alicante. 4-9 de Octubre 1993. Vol. 1. Diputación Provincial de Alicante, Alicante, pp. 119–138.

Zozaya, J., 1980. Aperçu générale sur la céramique espagnole, in: La Céramique Médiévale En Mediterranée Occidentale (X-Xv Siècles), 11-14 Septembre, Valbonne, France. Édition du centre national de la recherche scientifique, Valbonne, pp. 265–296.

Zozaya, J., Aparicio Yague, A., 2003. Análises de cerámicas Andalusíes, in: Bakirtizis, C. (Ed.), VIIe Congrés International Sur La Céramique Médiévale En Méditerranée, Thessaloniki, 11-16 Octobre 1999. Édition de la Caisse des Recettes Archéologiques, Athenes, pp. 341–350.

Zozaya, J., Retuerce Velasco, M., Aparicio Yague, A., 1995. Cerámica andalusi de reflejo dorado: 1195-1212, in: El Hraîki, R., Erbati, E. (Eds.), Actes Du 5éme Colloque Sur La Céramique Médiévale, Rabat 11-17 Novembre 1991. Dar al Manahil (Ministère des Affaires Culturelles), Rabat, pp. 121–124.

Annexes

Caliph: Comprehensive archaeological and laboratory investigation of Islamic pottery in Portuguese History

Annex 1 - section 5.1

Annexes are inserted in the following order:

- Ceramics sample list with samples laboratory reference (L.R.), samples typology and decoration style, sample's function and samples archaeological reference.
- PLM description of ceramic thin sections with matrix, porosity, and temper characteristics.
- XRPD data for ceramics, raw material and XRD oriented aggregate data of raw materials.
- XRF and ICP-MS data for ceramics and raw materials.

Table 1, annex 1. Ceramics sample list with samples laboratory reference (L.R.), samples typology and sample decoration style, sample's function and samples archaeological reference.

L.R.	Typology - Decoration style	Function	Archaeological Reference (Arruda and Viegas 1999)
1	Jug - White painted	Kitchen	Alc. Sant., 2080, corte 2, I9, fossa 1
2	Glass - White painted	Kitchen	Alc. Sant., 2079, corte 2, I9, fossa 1
3	Bottle - Monochromatic glaze	Container	Alc. Sant., 2116, corte 2, I9, fossa 1
4	Bottle - Undecorated ceramic	Container	Alc. Sant.,2082, corte 2, I9, fossa 1
5	Jar - Monochromatic glaze	Container	Alc. Sant., 2087, corte 2, I9, fossa 1
6	Jar - Undecorated ceramic	Container	Alc. Sant., 2115, corte 2, I9, fossa 3
7	Bowl - Monochromatic glaze	Kitchen	Alc. Sant., 2062, corte 2, I9, fossa 1
8	Bowl - Monochromatic glaze	Kitchen	Alc. Sant., 2063, corte 2, I9, fossa 1
9	Bowl, *Corda Seca - Polychromatic glaze*	Kitchen	Alc. Sant., 2085, corte 2, I9, fossa 1
11	Bowl, *Corda Seca - Polychromatic glaze*	Kitchen	Alc. Sant., 2086, corte 2, I9, fossa 1
11	Bowl - Undecorated ceramic	Kitchen	Alc. Sant., 2055, corte 2, I9, fossa 1
12	Bowl - Undecorated ceramic	Kitchen	Alc. Sant., 2016, corte 2, I9, fossa 1
13	Cup - White painted	Kitchen	Alc. Sant., 1998, corte 2, I9, fossa 1
14	Big bowl - Monochromatic glaze	Kitchen	Alc. Sant., 2068, corte 2, I9, fossa 1
15	Big bowl - Monochromatic glaze	Kitchen	Alc. Sant., 2070, corte 2, I9, fossa 1
16	Big bowl - Monochromatic glaze	Kitchen	Alc. Sant., 2066, corte 2, I9, fossa 1
17	Big bowl - Undecorated ceramic	Kitchen	Alc. Sant., 2012, corte 2, I9, fossa 1
18	Big bowl - Undecorated ceramic	Kitchen	Alc. Sant., 2017, corte 2, I9, fossa 1
19	Cooking pan - Monochromatic glaze	Fire	Alc. Sant., 2061, corte 2, I9, fossa 1
20	Cooking pan - Monochromatic glaze	Fire	Alc. Sant., 2067, corte 2, I9, fossa 1
21	Cooking pan - Undecorated ceramic	Fire	Alc. Sant., 1994, corte 2, I9, fossa 1
22	Cooking Pot - White painted	Fire	Alc. Sant., 1911, corte 2, K9, fossa 3
23	Cooking Pot - White painted	Fire	Alc. Sant., 1926, corte 2, K9, fossa 2
24	Cooking Pot - White painted	Fire	Alc. Sant., 2025, corte 2, I9, fossa 1
25	Cooking Pot - Undecorated ceramic	Fire	Alc. Sant., 2020, corte 2, I11, fossa 4
26	Cooking Pot - Undecorated ceramic	Fire	Alc. Sant., 2004, corte 2, I11, fossa 4
27	Cooking Pot - Undecorated ceramic	Fire	Alc. Sant., 2041, corte 2, I11, fossa 4
28	Big Jar - Undecorated ceramic	Container	Alc. Sant., 2081, corte 2, I9, fossa 1
29	Big Jar - White painted	Container	Alc. Sant., 2026, corte 2, I9, fossa 1
30	Big earth. Pot - Incised decoration	Container	Alc. Sant., 2039, corte 2, I11 banq. sul, fossa 4
31	Big earth. Pot - Incised decoration	Container	Alc. Sant., 2022, corte 2, I11, banq. sul, fossa 4
32	Big earth. Pot - Undecorated ceramic	Container	Alc. Sant., 2046, corte 2, I9, fossa 1
33	Earth. Pot - Undecorated ceramic	Container	Alc. Sant.,1953, corte 2, J8, fossa 1
34	Earth. Pot - Undecorated ceramic	Container	Alc. Sant., 2036, corte 2, I9, fossa 3
35	Basine - Undecorated ceramic	Kitchen	Alc. Sant., 2050, corte 2, I9, fossa 1
36	Lid - Undecorated ceramic	Fire	Alc. Sant., 2056, corte 2, I9, fossa 1
37	Small lantern - Monochromatic glaze	Spec. Function	Alc. Sant., 2094, corte 2, K9, fossa 1
38	Clay charcoal braizer - Undecorated ceramic	Fire	Alc. Sant., 2091, corte 2, I9, fossa 1
39	Pot support - Undecorated ceramic	Spec. Function	Alc. Sant., 2093, corte 2, I9, fossa 1
40	Glass - White painted	Kitchen	Alc. Sant., 2078, corte 2, I9, fossa 1
41	Glass - White painted	Kitchen	Alc. Sant., 1937, corte 2, K9, fossa 3
42	Alcatruz - Undecorated ceramic	Container	Alc. Sant., 2097, corte 2, I9, fossa 1

Table 2, annex 1. PLM description of ceramic thin sections; ceramic matrix, porosity, part 1

L.R.	Fabric	Subgroup	Matrix						Porosity
			Colour	Homogeneity/heterogeneity	Fe / Ca rich matrix	Matrix Activity	Clay pellets	Oxides	Description
1	1	A	Red	H.Hom.	Fe	Moderate	X	X	Mega vughs, meso vesicles and chanels
2	1	A	Red	H.Hom.	Fe	Moderate	X	X	Macro vughs, meso vesicles and channels
3	2	A	Gray-Brown	M.Het.	Fe-S.Ca	Slightly active		X	Meso vughs, meso-micro vesicles
4	1	A	Red	H.Hom.	Fe	Moderate	X	X	Macro-meso vughs, meso-micro vesicles
5	3	A	Gray	H.Hom.	H.Ca	Moderate		X	Macro-meso planar voids, meso vesicles
6	1	A	Red	H.Hom.	Fe-S.Ca	Moderate	X	X	Macro vughs and planar voids, meso vesicles
7	2	A	Gray-Brown	H.Hom.	Fe-S.Ca	Moderate		X	Macro vughs, meso vesicles
8	2	A	Gray-Brown	H.Hom.	Fe-S.Ca	Not active		X	Meso channels and vesicles
9	3	A	Gray-Brown	H.Hom.	H.Ca	Slightly active		X	Meso-micro vesicles
11	3	B	Gray-Brown	H.Hom.	H.Ca	Slightly active		X	Meso vesicles
11	3	B	Gray-Brown	H.Hom.	H.Ca	Slightly active		X	Meso-micro vesicles
12	1	A	Red	H.Hom.	Fe	Moderate		X	Meso-macro channels, meso vesicles
13	1	C	Red	H.Hom.	Fe	Moderate	X	X	Meso-macro channels, vesicles and vughs
14	2	A	Gray-Brown	S.Het.	Fe	Moderate		X	Macro-meso vesicles and channels
15	2	A	Gray-Brown	S.Het.	Fe	Moderate		X	Macro-meso vughs, meso vesicles and channels
16	2	A	Gray-Brown	S.Het.	Fe-S.Ca	Moderate		X	Meso vesicles and vughs
17	1	B	Red	M.Het.	Fe	Moderate		X	Mega vughs, macro-meso vesicles and channels
18	1	A	Red	H.Hom.	Fe	Slightly active	X	X	Macro-meso channels and vesicles
19	1	B	Red	H.Hom.	Fe	Slightly active		X	Meso channels and vesicles
20	1	B	Red	H.Hom.	Fe	Moderate	X	X	Meso channels and vesicles
21	1	A	Red	S.Het.	Fe	Slightly active	X	X	Meso-macro vughs and channels, meso vesicles
22	1	A	Red	H.Hom.	Fe	Moderate		X	Meso channels and vesicles

Table 3, annex 1. PLM description of ceramic thin sections; ceramic matrix, porosity, part 2.

L.R.	Fabric	Subgroup	Matrix						Porosity
			Colour	Homogeneity/heterogeneity	Fe / Ca rich matrix	Matrix Activity	Clay pellets	Oxides	Description
23	**1**	**C**	Brown	S.Het.	Fe	Slightly active	X	X	Meso channels and vesicles
24	**1**	**B**	Brown	H.Hom.	Fe	Slightly active	X	X	Meso channels, vesicles and vughs
25	**1**	**A**	Red	H.Hom.	Fe	Slightly active	X	X	Meso channels and vesicles
26	**1**	**A**	Red	S.Het.	Fe	Not active	X	X	Macro-meso channels, meso vesicles
27	**1**	**B**	Dark brown	M.Hom.	Fe	Slightly active		X	Macro vughs, meso vesicles
28	**1**	**B**	Red	H.Hom.	Fe	Slightly active	X	X	Macro-meso vughs and vesicles
29	**1**	**A**	Red	S.Hom.	Fe	Moderate	X	X	Macro-meso vughs, channels and vesicles
30	**1**	**B**	Red-brown	S.Het.	Fe	Moderate		X	Meso vesicles
31	**1**	**A**	Red	M.Hom.	Fe	Moderate	X	X	Macro-meso channels, meso vesicles
32	**1**	**A**	Red	H.Hom.	Fe	Moderate		X	Macro-meso vughs, meso channels and vesicles
33	**1**	**A**	Red-Gray	M.Het.	Fe-S.Ca	Moderate		X	Macro-meso channels
34	**1**	**A**	Red	M.Hom.	Fe	Moderate	X	X	Meso channels and vesicles
35	**1**	**A**	Red	S.Hom.	Fe	Moderate	X	X	Macro meso vughs, channels, vesicles
36	**3**	**B**	Gray-Brown	M.Hom.	H.Ca	Slightly active		X	Meso-micro vesicles
37	**2**	**A**	Gray-Brown	S.Het.	Fe-S.Ca	Moderate		X	Meso vesicles
38	**1**	**A**	Red	M.Hom.	Fe	Slightly active	X	X	Mega planar voids, meso vesicles
39	**1**	**B**	Red	H.Hom.	Fe	Slightly active		X	Macro-meso channels and vesicles
40	**1**	**C**	Red	H.Hom.	Fe	Slightly active	X	X	Macro-meso channels and vesicles
41	**1**	**C**	Red	H.Hom.	Fe	Slightly active	X	X	Macro-meso channels, vughs and vesicles
42	**1**	**C**	Red	H.Hom.	Fe	Slightly active	X	X	Meso channels and vesicles

Table 4, annex 1. PLM description of ceramic thin sections; temper, part 1

L.R.	Fabric	Subgroup	Temper									
			Shape	Roundness	Packing	Max size mm	Alignment	Sorting	Grain size distribution	Temper %	Minerals	Rock fragments
1	1	A	Eq&El	SR-SA	Open spaced	1.2	Weak	Moderate	Unimodal	14.25	Quartz, K-Fldspar, Plagioclase, Muscovite	Quartzite
2	1	A	Eq&El	SR-SA	Open spaced	1	Weak	Poor	Unimodal	11.04	Quartz, K-Fldspar, Plagioclase, Muscovite	Quartzite, Limestone
3	2	A	Eq&El	R-SR	Open spaced	0.65	Weak	Moderate	Unimodal	6.01	Quartz, K-Fldspar, Plagioclase, Muscovite, Post depositonal calcite	
4	1	A	Eq&El	SR-SA	Open spaced	1.1	Moderate	Poor	Unimodal	9.3	Quartz, K-Fldspar, Plagioclase, Muscovite	Quartzite, Sandstone
5	3	A	Eq&El	R-SR	Open spaced	0.45	Moderate	Moderate	Unimodal	2.93	Quartz, K-Fldspar, Muscovite, Secondary calcite, Foraminifera microfosils	
6	1	A	Eq&El	SR-SA	Open spaced	1.45	Moderate	Poor	Unimodal	13.92	Quartz, K-Fldspar, Plagioclase, Muscovite, Post depositonal calcite, Tourmaline	Quartzite
7	2	A	Eq&El	SR-SA	Open spaced	0.5	Weak	Moderate	Unimodal	12	Quartz, K-Fldspar, Plagioclase, Muscovite	
8	2	A	Eq&El	SR-SA	Open spaced	0.5	Moderate	Moderate	Unimodal	9.15	Quartz, Muscovite	
9	3	A	Eq&El	R	Open spaced	0.15	Strong	Well	Unimodal	1.56	Quartz, K-Fldspar, Plagioclase, Muscovite, Grog,	Schist
11	3	B	Eq&El	R-SR	Double spaced	0.38	Strong	Well	Unimodal	6.67	Quartz, K-Fldspar, Plagioclase, Muscovite, Secondary calcite	Quartzite
11	3	B	Eq&El	SR-SA	Open spaced	0.95	Strong	Well	Unimodal	2.65	Quartz, K-Fldspar, Plagioclase, Muscovite, Secondary calcite, Foraminifera microfossils, Shell	Quartzite, Limestone
12	1	A	Eq&El	SR-A	Open spaced	1.55	Moderate	Poor	Unimodal	9.32	Quartz, K-Fldspar, Muscovite, Secondary calcite	Quartzite, Limestone
13	1	C	Eq&El	SR-SA	Double spaced	0.93	Moderate	Moderate	Unimodal	12.14	Quartz, K-Fldspar, Plagioclase, Muscovite, Tourmaline	Quartzite, Granite
14	2	A	Eq&El	SR-A	Double spaced	0.7	Moderate	Moderate	Unimodal	11.01	Quartz, K-Fldspar, Plagioclase, Muscovite, Tourmaline	

Table 5, annex 1. PLM description of ceramic thin sections; temper, part 2

L.R.	Fabric	Subgroup	Temper									
			Shape	Roundness	Packing	Max size mm	Alignment	Sorting	Grain size distribution	Temper %	Minerals	Rock fragments
15	2	A	Eq&El	R-SR	Open spaced	0.53	Moderate	Moderate	Unimodal	5.49	Quartz, K-Fldspar, Plagioclase, Muscovite	
16	2	A	Eq&El	SR-SA	Open spaced	1	Strong	Moderate	Unimodal	7.5	Quartz, K-Fldspar, Plagioclase, Muscovite	
17	1	B	Eq&El	SR-A	Single spaced	2	Weak	Poor	Unimodal	14.2	Quartz, K-Fldspar, Plagioclase, Muscovite	Quartzite, Limestone
18	1	A	Eq&El	SR-SA	Open spaced	1.03	Moderate	Moderate	Unimodal	5.39	Quartz, K-Fldspar, Muscovite	Quartzite
19	1	B	Eq&El	SR-SA	Close spaced	0.67	Strong	Well	Unimodal	20.81	Quartz, K-Fldspar, Plagioclase, Muscovite, Tourmaline	Quartzite, Sandstone
20	1	B	Eq&El	SR-SA	Close spaced	0.52	Strong	Well	Unimodal	19.49	Quartz, K-Fldspar, Plagioclase, Muscovite, Tourmaline	Quartzite
21	1	A	Eq&El	SR-SA	Open spaced	1.52	Moderate	Moderate	Unimodal	6.6	Quartz, K-Fldspar, Muscovite	Quartzite
22	1	A	Eq&El	R-SA	Open spaced	0.72	Moderate	Poor	Unimodal	5.6	Quartz, K-Fldspar, Muscovite	Quartzite
23	1	C	Eq&El	SR-A	Double spaced	1	Moderate	Poor	Unimodal	15.82	Quartz, K-Fldspar, Muscovite	Quartzite, Granite, Sandstone
24	1	B	Eq&El	SR-A	Single spaced	1.45	Strong	Moderate	Unimodal	14.01	Quartz, K-Fldspar, Plagioclase, Muscovite, Tourmaline, Grog	Quartzite
25	1	A	Eq&El	SR-A	Double spaced	0.8	Moderate	Poor	Unimodal	7.13	Quartz, K-Fldspar, Plagioclase, Muscovite	Granite
26	1	A	Eq&El	SR-A	Open spaced	0.87	Weak	Poor	Unimodal	4.2	Quartz, K-Fldspar, Plagioclase, Muscovite	Quartzite
27	1	B	Eq&El	SR-A	Close spaced	1.38	Moderate	Moderate	Unimodal	14.35	Quartz, K-Fldspar, Plagioclase, Muscovite	Quartzite
28	1	B	Eq&El	SR-A	Single spaced	0.7	Weak	Poor	Unimodal	15.4	Quartz, K-Fldspar, Plagioclase, Muscovite, Tourmaline	Limestone

Table 6, annex 1. PLM description of ceramic thin sections; temper, part 3

L.R.	Fabric	Subgroup	Temper									
			Shape	Roundness	Packing	Max size mm	Alignment	Sorting	Grain size distribution	Temper %	Minerals	Rock fragments
29	1	A	Eq&El	SR-A	Double spaced	1	Moderate	Poor	Unimodal	11.43	Quartz, K-Fldspar, Muscovite	Quartzite, Granite
30	1	B	Eq&El	SR-A	Close spaced	1.65		Poor	Unimodal	17.8	Quartz, K-Fldspar, Plagioclase, Muscovite, Tourmaline	Quartzite
31	1	A	Eq&El	SR-A	Open spaced	1.16	Weak	Poor	Unimodal	5.64	Quartz, K-Fldspar, Plagioclase, Muscovite	Quartzite
32	1	A	Eq&El	SR-A	Single spaced	1.6	Weak	Very poor	Unimodal	16.77	Quartz, K-Fldspar, Muscovite, Tourmaline	Quartzite, Limestone
33	1	A	Eq&El	SR-A	Single spaced	1.12	Weak	Very poor	Unimodal	18.4	Quartz, K-Fldspar, Muscovite	Quartzite, Limestone
34	1	A	Eq&El	SR-A	Double spaced	1.33	Moderate	Poor	Unimodal	14.24	Quartz, K-Fldspar, Plagioclase, Muscovite, Tourmaline	Quartzite
35	1	A	Eq&El	SR-A	Double spaced	1.58	Weak	Poor	Unimodal	11.57	Quartz, K-Fldspar, Muscovite	Quartzite
36	3	B	Eq&El	SR-A	Open spaced	0.64	Moderate	Poor	Unimodal	8.35	Quartz, K-Fldspar, Plagioclase, Muscovite, Biotite, Green-Brown Amphibole, Secondary calcite, Formanifera microfossils	Quartzite, Limestone
37	2	A	Eq&El	SR-A	Open spaced	0.67	Weak	Moderate	Unimodal	11.87	Quartz, K-Fldspar, Plagioclase, Muscovite, Post depositonal calcite	Quartzite, Granite
38	1	A	Eq&El	SR-A	Single spaced	2.2	Weak	Very poor	Unimodal	13.2	Quartz, K-Fldspar, Plagioclase, Muscovite	Quartzite
39	1	B	Eq&El	SR-A	Single spaced	1.52	Weak	Very poor	Unimodal	17.76	Quartz, K-Fldspar, Plagioclase, Muscovite	Quartzite, Limestone
40	1	C	Eq&El	SR-A	Double spaced	1.7	Moderate	Moderate	Unimodal	13.24	Quartz, K-Fldspar, Plagioclase, Muscovite, Post depositional calcite, Tourmaline	Quartzite, Schist
41	1	C	Eq&El	SR-SA	Open spaced	0.85	Weak	Poor	Unimodal	8.08	Quartz, K-Fldspar, Plagioclase, Muscovite, Grog	Quartzite
42	1	C	Eq&El	SR-SA	Open spaced	0.57	Moderate	Poor	Unimodal	12.33	Quartz, K-Fldspar, Plagioclase, Muscovite	Quartzite

Table 7, annex 1. XRPD results of Islamic ceramics from the Santarém Alcaçova. Samples are devided into two different group, A and B (i.e. silica rich and calcium rich, respectively).

L.R.- XRPD Group	Quartz	Illite/Muscovite	K-Feldspars	Plagioclase	Anatase	Calcite	Analcime	Tourmaline	Hematite	magnetite	Mullite	Pryroxene	Akermanite	Ghelenite	Phlogopite	Vermiculite	Smectite
1 - Group A	69	11	15	4					1								TR
2 - Group A	69	14	8	6		2			1								
3 - Group A	65	11	17	6		2											
4 - Group A	76		14	5	1				1		4						
5 - Group B	23		14	20		6	6		2			20	8				
6 - Group A	52	17	24	6					1								
7 - Group A	74	11	13	4													
8 - Group A	78	7	13	2													
9 - Group B	33			30					2	TR		24		6	4		
11 - Group B	44		15	9		4			1			15		12			
11 - Group B	35	12	19	5		15		3				8		4			
12 - Group A	76	11	11	2		2			1								
13 - Group A	59	17	16	7					1								
14 - Group A	70	11	16	5													
15 - Group A	75	11	8	6		1											
16 - Group A	69	11	16	4		1											
17 - Group A	61	17	20	2													
18 - Group A	60	22	13	3		2			1								
19 - Group A	58	11	24	6					1								
20 - Group A	44	12	27	15					1								
21 - Group A	57	20	16	7													
22 - Group A	60	17	22						1								
23 - Group A	76	2	16	2	1				1		3						
24 - Group A	71	13	11	6													
25 - Group A	59	14	19	8					1								
26 - Group A	61	17	16	6													
27 - Group A	72	1	19	3	1	1			1		2						
28 - Group A	57	13	19	11					1								
29 - Group A	66	8	26	TR					1								
30 - Group A	56	15	20	8					1								
31 - Group A	48	20	28	5													
32 - Group A	50	35	12	2		Tr										Tr	
33 - Group A	51	22	18	9													
34 - Group A	54	18	23	4					1								
35 - Group A	70	14	13			1			1								
36 - Group B	31	13	24	7		20			1			4					
37 - Group A	73	11	11	2		4											
38 - Group A	66	9	20	5					TR								
39 - Group A	65	11	16	7					1								
40 - Group A	66	11	17	5	1				1								
41 - Group A	62	15	16	6					1								
42 - Group A	55	19	17	7	1				1								

Table 8, annex 1. XRPD and XRD oriented aggregate results of raw materials, part 1.

Laboratory reference	Sediment tratment	Quartz	Illite/Muscovite	K-Feldspars	Plagioclase	Anatase	Calcite	Halite	Vermiculite	Kaolinite	Smectite	Chlorite	Chlorite/smectite	∑Tectosilicates	∑Phyllosilicates
Ca1	**Untreated raw material, URM**	36	47	7	2	1				8	Tr			45	55
	<500	45	41	7	2	1				5	Tr			54	46
	<250	30	46	13	2	1				8	Tr			45	54
	<125	35	46	8	2	1				8	Tr			45	54
	<63	35	47	8	2	1				7	Tr			45	54
	Oriented aggregate, OM		XXXX							XX	Tr - Nontronite				
Ca2	**Untreated raw material, URM**	40	42	7	5		Tr	Tr		2	Tr	4		52	48
	<500	41	37	13	2		1	Tr		2	Tr	3		56	42
	<250	29	37	15	11		Tr	Tr		3	Tr	6		55	46
	<125	28	41	8	9		1	Tr		4	Tr	9		45	54
	<63	32	42	8	4		1	Tr		4	Tr	9		44	55
	Oriented aggregate, OM		XXX							X	Nontronite- X	XX			
Ca3	**Untreated raw material, URM**	47	32	14	2		2			1				63	33
	<500	39	36	13	9		1			2				61	38
	<250	43	35	15	4		1			2				62	37
	<125	43	45	7	2		1		Tr	2				52	47
	<63	27	53	13	3		1		Tr	2				43	55
	Oriented aggregate, OM		XXXX						X	X					
Ca4	**Untreated raw material, URM**	47	34	14	1			Tr	2	1	X			62	37
	<500	46	34	14	1			Tr	3	1	X			61	38
	<250	46	36	13	1			Tr	3	1	X			60	40
	<125	46	36	11	1			Tr	4	2	X			58	42
	<63	46	37	7	1			Tr	6	3	X			54	46
	Oriented aggregate, OM		XXX						XX	X	Saponite- XX				
Ca5	**Untreated raw material, URM**	46	37	8	4				1	4				58	42
	<500	48	38	7	3				1	3				58	42
	<250	45	38	8	5				1	4				58	43
	<125	45	38	7	4				1	4				56	43
	<63	47	38	7	4				1	3				58	42
	Oriented aggregate, OM		XXX						XX	XX	Saponite - XX				

Table 9, annex 1. XRPD and XRD oriented aggregate results of raw materials, part

Laboratory reference	Sediment tratment	Quartz	Illite/Muscovite	K-Feldspars	Plagioclase	Anatase	Calcite	Halite	Vermiculite	Kaolinite	Smectite	Chlorite	Chlorite/smectite	∑Tectosilicates	∑Phyllosilicates
Ca6	Untreated raw material, URM	30	36	9	13		5		5	2	Tr			52	43
	<500	36	40	11	5		2		5	2	Tr			51	47
	<250	36	35	13	9		1		4	1	Tr			58	40
	<125	35	37	8	7		2		7	2	Tr			50	46
	<63	31	37	8	7		4		9	3	Tr			46	49
	Oriented aggregate, OM		XXXX						X	X	Nontronite- X				
Ca7	Untreated raw material, URM	46	37	11	2	1				3	1		Tr	58	41
	<500	50	38	7	2	1				2	Tr		Tr	59	40
	<250	34	46	12	2	1				4	1		Tr	48	51
	<125	42	41	9	3	1				3	1		Tr	54	45
	<63	39	44	9	2	1				4	1		Tr	50	49
	Oriented aggregate, OM		XXX							XX	Saponite- XX		XX		
Ca8	Untreated raw material, URM	42	34	17	5		1		Tr	1	Tr			64	35
	<500	42	31	17	8		Tr		Tr	1	Tr			67	32
	<250	42	36	15	6				Tr	1	Tr			63	37
	<125	38	42	11	7	1	Tr		Tr	2	Tr			55	44
	<63	30	42	11	4	Tr	1		4	5	4			44	55
	Oriented aggregate, OM		XXX						XX	X	Montmo.te - XX				
Ca9	Untreated raw material, URM	46	30	14	4				5	1	Tr			64	36
	<500	49	36	11	1				2	1	Tr			60	39
	<250	49	37	7	2				3	1	Tr			58	41
	<125	48	37	7	3				4	1	Tr			58	42
	<63	43	37	7	4				6	3	Tr			54	46
	Oriented aggregate, OM		XXX						XX	XX	Montmo.te - XX				

Table 10, annex 1. Ceramic samples chemical composition obtained by XRF, major oxides, part 1

Laboratory reference – Chemical group	Major oxides and L.O.I												
		Na_2O	MgO	Al_2O_3	SiO_2	P_2O_5	S	K_2O	CaO	TiO_2	Fe_2O_3	MnO	LOI	Sum
1 - Group 1	**wt%**	0.26	1.03	19.40	66.20	0.099	0.025	3.05	0.61	0.86	5.95	0.040	2.59	110.13
	Err. ±	*0.05*	*0.02*	*0.04*	*0.04*	*0.004*	*0.001*	*0.05*	*0.02*	*0.01*	*0.01*	*0.003*		
2 - Group 1	**wt%**	0.31	1.03	19.70	64.20	0.123	0.016	2.98	1.08	0.87	6.27	0.038	2.23	98.85
	Err. ±	*0.04*	*0.02*	*0.04*	*0.04*	*0.004*	*0.001*	*0.05*	*0.02*	*0.01*	*0.01*	*0.003*		
3 - Group 2	**wt%**	0.37	0.59	17.70	71.50	0.116	0.153	2.76	1.11	1.18	1.62	0.011	2.9	99.99
	Err. ±	*0.05*	*0.03*	*0.04*	*0.04*	*0.004*	*0.001*	*0.06*	*0.03*	*0.02*	*0.01*	*0.003*		
4 - Group 1	**wt%**	0.30	1.08	19.60	65.50	0.099	0.012	3.03	0.71	0.90	6.18	0.052	1.06	98.52
	Err. ±	*0.04*	*0.02*	*0.04*	*0.04*	*0.004*	*0.001*	*0.05*	*0.02*	*0.01*	*0.01*	*0.003*		
5 - Group 3	**wt%**	1.38	2.94	14.11	45.70	0.396	0.255	1.25	18.11	0.60	4.92	0.000	9.43	99.07
	Err. ±	*0.05*	*0.03*	*0.03*	*0.03*	*0.005*	*0.002*	*0.04*	*0.05*	*0.01*	*0.01*	*0.003*		
6 - Group 1	**wt%**	0.28	0.81	17.80	66.80	0.146	0.016	3.37	0.63	0.71	5.47	0.011	3.22	99.26
	Err. ±	*0.04*	*0.02*	*0.04*	*0.04*	*0.004*	*0.001*	*0.05*	*0.02*	*0.01*	*0.01*	*0.003*		
7 - Group 2	**wt%**	0.41	0.47	15.40	75.20	0.118	0.022	2.49	0.24	1.09	1.39	0.011	1.43	98.27
	Err. ±	*0.04*	*0.02*	*0.03*	*0.04*	*0.003*	*0.001*	*0.05*	*0.02*	*0.01*	*0.00*	*0.003*		
8 - Group 2	**wt%**	0.48	0.56	15.90	74.30	0.112	0.035	2.64	0.39	1.16	1.63	0.016	0.84	98.06
	Err. ±	*0.04*	*0.02*	*0.03*	*0.04*	*0.003*	*0.001*	*0.05*	*0.02*	*0.01*	*0.00*	*0.003*		
9 - Group 3	**wt%**	1.36	3.07	18.90	47.40	0.377	0.045	2.91	14.20	0.61	6.03	0.000	2.12	97.02
	Err. ±	*0.05*	*0.03*	*0.04*	*0.03*	*0.003*	*0.001*	*0.05*	*0.05*	*0.01*	*0.01*	*0.002*		
11 - Group 3	**wt%**	0.53	2.16	11.90	52.70	0.416	0.120	2.16	15.40	0.55	4.40	0.000	7.31	97.64
	Err. ±	*0.05*	*0.03*	*0.03*	*0.03*	*0.005*	*0.001*	*0.04*	*0.05*	*0.01*	*0.01*	*0.003*		
11 - Group 3	**wt%**	0.94	1.86	11.70	41.30	0.627	0.123	3.40	19.60	0.81	3.80	0.038	13.65	97.85
	Err. ±	*0.05*	*0.03*	*0.03*	*0.03*	*0.005*	*0.001*	*0.05*	*0.05*	*0.01*	*0.01*	*0.003*		
12 - Group 1	**wt%**	0.28	1.02	19.60	65.11	0.114	0.012	3.09	0.57	0.87	6.00	0.028	1.22	97.89
	Err. ±	*0.04*	*0.02*	*0.04*	*0.04*	*0.004*	*0.001*	*0.05*	*0.02*	*0.01*	*0.01*	*0.003*		
13 - Group 1	**wt%**	0.30	1.03	18.80	65.40	0.118	0.014	3.11	0.63	0.79	5.92	0.052	2.63	98.77
	Err. ±	*0.04*	*0.02*	*0.04*	*0.04*	*0.004*	*0.001*	*0.05*	*0.02*	*0.01*	*0.01*	*0.003*		
14 - Group 2	**wt%**	0.35	0.56	18.00	72.11	0.098	0.189	2.81	0.22	1.20	1.52	0.011	1.47	98.53
	Err. ±	*0.04*	*0.02*	*0.04*	*0.04*	*0.004*	*0.001*	*0.05*	*0.02*	*0.01*	*0.00*	*0.003*		
15 - Group 2	**wt%**	0.31	0.54	17.40	72.70	0.113	0.053	2.74	0.24	1.21	1.59	0.008	1.36	98.25
	Err. ±	*0.04*	*0.02*	*0.03*	*0.04*	*0.003*	*0.001*	*0.05*	*0.02*	*0.01*	*0.00*	*0.003*		

Table 11, annex 1. Ceramic samples chemical composition obtained by XRF, major oxides, part 2.

Laboratory reference – Chemical group		Major oxides and L.O.I												
		Na_2O	MgO	Al_2O_3	SiO_2	P_2O_5	S	K_2O	CaO	TiO_2	Fe_2O_3	MnO	LOI	Sum
16 - Group 2	**wt%**	0.48	0.51	15.00	75.60	0.115	0.047	2.57	0.32	1.08	1.50	0.014	1.31	98.53
	Err. ±	*0.04*	*0.02*	*0.03*	*0.04*	*0.003*	*0.001*	*0.05*	*0.02*	*0.01*	*0.00*	*0.003*		
17 - Group 1	**wt%**	0.37	0.75	15.80	67.20	0.240	0.017	3.35	0.76	0.68	4.69	0.013	4.47	98.34
	Err. ±	*0.04*	*0.02*	*0.03*	*0.04*	*0.004*	*0.001*	*0.05*	*0.02*	*0.01*	*0.01*	*0.003*		
18 - Group 1	**wt%**	0.34	0.89	18.20	65.11	0.181	0.014	3.02	0.72	0.87	5.62	0.059	4.21	99.23
	Err. ±	*0.04*	*0.02*	*0.04*	*0.04*	*0.004*	*0.001*	*0.05*	*0.02*	*0.01*	*0.01*	*0.003*		
19 - Group 1	**wt%**	0.77	0.93	20.30	65.70	0.127	0.036	3.25	0.65	0.70	3.98	0.013	2.39	98.84
	Err. ±	*0.05*	*0.02*	*0.04*	*0.04*	*0.004*	*0.001*	*0.05*	*0.02*	*0.01*	*0.01*	*0.003*		
20 - Group 1	**wt%**	0.75	0.90	18.90	65.20	0.122	0.048	3.15	0.57	0.81	4.69	0.005	3.73	98.88
	Err. ±	*0.05*	*0.02*	*0.04*	*0.04*	*0.004*	*0.001*	*0.05*	*0.02*	*0.01*	*0.01*	*0.003*		
21 - Group 1	**wt%**	0.33	0.91	17.60	66.00	0.120	0.014	3.05	0.81	0.80	5.46	0.064	2.76	97.92
	Err. ±	*0.04*	*0.02*	*0.04*	*0.04*	*0.004*	*0.001*	*0.05*	*0.02*	*0.01*	*0.01*	*0.003*		
22 - Group 1	**wt%**	0.29	1.18	20.50	64.20	0.111	0.014	3.55	0.60	0.82	6.58	0.008	3.51	111.35
	Err. ±	*0.05*	*0.03*	*0.04*	*0.04*	*0.004*	*0.001*	*0.06*	*0.02*	*0.01*	*0.01*	*0.003*		
23 - Group 1	**wt%**	0.23	0.99	19.40	66.70	0.117	0.014	3.08	0.66	0.81	6.02	0.070	1.55	99.64
	Err. ±	*0.05*	*0.02*	*0.04*	*0.04*	*0.004*	*0.001*	*0.05*	*0.02*	*0.01*	*0.01*	*0.003*		
24 - Group 1	**wt%**	0.26	0.90	17.40	64.11	0.124	0.015	3.12	0.90	0.79	5.52	0.041	6.11	99.28
	Err. ±	*0.04*	*0.02*	*0.04*	*0.04*	*0.004*	*0.001*	*0.05*	*0.02*	*0.01*	*0.01*	*0.003*		
25 - Group 1	**wt%**	0.38	1.12	19.30	64.90	0.116	0.018	3.15	0.89	0.79	6.23	0.014	2.15	99.04
	Err. ±	*0.05*	*0.02*	*0.04*	*0.04*	*0.004*	*0.001*	*0.05*	*0.02*	*0.01*	*0.01*	*0.003*		
26 - Group 1	**wt%**	0.34	0.94	18.90	62.30	0.174	0.014	3.08	0.91	0.83	5.86	0.067	5.5	98.90
	Err. ±	*0.04*	*0.02*	*0.04*	*0.04*	*0.004*	*0.001*	*0.05*	*0.02*	*0.01*	*0.01*	*0.003*		
27 - Group 1	**wt%**	0.47	1.13	17.50	62.30	0.205	0.081	2.59	2.75	0.70	6.50	0.003	4.36	98.59
	Err. ±	*0.05*	*0.02*	*0.04*	*0.04*	*0.004*	*0.001*	*0.05*	*0.03*	*0.01*	*0.01*	*0.003*		
28 - Group 1	**wt%**	0.65	1.13	19.00	66.50	0.116	0.015	3.19	0.52	0.82	5.36	0.021	0.89	98.21
	Err. ±	*0.05*	*0.02*	*0.04*	*0.04*	*0.004*	*0.001*	*0.05*	*0.02*	*0.01*	*0.01*	*0.003*		
29 - Group 1	**wt%**	0.31	0.96	18.70	66.70	0.112	0.013	2.98	0.88	0.82	5.81	0.029	2.26	99.55
	Err. ±	*0.04*	*0.02*	*0.04*	*0.04*	*0.004*	*0.001*	*0.05*	*0.02*	*0.01*	*0.01*	*0.003*		
30 - Group 1	**wt%**	0.43	0.80	15.30	70.40	0.269	0.015	2.99	0.91	0.73	4.54	0.063	1.68	98.12
	Err. ±	*0.05*	*0.02*	*0.03*	*0.04*	*0.004*	*0.001*	*0.05*	*0.02*	*0.01*	*0.01*	*0.003*		

Table 12, annex 1. Ceramic samples chemical composition obtained by XRF, major oxides, part 3

Laboratory reference – Chemical group		Major oxides and L.O.I												
		Na_2O	MgO	Al_2O_3	SiO_2	P_2O_5	S	K_2O	CaO	TiO_2	Fe_2O_3	MnO	LOI	Sum
31 - Group 1	**wt%**	0.36	1.23	19.90	63.20	0.198	0.018	3.26	0.63	0.79	6.31	0.017	2.45	98.36
	Err. ±	*0.05*	*0.02*	*0.04*	*0.04*	*0.004*	*0.001*	*0.05*	*0.02*	*0.01*	*0.01*	*0.003*		
32 - Group 1	**wt%**	0.35	0.83	15.20	68.80	0.155	0.015	3.07	0.70	0.65	4.46	0.013	5.33	99.57
	Err. ±	*0.04*	*0.02*	*0.03*	*0.04*	*0.004*	*0.001*	*0.05*	*0.02*	*0.01*	*0.01*	*0.003*		
33 - Group 1	**wt%**	0.30	1.04	17.11	69.50	0.174	0.025	3.51	0.78	0.63	4.56	0.022	0.98	98.62
	Err. ±	*0.04*	*0.02*	*0.04*	*0.04*	*0.004*	*0.001*	*0.05*	*0.02*	*0.01*	*0.01*	*0.003*		
34 - Group 1	**wt%**	0.41	0.89	17.40	67.40	0.186	0.015	3.28	0.73	0.74	5.34	0.028	3.18	99.59
	Err. ±	*0.05*	*0.02*	*0.04*	*0.04*	*0.004*	*0.001*	*0.05*	*0.02*	*0.01*	*0.01*	*0.003*		
35 - Group 1	**wt%**	0.23	0.96	18.00	67.60	0.072	0.000	3.09	0.80	0.81	6.01	0.000	0.47	98.03
	Err. ±	*0.04*	*0.02*	*0.04*	*0.04*	*0.003*		*0.05*	*0.02*	*0.01*	*0.01*	*0.002*		
36 - Group 3	**wt%**	0.79	1.88	11.90	43.11	0.490	0.111	2.68	18.60	0.79	3.53	0.040	16.51	99.43
	Err. ±	*0.05*	*0.03*	*0.03*	*0.03*	*0.005*	*0.001*	*0.04*	*0.05*	*0.01*	*0.01*	*0.003*		
37 - Group 2	**wt%**	0.43	0.46	13.50	70.90	0.156	0.127	2.20	3.39	0.97	1.19	0.011	5.23	98.57
	Err. ±	*0.04*	*0.02*	*0.03*	*0.04*	*0.004*	*0.001*	*0.05*	*0.03*	*0.01*	*0.00*	*0.003*		
38 - Group 1	**wt%**	0.30	0.90	16.60	69.11	0.256	0.014	3.23	0.87	0.79	5.02	0.029	1.81	98.92
	Err. ±	*0.04*	*0.02*	*0.04*	*0.04*	*0.004*	*0.001*	*0.05*	*0.02*	*0.01*	*0.01*	*0.003*		
39 - Group 1	**wt%**	0.38	0.90	16.50	70.00	0.139	0.014	3.11	0.69	0.74	4.89	0.027	0.67	98.06
	Err. ±	*0.04*	*0.02*	*0.04*	*0.04*	*0.004*	*0.001*	*0.05*	*0.02*	*0.01*	*0.01*	*0.003*		
40 - Group 1	**wt%**	0.29	1.06	19.11	66.20	0.121	0.018	3.13	0.60	0.82	5.79	0.052	1	98.17
	Err. ±	*0.04*	*0.02*	*0.04*	*0.04*	*0.004*	*0.001*	*0.05*	*0.02*	*0.01*	*0.01*	*0.003*		
41 - Group 1	**wt%**	0.39	1.07	19.11	65.00	0.111	0.016	3.27	0.59	0.80	6.42	0.024	1.86	98.65
	Err. ±	*0.04*	*0.02*	*0.04*	*0.04*	*0.004*	*0.001*	*0.05*	*0.02*	*0.01*	*0.01*	*0.003*		
42 - Group 1	**wt%**	0.55	1.11	19.11	64.60	0.094	0.020	3.36	0.52	0.75	5.86	0.009	3.43	99.40
	Err. ±	*0.05*	*0.02*	*0.04*	*0.04*	*0.004*	*0.001*	*0.05*	*0.02*	*0.01*	*0.01*	*0.003*		
Mean Group 1	***wt%***	*0.37*	*0.98*	*18.32*	*66.06*	*0.143*	*0.019*	*3.15*	*0.79*	*0.78*	*5.58*	*0.030*	*2.66*	*98.89*
	St.Dev.	*0.14*	*0.12*	*1.40*	*2.04*	*0.050*	*0.014*	*0.18*	*0.39*	*0.07*	*0.68*	*0.021*	*1.47*	*0.73*
Mean Group 2	***wt%***	*0.40*	*0.53*	*16.13*	*73.19*	*0.114*	*0.090*	*2.60*	*0.84*	*1.13*	*1.49*	*0.012*	*2.08*	*98.60*
	St.Dev.	*0.06*	*0.04*	*1.53*	*1.72*	*0.018*	*0.061*	*0.19*	*1.08*	*0.08*	*0.15*	*0.002*	*1.42*	*0.59*
Mean Group 3	***wt%***	*1.00*	*2.38*	*13.50*	*46.04*	*0.461*	*0.131*	*2.48*	*17.18*	*0.67*	*4.54*	*0.016*	*9.40*	*97.80*
	St.Dev.	*0.33*	*0.52*	*2.90*	*3.94*	*0.091*	*0.068*	*0.73*	*2.04*	*0.11*	*0.89*	*0.019*	*5.11*	*0.87*

Table 13, annex 1. Ceramic samples chemical composition obtained by ICP-MS, trace elements, part 1.

Laboratory reference – Chemical group		Trace elements																	
		Sc	V	Co	Ni	Cu	Zn	Ga	Rb	Sr	Y	Zr	Nb	Cs	Ba	Hf	Pb	Th	U
1 - Group 1	**PPM**	14.13	123.01	12.55	40.80	37.52	111.11	26.16	193.54	32.18	20.19	111.09	16.65	12.47	497.00	2.90	62.88	12.09	2.31
	RSD	*4.29*	*1.20*	*3.24*	*1.87*	*1.76*	*1.47*	*0.64*	*2.25*	*1.46*	*1.06*	*0.32*	*0.96*	*4.70*	*3.11*	*3.45*	*4.76*	*0.65*	*0.96*
2 - Group 1	**PPM**	11.81	112.98	11.73	32.66	21.46	88.69	21.18	162.42	28.63	17.56	86.92	14.77	11.67	429.11	2.87	36.59	12.33	2.39
	RSD	*2.41*	*4.05*	*4.17*	*1.55*	*1.32*	*3.86*	*4.13*	*1.38*	*0.48*	*1.51*	*0.63*	*0.33*	*3.53*	*1.90*	*2.86*	*1.69*	*1.35*	*1.78*
3 - Group 2	**PPM**	11.97	75.38	3.78	14.89	22.14	36.58	21.69	163.80	63.79	31.45	80.00	26.34	11.61	363.43	2.53	5773.87	17.76	3.00
	RSD	*3.85*	*2.03*	*2.35*	*0.58*	*0.41*	*0.88*	*2.09*	*2.06*	*0.89*	*1.01*	*1.47*	*0.63*	*2.92*	*2.51*	*3.08*	*1.50*	*2.25*	*1.99*
4 - Group 1	**PPM**	14.21	117.51	12.78	37.85	27.37	99.47	24.07	192.97	32.25	22.35	98.08	17.11	13.55	460.40	3.20	47.60	14.30	2.46
	RSD	*2.14*	*3.94*	*3.11*	*0.91*	*2.23*	*2.40*	*2.38*	*0.95*	*0.45*	*1.63*	*2.38*	*0.99*	*2.80*	*1.88*	*3.71*	*0.88*	*3.53*	*2.35*
5 - Group 3	**PPM**	12.98	115.16	14.09	39.89	647.82	98.82	17.65	136.01	434.24	24.41	78.19	16.22	7.99	386.60	2.42	8543.24	11.99	1.88
	RSD	*3.61*	*0.87*	*2.37*	*0.64*	*1.56*	*1.07*	*2.01*	*2.13*	*1.32*	*0.93*	*1.22*	*0.87*	*2.27*	*2.17*	*2.21*	*1.92*	*3.21*	*1.91*
6 - Group 1	**PPM**	12.94	99.99	8.17	25.99	22.53	71.24	22.87	186.49	37.95	21.35	119.76	13.51	11.28	452.63	3.38	25.06	9.52	2.34
	RSD	*0.85*	*1.79*	*1.91*	*1.16*	*0.97*	*1.56*	*0.62*	*1.04*	*1.25*	*2.70*	*1.06*	*0.24*	*1.18*	*0.74*	*3.07*	*5.73*	*0.22*	*1.04*
7 - Group 2	**PPM**	7.55	43.67	2.59	9.30	32.00	21.72	13.59	123.32	42.55	14.95	59.65	18.90	6.90	256.27	1.87	508.23	11.98	2.14
	RSD	*3.40*	*0.87*	*1.32*	*2.26*	*1.21*	*1.92*	*1.28*	*1.08*	*1.22*	*0.50*	*0.60*	*1.26*	*4.50*	*1.58*	*2.72*	*1.03*	*1.71*	*2.67*
8 - Group 2	**PPM**	9.24	56.89	3.49	11.67	25.21	26.55	17.15	130.95	54.11	24.66	77.27	20.57	7.68	304.21	2.38	1199.90	15.86	2.77
	RSD	*2.61*	*1.82*	*2.46*	*1.07*	*0.63*	*2.28*	*0.83*	*0.50*	*1.36*	*1.03*	*3.00*	*1.27*	*3.55*	*2.65*	*5.52*	*4.92*	*6.63*	*5.29*
9 - Group 3	**PPM**	14.31	127.01	13.58	49.81	98.85	111.64	24.15	117.29	463.86	24.95	40.22	15.48	17.94	493.05	1.24	1795.60	13.99	2.39
	RSD	*2.09*	*1.74*	*1.99*	*1.41*	*1.45*	*3.04*	*1.77*	*0.62*	*3.19*	*1.46*	*1.20*	*0.68*	*1.42*	*1.84*	*1.94*	*0.81*	*3.83*	*1.98*
11 - Group 3	**PPM**	9.94	75.07	15.79	58.15	66.40	111.54	16.46	97.78	421.89	23.22	78.62	13.86	5.14	408.56	2.21	2129.57	8.80	1.87
	RSD	*1.53*	*0.35*	*0.86*	*1.02*	*2.06*	*1.00*	*1.87*	*0.68*	*0.20*	*0.89*	*1.35*	*1.31*	*2.90*	*1.48*	*1.74*	*0.33*	*0.74*	*1.00*
11 - Group 3	**PPM**	8.69	64.86	8.97	25.07	11.92	83.55	13.90	122.69	242.36	17.43	74.82	19.91	6.06	323.47	2.32	28.86	6.79	2.57
	RSD	*3.68*	*1.50*	*1.99*	*1.80*	*2.17*	*0.45*	*0.38*	*1.12*	*0.85*	*0.74*	*1.53*	*1.16*	*1.22*	*1.30*	*1.49*	*2.46*	*2.69*	*2.78*
12 - Group 1	**PPM**	12.72	115.26	11.15	32.35	24.64	92.56	23.26	178.82	27.99	25.59	120.91	15.82	12.56	451.27	3.90	58.60	13.77	2.85
	RSD	*1.20*	*2.70*	*2.17*	*2.78*	*2.83*	*2.06*	*1.44*	*1.82*	*1.59*	*2.51*	*1.90*	*1.85*	*2.89*	*1.95*	*1.95*	*3.46*	*3.45*	*2.31*
13 - Group 1	**PPM**	14.65	117.15	14.36	39.90	33.95	114.13	25.95	204.49	33.19	27.77	119.80	19.22	14.63	514.12	3.89	52.26	15.40	2.94
	RSD	*0.66*	*2.81*	*1.62*	*0.31*	*1.42*	*1.47*	*1.42*	*1.89*	*1.54*	*3.15*	*1.19*	*0.71*	*2.83*	*1.33*	*2.47*	*1.64*	*2.28*	*1.99*
14 - Group 2	**PPM**	12.21	68.21	3.99	14.98	23.89	30.25	22.60	161.41	59.53	29.49	84.95	27.85	8.41	357.19	2.61	6842.26	19.11	3.28
	RSD	*1.70*	*2.17*	*2.34*	*1.58*	*1.23*	*2.86*	*2.19*	*1.42*	*1.50*	*1.54*	*2.04*	*1.08*	*3.66*	*1.16*	*2.13*	*3.40*	*1.85*	*2.33*
15 - Group 2	**PPM**	11.22	61.20	3.21	13.12	24.49	27.00	18.87	141.72	52.16	24.27	84.62	22.27	8.51	309.68	2.60	1744.50	17.51	3.00
	RSD	*1.06*	*3.17*	*3.80*	*2.90*	*0.84*	*3.15*	*2.29*	*2.17*	*0.69*	*3.09*	*1.95*	*1.17*	*1.54*	*2.77*	*2.25*	*2.61*	*2.63*	*0.87*

Table 14, annex 1. Ceramic samples chemical composition obtained by ICP-MS, trace elements, part 2.

Laboratory reference - Chemical group		Trace elements																	
		Sc	V	Co	Ni	Cu	Zn	Ga	Rb	Sr	Y	Zr	Nb	Cs	Ba	Hf	Pb	Th	U
16 - Group 2	**PPM**	11.15	58.89	3.75	12.18	15.07	25.53	17.71	132.55	51.32	25.17	75.44	19.27	8.17	325.95	2.60	1744.50	17.51	3.00
	RSD	*3.32*	*1.38*	*2.20*	*1.70*	*5.79*	*0.66*	*2.13*	*3.68*	*0.62*	*4.81*	*1.55*	*1.11*	*1.74*	*1.66*	*2.25*	*2.61*	*2.63*	*0.87*
17 - Group 1	**PPM**	9.50	76.04	7.67	21.13	19.36	70.25	18.37	185.58	37.56	16.84	87.63	13.12	9.41	402.29	2.40	1502.45	14.08	2.77
	RSD	*1.40*	*1.66*	*1.67*	*1.70*	*0.73*	*1.93*	*0.83*	*1.22*	*2.73*	*2.41*	*0.33*	*0.67*	*0.92*	*1.90*	*2.71*	*4.02*	*1.21*	*1.88*
18 - Group 1	**PPM**	15.94	117.60	17.08	37.46	26.18	113.24	23.36	178.03	36.30	18.61	119.33	15.07	11.63	555.85	2.86	70.21	11.36	1.79
	RSD	*2.29*	*0.92*	*1.72*	*1.18*	*1.75*	*0.83*	*1.52*	*1.12*	*0.48*	*1.55*	*1.54*	*1.38*	*2.53*	*0.99*	*1.95*	*3.46*	*1.03*	*0.82*
19 - Group 1	**PPM**	14.78	116.46	11.68	30.40	35.86	85.02	26.27	211.06	71.95	24.70	88.86	16.77	13.60	407.04	3.51	36.72	11.33	2.29
	RSD	*1.75*	*1.91*	*1.25*	*1.82*	*1.82*	*0.77*	*0.78*	*1.06*	*0.41*	*0.92*	*1.32*	*1.08*	*1.51*	*1.94*	*2.17*	*2.49*	*0.18*	*2.05*
20 - Group 1	**PPM**	14.07	114.13	8.35	26.11	22.26	59.02	23.61	185.78	64.86	26.12	88.23	19.22	11.92	377.44	2.88	913.54	14.32	2.97
	RSD	*3.76*	*0.91*	*1.77*	*1.73*	*1.51*	*1.61*	*1.82*	*0.64*	*1.06*	*0.54*	*0.60*	*0.69*	*3.39*	*0.60*	*0.64*	*2.27*	*3.59*	*1.91*
21 - Group 1	**PPM**	11.33	95.57	9.37	29.11	25.55	83.97	20.37	174.90	31.91	23.57	114.52	14.25	11.58	416.70	2.86	1529.70	16.83	2.79
	RSD	*2.52*	*2.00*	*3.11*	*3.84*	*2.33*	*2.01*	*2.68*	*2.36*	*0.77*	*3.25*	*0.99*	*2.13*	*2.82*	*1.69*	*1.23*	*1.20*	*2.80*	*1.26*
22 - Group 1	**PPM**	15.92	116.56	12.03	37.04	28.24	99.12	26.32	192.22	32.12	17.50	113.32	14.62	12.78	477.12	3.38	38.34	13.00	2.54
	RSD	*0.54*	*1.18*	*1.59*	*1.63*	*0.23*	*0.39*	*0.07*	*0.70*	*0.97*	*2.53*	*1.83*	*1.08*	*2.03*	*2.26*	*2.22*	*1.03*	*0.58*	*1.98*
23 - Group 1	**PPM**	13.59	122.16	16.55	39.81	22.01	99.63	26.22	206.89	33.93	23.78	113.85	16.57	14.20	450.64	3.21	33.30	11.50	2.13
	RSD	*2.71*	*1.39*	*0.59*	*0.73*	*0.43*	*1.86*	*1.13*	*0.53*	*1.14*	*1.19*	*1.81*	*1.30*	*1.18*	*0.33*	*3.04*	*2.81*	*1.12*	*1.07*
24 - Group 1	**PPM**	12.16	113.17	12.25	37.01	28.09	94.05	23.23	183.48	38.26	22.62	119.07	15.07	12.28	465.59	3.22	34.41	12.11	1.94
	RSD	*4.30*	*1.14*	*0.69*	*0.38*	*1.45*	*1.15*	*1.46*	*1.39*	*2.96*	*1.19*	*2.89*	*0.86*	*2.35*	*0.76*	*5.82*	*1.19*	*2.62*	*1.19*
25 - Group 1	**PPM**	16.22	123.38	8.34	26.46	31.32	87.76	26.27	195.19	46.84	18.89	88.58	17.55	13.14	508.37	3.68	38.95	11.19	2.11
	RSD	*2.20*	*2.54*	*1.56*	*1.79*	*1.50*	*3.46*	*4.25*	*2.76*	*0.87*	*2.79*	*0.98*	*0.63*	*1.23*	*2.31*	*2.49*	*0.50*	*4.20*	*1.08*
26 - Group 1	**PPM**	12.95	111.09	13.85	36.73	25.26	110.69	22.51	184.96	37.37	25.75	124.32	15.34	11.01	525.18	2.77	40.50	13.84	2.76
	RSD	*1.84*	*1.80*	*1.66*	*1.44*	*1.06*	*1.69*	*1.26*	*0.76*	*1.22*	*2.40*	*1.11*	*2.15*	*2.49*	*1.14*	*3.91*	*5.90*	*3.23*	*3.98*
27 - Group 1	**PPM**	14.81	111.30	7.47	22.48	28.34	79.44	23.88	177.82	52.88	17.28	73.67	16.47	11.65	447.24	4.01	65.01	12.40	2.40
	RSD	*2.49*	*2.63*	*2.21*	*1.67*	*1.46*	*3.91*	*2.38*	*2.27*	*0.64*	*2.34*	*1.82*	*1.02*	*1.56*	*2.21*	*2.36*	*2.65*	*2.01*	*2.70*
28 - Group 1	**PPM**	12.94	116.62	9.43	29.04	19.48	76.08	24.67	198.80	53.64	23.34	95.60	17.46	12.28	357.04	2.45	68.83	13.67	2.95
	RSD	*11.52*	*12.00*	*12.96*	*14.32*	*11.66*	*11.24*	*12.52*	*11.53*	*1.70*	*11.30*	*0.94*	*9.31*	*1.04*	*1.40*	*1.23*	*5.99*	*1.13*	*2.21*
29 - Group 1	**PPM**	11.95	111.37	11.96	33.42	22.01	78.54	24.47	187.38	33.27	18.07	82.13	15.68	7.96	403.12	3.05	40.31	17.66	2.97
	RSD	*0.95*	*0.37*	*1.72*	*1.87*	*3.77*	*2.04*	*0.97*	*1.40*	*0.30*	*4.44*	*1.42*	*0.64*	*3.18*	*1.14*	*2.32*	*0.46*	*5.50*	*2.60*
30 - Group 1	**PPM**	9.54	81.74	11.55	24.22	21.63	69.79	18.27	183.87	43.32	23.86	91.15	13.65	11.81	366.59	2.57	30.41	11.51	1.83
	RSD	*3.08*	*2.59*	*2.25*	*1.16*	*1.74*	*1.17*	*1.47*	*3.16*	*0.97*	*2.11*	*0.40*	*0.84*	*5.69*	*0.67*	*4.05*	*2.00*	*2.46*	*1.91*

Table 15, annex 1. Ceramic samples chemical composition obtained by ICP-MS, trace elements, part 3

Laboratory reference - Chemical group		Trace elements																	
		Sc	V	Co	Ni	Cu	Zn	Ga	Rb	Sr	Y	Zr	Nb	Cs	Ba	Hf	Pb	Th	U
31 - Group 1	**PPM**	7.23	99.80	9.78	26.65	25.31	117.14	18.58	150.96	31.71	15.32	99.40	12.73	7.08	511.79	3.17	36.82	9.18	2.24
	RSD	*3.01*	*1.87*	*2.20*	*1.98*	*2.38*	*2.38*	*1.91*	*1.83*	*1.44*	*1.48*	*0.79*	*1.81*	*2.28*	*1.82*	*0.94*	*2.75*	*1.16*	*2.22*
32 - Group 1	**PPM**	11.08	85.05	8.11	21.26	22.40	71.94	19.59	187.18	41.27	15.93	111.94	11.94	11.71	438.57	3.29	30.96	9.44	2.09
	RSD	*1.99*	*1.32*	*1.68*	*0.53*	*0.67*	*1.42*	*0.86*	*0.81*	*1.33*	*0.86*	*1.05*	*0.65*	*1.90*	*1.69*	*2.92*	*2.43*	*1.87*	*0.86*
33 - Group 1	**PPM**	12.61	97.91	9.57	28.68	25.07	92.91	21.65	190.81	39.05	17.91	76.13	12.14	11.37	505.02	2.41	27.02	11.42	2.53
	RSD	*1.64*	*2.48*	*1.51*	*0.08*	*1.77*	*0.50*	*0.62*	*3.36*	*1.83*	*3.38*	*0.57*	*1.17*	*1.76*	*3.70*	*5.49*	*2.69*	*6.48*	*0.37*
34 - Group 1	**PPM**	13.50	113.39	11.68	33.51	27.16	87.84	23.38	191.52	39.83	28.57	119.69	17.22	11.84	506.93	3.84	49.32	14.85	2.60
	RSD	*3.37*	*2.21*	*2.00*	*0.33*	*0.94*	*2.69*	*3.27*	*2.51*	*1.11*	*0.66*	*0.51*	*0.71*	*2.70*	*2.25*	*2.36*	*1.74*	*4.92*	*2.61*
35 - Group 1	**PPM**	11.89	97.61	18.08	34.84	31.36	80.26	20.75	164.53	27.60	19.82	84.86	13.69	7.81	407.83	2.79	31.71	11.82	1.94
	RSD	*4.59*	*2.08*	*1.27*	*1.60*	*1.75*	*1.97*	*0.87*	*0.89*	*11.50*	*1.07*	*9.95*	*0.52*	*3.13*	*3.25*	*1.22*	*0.38*	*2.94*	*1.22*
36 - Group 3	**PPM**	7.83	56.23	8.86	23.24	11.29	73.96	12.60	118.12	223.53	16.79	72.87	18.14	5.36	294.53	2.34	23.60	7.23	2.51
	RSD	*4.30*	*1.12*	*1.19*	*1.35*	*2.77*	*1.35*	*1.66*	*2.11*	*0.09*	*1.56*	*0.56*	*1.31*	*2.56*	*0.99*	*1.93*	*2.11*	*0.69*	*1.21*
37 - Group 2	**PPM**	9.96	55.48	2.87	11.00	18.50	26.05	17.39	132.18	64.32	29.03	79.84	23.18	7.25	333.07	2.55	4348.63	16.07	2.77
	RSD	*2.78*	*3.23*	*4.51*	*2.17*	*2.23*	*3.92*	*3.11*	*2.52*	*1.51*	*2.16*	*1.74*	*1.68*	*1.13*	*3.30*	*1.80*	*2.12*	*1.86*	*2.00*
38 - Group 1	**PPM**	11.53	91.21	8.74	28.54	25.58	85.56	18.98	196.41	37.67	20.94	88.69	16.44	12.50	406.13	2.76	30.71	11.93	2.25
	RSD	*3.77*	*2.01*	*2.20*	*2.14*	*1.67*	*0.94*	*2.07*	*0.75*	*0.98*	*2.11*	*1.06*	*1.24*	*3.78*	*1.58*	*0.15*	*2.89*	*1.87*	*0.17*
39 - Group 1	**PPM**	11.56	84.12	11.65	30.35	23.36	79.62	20.03	176.78	35.57	18.23	77.55	14.13	11.12	413.45	2.54	42.11	13.45	2.12
	RSD	*1.42*	*2.36*	*2.09*	*1.30*	*1.00*	*2.75*	*2.15*	*1.84*	*0.45*	*1.37*	*2.50*	*0.84*	*4.64*	*5.14*	*3.07*	*4.59*	*2.11*	*2.84*
40 - Group 1	**PPM**	13.48	111.28	12.71	38.64	26.99	99.37	23.33	194.66	32.72	26.09	119.30	15.69	12.36	484.75	3.34	30.39	12.49	2.54
	RSD	*0.86*	*1.65*	*2.41*	*1.85*	*0.72*	*2.03*	*0.63*	*0.05*	*0.85*	*1.05*	*1.52*	*1.64*	*2.03*	*2.04*	*2.62*	*2.50*	*2.06*	*0.81*
41 - Group 1	**PPM**	12.82	112.34	12.94	33.13	26.42	87.18	22.67	173.38	31.12	25.00	120.94	14.58	11.72	440.58	3.86	40.69	12.78	2.41
	RSD	*1.95*	*0.88*	*2.51*	*2.16*	*1.47*	*0.83*	*1.45*	*0.51*	*0.54*	*2.09*	*0.88*	*0.67*	*0.98*	*1.69*	*2.89*	*1.49*	*5.33*	*3.53*
42 - Group 1	**PPM**	13.34	113.54	8.58	23.14	27.44	80.33	22.43	173.76	40.93	18.08	114.50	13.95	11.34	462.99	3.38	30.76	11.56	2.77
	RSD	*1.78*	*2.29*	*1.74*	*0.28*	*0.41*	*1.48*	*1.27*	*0.67*	*2.08*	*1.72*	*0.37*	*0.34*	*3.57*	*1.82*	*1.85*	*3.88*	*3.65*	*1.03*
Mean Group 1	**PPM**	*12.74*	*114.31*	*11.21*	*31.29*	*26.14*	*87.53*	*22.76*	*185.46*	*38.80*	*21.39*	*99.96*	*15.35*	*11.47*	*451.43*	*3.16*	*120.14*	*12.61*	*2.41*
	St.Dev.	*2.04*	*11.95*	*2.74*	*5.83*	*4.39*	*12.60*	*2.48*	*12.83*	*11.12*	*3.72*	*14.73*	*1.85*	*1.74*	*49.35*	*0.45*	*305.19*	*1.94*	*0.35*
Mean Group 2	**PPM**	*11.18*	*59.96*	*3.38*	*12.45*	*23.04*	*27.67*	*18.43*	*140.85*	*55.40*	*25.57*	*77.40*	*22.63*	*8.22*	*321.40*	*2.42*	*3131.41*	*16.05*	*2.82*
	St.Dev.	*1.47*	*9.29*	*0.48*	*1.91*	*4.97*	*4.32*	*2.80*	*14.64*	*7.18*	*5.03*	*7.94*	*3.18*	*1.12*	*33.55*	*0.24*	*2312.19*	*2.23*	*0.33*
Mean Group 3	**PPM**	*11.75*	*87.67*	*12.26*	*39.23*	*167.06*	*93.90*	*16.95*	*116.38*	*357.18*	*21.36*	*68.94*	*16.72*	*8.50*	*381.24*	*2.11*	*2504.18*	*9.56*	*2.25*
	St.Dev.	*2.49*	*28.18*	*2.83*	*13.61*	*242.72*	*13.43*	*4.02*	*12.96*	*112.52*	*3.52*	*14.52*	*2.11*	*4.83*	*69.47*	*0.44*	*3143.03*	*2.66*	*0.31*

Table 16, annex 1. Ceramic samples chemical composition obtained by ICP-MS, rare earth elements, part 1

Laboratory reference - Chemical group		Rare earth elements													
		La	Ce	Pr	Nd	Sm	Eu	Gd	Tb	Dy	Ho	Er	Tm	Yb	Lu
1 - Group 1	PPM	37.29	73.94	9.37	37.75	6.74	1.26	5.67	0.74	3.63	0.67	1.93	0.27	1.82	0.27
	RSD	*4.04*	*1.98*	*2.46*	*7.31*	*0.28*	*0.71*	*0.76*	*1.04*	*0.89*	*0.88*	*1.48*	*0.80*	*0.65*	*0.71*
2 - Group 1	PPM	26.14	59.90	7.43	30.11	6.50	1.04	4.94	0.66	3.37	0.61	1.80	0.31	2.06	0.30
	RSD	*1.95*	*1.52*	*1.77*	*2.22*	*1.96*	*1.83*	*0.08*	*0.24*	*0.92*	*0.29*	*0.40*	*0.88*	*1.20*	*1.99*
3 - Group 2	PPM	41.31	92.98	13.77	44.22	9.09	1.44	6.96	0.95	4.78	0.85	3.00	0.40	2.54	0.36
	RSD	*2.77*	*1.93*	*2.78*	*3.06*	*1.28*	*2.79*	*1.25*	*0.92*	*1.06*	*0.33*	*2.57*	*3.07*	*1.74*	*1.41*
4 - Group 1	PPM	33.09	72.18	9.00	34.82	7.99	1.28	6.00	0.78	3.93	0.73	2.11	0.37	2.35	0.36
	RSD	*2.40*	*1.06*	*2.34*	*2.77*	*2.49*	*2.70*	*2.12*	*1.61*	*1.48*	*2.31*	*1.30*	*4.90*	*3.28*	*2.42*
5 - Group 3	PPM	29.35	60.41	8.87	27.29	6.04	1.11	4.96	0.68	3.63	0.69	2.43	0.33	2.13	0.31
	RSD	*2.67*	*1.75*	*5.92*	*7.00*	*2.84*	*3.39*	*2.67*	*3.59*	*3.14*	*2.71*	*2.93*	*2.39*	*3.17*	*2.73*
6 - Group 1	PPM	26.42	58.41	6.72	25.93	4.98	1.03	4.48	0.64	3.52	0.69	2.04	0.30	1.96	0.30
	RSD	*1.66*	*2.08*	*2.43*	*1.07*	*0.62*	*0.30*	*0.66*	*0.98*	*0.28*	*1.11*	*0.41*	*0.46*	*0.66*	*0.57*
7 - Group 2	PPM	26.48	57.62	7.04	26.28	5.91	0.97	4.33	0.58	2.96	0.52	1.47	0.25	1.59	0.23
	RSD	*1.92*	*1.16*	*3.50*	*2.40*	*2.89*	*2.06*	*2.30*	*1.91*	*1.53*	*0.88*	*1.50*	*3.31*	*3.23*	*3.53*
8 - Group 2	PPM	36.27	78.54	9.34	35.29	7.97	1.36	6.26	0.89	4.80	0.87	2.45	0.40	2.54	0.36
	RSD	*2.14*	*2.01*	*3.21*	*2.47*	*4.98*	*2.00*	*0.52*	*0.65*	*0.38*	*0.29*	*0.64*	*4.91*	*3.45*	*4.82*
9 - Group 3	PPM	34.19	73.40	9.09	36.03	7.22	1.36	6.18	0.84	4.38	0.80	2.26	0.34	2.12	0.31
	RSD	*1.70*	*0.62*	*0.69*	*1.45*	*1.02*	*1.91*	*1.20*	*0.88*	*0.37*	*0.38*	*0.25*	*1.57*	*1.37*	*1.37*
11 - Group 3	PPM	30.90	62.89	7.45	27.82	5.00	1.09	4.79	0.68	3.65	0.72	2.06	0.29	1.85	0.27
	RSD	*1.32*	*2.28*	*3.46*	*2.17*	*1.44*	*0.25*	*0.90*	*0.72*	*0.22*	*0.83*	*0.71*	*0.71*	*1.68*	*0.57*
11 - Group 3	PPM	22.25	48.08	5.71	21.08	4.79	1.00	4.04	0.56	3.03	0.54	1.54	0.25	1.60	0.23
	RSD	*4.18*	*3.67*	*0.39*	*0.92*	*2.94*	*1.81*	*0.50*	*1.32*	*6.22*	*1.11*	*1.61*	*2.87*	*3.14*	*2.06*
12 - Group 1	PPM	28.53	68.98	8.17	31.27	7.25	1.11	5.54	0.80	4.39	0.83	2.44	0.44	2.85	0.43
	RSD	*4.69*	*3.84*	*0.65*	*1.76*	*3.27*	*2.02*	*0.46*	*1.89*	*0.98*	*0.99*	*0.32*	*3.82*	*3.24*	*3.62*
13 - Group 1	PPM	34.27	79.24	12.30	37.35	8.72	1.33	6.35	0.83	4.19	0.77	2.90	0.41	2.74	0.42
	RSD	*3.71*	*1.51*	*2.36*	*1.23*	*0.40*	*2.74*	*4.17*	*1.74*	*1.59*	*1.44*	*1.57*	*2.07*	*1.39*	*3.02*
14 - Group 2	PPM	46.93	112.60	15.16	47.94	11.24	1.65	7.58	0.99	4.77	0.85	2.94	0.38	2.41	0.34
	RSD	*2.87*	*1.99*	*2.31*	*2.02*	*2.36*	*4.96*	*1.73*	*2.09*	*1.20*	*0.34*	*2.72*	*1.84*	*3.81*	*1.60*
15 - Group 2	PPM	38.59	87.14	11.50	41.29	9.00	1.47	6.73	0.94	4.87	0.88	2.46	0.41	2.62	0.37
	RSD	*3.82*	*1.13*	*1.95*	*2.37*	*1.52*	*3.15*	*0.48*	*0.98*	*0.91*	*0.75*	*1.77*	*2.33*	*1.21*	*1.56*

Table 17, annex 1. Ceramic samples chemical composition obtained by ICP-MS, rare earth elements, part 2

Laboratory reference - Chemical group		Rare earth elements													
		La	Ce	Pr	Nd	Sm	Eu	Gd	Tb	Dy	Ho	Er	Tm	Yb	Lu
16 - Group 2	**PPM**	40.35	87.08	11.23	39.15	7.58	1.50	6.65	0.95	4.97	0.93	2.62	0.36	2.25	0.32
	RSD	*2.62*	*3.00*	*2.38*	*2.66*	*1.12*	*0.57*	*0.70*	*1.29*	*0.32*	*0.46*	*0.99*	*1.31*	*0.96*	*1.24*
17 - Group 1	**PPM**	22.81	54.55	6.79	25.60	5.64	0.87	4.20	0.55	2.82	0.51	1.51	0.26	1.77	0.27
	RSD	*2.95*	*1.67*	*3.64*	*3.47*	*1.88*	*3.46*	*0.97*	*0.94*	*1.83*	*1.11*	*0.79*	*1.41*	*1.13*	*1.53*
18 - Group 1	**PPM**	34.47	78.70	8.66	34.04	6.61	1.30	5.53	0.73	3.66	0.69	2.04	0.30	2.05	0.32
	RSD	*2.83*	*2.08*	*3.06*	*3.67*	*0.36*	*0.31*	*0.84*	*0.84*	*0.37*	*1.18*	*0.77*	*0.41*	*0.65*	*1.26*
19 - Group 1	**PPM**	31.52	72.99	11.51	31.86	7.06	1.24	5.26	0.71	3.67	0.68	2.49	0.34	2.24	0.32
	RSD	*2.02*	*1.42*	*3.63*	*1.35*	*1.64*	*1.52*	*1.64*	*1.72*	*1.28*	*1.74*	*3.29*	*2.16*	*1.26*	*2.92*
20 - Group 1	**PPM**	35.31	82.39	12.33	36.83	7.93	1.22	6.00	0.79	3.95	0.72	2.67	0.36	2.34	0.34
	RSD	*4.05*	*0.82*	*4.91*	*1.73*	*1.13*	*1.90*	*0.94*	*0.23*	*0.66*	*0.41*	*0.77*	*0.59*	*0.96*	*1.21*
21 - Group 1	**PPM**	26.74	60.26	7.51	29.86	6.80	1.01	5.07	0.71	3.78	0.71	2.07	0.37	2.43	0.37
	RSD	*1.79*	*2.67*	*4.90*	*1.36*	*1.42*	*0.89*	*1.50*	*1.37*	*0.87*	*0.60*	*0.71*	*2.24*	*1.72*	*1.16*
22 - Group 1	**PPM**	31.41	68.93	8.19	31.76	6.08	1.18	5.09	0.65	3.23	0.61	1.80	0.26	1.79	0.28
	RSD	*3.29*	*1.33*	*1.28*	*3.65*	*0.86*	*0.33*	*0.56*	*0.86*	*1.37*	*0.70*	*0.28*	*1.23*	*0.26*	*0.38*
23 - Group 1	**PPM**	35.43	80.71	9.03	34.68	6.46	1.21	5.77	0.79	4.04	0.77	2.21	0.31	2.06	0.31
	RSD	*2.83*	*1.16*	*3.03*	*2.91*	*1.64*	*1.53*	*0.63*	*1.04*	*0.26*	*0.60*	*0.46*	*1.26*	*0.75*	*1.12*
24 - Group 1	**PPM**	31.81	69.31	8.40	32.69	6.03	1.20	5.38	0.75	3.94	0.77	2.21	0.32	2.13	0.32
	RSD	*1.36*	*0.54*	*3.76*	*2.59*	*0.72*	*0.42*	*1.04*	*1.08*	*1.23*	*1.37*	*0.81*	*0.68*	*0.75*	*0.77*
25 - Group 1	**PPM**	29.99	67.08	11.13	32.73	6.95	1.11	5.02	0.63	2.95	0.53	1.92	0.26	1.76	0.26
	RSD	*3.72*	*1.24*	*4.38*	*0.82*	*4.26*	*3.45*	*1.08*	*0.88*	*1.33*	*1.37*	*2.76*	*3.34*	*3.72*	*3.73*
26 - Group 1	**PPM**	27.89	66.46	8.03	31.35	7.41	1.22	5.85	0.83	4.50	0.85	2.48	0.44	2.88	0.44
	RSD	*1.48*	*0.22*	*1.82*	*0.63*	*3.15*	*0.91*	*0.91*	*0.84*	*0.13*	*0.06*	*0.55*	*2.96*	*3.20*	*2.84*
27 - Group 1	**PPM**	29.25	65.39	9.92	30.18	6.63	1.01	4.59	0.58	2.67	0.47	1.74	0.24	1.57	0.23
	RSD	*4.46*	*3.88*	*3.20*	*2.16*	*1.80*	*3.11*	*2.85*	*2.20*	*3.77*	*3.21*	*0.70*	*5.74*	*1.22*	*5.43*
28 - Group 1	**PPM**	32.53	76.30	9.37	35.69	7.70	1.08	5.74	0.75	3.79	0.69	1.99	0.34	2.19	0.33
	RSD	*0.72*	*2.07*	*0.71*	*1.37*	*1.65*	*2.09*	*0.93*	*0.47*	*0.89*	*0.09*	*1.26*	*1.64*	*4.07*	*2.94*
29 - Group 1	**PPM**	33.77	73.91	8.78	34.38	6.35	1.20	5.37	0.69	3.39	0.62	1.77	0.24	1.58	0.23
	RSD	*0.58*	*1.36*	*1.60*	*2.45*	*1.35*	*0.96*	*0.37*	*0.26*	*0.69*	*0.73*	*1.41*	*0.37*	*0.47*	*1.90*
30 - Group 1	**PPM**	28.79	64.27	8.00	31.00	6.46	1.01	5.18	0.71	3.68	0.68	2.00	0.34	2.21	0.33
	RSD	*1.41*	*2.39*	*1.96*	*1.19*	*0.98*	*0.89*	*1.11*	*1.09*	*0.24*	*0.41*	*1.35*	*2.22*	*1.40*	*1.12*

Table 18, annex 1. Ceramic samples chemical composition obtained by ICP-MS, rare earth elements, part 3

Laboratory reference - Chemical group		Rare earth elements													
		La	Ce	Pr	Nd	Sm	Eu	Gd	Tb	Dy	Ho	Er	Tm	Yb	Lu
31 - Group 1	**PPM**	20.08	47.32	5.81	21.70	5.20	0.91	3.98	0.54	2.86	0.53	1.59	0.28	1.82	0.28
	RSD	*4.34*	*1.42*	*2.42*	*0.89*	*2.35*	*2.57*	*0.71*	*0.99*	*0.98*	*1.01*	*1.11*	*2.38*	*1.29*	*1.35*
32 - Group 1	**PPM**	24.73	53.89	6.63	25.49	4.51	0.88	3.89	0.54	2.76	0.53	1.58	0.23	1.58	0.24
	RSD	*1.66*	*0.59*	*4.48*	*3.28*	*0.93*	*1.04*	*0.63*	*0.99*	*0.59*	*1.24*	*0.16*	*1.00*	*1.73*	*1.23*
33 - Group 1	**PPM**	29.48	61.61	7.57	30.29	5.56	1.11	4.89	0.64	3.15	0.59	1.68	0.23	1.53	0.23
	RSD	*2.81*	*3.74*	*0.59*	*1.68*	*1.50*	*0.64*	*0.20*	*0.56*	*1.28*	*1.35*	*1.06*	*1.29*	*1.18*	*0.78*
34 - Group 1	**PPM**	32.53	72.62	11.86	34.83	7.68	1.19	5.84	0.80	4.23	0.80	2.94	0.42	2.73	0.40
	RSD	*1.82*	*2.35*	*4.31*	*1.37*	*1.99*	*0.77*	*2.04*	*0.92*	*0.68*	*0.26*	*2.90*	*2.26*	*3.44*	*1.69*
35 - Group 1	**PPM**	28.12	81.66	8.37	34.07	7.50	1.18	5.70	0.73	3.61	0.65	1.90	0.32	2.15	0.32
	RSD	*2.73*	*0.35*	*1.85*	*4.01*	*1.05*	*1.89*	*2.21*	*1.33*	*0.91*	*1.51*	*1.55*	*1.12*	*0.91*	*1.94*
36 - Group 3	**PPM**	21.40	46.21	5.72	21.41	4.82	0.95	4.02	0.57	3.05	0.57	1.60	0.26	1.61	0.24
	RSD	*4.76*	*1.98*	*2.12*	*1.13*	*0.11*	*1.48*	*1.30*	*0.88*	*0.64*	*1.65*	*0.81*	*0.70*	*1.25*	*1.63*
37 - Group 2	**PPM**	35.54	80.49	12.45	35.48	8.48	1.29	6.15	0.87	4.51	0.82	3.01	0.41	2.65	0.38
	RSD	*2.18*	*2.61*	*3.75*	*2.45*	*2.30*	*3.20*	*0.32*	*1.08*	*1.32*	*0.14*	*2.75*	*2.78*	*2.19*	*1.32*
38 - Group 1	**PPM**	26.34	58.98	9.53	29.53	6.55	0.99	4.76	0.64	3.25	0.60	2.21	0.30	1.97	0.29
	RSD	*3.47*	*1.59*	*3.07*	*3.61*	*0.79*	*2.24*	*0.44*	*1.90*	*0.63*	*1.90*	*1.44*	*1.60*	*1.40*	*0.42*
39 - Group 1	**PPM**	30.78	65.72	8.53	32.71	7.32	1.14	5.39	0.68	3.39	0.61	1.73	0.30	1.92	0.30
	RSD	*7.44*	*3.60*	*2.84*	*1.44*	*2.51*	*4.03*	*1.25*	*1.77*	*1.95*	*1.11*	*2.08*	*2.98*	*3.61*	*2.06*
40 - Group 1	**PPM**	31.56	67.71	8.82	34.19	7.51	1.25	5.95	0.82	4.24	0.79	2.30	0.39	2.55	0.38
	RSD	*1.78*	*1.41*	*1.20*	*1.55*	*1.70*	*2.06*	*0.43*	*0.72*	*0.55*	*0.26*	*0.23*	*1.68*	*2.24*	*1.99*
41 - Group 1	**PPM**	25.97	67.90	7.51	29.14	6.63	1.07	5.28	0.77	4.20	0.79	2.34	0.42	2.71	0.41
	RSD	*1.17*	*0.63*	*2.54*	*2.19*	*2.90*	*3.51*	*1.12*	*1.39*	*1.72*	*0.89*	*1.35*	*2.57*	*2.22*	*2.61*
42 - Group 1	**PPM**	27.42	61.50	7.65	29.19	6.52	1.09	4.81	0.65	3.27	0.60	1.76	0.32	2.08	0.33
	RSD	*1.39*	*3.23*	*2.93*	*3.04*	*1.79*	*0.53*	*0.75*	*2.55*	*0.88*	*1.56*	*0.82*	*3.69*	*2.39*	*3.76*
Mean Group 1	**PPM**	*29.82*	*67.76*	*8.66*	*31.70*	*6.71*	*1.12*	*5.25*	*0.70*	*3.60*	*0.67*	*2.07*	*0.32*	*2.13*	*0.32*
	St.Dev.	*3.92*	*8.60*	*1.51*	*3.67*	*0.92*	*0.12*	*0.61*	*0.08*	*0.50*	*0.11*	*0.37*	*0.06*	*0.39*	*0.06*
Mean Group 2	**PPM**	*37.92*	*83.78*	*11.21*	*38.52*	*8.32*	*1.38*	*6.38*	*0.88*	*4.52*	*0.82*	*2.56*	*0.37*	*2.37*	*0.34*
	St.Dev.	*5.83*	*13.01*	*2.57*	*6.53*	*1.27*	*0.20*	*0.95*	*0.13*	*0.65*	*0.12*	*0.50*	*0.05*	*0.34*	*0.05*
Mean Group 3	**PPM**	*27.62*	*58.20*	*7.37*	*26.73*	*5.57*	*1.11*	*4.80*	*0.67*	*3.55*	*0.66*	*1.98*	*0.29*	*1.86*	*0.27*
	St.Dev.	*4.99*	*11.04*	*1.46*	*5.44*	*0.94*	*0.14*	*0.79*	*0.11*	*0.49*	*0.11*	*0.35*	*0.04*	*0.24*	*0.03*

Table 19, annex 1. Ceramic samples, calculated values, part 1.

Laboratory reference - Chemical group		Calculated values														
		SiO_2/Al_2O_3	Fe_2O_3/TiO_2	Zr/U	Hf/U	Ce_{CN}	Eu_{CN}	Ce_{CN}/Eu_{CN}	Ce_{CN} anomly	EU_{CN} anomaly	$LREE_{CN}$	$MREE_{CN}$	$HREE_{CN}$	$LREE_{CN}/MREE_{CN}$	$LREE_{CN}/HREE_{CN}$	Sum REE_{CN}
1 - Group 1	PPM	3.41	6.89	43.84	1.26	120.62	22.31	5.41	0.96	0.62	507.12	98.20	45.51	5.16	11.14	650.83
2 - Group 1	PPM	3.26	7.18	36.30	1.20	97.72	18.44	5.30	1.04	0.56	397.90	86.38	48.71	4.61	8.17	532.99
3 - Group 2	PPM	4.04	1.37	26.65	0.84	151.68	25.49	5.95	0.94	0.55	632.55	121.76	65.38	5.20	9.67	819.69
4 - Group 1	PPM	3.34	6.89	39.94	1.30	117.74	22.66	5.20	1.01	0.56	484.50	113.65	57.02	4.67	8.50	645.17
5 - Group 3	PPM	3.24	8.21	41.55	1.28	98.55	19.55	5.04	0.91	0.61	418.45	90.77	54.64	4.61	7.66	563.86
6 - Group 1	PPM	3.75	7.66	46.89	1.45	95.29	18.30	5.21	1.06	0.67	369.56	85.58	48.88	4.32	7.56	504.02
7 - Group 2	PPM	4.88	1.28	27.89	0.88	93.99	17.20	5.46	1.02	0.58	378.98	76.75	38.34	4.94	9.88	494.07
8 - Group 2	PPM	4.67	1.41	27.85	0.86	128.12	24.09	5.32	1.03	0.59	512.86	115.75	62.17	4.43	8.25	690.79
9 - Group 3	PPM	2.51	9.90	16.79	0.52	119.73	24.12	4.96	1.01	0.62	489.62	111.89	53.78	4.42	9.11	654.29
11 - Group 3	PPM	4.43	8.03	42.08	1.18	112.59	19.32	5.31	1.00	0.68	407.88	90.14	47.18	4.52	8.65	545.19
11 - Group 3	PPM	3.53	4.67	29.11	0.90	78.44	17.70	4.43	1.03	0.69	312.31	75.69	39.17	4.13	7.97	427.17
12 - Group 1	PPM	3.32	6.91	42.45	1.37	112.53	19.72	5.71	1.09	0.53	438.38	112.72	68.11	4.27	6.44	609.22
13 - Group 1	PPM	3.48	7.47	40.81	1.33	129.27	23.56	5.49	0.93	0.54	547.05	119.73	69.06	4.99	7.92	725.84
14 - Group 2	PPM	4.01	1.27	25.88	0.79	167.38	29.35	5.70	0.93	0.57	702.88	129.90	62.85	5.41	11.18	895.64
15 - Group 2	PPM	4.18	1.31	28.18	0.87	142.16	26.08	5.45	1.05	0.58	569.31	121.66	63.46	4.68	8.97	754.43

Table 20, annex 1. Ceramic samples, calculated values, part 2.

Laboratory reference - Chemical group		Calculated values														
		SiO_2/Al_2O_3	Fe_2O_3/TiO_2	Zr/U	Hf/U	Ce_{CN}	Eu_{CN}	Ce_{CN}/Eu_{CN}	Ce_{CN} anomly	EU_{CN} anomaly	$LREE_{CN}$	$MREE_{CN}$	$HREE_{CN}$	$LREE_{CN}/MREE_{CN}$	$LREE_{CN}/HREE_{CN}$	Sum REE_{CN}
16 - Group 2	**PPM**	5.04	1.39	27.22	0.86	142.06	26.68	5.32	1.04	0.64	559.36	123.80	57.86	4.52	9.67	741.02
17 - Group 1	**PPM**	4.25	6.88	48.90	1.59	88.99	15.54	5.73	1.06	0.55	352.54	72.71	41.89	4.85	8.42	467.15
18 - Group 1	**PPM**	3.58	6.44	47.65	1.53	128.39	23.02	5.58	1.11	0.65	486.28	98.47	50.44	4.94	9.64	635.19
19 - Group 1	**PPM**	3.24	5.71	29.93	0.97	119.07	21.97	5.42	0.97	0.62	482.67	95.52	56.53	5.05	8.54	634.71
20 - Group 1	**PPM**	3.45	5.76	31.59	1.02	134.41	21.63	6.21	0.96	0.54	550.48	112.87	59.79	5.35	9.21	713.14
21 - Group 1	**PPM**	3.75	6.83	41.15	1.33	98.30	18.00	5.46	1.03	0.53	403.33	91.52	58.09	4.41	6.94	552.93
22 - Group 1	**PPM**	3.13	8.06	48.40	1.50	112.44	20.93	5.37	1.04	0.65	443.87	88.96	44.21	4.99	11.04	577.04
23 - Group 1	**PPM**	3.44	7.42	58.65	1.66	131.66	21.48	6.13	1.09	0.60	498.03	112.76	51.57	4.85	9.66	652.35
24 - Group 1	**PPM**	3.68	6.97	56.48	1.74	113.07	21.29	5.31	1.03	0.64	450.07	99.18	53.08	4.54	8.48	602.32
25 - Group 1	**PPM**	3.36	7.94	32.15	1.01	119.43	19.48	5.62	0.93	0.57	463.69	83.81	44.31	5.53	11.46	591.80
26 - Group 1	**PPM**	3.30	7.09	51.87	1.67	118.42	21.67	5.00	1.07	0.56	431.31	117.96	69.17	3.99	6.24	608.44
27 - Group 1	**PPM**	3.56	9.26	24.94	0.83	116.68	17.89	5.96	0.93	0.56	447.79	76.38	39.88	5.86	11.23	564.05
28 - Group 1	**PPM**	3.50	6.50	32.16	1.03	124.46	19.23	6.47	1.06	0.50	492.76	96.86	53.05	5.09	9.29	642.68
29 - Group 1	**PPM**	3.57	7.13	44.98	1.41	120.58	21.34	5.65	1.04	0.63	475.77	92.76	40.32	5.13	11.80	608.84
30 - Group 1	**PPM**	4.60	6.23	43.86	1.37	114.85	17.89	5.86	1.02	0.53	424.11	91.04	53.37	4.66	7.95	568.51

Table 21, annex 1. Ceramic samples, calculated values, part 3.

Laboratory reference - Chemical group		Calculated values														
		SiO_2/Al_2O_3	Fe_2O_3/TiO_2	Zr/U	Hf/U	Ce_{CN}	Eu_{CN}	Ce_{CN}/Eu_{CN}	Ce_{CN} anomly	EU_{CN} anomaly	$LREE_{CN}$	$MREE_{CN}$	$HREE_{CN}$	$LREE_{CN}/MREE_{CN}$	$LREE_{CN}/HREE_{CN}$	Sum REE_{CN}
31 - Group 1	**PPM**	3.18	8.02	44.42	1.42	77.19	16.25	4.75	1.06	0.61	307.11	72.72	43.78	4.22	7.02	423.61
32 - Group 1	**PPM**	4.53	6.82	53.05	1.57	87.91	15.61	5.63	1.02	0.64	349.94	71.01	38.82	4.93	9.02	459.76
33 - Group 1	**PPM**	4.06	7.28	30.08	0.95	110.50	19.48	5.16	1.00	0.64	411.37	85.36	38.85	4.81	11.56	534.58
34 - Group 1	**PPM**	3.87	7.26	46.09	1.48	118.47	21.18	5.59	0.93	0.54	500.90	114.59	68.61	4.79	7.30	674.11
35 - Group 1	**PPM**	3.76	7.43	43.71	1.44	133.22	20.92	6.37	1.29	0.55	467.27	96.38	51.12	4.85	9.14	614.77
36 - Group 3	**PPM**	3.95	4.45	29.01	0.93	75.38	16.96	4.44	1.01	0.66	306.76	75.63	39.96	4.06	7.68	422.34
37 - Group 2	**PPM**	5.25	1.23	28.87	0.92	131.31	22.96	5.72	0.93	0.55	550.39	111.31	67.20	4.94	8.19	728.90
38 - Group 1	**PPM**	4.16	6.35	39.35	1.23	96.22	17.59	5.47	0.90	0.54	418.89	83.47	50.20	5.02	8.34	552.56
39 - Group 1	**PPM**	4.24	6.65	36.51	1.20	117.21	20.30	5.28	0.98	0.55	450.01	90.97	46.94	4.95	9.59	587.93
40 - Group 1	**PPM**	3.47	7.11	43.09	1.32	111.46	22.17	4.98	0.98	0.57	464.16	116.48	61.56	4.36	7.54	632.20
41 - Group 1	**PPM**	3.40	8.03	50.26	1.61	111.77	19.05	5.81	1.18	0.55	409.88	98.47	65.05	4.16	6.30	573.41
42 - Group 1	**PPM**	3.38	7.82	37.70	1.22	110.32	19.37	5.18	1.03	0.59	406.36	85.61	50.45	4.75	8.05	542.42
Mean Group 1	**PPM**	3.63	7.13	42.24	1.33	*111.54*	*19.94*	5.54	*1.03*	*0.58*	*444.40*	*92.74*	*52.28*	4.80	*8.68*	*589.42*
	St.Dev.	0.39	0.72	8.03	0.23	*14.03*	*2.13*	0.40	*0.08*	*0.05*	*55.39*	*11.60*	*9.21*	0.41	*1.46*	*68.76*
Mean Group 2	**PPM**	4.58	1.32	27.50	0.86	*136.67*	*24.55*	5.56	*0.99*	*0.58*	*558.05*	*114.42*	*59.61*	4.87	*9.40*	*732.08*
	St.Dev.	0.47	0.06	0.93	0.04	*21.22*	*3.54*	0.22	*0.05*	*0.03*	*93.21*	*16.32*	*9.09*	0.33	*0.97*	*115.49*
Mean Group 3	**PPM**	3.53	7.05	31.71	0.96	*94.94*	*19.53*	4.84	*0.99*	*0.65*	*387.00*	*88.62*	*46.94*	4.35	*8.21*	*522.57*
	St.Dev.	0.65	2.14	9.39	0.27	*16.38*	*2.49*	0.35	*0.04*	*0.03*	*69.24*	*12.95*	*6.56*	0.22	*0.57*	*88.00*

Table 22, annex 1. Sediment samples chemical composition obtained by XRF and L.O.I., major oxides, part 1.

Laboratory reference - Sediment tratment		Major oxides and L.O.I												
		Na_2O	MgO	Al_2O_3	SiO_2	P_2O_5	S	K_2O	CaO	TiO_2	Fe_2O_3	MnO	LOI	Sum
Ca1-URM	wt%	0.22	0.57	20.30	65.70	0.079	0.018	2.92	0.07	1.07	1.26	0.003	7.32	99.54
	Err. ±	*0.04*	*0.02*	*0.04*	*0.04*	*0.003*	*0.001*	*0.05*	*0.02*	*0.01*	*0.00*	*0.003*		
Ca1<500 µm	wt%	0.21	0.48	16.50	70.90	0.087	0.031	2.35	0.12	0.96	1.50	0.006	6.16	99.30
	Err. ±	*0.04*	*0.02*	*0.03*	*0.04*	*0.003*	*0.001*	*0.05*	*0.02*	*0.01*	*0.00*	*0.003*		
Ca1<250 µm	wt%	0.18	0.54	18.11	68.30	0.088	0.030	2.62	0.14	1.07	1.58	0.009	6.90	99.56
	Err. ±	*0.04*	*0.02*	*0.04*	*0.04*	*0.003*	*0.001*	*0.05*	*0.02*	*0.01*	*0.00*	*0.003*		
Ca1<125 µm	wt%	0.15	0.56	19.30	66.60	0.088	0.030	2.75	0.13	1.15	1.56	0.002	7.16	99.48
	Err. ±	*0.04*	*0.02*	*0.04*	*0.04*	*0.003*	*0.001*	*0.05*	*0.02*	*0.01*	*0.00*	*0.003*		
Ca1<63 µm	wt%	0.23	0.55	20.00	65.20	0.076	0.028	2.81	0.13	1.15	1.56	0.005	7.44	99.18
	Err. ±	*0.04*	*0.02*	*0.04*	*0.04*	*0.003*	*0.001*	*0.05*	*0.02*	*0.01*	*0.00*	*0.003*		
Mean Ca1	***wt%***	***0.20***	***0.54***	***18.84***	***67.34***	***0.08***	***0.028***	***2.69***	***0.12***	***1.08***	***1.49***	***0.00***	***7.00***	***99.41***
	St.Dev.	***0.03***	***0.03***	***1.39***	***2.07***	***0.01***	***0.005***	***0.20***	***0.02***	***0.07***	***0.12***	***0.00***	***0.46***	***0.15***
Ca2-URM	wt%	1.93	1.64	14.40	67.70	0.114	0.022	3.02	0.54	0.74	4.77	0.024	6.48	111.38
	Err. ±	*0.05*	*0.02*	*0.03*	*0.04*	*0.003*	*0.001*	*0.05*	*0.02*	*0.01*	*0.01*	*0.002*		
Ca2<500 µm	wt%	1.12	1.51	13.40	69.40	0.122	0.017	2.83	1.17	0.69	4.26	0.034	5.94	110.49
	Err. ±	*0.05*	*0.02*	*0.03*	*0.04*	*0.003*	*0.001*	*0.05*	*0.02*	*0.01*	*0.01*	*0.002*		
Ca2<250 µm	wt%	1.02	1.55	13.50	69.11	0.123	0.016	2.70	1.16	0.76	4.44	0.032	6.31	110.71
	Err. ±	*0.05*	*0.02*	*0.03*	*0.04*	*0.003*	*0.001*	*0.05*	*0.02*	*0.01*	*0.01*	*0.002*		
Ca2<125 µm	wt%	0.89	1.80	14.20	66.80	0.121	0.013	2.51	1.25	0.87	5.01	0.036	7.01	110.52
	Err. ±	*0.05*	*0.02*	*0.03*	*0.04*	*0.003*	*0.001*	*0.04*	*0.02*	*0.01*	*0.01*	*0.002*		
Ca2<63 µm	wt%	0.79	2.06	15.40	63.60	0.120	0.015	2.56	1.35	0.97	5.69	0.043	8.30	110.89
	Err. ±	*0.05*	*0.02*	*0.03*	*0.04*	*0.003*	*0.001*	*0.04*	*0.02*	*0.01*	*0.01*	*0.002*		
Mean Ca2	***wt%***	***1.15***	***1.71***	***14.18***	***67.32***	***0.120***	***0.016***	***2.72***	***1.09***	***0.81***	***4.83***	***0.034***	***6.81***	***110.80***
	St.Dev.	***0.41***	***0.20***	***0.72***	***2.09***	***0.003***	***0.003***	***0.19***	***0.28***	***0.11***	***0.50***	***0.006***	***0.82***	***0.33***
Ca3-URM	wt%	0.45	0.46	8.77	77.40	0.165	0.025	2.91	2.47	0.46	2.04	0.025	5.93	111.11
	Err. ±	*0.04*	*0.02*	*0.02*	*0.04*	*0.003*	*0.001*	*0.05*	*0.03*	*0.01*	*0.01*	*0.002*		
Ca3<500 µm	wt%	0.55	0.74	11.70	70.00	0.177	0.027	2.89	2.08	0.75	3.25	0.044	8.46	110.66
	Err. ±	*0.05*	*0.02*	*0.03*	*0.04*	*0.004*	*0.001*	*0.05*	*0.03*	*0.01*	*0.01*	*0.002*		
Ca3<250 µm	wt%	0.60	0.72	11.60	69.50	0.174	0.028	2.93	2.09	0.73	3.26	0.041	8.51	110.18
	Err. ±	*0.05*	*0.02*	*0.03*	*0.04*	*0.003*	*0.001*	*0.05*	*0.03*	*0.01*	*0.01*	*0.002*		
Ca3<125 µm	wt%	0.59	0.80	12.50	68.11	0.178	0.028	2.80	2.12	0.84	3.66	0.045	9.26	110.91
	Err. ±	*0.05*	*0.02*	*0.03*	*0.04*	*0.004*	*0.001*	*0.04*	*0.03*	*0.01*	*0.01*	*0.002*		
Ca3<63 µm	wt%	0.56	0.96	13.40	65.20	0.178	0.027	2.82	2.09	0.93	4.11	0.050	11.37	110.69
	Err. ±	*0.04*	*0.02*	*0.03*	*0.04*	*0.004*	*0.001*	*0.05*	*0.03*	*0.01*	*0.01*	*0.002*		
Mean Ca3	***wt%***	***0.55***	***0.74***	***11.59***	***70.04***	***0.174***	***0.027***	***2.87***	***2.17***	***0.74***	***3.26***	***0.041***	***8.51***	***110.71***
	St.Dev.	***0.05***	***0.16***	***1.55***	***4.04***	***0.005***	***0.001***	***0.05***	***0.15***	***0.16***	***0.69***	***0.009***	***1.46***	***0.31***
Ca4-URM	wt%	0.20	0.41	9.07	79.20	0.092	0.003	2.99	0.33	0.44	3.01	0.055	4.99	110.79
	Err. ±	*0.04*	*0.02*	*0.03*	*0.04*	*0.003*	*0.001*	*0.05*	*0.02*	*0.01*	*0.01*	*0.002*		
Ca4<500 µm	wt%	0.29	0.56	11.20	73.40	0.111	0.001	3.18	0.55	0.65	3.65	0.068	5.59	99.25
	Err. ±	*0.04*	*0.02*	*0.03*	*0.04*	*0.003*	*0.001*	*0.05*	*0.02*	*0.01*	*0.01*	*0.002*		
Ca4<250 µm	wt%	0.30	0.61	11.60	72.11	0.115	0.004	2.92	0.58	0.81	4.06	0.073	5.95	99.11
	Err. ±	*0.04*	*0.02*	*0.03*	*0.04*	*0.003*	*0.001*	*0.05*	*0.02*	*0.01*	*0.01*	*0.002*		
Ca4<125 µm	wt%	0.33	0.75	13.30	67.40	0.134	0.003	2.45	0.81	1.02	5.19	0.099	7.97	99.45
	Err. ±	*0.04*	*0.02*	*0.03*	*0.04*	*0.004*	*0.001*	*0.04*	*0.02*	*0.01*	*0.01*	*0.003*		
Ca4<63 µm	wt%	0.21	0.96	16.30	59.40	0.122	0.011	2.12	1.16	0.99	6.75	0.120	11.01	99.16
	Err. ±	*0.04*	*0.02*	*0.04*	*0.04*	*0.004*	*0.001*	*0.04*	*0.02*	*0.01*	*0.01*	*0.003*		
Mean Ca4	***wt%***	***0.27***	***0.66***	***12.29***	***70.30***	***0.111***	***0.004***	***2.73***	***0.69***	***0.78***	***4.53***	***0.083***	***7.11***	***99.55***
	St.Dev.	***0.05***	***0.19***	***2.41***	***6.62***	***0.015***	***0.003***	***0.39***	***0.28***	***0.22***	***1.32***	***0.023***	***2.20***	***0.63***
Ca5-URM	wt%	0.48	1.20	17.11	62.00	0.093	0.014	2.70	0.33	0.91	6.52	0.017	7.96	99.32
	Err. ±	*0.05*	*0.02*	*0.04*	*0.04*	*0.004*	*0.001*	*0.05*	*0.02*	*0.01*	*0.01*	*0.003*		
Ca5<500 µm	wt%	0.42	1.23	17.50	61.50	0.087	0.012	2.70	0.36	0.93	6.05	0.021	7.95	98.76
	Err. ±	*0.04*	*0.02*	*0.04*	*0.04*	*0.003*	*0.001*	*0.05*	*0.02*	*0.01*	*0.01*	*0.003*		
Ca5<250 µm	wt%	0.40	1.26	17.70	62.11	0.084	0.011	2.67	0.30	0.96	6.08	0.023	8.03	99.62
	Err. ±	*0.05*	*0.02*	*0.04*	*0.04*	*0.004*	*0.001*	*0.05*	*0.02*	*0.01*	*0.01*	*0.003*		
Ca5<125 µm	wt%	0.35	1.22	17.30	62.70	0.089	0.013	2.66	0.35	0.98	5.98	0.024	7.86	99.52
	Err. ±	*0.05*	*0.02*	*0.04*	*0.04*	*0.004*	*0.001*	*0.05*	*0.02*	*0.01*	*0.01*	*0.003*		
Ca5<63 µm	wt%	0.40	1.26	17.70	62.11	0.084	0.011	2.63	0.34	1.01	6.11	0.026	7.86	99.52
	Err. ±	*0.05*	*0.02*	*0.04*	*0.04*	*0.004*	*0.001*	*0.05*	*0.02*	*0.01*	*0.01*	*0.003*		
Mean Ca5	***wt%***	***0.41***	***1.23***	***17.46***	***62.08***	***0.087***	***0.012***	***2.67***	***0.34***	***0.96***	***6.15***	***0.022***	***7.93***	***99.35***
	St.Dev.	***0.04***	***0.02***	***0.23***	***0.38***	***0.004***	***0.001***	***0.03***	***0.02***	***0.04***	***0.19***	***0.003***	***0.06***	***0.31***

Table 23, annex 1. Sediment samples chemical composition obtained by XRF and L.O.I., major oxides, part 2.

Laboratory reference - Sediment tratment		Major oxides and L.O.I												
		Na_2O	MgO	Al_2O_3	SiO_2	P_2O_5	S	K_2O	CaO	TiO_2	Fe_2O_3	MnO	LOI	Sum
Ca6-URM	wt%	2.07	0.78	11.90	64.60	0.142	0.049	2.63	6.81	0.56	3.07	0.015	9.98	111.61
	Err. ±	*0.05*	*0.02*	*0.03*	*0.04*	*0.00*	*0.00*	*0.04*	*0.04*	*0.01*	*0.01*	*0.002*		
Ca6<500 µm	wt%	0.76	0.78	11.60	72.80	0.123	0.021	2.82	2.03	0.61	3.40	0.020	5.85	110.81
	Err. ±	*0.05*	*0.02*	*0.03*	*0.04*	*0.003*	*0.001*	*0.04*	*0.02*	*0.01*	*0.01*	*0.002*		
Ca6<250 µm	wt%	1.34	0.80	11.60	72.30	0.125	0.026	2.55	2.05	0.69	3.55	0.023	6.08	111.13
	Err. ±	*0.05*	*0.02*	*0.03*	*0.04*	*0.003*	*0.001*	*0.04*	*0.03*	*0.01*	*0.01*	*0.002*		
Ca6<125 µm	wt%	0.71	1.01	12.80	67.40	0.122	0.024	2.24	2.94	0.86	4.29	0.022	8.40	110.82
	Err. ±	*0.05*	*0.02*	*0.03*	*0.04*	*0.003*	*0.001*	*0.04*	*0.03*	*0.01*	*0.01*	*0.002*		
Ca6<63 µm	wt%	2.07	1.18	14.60	60.30	0.121	0.037	2.27	4.22	0.87	5.08	0.021	11.89	111.66
	Err. ±	*0.06*	*0.02*	*0.03*	*0.04*	*0.003*	*0.001*	*0.04*	*0.03*	*0.01*	*0.01*	*0.002*		
Mean Ca6	***wt%***	***1.39***	***0.91***	***12.30***	***67.48***	***0.127***	***0.032***	***2.50***	***3.61***	***0.72***	***3.88***	***0.020***	***8.24***	***111.21***
	St.Dev.	***0.60***	***0.16***	***1.30***	***4.72***	***0.008***	***0.011***	***0.22***	***1.79***	***0.13***	***0.72***	***0.003***	***2.02***	***0.37***
Ca7-URM	wt%	0.36	1.09	14.90	68.90	0.089	0.014	2.42	0.47	1.00	3.61	0.017	7.54	110.41
	Err. ±	*0.04*	*0.02*	*0.03*	*0.04*	*0.003*	*0.001*	*0.04*	*0.02*	*0.01*	*0.01*	*0.002*		
Ca7<500 µm	wt%	0.39	1.00	13.70	71.90	0.099	0.014	2.43	0.47	0.98	3.18	0.019	6.46	110.64
	Err. ±	*0.04*	*0.02*	*0.03*	*0.04*	*0.003*	*0.001*	*0.04*	*0.02*	*0.01*	*0.01*	*0.002*		
Ca7<250 µm	wt%	0.39	0.97	13.50	72.30	0.097	0.014	2.36	0.45	0.99	3.13	0.014	6.41	110.62
	Err. ±	*0.04*	*0.02*	*0.03*	*0.04*	*0.003*	*0.001*	*0.04*	*0.02*	*0.01*	*0.01*	*0.002*		
Ca7<125 µm	wt%	0.41	0.96	13.40	72.30	0.099	0.014	2.24	0.44	1.05	3.12	0.017	6.41	110.46
	Err. ±	*0.04*	*0.02*	*0.03*	*0.04*	*0.003*	*0.001*	*0.04*	*0.02*	*0.01*	*0.01*	*0.002*		
Ca7<63 µm	wt%	0.40	1.11	14.60	69.60	0.113	0.014	2.24	0.52	1.13	3.47	0.017	7.29	110.50
	Err. ±	*0.04*	*0.02*	*0.03*	*0.04*	*0.003*	*0.001*	*0.04*	*0.02*	*0.01*	*0.01*	*0.002*		
Mean Ca7	***wt%***	***0.39***	***1.03***	***14.02***	***71.00***	***0.097***	***0.014***	***2.34***	***0.47***	***1.03***	***3.30***	***0.017***	***6.82***	***110.53***
	St.Dev.	***0.02***	***0.06***	***0.61***	***1.45***	***0.005***	***0.000***	***0.08***	***0.03***	***0.06***	***0.20***	***0.002***	***0.49***	***0.09***
Ca8-URM	wt%	0.56	0.58	11.20	76.20	0.083		2.71	0.27	0.65	3.13	0.00	3.95	99.32
	Err. ±	*0.04*	*0.02*	*0.03*	*0.04*	*0.003*		*0.05*	*0.02*	*0.01*	*0.01*	*0.004*		
Ca8<500 µm	wt%	0.48	0.47	11.50	78.11	0.085		3.12	0.25	0.37	2.66	0.000	3.50	99.53
	Err. ±	*0.04*	*0.02*	*0.03*	*0.04*	*0.003*		*0.05*	*0.02*	*0.01*	*0.01*	*0.005*		
Ca8<250 µm	wt%	0.60	0.53	11.20	75.80	0.089		2.56	0.33	0.56	3.23	0.000	4.48	99.38
	Err. ±	*0.04*	*0.02*	*0.03*	*0.04*	*0.003*		*0.05*	*0.02*	*0.01*	*0.01*	*0.006*		
Ca8<125 µm	wt%	0.70	0.84	15.80	63.90	0.154		2.14	0.52	1.17	5.45	0.000	7.56	98.24
	Err. ±	*0.04*	*0.02*	*0.03*	*0.04*	*0.004*		*0.04*	*0.02*	*0.01*	*0.01*	*0.009*		
Ca8<63 µm	wt%	0.33	1.08	20.80	53.00	0.113		2.35	0.72	0.84	7.11	0.000	11.67	98.01
	Err. ±	*0.04*	*0.02*	*0.04*	*0.04*	*0.004*		*0.04*	*0.02*	*0.01*	*0.01*	*0.013*		
Mean Ca8	***wt%***	***0.53***	***0.70***	***13.90***	***69.40***	***0.115***		***2.58***	***0.42***	***0.72***	***4.32***	***0.000***	***6.23***	***98.90***
	St.Dev.	***0.13***	***0.23***	***3.93***	***9.61***	***0.027***		***0.33***	***0.18***	***0.27***	***1.70***	***0.000***	***3.07***	***0.64***
Ca9-URM	wt%	0.48	0.52	11.40	79.00	0.120	0.016	2.53	0.32	0.56	2.81	0.069	4.41	111.23
	Err. ±	*0.04*	*0.02*	*0.03*	*0.04*	*0.003*	*0.001*	*0.04*	*0.02*	*0.01*	*0.01*	*0.002*		
Ca9<500 µm	wt%	0.54	0.66	12.20	75.00	0.116	0.014	2.76	0.42	0.71	3.36	0.056	5.40	111.24
	Err. ±	*0.04*	*0.02*	*0.03*	*0.04*	*0.003*	*0.001*	*0.05*	*0.02*	*0.01*	*0.01*	*0.002*		
Ca9<250 µm	wt%	0.53	0.74	13.00	73.00	0.120	0.016	2.51	0.46	0.86	3.78	0.064	6.14	111.21
	Err. ±	*0.05*	*0.02*	*0.03*	*0.04*	*0.003*	*0.001*	*0.05*	*0.02*	*0.01*	*0.01*	*0.002*		
Ca9<125 µm	wt%	0.52	0.81	14.00	69.90	0.122	0.017	2.38	0.50	1.00	4.34	0.067	7.04	110.69
	Err. ±	*0.04*	*0.02*	*0.03*	*0.04*	*0.003*	*0.001*	*0.04*	*0.02*	*0.01*	*0.01*	*0.002*		
Ca9<63 µm	wt%	0.40	0.97	15.50	66.30	0.113	0.017	2.46	0.54	1.07	4.95	0.064	8.27	110.65
	Err. ±	*0.04*	*0.02*	*0.03*	*0.04*	*0.003*	*0.001*	*0.04*	*0.02*	*0.01*	*0.01*	*0.002*		
Mean Ca9	***wt%***	***0.49***	***0.74***	***13.02***	***72.64***	***0.12***	***0.016***	***2.53***	***0.45***	***0.84***	***3.85***	***0.064***	***6.25***	***111.00***
	St.Dev.	***0.05***	***0.15***	***1.71***	***4.33***	***0.00***	***0.001***	***0.13***	***0.07***	***0.19***	***0.75***	***0.005***	***1.33***	***0.27***

Table 24, annex 1. Sediment samples chemical composition obtained by ICP-MS, trace elements, part 1.

Laboratory reference - Sediment tratment		Trace elements																	
		Sc	V	Co	Ni	Cu	Zn	Ga	Rb	Sr	Y	Zr	Nb	Cs	Ba	Hf	Pb	Th	U
Ca1-URM	PPM	17.71	126.84	4.04	17.02	33.97	41.60	28.48	155.19	29.16	30.47	192.26	19.65	15.80	512.22	5.46	14.91	17.50	9.97
	RSD	*0.49*	*0.08*	*1.12*	*1.84*	*0.75*	*0.98*	*1.63*	*0.83*	*1.60*	*2.11*	*2.38*	*0.94*	*0.74*	*4.57*	*0.93*	*1.26*	*4.72*	*0.85*
Ca1<500 µm	PPM	13.20	111.66	4.00	15.90	26.09	51.37	23.83	142.78	29.39	25.62	171.94	17.12	14.76	419.17	4.86	18.33	13.03	6.65
	RSD	*4.23*	*1.14*	*1.66*	*2.26*	*1.44*	*1.20*	*1.69*	*1.14*	*1.34*	*1.16*	*0.36*	*1.08*	*1.57*	*1.53*	*1.97*	*0.84*	*1.33*	*1.29*
Ca1<250 µm	PPM	14.76	118.74	3.96	16.54	26.77	39.11	25.06	155.09	29.58	29.44	196.92	19.58	15.34	451.83	5.44	20.76	15.90	7.71
	RSD	*1.79*	*1.03*	*1.16*	*2.08*	*2.23*	*2.31*	*1.01*	*1.13*	*0.74*	*0.77*	*2.91*	*1.92*	*3.34*	*0.29*	*1.82*	*2.39*	*2.38*	*2.53*
Ca1<125 µm	PPM	15.98	114.82	4.08	17.58	29.37	42.26	26.39	156.87	28.97	30.88	217.77	21.11	15.99	480.00	5.75	21.27	16.31	8.69
	RSD	*2.12*	*0.38*	*1.34*	*0.96*	*1.19*	*1.85*	*0.70*	*1.72*	*1.18*	*1.37*	*1.83*	*2.06*	*3.02*	*1.97*	*1.20*	*3.42*	*2.34*	*3.49*
Ca1<63 µm	PPM	17.04	123.15	4.13	18.33	32.50	48.76	27.19	156.99	29.56	32.37	225.21	20.99	15.70	515.12	6.09	21.58	18.55	9.58
	RSD	*1.51*	*0.14*	*1.73*	*1.02*	*0.78*	*1.37*	*0.58*	*0.94*	*1.46*	*1.84*	*0.68*	*1.26*	*1.85*	*1.32*	*1.11*	*3.37*	*2.69*	*4.88*
Mean Ca1	PPM	***15.74***	***115.04***	***4.04***	***17.08***	***29.74***	***44.62***	***26.19***	***153.38***	***29.33***	***29.76***	***200.82***	***19.69***	***15.52***	***475.67***	***5.52***	***19.37***	***16.26***	***8.52***
	St.Dev.	***1.62***	***9.21***	***0.06***	***0.84***	***3.09***	***4.64***	***1.62***	***5.36***	***0.24***	***2.27***	***19.00***	***1.44***	***0.43***	***36.53***	***0.41***	***2.51***	***1.86***	***1.22***
Ca2-URM	PPM	11.46	98.73	11.99	33.24	21.79	98.71	21.51	167.62	54.57	19.21	155.80	15.52	11.54	412.27	4.54	19.70	12.52	2.68
	RSD	*1.81*	*0.81*	*0.36*	*1.67*	*0.42*	*0.68*	*0.80*	*0.47*	*0.69*	*2.91*	*4.36*	*0.09*	*2.89*	*3.63*	*0.49*	*4.53*	*3.13*	*1.20*
Ca2<500 µm	PPM	9.39	86.32	11.89	29.35	21.66	88.09	20.07	176.11	62.57	24.09	162.06	14.85	11.15	397.26	4.54	30.04	15.00	3.12
	RSD	*0.20*	*0.91*	*0.29*	*1.11*	*1.29*	*0.84*	*1.12*	*1.08*	*1.29*	*1.60*	*3.61*	*1.00*	*0.41*	*2.28*	*2.30*	*3.72*	*0.83*	*2.16*
Ca2<250 µm	PPM	9.74	92.64	11.59	31.27	22.85	123.11	20.37	163.40	61.44	23.65	166.61	15.79	11.36	400.03	4.68	23.71	16.21	3.15
	RSD	*3.14*	*0.32*	*0.36*	*0.28*	*0.33*	*0.65*	*1.39*	*0.73*	*0.77*	*1.18*	*3.55*	*0.58*	*1.14*	*2.00*	*4.94*	*3.57*	*5.81*	*5.24*
Ca2<125 µm	PPM	11.40	113.26	12.57	34.30	25.27	112.13	21.58	149.48	63.14	29.58	224.80	17.39	11.25	452.24	6.45	27.24	22.71	4.23
	RSD	*1.44*	*1.16*	*0.92*	*1.20*	*1.83*	*1.40*	*2.15*	*0.60*	*0.68*	*0.73*	*3.45*	*1.37*	*4.20*	*6.96*	*11.85*	*11.51*	*13.67*	*9.59*
Ca2<63 µm	PPM	12.01	122.29	14.16	38.87	28.40	117.92	23.49	147.40	68.92	27.64	223.79	17.77	11.62	448.72	6.22	27.72	19.57	4.12
	RSD	*8.17*	*0.04*	*0.99*	*1.64*	*0.97*	*1.12*	*0.73*	*1.78*	*1.35*	*11.82*	*7.82*	*1.06*	*1.53*	*0.58*	*1.01*	*2.02*	*5.58*	*0.67*
Mean Ca2	PPM	***11.60***	***110.65***	***12.24***	***33.40***	***23.99***	***115.99***	***21.41***	***160.80***	***62.13***	***24.83***	***186.61***	***16.26***	***11.19***	***422.11***	***5.29***	***25.68***	***17.20***	***3.46***
	St.Dev.	***0.99***	***12.24***	***1.11***	***3.21***	***2.56***	***12.83***	***1.20***	***11.91***	***4.58***	***3.58***	***30.96***	***1.12***	***0.31***	***23.74***	***0.86***	***3.61***	***3.57***	***0.61***
Ca3-URM	PPM	11.40	82.28	11.14	25.89	28.64	116.07	18.80	152.62	37.89	27.57	202.49	16.07	9.67	416.20	5.99	51.87	20.40	4.09
	RSD	*0.43*	*0.26*	*0.78*	*1.65*	*0.62*	*1.64*	*0.94*	*0.99*	*1.44*	*1.41*	*6.42*	*0.65*	*2.39*	*0.74*	*4.02*	*0.71*	*1.70*	*2.04*
Ca3<500 µm	PPM	11.13	74.69	11.12	23.43	26.24	85.04	17.64	145.83	38.09	25.65	177.12	15.74	8.97	384.60	5.42	49.82	18.64	3.61
	RSD	*4.70*	*1.42*	*1.89*	*2.28*	*1.68*	*0.97*	*0.45*	*1.74*	*0.76*	*1.71*	*2.27*	*1.39*	*1.47*	*2.08*	*1.72*	*2.69*	*5.61*	*2.02*
Ca3<250 µm	PPM	8.84	66.68	9.29	21.46	23.81	81.89	16.18	152.31	39.55	25.83	157.31	14.20	8.46	384.78	4.73	44.99	16.34	3.36
	RSD	*2.48*	*0.21*	*1.45*	*0.50*	*2.07*	*0.92*	*0.40*	*1.01*	*2.03*	*0.65*	*3.56*	*1.51*	*1.58*	*1.03*	*1.94*	*2.69*	*2.48*	*1.55*
Ca3<125 µm	PPM	8.68	68.30	9.43	21.88	23.87	84.78	16.91	145.05	38.08	23.97	155.84	14.61	8.38	366.68	4.47	44.60	19.97	3.36
	RSD	*1.94*	*0.33*	*0.44*	*0.68*	*1.06*	*1.02*	*1.89*	*1.98*	*2.55*	*0.68*	*2.17*	*1.14*	*3.70*	*1.91*	*0.97*	*2.68*	*1.44*	*1.41*
Ca3<63 µm	PPM	5.30	41.49	6.34	13.56	15.31	49.17	11.25	145.55	40.42	14.77	91.59	8.85	6.57	342.04	2.80	38.32	11.11	2.02
	RSD	*1.61*	*1.03*	*0.60*	*0.88*	*0.77*	*0.95*	*0.37*	*0.67*	*1.29*	*1.70*	*1.34*	*0.55*	*2.84*	*3.68*	*2.49*	*4.97*	*1.52*	*1.73*
Mean Ca3	PPM	***8.87***	***66.69***	***9.27***	***21.24***	***23.58***	***81.39***	***16.15***	***148.27***	***38.81***	***23.56***	***156.87***	***13.89***	***8.41***	***378.86***	***4.68***	***45.92***	***17.09***	***3.29***
	St.Dev.	***2.04***	***13.74***	***1.60***	***4.14***	***4.50***	***18.29***	***2.60***	***3.43***	***1.00***	***4.54***	***36.75***	***2.62***	***1.03***	***24.36***	***1.08***	***4.71***	***3.77***	***0.69***

Table 25, annex 1. Sediment samples chemical composition obtained by ICP-MS, trace elements, part 2.

Laboratory reference - Sediment tratment		Trace elements																	
		Sc	V	Co	Ni	Cu	Zn	Ga	Rb	Sr	Y	Zr	Nb	Cs	Ba	Hf	Pb	Th	U
Ca4-URM	PPM	4.81	41.50	8.13	14.76	9.43	47.51	13.81	162.59	38.85	16.76	126.61	11.17	7.98	387.65	3.76	27.44	15.23	2.50
	RSD	*5.75*	*0.82*	*0.85*	*0.99*	*0.76*	*0.87*	*1.11*	*0.37*	*0.59*	*1.46*	*0.52*	*0.43*	*3.45*	*1.20*	*2.94*	*5.18*	*5.01*	*2.82*
Ca4<500 µm	PPM	5.49	46.58	11.88	20.18	11.54	54.03	15.15	165.33	40.64	22.82	139.37	13.15	7.99	394.35	3.88	32.11	22.47	4.06
	RSD	*0.42*	*0.95*	*0.27*	*0.83*	*1.44*	*0.52*	*0.94*	*0.56*	*0.12*	*0.67*	*0.62*	*0.99*	*1.04*	*3.04*	*4.09*	*1.59*	*6.87*	*3.23*
Ca4<250 µm	PPM	5.79	53.08	12.32	22.57	13.22	59.69	17.11	160.68	38.82	27.82	183.54	14.94	8.68	392.21	4.92	32.38	36.93	5.14
	RSD	*3.20*	*0.82*	*1.79*	*0.86*	*0.73*	*0.71*	*0.30*	*0.79*	*0.92*	*2.65*	*2.34*	*0.65*	*1.90*	*6.31*	*2.51*	*3.87*	*3.59*	*2.31*
Ca4<125 µm	PPM	7.63	67.92	17.11	29.14	16.47	75.31	20.32	141.00	34.30	37.66	304.11	18.74	8.73	376.12	7.98	34.78	44.22	6.51
	RSD	*2.26*	*1.88*	*1.52*	*0.99*	*1.36*	*1.94*	*1.38*	*1.16*	*1.25*	*0.83*	*0.79*	*0.82*	*6.29*	*5.95*	*3.43*	*3.86*	*2.04*	*3.99*
Ca4<63 µm	PPM	9.45	88.96	24.14	38.86	20.96	93.81	23.53	133.09	29.60	38.41	308.69	17.55	9.89	389.54	8.17	37.99	35.38	5.90
	RSD	*4.27*	*0.76*	*0.67*	*1.29*	*1.11*	*0.31*	*0.62*	*0.41*	*1.48*	*1.91*	*3.51*	*0.42*	*1.72*	*1.68*	*3.68*	*2.96*	*4.07*	*3.67*
Mean Ca4	PPM	***6.63***	***59.61***	***14.52***	***25.11***	***14.32***	***66.07***	***17.98***	***152.54***	***36.44***	***28.69***	***212.46***	***15.11***	***8.66***	***387.97***	***5.74***	***32.94***	***30.85***	***4.82***
	St.Dev.	***1.69***	***17.15***	***5.63***	***8.29***	***4.04***	***16.64***	***3.54***	***12.98***	***4.01***	***8.39***	***79.00***	***2.78***	***0.69***	***6.35***	***1.95***	***3.47***	***11.49***	***1.42***
Ca5-URM	PPM	13.22	133.47	14.92	41.86	33.90	96.41	24.80	178.49	33.70	29.20	199.45	17.23	12.98	437.93	5.37	28.90	16.86	4.15
	RSD	*4.95*	*0.52*	*0.46*	*1.96*	*1.03*	*1.26*	*1.42*	*0.84*	*1.35*	*2.89*	*0.55*	*0.66*	*3.08*	*1.45*	*2.83*	*3.77*	*2.68*	*2.33*
Ca5<500 µm	PPM	14.32	129.32	12.38	41.01	30.86	98.11	24.65	184.48	33.81	30.27	208.47	17.14	13.76	417.91	5.57	33.48	16.14	3.82
	RSD	*0.64*	*1.50*	*1.35*	*1.01*	*1.82*	*1.17*	*1.31*	*0.83*	*1.72*	*0.62*	*4.18*	*1.32*	*4.22*	*4.29*	*4.32*	*2.17*	*6.19*	*5.06*
Ca5<250 µm	PPM	13.90	128.95	12.74	40.94	37.46	96.58	24.77	180.08	33.94	30.48	206.78	17.43	13.55	412.95	5.56	31.24	15.79	3.81
	RSD	*1.88*	*0.64*	*1.53*	*0.97*	*0.71*	*2.00*	*0.24*	*1.30*	*1.71*	*1.99*	*2.70*	*1.41*	*2.33*	*1.45*	*1.11*	*0.95*	*5.71*	*0.98*
Ca5<125 µm	PPM	13.96	128.39	13.73	40.85	31.28	99.62	24.72	176.18	35.45	29.31	203.99	18.20	13.33	411.60	5.49	30.80	16.48	3.78
	RSD	*1.27*	*0.76*	*0.87*	*1.61*	*0.86*	*1.11*	*0.78*	*0.33*	*0.79*	*1.61*	*2.65*	*0.25*	*3.48*	*2.28*	*2.64*	*1.65*	*3.11*	*3.83*
Ca5<63 µm	PPM	14.08	130.54	11.84	41.20	31.02	112.79	24.73	171.51	35.03	31.38	219.36	18.15	13.55	437.25	5.71	30.98	17.23	4.08
	RSD	*1.06*	*1.32*	*1.09*	*0.69*	*1.63*	*1.50*	*0.33*	*1.46*	*1.01*	*2.35*	*2.93*	*1.39*	*0.78*	*1.92*	*1.31*	*3.99*	*2.33*	*0.35*
Mean Ca5	PPM	***13.90***	***130.13***	***13.12***	***41.17***	***32.90***	***98.70***	***24.73***	***178.15***	***34.39***	***30.13***	***207.61***	***17.63***	***13.43***	***423.33***	***5.54***	***31.08***	***16.50***	***3.93***
	St.Dev.	***0.37***	***1.81***	***1.09***	***0.36***	***2.54***	***2.35***	***0.05***	***4.29***	***0.71***	***0.80***	***6.62***	***0.45***	***0.26***	***11.88***	***0.11***	***1.46***	***0.51***	***0.15***
Ca6-URM	PPM	7.34	51.17	7.35	18.15	12.92	62.32	15.40	161.70	32.55	18.50	127.39	13.25	11.27	302.76	3.52	17.31	9.85	2.14
	RSD	*2.16*	*0.86*	*0.71*	*2.18*	*1.59*	*1.19*	*0.76*	*1.57*	*0.88*	*1.32*	*3.00*	*1.78*	*4.63*	*1.54*	*0.31*	*0.64*	*3.73*	*0.27*
Ca6<500 µm	PPM	7.38	53.57	8.42	19.23	13.02	62.09	16.57	166.61	33.26	19.77	140.56	13.42	11.69	312.81	3.78	19.98	13.57	2.23
	RSD	*2.51*	*0.72*	*1.27*	*1.35*	*3.78*	*2.19*	*0.99*	*1.26*	*0.67*	*0.85*	*1.56*	*1.69*	*2.69*	*1.59*	*0.87*	*2.99*	*2.89*	*0.90*
Ca6<250 µm	PPM	7.80	57.25	7.91	20.97	14.06	68.62	16.75	149.24	32.95	24.41	176.39	14.99	11.51	316.23	4.42	19.40	14.11	2.59
	RSD	*2.66*	*0.63*	*1.01*	*1.15*	*2.11*	*1.34*	*0.71*	*1.40*	*0.74*	*1.09*	*2.13*	*2.48*	*1.99*	*1.93*	*1.33*	*2.04*	*3.89*	*0.34*
Ca6<125 µm	PPM	9.33	70.18	8.64	24.40	15.59	81.43	18.62	134.58	34.41	30.59	232.05	16.96	11.52	326.47	6.08	19.99	20.34	3.92
	RSD	*3.78*	*1.17*	*0.89*	*0.47*	*1.18*	*1.07*	*1.49*	*1.16*	*0.53*	*0.65*	*1.94*	*1.26*	*1.70*	*1.17*	*2.84*	*0.53*	*4.00*	*2.18*
Ca6<63 µm	PPM	11.45	84.03	9.66	29.02	18.11	94.72	20.97	127.86	34.37	34.30	270.18	16.51	11.95	378.11	6.87	19.95	20.23	4.02
	RSD	*1.77*	*0.40*	*0.50*	*0.20*	*0.77*	*0.24*	*0.45*	*1.02*	*0.45*	*0.42*	*2.76*	*1.37*	*0.41*	*2.51*	*0.89*	*1.67*	*1.95*	*1.39*
Mean Ca6	PPM	***8.66***	***63.24***	***8.39***	***22.35***	***14.74***	***73.83***	***17.66***	***148.00***	***33.51***	***25.52***	***189.31***	***15.03***	***11.99***	***327.27***	***4.93***	***19.33***	***15.62***	***2.98***
	St.Dev.	***1.57***	***12.29***	***0.77***	***3.95***	***1.94***	***12.58***	***1.95***	***14.97***	***0.75***	***6.11***	***54.30***	***1.53***	***0.45***	***26.52***	***1.31***	***1.03***	***4.08***	***0.82***

Table 26, annex 1. Sediment samples chemical composition obtained by ICP-MS, trace elements, part 3.

Laboratory reference - Sediment tratment		Trace elements																	
		Sc	V	Co	Ni	Cu	Zn	Ga	Rb	Sr	Y	Zr	Nb	Cs	Ba	Hf	Pb	Th	U
Ca7-URM	PPM	12.24	110.27	8.05	30.97	22.03	99.77	21.22	123.97	34.44	33.65	272.86	19.06	9.05	360.00	7.70	24.15	22.79	5.51
	RSD	*3.02*	*1.35*	*2.52*	*1.18*	*0.41*	*0.61*	*1.29*	*1.53*	*0.51*	*1.64*	*5.46*	*1.31*	*8.88*	*7.26*	*5.68*	*9.57*	*6.81*	*5.63*
Ca7<500 µm	PPM	11.84	87.74	8.07	28.05	20.51	89.41	19.55	132.01	33.29	31.93	247.76	18.64	11.18	356.03	7.17	24.04	23.64	5.13
	RSD	*2.07*	*1.39*	*1.18*	*0.73*	*0.62*	*0.53*	*1.04*	*0.89*	*1.02*	*1.44*	*1.11*	*0.67*	*5.79*	*1.85*	*3.73*	*6.22*	*3.33*	*3.29*
Ca7<250 µm	PPM	11.90	87.86	8.65	27.89	20.26	88.74	19.56	142.01	32.76	31.69	235.25	17.73	11.01	353.05	6.81	24.07	18.45	4.53
	RSD	*1.12*	*0.40*	*0.80*	*0.80*	*0.64*	*0.57*	*1.27*	*0.83*	*0.92*	*2.04*	*1.74*	*0.64*	*2.09*	*1.19*	*3.48*	*0.27*	*2.76*	*4.47*
Ca7<125 µm	PPM	11.87	88.69	12.24	28.78	20.85	92.11	20.00	145.28	33.15	29.69	222.71	17.81	11.34	356.72	6.80	26.14	19.47	4.75
	RSD	*1.42*	*0.97*	*1.63*	*1.18*	*0.73*	*0.42*	*0.24*	*1.34*	*0.40*	*1.36*	*3.32*	*0.59*	*2.29*	*1.69*	*2.42*	*3.54*	*5.23*	*3.02*
Ca7<63 µm	PPM	12.12	114.99	8.98	28.04	20.35	111.06	22.44	149.00	34.76	27.65	204.49	18.31	11.42	395.04	6.16	22.80	16.87	4.21
	RSD	*1.90*	*0.11*	*0.55*	*1.31*	*0.86*	*0.88*	*2.43*	*0.99*	*0.69*	*3.79*	*1.30*	*0.38*	*0.73*	*1.71*	*2.84*	*5.88*	*5.33*	*2.97*
Mean Ca7	PPM	***11.39***	***93.91***	***9.20***	***28.74***	***20.80***	***96.22***	***20.56***	***138.46***	***33.68***	***30.92***	***236.61***	***18.31***	***11.60***	***364.17***	***6.93***	***24.24***	***20.24***	***4.83***
	St.Dev.	***0.64***	***7.28***	***1.56***	***1.15***	***0.65***	***8.39***	***1.12***	***9.18***	***0.78***	***2.06***	***23.09***	***0.50***	***0.89***	***15.59***	***0.51***	***1.07***	***2.58***	***0.45***
Ca8-URM	PPM	6.11	44.44	7.40	21.73	15.54	62.57	14.78	162.03	27.98	21.15	160.40	14.82	11.23	477.33	4.68	26.29	16.95	3.63
	RSD	*2.36*	*0.85*	*0.56*	*1.83*	*1.24*	*0.69*	*0.95*	*1.62*	*1.67*	*1.58*	*4.34*	*1.31*	*4.18*	*1.70*	*1.29*	*3.37*	*3.91*	*1.39*
Ca8<500 µm	PPM	4.11	36.78	7.28	16.25	13.52	44.41	12.83	168.39	29.88	13.52	76.23	8.33	8.63	719.17	2.24	25.03	5.57	1.75
	RSD	*3.42*	*1.60*	*0.87*	*2.08*	*0.35*	*0.92*	*0.78*	*0.46*	*0.31*	*1.00*	*0.88*	*0.31*	*2.76*	*1.72*	*1.34*	*1.47*	*0.57*	*0.81*
Ca8<250 µm	PPM	5.01	47.52	9.52	20.69	16.90	53.40	13.99	124.50	26.48	16.46	120.03	11.75	7.85	898.25	3.54	25.07	9.55	2.60
	RSD	*0.52*	*0.69*	*0.74*	*2.21*	*2.49*	*3.46*	*0.86*	*2.72*	*0.36*	*0.64*	*2.79*	*2.15*	*0.43*	*2.00*	*1.68*	*1.61*	*5.46*	*1.51*
Ca8<125 µm	PPM	8.82	83.79	21.87	33.12	26.01	89.97	22.16	111.27	35.70	46.50	536.87	22.91	8.13	2390.08	11.86	51.89	45.66	11.05
	RSD	*3.40*	*0.95*	*0.48*	*1.86*	*1.48*	*1.27*	*0.37*	*1.68*	*0.91*	*1.70*	*35.39*	*1.27*	*2.82*	*2.55*	*1.53*	*2.86*	*1.40*	*1.92*
Ca8<63 µm	PPM	9.04	114.84	34.58	43.99	33.66	113.32	25.31	90.95	37.90	24.66	262.29	11.42	5.11	4120.75	7.56	85.87	19.22	5.61
	RSD	*2.06*	*0.75*	*0.42*	*0.88*	*0.61*	*0.67*	*1.11*	*1.39*	*1.52*	*1.09*	*2.80*	*1.92*	*1.61*	*2.03*	*0.70*	*3.22*	*3.92*	*0.68*
Mean Ca8	PPM	***6.62***	***65.48***	***16.13***	***27.16***	***21.13***	***70.73***	***17.82***	***131.23***	***31.59***	***24.46***	***231.16***	***13.84***	***7.99***	***1721.11***	***5.98***	***42.83***	***19.39***	***4.73***
	St.Dev.	***1.99***	***29.53***	***11.69***	***11.09***	***7.59***	***22.32***	***4.97***	***29.79***	***4.44***	***11.67***	***164.80***	***4.98***	***1.66***	***1373.59***	***3.43***	***23.84***	***14.03***	***2.96***
Ca9-URM	PPM	6.26	56.17	8.62	18.92	13.18	58.09	14.82	165.14	30.85	17.07	112.37	11.81	9.23	379.19	3.38	25.89	13.56	2.43
	RSD	*3.71*	*1.94*	*1.94*	*1.25*	*0.62*	*0.52*	*1.34*	*0.15*	*1.03*	*1.11*	*1.37*	*0.26*	*1.19*	*2.34*	*2.01*	*2.27*	*4.80*	*1.55*
Ca9<500 µm	PPM	7.87	70.09	9.47	22.47	16.19	71.71	18.25	187.67	34.43	25.82	174.43	14.52	11.43	415.66	4.80	30.71	19.50	3.33
	RSD	*2.91*	*0.53*	*0.47*	*1.15*	*1.01*	*1.20*	*2.70*	*1.82*	*1.41*	*0.09*	*2.04*	*0.28*	*4.40*	*1.37*	*2.41*	*2.41*	*0.81*	*2.41*
Ca9<250 µm	PPM	8.77	78.45	11.29	25.27	17.95	81.37	19.90	175.73	34.70	29.76	229.98	17.83	11.14	408.91	6.19	29.27	21.83	3.72
	RSD	*1.70*	*1.07*	*1.02*	*0.87*	*0.68*	*1.25*	*1.25*	*0.95*	*0.23*	*0.51*	*4.66*	*0.69*	*2.98*	*2.65*	*1.74*	*2.74*	*2.29*	*1.44*
Ca9<125 µm	PPM	11.43	91.89	11.56	29.27	20.05	92.27	22.06	169.39	34.03	35.45	266.01	18.50	13.52	477.07	7.97	32.48	30.36	5.15
	RSD	*2.82*	*1.21*	*1.57*	*0.85*	*1.78*	*1.39*	*1.45*	*1.23*	*1.99*	*2.66*	*5.06*	*3.50*	*7.17*	*6.67*	*8.73*	*7.91*	*7.34*	*8.80*
Ca9<63 µm	PPM	11.99	116.59	12.35	33.17	22.30	116.03	24.17	170.69	33.92	35.71	277.51	19.80	12.93	486.08	7.42	30.87	24.71	4.56
	RSD	*2.68*	*2.09*	*0.95*	*0.83*	*0.70*	*1.25*	*0.39*	*0.94*	*0.71*	*1.34*	*0.84*	*1.46*	*1.47*	*3.47*	*1.54*	*1.99*	*2.02*	*1.27*
Mean Ca9	PPM	***9.06***	***80.64***	***11.46***	***25.82***	***17.93***	***81.90***	***19.84***	***173.73***	***33.59***	***28.76***	***212.06***	***16.49***	***11.65***	***433.38***	***5.95***	***29.84***	***21.99***	***3.84***
	St.Dev.	***1.99***	***17.41***	***1.36***	***5.00***	***3.14***	***16.50***	***3.20***	***7.75***	***1.40***	***6.92***	***61.43***	***2.92***	***1.50***	***41.32***	***1.68***	***2.22***	***5.56***	***0.95***

Table 27, annex 1. Sediment samples chemical composition obtained by ICP-MS, rare earth elements, part 1.

Laboratory reference - Sediment treatment	PPM	Rare earth elements													
		La	Ce	Pr	Nd	Sm	Eu	Gd	Tb	Dy	Ho	Er	Tm	Yb	Lu
Ca1-URM	PPM	40.70	96.60	11.90	44.47	8.46	1.62	7.44	1.02	5.59	1.08	3.16	0.51	3.01	0.50
	RSD	*3.39*	*5.35*	*3.15*	*1.67*	*3.02*	*3.02*	*2.22*	*2.85*	*2.71*	*2.69*	*2.70*	*0.73*	*3.25*	*1.49*
Ca1<500 µm	PPM	36.53	81.44	9.99	34.27	6.91	1.30	5.98	0.82	4.55	0.89	2.60	0.41	2.48	0.41
	RSD	*3.84*	*1.90*	*2.39*	*1.99*	*1.58*	*1.72*	*2.27*	*2.22*	*1.81*	*2.20*	*1.86*	*2.00*	*2.29*	*1.53*
Ca1<250 µm	PPM	37.93	85.69	11.26	37.64	7.34	1.41	6.57	0.92	5.14	1.01	2.97	0.48	2.78	0.47
	RSD	*2.00*	*2.56*	*2.31*	*6.08*	*2.77*	*2.67*	*2.83*	*2.77*	*2.24*	*2.45*	*2.15*	*2.40*	*2.66*	*1.61*
Ca1<125 µm	PPM	41.23	91.59	11.47	42.48	8.03	1.51	7.04	0.99	5.48	1.08	3.15	0.50	2.98	0.49
	RSD	*1.16*	*2.37*	*0.74*	*5.67*	*1.41*	*2.03*	*2.88*	*2.42*	*1.77*	*1.85*	*2.89*	*1.20*	*2.64*	*0.71*
Ca1<63 µm	PPM	44.19	113.41	12.11	46.35	8.80	1.63	7.71	1.07	5.89	1.13	3.33	0.53	3.16	0.52
	RSD	*1.05*	*1.49*	*2.47*	*1.87*	*0.45*	*1.59*	*1.02*	*0.80*	*0.99*	*1.05*	*0.87*	*1.01*	*1.25*	*1.20*
Mean Ca1	**PPM**	***40.12***	***91.75***	***11.14***	***41.04***	***7.91***	***1.49***	***6.95***	***0.96***	***5.33***	***1.04***	***3.04***	***0.49***	***2.88***	***0.48***
	St.Dev.	***2.67***	***7.78***	***0.86***	***4.46***	***0.70***	***0.13***	***0.62***	***0.09***	***0.46***	***0.08***	***0.25***	***0.04***	***0.24***	***0.04***
Ca2-URM	PPM	29.46	65.72	11.47	33.59	5.78	0.99	4.79	0.64	3.28	0.61	1.86	0.33	1.82	0.27
	RSD	*3.97*	*3.63*	*3.94*	*1.45*	*1.15*	*1.94*	*2.89*	*3.24*	*0.31*	*0.26*	*2.06*	*3.29*	*3.11*	*0.60*
Ca2<500 µm	PPM	32.69	73.92	12.16	34.54	6.19	0.99	5.14	0.71	3.80	0.72	2.17	0.38	2.04	0.30
	RSD	*3.14*	*2.90*	*1.66*	*1.08*	*1.47*	*3.05*	*0.63*	*0.86*	*0.93*	*0.59*	*0.79*	*3.09*	*0.66*	*0.73*
Ca2<250 µm	PPM	33.88	77.33	12.39	36.81	6.74	1.02	5.52	0.76	3.90	0.73	2.16	0.36	2.00	0.29
	RSD	*2.44*	*3.30*	*5.19*	*3.43*	*0.98*	*0.81*	*0.29*	*0.86*	*0.25*	*1.29*	*0.16*	*3.73*	*0.94*	*0.50*
Ca2<125 µm	PPM	42.94	113.86	16.72	51.14	9.08	1.25	7.35	0.99	5.02	0.92	2.75	0.46	2.53	0.38
	RSD	*0.81*	*7.76*	*9.76*	*5.72*	*6.69*	*9.42*	*7.09*	*6.67*	*7.09*	*6.08*	*6.77*	*11.60*	*7.09*	*7.73*
Ca2<63 µm	PPM	40.68	90.27	14.70	43.00	7.91	1.18	6.41	0.86	4.51	0.83	2.51	0.43	2.40	0.36
	RSD	*1.94*	*3.66*	*4.74*	*1.89*	*0.45*	*4.26*	*1.85*	*0.73*	*1.40*	*1.21*	*3.31*	*1.76*	*0.89*	*3.73*
Mean Ca2	**PPM**	***35.93***	***82.22***	***13.29***	***39.81***	***7.14***	***1.09***	***5.84***	***0.79***	***4.11***	***0.76***	***2.29***	***0.39***	***2.16***	***0.32***
	St.Dev.	***5.07***	***13.40***	***2.18***	***6.54***	***1.20***	***0.11***	***0.93***	***0.12***	***0.60***	***0.11***	***0.31***	***0.05***	***0.26***	***0.04***
Ca3-URM	PPM	47.67	116.26	15.20	51.08	9.21	1.40	7.43	1.00	5.16	0.96	2.85	0.44	2.72	0.42
	RSD	*1.41*	*2.09*	*1.84*	*4.07*	*1.72*	*0.58*	*2.59*	*1.34*	*2.15*	*1.65*	*2.71*	*3.42*	*1.55*	*1.80*
Ca3<500 µm	PPM	40.33	89.22	13.74	42.08	7.82	1.17	6.34	0.86	4.53	0.85	2.52	0.41	2.37	0.36
	RSD	*2.08*	*1.97*	*1.82*	*2.25*	*1.42*	*2.32*	*0.37*	*0.74*	*0.43*	*0.41*	*0.39*	*2.31*	*0.64*	*1.02*
Ca3<250 µm	PPM	35.61	74.52	11.76	37.22	6.78	1.06	5.60	0.78	4.31	0.82	2.48	0.41	2.34	0.35
	RSD	*2.87*	*6.07*	*2.79*	*3.62*	*0.47*	*4.18*	*1.57*	*0.81*	*0.55*	*1.13*	*0.35*	*1.30*	*0.82*	*0.72*
Ca3<125 µm	PPM	40.57	89.57	13.49	42.59	7.61	1.07	6.07	0.81	4.18	0.77	2.28	0.36	2.07	0.31
	RSD	*2.91*	*2.18*	*1.72*	*3.12*	*1.26*	*1.12*	*2.77*	*2.44*	*1.49*	*2.68*	*1.87*	*1.36*	*1.37*	*2.20*
Ca3<63 µm	PPM	21.80	46.37	7.08	23.03	4.19	0.71	3.48	0.48	2.49	0.47	1.38	0.22	1.29	0.19
	RSD	*3.21*	*1.68*	*3.34*	*4.97*	*1.04*	*1.98*	*1.22*	*1.80*	*1.01*	*1.38*	*0.99*	*1.61*	*1.86*	*0.75*
Mean Ca3	**PPM**	***37.19***	***81.19***	***12.25***	***39.20***	***7.12***	***1.08***	***5.78***	***0.79***	***4.13***	***0.77***	***2.30***	***0.37***	***2.16***	***0.32***
	St.Dev.	***8.61***	***20.11***	***2.81***	***9.23***	***1.66***	***0.22***	***1.30***	***0.17***	***0.89***	***0.17***	***0.49***	***0.08***	***0.48***	***0.07***

Table 28, annex 1. Sediment samples chemical composition obtained by ICP-MS, rare earth elements, part 2.

Laboratory reference - Sediment treatment	PPM	Rare earth elements													
		La	Ce	Pr	Nd	Sm	Eu	Gd	Tb	Dy	Ho	Er	Tm	Yb	Lu
Ca4-URM	PPM	28.87	61.75	8.03	30.06	5.28	0.81	4.27	0.56	2.73	0.49	1.46	0.25	1.33	0.20
	RSD	*1.59*	*1.65*	*3.54*	*1.78*	*1.36*	*2.22*	*1.61*	*2.17*	*0.88*	*1.61*	*2.57*	*1.13*	*1.41*	*1.52*
Ca4<500 µm	PPM	38.32	81.68	11.88	41.65	7.07	0.92	5.74	0.75	3.60	0.65	1.85	0.31	1.63	0.24
	RSD	*1.89*	*3.17*	*4.98*	*1.44*	*2.32*	*2.63*	*1.25*	*1.08*	*1.18*	*0.78*	*1.42*	*3.75*	*1.91*	*1.09*
Ca4<250 µm	PPM	61.84	131.97	17.01	66.08	11.89	1.12	8.54	1.02	4.67	0.80	2.31	0.37	1.96	0.29
	RSD	*0.99*	*1.85*	*4.02*	*3.92*	*0.61*	*2.01*	*0.93*	*1.14*	*1.35*	*0.98*	*1.54*	*3.46*	*1.22*	*0.66*
Ca4<125 µm	PPM	78.95	172.41	21.54	84.05	13.91	1.39	11.99	1.35	6.16	1.09	3.18	0.53	2.75	0.41
	RSD	*3.64*	*4.83*	*0.76*	*2.31*	*2.66*	*4.33*	*2.91*	*3.22*	*2.58*	*2.69*	*3.07*	*3.39*	*2.29*	*1.79*
Ca4<63 µm	PPM	64.78	143.05	18.47	72.19	12.37	1.56	11.07	1.30	6.24	1.13	3.34	0.55	3.00	0.45
	RSD	*1.41*	*2.12*	*0.57*	*1.44*	*0.70*	*1.13*	*0.79*	*0.82*	*1.01*	*0.83*	*1.33*	*3.72*	*1.64*	*2.00*
Mean Ca4	**PPM**	***54.55***	***118.17***	***15.19***	***58.80***	***9.90***	***1.16***	***7.92***	***1.00***	***4.68***	***0.83***	***2.43***	***0.40***	***2.13***	***0.32***
	St.Dev.	***18.31***	***40.66***	***4.99***	***19.95***	***3.24***	***0.28***	***2.55***	***0.31***	***1.39***	***0.25***	***0.73***	***0.12***	***0.64***	***0.11***
Ca5-URM	PPM	39.51	86.32	11.67	41.63	7.77	1.34	6.51	0.90	4.69	0.89	2.68	0.46	2.58	0.38
	RSD	*1.07*	*0.65*	*2.18*	*2.07*	*0.39*	*2.01*	*1.73*	*0.67*	*1.11*	*0.31*	*0.73*	*3.06*	*1.03*	*1.80*
Ca5<500 µm	PPM	35.70	75.51	11.49	38.95	7.12	1.26	6.17	0.88	4.67	0.90	2.69	0.48	2.60	0.39
	RSD	*2.85*	*0.70*	*4.77*	*4.47*	*0.73*	*2.37*	*0.99*	*1.14*	*1.23*	*0.83*	*1.02*	*5.13*	*0.65*	*0.87*
Ca5<250 µm	PPM	38.09	78.33	11.16	38.56	7.04	1.28	6.07	0.86	4.62	0.89	2.70	0.49	2.57	0.38
	RSD	*4.48*	*3.17*	*1.72*	*0.64*	*0.69*	*4.90*	*2.43*	*1.33*	*1.86*	*2.04*	*1.98*	*0.23*	*0.84*	*1.20*
Ca5<125 µm	PPM	39.82	82.87	11.86	40.23	7.50	1.33	6.27	0.87	4.50	0.86	2.67	0.46	2.51	0.38
	RSD	*1.83*	*3.41*	*2.16*	*1.40*	*1.34*	*1.32*	*1.15*	*1.89*	*1.39*	*0.77*	*3.93*	*4.05*	*2.25*	*2.56*
Ca5<63 µm	PPM	41.07	85.07	11.11	43.74	7.91	1.36	6.65	0.93	4.93	0.92	2.79	0.49	2.66	0.40
	RSD	*2.62*	*4.99*	*1.20*	*3.92*	*1.19*	*2.00*	*1.74*	*1.28*	*1.02*	*1.48*	*0.90*	*1.17*	*1.97*	*1.23*
Mean Ca5	**PPM**	***38.84***	***81.62***	***11.65***	***40.62***	***7.47***	***1.31***	***6.33***	***0.89***	***4.68***	***0.89***	***2.71***	***0.48***	***2.58***	***0.39***
	St.Dev.	***1.83***	***4.09***	***0.32***	***1.89***	***0.34***	***0.04***	***0.21***	***0.03***	***0.14***	***0.02***	***0.05***	***0.01***	***0.05***	***0.01***
Ca6-URM	PPM	25.55	54.25	8.08	25.58	4.80	0.79	4.32	0.56	3.09	0.60	2.09	0.27	1.65	0.26
	RSD	*0.64*	*2.87*	*3.21*	*0.14*	*0.42*	*0.70*	*0.24*	*1.03*	*1.30*	*1.15*	*2.70*	*2.09*	*1.32*	*2.14*
Ca6<500 µm	PPM	32.39	73.53	11.31	32.38	5.83	0.85	4.97	0.61	3.17	0.61	2.11	0.27	1.64	0.26
	RSD	*3.14*	*2.78*	*5.49*	*3.98*	*2.00*	*1.26*	*1.01*	*2.49*	*2.44*	*1.77*	*4.26*	*1.24*	*1.30*	*0.92*
Ca6<250 µm	PPM	32.75	72.51	11.39	34.01	6.33	0.87	5.49	0.72	3.89	0.76	2.57	0.34	2.11	0.33
	RSD	*0.84*	*0.25*	*1.14*	*5.60*	*1.82*	*0.65*	*0.68*	*1.59*	*1.83*	*1.36*	*1.90*	*0.95*	*2.26*	*0.80*
Ca6<125 µm	PPM	48.99	118.78	15.53	49.03	9.12	1.15	7.93	0.99	5.12	0.99	3.33	0.43	2.63	0.42
	RSD	*1.05*	*2.66*	*6.81*	*1.40*	*0.76*	*0.57*	*1.74*	*1.11*	*0.61*	*0.41*	*1.26*	*2.71*	*0.93*	*1.64*
Ca6<63 µm	PPM	44.89	112.11	14.15	47.34	8.92	1.20	7.91	1.03	5.60	1.09	3.66	0.49	3.11	0.50
	RSD	*1.88*	*3.24*	*2.23*	*1.67*	*1.12*	*0.36*	*0.39*	*1.80*	*1.25*	*1.39*	*0.63*	*0.34*	*0.38*	*0.47*
Mean Ca6	**PPM**	***36.91***	***82.23***	***11.69***	***37.67***	***7.00***	***0.97***	***6.13***	***0.78***	***4.17***	***0.81***	***2.75***	***0.36***	***2.23***	***0.36***
	St.Dev.	***8.68***	***20.26***	***2.74***	***9.06***	***1.72***	***0.17***	***1.51***	***0.19***	***1.02***	***0.20***	***0.64***	***0.09***	***0.57***	***0.09***

Table 29, annex 1. Sediment samples chemical composition obtained by ICP-MS, rare earth elements, part 3.

Laboratory reference - Sediment treatment	PPM	Rare earth elements													
		La	Ce	Pr	Nd	Sm	Eu	Gd	Tb	Dy	Ho	Er	Tm	Yb	Lu
Ca7-URM	PPM	52.71	111.91	15.97	51.39	9.58	1.41	7.80	1.07	5.71	1.06	3.18	0.51	3.04	0.46
	RSD	*2.19*	*5.37*	*7.99*	*7.84*	*7.33*	*4.09*	*7.13*	*8.20*	*7.24*	*6.89*	*7.88*	*5.85*	*7.30*	*4.82*
Ca7<500 µm	PPM	51.75	119.02	16.33	51.34	9.61	1.34	7.77	1.07	5.67	1.06	3.14	0.49	2.94	0.44
	RSD	*1.86*	*4.30*	*2.17*	*3.38*	*1.34*	*2.95*	*0.53*	*0.58*	*0.80*	*1.29*	*0.73*	*3.45*	*1.26*	*0.30*
Ca7<250 µm	PPM	43.91	95.68	13.84	45.31	8.23	1.34	6.87	0.98	5.38	1.03	3.12	0.50	2.95	0.44
	RSD	*2.78*	*3.97*	*2.83*	*1.72*	*1.51*	*3.52*	*1.19*	*0.88*	*0.21*	*0.21*	*0.55*	*3.84*	*2.04*	*2.07*
Ca7<125 µm	PPM	42.60	90.83	14.21	42.77	8.00	1.28	6.66	0.94	5.09	0.97	2.91	0.49	2.74	0.41
	RSD	*1.81*	*2.46*	*3.82*	*0.84*	*0.51*	*1.26*	*1.62*	*1.47*	*1.28*	*0.43*	*1.60*	*2.91*	*1.34*	*1.27*
Ca7<63 µm	PPM	41.80	87.14	13.78	41.93	7.68	1.29	6.25	0.87	4.64	0.88	2.66	0.45	2.52	0.38
	RSD	*0.35*	*3.36*	*5.86*	*5.53*	*0.02*	*3.61*	*0.41*	*1.06*	*0.42*	*0.07*	*1.11*	*3.92*	*0.04*	*0.24*
Mean Ca7	PPM	***46.55***	***98.72***	***14.83***	***46.55***	***8.62***	***1.33***	***7.07***	***0.99***	***5.30***	***1.00***	***3.00***	***0.49***	***2.84***	***0.43***
	St.Dev.	***4.69***	***9.60***	***1.11***	***4.09***	***0.82***	***0.05***	***0.62***	***0.08***	***0.40***	***0.07***	***0.20***	***0.02***	***0.19***	***0.03***
Ca8-URM	PPM	34.81	76.14	11.05	34.76	6.42	0.80	5.65	0.69	3.62	0.70	2.41	0.31	1.91	0.31
	RSD	*0.65*	*2.19*	*2.02*	*0.55*	*1.61*	*0.53*	*1.08*	*2.04*	*1.38*	*2.14*	*1.81*	*0.18*	*2.14*	*0.83*
Ca8<500 µm	PPM	13.90	30.75	3.88	12.67	2.57	0.59	2.49	0.36	2.11	0.43	1.51	0.20	1.27	0.19
	RSD	*0.93*	*0.93*	*3.38*	*1.49*	*0.65*	*1.79*	*0.50*	*2.46*	*1.59*	*1.87*	*2.91*	*1.34*	*1.19*	*1.02*
Ca8<250 µm	PPM	20.68	53.14	6.36	19.47	3.88	0.68	3.57	0.48	2.72	0.55	1.90	0.25	1.56	0.24
	RSD	*1.24*	*2.31*	*2.25*	*3.66*	*3.86*	*0.50*	*2.00*	*2.53*	*4.07*	*3.59*	*3.54*	*2.07*	*4.77*	*2.26*
Ca8<125 µm	PPM	87.20	208.70	26.38	86.25	16.11	1.61	14.16	1.65	8.13	1.55	5.25	0.69	4.23	0.69
	RSD	*1.88*	*2.83*	*1.40*	*6.56*	*2.79*	*0.28*	*1.43*	*2.65*	*2.32*	*2.08*	*1.59*	*1.95*	*2.30*	*2.21*
Ca8<63 µm	PPM	38.42	97.76	12.32	45.24	8.65	1.79	7.72	0.99	5.07	0.97	3.15	0.41	2.70	0.43
	RSD	*2.83*	*0.92*	*3.44*	*0.48*	*2.14*	*0.17*	*0.37*	*1.00*	*2.03*	*1.73*	*2.24*	*0.66*	*1.35*	*0.46*
Mean Ca8	PPM	***39.00***	***93.30***	***12.00***	***39.68***	***7.52***	***1.11***	***6.72***	***0.83***	***4.33***	***0.84***	***2.84***	***0.37***	***2.33***	***0.37***
	St.Dev.	***25.72***	***61.90***	***7.81***	***25.93***	***4.77***	***0.50***	***4.13***	***0.46***	***2.15***	***0.40***	***1.32***	***0.17***	***1.06***	***0.18***
Ca9-URM	PPM	29.05	62.28	7.48	29.62	5.12	0.81	4.12	0.54	2.73	0.50	1.52	0.26	1.39	0.21
	RSD	*2.84*	*1.48*	*5.70*	*2.57*	*1.86*	*2.82*	*1.79*	*0.59*	*1.72*	*1.65*	*0.99*	*2.37*	*1.05*	*0.39*
Ca9<500 µm	PPM	39.55	85.59	11.41	41.67	6.94	0.96	5.74	0.78	3.98	0.75	2.25	0.39	2.05	0.30
	RSD	*6.03*	*4.11*	*6.49*	*0.75*	*1.34*	*2.97*	*1.30*	*1.28*	*1.49*	*1.14*	*0.75*	*1.85*	*1.25*	*1.80*
Ca9<250 µm	PPM	45.76	97.37	12.42	47.16	8.32	1.09	6.70	0.90	4.55	0.86	2.56	0.45	2.34	0.34
	RSD	*2.42*	*2.99*	*1.57*	*4.60*	*2.20*	*1.70*	*1.68*	*1.82*	*1.83*	*0.91*	*2.11*	*0.73*	*1.99*	*2.16*
Ca9<125 µm	PPM	59.50	125.60	16.23	61.09	11.72	1.38	8.84	1.20	6.03	1.14	3.40	0.59	3.08	0.45
	RSD	*11.61*	*8.29*	*11.05*	*8.14*	*9.15*	*9.20*	*8.30*	*7.98*	*8.70*	*7.84*	*9.50*	*8.51*	*7.09*	*7.53*
Ca9<63 µm	PPM	53.48	116.83	14.55	56.97	11.14	1.43	8.28	1.11	5.64	1.06	3.13	0.54	2.86	0.42
	RSD	*1.90*	*0.83*	*1.05*	*1.84*	*0.32*	*1.49*	*1.12*	*1.08*	*1.05*	*1.25*	*1.00*	*2.07*	*0.99*	*0.46*
Mean Ca9	PPM	***45.47***	***97.53***	***12.22***	***47.30***	***8.25***	***1.14***	***6.74***	***0.90***	***4.59***	***0.86***	***2.57***	***0.44***	***2.35***	***0.35***
	St.Dev.	***11.64***	***22.56***	***3.08***	***11.21***	***2.06***	***0.24***	***1.71***	***0.24***	***1.18***	***0.23***	***0.67***	***0.12***	***0.60***	***0.09***

Table 30, annex 1. Sediment samples, calculated values, part 1.

Laboratory reference - Sediment treatment		Calculated values														
		SiO_2/Al_2O_3	Fe_2O_3/TiO_2	Zr/U	Hf/U	Ce_{CN}	Eu_{CN}	Ce_{CN}/Eu_{CN}	Ce_{CN} anomly	EU_{CN} anomaly	$LREE_{CN}$	$MREE_{CN}$	$HREE_{CN}$	$LREE_{CN}/MREE_{CN}$	$LREE_{CN}/HREE_{CN}$	Sum REE_{CN}
Ca1-URM	**a.u.**	3.24	1.18	19.29	0.55	157.58	28.76	5.48	1.06	0.62	612.02	136.93	79.58	4.47	7.69	828.53
Ca1<500 µm	**a.u.**	4.30	1.56	25.87	0.73	132.85	23.02	5.77	1.03	0.61	516.31	111.62	64.80	4.67	7.97	691.74
Ca1<250 µm	**a.u.**	3.77	1.48	25.53	0.70	139.79	25.00	5.59	1.05	0.62	542.35	122.82	74.38	4.42	7.29	739.55
Ca1<125 µm	**a.u.**	3.45	1.36	25.07	0.66	149.41	26.75	5.59	1.02	0.61	594.11	131.52	78.51	4.52	7.57	804.15
Ca1<63 µm	**a.u.**	3.26	1.36	23.52	0.64	168.70	28.98	5.82	1.08	0.60	646.44	141.98	83.09	4.55	7.78	871.50
Mean Ca1	**a.u.**	***3.60***	***1.39***	***23.86***	***0.66***	***149.67***	***26.50***	***5.65***	***1.05***	***0.61***	***582.25***	***128.77***	***76.07***	***4.52***	***7.66***	***787.09***
	St.Dev.	***0.40***	***0.13***	***2.42***	***0.06***	***12.69***	***2.27***	***0.13***	***0.02***	***0.01***	***47.09***	***11.08***	***6.28***	***0.09***	***0.23***	***64.01***
Ca2-URM	**a.u.**	4.70	6.43	58.13	1.69	117.21	17.59	6.11	0.91	0.57	456.93	84.00	51.85	5.44	8.81	592.78
Ca2<500 µm	**a.u.**	5.18	6.17	51.89	1.45	120.58	17.60	6.85	0.90	0.54	506.96	91.72	55.08	5.53	9.20	653.76
Ca2<250 µm	**a.u.**	5.12	5.83	52.97	1.49	126.15	18.14	6.95	0.91	0.51	528.76	96.01	54.70	5.51	9.67	679.47
Ca2<125 µm	**a.u.**	4.70	5.75	53.11	1.52	169.44	22.17	7.64	0.94	0.47	704.00	123.74	62.83	5.69	11.21	890.57
Ca2<63 µm	**a.u.**	4.13	5.85	54.30	1.51	147.26	20.89	7.05	0.89	0.50	624.86	111.50	54.15	5.65	11.54	789.51
Mean Ca2	**a.u.**	**4.77**	**6.01**	**54.08**	**1.53**	***134.13***	***19.28***	**6.92**	***0.91***	***0.52***	***564.30***	***111.19***	***55.72***	**5.56**	**11.09**	***721.22***
	St.Dev.	***0.38***	***0.26***	***2.16***	***0.08***	***21.87***	***1.90***	***0.49***	***0.02***	***0.04***	***88.61***	***14.20***	***3.73***	***0.09***	***1.09***	***115.96***
Ca3-URM	**a.u.**	8.83	4.41	49.48	1.46	173.34	24.79	6.99	0.96	0.51	712.23	128.41	64.75	5.55	11.00	905.39
Ca3<500 µm	**a.u.**	5.98	4.36	49.08	1.50	145.54	20.78	7.00	0.92	0.51	608.65	111.38	60.17	5.51	11.12	779.21
Ca3<250 µm	**a.u.**	5.99	4.48	46.80	1.41	121.57	18.86	6.45	0.88	0.53	525.88	111.20	58.71	5.20	8.96	685.79
Ca3<125 µm	**a.u.**	5.45	4.38	46.34	1.33	146.11	18.96	7.71	0.93	0.48	607.22	112.92	58.45	5.90	11.39	768.58
Ca3<63 µm	**a.u.**	4.87	4.41	45.35	1.39	75.65	12.54	6.03	0.90	0.56	322.62	61.99	41.78	5.20	7.72	426.39
Mean Ca3	**a.u.**	**6.22**	**4.41**	**47.41**	**1.42**	***132.44***	***19.19***	**6.84**	***0.92***	***0.52***	***555.32***	***110.98***	***56.77***	**5.47**	**9.64**	***713.07***
	St.Dev.															

Table 31, annex 1. Sediment samples, calculated values, part 2.

Laboratory reference - Sediment treatment		Calculated values														
		SiO_2/Al_2O_3	Fe_2O_3/TiO_2	Zr/U	Hf/U	Ce_{CN}	Eu_{CN}	Ce_{CN}/Eu_{CN}	Ce_{CN} anomly	EU_{CN} anomaly	$LREE_{CN}$	$MREE_{CN}$	$HREE_{CN}$	$LREE_{CN}/MREE_{CN}$	$LREE_{CN}/HREE_{CN}$	Sum REE_{CN}
Ca4-URM	**a.u.**	8.73	6.90	50.66	1.50	110.74	14.44	6.98	0.98	0.52	411.51	71.42	35.41	5.75	11.59	517.34
Ca4<500 µm	**a.u.**	6.55	5.59	34.31	0.96	133.25	16.32	8.17	0.97	0.44	551.06	92.37	43.88	5.97	12.56	687.31
Ca4<250 µm	**a.u.**	6.22	5.04	35.71	0.96	215.28	19.88	11.83	0.98	0.35	877.61	124.87	53.30	7.03	16.47	1155.78
Ca4<125 µm	**a.u.**	5.07	5.09	46.71	1.23	281.25	24.61	11.43	1.01	0.34	1124.42	162.27	75.26	6.93	14.94	1361.95
Ca4<63 µm	**a.u.**	3.64	6.81	52.35	1.39	233.35	27.69	8.43	1.00	0.43	947.30	160.29	79.74	5.91	11.88	1187.33
Mean Ca4	**a.u.**	**6.04**	**5.89**	**43.95**	**1.21**	***192.77***	***20.59***	**9.16**	***0.99***	***0.42***	***782.18***	***122.25***	***57.52***	***6.32***	***13.49***	***961.94***
	St.Dev.	***1.69***	***0.82***	***7.54***	***0.22***	***66.32***	***4.96***	***1.69***	***0.02***	***0.07***	***262.70***	***36.14***	***17.33***	***0.55***	***1.90***	***313.91***
Ca5-URM	**a.u.**	3.63	7.20	48.11	1.30	140.82	23.86	5.90	1.02	0.58	566.03	117.11	67.06	4.83	8.44	750.19
Ca5<500 µm	**a.u.**	3.51	6.52	54.59	1.46	123.18	22.33	5.52	0.94	0.58	520.17	112.98	68.19	4.60	7.63	701.34
Ca5<250 µm	**a.u.**	3.51	6.37	54.22	1.46	127.79	22.74	5.62	0.96	0.60	529.97	112.28	68.05	4.72	7.79	711.31
Ca5<125 µm	**a.u.**	3.62	6.13	54.01	1.45	135.18	23.69	5.71	0.96	0.59	558.88	113.36	66.34	4.93	8.43	738.57
Ca5<63 µm	**a.u.**	3.51	6.04	53.75	1.40	138.78	24.07	5.76	0.96	0.57	580.92	120.19	70.01	4.83	8.30	771.13
Mean Ca5	**a.u.**	**3.56**	**6.45**	**52.93**	**1.41**	***133.15***	***23.34***	**5.70**	***0.97***	***0.58***	***551.20***	***115.18***	***67.93***	**4.78**	**8.12**	***734.31***
	St.Dev.	**0.06**	**0.41**	**2.43**	**0.06**	***6.68***	***0.68***	**0.13**	***0.02***	***0.01***	***22.70***	***3.01***	***1.24***	**0.11**	**0.34**	***25.65***
Ca6-URM	**a.u.**	5.93	5.49	59.45	1.64	88.50	13.98	6.33	0.91	0.53	371.78	74.95	44.75	4.96	8.31	491.48
Ca6<500 µm	**a.u.**	6.28	5.54	62.91	1.69	119.96	15.01	7.99	0.97	0.48	477.95	80.99	44.98	5.90	11.63	603.92
Ca6<250 µm	**a.u.**	6.23	5.18	68.23	1.71	118.28	15.48	7.64	0.95	0.45	485.55	92.78	56.27	5.23	8.63	634.61
Ca6<125 µm	**a.u.**	5.27	4.97	59.15	1.55	177.46	20.42	8.69	0.95	0.41	720.43	126.70	71.81	5.69	11.03	918.94
Ca6<63 µm	**a.u.**	4.13	5.83	67.13	1.71	166.55	21.40	7.78	0.98	0.44	672.32	132.41	82.28	5.08	8.17	887.00
Mean Ca6	**a.u.**	**5.57**	**5.40**	**63.37**	**1.66**	***134.15***	***17.26***	**7.69**	***0.95***	***0.46***	***545.61***	***111.57***	***60.02***	**5.37**	**9.15**	***707.19***
	St.Dev.	**0.80**	**0.30**	**3.77**	**0.06**	***33.05***	***3.04***	**0.77**	***0.02***	***0.04***	***130.40***	***23.63***	***14.88***	**0.36**	**0.99**	***167.11***

Table 32, annex 1. Sediment samples, calculated values, part 3.

Laboratory reference - Sediment treatment		Calculated values														
		SiO_2/Al_2O_3	Fe_2O_3/TiO_2	Zr/U	Hf/U	Ce_{CN}	Eu_{CN}	Ce_{CN}/Eu_{CN}	Ce_{CN} anomly	EU_{CN} anomaly	$LREE_{CN}$	$MREE_{CN}$	$HREE_{CN}$	$LREE_{CN}/MREE_{CN}$	$LREE_{CN}/HREE_{CN}$	Sum REE_{CN}
Ca7-URM	**a.u.**	4.62	3.63	49.52	1.40	180.94	25.04	7.23	0.92	0.50	752.63	136.64	78.11	5.51	9.64	967.36
Ca7<500 µm	**a.u.**	5.25	3.25	48.33	1.40	177.85	23.78	7.48	0.91	0.47	749.43	134.93	75.74	5.55	9.90	960.09
Ca7<250 µm	**a.u.**	5.36	3.16	51.98	1.51	156.08	23.75	6.57	0.94	0.54	645.24	126.22	76.09	5.11	8.48	847.54
Ca7<125 µm	**a.u.**	5.40	2.97	46.86	1.43	148.17	22.65	6.54	0.89	0.53	628.61	120.70	71.85	5.21	8.75	821.16
Ca7<63 µm	**a.u.**	4.77	3.07	48.53	1.46	142.16	22.83	6.23	0.88	0.57	611.70	113.28	65.93	5.39	9.26	789.91
Mean Ca7	**a.u.**	**5.08**	**3.22**	**49.04**	**1.44**	***161.04***	***23.61***	**6.81**	***0.91***	***0.52***	***677.32***	***126.35***	***73.54***	**5.35**	**9.20**	***877.22***
	St.Dev.	**0.32**	**0.23**	**1.70**	**0.04**	***15.65***	***0.85***	**0.47**	***0.02***	***0.03***	***61.17***	***8.74***	***4.31***	**0.17**	**0.53**	***72.99***
Ca8-URM	**a.u.**	6.80	4.82	44.17	1.29	124.21	14.25	8.72	0.94	0.41	509.57	89.15	52.14	5.72	9.77	650.86
Ca8<500 µm	**a.u.**	7.44	7.29	43.54	1.28	50.16	11.54	4.76	1.01	0.72	195.76	49.43	33.46	3.96	5.85	278.65
Ca8<250 µm	**a.u.**	6.77	5.73	46.22	1.36	86.68	12.16	7.13	1.12	0.56	311.33	64.50	41.48	4.83	7.51	417.31
Ca8<125 µm	**a.u.**	4.04	4.66	53.43	1.18	340.45	28.62	11.89	1.05	0.33	1290.13	207.05	115.17	6.23	11.20	1612.36
Ca8<63 µm	**a.u.**	2.55	8.50	46.75	1.35	159.48	31.75	5.02	1.09	0.67	611.74	136.31	70.33	4.49	8.70	818.38
Mean Ca8	**a.u.**	**5.52**	**6.20**	**46.82**	**1.29**	***152.20***	***19.46***	**7.50**	***1.04***	***0.53***	***583.71***	***119.29***	***62.52***	**5.04**	**8.61**	***755.51***
	St.Dev.	**1.89**	**1.48**	**3.52**	**0.06**	***110.97***	***8.89***	**2.63**	***0.06***	***0.15***	***382.11***	***57.07***	***29.08***	**0.82**	**1.84**	***467.09***
Ca9-URM	**a.u.**	7.60	5.04	46.23	1.39	111.59	14.32	7.09	1.02	0.54	404.19	70.33	36.98	5.75	11.93	511.50
Ca9<500 µm	**a.u.**	6.15	4.71	52.32	1.44	139.63	17.14	8.15	1.02	0.47	556.75	97.35	54.65	5.72	11.19	708.75
Ca9<250 µm	**a.u.**	5.62	4.40	61.82	1.66	158.84	19.43	8.17	0.99	0.45	645.17	112.22	62.58	5.75	11.31	819.97
Ca9<125 µm	**a.u.**	4.99	4.36	51.69	1.55	204.89	24.52	8.36	0.98	0.43	837.00	147.45	82.90	5.68	11.11	1167.35
Ca9<63 µm	**a.u.**	4.28	4.63	60.82	1.63	190.58	25.44	7.49	1.01	0.48	766.18	140.13	76.31	5.47	11.04	982.62
Mean Ca9	**a.u.**	**5.73**	**4.63**	**54.58**	**1.53**	***159.11***	***20.17***	**7.85**	***1.00***	***0.47***	***641.86***	***113.49***	***62.68***	***5.67***	***11.31***	***818.04***
	St.Dev.	***1.12***	***0.25***	***5.91***	***0.11***	***36.81***	***4.26***	***0.48***	***0.02***	***0.04***	***153.15***	***28.24***	***16.25***	***0.11***	***0.32***	***197.56***

Annexe 2 - section 5.2

Annexes are inserted in the following order:

- Ceramics sample list with samples archaeological reference, archaeological context of discovery, chronology, samples typology and decoration style, samples function and provenance.
- PLM description of ceramic thin sections with matrix, porosity, and temper characteristics.
- XRF and ICP-MS data for ceramics

Table 1, annex 2. List of the ceramic samples analysed with the indication of the sample reference, the recovering context (stratigraphic unit, [U.S.]), the chronology, the typology, the decoration and the archaeological site. SICh = Church of Santa Iria, RCO = Avenida 5 de Outubro, n.º 2-8, RJA = Rua João de Afonso.

Sample reference [U.S.]-n°	Archaeological context-[U.S.]	Chronology - century	Typology	Function	Decoration	Arch. site
LSI04-228	*Silo*	*8th - 9th*	*Pot*	*Fire ceramic*	*Unpainted*	*SICh*
LSI04-229	*Silo*	*8th - 9th*	*Pot*	*Fire ceramic*	*Unpainted*	*SICh*
LSI04-232	*Silo*	*8th - 9th*	*Pot*	*Fire ceramic*	*Unpainted*	*SICh*
LSI04-233	*Silo*	*8th - 9th*	*Pot*	*Fire ceramic*	*Unpainted*	*SICh*
LSI04-236	*Silo*	*8th - 9th*	*Pot*	*Fire ceramic*	*Unpainted*	*SICh*
[1368]-11000	*Kiln 1-[1720]*	*11th - 12th*	*Unclassified ceramic samples*	*-*	*White painted*	*RCO*
[1368-11002	*Kiln 1-[1720]*	*11th - 12th*	*Unclassified ceramic samples*	*-*	*White painted*	*RCO*
[1368]-11004	*Kiln 1-[1720]*	*11th - 12th*	*Unclassified ceramic samples*	*-*	*White painted*	*RCO*
[1368]-9999	*Kiln 1-[1720]*	*11th - 12th*	*Unclassified ceramic samples*	*-*	*White painted*	*RCO*
[1335]-9818	*Kiln 1-[1720]*	*11th - 12th*	*Unclassified ceramic samples*	*-*	*Unpainted*	*RCO*
[2041]-13884	*Kiln 2-[2046]*	*11th - 12th*	*Unclassified ceramic samples*	*-*	*White painted*	*RCO*
[2041]-13885	*Kiln 2-[2046]*	*11th - 12th*	*Unclassified ceramic samples*	*-*	*White painted*	*RCO*
[1117]-8202	*Silo-[2467]*	*11th - 12th*	*Bowl*	*Kitchen ceramic*	*White painted*	*RCO*
[1117]-8209	*Silo-[2467]*	*11th - 12th*	*Jug*	*Liquid container*	*CSP*	*RCO*
[1117]-8197	*Silo-[2467]*	*11th - 12th*	*Jug*	*Liquid container*	*Unpainted*	*RCO*
[973]-7561	*Silo-[2467]*	*11th - 12th*	*Jug*	*Liquid container*	*Unpainted*	*RCO*
[1359]-9939	*Silo-[1378]*	*11th - 12th*	*Bowl*	*Kitchen ceramic*	*Unpainted*	*RCO*
[1359]-9930	*Silo-[1378]*	*11th - 12th*	*Pan*	*Fire ceramic*	*Unpainted*	*RCO*
[473]-4458	*Silo-[470]*	*11th - 12th*	*Jug*	*Liquid container*	*White painted*	*RCO*
[473]-4453	*Silo-[470]*	*11th - 12th*	*Pot*	*Fire ceramic*	*White painted*	*RCO*
[1130]-7712	*Kiln 3-[1576]*	*12th - 13th*	*Unclassified ceramic samples*	*-*	*White painted*	*RCO*
[1130]-7716	*Kiln 3-[1576]*	*12th - 13th*	*Unclassified ceramic samples*	*-*	*White painted*	*RCO*
[1130]-7714	*Kiln 3-[1576]*	*12th - 13th*	*Unclassified ceramic samples*	*-*	*Unpainted*	*RCO*
[91]-1977	*Silo-[2466]*	*13th*	*Jug*	*Liquid container*	*Unpainted*	*RCO*
[91]-1980	*Silo-[2466]*	*13th*	*Pot*	*Fire ceramic*	*Unpainted*	*RCO*
[91]-1992	*Silo-[2466]*	*13th*	*Cover*	*Fire ceramic*	*White painted*	*RCO*
[91]-1994	*Silo-[2466]*	*13th*	*Cooker*	*Fire ceramic*	*White painted*	*RCO*
[973]-7560	*Silo-[2467]*	*11th - 12th*	*Jug*	*Liquid container*	*Red painted*	*RCO*
[508]-4967	*Silo-[520]*	*11th - 12th*	*Bowl*	*Kitchen ceramic*	*Mon. Glaze*	*RCO*
[2244]-15043	*Silo-[2171]*	*13th*	*Jug*	*Liquid container*	*Unpainted*	*RCO*
[2171]-14751	*Silo-[2171]*	*13th*	*Bowl*	*Kitchen ceramic*	*Honey and black*	*RCO*
[571]-5517	*Silo-[476]*	*12th - 13th*	*Pot*	*Fire ceramic*	*Unpainted*	*RCO*
[571]-5516	*Silo-[476]*	*12th - 13th*	*Jug*	*Liquid container*	*Red painted*	*RCO*
[1]-15467	*Surface cleaning-[1]*	*15th - 16th*	*Undetermined*	*-*	*White painted*	*RCO*
[939]-7351	*Metal. Activity-[939]*	*15th*	*Jug*	*Liquid container*	*White painted*	*RCO*
Vala37	*Kiln 4-[11]*	*11th - 12th*	*Bowl*	*Kitchen ceramic*	*CST*	*RJA*

Table 2, annex 2. Ceramic samples matrix and porosity characteristics. H.HOM., highly homogeneous – M.HOM., moderately homogeneous – S.HOM., slightly homogeneous – H.HET., highly heterogeneous – M.HET., moderately heterogeneous – S.HET., slightly heterogeneous. Fe- Ca rich matrix: Fe, iron rich matrix – S.Ca, slightly calcitic – M. Ca, moderately calcitic – H.Ca., Highly calcitic. Part 1.

Sample reference [U.S.]-n°	Fabric	Subgroup	Matrix						Porosity
			Colour	Homogeneity/heterogeneity	Fe / Ca rich matrix	Matrix Activity	Clay pellets	Oxides	Description
LSI04-233	***1***	***B***	Red brown	H.Hom.	Fe	Moderate		X	Meso-macro vughs and elongated voids
LSI04-229	***1***	***B***	Red-brown	M.Hom.	Fe	Moderate		X	Meso vesicles, channels and voids
LSI04-228	***1***	***B***	Brown	S.Hom.	Fe	Slightly active		X	Macro and mega vughs, and channels
LSI04-236	***1***	***B***	Brown-red	M.Hom.	Fe	Slightly active	X	X	Macro and mega vughs and channels
LSI04-232	***1***	***B***	Brown-red	M.Hom.	Fe	Moderate		X	Meso-macro vughs and vesicles
[1368]-11000	***1***	***A***	Red	M.Hom.	Fe	Moderate	X	X	Meso-macro vughs-channels and vesicles + macro elongated voids
[1368]-11002	***2***	***B***	Brown	S.Het.	S.Ca	Moderate		X	Meso vughs and voids + macro elongated and planar voids
[1368]-11004	***2***	***B***	Brown	S.Het.	S.Ca	Moderate		X	Meso vughs, vesicles and planar voids
[1368]-9999	***1***	***A***	Red	M.Hom.	Fe	Moderate	X	X	Meso vesicles, vughs, channels
[1335]-9818	***ND***	***ND***	Red-light brown	H.Het.	Fe+H.Ca	Highly active	X	X	Meso vesicles, vughs, planar voids
[2041]-13884	***1***	***A***	Red	M.Hom.	Fe	Moderate	X	X	Meso vesicles, vughs + meso-macro planar voids, channels
[2041]-13885	***2***	***B***	Brown	S.Het.	S.Ca	Moderate		X	Meso vughs, vesicles channels and planar voids
[1117]-8202	***1***	***A***	Red brown	S.Hom.	Fe	Moderate		X	Meso vesicles + meso/macro vughs and channels
[1117]-8197	***1***	***C***	Red	M.Hom.	Fe	Moderate			Meso vesicles + meso/macro vughs
[973]-7561	***1***	***C***	Red	M.Hom.	Fe	Moderate		X	Meso vesicles, vughs, planar voids
[1359]-9939	***1***	***B***	Red	M.Hom.	Fe	Slightly active	X	X	Meso vesicles + meso/macro vughs
[1359]-9930	***2***	***B***	Brown-gray	S.Het.	S.Ca	Slightly active	X	X	Meso vughs, planar void, channels
[473]-4458	***1***	***C***	Red	M.Hom.	Fe	Moderate	X	X	Meso vesicles, vughs
[473]-4453	***2***	***C***	Brown	M.Hom.	S.Ca	Moderate	X	X	Meso veschicles + meso macro vughs
[1130]-7712	***2***	***B***	Brown-gray	S.Het.	S.Ca	Slightly active	X	X	Meso vesicles, vughs channels, planar voids
[1130]-7714	***2***	***C***	Brown	S.Het.	S.Ca	Slightly active	X	X	Meso vesicles, channels, vughs + macro/mega planar voids and vughs
[1130]-7716	***2***	***C***	Brown	S.Het.	S.Ca	Slightly active	X	X	Meso/macro vesicles, vughs

Table 3, annex 2. Ceramic samples matrix and porosity characteristics. H.HOM., highly homogeneous – M.HOM., moderately homogeneous – S.HOM., slightly homogeneous – H.HET., highly heterogeneous – M.HET., moderately heterogeneous – S.HET., slightly heterogeneous. Fe- Ca rich matrix: Fe, iron rich matrix – S.Ca, slightly calcitic – M. Ca, moderately calcitic – H.Ca., Highly calcitic. Part 2.

Sample reference [U.S.]-n°	Fabric	Subgroup	Matrix						Porosity
			Colour	Homogeneity/heterogeneity	Fe / Ca rich matrix	Matrix Activity	Clay pellets	Oxides	Description
[91]-1977	2	C	Red brown	M.Hom.	Fe	Slightly active	X	X	Meso vughs, channels
[91]-1980	1	C	Red brown	S.Het.	S.Ca	Moderate	X	X	Meso/macro vughs + meso channels planar voids, vesicles
[91]-1992	2	A	Red brown	M.Hom.	Fe	Moderate	X	X	Meso vughs, vesicles, planar voids
[91]-1994	1	C	Red-brown	S.Het.	S.Ca	Moderate	X	X	Meso vesicles, vughs channels, planar voids
[1117]-8209	2	B	Brown	H.Hom.	S.Ca	Moderate	X	X	Meso vesicles, vughs
[973]-7560	1	A	Red brown	H.Hom.	Fe	Moderate	X	X	Meso vesicles, vughs, channels
[508]-4967	2	B	Brown	H.Hom.	S.Ca	Moderate		X	Meso vughs, channels
[2244]-15043	1	B	Brown dark red	M.Het.	Fe	Moderate	X	X	Meso vesicles, vughs + meso/macro/mega channels
[2171]-14751	2	C	Gray brown	H.Hom.	Fe/S.Ca	Moderate		X	Meso vesicles, planar voids, vughs
[571]-5117	1	B	Brown	M.Hom.	Fe	Moderate		X	Meso vughs
[571]-5116	2	A	Light brown	H.Hom.	S.Ca	Moderate		X	Meso/macro vughs, vescicles, planar voids
Vala 37	1	A	Brown red	S.Hom.	S.Ca	Moderate	X	X	Meso vesicles + meso/macro vughs
[1]-15467	2	A	Light brown	H.Hom.	S.Ca	Moderate		X	Meso/macro vughs, vesicles, planar void + mega channels
[939]-7351	1	C	Red	M.Hom.	Fe	Moderate	X	X	Meso vesicles, vughs, channels

Table 4, annex 2. Ceramic samples temper characteristics. Main grain shape: Eq&El, mainly equal (rounded) and elongated grains – El&Eq, mainly elongated and equal grains. Roundness: VA, very angular – A, angular – SA, sub angular – SR, sub rounded – R, rounded – WR, well rounded. Packing: CS, close spaced – SS, single spaced – DS, double spaced – OS, open spaced. Sorting: VP, very poor – P, poor – M, moderate – W, well. Grain size distribution (G.S.D.): U, unimodal – B, bimodal. Part 1.

Sample ref.-[U.S.]-n°	Fabric	Subgroup	Temper									
			Shape	Roundness	Packing	Max size mm	Alignment	Sorting	Grain size distribution	Temper %	Minerals	Rock frag.
LSI04-233	1	B	Eq&el	R-A	DS-OS	2.4	Weak	Poor	U	9.50	Quartz, K-Fldspar, Plagioclase, Muscovite, Tourmaline, Secondary calcite	Quartzite, Sandstone
LSI04-229	1	B	Eq&el	R-A	DS-OS	1.65	Weak	Poor	U	14.54	Quartz, K-Fldspar, Plagioclase, Muscovite, Tourmaline, Secondary calcite, Grog	Quartzite
LSI04-228	1	B	Eq&el	R –SA	DS-OS	1.77	Weak	Poor	U	11.91	Quartz, K-Fldspar, Plagioclase, Muscovite, Tourmaline	Quartzite
LSI04-236	1	B	Eq&el	R-SA	DS-OS	2.11	Weak	Poor	U	12.52	Quartz, K-Fldspar, Plagioclase, Muscovite	Quartzite
LSI04-232	1	B	Eq&el	R-SA	DS-OS	0.99	Weak	Moderate	U	11.55	Quartz, K-Fldspar, Plagioclase, Muscovite, Tourmaline	Quartzite, Granite
[1368]-11000	1	A	Eq&el	R-SA	DS-OS	1.38	Weak	Moderate	U	8.36	Quartz, K-Fldspar, Plagioclase, Muscovite, Grog	Quartzite, Sandstone
[1368]-11002	2	B	Eq&el	R-SA	DS-OS	0.98	Weak	Moderate	U	9.57	Quartz, K-Fldspar, Muscovite, Secondary calcite	Quartzite, Limestone
[1368]-11004	2	B	Eq&el	R-SA	DS-OS	0.84	Weak	Well	U	5.09	Quartz, K-Fldspar, Muscovite, Secondary calcite	Quartzite, Limestone
[1368]-9999	1	A	Eq&el	R-SA	DS-OS	1.19	Moderate	Poor	U	11.56	Quartz, K-Fldspar, Plagioclase, Muscovite	Quartzite
[1335]-9818	ND	ND	Eq&el	R-SA	DS-OS	1.41	Weak	Poor	U	4.3	Quartz, K-Fldspar, Plagioclase, Muscovite, Tourmaline, Grog, Shell	Quartzite, Sandstone , Limestone, Biosparite, Intrasparite
[2041]-13884	1	A	Eq&el	R-SA	DS-OS	2.13	Weak	Poor	U	9.40	Quartz, K-Fldspar, Plagioclase, Muscovite, Tourmaline, Secondary calcite, Grog	Quartzite
[2041]-13885	2	B	Eq&el	R-SA	DS-OS	0.9	Moderate	Poor	U	11.75	Quartz, K-Fldspar, Plagioclase, Muscovite, Sec. calcite	Quartzite, Limestone
[1117]-8202	1	A	Eq&el	R-SA	DS-OS	1.92	Moderate	Poor	U	11.16	Quartz, K-Fldspar, Plagioclase, Muscovite	Quartzite, Sandstone
[1117]-8197	1	C	Eq&el	SR-SA	CS	1.07	Moderate	Well	U	8.44	Quartz, K-Fldspar, Plagioclase, Muscovite, Tourmaline, Grog	Quartzite, Sandstone , Limestone
[973]-7561	1	C	Eq&el	SR-SA	CS	1.07	Moderate	Well	U	17.33	Quartz, K-Fldspar, Plagioclase, Muscovite, Tourmaline	Quartzite, Sandstone
[1359]-9939	1	B	Eq&el	R-SA	SS-DS	1.11	Weak	Moderate	U	12.54	Quartz, K-Fldspar, Plagioclase, Muscovite	Quartzite
[1359]-9930	2	B	Eq&el	R-SA	DS-OS	1.31	Moderate	Moderate	U	11.43	Quartz, K-Fldspar, Plagioclase, Muscovite	Quartzite, Sandstone , Schist
[473]-4458	1	C	Eq&el	R-SA	CS	1.05	Moderate	Well	U	14.65	Quartz, K-Fldspar, Plagioclase, Muscovite, Tourmaline	Quartzite, Sandstone , Limestone
[473]-4453	2	C	Eq&el	R-SA	DS-OS	1.49	Weak	Poor	U	5.77	Quartz, K-Fldspar, Plagioclase, Muscovite	Quartzite, Sandstone

Table 5, annex 2. Ceramic samples temper characteristics. Main grain shape: Eq&El, mainly equal (rounded) and elongated grains – El&Eq, mainly elongated and equal grains. Roundness: VA, very angular – A, angular – SA, sub angular – SR, sub rounded – R, rounded – WR, well rounded. Packing: CS, close spaced – SS, single spaced – DS, double spaced – OS, open spaced. Sorting: VP, very poor – P, poor – M, moderate – W, well. Grain size distribution (G.S.D.): U, unimodal – B, bimodal. Part 2.

Sample ref.- [U.S.]-n°	Fabric	Subgroup	Temper									
			Shape	Roundness	Packing	Max size mm	Alignment	Sorting	Grain size distribution	Temper %	Minerals	Rock frag.
[1130]-7712	2	B	Eq&el	R-A	SS-DS	1.42	Weak	Poor	U	11.74	Quartz, K-Fldspar, Muscovite, Secondary calcite	Quartzite, Sandstone , Limestone
[1130]-7714	2	C	Eq&el	R-SA	DS-OS	0.6	Moderate	Poor	U	7.56	Quartz, K-Fldspar, Muscovite, Secondary calcite	Sandstone
[1130]-7716	2	C	Eq&el	R-SA	DS-OS	1.77	Weak	Poor	U	11.01	Quartz, K-Fldspar, Muscovite, Secondary calcite	Quartzite, Sandstone , Limestone
[91]-1977	2	C	Eq&el	R-SA	SS-DS	1.98	Moderate	Moderate	U	11.9	Quartz, K-Fldspar, Plagioclase, Muscovite	Quartzite, Sandstone
[91]-1980	1	C	Eq&el	R-SA	SS-DS	1.03	Moderate	Poor	U	8.75	Quartz, K-Fldspar, Plagioclase, Muscovite, Tourmaline	Quartzite, Limestone
[91]-1992	2	A	Eq&el	R-SA	DS-OS	0.83	Weak	Poor	U	7.62	Quartz, K-Fldspar, Plagioclase, Muscovite, Tourmaline	Quartzite
[91]-1994	1	C	Eq&el	R-SA	DS-OS	1.34	Weak	Poor	U	11.71	Quartz, K-Fldspar, Plagioclase, Muscovite	Quartzite, Sandstone
[1117]-8209	2	B	Eq&el	R-SA	OS	0.82	Weak	Moderate	U	11.17	Quartz, K-Fldspar, Plagioclase, Muscovite, Tourmaline	Quartzite, Limestone
[973]-7560	1	A	Eq&El	R-SR	OS	0.42	Weak	Moderate	U	7.54	Quartz, K-Fldspar, Muscovite, Grog	Quartzite, Limestone, Biosparite
[508]-4967	2	B	Eq&el	R-SA	DS-OS	0.56	Moderate	Poor	U	7.55	Quartz, K-Fldspar, Muscovite, Tourmaline	Quartzite
[2244]-15043	1	B	Eq&el	SR-A	SS-DS	1.18	Moderate	Very poor	U	18.52	Quartz, K-Fldspar, Muscovite, Tourmaline, Secondary calcite	Quartzite, Granite
[2171]-14751	2	C	Eq&el	R-SA	DS-OS	0.68	Moderate	Poor	U	5.36	Quartz, K-Fldspar, Plagioclase, Muscovite, Secondary calcite	Quartzite, Limestone
[571]-5117	1	B	Eq&el	R-SR	CS-SS	0.5	Moderate	Well	U	24.9	Quartz, K-Fldspar, Plagioclase, Muscovite, Tourmaline	Quartzite
[571]-5116	2	A	Eq&el	R-SA	DS-OS	0.82	Weak	Poor	U	11.70	Quartz, Plagioclase, Tourmaline, Secondary calcite	Quartzite, Granite , Limestone
Vala 37	1	A	Eq&el	R-SA	DS-OS	0.60	Moderate	Poor	U	9.4	Quartz, K-Fldspar, Plagioclase, Muscovite, Biotite, Tourmaline , Secondary calcite, Grog	Quartzite, Sandstone
[1]-15467	2	A	Eq&el	R-SA	DS-OS	0.77	Moderate	Moderate	U	16.1	Quartz, K-Fldspar, Plagioclase, Muscovite, Biotite, Tourmaline , Secondary calcite	Quartzite, Granite, Schist
[939]-7351	1	C	Eq&el	R-SA	DS-OS	0.95	Moderate	Poor	U	11.69	Quartz, K-Fldspar, Muscovite, Biotite	Quartzite

Table 6, annex 2. Ceramic samples chemical composition, major oxides obtained by XRF and L.O.I, part 1.

Sample reference – [U.S.]-n°	Major oxides and L.O.I													
		Na_2O	MgO	Al_2O_3	SiO_2	P_2O_5	S	K_2O	CaO	TiO_2	Fe_2O_3	MnO	LOI	Sum
LSI04-233	**wt%**	0.22	1.01	17.80	67.60	0.14	0.044	3.65	1.05	0.83	0.01	6.13	3.31	101.79
	Err. ±	0.06	*0.03*	*0.05*	*0.05*	*0.01*	*0.001*	*0.05*	*0.02*	*0.01*	*0.002*	*0.01*		
LSI04-232	**wt%**	0.64	0.97	15.00	69.30	0.33	0.038	2.84	0.85	0.74	1.44	4.75	3.71	100.61
	Err. ±	*0.07*	*0.03*	*0.04*	0.05	*0.01*	*0.001*	*0.05*	*0.02*	*0.01*	*0.002*	*0.01*		
LSI04-228	**wt%**	0.62	0.94	15.30	66.11	1.38	0.056	3.46	1.99	0.59	0.02	5.07	4.52	100.06
	Err. ±	*0.07*	*0.03*	*0.04*	*0.05*	*0.01*	*0.001*	*0.05*	*0.03*	*0.01*	*0.002*	*0.01*		
LSI04-229	**wt%**	0.35	1.14	16.80	66.70	0.32	0.047	3.83	0.83	0.64	0.02	5.05	5.04	100.76
	Err. ±	*0.07*	*0.03*	*0.05*	*0.05*	*0.01*	*0.001*	*0.05*	*0.02*	*0.01*	*0.002*	*0.01*		
LSI04-236	**wt%**	0.63	1.24	15.40	67.90	0.18	0.042	3.47	0.82	0.78	0.01	5.91	4.70	101.08
	Err. ±	*0.07*	*0.03*	*0.05*	*0.05*	*0.01*	*0.001*	*0.05*	*0.02*	*0.01*	*0.002*	*0.01*		
[1335]-9818	**wt%**	0.30	0.97	18.00	62.30	0.18	0.041	3.42	2.75	0.75	0.02	5.99	6.97	101.68
	Err. ±	*0.06*	*0.03*	*0.05*	*0.05*	*0.01*	*0.001*	*0.05*	*0.03*	*0.01*	*0.002*	*0.01*		
[1368]-9999	**wt%**	0.33	1.02	18.20	68.20	0.05	0.098	3.25	0.78	0.77	0.03	6.13	2.72	101.57
	Err. ±	*0.06*	*0.03*	*0.05*	*0.05*	*0.01*	*0.001*	*0.05*	*0.02*	*0.01*	*0.002*	*0.01*		
[2041]-13884	**wt%**	0.21	1.04	18.60	67.20	0.05	0.039	3.31	0.75	0.79	0.06	6.04	3.15	101.24
	Err. ±	*0.07*	*0.03*	*0.05*	*0.05*	*0.01*	*0.001*	*0.05*	*0.02*	*0.01*	*0.002*	*0.01*		
[1368]-11000	**wt%**	0.23	1.04	17.80	67.40	0.05	0.037	3.29	0.69	0.72	0.03	5.86	3.16	100.31
	Err. ±	*0.06*	*0.03*	*0.05*	*0.05*	*0.01*	*0.001*	*0.05*	*0.02*	*0.01*	*0.002*	*0.01*		
[1368]-11002	**wt%**	0.54	1.02	18.70	67.11	0.04	0.037	3.77	0.74	0.75	0.04	5.90	1.46	100.09
	Err. ±	*0.07*	*0.03*	*0.05*	*0.05*	*0.01*	*0.001*	*0.05*	*0.02*	*0.01*	*0.002*	*0.01*		
[1368]-11004	**wt%**	0.20	1.04	19.50	67.50	0.04	0.034	3.20	0.66	0.84	0.02	6.53	1.53	101.11
	Err. ±	*0.06*	*0.03*	*0.05*	*0.05*	*0.01*	*0.001*	*0.05*	*0.02*	*0.01*	*0.002*	*0.01*		
[2041]-13885	**wt%**	0.27	1.15	19.70	66.30	0.04	0.034	3.32	0.85	0.80	0.02	6.31	1.43	100.22
	Err. ±	*0.06*	*0.03*	*0.05*	*0.05*	*0.01*	*0.001*	*0.05*	*0.02*	*0.01*	*0.002*	*0.01*		
[973]-7560	**wt%**	0.81	1.20	19.20	68.80	0.06	0.046	3.88	0.67	1.05	0.00	3.57	2.33	101.62
	Err. ±	*0.07*	*0.03*	*0.05*	*0.05*	*0.01*	*0.001*	*0.05*	*0.02*	*0.01*	*0.002*	*0.01*		
Vala 37	**wt%**	0.31	1.25	17.60	65.50	0.08	0.111	3.32	1.11	0.82	0.03	5.80	6.11	102.01
	Err. ±	*0.07*	*0.03*	*0.05*	*0.05*	*0.01*	*0.002*	*0.05*	*0.02*	*0.01*	*0.002*	*0.01*		
[1117]-8209	**wt%**	0.99	0.91	18.90	63.30	0.60	0.115	3.38	0.89	0.69	0.01	3.66	6.33	99.78
	Err. ±	*0.07*	*0.03*	*0.05*	*0.05*	*0.01*	*0.002*	*0.05*	*0.02*	*0.01*	*0.002*	*0.01*		
[508]-4967	**wt%**	0.40	0.81	18.20	71.60	0.06	0.200	3.36	0.37	0.93	0.01	2.58	1.48	99.99
	Err. ±	*0.07*	*0.03*	*0.05*	*0.05*	*0.01*	*0.002*	*0.05*	*0.02*	*0.01*	*0.002*	*0.01*		
[473]-4458	**wt%**	0.62	1.20	16.11	72.30	0.05	0.041	3.37	0.55	0.62	0.01	4.46	1.12	100.44
	Err. ±	*0.07*	*0.03*	*0.05*	*0.05*	*0.01*	*0.001*	*0.05*	*0.02*	*0.01*	*0.002*	*0.01*		
[973]-7561	**wt%**	0.73	1.04	15.50	72.40	0.07	0.037	3.20	0.53	0.58	0.01	4.77	1.33	100.20
	Err. ±	*0.07*	*0.03*	*0.04*	*0.05*	*0.01*	*0.001*	*0.05*	*0.02*	*0.01*	*0.002*	*0.01*		
[1117]-8197	**wt%**	0.27	0.96	16.60	69.80	0.06	0.040	3.09	0.80	0.68	0.02	5.27	2.96	100.55
	Err. ±	*0.06*	*0.03*	*0.05*	*0.05*	*0.01*	*0.001*	*0.05*	*0.02*	*0.01*	*0.002*	*0.01*		
[1359]-9939	**wt%**	0.30	1.02	17.20	66.70	0.09	0.036	3.13	0.69	0.72	0.03	5.63	4.04	99.58
	Err. ±	*0.06*	*0.03*	*0.05*	*0.05*	*0.01*	*0.001*	*0.05*	*0.02*	*0.01*	*0.002*	*0.01*		
[473]-4453	**wt%**	0.35	1.20	19.90	67.00	0.09	0.036	3.06	0.64	0.79	0.01	6.81	1.46	101.35
	Err. ±	*0.07*	*0.03*	*0.05*	*0.05*	*0.01*	*0.001*	*0.05*	*0.02*	*0.01*	*0.002*	*0.01*		
[1117]-8202	**wt%**	0.42	1.22	16.90	68.40	0.11	0.037	3.35	0.63	0.65	0.02	5.41	3.33	100.46
	Err. ±	*0.07*	*0.03*	*0.05*	*0.05*	*0.01*	*0.001*	*0.05*	*0.02*	*0.01*	*0.002*	*0.01*		

Table 7, annex 2. Ceramic samples chemical composition, major oxides obtained by XRF and L.O.I, part 2.

Sample reference – [U.S.]-n°	Major oxides and L.O.I													
		Na_2O	MgO	Al_2O_3	SiO_2	P_2O_5	S	K_2O	CaO	TiO_2	Fe_2O_3	MnO	LOI	Sum
[1359]-9930	**wt%**	0.39	1.15	17.60	65.60	0.25	0.039	3.06	1.06	0.73	0.01	6.37	5.28	101.54
	Err. ±	*0.07*	*0.03*	*0.05*	*0.05*	*0.01*	*0.001*	*0.05*	*0.02*	*0.01*	*0.002*	*0.01*		
[1130]-7712	**wt%**	0.29	1.17	18.80	68.11	0.06	0.033	3.30	0.80	0.73	0.03	5.82	1.40	100.53
	Err. ±	*0.06*	*0.03*	*0.05*	*0.05*	*0.01*	*0.001*	*0.05*	*0.02*	*0.01*	*0.002*	*0.01*		
[1130]-7714	**wt%**	0.31	1.12	19.20	68.00	0.04	0.035	3.29	0.74	0.73	0.02	6.12	0.50	100.12
	Err. ±	*0.07*	*0.03*	*0.05*	*0.05*	*0.01*	*0.001*	*0.05*	*0.02*	*0.01*	*0.002*	*0.01*		
[1130]-7716	**wt%**	0.30	1.09	18.80	68.00	0.05	0.035	3.18	0.77	0.78	0.03	5.86	1.83	100.73
	Err. ±	*0.06*	*0.03*	*0.05*	*0.05*	*0.01*	*0.001*	*0.05*	*0.02*	*0.01*	*0.002*	*0.01*		
[571]-5116	**wt%**	0.33	0.92	26.50	64.30	0.09	0.045	2.19	0.52	0.75	0.01	2.33	3.12	101.11
	Err. ±	*0.06*	*0.03*	*0.06*	*0.05*	*0.01*	*0.001*	*0.04*	*0.02*	*0.01*	*0.002*	*0.01*		
[2244]-15043	**wt%**	0.61	1.66	17.11	62.90	0.13	0.039	3.91	1.00	0.77	0.03	6.30	4.72	99.17
	Err. ±	*0.07*	*0.03*	*0.05*	*0.05*	*0.01*	*0.001*	*0.05*	*0.02*	*0.01*	*0.002*	*0.01*		
[2171]-14751	**wt%**	0.75	1.23	20.00	66.80	0.11	0.121	3.74	0.87	0.97	n.d	3.55	2.19	100.33
	Err. ±	*0.07*	*0.03*	*0.05*	*0.05*	*0.01*	*0.002*	*0.05*	*0.02*	*0.01*	*n.d*	*0.01*		
[571]-5117	**wt%**	0.26	0.75	15.70	73.60	0.17	0.040	4.04	0.62	0.60	0.02	3.40	2.50	101.70
	Err. ±	*0.06*	*0.03*	*0.04*	*0.05*	*0.01*	*0.001*	*0.05*	*0.02*	*0.01*	*0.002*	*0.01*		
[91]-1977	**wt%**	0.22	0.90	17.30	70.50	0.07	0.035	2.67	0.88	0.81	0.03	5.35	2.08	100.86
	Err. ±	*0.07*	*0.03*	*0.05*	*0.05*	*0.01*	*0.001*	*0.05*	*0.02*	*0.01*	*0.002*	*0.01*		
[91]-1980	**wt%**	0.45	1.23	19.60	67.11	0.04	0.050	3.17	0.43	0.78	0.01	6.62	1.50	100.98
	Err. ±	*0.07*	*0.03*	*0.05*	*0.05*	*0.01*	*0.001*	*0.05*	*0.02*	*0.01*	*0.002*	*0.01*		
[91]-1992	**wt%**	0.32	1.52	20.80	65.40	0.04	0.041	3.21	0.55	0.78	0.02	7.30	1.12	101.09
	Err. ±	*0.07*	*0.03*	*0.05*	*0.05*	*0.01*	*0.001*	*0.05*	*0.02*	*0.01*	*0.002*	*0.01*		
[91]-1994	**wt%**	0.39	1.05	18.20	67.70	0.07	0.038	3.31	0.42	0.75	0.01	6.87	2.33	101.14
	Err. ±	*0.07*	*0.03*	*0.05*	*0.05*	*0.01*	*0.001*	*0.05*	*0.02*	*0.01*	*0.002*	*0.01*		
[939]-7351	**wt%**	0.48	0.90	18.00	67.20	0.05	0.044	3.25	0.62	0.73	0.01	5.94	2.95	100.17
	Err. ±	*0.07*	*0.03*	*0.05*	*0.05*	*0.01*	*0.001*	*0.05*	*0.02*	*0.01*	*0.002*	*0.01*		
[1]-15467	**wt%**	0.64	0.92	22.11	65.90	0.09	0.046	3.45	0.63	0.94	0.01	3.12	3.58	101.42
	Err. ±	*0.07*	*0.03*	*0.05*	*0.05*	*0.01*	*0.001*	*0.05*	*0.02*	*0.01*	*0.002*	*0.01*		

Table 8, annex 2. Ceramic samples chemical composition, traces elements obtained by ICP-MS, part 1.

Sample reference – [U.S.]-n°		Trace elements																
		Sc	V	Co	Ni	Cu	Zn	Ga	Rb	Sr	Y	Zr	Nb	Cs	Ba	Hf	Th	U
LSI04-233	**PPM**	13.38	81.90	13.33	34.32	18.97	119.96	24.56	223.88	54.19	24.15	76.68	18.20	18.97	404.09	2.30	19.51	2.23
	RSD	*1.75*	*0.70*	*1.66*	*0.67*	*0.42*	*0.71*	*2.76*	*1.39*	*1.57*	*0.72*	*0.26*	*1.39*	*4.81*	*4.09*	*1.20*	*5.52*	*1.00*
LSI04-232	**PPM**	11.04	75.19	8.21	18.17	20.56	88.83	20.35	160.20	49.24	20.58	119.11	14.37	9.30	552.42	2.92	14.21	2.26
	RSD	*0.12*	*0.34*	*1.76*	*2.39*	*0.95*	*1.03*	*1.59*	*0.76*	*1.42*	*1.31*	*0.40*	*0.41*	*0.46*	*1.14*	*1.43*	*3.83*	*4.56*
LSI04-228	**PPM**	11.92	78.96	9.89	23.54	63.58	99.81	19.19	164.42	74.68	17.32	72.14	11.41	8.94	745.49	2.04	11.33	1.74
	RSD	*1.24*	*1.28*	*0.11*	*2.55*	*0.40*	*0.86*	*2.08*	*0.44*	*0.73*	*0.23*	*0.67*	*1.59*	*0.78*	*0.52*	*1.73*	*1.44*	*2.00*
LSI04-229	**PPM**	12.83	92.22	9.77	26.70	23.30	115.55	21.70	196.24	51.37	21.16	114.45	12.69	11.17	581.51	3.16	11.18	2.19
	RSD	*3.92*	*1.28*	*0.39*	*1.70*	*0.94*	*0.83*	*2.46*	*1.29*	*0.21*	*0.93*	*0.71*	*1.07*	*0.47*	*1.78*	*1.04*	*2.12*	*1.13*
LSI04-236	**PPM**	12.49	91.90	9.06	27.39	20.64	117.84	20.71	178.00	58.89	19.29	118.97	15.78	9.20	466.43	2.71	11.01	2.38
	RSD	*1.32*	*1.00*	*2.14*	*4.00*	*1.24*	*0.55*	*4.12*	*0.76*	*0.08*	*0.96*	*0.60*	*1.46*	*0.35*	*0.76*	*1.39*	*2.94*	*2.13*
[1335]-9818	**PPM**	13.78	117.06	8.70	36.86	31.77	90.18	22.41	157.77	27.04	28.66	153.80	15.49	11.78	496.85	2.97	11.95	1.95
	RSD	*5.07*	*5.44*	*4.97*	*7.70*	*0.86*	*2.94*	*2.64*	*5.08*	*1.32*	*3.07*	*5.18*	*2.77*	*0.75*	*0.71*	*0.67*	*0.82*	*1.59*
[1368]-9999	**PPM**	12.90	111.53	12.63	42.77	56.18	114.08	22.87	184.31	25.53	28.72	149.34	16.78	13.08	534.05	2.78	13.56	2.00
	RSD	*6.94*	*3.13*	*3.46*	*4.77*	*1.09*	*2.17*	*6.04*	*3.63*	*2.24*	*0.74*	*4.69*	*1.71*	*1.06*	*2.41*	*0.33*	*0.94*	*0.43*
[2041]-13884	**PPM**	13.92	112.15	64.75	50.88	33.72	96.06	25.60	191.70	26.11	32.97	156.12	16.98	14.01	585.33	2.92	13.36	2.11
	RSD	*2.16*	*3.74*	*3.89*	*5.49*	*1.02*	*2.65*	*5.36*	*4.09*	*2.29*	*3.79*	*3.32*	*3.09*	*1.84*	*1.23*	*0.59*	*1.56*	*0.43*
[1368]-11000	**PPM**	15.17	93.02	15.40	40.15	41.78	84.72	19.03	181.20	22.70	25.24	130.65	14.53	11.15	476.93	3.50	11.97	2.30
	RSD	*5.06*	*3.22*	*3.12*	*1.80*	*1.94*	*2.00*	*5.45*	*2.55*	*1.26*	*1.16*	*1.21*	*1.16*	*0.67*	*0.91*	*0.57*	*0.96*	*1.23*
[1368]-11002	**PPM**	19.00	115.66	18.21	38.95	27.37	93.09	22.19	211.54	27.41	30.65	142.05	16.76	14.44	567.36	3.97	12.82	2.84
	RSD	*11.75*	*1.99*	*1.18*	*0.48*	*1.73*	*0.58*	*4.11*	*0.80*	*2.98*	*2.46*	*0.43*	*4.00*	*1.86*	*2.01*	*2.62*	*1.71*	*1.81*
[1368]-11004	**PPM**	17.67	116.62	9.76	37.03	49.02	83.18	23.64	193.61	23.40	28.80	137.47	16.98	13.69	521.61	3.89	12.87	2.81
	RSD	*8.81*	*3.60*	*1.29*	*3.18*	*3.32*	*0.60*	*3.45*	*3.19*	*2.46*	*1.12*	*4.21*	*0.79*	*1.78*	*4.02*	*7.17*	*2.26*	*2.75*
[2041]-13885	**PPM**	18.12	119.09	11.68	43.29	46.20	87.24	23.35	204.48	25.81	33.29	158.11	17.22	14.39	546.94	4.39	12.81	3.09
	RSD	*1.51*	*3.54*	*2.91*	*4.28*	*3.22*	*2.99*	*6.62*	*3.32*	*1.72*	*1.33*	*6.68*	*0.57*	*2.13*	*3.03*	*2.46*	*2.28*	*2.52*
[973]-7560	**PPM**	17.00	117.78	4.58	12.57	28.98	59.89	25.61	189.47	82.11	18.70	137.11	21.23	11.60	473.53	3.75	12.90	3.30
	RSD	*3.71*	*0.65*	*1.21*	*4.49*	*1.08*	*2.14*	*4.65*	*0.57*	*0.75*	*1.72*	*3.06*	*0.75*	*0.59*	*1.07*	*0.99*	*2.60*	*1.64*
Vala 37	**PPM**	14.60	115.22	11.75	32.72	250.99	96.42	22.61	196.18	31.48	23.06	148.61	18.72	11.68	427.30	3.54	13.12	2.96
	RSD	*0.73*	*2.98*	*6.19*	*3.65*	*4.31*	*0.93*	*4.57*	*3.47*	*4.43*	*1.69*	*5.19*	*1.11*	*0.71*	*1.50*	*4.81*	*1.44*	*2.49*
[1117]-8209	**PPM**	11.58	81.16	6.83	24.77	181.04	85.90	23.17	176.45	52.44	34.25	110.66	17.49	9.78	503.77	2.49	14.73	3.84
	RSD	*8.84*	*2.27*	*3.49*	*0.53*	*1.24*	*0.51*	*7.01*	*0.82*	*0.89*	*1.49*	*2.30*	*1.75*	*2.49*	*2.85*	*1.84*	*4.83*	*5.23*
[508]-4967	**PPM**	11.55	71.92	7.11	14.45	111.02	51.32	21.57	205.72	60.06	26.43	114.98	23.96	11.53	449.71	2.45	17.11	3.59
	RSD	*6.18*	*3.31*	*4.11*	*2.69*	*3.53*	*2.54*	*6.07*	*2.50*	*3.23*	*1.36*	*8.09*	*3.31*	*0.94*	*3.40*	*3.34*	*2.07*	*2.85*
[473]-4458	**PPM**	11.02	76.93	9.08	26.25	20.03	82.63	22.28	180.34	43.11	23.53	113.20	13.30	11.82	454.39	2.59	12.25	2.09
	RSD	*4.80*	*3.35*	*5.35*	*3.33*	*0.59*	*1.65*	*2.11*	*2.82*	*1.08*	*1.44*	*3.78*	*3.40*	*0.26*	*0.99*	*1.01*	*0.69*	*0.54*
[973]-7561	**PPM**	11.15	78.00	11.15	27.80	22.22	74.52	20.89	182.31	45.79	24.87	96.60	13.92	11.89	411.93	2.00	14.30	2.24
	RSD	*3.07*	*0.94*	*2.11*	*2.56*	*1.04*	*1.29*	*2.21*	*0.24*	*2.22*	*0.05*	*2.07*	*2.89*	*0.87*	*1.48*	*1.51*	*0.77*	*1.24*

Table 9, annex 2. Ceramic samples chemical composition, traces elements obtained by ICP-MS, part 2.

Sample reference – [U.S.]-n°		Trace elements																
		Sc	V	Co	Ni	Cu	Zn	Ga	Rb	Sr	Y	Zr	Nb	Cs	Ba	Hf	Th	U
[1117]-8197	PPM	12.08	87.35	15.60	31.90	29.87	83.84	21.91	197.55	28.09	25.02	144.74	16.45	11.80	448.94	2.68	12.23	1.65
	RSD	*11.25*	*3.78*	*3.87*	*4.23*	*0.96*	*1.35*	*1.78*	*3.60*	*0.53*	*4.11*	*8.88*	*2.94*	*1.02*	*1.82*	*0.73*	*1.38*	*0.43*
[1359]-9939	PPM	13.17	111.12	15.04	34.42	28.28	81.07	22.16	188.19	26.85	29.34	156.69	15.89	13.71	552.52	3.01	14.33	2.09
	RSD	*7.27*	*5.11*	*5.81*	*4.77*	*2.37*	*2.83*	*3.65*	*6.88*	*2.12*	*3.11*	*7.34*	*3.11*	*9.36*	*7.76*	*0.87*	*9.93*	*1.34*
[473]-4453	PPM	18.83	118.74	9.33	30.26	29.55	81.14	22.89	194.86	28.76	29.77	148.02	17.41	14.33	521.33	4.33	14.38	3.19
	RSD	*7.62*	*2.70*	*1.51*	*0.42*	*0.67*	*2.53*	*0.26*	*3.54*	*1.14*	*1.58*	*1.72*	*0.44*	*0.22*	*3.73*	*1.84*	*0.67*	*1.26*
[1117]-8202	PPM	14.38	92.39	12.03	34.98	38.85	80.77	19.78	185.31	32.42	26.84	130.11	15.09	11.32	495.30	3.73	14.36	2.96
	RSD	*4.93*	*1.46*	*1.96*	*2.75*	*1.22*	*0.84*	*4.31*	*2.29*	*1.49*	*1.64*	*1.83*	*1.73*	*2.14*	*5.32*	*1.18*	*1.81*	*2.56*
[1359]-9930	PPM	18.19	125.69	20.21	39.27	356.99	111.59	22.43	200.75	30.89	27.30	149.90	16.39	12.78	569.02	4.03	13.55	3.06
	RSD	*6.77*	*3.53*	*3.74*	*2.73*	*2.56*	*3.75*	*1.27*	*1.99*	*2.66*	*1.45*	*3.53*	*0.69*	*1.02*	*5.17*	*2.11*	*1.03*	*0.82*
[1130]-7712	PPM	16.57	115.27	11.37	40.46	35.93	114.73	25.68	195.08	31.12	29.23	127.02	16.27	13.74	547.94	2.70	11.75	2.13
	RSD	*6.99*	*5.42*	*11.04*	*6.67*	*1.24*	*3.55*	*6.84*	*5.43*	*3.20*	*2.25*	*4.73*	*1.90*	*0.50*	*1.90*	*0.42*	*0.59*	*1.28*
[1130]-7714	PPM	14.95	117.12	13.42	40.37	19.02	113.51	24.94	190.73	27.11	31.37	137.42	15.40	13.04	497.88	2.76	11.63	2.06
	RSD	*5.60*	*5.67*	*6.09*	*5.07*	*2.03*	*1.00*	*1.93*	*6.55*	*1.05*	*3.11*	*5.03*	*3.50*	*0.94*	*0.68*	*0.52*	*1.21*	*1.35*
[1130]-7716	PPM	16.25	129.96	11.33	41.79	18.09	115.84	27.94	194.91	28.67	31.95	128.74	18.29	13.85	537.09	2.61	12.63	2.16
	RSD	*1.55*	*1.82*	*1.45*	*1.13*	*0.87*	*2.56*	*2.62*	*1.69*	*2.88*	*1.08*	*1.40*	*3.04*	*1.47*	*0.35*	*1.71*	*0.99*	*2.91*
[571]-5116	PPM	11.45	74.46	9.42	24.51	20.25	35.30	25.32	127.96	55.61	19.35	92.03	16.64	9.83	285.98	2.37	13.45	2.37
	RSD	*1.63*	*2.59*	*1.85*	*2.47*	*2.80*	*3.50*	*4.66*	*1.50*	*0.59*	*1.05*	*1.79*	*1.61*	*1.28*	*2.43*	*4.27*	*1.06*	*1.16*
[2244]-15043	PPM	13.99	94.16	14.92	35.11	54.86	79.25	23.44	215.84	48.46	22.23	81.47	19.23	18.12	661.78	2.16	12.55	2.13
	RSD	*2.97*	*3.24*	*4.71*	*1.65*	*4.06*	*1.64*	*1.94*	*4.54*	*5.65*	*1.79*	*5.29*	*1.21*	*0.91*	*1.89*	*4.62*	*3.26*	*1.73*
[2171]-14751	PPM	6.04	42.84	3.77	9.25	82.99	92.36	17.11	217.84	46.56	16.53	72.09	19.13	13.02	271.74	1.91	16.43	4.66
	RSD	*14.47*	*3.19*	*11.73*	*2.52*	*4.47*	*1.03*	*3.87*	*5.41*	*6.02*	*3.58*	*4.23*	*2.83*	*0.61*	*4.50*	*6.35*	*1.11*	*2.60*
[571]-5117	PPM	15.21	111.70	4.61	16.81	28.80	47.52	25.21	177.39	82.66	22.69	148.51	24.81	11.17	470.17	3.58	12.91	4.99
	RSD	*3.02*	*1.58*	*6.82*	*4.55*	*4.61*	*5.65*	*2.58*	*3.76*	*3.27*	*1.08*	*3.60*	*2.21*	*1.07*	*3.69*	*4.85*	*3.29*	*3.04*
[91]-1977	PPM	15.63	92.98	11.42	33.25	24.38	63.85	21.61	204.87	28.85	25.95	121.05	17.23	13.36	448.72	3.45	14.60	2.48
	RSD	*0.91*	*5.09*	*5.66*	*4.55*	*5.40*	*1.84*	*2.23*	*5.15*	*4.24*	*1.70*	*6.21*	*1.28*	*0.62*	*3.43*	*1.53*	*1.37*	*1.02*
[91]-1980	PPM	17.37	118.16	7.21	28.06	48.35	77.48	23.81	192.27	33.40	23.61	137.38	15.41	12.41	674.22	3.67	12.00	3.79
	RSD	*3.30*	*1.02*	*1.96*	*0.83*	*1.88*	*1.47*	*1.89*	*0.73*	*0.78*	*4.63*	*4.87*	*1.75*	*0.87*	*2.36*	*1.92*	*0.89*	*0.93*
[91]-1992	PPM	20.75	135.90	17.34	45.02	37.70	93.41	26.55	203.36	31.18	27.21	141.05	16.00	14.31	584.57	3.81	12.22	2.96
	RSD	*11.56*	*2.48*	*0.78*	*1.18*	*1.59*	*1.91*	*2.15*	*2.39*	*0.70*	*1.97*	*6.20*	*2.58*	*0.53*	*1.08*	*1.50*	*0.91*	*1.06*
[91]-1994	PPM	16.88	116.36	13.82	32.00	44.78	80.61	22.22	197.92	30.26	27.13	135.77	15.78	13.12	506.37	3.99	14.11	4.65
	RSD	*6.57*	*1.36*	*0.97*	*4.83*	*0.71*	*2.44*	*4.39*	*2.01*	*0.83*	*2.50*	*2.41*	*2.16*	*1.11*	*3.95*	*0.40*	*1.01*	*1.47*
[939]-7351	PPM	14.63	94.42	5.54	20.37	25.11	79.13	23.31	187.06	40.60	22.60	121.63	13.90	9.74	501.65	3.30	11.21	2.21
	RSD	*1.46*	*0.94*	*0.44*	*4.43*	*1.24*	*0.64*	*0.93*	*1.39*	*1.56*	*0.79*	*1.15*	*1.62*	*1.42*	*1.73*	*3.17*	*3.06*	*1.67*
[1]-15467	PPM	16.88	93.82	12.34	24.28	27.84	63.14	26.16	197.05	64.07	26.63	98.12	17.89	11.26	392.02	2.64	12.36	2.26
	RSD	*2.42*	*0.67*	*1.35*	*5.99*	*1.60*	*4.15*	*2.92*	*0.82*	*0.36*	*1.67*	*0.93*	*1.15*	*0.92*	*1.65*	*2.07*	*2.32*	*2.52*

Table 10, annex 2. Ceramic samples chemical composition, rare earth elements obtained by ICP-MS, part 1.

Sample reference – [U.S.]-n°		Rare earth elements														
		La	Ce	Pr	Nd	Sm	Eu	Gd	Tb	Dy	Ho	Er	Tm	Yb	Lu
LSI04-233	PPM	44.64	118.67	11.01	40.18	7.89	1.20	6.66	0.95	4.95	0.93	2.62	0.37	2.41	0.35
	RSD	*1.37*	*0.88*	*0.70*	*0.47*	*0.75*	*1.03*	*0.70*	*0.74*	*2.34*	*1.69*	*1.20*	*1.45*	*0.62*	*3.21*
LSI04-232	PPM	37.96	83.03	9.82	36.51	7.18	1.13	5.84	0.79	3.99	0.75	2.09	0.30	1.95	0.30
	RSD	*2.37*	*0.51*	*0.63*	*0.53*	*1.79*	*1.37*	*0.72*	*1.18*	*5.60*	*5.24*	*1.53*	*4.21*	*0.79*	*5.02*
LSI04-228	PPM	48.39	59.03	11.27	38.88	6.99	1.21	5.37	0.72	3.39	0.64	1.75	0.24	1.55	0.24
	RSD	*4.77*	*1.74*	*1.52*	*0.66*	*0.44*	*0.31*	*1.11*	*1.50*	*1.79*	*1.07*	*0.60*	*1.18*	*0.92*	*3.48*
LSI04-229	PPM	31.39	65.45	8.15	31.08	6.18	1.11	5.12	0.77	4.09	0.80	2.28	0.33	2.17	0.33
	RSD	*0.65*	*1.40*	*0.75*	*0.54*	*0.12*	*0.48*	*2.26*	*2.06*	*1.69*	*1.72*	*0.66*	*1.32*	*0.72*	*2.82*
LSI04-236	PPM	34.71	72.60	8.41	31.24	6.14	1.16	5.17	0.70	3.54	0.68	1.88	0.27	1.73	0.27
	RSD	*1.88*	*1.06*	*0.89*	*0.51*	*0.64*	*0.79*	*0.71*	*1.02*	*1.23*	*1.90*	*1.58*	*2.02*	*1.15*	*1.93*
[1335]-9818	PPM	31.79	67.07	8.04	31.53	6.43	0.96	4.43	0.68	5.37	1.05	2.20	0.46	2.09	0.31
	RSD	*2.17*	*1.26*	*0.83*	*0.94*	*0.71*	*0.99*	*0.63*	*0.55*	*1.01*	*0.67*	*0.66*	*1.30*	*0.29*	*1.48*
[1368]-9999	PPM	38.03	80.31	9.46	36.91	7.50	1.05	4.78	0.70	5.53	1.06	2.11	0.45	1.99	0.30
	RSD	*2.13*	*2.07*	*0.73*	*0.71*	*1.23*	*0.23*	*1.11*	*0.66*	*0.76*	*1.12*	*0.62*	*1.21*	*0.69*	*1.12*
[2041]-13884	PPM	40.95	127.73	11.11	39.22	8.07	1.13	5.22	0.76	6.30	1.22	2.31	0.52	2.16	0.33
	RSD	*1.74*	*2.54*	*1.75*	*1.63*	*1.43*	*0.37*	*0.21*	*0.35*	*1.65*	*1.06*	*0.87*	*2.27*	*1.11*	*0.85*
[1368]-11000	PPM	34.23	70.48	8.23	31.59	6.36	0.84	3.79	0.55	4.76	0.91	2.75	0.39	2.61	0.39
	RSD	*5.61*	*2.32*	*0.81*	*0.74*	*1.57*	*1.11*	*0.54*	*0.86*	*1.17*	*1.14*	*0.49*	*0.78*	*0.82*	*0.83*
[1368]-11002	PPM	37.14	86.47	9.29	35.52	7.21	0.98	4.43	0.65	5.62	1.09	3.33	0.47	3.11	0.47
	RSD	*1.99*	*4.43*	*1.54*	*1.05*	*1.43*	*1.12*	*0.77*	*0.75*	*1.65*	*0.45*	*1.59*	*1.51*	*0.08*	*1.39*
[1368]-11004	PPM	39.33	80.35	9.29	35.39	7.09	0.91	4.19	0.60	5.29	1.01	3.08	0.43	2.91	0.44
	RSD	*1.76*	*3.87*	*1.97*	*1.74*	*1.15*	*0.41*	*0.99*	*0.58*	*1.56*	*1.67*	*1.63*	*0.86*	*2.40*	*1.72*
[2041]-13885	PPM	40.07	75.22	9.60	36.94	7.57	0.98	4.40	0.65	6.03	1.16	3.50	0.49	3.31	0.50
	RSD	*1.83*	*3.59*	*2.39*	*2.57*	*2.88*	*1.08*	*0.99*	*0.60*	*2.47*	*1.47*	*1.97*	*2.52*	*2.50*	*2.88*
[973]-7560	PPM	38.63	81.33	9.68	36.36	7.08	1.25	5.50	0.75	3.90	0.74	2.14	0.31	2.06	0.32
	RSD	*0.97*	*3.31*	*0.61*	*0.97*	*0.35*	*0.55*	*0.92*	*1.62*	*0.17*	*1.80*	*2.62*	*1.52*	*0.56*	*2.02*
Vala 37	PPM	32.36	67.03	7.73	30.92	6.12	1.22	5.68	0.83	3.98	0.77	2.34	0.33	2.20	0.32
	RSD	*0.69*	*3.20*	*1.09*	*1.58*	*2.85*	*3.80*	*3.00*	*12.17*	*3.94*	*3.58*	*4.52*	*5.19*	*5.44*	*5.30*
[1117]-8209	PPM	41.57	85.66	9.56	38.04	7.48	1.50	7.30	1.02	5.17	0.99	2.99	0.40	2.59	0.37
	RSD	*1.59*	*0.53*	*2.91*	*3.41*	*4.18*	*7.73*	*8.56*	*7.70*	*3.68*	*3.14*	*1.69*	*1.79*	*3.03*	*1.20*
[508]-4967	PPM	39.98	81.31	9.15	35.81	7.03	1.37	6.45	0.90	4.45	0.84	2.51	0.33	2.13	0.31
	RSD	*2.74*	*4.12*	*2.16*	*3.44*	*5.22*	*5.31*	*6.77*	*4.63*	*4.87*	*4.83*	*7.23*	*4.56*	*3.21*	*2.03*
[473]-4458	PPM	33.44	71.58	8.39	33.20	6.66	1.04	4.79	0.68	4.60	0.87	2.00	0.37	1.82	0.27
	RSD	*2.55*	*0.75*	*0.84*	*0.90*	*0.55*	*0.51*	*0.32*	*0.23*	*0.66*	*0.82*	*0.32*	*1.08*	*0.74*	*0.80*
[973]-7561	PPM	39.34	88.13	11.05	39.97	8.00	1.11	5.46	0.74	4.84	0.89	1.97	0.36	1.73	0.25
	RSD	*1.98*	*1.38*	*1.32*	*0.83*	*0.97*	*0.39*	*0.87*	*0.71*	*0.38*	*0.41*	*0.66*	*0.96*	*0.44*	*0.83*

Table 11, annex 2. Ceramic samples chemical composition, rare earth elements obtained by ICP-MS, part 2.

Sample reference – [U.S.]-n°		Rare earth elements													
		La	Ce	Pr	Nd	Sm	Eu	Gd	Tb	Dy	Ho	Er	Tm	Yb	Lu
[1117]-8197	PPM	32.61	72.67	8.08	31.26	6.24	0.94	4.28	0.62	4.62	0.89	1.93	0.38	1.82	0.27
	RSD	*0.88*	*1.98*	*1.40*	*1.47*	*1.14*	*0.76*	*0.02*	*0.94*	*1.54*	*1.43*	*0.83*	*1.24*	*0.58*	*0.89*
[1359]-9939	PPM	40.19	87.81	9.97	38.78	7.76	1.06	4.99	0.74	6.11	1.19	2.33	0.51	2.20	0.33
	RSD	*11.31*	*9.66*	*9.98*	*11.19*	*11.27*	*0.52*	*1.08*	*1.14*	*11.11*	*11.67*	*0.48*	*8.96*	*0.77*	*1.13*
[473]-4453	PPM	39.25	85.25	9.85	38.15	7.74	0.99	4.43	0.64	5.77	1.11	3.38	0.48	3.19	0.49
	RSD	*3.69*	*2.13*	*0.30*	*0.05*	*0.47*	*0.79*	*0.73*	*0.24*	*1.14*	*0.67*	*1.22*	*1.29*	*0.51*	*3.02*
[1117]-8202	PPM	38.26	77.23	9.20	35.16	6.99	0.85	4.00	0.57	4.97	0.94	2.85	0.39	2.67	0.41
	RSD	*1.09*	*3.92*	*2.23*	*2.96*	*2.92*	*0.30*	*1.12*	*0.91*	*3.05*	*2.49*	*1.58*	*2.65*	*2.09*	*3.27*
[1359]-9930	PPM	41.36	81.70	9.81	37.72	7.59	0.97	4.39	0.61	5.21	0.98	2.99	0.42	2.82	0.43
	RSD	*2.21*	*2.96*	*0.79*	*0.52*	*1.11*	*0.71*	*0.72*	*0.09*	*1.17*	*1.86*	*0.95*	*0.66*	*0.56*	*1.28*
[1130]-7712	PPM	36.28	78.91	8.86	35.15	7.19	1.21	5.31	0.79	5.54	1.06	2.40	0.45	2.26	0.33
	RSD	*2.80*	*1.50*	*0.78*	*1.15*	*0.80*	*1.08*	*0.20*	*0.34*	*0.93*	*0.32*	*0.84*	*1.65*	*3.68*	*0.77*
[1130]-7714	PPM	36.75	70.22	9.22	36.82	7.55	1.21	5.45	0.81	5.85	1.14	2.50	0.48	2.33	0.34
	RSD	*1.66*	*1.57*	*1.34*	*1.71*	*2.17*	*0.70*	*0.35*	*0.58*	*1.24*	*1.14*	*0.73*	*1.60*	*0.09*	*0.77*
[1130]-7716	PPM	39.01	76.04	9.63	37.97	7.68	1.21	5.46	0.81	5.99	1.15	2.51	0.48	2.29	0.34
	RSD	*2.68*	*1.40*	*1.45*	*1.26*	*2.15*	*0.50*	*0.75*	*0.44*	*1.23*	*1.81*	*0.48*	*1.72*	*0.56*	*1.11*
[571]-5116	PPM	36.25	64.89	7.61	29.23	5.59	1.34	4.98	0.69	3.45	0.66	1.94	0.27	1.72	0.25
	RSD	*3.09*	*2.06*	*2.70*	*3.52*	*4.46*	*5.36*	*8.12*	*9.00*	*7.83*	*8.19*	*7.39*	*5.05*	*5.24*	*3.40*
[2244]-15043	PPM	33.74	70.27	7.47	28.91	5.64	1.32	5.37	0.77	3.87	0.73	2.18	0.30	1.95	0.28
	RSD	*3.71*	*0.98*	*1.46*	*1.48*	*3.01*	*0.98*	*2.81*	*1.80*	*3.57*	*3.81*	*3.22*	*2.89*	*3.98*	*3.26*
[2171]-14751	PPM	29.91	63.17	6.92	26.56	5.11	0.83	4.57	0.61	2.90	0.53	1.51	0.21	1.32	0.19
	RSD	*3.40*	*2.19*	*0.19*	*0.66*	*1.72*	*2.91*	*4.00*	*3.32*	*2.31*	*3.75*	*4.27*	*2.75*	*4.33*	*3.57*
[571]-5117	PPM	30.63	65.23	7.09	28.12	5.67	1.24	5.16	0.75	3.93	0.78	2.37	0.34	2.23	0.34
	RSD	*4.47*	*2.49*	*1.01*	*2.19*	*3.49*	*3.58*	*5.40*	*6.09*	*5.88*	*6.90*	*7.18*	*7.34*	*5.14*	*6.71*
[91]-1977	PPM	41.76	86.39	11.26	39.35	7.83	1.03	4.82	0.67	5.03	0.96	2.85	0.41	2.67	0.41
	RSD	*2.90*	*3.21*	*0.80*	*0.63*	*1.07*	*0.62*	*0.11*	*0.57*	*0.42*	*0.15*	*0.91*	*1.70*	*1.87*	*1.18*
[91]-1980	PPM	33.49	78.55	8.27	32.28	6.49	0.96	3.93	0.55	4.26	0.82	2.54	0.36	2.51	0.38
	RSD	*4.43*	*0.28*	*1.11*	*0.92*	*1.06*	*0.29*	*0.43*	*1.33*	*0.58*	*0.42*	*1.81*	*1.34*	*0.68*	*2.32*
[91]-1992	PPM	39.74	80.56	9.57	37.50	7.51	1.06	4.56	0.62	4.92	0.94	2.86	0.40	2.73	0.42
	RSD	*4.11*	*2.71*	*0.69*	*0.62*	*0.55*	*1.46*	*0.65*	*0.25*	*0.49*	*0.25*	*1.37*	*1.23*	*0.67*	*1.42*
[91]-1994	PPM	43.46	92.61	11.38	39.94	7.94	1.02	4.65	0.64	5.35	1.00	3.04	0.42	2.87	0.44
	RSD	*2.13*	*4.12*	*0.82*	*0.71*	*0.79*	*0.61*	*0.59*	*0.60*	*0.87*	*0.89*	*0.24*	*0.95*	*0.38*	*2.43*
[939]-7351	PPM	31.99	65.82	8.08	31.22	6.15	1.11	5.08	0.78	4.23	0.85	2.43	0.35	2.33	0.36
	RSD	*2.88*	*1.31*	*1.12*	*0.84*	*1.02*	*1.23*	*1.78*	*2.43*	*2.67*	*1.77*	*3.79*	*2.40*	*1.19*	*3.74*
[1]-15467	PPM	41.22	87.15	11.27	38.24	7.57	1.49	6.20	0.95	5.09	1.02	2.87	0.40	2.53	0.38
	RSD	*3.11*	*3.01*	*3.47*	*1.89*	*2.54*	*1.05*	*0.89*	*3.12*	*2.33*	*1.03*	*2.22*	*2.42*	*1.42*	*2.24*

Table 12, annex 2. Ceramic samples calculated values.

Sample reference – [U.S.]-n°		Calculated values														
		SiO_2/Al_2O_3	Fe_2O_3/TiO_2	Zr/U	Hf/U	Ce_{CN}	Eu_{CN}	Ce_{CN}/Eu_{CN}	Ce_{CN} anomly	EU_{CN} anomaly	$LREE_{CN}$	$MREE_{CN}$	$HREE_{CN}$	$LREE_{CN}/MREE_{CN}$	$LREE_{CN}/HREE_{CN}$	Sum REE_{CN}
LSI04-233	**a.u.**	3.80	7.43	34.39	1.03	177.27	21.37	8.29	1.19	0.53	625.53	118.40	60.42	5.28	11.35	804.34
LSI04-232	**a.u.**	4.62	6.38	48.36	1.29	135.45	20.16	6.72	1.04	0.60	529.85	111.40	49.33	5.23	11.74	680.58
LSI04-228	**a.u.**	4.32	8.59	41.53	1.18	96.30	21.58	4.46	0.64	0.60	543.46	93.93	39.97	5.79	13.60	677.36
LSI04-229	**a.u.**	3.97	7.94	52.24	1.44	116.77	19.79	5.40	0.99	0.63	436.75	98.12	54.39	4.45	8.03	589.26
LSI04-236	**a.u.**	4.41	7.57	45.88	1.14	118.44	20.57	5.76	1.03	0.55	465.40	92.75	44.15	5.02	11.54	602.30
[1335]-9818	**a.u.**	3.46	8.04	78.74	1.52	119.41	17.11	6.39	1.02	0.53	442.58	99.40	58.11	4.45	7.62	600.09
[1368]-9999	**a.u.**	3.75	8.01	74.80	1.39	131.00	18.58	7.05	1.02	0.53	524.84	114.00	56.03	5.05	9.37	684.86
[2041]-13884	**a.u.**	3.61	7.67	73.87	1.38	208.37	20.11	11.37	1.52	0.52	630.30	115.29	62.16	5.47	11.14	807.74
[1368]-11000	**a.u.**	3.79	8.14	56.90	1.52	114.98	14.95	7.69	1.02	0.53	460.14	85.36	65.11	5.39	7.07	611.60
[1368]-11002	**a.u.**	3.59	7.90	50.03	1.40	141.06	17.41	8.11	1.13	0.51	524.26	110.67	78.36	5.21	6.69	703.29
[1368]-11004	**a.u.**	3.46	7.78	48.94	1.38	131.07	16.18	8.11	1.02	0.52	522.51	93.98	72.54	5.56	7.20	689.04
[2041]-13885	**a.u.**	3.37	7.94	51.16	1.42	122.71	17.43	7.04	0.93	0.61	527.27	113.26	82.52	5.11	6.39	713.04
[973]-7560	**a.u.**	3.58	3.40	41.56	1.14	132.68	22.24	5.97	1.02	0.63	527.34	110.06	51.55	5.27	11.23	678.95
Vala37-[11]	**a.u.**	3.72	7.11	50.19	1.19	119.34	21.65	5.05	1.02	0.62	438.26	113.59	54.71	4.23	8.01	596.56
[1117]-8209	**a.u.**	3.35	5.27	26.18	0.65	139.75	26.65	5.24	1.04	0.62	551.93	130.77	65.97	4.22	8.37	748.67
[508]-4697	**a.u.**	3.93	2.77	29.24	0.68	132.64	24.33	5.45	1.03	0.56	525.73	115.12	55.11	4.57	9.54	695.94
[473]-4458	**a.u.**	4.49	7.24	54.15	1.24	116.77	18.49	6.31	1.03	0.51	465.87	96.20	49.63	4.84	9.39	611.70
[937]-7561	**a.u.**	4.67	8.17	43.05	0.89	143.77	19.76	7.28	1.07	0.55	559.58	113.51	47.84	5.41	11.70	711.93
[1117]-8197	**a.u.**	4.20	7.78	87.57	1.62	118.55	16.69	7.11	1.08	0.52	453.87	90.62	50.02	5.01	9.07	594.51
[1359]-9939	**a.u.**	3.88	7.86	74.99	1.44	143.25	18.87	7.59	1.06	0.51	557.53	111.13	62.39	5.02	8.94	731.06
[473]-4453	**a.u.**	3.37	8.58	46.41	1.36	139.07	17.51	7.94	1.05	0.49	546.62	111.37	80.04	5.39	6.83	728.03
[1117]-8202	**a.u.**	4.05	8.37	43.88	1.26	125.98	15.07	8.36	1.00	0.51	511.70	88.35	66.70	5.78	7.66	665.75
[1359]-9930	**a.u.**	3.73	8.73	48.96	1.32	133.27	17.15	7.77	0.98	0.60	547.27	95.33	70.44	5.74	7.77	713.04
[1130]-7712	**a.u.**	3.62	7.97	59.61	1.27	128.73	21.55	5.97	1.06	0.57	502.86	112.00	60.76	4.49	8.28	675.62
[1130]-7714	**a.u.**	3.54	8.38	66.71	1.34	114.56	21.41	5.35	0.92	0.57	500.53	115.88	63.43	4.32	7.89	679.85
[1130]-7716	**a.u.**	3.62	7.50	59.60	1.21	124.05	21.54	5.76	0.95	0.77	527.41	116.96	63.17	4.51	8.35	707.54
[571]-5116	**a.u.**	2.43	3.09	38.91	1.00	115.86	23.81	4.45	0.94	0.73	442.60	93.98	43.91	4.71	11.08	580.49
[2244]-15043	**a.u.**	3.68	8.21	38.32	1.02	114.64	23.50	4.88	1.07	0.70	438.87	110.86	49.46	4.35	8.87	589.20
[2171]-14751	**a.u.**	3.34	3.66	29.77	0.72	116.40	22.08	4.82	1.07	0.53	411.89	99.18	55.99	4.15	7.36	567.05
[571]-5517	**a.u.**	4.69	5.67	15.47	0.41	113.05	14.78	6.97	1.06	0.51	396.46	76.09	33.54	5.21	11.82	506.09
[91]-1977	**a.u.**	4.08	6.62	48.78	1.39	140.93	18.35	7.68	1.01	0.58	566.75	99.14	67.51	5.72	8.40	733.39
[91]-1980	**a.u.**	3.42	8.51	36.22	0.97	128.15	17.12	7.48	1.14	0.55	473.11	84.42	61.60	5.60	7.68	619.13
[91]-1992	**a.u.**	3.14	9.35	47.70	1.29	131.42	18.76	7.00	1.00	0.51	535.06	95.96	68.25	5.58	7.84	699.27
[91]-1994	**a.u.**	3.72	9.22	29.19	0.86	151.07	18.15	8.32	1.05	0.60	587.31	99.27	71.74	5.92	8.19	758.31
[939]-7315	**a.u.**	3.73	8.11	55.12	1.49	117.37	19.51	5.50	0.99	0.66	439.23	99.36	58.53	4.42	7.50	597.12
[1]-15467	**a.u.**	2.98	3.33	43.37	1.17	142.17	26.40	5.39	1.02	0.65	561.60	123.29	65.35	4.56	8.59	750.24

Annexe 3 - section 5.3

Annexes are inserted in the following order:

- Ceramics sample list with samples laboratory reference (L.R.), samples typology and decoration style, samples function and samples archaeological reference.
- PLM description of ceramic thin sections with matrix, porosity, and temper characteristics.
- XRF data for ceramics and raw materials.
- Physical and mechanical data for each singular sample.

Table 1, annex 3. Archaeological ceramic sample list from Rua 5 de Outubro, Santarém (RCO).

[S.U]-Ref.	*Arc. Context/S.U.*	*Chronology - century*	*Typology*	*Function*	*Decoration*	*Arch. Site-Site*
[509]-4724	[583]	*11th - 12th*	Pot	Fire ceramics	White Painted	RCO
[504]-4665	[520]	*11th - 12th*	Pan	Fire ceramics	Unpainted	RCO
[1666]-12037	[1667]	*11th - 12th*	Lid	Fire ceramics	White Painted	RCO
[504]-4660	[520]	*11th - 12th*	Big Jug	Food, liquid containers	White Painted	RCO
[504]-4666	[520]	*11th - 12th*	Jug	Food, liquid containers	White Painted	RCO
[475]-4467	[476]	*11th - 12th*	Big earthen pot	Food, liquid containers	Unpainted	RCO
[504]-4663	[520]	*11th - 12th*	Bowl	Table ceramics	White Painted	RCO
[504]-4664	[520]	*11th - 12th*	Bowl	Table ceramics	White Painted	RCO
[91]-1978	[2466]	*12th - 13th*	Pot	Fire ceramics	Unpainted	RCO
[2244]-15045	[2172]	*12th - 13th*	Pan	Fire ceramics	Unpainted	RCO
[91]-1983	[2466]	*12th - 13th*	Lid	Fire ceramics	Unpainted	RCO
[2244]-15029	[2172]	*12th - 13th*	Big Jug	Food, liquid containers	White Painted	RCO
[91]-1981	[2466]	*12th - 13th*	Jug	Food, liquid containers	Unpainted	RCO
[91]-1979	[2466]	*12th - 13th*	Big earthen pot	Food, liquid containers	Unpainted	RCO
[91]-1985	[2466]	*12th - 13th*	Bowl	Table ceramics	Unpainted	RCO
[829]-6952	[828]	*13th - 14th*	Pot	Fire ceramics	Unpainted	RCO
[829]-6953	[828]	*13th - 14th*	Pan	Fire ceramics	Unpainted	RCO
[829]-6950	[828]	*13th - 14th*	Lid	Fire ceramics	Unpainted	RCO
[829]-6966	[828]	*13th - 14th*	Jug	Food, liquid containers	White Painted	RCO
[829]-6947	[828]	*13th - 14th*	Bowl	Table ceramics	Unpainted	RCO
[829]-6962	[828]	*13th - 14th*	Bowl	Table ceramics	Unpainted	RCO
[2058]-14121	[2059]	*15th - 16th*	Pot	Fire ceramics	Unpainted	RCO
[2096]-14392	[2059]	*15th - 16th*	Pan	Fire ceramics	Unpainted	RCO
[2058]-14124	[2059]	*15th - 16th*	Lid	Fire ceramics	Unpainted	RCO
[2096]-14374	[2059]	*15th - 16th*	Big earthen pot	Food, liquid containers	Unpainted	RCO
[2096]-14381	[2059]	*15th - 16th*	Bowl	Table ceramics	Unpainted	RCO
[2058]-14122	[2059]	*15th - 16th*	Bowl	Table ceramics	Unpainted	RCO

Table 2, annex 3. Traditional ceramic samples list from Muge (MG).

[S.U]-Ref.	*Arc. Context/S.U.*	*Chronology - century*	*Typology*	*Function*	*Decoration*	*Arch. Site-Site*
Trd-1	Atelier	Contemporary	Pot Lid	Fire ceramics	Unglazed	MG
Trd-2	Atelier	Contemporary	Pot	Fire ceramics	Glazed	MG
Trd-2a	Atelier	Contemporary	Pot (Bottom)	Fire ceramics	Glazed	MG
Trd-3	Atelier	Contemporary	Chestnut roaster	Fire ceramics	Unglazed	MG
Trd-4	Atelier	Contemporary	*Tacho*	Fire ceramics	Glazed	MG
Trd-5	Atelier	Contemporary	*Tacho* Lid	Fire ceramics	Glazed	MG
Trd-6	Atelier	Contemporary	Jug	Food, liquid containers	Unglazed	MG
Trd-6a	Atelier	Contemporary	Jug (Bottom)	Food, liquid containers	Unglazed	MG
Trd-7	Atelier	Contemporary	Jug lid	Food, liquid containers	Unglazed	MG
Trd-8	Atelier	Contemporary	Water costrel	Food, liquid containers	Unglazed	MG
Trd-8a	Atelier	Contemporary	Water costrel (Bottom)	Food, liquid containers	Unglazed	MG
Trd-9	Atelier	Contemporary	Water costrel Lid	Food, liquid containers	Unglazed	MG
Trd-11	Atelier	Contemporary	Glazed plate	Table ceramics	Glazed	MG
Trd-11	Atelier	Contemporary	Painted plate	Table ceramics	Unglazed	MG
Trd-12	Atelier	Contemporary	Green bowl	Table ceramics	Glazed	MG
Trd-13	Atelier	Contemporary	Bowl	Table ceramics	Glazed	MG
Trd-14	Atelier	Contemporary	Yellow bowl	Table ceramics	Glazed	MG

Table 3, annex 3. Ceramic samples matrix and porosity characteristics. H.HOM., highly homogeneous – M.HOM., moderately homogeneous – S.HOM., slightly homogeneous – H.HET., highly heterogeneous – M.HET., moderately heterogeneous – S.HET., slightly heterogeneous. Fe- Ca rich matrix: Fe, iron rich matrix – S.Ca, slightly calcitic – M. Ca, moderately calcitic – H.Ca., Highly calcitic. Part 1.

Sample ref. [U.S.]-n°	Fabric	Subgroup	Matrix						Porosity
			Colour	Homogeneity/ heterogeneity	Fe / Ca rich matrix	Matrix Activity	Clay pellets	Oxides	Description
[509]-4724	1	A	Red	H.Hom.	Fe	Moderate		X	Macro vughs and meso-micro vesicles
[504]-4665	1	B	Red-brown	M.Hom.	Fe	Moderate		X	Macro-meso vesicles, channels and planar voids
[1666]-12037	1	A	Red	H.Hom.	Fe	Moderate		X	Meso vughs and meso-micro vesicles
[504]-4660	2	A	Brown-grey	S.Het.	S.Ca.	Moderate	X	X	Meso-micro planar voids
[504]-4666	1	A	Brown-grey	S.Het.	Fe	Moderate		X	Meso vughs, planar voids and vesicles
[475]-4467	1	A	Red	H.Hom.	Fe	Not active	X	X	Mega-meso vughs and planar voids
[504]-4663	1	A	Red	H.Hom.	Fe	Moderate	X	X	Meso planar voids and micro vesicles
[504]-4664	1	A	Red	H.Hom.	Fe	Moderate		X	Meso channels and vesicles
[91]-1978	1	B	Red	M.Hom.	Fe	Not active	X	X	Macro-meso vughs and macro-meso planar voids and vesicles
[2244]-15045	1	B	Red	M.Hom.	Fe	Moderate	X	X	Macro-meso channels and planar voids
[91]-1983	1	B	Red	M.Hom.	Fe	Moderate	X	X	Macro-micro planar voids and micro vesicles
[2244]-15029	1	A	Red-brown	M.Hom.	Fe	Moderate	X	X	Mega-meso planar voids planar voids and meso-micro vesicles
[91]-1981	1	A	Red	H.Hom.	Fe	Moderate	X	X	Macro vughs, meso planar voids and micro vesicles
[91]-1979	1	A	Red-brown	S.Het.	Fe	Moderate	X	X	Macro-meso planar voids and channels and micro vesicles
[91]-1985	1	A	Red	M.Hom.	Fe	Moderate	X	X	Macro channels and planar voids, micro vesicles
[829]-6952	2	B	Brown-grey	S.Het.	S.Ca.	Moderate	X	X	Mega-meso vughs and meso vughs
[829]-6953	1	A	Red-brown	M.Hom.	Fe	Moderate	X	X	Mega-macro planar voids, channels and vesicles
[829]-6950	1	B	Brown-grey	M.Hom.	Fe	Moderate	X	X	Macro-meso vughs, meso-micro planar voids and vesicles
[829]-6966	1	A	Red	H.Hom.	Fe	Moderate	X	X	Meso-micro vesicles and channels
[829]-6947	2	A	Brown-grey	S.Hom.	S.Ca.	Moderate	X	X	Macro-micro vesicles, channels and planar voids
[829]-6962	1	A	Red-brown	M.Hom.	Fe	Moderate		X	Macro vughs, meso-micro planar voids, channels and vesicles

Table 4, annex 3. Ceramic samples matrix and porosity characteristics. H.HOM., highly homogeneous – M.HOM., moderately homogeneous – S.HOM., slightly homogeneous – H.HET., highly heterogeneous – M.HET., moderately heterogeneous – S.HET., slightly heterogeneous. Fe- Ca rich matrix: Fe, iron rich matrix – S.Ca, slightly calcitic – M. Ca, moderately calcitic – H.Ca., Highly calcitic. Part 2.

Sample ref. [U.S.]-n°	Fabric	Subgroup	Matrix						Porosity
			Colour	Homogeneity/ heterogeneity	Fe / Ca rich matrix	Matrix Activity	Clay pellets	Oxides	Description
[2058]-14121	1	B	Red	H.Hom.	Fe	Moderate	X	X	Macro vughs, meso-micro planar voids and vesicles
[2096]-14392	1	A	Red	H.Hom.	Fe	Moderate	X	X	Meso planar voids and vesicles
[2058]-14124	2	A	Brown-grey	S.Het.	S.Ca.	Moderate	X	X	Macro-meso planar voids, vughs and channels
[2096]-14374	1	A	Red	H.Hom.	Fe	Moderate	X	X	Mega-macro vughs, macro-meso planar voids and vesicles
[2096]-14381	1	A	Red-grey	S.Het.	Fe	Moderate	X	X	Macro-meso planar voids, channels and vughs
[2058]-14122	1	A	Red	H.Hom.	Fe	Moderate	X	X	Meso planar voids and vesicles
Trd-1	3	-	Red	H.Hom.	Fe	Slightly active		X	Macro-meso planar voids, meso-micro vesicles
Trd-2	3	-	Red	H.Hom.	Fe	Slightly active		X	Macro-meso channels and vughs, meso-micro vesicles
Trd-2a	3		Red	H.Hom.	Fe	Slightly active	X	X	Meso-micro vughs and vesicles
Trd-3	3	-	Red	H.Hom.	Fe	Slightly active	X	X	Meso-micro vughs and vesicles
Trd-4	3	-	Red	H.Hom.	Fe	Slightly active		X	Meso channels and vesicles
Trd-5	3	-	Red	H.Hom.	Fe	Slightly active		X	Macro vughs, meso channels and vesicles
Trd-6	3	-	Red	H.Hom.	Fe	Slightly active	X	X	Meso-micro vughs and vesicles
Trd-6a	3		Red	H.Hom.	Fe	Slightly active		X	Macro-meso vughs and micro vesicles
Trd-7	3	-	Red	H.Hom.	Fe	Slightly active		X	Macro channels, meso-micro vesicles
Trd-8	3	-	Red	H.Hom.	Fe	Slightly active	X	X	Macro-meso vughs and micro vesicles
Trd-8a	3		Red	H.Hom.	Fe	Slightly active	X	X	Meso-micro vughs and vesicles
Trd-9	3	-	Red	H.Hom.	Fe	Slightly active		X	Meso vesicles and channels
Trd-11	3	-	Red	H.Hom.	Fe	Slightly active		X	Macro vughs, macro-meso channels and vesicles
Trd-11	3	-	Red	H.Hom.	Fe	Slightly active		X	Meso-micro vughs and vesicles
Trd-12	3	-	Red	H.Hom.	Fe	Slightly active		X	Meso vesicles and channels
Trd-13	3	-	Red	H.Hom.	Fe	Slightly active		X	Macro-meso channels, meso-micro vesicles
Trd-14	3	-	Red	H.Hom.	Fe	Slightly active	X	X	Meso-micro vesicles and channels

Table 5, annex 3. Ceramic samples temper characteristics. Main grain shape: Eq&El, mainly equal (rounded) and elongated grains – El&Eq, mainly elongated and equal grains. Roundness: VA, very angular – A, angular – SA, sub angular – SR, sub rounded – R, rounded – WR, well rounded. Packing: CS, close spaced – SS, single spaced – DS, double spaced – OS, open spaced. Sorting: VP, very poor – P, poor – M, moderate – W, well. Grain size distribution (G.S.D.): U, unimodal – B, bimodal. Part 1.

Sample reference-[U.S.]-nº	Fabric	Subgroup	Temper									
			Shape	Roundness	Packing	Max size mm	Alignment	Sorting	Grain size distribution	Temper %	Minerals	Rock fragments
[509]-4724	1	A	Eq&El	SR-A	OS	0.4	Moderate	Moderate	U	6.96	Quartz, K-Fldspar, Plagioclase, Muscovite, Tourmaline	Quartzite
[504]-4665	1	B	Eq&El	SR-A	SS	0.9	Moderate	Moderate	U	16.87	Quartz, K-Fldspar, Plagioclase, Muscovite, Calcite	Quartzite, Granite
[1666]-12037	1	A	Eq&El	SR-A	DS	0.6	Moderate	Moderate	U	9.59	Quartz, K-Fldspar, Muscovite, Tournaline	Quartzite
[504]-4660	2	A	Eq&El	SR-A	SS	1.4	Weak	Very poor	U	17.86	Quartz, K-Fldspar, Plagioclase, Muscovite, Secondry calcite	Quartzite, Sandostone, Biomicrite, Intramicrite
[504]-4666	1	A	Eq&El	SR-A	SS	0.7	Weak	Poor	U	12.27	Quartz, K-Fldspar, Muscovite, Secondary Calcite	Quartzite, Limestone
[475]-4467	1	A	Eq&El	SR-A	SS	2.3	Weak	Very poor	U	19.54	Quartz, K-Fldspar, Plagioclase, Muscovite, Tourmaline	Quartzite, Sandstone
[504]-4663	1	A	Eq&El	SR-A	DS	1	Moderate	Moderate	U	12.15	Quartz, K-Fldspar, Muscovite	Quartzite, Granite
[504]-4664	1	A	Eq&El	SR-A	DS	0.65	Moderate	Moderate	U	8.99	Quartz, K-Fldspar, Muscovite	Quartzite, Granite
[91]-1978	1	B	Eq&El	SR-A	SS	0.4	Weak	Poor	U	11.43	Quartz, K-Fldspar, Plagioclase, Muscovite,	Quartzite, Granite
[2244]-15045	1	B	Eq&El	SR-A	SS	1	Moderate	Poor	U	11.30	Quartz, K-Fldspar, Plagioclase, Muscovite, Tourmaline, Secondry calcite	Quartzite, Granite, Sandstone, Limestone
[91]-1983	1	B	Eq&El	SR-A	SS	1	Weak	Poor	U	11.72	Quartz, K-Fldspar, Muscovite	Quartzite, Limestone
[2244]-15029	1	A	Eq&El	SR-A	DS	0.7	Moderate	Moderate	U	9.55	Quartz, K-Fldspar, Plagioclase, Muscovite, Tourmaline	Quartzite, Granite
[91]-1981	1	A	Eq&El	SR-A	OS	0.7	Weak	Moderate	U	7.11	Quartz, K-Fldspar, Muscovite	Quartzite
[91]-1979	1	A	Eq&El	SR-A	SS	2	Weak	Very poor	U	13.34	Quartz, K-Fldspar, Plagioclase, Muscovite, Tourmaline	Quartzite, Granite
[91]-1985	1	A	Eq&El	SR-A	OS	1.2	Moderate	Poor	U	6.54	Quartz, K-Fldspar, Muscovite, Tourmaline	Quartzite, Granite
[829]-6952	2	B	Eq&El	SR-A	DS	0.9	Weak	Poor	U	9.46	Quartz, K-Fldspar, Muscovite, Secondry calcite	Quartzite, Granite
[829]-6953	1	A	Eq&El	SR-A	SS	0.9	Moderate	Very poor	U	13.95	Quartz, K-Fldspar, Plagioclase, Muscovite,	Quartzite, Granite
[829]-6950	1	B	Eq&El	SR-A	SS	1	Moderate	Poor	U	13.57	Quartz, K-Fldspar, Muscovite, Tourmaline	Quartzite, Sandstone
[829]-6966	1	A	Eq&El	R-SA	OS	0.3	Moderate	Moderate	U	4.73	Quartz, K-Fldspar, Muscovite	Quartzite
[829]-6947	2	A	Eq&El	R-SA	CS	0.5	Moderate	Well	U	20.60	Quartz, K-Fldspar, Plagioclase, Muscovite, Tourmaline, Secondry calcite	Quartzite, Limestone
[829]-6962	1	A	Eq&El	R-SA	SS	0.6	Moderate	Moderate	U	11.22	Quartz, K-Fldspar, Plagioclase, Muscovite, Tourmaline	Quartzite, Granite

Table 6, annex 3. Ceramic samples temper characteristics. Main grain shape: Eq&El, mainly equal (rounded) and elongated grains – El&Eq, mainly elongated and equal grains. Roundness: VA, very angular – A, angular – SA, sub angular – SR, sub rounded – R, rounded – WR, well rounded. Packing: CS, close spaced – SS, single spaced – DS, double spaced – OS, open spaced. Sorting: VP, very poor – P, poor – M, moderate – W, well. Grain size distribution (G.S.D.): U, unimodal – B, bimodal. Part 2.

Sample ref.-[U.S.]-n°	Fabric	Subgroup	Temper										
			Shape	Roundness	Packing	Max size mm	Alignment	Sorting	Grain size distribution	Temper %	Minerals	Rock frag.
[2058]-14374	1	A	Eq&El	SR-A	SS	1.15	Weak	Moderate	U	14.77	Quartz, K-Fldspar, Plagioclase, Muscovite, Biotite, Tourmaline	Quartzite, Granite, Sandsotne
[2096]-14392	1	B	Eq&El	SR-A	DS	0.9	Moderate	Moderate	U	11.87	Quartz, K-Fldspar, Plagioclase, Muscovite, Tourmaline, Calcite	Quartzite, Granite
[2058]-14124	1	A	Eq&El	SR-A	SS	0.8	Weak	Poor	U	14.66	Quartz, K-Fldspar, Plagioclase, Muscovite, Tourmaline, Secondary calcite	Quartzite, Granite
[2096]-14381	2	A	Eq&El	SR-A	CS	1.3	Weak	Very poor	U	20.25	Quartz, K-Fldspar, Plagioclase, Muscovite, Biotite	Quartzite, Granite, Sandstone
[2096]-14121	1	A	Eq&El	SR-A	SS	0.85	Weak	Poor	U	11.66	Quartz, K-Fldspar, Plagioclase, Muscovite	Quartzite, Granite, Schist
[2058]-14122	1	A	Eq&El	SR-A	SS	0.6	Moderate	Poor	U	14.74	Quartz, K-Fldspar, Plagioclase, Muscovite, Biotite	Quartzite
Trd-1	3		Eq&El	SR-A	DS	0.6	Strong	Well	U	6.54	Quartz, K-Fldspar, Muscovite	Quartzite
Trd-2	3		Eq&El	SR-A	SS	0.4	Strong	Well	U	11.28	Quartz, K-Fldspar, Muscovite	Quartzite
Trd-2a	3		Eq&El	SR-A	SS	1.3	Strong	Well	U	12.11	Quartz, K-Fldspar, Muscovite	Quartzite
Trd-3	3		Eq&El	SR-A	SS	1	Strong	Well	U	11.62	Quartz, K-Fldspar, Plagioclase, Muscovite	Quartzite
Trd-4	3		Eq&El	SR-A	SS	0.85	Strong	Well	U	11.63	Quartz, K-Fldspar, Plagioclase, Muscovite	Quartzite
Trd-5	3		Eq&El	SR-A	DS	1.3	Strong	Well	U	7.60	Quartz, K-Fldspar, Muscovite, Tourmaline	
Trd-6	3		Eq&El	SR-A	SS	0.7	Strong	Well	U	13.12	Quartz, K-Fldspar, Muscovite	Quartzite
Trd-6a	3		Eq&El	SR-A	DS	1.3	Strong	Moderate	U	7.59	Quartz, K-Fldspar, Muscovite	
Trd-7	3		Eq&El	SR-A	SS	0.4	Strong	Well	U	12.78	Quartz, K-Fldspar, Muscovite	
Trd-8	3		Eq&El	SR-A	SS	1.15	Moderate	Moderate	U	11.22	Quartz, K-Fldspar, Muscovite, Tourmaline	Quartzite
Trd-8a	3		Eq&El	SR-A	SS	1.3	Strong	Moderate	U	11.53	Quartz, K-Fldspar, Muscovite	Quartzite
Trd-9	3		Eq&El	SR-A	SS	1.3	Strong	Well	U	12.38	Quartz, K-Fldspar, Muscovite, Tourmaline	Quartzite
Trd-11	3		Eq&El	SR-A	SS	0.85	Strong	Moderate	U	12.59	Quartz, K-Fldspar, Plagioclase, Muscovite	Quartzite
Trd-11	3		Eq&El	SR-A	SS	1	Moderate	Well	U	8.39	Quartz, K-Fldspar, Muscovite	Quartzite
Trd-12	3		Eq&El	SR-A	SS	0.6	Moderate	Well	U	8.75	Quartz, K-Fldspar, Muscovite	Quartzite
Trd-13	3		Eq&El	SR-A	SS	0.7	Strong	Moderate	U	11.40	Quartz, K-Fldspar, Plagioclase, Muscovite, Tourmaline	Quartzite
Trd-14	3		Eq&El	SR-A	SS	1	Strong	Well	U	14.02	Quartz, K-Fldspar, Plagioclase, Muscovite, Tourmaline	Quartzite

Table 7, annex 3. Archaeological ceramic samples chemical composition, major oxides obtained by XRF and L.O.I., Part 1.

Sample ref. – [U.S.]-n°	Major oxides and L.O.I													
		Na_2O	MgO	Al_2O_3	SiO_2	P_2O_5	S	K_2O	CaO	TiO_2	MnO	Fe_2O_3	LOI	Sum
[509]-4724	**wt%**	0.39	1.07	17.90	67.00	0.08	0.04	3.22	0.84	0.76	0.011	5.59	2.17	99.07
	Err. ±	*0.07*	*0.03*	*0.05*	*0.05*	*0.01*	*0.001*	*0.05*	*0.02*	*0.01*	*0.002*	*0.01*		
[504]-4665	**wt%**	0.42	0.98	16.40	67.11	0.18	0.03	3.19	0.89	0.69	0.014	5.36	4.73	99.99
	Err. ±	*0.07*	*0.03*	*0.05*	*0.05*	*0.01*	*0.001*	*0.05*	*0.02*	*0.01*	*0.002*	*0.01*		
[1666]-12037	**wt%**	0.40	0.91	17.30	65.20	0.17	0.03	2.71	0.73	0.67	0.009	6.18	5.03	99.34
	Err. ±	*0.07*	*0.03*	*0.05*	*0.05*	*0.01*	*0.001*	*0.05*	*0.02*	*0.01*	*0.002*	*0.01*		
[504]-4660	**wt%**	0.30	0.93	18.90	69.80	0.05	0.04	3.19	0.44	0.62	0.009	6.26	1.11	111.64
	Err. ±	*0.07*	*0.03*	*0.05*	*0.05*	*0.01*	*0.001*	*0.05*	*0.02*	*0.01*	*0.002*	*0.01*		
[504]-4666	**wt%**	0.30	1.07	17.70	68.00	0.04	0.03	2.95	0.58	0.71	0.023	5.72	2.80	99.92
	Err. ±	*0.06*	*0.03*	*0.05*	*0.05*	*0.01*	*0.001*	*0.05*	*0.02*	*0.01*	*0.002*	*0.01*		
[473]-4467	**wt%**	0.16	0.94	16.60	73.20	0.03	0.04	2.98	0.57	0.59	0.014	5.23	1.00	111.34
	Err. ±	*0.07*	*0.03*	*0.05*	*0.05*	*0.01*	*0.001*	*0.05*	*0.02*	*0.01*	*0.002*	*0.01*		
[504]-4663	**wt%**	0.36	0.97	17.80	68.30	0.09	0.04	3.31	0.66	0.75	0.008	6.19	2.43	110.91
	Err. ±	*0.07*	*0.03*	*0.05*	*0.05*	*0.01*	*0.001*	*0.05*	*0.02*	*0.01*	*0.002*	*0.01*		
[504]-4664	**wt%**	0.46	1.17	17.90	68.00	0.12	0.04	3.16	0.90	0.83	0.019	6.33	0.96	99.89
	Err. ±	*0.07*	*0.03*	*0.05*	*0.05*	*0.01*	*0.001*	*0.05*	*0.02*	*0.01*	*0.002*	*0.01*		
[91]-1978	**wt%**	0.49	1.15	19.11	65.80	0.08	0.05	3.36	0.92	0.68	0.004	6.31	2.78	110.73
	Err. ±	*0.07*	*0.03*	*0.05*	*0.05*	*0.01*	*0.001*	*0.05*	*0.02*	*0.01*	*0.002*	*0.01*		
[2244]-15045	**wt%**	0.50	1.15	18.50	65.00	0.11	0.05	3.17	1.16	0.71	0.008	6.28	2.62	99.24
	Err. ±	*0.07*	*0.03*	*0.05*	*0.05*	*0.01*	*0.001*	*0.05*	*0.02*	*0.01*	*0.002*	*0.01*		
[91]-1983	**wt%**	0.37	1.15	18.70	67.70	0.16	0.04	2.91	0.68	0.75	0.015	5.91	1.15	99.53
	Err. ±	*0.07*	*0.03*	*0.05*	*0.05*	*0.01*	*0.001*	*0.05*	*0.02*	*0.01*	*0.002*	*0.01*		
[2244]-15029	**wt%**	0.28	0.96	17.20	68.50	0.29	0.04	3.15	1.12	0.79	0.040	5.43	1.66	99.45
	Err. ±	*0.06*	*0.03*	*0.05*	*0.05*	*0.01*	*0.001*	*0.05*	*0.02*	*0.01*	*0.002*	*0.01*		
[91]-1981	**wt%**	0.40	1.04	18.70	64.60	0.11	0.04	3.11	0.73	0.82	0.006	6.36	2.54	98.46
	Err. ±	*0.07*	*0.03*	*0.05*	*0.05*	*0.01*	*0.001*	*0.05*	*0.02*	*0.01*	*0.002*	*0.01*		
[91]-1979	**wt%**	0.32	1.05	18.70	68.11	0.11	0.04	3.09	0.47	0.67	0.008	6.04	2.04	110.63
	Err. ±	*0.06*	*0.03*	*0.05*	*0.05*	*0.01*	*0.001*	*0.05*	*0.02*	*0.01*	*0.002*	*0.01*		
[91]-1985	**wt%**	0.20	1.27	20.20	65.60	0.06	0.04	3.47	0.55	0.74	0.006	6.92	1.49	110.55
	Err. ±	*0.07*	*0.03*	*0.05*	*0.05*	*0.01*	*0.001*	*0.05*	*0.02*	*0.01*	*0.002*	*0.01*		
[829]-6952	**wt%**	0.77	1.22	20.20	66.60	0.11	0.04	3.34	0.66	0.70	0.005	6.56	1.00	111.20
	Err. ±	*0.07*	*0.03*	*0.05*	*0.05*	*0.01*	*0.001*	*0.05*	*0.02*	*0.01*	*0.002*	*0.01*		
[829]-6953	**wt%**	0.36	1.09	19.40	66.20	0.42	0.05	2.98	0.79	0.69	0.018	5.55	1.86	99.41
	Err. ±	*0.07*	*0.03*	*0.05*	*0.05*	*0.01*	*0.001*	*0.05*	*0.02*	*0.01*	*0.002*	*0.01*		
[829]-6950	**wt%**	0.58	1.11	18.00	66.90	0.21	0.04	3.09	0.79	0.75	0.009	6.01	2.41	99.89
	Err. ±	*0.07*	*0.03*	*0.05*	*0.05*	*0.01*	*0.001*	*0.05*	*0.02*	*0.01*	*0.002*	*0.01*		
[829]-6966	**wt%**	0.30	1.22	19.80	67.11	0.06	0.04	3.23	0.48	0.78	0.006	6.73	1.56	111.30
	Err. ±	*0.07*	*0.03*	*0.05*	*0.05*	*0.01*	*0.001*	*0.05*	*0.02*	*0.01*	*0.002*	*0.01*		
[829]-6947	**wt%**	0.92	1.00	22.90	65.50	0.23	0.04	3.23	0.99	0.69	0.009	3.23	2.06	110.80
	Err. ±	*0.07*	*0.03*	*0.05*	*0.05*	*0.01*	*0.001*	*0.05*	*0.02*	*0.01*	*0.002*	*0.01*		
[829]-6962	**wt%**	0.92	1.07	18.11	67.60	0.40	0.05	2.82	0.71	0.70	0.007	6.21	1.32	99.90
	Err. ±	*0.07*	*0.03*	*0.05*	*0.05*	*0.01*	*0.001*	*0.05*	*0.02*	*0.01*	*0.002*	*0.01*		

Table 8, annex 3. Archaeological ceramic samples chemical composition, major oxides obtained by XRF and L.O.I., Part 2.

Sample ref. – [U.S.]-n°	Major oxides and L.O.I													
		Na_2O	MgO	Al_2O_3	SiO_2	P_2O_5	S	K_2O	CaO	TiO_2	MnO	Fe_2O_3	LOI	Sum
[2058]-14121	**wt%**	0.46	1.01	16.80	70.70	0.06	0.04	2.62	0.44	0.76	0.008	5.82	1.49	110.21
	Err. ±	*0.07*	*0.03*	*0.05*	*0.05*	*0.01*	*0.001*	*0.05*	*0.02*	*0.01*	*0.002*	*0.01*		
[2096]-14392	**wt%**	0.46	1.03	17.00	67.30	0.12	0.07	2.82	1.77	0.66	0.009	5.52	2.67	99.43
	Err. ±	*0.07*	*0.03*	*0.05*	*0.05*	*0.01*	*0.001*	*0.05*	*0.03*	*0.01*	*0.002*	*0.01*		
[2058]-14124	**wt%**	0.65	1.18	17.40	63.60	0.11	0.08	3.27	3.59	0.57	0.026	5.24	3.77	99.48
	Err. ±	*0.07*	*0.03*	*0.05*	*0.05*	*0.01*	*0.002*	*0.05*	*0.03*	*0.01*	*0.002*	*0.01*		
[2096]-14374	**wt%**	0.51	0.80	15.11	72.20	0.07	0.03	3.13	0.60	0.55	0.011	4.48	2.41	99.89
	Err. ±	*0.07*	*0.03*	*0.04*	*0.05*	*0.01*	*0.001*	*0.05*	*0.02*	*0.01*	*0.002*	*0.01*		
[2096]-14381	**wt%**	0.57	1.06	17.70	71.00	0.05	0.05	2.73	0.51	0.69	0.006	5.83	1.01	111.19
	Err. ±	*0.07*	*0.03*	*0.05*	*0.05*	*0.01*	*0.001*	*0.05*	*0.02*	*0.01*	*0.002*	*0.01*		
[2096]-14122	**wt%**	0.40	0.95	18.50	68.60	0.05	0.04	3.03	0.64	0.81	0.038	6.23	2.06	111.35
	Err. ±	*0.07*	*0.03*	*0.05*	*0.05*	*0.01*	*0.001*	*0.05*	*0.02*	*0.01*	*0.002*	*0.01*		

Table 9, annex 3. Traditional ceramic samples chemical composition, major oxides obtained by XRF and L.O.I.

Sample ref. – [U.S.]-n°	Major oxides and L.O.I													
		Na_2O	MgO	Al_2O_3	SiO_2	P_2O_5	S	K_2O	CaO	TiO_2	MnO	Fe_2O_3	LOI	Sum
Trd-1	**wt%**	0.67	1.46	19.90	66.90	0.04	0.04	3.11	0.35	0.76	0.011	6.59	0.80	110.62
	Err. ±	*0.07*	*0.03*	*0.05*	*0.05*	*0.01*	*0.001*	*0.05*	*0.02*	*0.01*	*0.002*	*0.01*		
Trd-2	**wt%**	0.70	1.36	18.30	67.11	0.04	0.11	3.11	0.41	0.71	0.013	5.95	1.95	99.74
	Err. ±	*0.07*	*0.03*	*0.05*	*0.05*	*0.01*	*0.002*	*0.05*	*0.02*	*0.01*	*0.002*	*0.01*		
Trd-2a	**wt%**	0.74	1.29	18.70	67.70	0.115	0.02	3.17	0.35	0.79	0.019	6.00	1.06	99.94
	Err. ±	*0.05*	*0.02*	*0.04*	*0.04*	*0.003*	*0.001*	*0.05*	*0.02*	*0.01*	*0.002*	*0.01*		
Trd-3	**wt%**	0.75	1.42	19.00	67.11	0.04	0.05	3.09	0.38	0.76	0.014	6.30	1.32	110.23
	Err. ±	*0.07*	*0.03*	*0.05*	*0.05*	*0.01*	*0.001*	*0.05*	*0.02*	*0.01*	*0.002*	*0.01*		
Trd-4	**wt%**	0.85	1.33	18.50	67.40	0.04	0.19	2.80	0.37	0.73	0.015	6.23	1.43	99.89
	Err. ±	*0.07*	*0.03*	*0.05*	*0.05*	*0.01*	*0.002*	*0.05*	*0.02*	*0.01*	*0.002*	*0.01*		
Trd-5	**wt%**	0.80	1.31	18.60	67.90	0.112	0.02	2.94	0.34	0.82	0.018	6.27	0.87	99.99
	Err. ±	*0.05*	*0.02*	*0.04*	*0.04*	*0.003*	*0.001*	*0.05*	*0.02*	*0.01*	*0.002*	*0.01*		
Trd-6	**wt%**	0.56	1.35	17.90	67.30	0.05	0.04	2.85	0.38	0.76	0.012	6.27	2.48	99.95
	Err. ±	*0.07*	*0.03*	*0.05*	*0.05*	*0.01*	*0.001*	*0.05*	*0.02*	*0.01*	*0.002*	*0.01*		
Trd-6a	**wt%**	0.68	1.28	18.20	66.80	0.0985	0.02	2.96	0.30	0.81	0.016	6.25	2.61	110.02
	Err. ±	*0.05*	*0.02*	*0.04*	*0.04*	*0.003*	*0.001*	*0.05*	*0.02*	*0.01*	*0.002*	*0.01*		
Trd-7	**wt%**	0.78	1.27	17.80	68.50	0.04	0.04	3.02	0.41	0.76	0.015	5.89	1.35	99.87
	Err. ±	*0.07*	*0.03*	*0.05*	*0.05*	*0.01*	*0.001*	*0.05*	*0.02*	*0.01*	*0.002*	*0.01*		
Trd-8	**wt%**	0.73	1.39	18.70	68.70	0.04	0.04	3.04	0.34	0.69	0.013	6.58	0.97	111.23
	Err. ±	*0.07*	*0.03*	*0.05*	*0.05*	*0.01*	*0.001*	*0.05*	*0.02*	*0.01*	*0.002*	*0.01*		
Trd-8a	**wt%**	0.67	1.27	18.40	68.20	0.11	0.02	3.05	0.34	0.76	0.020	6.35	1.12	110.30
	Err. ±	*0.05*	*0.02*	*0.04*	*0.04*	*0.003*	*0.001*	*0.05*	*0.02*	*0.01*	*0.002*	*0.01*		
Trd-9	**wt%**	0.73	1.30	17.40	69.40	0.04	0.05	2.85	0.42	0.78	0.014	5.48	1.57	110.03
	Err. ±	*0.07*	*0.03*	*0.05*	*0.05*	*0.01*	*0.001*	*0.05*	*0.02*	*0.01*	*0.002*	*0.01*		
GTrd-11	**wt%**	0.72	1.33	18.30	69.20	0.04	0.19	3.03	0.38	0.69	0.015	6.25	0.49	110.63
	Err. ±	*0.07*	*0.03*	*0.05*	*0.05*	*0.01*	*0.002*	*0.05*	*0.02*	*0.01*	*0.002*	*0.01*		
Trd-11	**wt%**	0.80	1.39	18.40	67.40	0.04	0.04	2.86	0.36	0.76	0.013	6.12	2.31	110.49
	Err. ±	*0.07*	*0.03*	*0.05*	*0.05*	*0.01*	*0.001*	*0.05*	*0.02*	*0.01*	*0.002*	*0.01*		
Trd-12	**wt%**	0.72	1.17	17.80	67.90	0.04	0.37	2.83	0.47	0.77	0.016	5.62	1.86	99.56
	Err. ±	*0.07*	*0.03*	*0.05*	*0.05*	*0.01*	*0.002*	*0.05*	*0.02*	*0.01*	*0.002*	*0.01*		
Trd-13	**wt%**	0.74	1.30	18.30	68.11	0.05	0.27	3.00	0.36	0.69	0.015	6.40	0.70	99.92
	Err. ±	*0.07*	*0.03*	*0.05*	*0.05*	*0.01*	*0.002*	*0.05*	*0.02*	*0.01*	*0.002*	*0.01*		
Trd-14	**wt%**	0.61	1.28	17.70	68.11	0.04	0.21	2.92	0.38	0.67	0.011	6.00	1.99	99.91
	Err. ±	*0.07*	*0.03*	*0.05*	*0.05*	*0.01*	*0.002*	*0.05*	*0.02*	*0.01*	*0.002*	*0.01*		

Table 10, annex 3. Sediment samples (WC – weak clay; SC – strong clay) chemical composition, major oxides obtained by XRF and L.O.I.

Raw materials	Major oxides and L.O.I													
		Na_2O	MgO	Al_2O_3	SiO_2	P_2O_5	S	K_2O	CaO	TiO_2	MnO	Fe_2O_3	LOI	Sum
SC raw	**wt%**	0.33	1.01	15.20	65.90	0.087	0.03	2.96	0.23	0.57	0.016	5.29	8.89	110.51
***ERR* ±**	***Err.* ±**	*0.04*	*0.02*	*0.03*	*0.04*	*0.004*	*0.001*	*0.05*	*0.02*	*0.01*	*0.003*	*0.01*		
SC < 63µm fraction	**wt%**	0.34	1.34	19.90	56.60	0.086	0.02	2.98	0.24	0.80	0.017	6.90	12.21	111.43
***ERR* ±**	***Err.* ±**	*0.04*	*0.02*	*0.04*	*0.04*	*0.004*	*0.001*	*0.05*	*0.02*	*0.01*	*0.003*	*0.01*		
WC raw	**wt%**	1.37	1.23	17.20	60.50	0.110	0.02	2.64	0.31	0.78	0.014	6.43	9.50	110.11
***ERR* ±**	***Err.* ±**	*0.05*	*0.02*	*0.03*	*0.04*	*0.003*	*0.001*	*0.04*	*0.02*	*0.01*	*0.002*	*0.01*		
WC < 63µm fraction	**wt%**	0.72	1.20	17.11	61.60	0.098	0.02	2.50	0.36	0.88	0.019	6.11	11.29	110.89
***ERR* ±**	***Err.* ±**	*0.05*	*0.02*	*0.03*	*0.04*	*0.003*	*0.001*	*0.04*	*0.02*	*0.01*	*0.002*	*0.01*		

Table 11, annex 3. Physical and mechanical properties of traditional fire ceramics; The table shows the single characteristics of each untreated sample (with glaze and without glaze) and fired at 750 °C and 1100 °C (the glaze layer was removed prior to perform experimental firing).

Function	Samples and fragments	Apparent density	Real density	Density of the solid	Total Porosity	Open porosity to water	Open porosity to Helium	Closed porosity to Helium	Weight imbibition coefficient	Saturation index	PLT Strength index
	Fragment	***g/cm³***	***g/cm³***	***g/cm³***	***%***	***%***	***%***	***%***	***%***	***%***	***(MPa)***
		ρ_B	**ρ_R**	**ρ_S**	**ΦT**	**$\Phi_o H2O$**	**ΦoHe**	**ΦcHe**	**ICw**	**SI**	**$Is_{(50)}$**
Fire ceramics	*Pot, bottom-glaze*	1.86	2.67	2.73	32.5	26.1	30.3	2.2	14.0	32.5	2.08
	Pot, bottom-no glaze	1.84	2.60	2.68	32.5	24.2	29.3	3.1	13.1	32.5	2.46
	Pot, bottom-no glaze 750 °C	1.86	2.57	2.77	35.6	24.3	27.7	7.9	13.0	35.6	4.54
	Pot, bottom-no glaze 1100 °C	1.93	2.67	2.75	30.9	20.9	27.9	3.0	11.8	30.9	3.54
	Pot, wall-glaze	1.86	2.67	2.75	33.5	25.7	30.4	3.1	13.8	33.5	3.12
	Pot, wall-no glaze	1.86	2.59	2.67	31.3	26.3	28.0	3.3	14.1	31.3	4.27
	Pot, wall-no glaze 750 °C	1.87	2.64	2.65	29.5	24.6	29.0	0.5	13.1	29.5	3.19
	Pot, wall-no glaze 1100 °C	1.94	2.56	2.59	25.2	21.1	24.1	1.1	11.8	25.2	4.48
	Pot lid	1.87	2.69	2.73	31.7	24.1	30.6	1.2	12.9	31.7	3.62
	Pot lid 750 °C	1.84	2.75	2.83	36.0	26.5	33.3	2.7	14.4	36.0	1.89
	Pot lid 1100 °C	1.90	2.58	2.73	32.1	22.1	26.1	6.1	11.6	32.1	2.16
	Chestnust roaster	1.86	2.60	2.65	30.1	26.3	28.4	1.7	14.1	30.1	3.66
	Chestnust roaster 750 °C	1.86	2.58	2.63	29.6	25.6	28.0	1.7	13.7	29.6	3.41
	Chestnust roaster 1100 °C	1.97	2.63	2.85	33.6	18.4	25.0	8.6	9.3	33.6	1.89
	Tacho glaze	1.84	2.73	2.80	34.9	28.4	32.5	2.4	15.3	34.9	3.04
	Tacho-no glaze	1.84	2.69	2.76	34.4	28.3	31.5	2.9	15.3	34.4	2.23
	Tacho-no glaze 750 °C	1.84	2.60	2.67	31.9	27.3	29.2	2.7	14.8	31.9	3.05
	Tacho-no glaze 1100 °C	1.91	2.52	2.65	29.6	23.4	24.2	5.3	12.2	29.6	11.63
	Tacho lid-glaze	1.88	2.70	2.74	31.9	27.5	30.3	1.6	14.6	31.9	2.21
	Tacho lid-no glaze	1.84	2.54	2.70	34.0	27.4	27.6	6.4	14.9	34.0	1.64
	Tacho lid-no glaze 750 °C	1.98	2.73	2.78	29.2	26.5	27.4	1.8	13.3	29.2	1.99
	Tacho lid-no glaze 1100 °C	1.94	2.57	2.68	28.6	21.8	24.3	4.2	11.2	28.6	1.59

Table 12, annex 3. Physical and mechanical properties of traditional kitchen ceramics; The table shows the single characteristics of each samples untreated sample (with glaze and without glaze) and fired at 750 °C and 1100 °C (the glaze layer was removed prior to perform experimental firing).

Function	Samples and fragments	Apparent density	Real density	Density of the solid	Total Porosity	Open porosity to water	Open porosity to helium	Closed porosity to He	Weight imbibition coefficient	Saturation index	PLT Strength index
	Fragment	***g/cm³***	***g/cm³***	***g/cm³***	***%***	***%***	***%***	***%***	***%***	***%***	***(MPa)***
		ρ_B	ρ_R	ρ_S	ΦT	Φ_0H2O	ΦoHe	ΦcHe	ICw	SI	$Is_{(50)}$
Kitchen ceramics	*Glazed plate*	1.88	2.66	2.74	32.1	25.4	29.3	2.8	13.4	86.6	4.00
	Glazed plate-no glaze	1.87	2.63	2.69	31.1	27.1	28.8	2.3	14.5	94.2	3.40
	Glazed plate-no glaze 750 °C	1.88	2.68	2.76	33.1	23.4	29.8	3.3	12.4	78.4	3.72
	Glazed plate-no glaze 1100 °C	1.95	2.55	2.66	28.0	20.8	23.8	4.2	11.7	87.5	3.00
	Painted plate	1.83	2.58	2.64	31.3	28.5	29.0	2.3	15.5	98.2	1.36
	Painted plate 750 °C	1.99	2.74	2.82	30.4	26.3	27.3	3.2	13.2	96.3	3.20
	Painted plate 1100 °C	2.02	2.66	2.89	32.7	21.5	23.9	8.8	11.6	90.0	3.85
	Green bowl-glaze	1.92	2.60	2.77	32.8	25.4	26.2	6.6	13.2	97.0	1.43
	Green bowl-no glaze	1.84	2.62	2.80	36.4	27.9	29.5	6.9	15.1	94.7	1.65
	Green bowl-no glaze 750 °C	1.89	2.60	2.67	30.3	25.3	27.4	2.9	13.4	92.4	2.36
	Green bowl-no glaze 1100 °C	1.95	2.60	2.74	30.5	23.0	25.2	5.3	11.8	91.4	2.48
	Bowl-glaze	1.90	2.68	2.75	32.0	26.9	29.4	2.6	14.2	91.6	3.00
	Bowl-no glaze	1.87	2.74	2.80	33.9	27.8	31.8	2.1	14.8	87.5	2.62
	Bowl-no glaze 750 °C	1.88	2.69	2.78	33.5	26.7	30.3	3.2	14.2	88.0	1.99
	Bowl-no glaze 1100 °C	1.97	2.63	2.65	25.9	21.5	25.2	0.7	11.9	85.3	4.43
	Yellow bowl-glaze	1.87	2.68	2.80	34.9	27.4	30.1	4.8	14.6	91.2	2.63
	Yellow bowl-no glaze	1.87	2.62	2.78	34.8	27.1	28.6	6.2	14.5	94.7	2.95
	Yellow bowl-no glaze 750°C	1.87	2.55	2.70	32.5	26.6	26.6	5.9	14.2	110.0	3.59
	Yellow bowl-no glaze 1100 °C	1.95	2.64	2.82	33.2	21.1	26.2	7.0	11.8	80.7	3.09

Table 13, annex 3. Physical and mechanical properties of traditional food-liquid containers; The table shows the single characteristics of each samples untreated sample (with glaze and without glaze) and fired at 750 °C and 1100 °C (the glaze layer was removed prior to perform experimental firing).

Function	Samples and fragments	Apparent density	Real density	Density of the solid	Total Porosity	Open porosity to water	Open porosity to helium	Closed porosity to He	Weight imbibition coefficient	Saturation index	PLT Strength index
	Fragment	***g/cm³***	***g/cm³***	***g/cm³***	***%***	***%***	***%***	***%***	***%***	***%***	***(MPa)***
		ρ_B	**ρ_R**	**ρ_S**	**ΦT**	**Φ_0H2O**	**ΦoHe**	**ΦcHe**	**ICw**	**SI**	**$Is_{(50)}$**
Food, liquid containers	*Jug*	34.8	27.9	30.1	4.6	15.0	92.5	34.8	27.9	30.1	4.6
	Jug 750 °C	34.0	27.1	28.9	5.1	14.7	93.9	34.0	27.1	28.9	5.1
	Jug 1100 °C	36.0	27.0	33.6	2.4	14.6	80.4	36.0	27.0	33.6	2.4
	Jug, bottom	28.4	20.8	25.9	2.5	11.7	80.3	28.4	20.8	25.9	2.5
	Jug, bottom 750 °C	34.4	25.7	30.2	4.2	13.7	85.1	34.4	25.7	30.2	4.2
	Jug, bottom 1100 °C	34.1	27.5	32.3	1.8	14.8	85.0	34.1	27.5	32.3	1.8
	Jug lid	29.7	20.5	27.8	1.9	11.5	73.7	29.7	20.5	27.8	1.9
	Jug lid 750 °C	37.4	27.3	34.0	3.4	15.0	80.3	37.4	27.3	34.0	3.4
	Jug lid 1100 °C	37.3	28.1	34.0	3.2	15.4	82.5	37.3	28.1	34.0	3.2
	Water costrel, bottom	33.3	22.1	28.4	4.9	11.9	77.9	33.3	22.1	28.4	4.9
	Water costrel, bottom 750 °C	31.1	26.5	30.3	0.9	14.1	87.4	31.1	26.5	30.3	0.9
	Water costrel, bottom 1100 °C	36.1	25.6	31.5	4.7	13.7	81.4	36.1	25.6	31.5	4.7
	Water costrel, wall	32.1	20.5	25.3	6.9	11.4	81.2	32.1	20.5	25.3	6.9
	Water costrel, wall 750 °C	31.4	25.2	30.6	0.8	14.1	82.5	31.4	25.2	30.6	0.8
	Water costrel, wall 1100 °C	30.8	24.7	29.9	1.0	13.1	82.7	30.8	24.7	29.9	1.0
	Water costrel lid	30.0	21.0	24.9	5.2	11.7	84.3	30.0	21.0	24.9	5.2
	Water costrel lid 750 °C	36.0	29.0	33.2	2.8	15.9	87.5	36.0	29.0	33.2	2.8
	Water costrel lid 1100 °C	33.4	27.9	31.4	2.0	15.1	88.9	33.4	27.9	31.4	2.0

Table 14, annex 3. Physical and mechanical properties of archaeological ceramics. Part 1.

Century	Function	Samples	Typology	Apparent density	Real density	Density of the solid	Total Porosity	Open porosity to water	Open porosity to helium	Closed porosity to He	Weight imbibition coefficient	Saturation index	PLT Strength index
				g/cm³	*g/cm³*	*g/cm³*	*%*	*%*	*%*	*%*	*%*	*%*	*(MPa)*
				ρ_B	ρ_R	ρ_S	ΦT	$\Phi_o H2O$	ΦoHe	ΦcHe	ICw	SI	$Is_{(50)}$
11th-12th	Fire	[509]-4724	Pot	1.98	2.56	2.65	25.9	21.3	22.4	3.5	11.8	95.3	2.81
		[504]-4665	Pan	1.95	2.57	2.62	26.3	22.4	24.0	2.3	11.4	93.1	2.38
		[1666]-12037	Lid	1.89	2.56	2.60	27.8	22.0	26.2	1.6	11.6	84.0	1.24
	Food, liquid containers	[504]-4660	Big jug	2.00	2.64	2.75	28.5	17.3	24.3	4.2	8.7	71.3	2.13
		[504]-4666	Jug	1.99	2.64	2.74	28.3	21.2	24.4	3.9	11.6	86.8	3.46
		[475]-4467	Big earthen pot	1.85	2.59	2.60	28.8	26.3	28.4	0.4	14.2	92.5	1.47
	Kitchen ceramics	[504-4663	Bowl	1.90	2.68	2.77	32.4	26.4	29.3	3.1	14.1	90.2	2.75
		[504]-4664	Bowl	1.89	2.66	2.80	34.5	25.6	29.2	5.3	13.6	87.7	3.52
12th - 13th	Fire ceramics	[91]-1978	Pot	1.91	2.59	2.62	27.4	23.8	26.1	1.2	12.4	90.9	7.07
		[2244]-15045	Pan	1.88	2.65	2.74	32.3	26.7	29.1	3.2	14.1	91.7	4.54
		[91]-1983	Lid	1.96	2.67	2.69	27.3	21.3	26.5	0.8	11.8	80.2	2.70
	Food, liquid containers	[2244]-15029	Big jug	1.98	2.57	2.63	25.5	22.1	22.9	2.6	11.1	96.4	3.67
		[91]-1981	Jug	1.91	2.55	2.76	33.2	24.2	25.3	7.9	13.2	95.6	2.51
		[91]-1979	Big earthen pot	1.90	2.64	2.74	31.8	23.6	28.0	3.9	12.4	84.5	3.49
	Kitchen ceramics	[91]-1985	Bowl	1.85	2.63	2.77	35.2	26.3	29.6	5.6	14.2	88.8	4.50

Table 15, annex 3. Physical and mechanical properties of archaeological ceramics. Part 2.

Century	Function	Samples	Typology	Apparent density	Real density	Density of the solid	Total Porosity	Open porosity to water	Open porosity to helium	Closed porosity to He	Weight imbibition coefficient	Saturation index	PLT Strength index
				g/cm³	*g/cm³*	*g/cm³*	*%*	*%*	*%*	*%*	*%*	*%*	*(MPa)*
				ρ_B	ρ_R	ρ_S	ΦT	$\Phi_o H2O$	ΦoHe	ΦcHe	ICw	SI	$Is_{(50)}$
13th – 14th	Fire ceramics	[829]-6952	Pot	1.96	2.70	2.75	29.0	22.3	27.3	1.7	11.3	81.9	4.07
		[829]-6953	Pan	1.94	2.62	2.72	30.0	22.4	26.0	4.0	11.6	86.3	2.89
		[829]-6950	Lid	1.95	2.52	2.68	29.2	20.7	22.8	6.4	11.6	90.9	5.25
	Food, liquid containers	[829]-6966	Jug	1.87	2.73	2.77	32.8	28.7	31.5	1.3	15.3	91.2	4.17
	Kitchen ceramics	[829]-6947	Bowl	1.84	2.60	2.76	35.3	22.5	29.0	6.3	12.2	77.8	1.25
		[829]-6962	Bowl	1.92	2.40	2.64	29.7	18.4	19.8	9.9	9.8	93.1	3.83
15th – 16th	Fire ceramics	[2058]-14121	Pot	1.88	2.65	2.68	30.2	24.1	29.2	1.1	13.0	82.6	2.36
		[2096]-14392	Pan	1.92	2.64	2.72	30.6	26.4	27.3	3.3	13.8	96.6	3.85
		[2058]-14124	Lid	2.05	2.64	2.68	24.0	21.2	22.4	1.6	13.2	94.5	3.72
	Food, liquid containers	[2096]-14374	Big earthen pot	1.91	2.68	2.68	28.8	26.3	28.8	0.0	13.8	91.6	1.08
	Kitchen ceramics	[2096]-14381	Bowl	1.92	2.55	2.65	28.8	20.2	24.8	4.1	11.8	81.7	2.79
		[2058]-14122	Bowl	1.89	2.69	2.74	31.5	28.2	29.8	1.7	14.9	94.6	2.47

Table 16, annex 3. Medium values with standard deviation for physical and mechanical properties of traditional kitchen ceramics with glaze and without glaze

Function	***Glaze-no glaze***		**Apparent density**	**Real density density**	**Density of the solid**	**Total Porosity**	**Open porosity to water**	**Open porosity to helium**	**Closed porosity to He**	**Weight imbibition coefficient**	**Saturation index**	**PLT Strength index**
			g/cm³	***g/cm³***	***g/cm³***	***%***	***%***	***%***	***%***	***%***	***%***	***(MPa)***
			ρB	**ρR**	**ρS**	**ΦT**	**ΦH_2O**	**ΦoHe**	**ΦcHe**	**ICw**	**SI**	**$Is_{(50)}$**
Kitchen ceramics	**Glaze**	***Average***	1.89	2.66	2.77	32.9	26.3	28.7	4.2	13.8	91.6	2.76
		St. dev.	0.02	0.03	0.02	1.1	0.9	1.5	1.6	0.6	3.7	0.92
Kitchen ceramics	**No glaze**	***Average***	1.86	2.65	2.77	34.1	27.5	29.7	4.4	14.7	92.8	2.65
		St. dev.	0.01	0.05	0.05	1.9	0.4	1.3	2.2	0.3	3.0	0.64

Annexe 4 - section 5.4

Annexes are inserted in the following order:

- Ceramics sample list with samples typology, decoration style, function and archaeological reference.
- PLM description of ceramic thin sections with matrix, porosity, and temper characteristics.
- XRF data.
- ICP-MS data.
- SEM-EDS BSE images and elemental mapping (i.e. for selected samples) distribution analysis results;
- SEM-EDS data table, spot/area chemical analysis

Table 1, annex 4. Ceramic samples included in section 5.4. The table reports samples archaeological reference, typology, decoration pattern, chronology, period, and the name of the of the archaeological site where the samples have been discovered at Mértola.

Sample Ref.	Typology-dec.	Iconography	Century	Period	Arch. Site
RDC-118-2014-0001	Kiln rod with green glaze	None	2nd half 12th	Almohad	Rua Dr. Afonso Costa
RDC-118-2014-0002	Kiln rod	None	2nd half 12th	Almohad	Rua Dr. Afonso Costa
RDC-118-2014-0003	Kiln rod	None	2nd half 12th	Almohad	Rua Dr. Afonso Costa
RDC-118-2014-0004	Kiln rod	None	2nd half 12th	Almohad	Rua Dr. Afonso Costa
RDC-118-2014-0005	Kiln rod	None	2nd half 12th	Almohad	Rua Dr. Afonso Costa
RDC-118-2014-0006	Kiln rod	None	2nd half 12th	Almohad	Rua Dr. Afonso Costa
RDC-118-2014-0007	Kiln rod	None	2nd half 12th	Almohad	Rua Dr. Afonso Costa
RDC-118-2014-0008	Kiln rod	None	2nd half 12th	Almohad	Rua Dr. Afonso Costa
R25A-02-SXV-94	Kiln waste, Jar	White painted	1st half 13th	Almohad	Rua 25 de Abril
CRVM-0357	Bowl, GB	Eternal knot	2nd half 11th - early 11th	Caliphal	*Alcaçova*, Criptoportic A
CRVM-623	Bowl, GB	Geometric	2nd half 11th	Caliphal	*Alcaçova*
CRVM-666	Bowl, GB	Vegetal-lotus flower	2nd half 11th	Caliphal	*Alcaçova*
CRVM-642	Bowl, GB	Epigraphic	11th	Taifa	Castle hillside
CRVM-1197	Bowl, GB	Vegetalist	11th	Taifa	*Alcaçova*, Criptoportic A
CRVM-1659	Bowl, GB	Geometric	11th	Taifa	*Alcaçova*, Criptoportic A
CRVM-1668	Bowl, GB	Bands and points	11th	Taifa	*Alcaçova*
CRVM-1671	Bowl, GB	Fitomorphic	11th	Taifa	*Alcaçova*
LVG-02-SXVIII-187	Bowl, GB	Zoomorphic	11th	Taifa	Largo Vasco da Gama
CRVM-1665	Bowl, GB	Zoomorphic	1st half 12th	Almoravid	Castle
CRVM-1666	Bowl, GB	Zoomorphic	1st half 12th	Almoravid	Castle
CRVM-1670	Bowl, GB	Zoomorphic	1st half 12th	Almoravid	Castle hillside
CRVM-1667	Bowl, GB	Not determined	2nd half 12th	Almohad	Castle
CRVM-1669	Bowl, GB	Epigraphic	2nd half 12th	Almohad	Castle hillside
CRVM-223	Bowl, GB	Zoomorphic	2nd half 12th	Almohad	Castle hillside
CRVM-0670	Bowl, GB	Fitomorphic	2nd half 12th – early 13th	Almohad	Castle hillside
CRCSP-0030	Jug, CSP	Epigraphic	1st half 12th	Almoravid	Indetermined
CRCSP-0031	Jug, CSP	Fitomorphic	12th	Almoravid	Indetermined
CRCSP-0028	Jug, CSP	Geometric	1st half 12th	Almoravid	*Alcaçova*, Criptoportic A
CRCSP-0027	Jug, CSP	Fitomorphic	1st half 12th	Almoravid	*Alcaçova*, Criptoportic A
CRCSP-0021	Jug, CSP	Fitomorphic	12th	Almoravid	*Alcaçova*, Criptoportic A
CRCSP-0029	Jug, CSP	Fitomorphic	12th	Almohad	Indetermined
CRVF-0003	Lid-HB	Fitomorphic	End 12th – beginning 13th	Almohad	*Alcaçova*, Criptoportic A

Table 2, annex 4. Ceramic paste, porosity and temper characteristic of the kiln rods (KR) and of the white painted (WP) fragment. Matrix homogeneity/heterogeneity: H.HOM., highly homogeneous – M.HOM., moderately homogeneous – S.HOM., slightly homogeneous – H.HET., highly heterogeneous – M.HET., moderately heterogeneous – S.HET., slightly heterogeneous. Fe- Ca rich matrix: Fe, iron rich matrix – S.Ca, slightly calcitic – M. Ca, moderately calcitic – H.Ca., Highly calcitic. Matrix activity: S, slightly active – M, moderately active – H, highly active – I, isotropic. Alignment: W, weak – M, moderate. Main grain shape: Eq&El, mainly equal (rounded) and elongated grains – El&Eq, mainly elongated and equal grains. Roundness: VA, very angular – A, angular – SA, sub angular – SR, sub rounded – R, rounded – WR, well rounded. Packing: CS, close spaced – SS, single spaced – DS, double spaced – OS, open spaced. Sorting: VP, very poor – P, poor – M, moderate – W, well. Grain size distribution (G.S.D.): U, unimodal – B, bimodal.

SAMPLE	Typology	Fabric	Ceramic paste						Porosity		Temper							
			Colour	Hom. – Het.	Fe- Ca rich matrix	Activity	Oxides	%	Description	%	Shape	Roundness	Packing	Max size µm	Alignment	Sorting	G.S.D.	%
RDC-118-2014-0001	*KR*	I	Red	M.HOM	Fe	S	X	71.14	Micro-macro planar voids and channels	9.21	Eq&El	A-R	CS	4000	W	P	BM	19.65
RDC-118-2014-0002	*KR*	I	Red	M.HOM	Fe	I	X	71.21	Micro-macro planar voids and channels	7.14	Eq&El	A-R	CS	5000	W	VP	BM	21.65
RDC-118-2014-0003	*KR*	I	Red	M.HOM	Fe	S	X	75.56	Meso-mega planar voids, channels, vughs	6.11	Eq&El	A-R	CS	2500	W	P	BM	18.33
RDC-118-2014-0004	*KR*	I	Red	M.HOM	Fe	I	X	72.43	Micro planar voids, meso-mega vughs and channels	9.9	Eq&El	A-R	CS	4000	W	P	BM	17.67
RDC-118-2014-0005	*KR*	I	Red	M.HOM	Fe	I	X	71.79	Micro channels, meso-macro vughs	7.16	Eq&El	A-R	CS	2500	W	P	BM	21.05
RDC-118-2014-0006	*KR*	I	Red	M.HOM	Fe	I	X	70.44	Micro channels, meso-macro vughs	11.24	Eq&El	A-R	CS	5000	W	P	BM	19.32
RDC-118-2014-0007	*KR*	I	Red	M.HOM	Fe	I	X	75.49	Micro channels and vesicles, meso-macro vughs and channels	9.21	Eq&El	A-R	CS	4000	W	M	BM	15.3
RDC-118-2014-0008	*KR*	I	Red	M.HOM	Fe	I	X	71.04	Micro vesicles, meso-macro vughs and channels	7.5	Eq&El	A-R	CS	4500	W	P	BM	21.46
R25A-02-SXV-94	*WP*	I	Red	M.HOM	Fe	S	X	65.99	Meso planar voids, vughs and channels	13.78	Eq&El	A-WR	CS	3000	M	M	BM	20.23

Table 3, annex 4. Ceramic paste, porosity and temper characteristic of green and brown (GB) ceramics. Matrix homogeneity/heterogeneity: H.HOM., highly homogeneous – M.HOM., moderately homogeneous – S.HOM., slightly homogeneous – H.HET., highly heterogeneous – M.HET., moderately heterogeneous – S.HET., slightly heterogeneous. Fe- Ca rich matrix: Fe, iron rich matrix – S.Ca, slightly calcitic – M. Ca, moderately calcitic – H.Ca., Highly calcitic. Matrix activity: S, slightly active – M, moderately active – H, highly active – I, isotropic. Alignment: W, weak – M, moderate. Main grain shape: Eq&El, mainly equal (rounded) and elongated grains – El&Eq, mainly elongated and equal grains. Roundness: VA, very angular – A, angular – SA, sub angular – SR, sub rounded – R, rounded – WR, well rounded. Packing: CS, close spaced – SS, single spaced – DS, double spaced – OS, open spaced. Sorting: VP, very poor – P, poor – M, moderate – W, well. Grain size distribution (G.S.D.): U, unimodal – B, bimodal.

SAMPLE	Typology	Fabric	Ceramic paste						Porosity		Temper							
			Colour	Hom. – Het.	Fe- Ca rich matrix	Activity	Oxides	%	Description	%	Shape	Roundness	Packing	Max size µm	Alignment	Sorting	G.S.D.	%
CRVM-0357	GB	Ia	Buffy-Red	M. HET	M. Ca	I	X	84.26	Meso vesicles and vughs, macro channels	1.62	Eq&El	WR	DS	300	M	M/W	U	14.12
CRVM-623	GB	Ia	Buffy-Red	M. HET	M. Ca	S	X	91.73	Meso vesicles and vughs	4.48	Eq&El	SR-WR	OS	450	W	M	U	3.79
CRVM-642	GB	Ia	Buffy-Red	H. HET	M. Ca	S	X	86.49	Meso vesicles and vughs	2.05	Eq&El	SA-WR	DS	650	M	M	BM	11.46
CRVM-666	GB	Ia	Buffy-Red	M. HET	M. Ca	S	X	92.23	Meso vesicles and vughs, macro channels	1.66	Eq&El	A-WR	DS	1110	M	M/W	BM	6.11
CRVM-1197	GB	III	Buffy	S. HOM	H. Ca	I		90.67	Micro-meso vesicles	2.53	Eq&El	A-WR	OS	411	M	M	BM	6.8
CRVM-1659	GB	II	Buffy	M. HOM	H. Ca	I	X	77	Micro-meso planar voids, vesicles, vughs and meso channels	11.03	Eq&El	WR	SS	820	M	P	BM	11.97
CRVM-1668	GB	Ia	Buffy-Red	M. HET	M. Ca	I	X	86.22	Micro-meso vesicles and vughs	4.28	Eq&El	SR-WR	DS	400	M	M	BM	9.50
CRVM-1671	GB	Ia	Buffy-Red	H. HET	M. Ca	I	X	88.34	Micro-macro vesicles and vughs	1.53	Eq&El	A-WR	DS	430	M	M	BM	11.13
LVG-02-SXVIII-187	GB	Ia	Buffy-Red	H. HET	M. Ca	I	X	91.88	Micro-macro vesicles and vughs	6.59	Eq&El	SR-WR	OS	500	W	M	BM	1.53
CRVM-1665	GB	III	Buffy	H. HOM	H. Ca	I	X	89.27	Micro-macro vesicles, vughs and channels	3.22	Eq&El	A-WR	DS	1150	M	M	BM	7.51
CRVM-1666	GB	Ia	Buffy-Red	M. HET	M. Ca	S	X	82.3	Micro-meso vesicles, vughs and channels	3.96	Eq&El	SA-WR	SS	650	M	M	BM	13.74
CRVM-1670	GB	III	Buffy-Gray	H.HOM	H. Ca	S	X	87.94	Micro-macro vesicles, channels and vughs	4.22	Eq&El	A-WR	DS	600	M	P	BM	7.84
CRVM-1667	GB	Ia	Buffy-Red	H. HET	M. Ca	S	X	82.22	Micro-meso vesicles, vughs and mega channels	4.59	Eq&El	SA-WR	SS	750	M	M	BM	13.19
CRVM-1669	GB	Ia	Buffy-Red	H. HET	M. Ca	S	X	84.34	Micro-meso vesicles, vughs and channels	4.6	Eq&El	SA-WR	SS	780	M	M	BM	11.06
CRVM-223	GB	I	Red	S.HET	Fe	I	X	72.14	Micro-meso vesicles and vughs	11.86	Eq&El	A-SR	DS	911	W	M	U	17
CRVM-0670	GB	I	Red	M.HOM	Fe	S	X	74.79	Micro-meso vesicles, vughs and channels	8.85	Eq&El	A-SR	SS	611	W	P	U	16.36

Table 4, annex 4. Ceramic paste, porosity and temper characteristic of honey and black (HB) and of partial corda seca (CSP) ceramics. Matrix homogeneity/heterogeneity: H.HOM., highly homogeneous – M.HOM., moderately homogeneous – S.HOM., slightly homogeneous – H.HET., highly heterogeneous – M.HET., moderately heterogeneous – S.HET., slightly heterogeneous. Fe- Ca rich matrix: Fe, iron rich matrix – S.Ca, slightly calcitic – M. Ca, moderately calcitic – H.Ca., Highly calcitic. Matrix activity: S, slightly active – M, moderately active – H, highly active – I, isotropic. Alignment: W, weak – M, moderate. Main grain shape: Eq&El, mainly equal (rounded) and elongated grains – El&Eq, mainly elongated and equal grains. Roundness: VA, very angular – A, angular – SA, sub angular – SR, sub rounded – R, rounded – WR, well rounded. Packing: CS, close spaced – SS, single spaced – DS, double spaced – OS, open spaced. Sorting: VP, very poor – P, poor – M, moderate – W, well. Grain size distribution (G.S.D.): U, unimodal – B, bimodal.

SAMPLE	Typology	Fabric	Ceramic paste						Porosity		Temper							
			Colour	Hom. – Het.	Fe- Ca rich matrix	Activity	Oxides	%	Description	%	Shape	Roundness	Packing	Max size µm	Alignment	Sorting	G.S.D.	%
CRVF-0003	*HB*	Ib	Red	M.HOM	Fe	S	X	89.41	Micro-meso vesicles and vughs	4.39	Eq&El	SA-SR	OS	700	W	P	BM	6.2
CSP-0021	*CSP*	Ia	Buffy-Red	M.HET	M.Ca	I	X	91.14	Micro-meso vesicles and vughs	2.54	Eq&El	A-SR	OS	225	M	W	U	6.32
CSP-0027	*CSP*	Ia	Buffy-Red	S.HOM	Fe/S. Ca	S		84.76	Micro-meso vesicles, vughs and channels	6.5	Eq&El	A-SR	DS	211	M	M	U	8.74
CSP-0028	*CSP*	Ib	Red	S.HOM	Fe/S. Ca	S	X	87.15	Micro-meso vesicles, vughs and channels	3.12	Eq&El	SA-SR	DS	620	M	P	BM	9.73
CSP-0029	*CSP*	III	Buffy	H.HOM	H. Ca	I	X	91.57	Meso vughs and vesicles	5.12	Eq&El	SA-R	OS	450	M	W	BM	3.31
CSP-0030	*CSP*	Ia	Red	M.HOM	Fe/S. Ca	S	X	93.3	Micro-meso vesicles	0.25	Eq&El	A-SR	DS	150	W	M	U	6.35
CSP-0031	*CSP*	Ib	Red	M.HOM	Fe/S. Ca	S	X	91.19	Meso vughs and vesicles	3.89	Eq&El	SA-SR	OS	440	M	P	BM	4.92

Table 5, annex 4. Major oxides chemical composition and L.O.I. of kiln rods and the white painted ceramics obtained by XRF.

Sample Name	Formula	Na_2O	MgO	Al_2O_3	SiO_2	P_2O_5	K_2O	CaO	TiO_2	Fe_2O_3	MnO	PbO	S	LOI	SUM
RDC-118-2014-0001	wt%	1.12	1.45	16.60	66.60	0.380	2.18	1.36	0.76	6.24	0.123	0.011	0.003	2.9	99.73
	Err. ±	0.05	0.03	0.04	0.04	0.004	0.04	0.02	0.01	0.01	0.003	0.002	0.001		
RDC-118-2014-0002	wt%	1.23	1.25	16.40	68.30	0.186	2.16	0.83	0.74	6.22	0.117	0.015	0.002	3.2	110.64
	Err. ±	0.05	0.02	0.03	0.04	0.004	0.04	0.02	0.01	0.01	0.003	0.002	0.001		
RDC-118-2014-0003	wt%	1.12	1.32	16.40	66.90	0.175	2.07	2.19	0.73	6.05	0.113	0.006	0.006	2.31	99.38
	Err. ±	0.05	0.02	0.04	0.04	0.004	0.04	0.03	0.01	0.01	0.003	0.002	0.001		
RDC-118-2014-0004	wt%	1.22	1.34	16.60	67.00	0.252	2.17	0.86	0.76	6.31	0.111	0.022	0.003	3.2	99.85
	Err. ±	0.05	0.02	0.04	0.04	0.004	0.04	0.02	0.01	0.01	0.003	0.002	0.001		
RDC-118-2014-0005	wt%	1.25	1.46	16.70	68.60	0.115	2.16	0.72	0.79	6.52	0.117	0.118	0.049	1.43	110.02
	Err. ±	0.05	0.02	0.04	0.04	0.003	0.04	0.02	0.01	0.01	0.003	0.002	0.001		
RDC-118-2014-0006	wt%	1.15	1.38	16.80	68.40	0.141	2.26	0.84	0.78	6.46	0.112	0.070	0.017	1.1	99.51
	Err. ±	0.05	0.02	0.04	0.04	0.004	0.04	0.02	0.01	0.01	0.003	0.002	0.001		
RDC-118-2014-0007	wt%	1.07	1.31	16.60	66.80	0.111	2.32	0.74	0.78	6.69	0.143	0.144	0.033	3	99.74
	Err. ±	0.04	0.02	0.04	0.04	0.004	0.04	0.02	0.01	0.01	0.004	0.003	0.001		
RDC-118-2014-0008	wt%	1.39	1.28	16.60	66.80	0.275	2.15	0.94	0.78	6.37	0.113	0.011	0.003	3.31	110.03
	Err. ±	0.05	0.02	0.03	0.04	0.004	0.04	0.02	0.01	0.01	0.003	0.002	0.001		
R25A-02-SXV-94	wt%	1.12	1.59	18.60	66.00	0.092	2.45	0.59	0.81	7.13	0.115	0.003	0.002	2.03	110.53
	Err. ±	0.05	0.03	0.04	0.04	0.004	0.04	0.02	0.01	0.01	0.003	0.002	0.001		

Table 6, annex 4. Major oxides chemical composition and L.O.I. of green and brown ceramics obtained by XRF.

Sample Name	Formula	Na_2O	MgO	Al_2O_3	SiO_2	P_2O_5	K_2O	CaO	TiO_2	Fe_2O_3	MnO	PbO	S	LOI	SUM
CRVM-0357	wt%	0.86	2.35	15.11	53.30	1.850	3.29	11.80	0.68	5.42	0.124	0.615	0.232	3.89	99.51
	Err. ±	0.05	0.03	0.04	0.04	0.006	0.05	0.04	0.01	0.01	0.003	0.004	0.002		
CRVM-623	wt%	0.95	3.46	16.20	49.20	0.933	2.25	15.11	0.65	6.08	0.174	1.161	0.345	4.35	110.85
	Err. ±	0.05	0.03	0.04	0.04	0.005	0.04	0.05	0.01	0.01	0.004	0.005	0.002		
CRVM-642	wt%	0.62	2.69	14.90	55.70	0.652	2.75	12.90	0.70	5.44	0.194	0.514	0.175	2.39	99.63
	Err. ±	0.04	0.03	0.03	0.04	0.005	0.04	0.05	0.01	0.01	0.004	0.003	0.002		
CRVM-666	wt%	0.66	3.60	13.60	47.80	0.514	2.97	17.80	0.57	4.76	0.141	1.110	0.391	5.52	99.42
	Err. ±	0.05	0.03	0.03	0.03	0.005	0.05	0.05	0.01	0.01	0.004	0.005	0.002		
CRVM-1197	wt%	1.22	2.99	14.90	48.90	3.500	1.58	15.40	0.63	5.32	0.155	0.993	0.299	3.71	99.59
	Err. ±	0.05	0.03	0.04	0.04	0.008	0.04	0.05	0.01	0.01	0.004	0.005	0.002		
CRVM-1659	wt%	0.85	1.89	11.60	58.50	2.320	0.99	13.80	0.59	4.41	0.122	0.744	0.206	4.78	110.80
	Err. ±	0.04	0.03	0.03	0.04	0.006	0.04	0.05	0.01	0.01	0.004	0.004	0.002		
CRVM-1668	wt%	0.61	3.08	13.43	48.40	0.801	2.61	16.50	0.53	4.74	0.189	0.524	0.189	8.4	110.00
	Err. ±	0.04	0.03	0.03	0.03	0.005	0.04	0.05	0.01	0.01	0.004	0.003	0.002		
CRVM-1671	wt%	0.73	3.19	14.20	50.00	0.550	2.89	16.11	0.58	5.11	0.138	0.249	0.123	5.96	99.82
	Err. ±	0.05	0.03	0.03	0.04	0.004	0.04	0.05	0.01	0.01	0.004	0.003	0.001		
LVG-02-SXVIII-187	wt%	0.90	3.70	14.11	46.11	1.840	2.40	16.30	0.63	5.12	0.213	0.689	0.200	7.54	99.72
	Err. ±	0.05	0.03	0.03	0.03	0.006	0.04	0.05	0.01	0.01	0.004	0.004	0.002		
CRVM-1665	wt%	1.51	1.85	15.20	56.11	0.459	1.59	11.90	0.67	5.84	0.113	0.161	0.371	3.1	110.86
	Err. ±	0.05	0.03	0.03	0.04	0.004	0.04	0.04	0.01	0.01	0.003	0.005	0.002		
CRVM-1666	wt%	0.68	2.67	14.00	46.11	3.860	2.91	14.70	0.63	5.21	0.464	0.494	0.148	7.7	99.56
	Err. ±	0.05	0.03	0.03	0.03	0.008	0.04	0.05	0.01	0.01	0.006	0.003	0.002		
CRVM-1670	wt%	1.63	1.88	16.40	55.00	0.488	1.72	12.20	0.74	6.24	0.113	0.833	0.311	1.74	99.30
	Err. ±	0.05	0.03	0.04	0.04	0.004	0.04	0.04	0.01	0.01	0.003	0.004	0.002		
CRVM-1667	wt%	0.50	2.32	15.60	58.60	0.778	2.94	11.90	0.69	5.51	0.182	0.411	0.148	1.25	110.82
	Err. ±	0.04	0.03	0.03	0.04	0.005	0.04	0.04	0.01	0.01	0.004	0.003	0.002		
CRVM-1669	wt%	0.46	3.46	11.60	47.40	0.435	2.47	17.50	0.53	4.12	0.119	0.457	0.229	11.9	99.67
	Err. ±	0.04	0.03	0.03	0.03	0.004	0.04	0.05	0.01	0.01	0.003	0.003	0.002		

Sample Name	Formula	Na_2O	MgO	Al_2O_3	SiO_2	P_2O_5	K_2O	CaO	TiO_2	Fe_2O_3	MnO	PbO	S	LOI	SUM
CRVM-223	wt%	0.37	1.69	15.50	63.90	0.381	3.00	6.85	0.76	5.51	0.205	0.129	0.046	1.3	99.64
	Err. ±	0.04	0.03	0.04	0.04	0.004	0.05	0.04	0.01	0.01	0.004	0.002	0.001		
CRVM-0670	wt%	0.45	1.71	15.40	63.40	0.297	2.98	7.40	0.75	5.40	0.195	0.164	0.068	1.5	99.72
	Err. ±	0.04	0.03	0.04	0.04	0.004	0.05	0.04	0.01	0.01	0.004	0.003	0.001		

Table 7, annex 4. Major oxides chemical composition and L.O.I. of honey and black and partial corda seca ceramics obtained by XRF.

Sample Name	Formula	Na_2O	MgO	Al_2O_3	SiO_2	P_2O_5	K_2O	CaO	TiO_2	Fe_2O_3	MnO	PbO	S	LOI	SUM
CRCSP-0030	wt%	0.45	0.76	15.00	44.11	11.400	2.75	3.26	0.67	6.00	0.125	0.127	0.143	14.62	99.40
	Err. ±	0.04	0.02	0.03	0.03	0.012	0.05	0.03	0.01	0.01	0.003	0.003	0.002		
CRCSP-0031	wt%	0.84	3.12	16.60	57.50	0.472	2.92	8.47	0.74	6.08	0.235	0.218	0.080	2.51	99.79
	Err. ±	0.05	0.03	0.04	0.04	0.004	0.05	0.04	0.01	0.01	0.004	0.003	0.001		
CRCSP-0028	wt%	0.81	1.71	14.80	53.30	6.200	2.57	4.73	0.71	5.86	0.240	0.162	0.062	8.7	99.85
	Err. ±	0.05	0.03	0.03	0.04	0.009	0.05	0.03	0.01	0.01	0.005	0.003	0.001		
CRCSP-0027	wt%	1.21	3.17	17.90	50.80	0.378	3.29	12.70	0.60	5.95	0.142	0.386	0.135	3.2	99.86
	Err. ±	0.05	0.03	0.04	0.04	0.004	0.05	0.05	0.01	0.01	0.004	0.003	0.001		
CRCSP-0021	wt%	1.06	2.48	17.70	48.20	2.130	2.99	12.90	0.60	5.81	0.152	0.354	0.138	5.09	99.60
	Err. ±	0.05	0.03	0.04	0.03	0.006	0.05	0.05	0.01	0.01	0.004	0.003	0.002		
CRCSP-0029	wt%	1.40	3.13	15.70	50.80	0.681	1.72	15.50	0.66	5.58	0.165	0.099	0.064	4.41	99.91
	Err. ±	0.05	0.03	0.03	0.03	0.005	0.04	0.05	0.01	0.01	0.004	0.002	0.001		
CRVF-0003	wt%	0.61	2.65	17.40	57.30	2.180	3.61	3.72	0.76	6.68	0.292	0.527	0.134	3.9	99.76
	Err. ±	0.04	0.03	0.04	0.04	0.006	0.05	0.03	0.01	0.01	0.005	0.004	0.002		

Table 8, annex 4. Trace elements concentration of kiln rods and the white painted fragment obtained by ICP-MS.

Sample ref.		Sc	V	Mn	Co	Ni	Cu	Zn	Ga	Rb	Sr	Y	Zr	Nb	Cs	Ba	Hf	Th	U
RDC-118-2014-0001	ppm	17.05	133.80	378.78	15.01	18.67	50.03	90.07	28.48	133.62	144.54	28.70	119.44	16.75	7.80	522.71	2.49	12.99	2.46
	RSD	2.43	1.44	1.37	0.22	0.51	1.21	1.20	4.72	1.85	1.35	1.08	0.69	1.65	1.20	1.85	1.79	2.19	2.80
RDC-118-2014-0002	ppm	14.28	128.46	384.88	13.97	18.88	56.00	87.16	27.13	124.89	168.36	26.73	130.31	16.15	6.70	526.61	2.48	12.40	2.35
	RSD	4.14	1.52	0.93	1.54	2.31	1.40	1.84	2.34	1.02	0.88	0.36	0.90	0.75	2.63	1.90	1.30	2.23	1.21
RDC-118-2014-0003	ppm	14.17	121.74	328.33	13.96	18.19	37.83	73.05	25.82	116.55	151.54	27.57	129.92	14.98	6.49	530.11	2.74	12.11	2.37
	RSD	9.68	1.13	1.48	0.86	0.24	1.31	1.64	3.24	1.11	1.31	0.71	1.81	1.51	3.11	2.21	2.09	0.67	1.04
RDC-118-2014-0004	ppm	14.63	127.28	335.03	13.54	16.19	40.90	90.35	26.07	119.84	158.31	25.04	114.84	15.32	6.86	528.84	2.40	11.85	2.28
	RSD	12.49	1.25	1.21	3.04	1.75	1.16	1.60	1.96	0.93	0.16	0.73	0.24	1.11	1.58	2.23	0.24	1.58	0.72
RDC-118-2014-0005	ppm	15.75	122.13	412.80	16.35	25.60	38.78	87.69	27.76	124.03	135.35	26.23	111.15	15.61	7.33	526.78	2.52	13.32	2.35
	RSD	4.61	1.17	0.69	0.69	4.33	1.37	1.08	3.04	1.42	0.63	1.73	1.07	1.86	0.57	1.83	1.11	0.93	1.39
RDC-118-2014-0006	ppm	15.87	120.11	380.15	15.56	29.85	45.23	87.53	25.54	118.23	135.59	25.90	113.49	14.88	6.99	494.48	2.49	12.85	2.47
	RSD	5.67	0.84	0.55	0.95	1.04	0.62	2.45	0.70	1.17	1.67	1.83	1.31	0.32	1.03	0.85	1.52	0.97	1.34
RDC-118-2014-0007	ppm	15.49	115.03	557.84	17.58	27.98	68.02	97.94	25.95	118.63	132.36	24.78	118.56	14.86	6.60	539.66	2.64	12.31	2.38
	RSD	4.83	1.43	1.40	0.80	2.48	1.19	1.32	3.83	0.85	1.58	0.85	0.87	1.45	1.75	3.15	2.98	1.40	2.82
RDC-118-2014-0008	ppm	17.27	138.59	358.50	15.17	19.79	43.13	86.75	28.69	131.92	146.95	28.82	127.11	17.24	7.91	535.08	2.66	14.48	2.59
	RSD	3.56	0.63	0.75	0.53	6.34	2.57	3.88	3.50	2.52	2.39	1.24	1.18	1.00	2.20	3.14	1.79	1.98	2.55
R25A-02-SXV-94	ppm	17.26	132.80	313.27	15.03	32.74	48.46	74.54	26.43	118.13	120.16	26.30	113.93	13.33	7.07	540.76	2.53	12.02	2.47
	RSD	6.36	1.87	1.14	3.44	4.41	0.77	1.04	1.87	1.02	1.59	1.73	1.71	1.56	0.53	0.68	0.61	0.55	0.51

Table 9, annex 4. Trace elements concentration of green and brown ceramics obtained by ICP-MS.

Sample ref.		Sc	V	Mn	Co	Ni	Cu	Zn	Ga	Rb	Sr	Y	Zr	Nb	Cs	Ba	Hf	Th	U
CRVM-0357	ppm	14.12	111.39	477.55	15.88	41.45	49.57	98.08	21.63	129.77	296.25	27.86	66.35	17.87	6.60	399.96	1.64	11.03	3.05
	RSD	5.34	1.77	1.67	3.31	0.65	2.78	0.58	2.77	1.38	1.05	1.34	0.57	1.91	2.29	1.95	1.86	0.73	0.25
CRVM-623	ppm	15.54	114.62	772.71	15.25	41.58	203.01	91.43	22.58	111.09	460.84	27.85	78.18	16.79	6.90	464.16	2.00	11.17	2.02
	RSD	3.86	1.45	0.99	1.54	1.71	3.11	1.28	3.40	0.65	0.34	2.05	5.04	1.61	1.78	1.46	1.67	0.43	1.04
CRVM-642	ppm	13.11	111.30	1426.03	18.74	26.64	89.04	125.82	23.54	135.00	420.67	31.98	97.94	17.89	8.01	395.71	1.91	11.92	2.43
	RSD	5.12	0.83	1.03	0.72	2.35	0.46	1.80	2.80	0.14	1.30	1.45	1.43	1.20	1.08	2.88	2.63	1.64	2.03
CRVM-666	ppm	6.98	43.25	362.36	6.91	17.78	28.86	56.79	11.93	56.90	233.56	13.54	37.23	7.81	3.11	185.99	0.93	4.90	0.97
	RSD	3.04	0.92	0.63	0.19	1.13	6.97	1.33	4.52	1.77	1.05	1.38	2.89	0.51	2.91	3.46	4.06	1.56	1.98
CRVM-1197	ppm	13.28	95.70	1580.56	37.08	45.05	303.65	451.02	19.91	97.01	527.70	26.06	69.89	14.29	6.57	458.26	1.79	9.90	2.07
	RSD	2.54	0.71	1.52	1.19	1.17	3.18	0.33	2.77	1.47	1.11	0.05	0.30	1.09	2.37	2.17	0.65	0.72	0.56
CRVM-1659	ppm	9.90	80.43	591.34	12.11	26.59	41.87	115.51	16.06	39.66	363.58	20.56	95.26	18.42	2.24	340.80	2.29	7.86	2.07
	RSD	2.59	1.01	0.52	0.92	3.18	1.97	1.36	2.66	1.15	0.89	2.15	1.03	0.80	0.66	3.32	0.44	0.82	1.38
CRVM-1668	ppm	11.44	75.04	814.89	11.63	28.46	47.08	88.73	16.66	89.18	385.20	22.92	66.18	12.98	5.29	390.87	1.69	8.49	1.73
	RSD	11.14	0.84	2.00	2.36	1.53	1.00	3.17	6.13	1.65	0.80	0.98	7.68	0.84	0.59	0.92	0.08	1.35	1.39
CRVM-1671	ppm	13.11	93.58	657.77	14.55	35.02	45.37	86.39	18.83	111.00	379.52	24.85	70.82	14.77	6.02	388.69	1.71	9.71	1.91
	RSD	3.65	1.31	0.49	2.34	1.11	1.50	1.73	4.64	1.11	0.11	3.28	4.28	1.84	2.93	1.40	1.56	0.60	1.69
LGV-02-SXVIII-187	ppm	12.04	79.69	727.80	14.38	33.69	58.65	118.73	17.31	71.51	372.28	22.51	63.03	13.42	5.87	524.86	1.63	8.79	1.65
	RSD	4.84	1.78	1.81	0.86	1.11	7.25	2.98	4.13	1.96	1.14	2.58	3.36	2.92	2.38	1.60	1.97	0.52	0.91
CRVM-1665	ppm	14.30	128.95	311.01	13.54	40.64	72.19	97.16	20.83	56.83	413.95	21.76	60.24	16.50	3.16	313.28	1.47	8.58	2.08
	RSD	4.98	0.30	0.97	2.43	1.36	6.16	1.16	6.03	1.06	1.31	3.72	1.37	2.30	2.37	2.78	1.82	0.68	0.97
CRVM-1666	ppm	12.83	80.65	1480.98	14.99	42.73	153.02	456.96	19.73	85.39	553.70	27.25	70.50	15.77	5.16	649.15	1.74	11.07	2.21
	RSD	3.44	0.20	0.42	3.24	1.92	3.24	0.71	4.05	0.69	0.55	1.11	2.11	1.76	0.84	3.65	1.53	1.38	1.59
CRVM-1670	ppm	17.49	176.93	388.50	17.75	35.90	354.91	131.17	28.11	81.91	567.40	28.51	111.96	20.84	6.66	315.56	2.21	11.61	2.37
	RSD	2.74	0.72	1.21	0.49	2.81	0.88	1.74	0.66	2.55	0.87	1.08	0.60	0.91	0.92	2.02	3.63	1.34	1.85
CRVM-1667	ppm	11.79	84.36	766.32	12.77	38.02	43.32	88.39	20.08	111.12	393.61	27.74	76.63	16.15	9.26	413.24	1.89	11.47	2.09
	RSD	3.19	1.06	0.78	1.34	2.19	4.75	0.67	0.73	0.79	2.11	2.11	7.45	2.13	3.78	1.29	1.17	0.30	0.39
CRVM-1669	ppm	12.42	115.13	659.31	15.77	17.53	57.97	115.29	21.35	127.48	543.63	29.24	89.71	17.40	7.32	356.40	1.78	11.74	2.44
	RSD	3.28	1.14	1.13	1.03	5.42	1.05	3.86	3.38	0.70	1.64	0.49	1.24	0.57	2.35	1.81	4.58	0.89	2.26

Sample ref.		Sc	V	Mn	Co	Ni	Cu	Zn	Ga	Rb	Sr	Y	Zr	Nb	Cs	Ba	Hf	Th	U
CRVM-223	ppm	13.72	99.58	1131.95	14.52	41.77	36.73	90.09	21.98	139.15	283.74	32.19	89.03	16.84	12.60	508.98	2.48	12.87	2.34
	RSD	4.63	2.33	0.78	0.88	1.91	2.07	1.06	3.44	1.61	2.07	0.67	3.87	2.17	2.92	0.65	3.15	1.22	2.05
CRVM-0670	ppm	12.45	115.61	986.24	14.37	42.14	36.58	87.97	22.21	143.39	292.39	33.65	97.03	16.83	12.81	518.16	2.68	12.96	2.30
	RSD	4.05	1.24	1.90	0.83	3.15	3.23	1.11	2.71	2.18	1.64	0.78	1.69	1.42	1.11	2.43	5.35	0.57	0.52

Table 10, annex 4. Trace elements concentration of CSP and honey and black ceramics obtained by ICP-MS.

Sample ref.		Sc	V	Mn	Co	Ni	Cu	Zn	Ga	Rb	Sr	Y	Zr	Nb	Cs	Ba	Hf	Th	U
CRCSP-0030	ppm	12.72	77.92	422.18	6.51	30.11	89.11	188.39	22.35	75.64	405.12	22.21	29.06	14.14	7.28	814.64	0.70	13.56	2.33
	RSD	5.35	1.98	2.48	3.40	0.71	1.16	2.20	1.63	0.88	1.15	0.84	12.45	0.94	2.53	0.47	2.30	0.71	1.82
CRCSP-0031	ppm	14.61	123.91	1234.71	19.13	65.89	76.62	111.76	24.02	143.13	353.58	28.69	95.24	19.31	8.71	547.55	2.50	13.45	2.45
	RSD	5.64	1.36	1.20	0.56	1.30	1.97	1.14	3.51	0.64	1.01	1.26	1.94	1.00	3.62	0.93	1.80	3.36	1.00
CRCSP-0028	ppm	13.35	92.29	1267.45	21.99	58.38	116.77	287.77	21.76	115.89	379.54	26.99	83.04	16.76	6.36	613.66	2.33	12.59	2.38
	RSD	7.15	3.07	1.67	0.20	6.27	5.50	0.55	6.04	4.68	4.98	1.09	0.07	5.61	1.57	0.87	3.05	1.54	2.85
CRCSP-0027	ppm	13.71	138.88	627.01	15.16	51.44	249.66	115.89	25.50	148.50	463.72	27.11	37.96	15.62	13.94	501.55	0.94	13.25	2.59
	RSD	4.81	1.30	2.16	1.61	2.86	2.56	3.24	2.21	2.74	2.46	1.95	5.33	1.64	1.18	1.08	1.38	0.92	0.39
CRCSP-0021	ppm	14.36	135.57	769.11	19.39	56.12	438.17	189.39	27.52	147.93	599.54	28.11	35.97	16.55	15.20	702.11	1.03	13.98	2.79
	RSD	3.06	2.26	1.32	1.00	2.33	3.34	1.41	4.11	2.90	3.11	1.83	3.77	2.98	3.22	1.47	4.36	2.19	2.72
CRCSP-0029	ppm	14.02	127.00	872.70	16.29	43.42	45.81	119.23	23.67	118.11	548.95	30.54	87.70	16.86	8.55	454.41	2.44	11.05	2.32
	RSD	6.70	6.77	6.20	7.67	6.33	5.70	7.92	6.71	6.46	7.11	1.72	7.94	6.25	4.24	1.15	3.56	3.25	2.68
CRVF-0003	ppm	16.39	125.96	1687.53	23.96	75.15	116.86	235.22	27.39	171.37	263.90	29.16	92.67	19.62	9.74	485.70	2.26	14.26	2.51
	RSD	6.63	6.68	3.85	2.35	5.96	6.01	4.05	3.93	5.07	5.04	1.09	8.82	5.50	1.62	2.67	3.60	1.80	0.93

Table 11, annex 4. REE chemical elements concentration of kiln rods and the white painted ceramics obtained by ICP-MS.

Sample ref.		La	Ce	Pr	Nd	Sm	Eu	Gd	Tb	Dy	Ho	Er	Tm	Yb	Lu
RDC-118-2014-0001	ppm	37.57	74.15	11.59	40.52	8.06	1.43	5.72	0.78	5.08	0.97	2.29	0.40	2.09	0.31
	RSD	2.31	1.92	2.70	2.74	3.45	4.90	3.42	3.51	4.12	3.70	3.70	2.52	2.88	3.24
RDC-118-2014-0002	ppm	34.12	67.67	11.24	39.36	7.61	1.28	5.14	0.68	4.60	0.87	1.95	0.35	1.81	0.27
	RSD	2.07	1.27	2.47	2.68	3.19	4.20	3.31	3.90	3.30	3.12	2.95	2.09	2.01	0.92
RDC-118-2014-0003	ppm	35.50	70.00	9.97	38.28	7.42	1.32	5.32	0.74	4.90	0.95	2.19	0.38	2.04	0.30
	RSD	2.07	4.11	2.43	2.81	2.51	1.77	2.83	3.54	1.96	1.57	0.87	2.22	2.19	2.98
RDC-118-2014-0004	ppm	34.39	68.14	9.66	37.20	7.13	1.25	5.03	0.68	4.54	0.85	1.96	0.35	1.81	0.27
	RSD	4.47	2.76	0.82	1.70	2.34	3.82	3.77	4.33	2.22	3.11	4.89	2.99	2.35	2.72
RDC-118-2014-0005	ppm	36.80	83.49	11.18	39.01	7.61	1.37	5.67	0.77	4.89	0.94	2.21	0.38	2.05	0.30
	RSD	2.50	0.53	3.00	3.54	2.75	1.59	2.19	2.21	2.90	3.61	4.39	3.16	4.85	4.25
RDC-118-2014-0006	ppm	36.23	77.69	9.71	37.32	7.27	1.31	5.35	0.74	4.77	0.91	2.17	0.38	2.00	0.30
	RSD	2.90	2.14	0.33	0.76	1.67	1.96	2.16	2.95	2.39	2.48	2.65	3.75	1.90	1.97
RDC-118-2014-0007	ppm	35.38	75.27	9.70	36.98	7.18	1.33	5.37	0.73	4.63	0.88	2.14	0.37	2.01	0.30
	RSD	0.75	2.69	3.09	3.11	4.37	5.23	4.29	3.67	5.33	3.60	3.11	1.95	0.51	2.21
RDC-118-2014-0008	ppm	39.87	76.53	11.99	42.55	8.23	1.46	5.86	0.81	5.33	1.01	2.31	0.42	2.15	0.31
	RSD	5.40	4.89	4.04	3.40	3.09	1.37	2.02	0.45	1.80	1.50	0.46	1.18	0.63	2.66
R25A-02-SXV-94	ppm	34.38	64.81	9.23	35.34	6.74	1.32	5.20	0.72	4.72	0.92	2.25	0.39	2.09	0.31
	RSD	0.11	3.02	1.71	1.74	1.65	4.47	1.48	1.35	1.30	1.67	1.59	1.37	0.98	0.14

Table 12, annex 4. REE chemical elements concentration of green and brown ceramics obtained by ICP-MS.

Sample ref.		La	Ce	Pr	Nd	Sm	Eu	Gd	Tb	Dy	Ho	Er	Tm	Yb	Lu
CRVM-0357	ppm	39.43	77.80	9.16	33.14	6.54	1.15	5.14	0.72	4.52	0.91	2.18	0.35	2.20	0.32
	RSD	0.40	1.94	0.57	0.54	0.58	0.99	1.02	0.26	0.54	0.60	1.86	0.29	0.14	1.19
CRVM-623	ppm	40.09	77.97	9.07	33.60	6.57	1.22	5.29	0.74	4.72	0.92	2.21	0.36	2.26	0.33
	RSD	0.52	0.16	1.02	0.41	0.81	0.55	0.14	0.53	1.30	1.92	1.22	0.76	0.50	1.94
CRVM-642	ppm	33.74	64.57	9.38	35.67	6.99	1.21	5.33	0.76	5.11	0.99	2.30	0.40	2.09	0.30
	RSD	0.34	2.08	1.32	1.62	1.89	2.61	1.89	2.52	3.52	2.58	2.00	3.97	2.23	1.93
CRVM-666	ppm	17.73	34.83	4.06	14.88	2.94	0.56	2.48	0.35	2.16	0.43	1.08	0.17	1.05	0.15
	RSD	3.25	1.47	1.83	1.23	1.83	0.79	0.21	0.19	1.60	1.55	0.63	3.38	1.62	1.41
CRVM-1197	ppm	33.77	72.38	7.80	29.26	5.71	1.15	5.06	0.71	4.40	0.87	2.29	0.35	2.27	0.33
	RSD	2.42	1.39	2.96	1.12	2.62	0.11	0.82	1.27	0.65	3.18	0.97	1.06	0.86	2.38
CRVM-1659	ppm	32.05	64.55	7.38	27.15	5.17	1.06	4.44	0.61	3.62	0.71	1.81	0.28	1.78	0.26
	RSD	1.32	0.92	1.20	1.78	2.58	0.58	0.51	1.13	0.52	1.80	1.20	0.99	0.84	0.93
CRVM-1668	ppm	29.35	57.12	6.95	25.42	5.09	1.00	4.35	0.62	3.79	0.76	1.94	0.30	1.88	0.27
	RSD	2.91	1.28	1.00	1.36	0.79	0.76	0.36	0.84	0.55	0.52	0.62	2.06	2.50	1.57
CRVM-1671	ppm	32.53	65.71	8.02	28.65	5.74	1.08	4.83	0.68	4.09	0.83	2.04	0.31	1.96	0.29
	RSD	1.16	2.90	0.41	0.77	0.51	1.72	0.89	0.57	0.52	1.57	0.46	0.26	0.55	0.64
LGV-02-SXVIII-187	ppm	31.56	60.04	7.22	26.19	5.21	1.06	4.49	0.64	3.75	0.76	1.93	0.29	1.83	0.27
	RSD	0.30	0.85	1.55	0.17	1.64	0.58	0.54	1.62	0.36	1.91	1.40	0.66	0.79	1.56
CRVM-1665	ppm	32.25	64.89	7.53	27.13	5.38	1.02	4.30	0.60	3.71	0.73	1.77	0.27	1.75	0.25
	RSD	0.78	2.23	0.26	1.20	0.02	0.98	0.89	0.66	0.67	0.62	1.65	1.43	0.84	1.21
CRVM-1666	ppm	36.77	71.43	8.40	30.78	6.11	1.17	4.97	0.70	4.41	0.90	2.15	0.35	2.19	0.32
	RSD	0.87	0.84	0.53	0.68	0.30	0.31	0.91	0.59	0.66	0.81	0.67	1.41	1.37	1.29
CRVM-1670	ppm	35.67	69.27	9.60	36.42	7.06	1.24	5.23	0.73	4.89	0.93	2.11	0.38	1.89	0.28
	RSD	4.39	1.78	2.44	2.78	3.66	4.04	3.60	3.33	4.54	3.37	3.62	3.81	2.66	2.85
CRVM-1667	ppm	36.60	70.34	8.59	31.21	6.24	1.17	5.19	0.72	4.28	0.87	2.17	0.33	2.11	0.31
	RSD	1.05	0.86	1.06	0.30	1.18	0.91	0.96	0.83	1.53	0.85	1.19	0.90	1.75	0.18
CRVM-1669	ppm	34.66	64.44	9.42	35.98	6.92	1.16	5.20	0.73	5.01	0.95	2.14	0.38	1.90	0.28
	RSD	1.94	2.24	2.92	2.75	3.07	1.01	1.25	1.63	3.07	3.17	2.67	1.59	2.52	3.28

Sample ref.		**La**	**Ce**	**Pr**	**Nd**	**Sm**	**Eu**	**Gd**	**Tb**	**Dy**	**Ho**	**Er**	**Tm**	**Yb**	**Lu**
CRVM-223	ppm	44.58	84.30	11.42	38.82	7.07	1.52	6.58	0.92	5.06	0.97	2.88	0.40	2.49	0.37
	RSD	0.61	1.98	2.61	1.04	1.74	0.19	1.87	2.30	1.46	0.52	1.12	2.69	0.57	0.83
CRVM-0670	ppm	43.45	84.45	9.93	37.56	6.81	1.52	6.60	0.92	5.02	0.97	2.85	0.40	2.53	0.37
	RSD	1.07	7.15	1.93	0.97	0.44	0.65	0.06	1.95	0.81	1.50	0.52	1.20	1.30	1.66

Table 13, annex 4. REE chemical elements concentration of CSP and honey and black ceramics obtained by ICP-MS.

Sample ref.		La	Ce	Pr	Nd	Sm	Eu	Gd	Tb	Dy	Ho	Er	Tm	Yb	Lu
CRCSP-0030	ppm	40.48	85.67	9.55	36.30	6.44	1.43	5.80	0.80	4.02	0.72	2.03	0.26	1.61	0.22
	RSD	2.01	1.23	3.01	3.48	0.40	0.78	0.64	6.66	0.21	1.68	0.84	1.62	2.01	2.20
CRCSP-0031	ppm	45.09	94.30	11.64	37.91	6.79	1.45	6.26	0.87	4.80	0.93	2.79	0.38	2.48	0.36
	RSD	0.80	0.33	1.02	4.43	0.69	1.12	0.08	0.18	0.40	0.81	2.59	1.28	1.91	1.68
CRCSP-0028	ppm	40.45	85.03	9.63	35.70	6.43	1.42	5.96	0.87	4.59	0.90	2.56	0.41	2.26	0.38
	RSD	1.19	0.76	5.51	1.82	1.04	1.41	0.70	3.18	5.66	3.15	3.08	3.79	0.74	3.57
CRCSP-0027	ppm	41.67	83.95	9.73	36.46	6.47	1.40	6.09	0.84	4.43	0.82	2.31	0.31	1.82	0.25
	RSD	1.71	1.37	3.55	1.75	0.79	1.02	0.57	0.14	1.19	2.61	1.12	3.49	1.62	1.35
CRCSP-0021	ppm	45.50	89.09	11.18	38.22	6.79	1.57	6.41	0.86	4.59	0.82	2.36	0.32	1.90	0.26
	RSD	0.62	0.97	1.43	3.35	2.28	9.00	2.75	1.04	2.82	0.61	5.83	2.00	5.56	1.40
CRCSP-0029	ppm	41.19	80.15	9.60	35.60	6.33	1.38	6.01	0.84	4.60	0.89	2.60	0.40	2.27	0.34
	RSD	1.14	3.96	1.90	2.55	1.08	1.75	0.81	1.27	1.53	1.88	0.39	3.81	1.69	5.31
CRVF-0003	ppm	46.82	96.34	11.81	38.27	6.85	1.40	6.31	0.86	4.58	0.87	2.56	0.36	2.35	0.34
	RSD	0.33	0.98	0.61	2.47	0.64	2.04	0.42	1.53	1.63	0.83	1.17	1.51	9.05	5.05

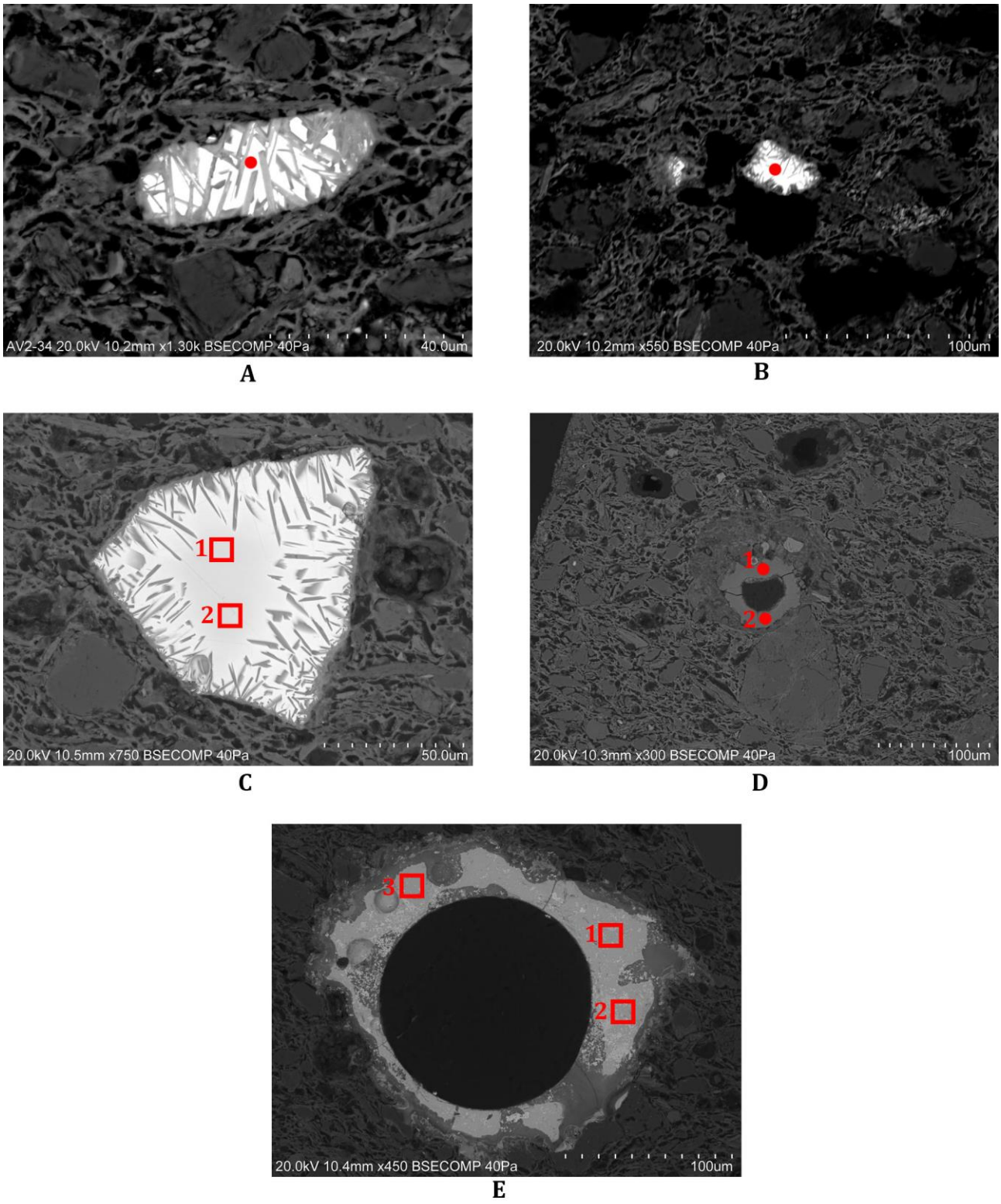

Image 1, annex 4. Features analysed by SEM-EDS on sample CRVM-0357.

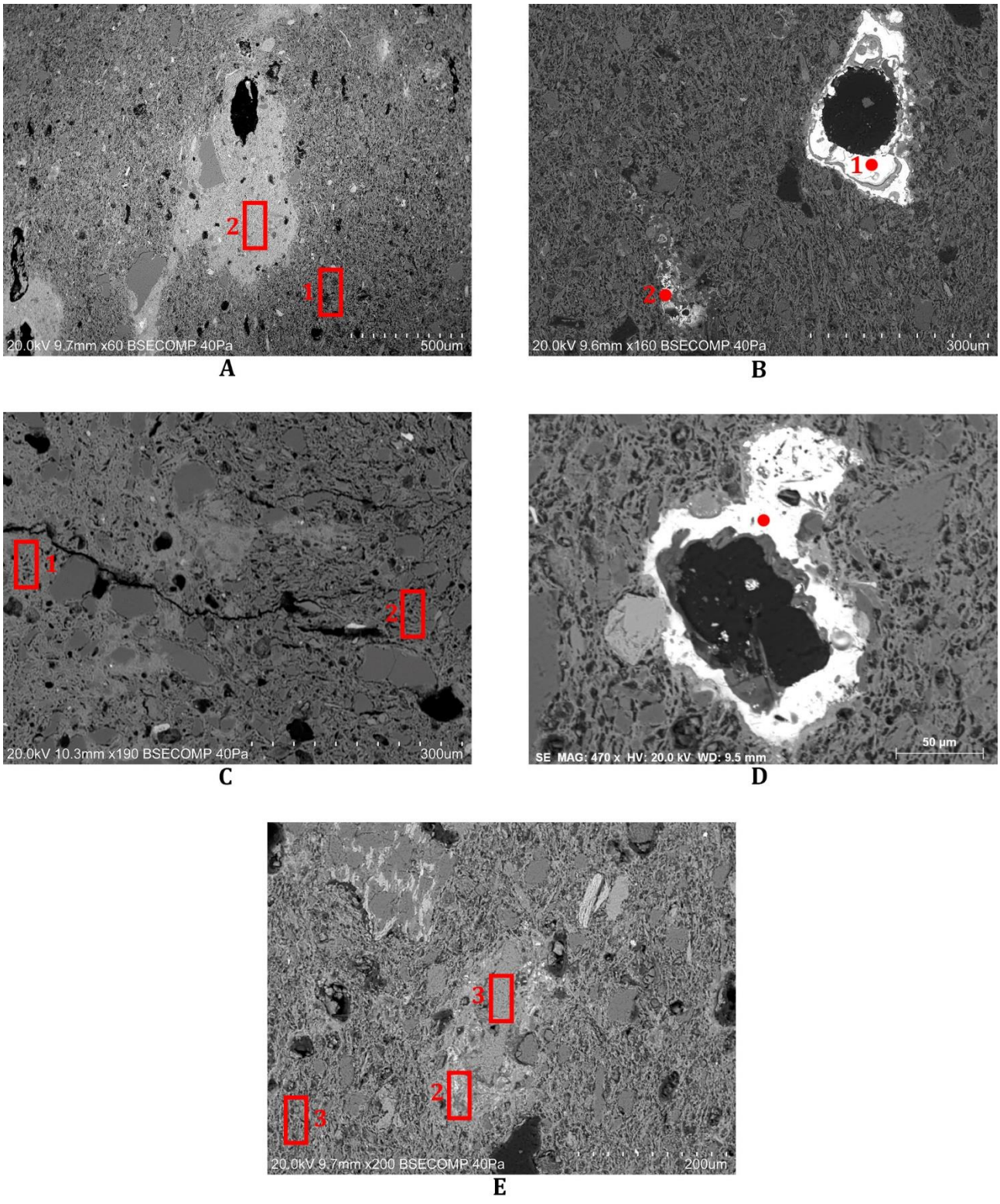

Image 2, annex 4. Features analysed by SEM-EDS on samples CRVM-623 (A, B) / 642 (C, D) / 666 (E).

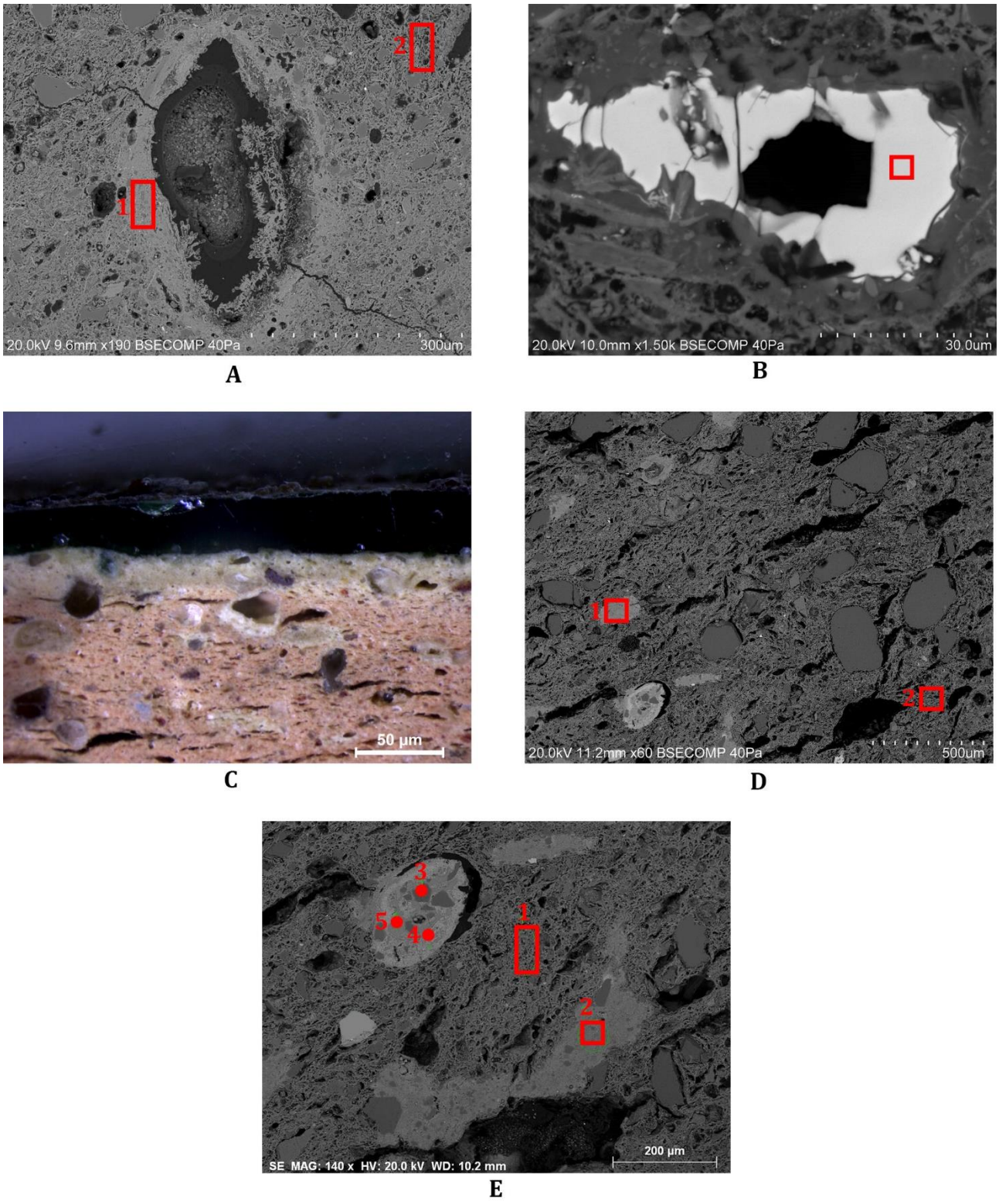

Image 3, annex 4. Features analysed by SEM-EDS on samples CRVM-1097 (A, B) / 1659 (C, D, E).

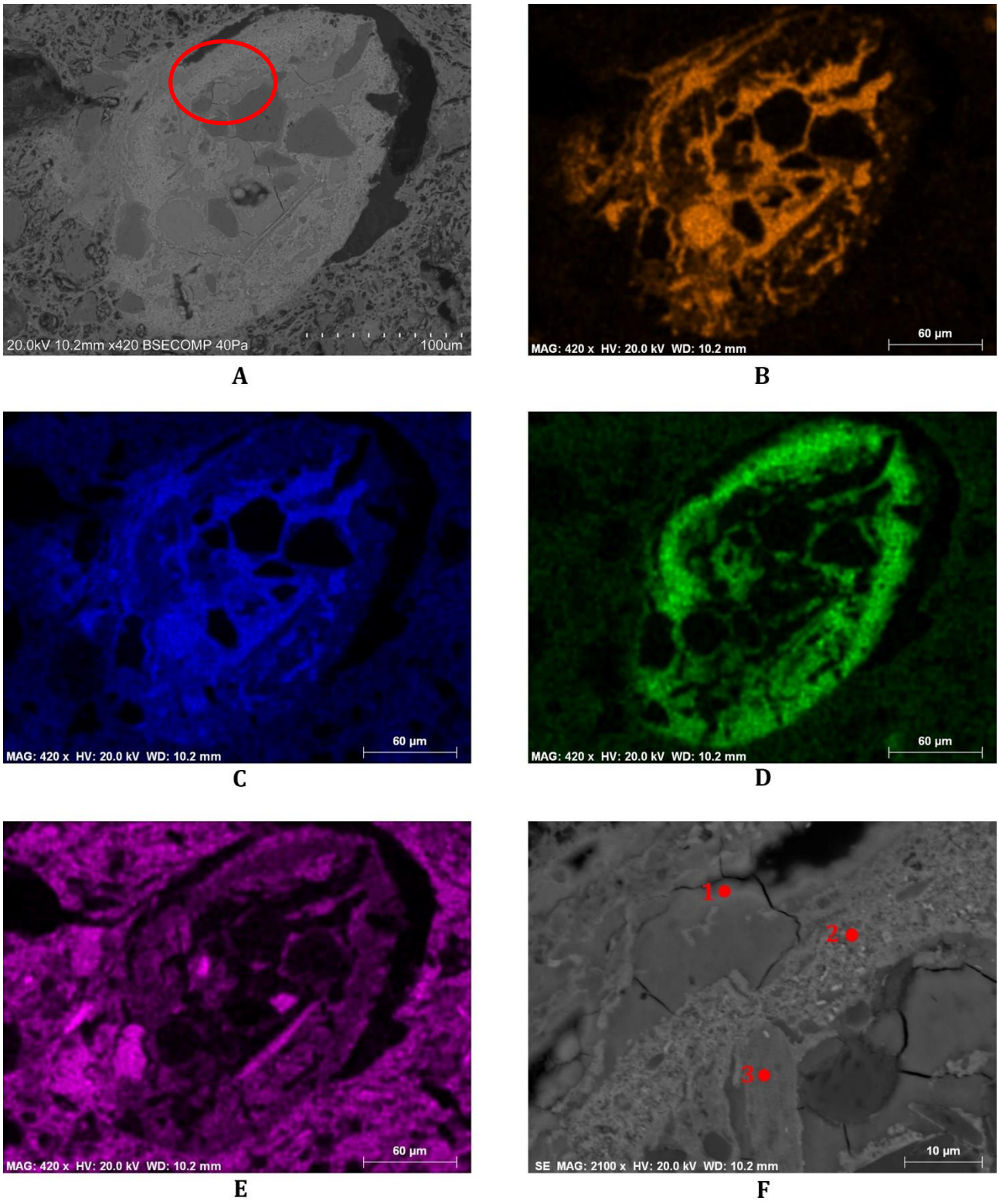

Image 4, annex 4. Features analysed by SEM-EDS on sample CRVM-1659 and elemental mapping distribution of P, (B), Ca (C), Fe (D) and Al (E). Picture F represent a magnified area of picture A (red circle).

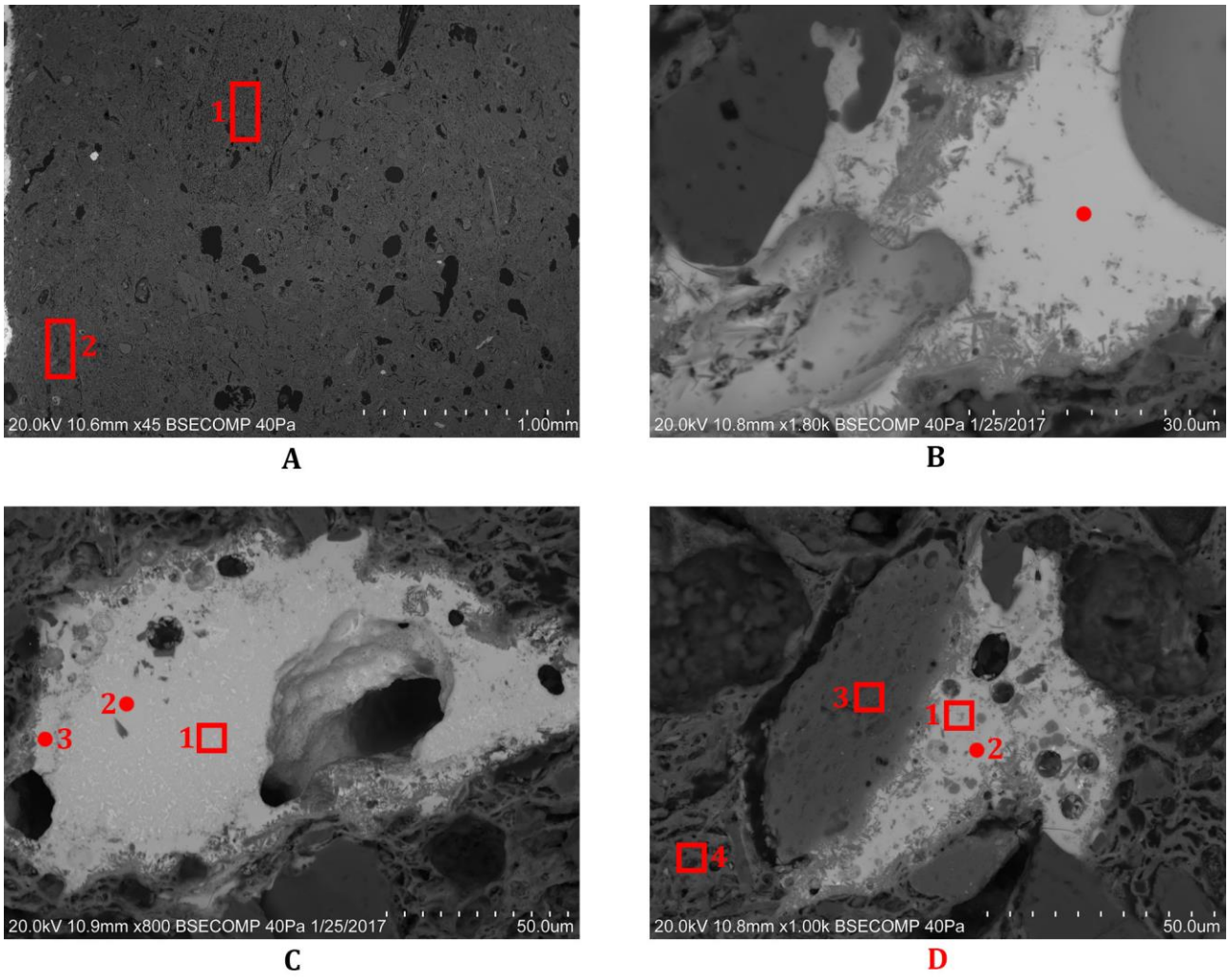

Image 5, annex 4. Features analysed by SEM-EDS on sample CRVM-1667.

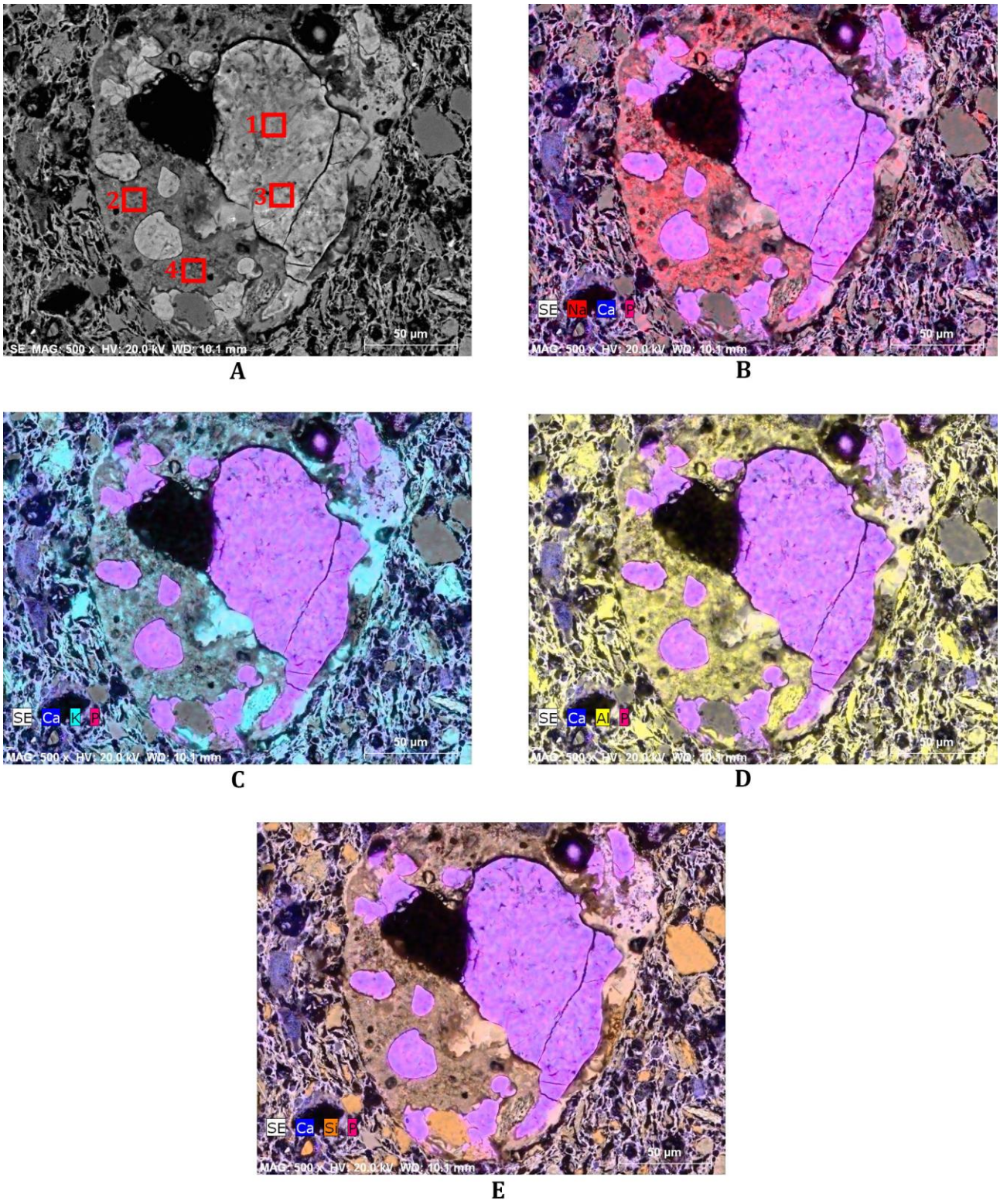

Image 6, annex 4. Fatures analysed by SEM-EDS on sample CRVM-1668.

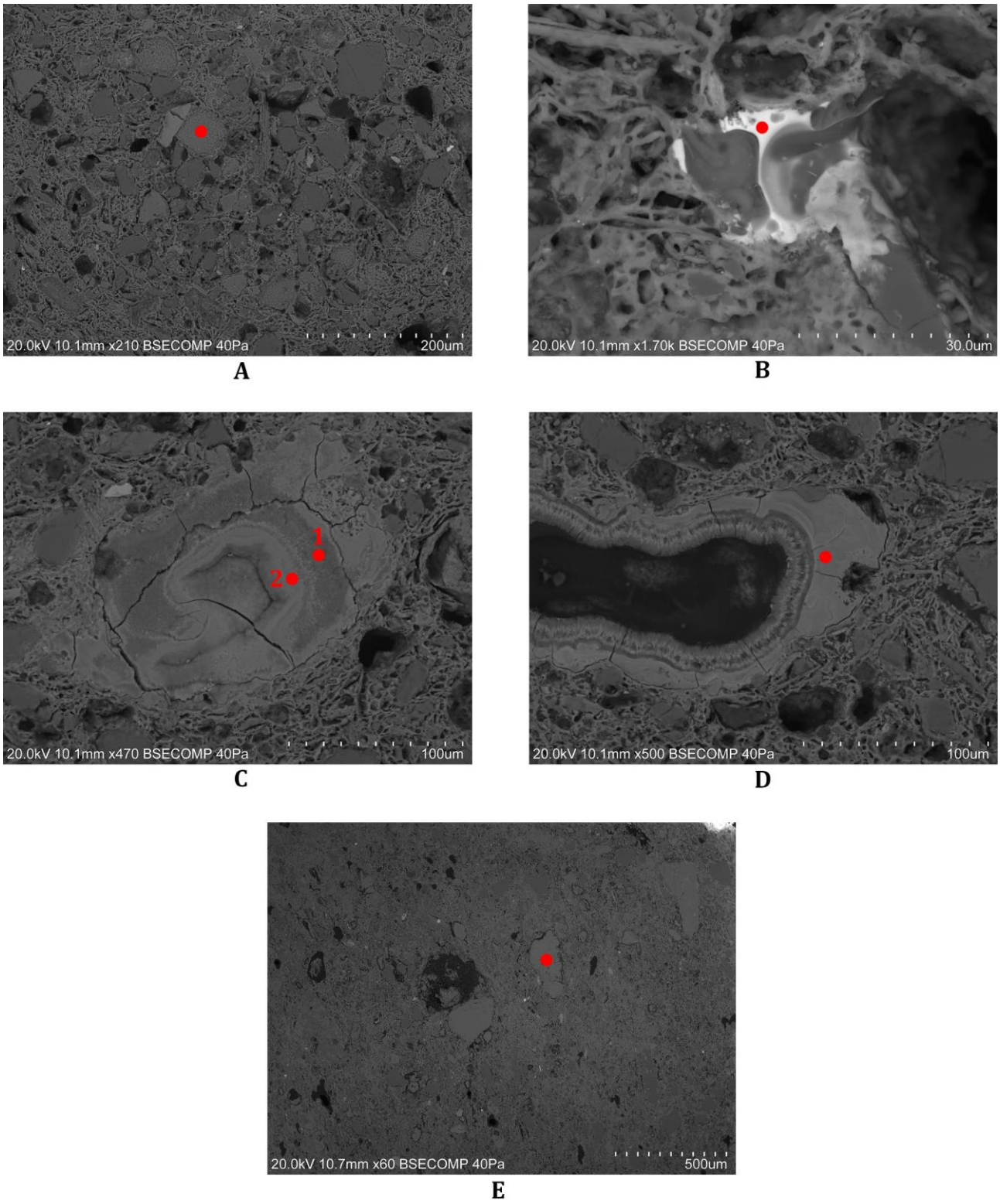

Image 7, annex 4. Features analysed by SEM-EDS on samples CRVM-1668 (A, B, C, D) / 1669 (E).

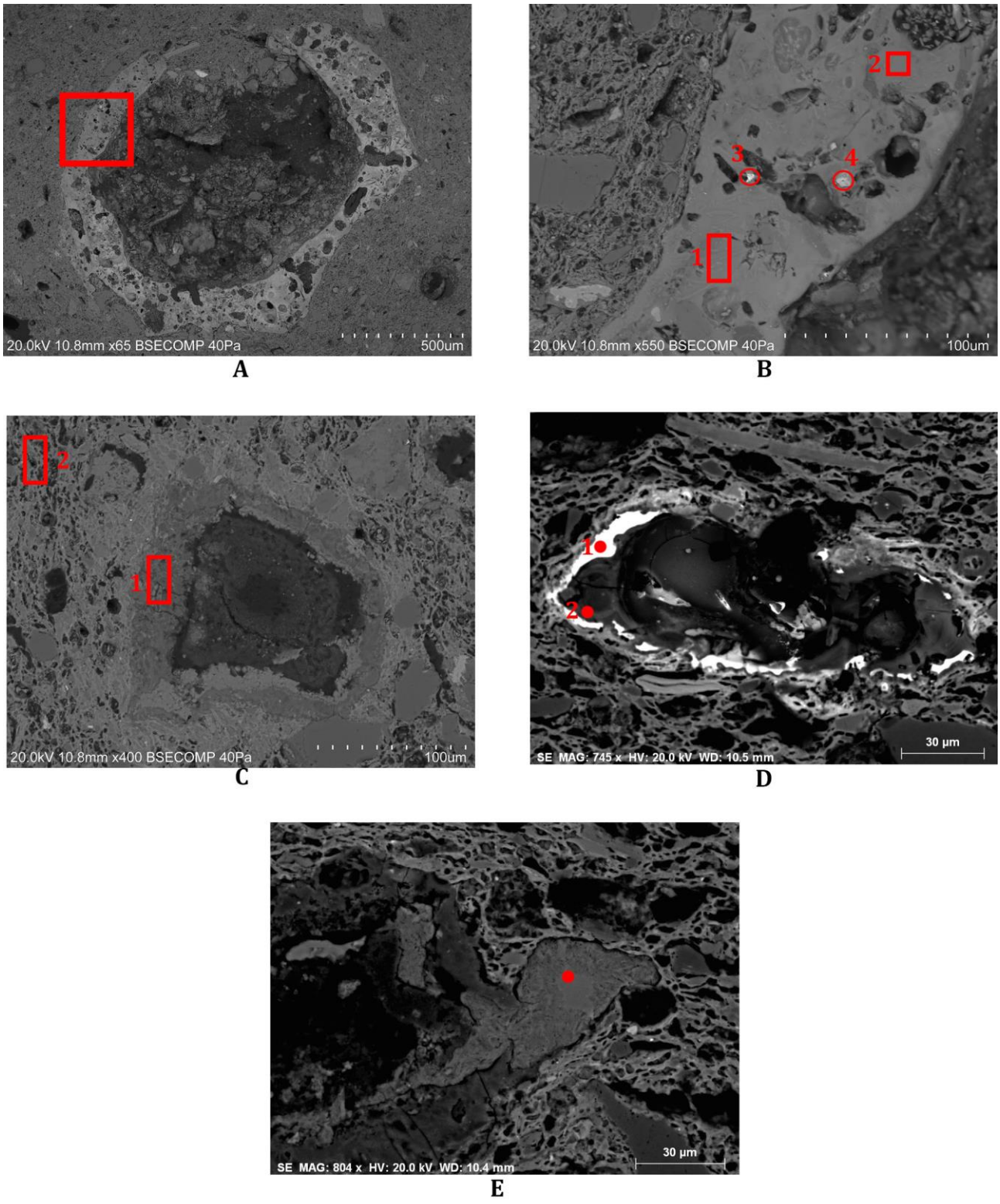

Image 8, annex 4. Features analysed by SEM-EDS on samples CRVM-1670 (A, B) / 1671 (C, D, E).

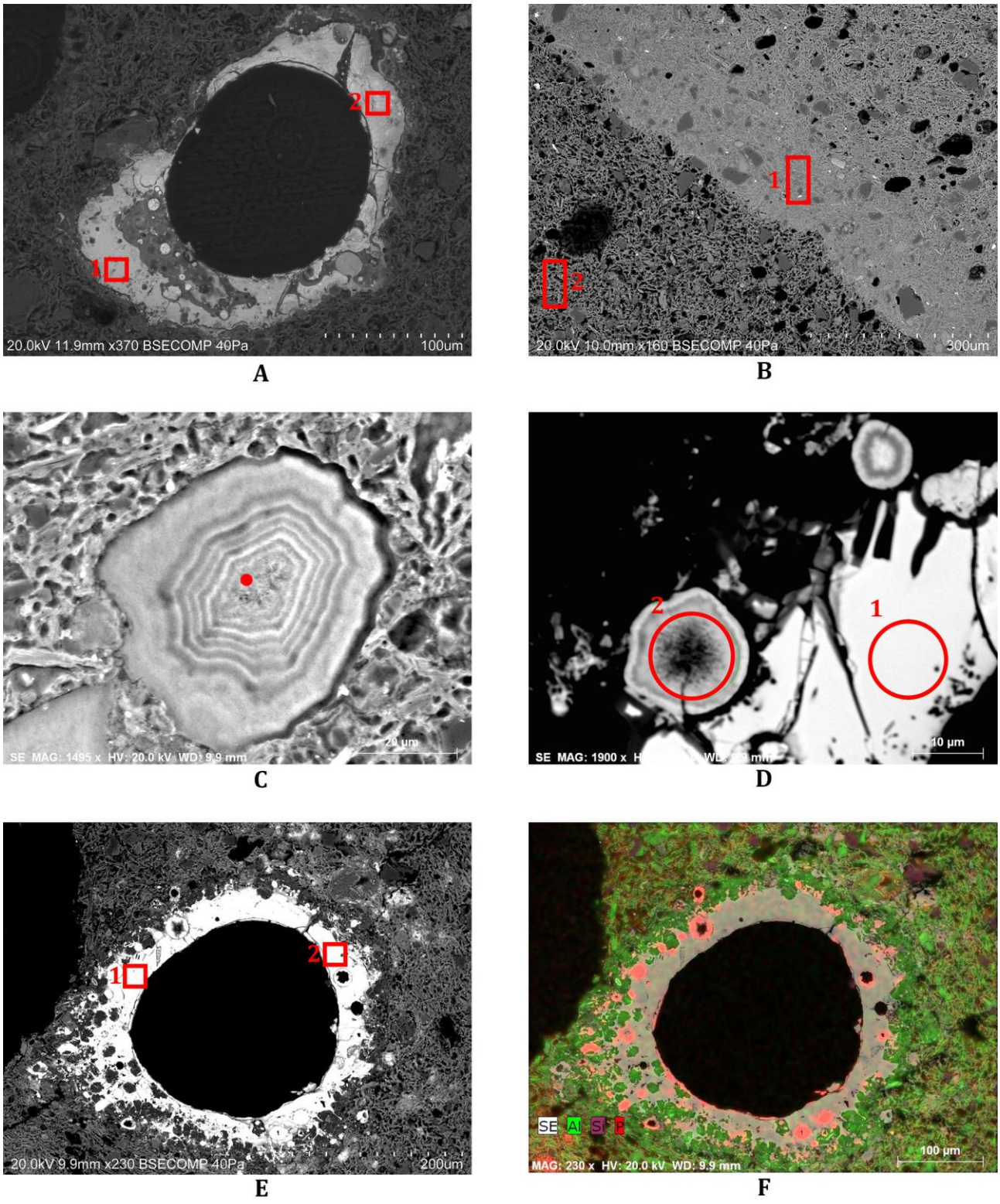

Image 9, annex 4. Features analysed by SEM-EDS on sample LVG-02-SXVIII-187

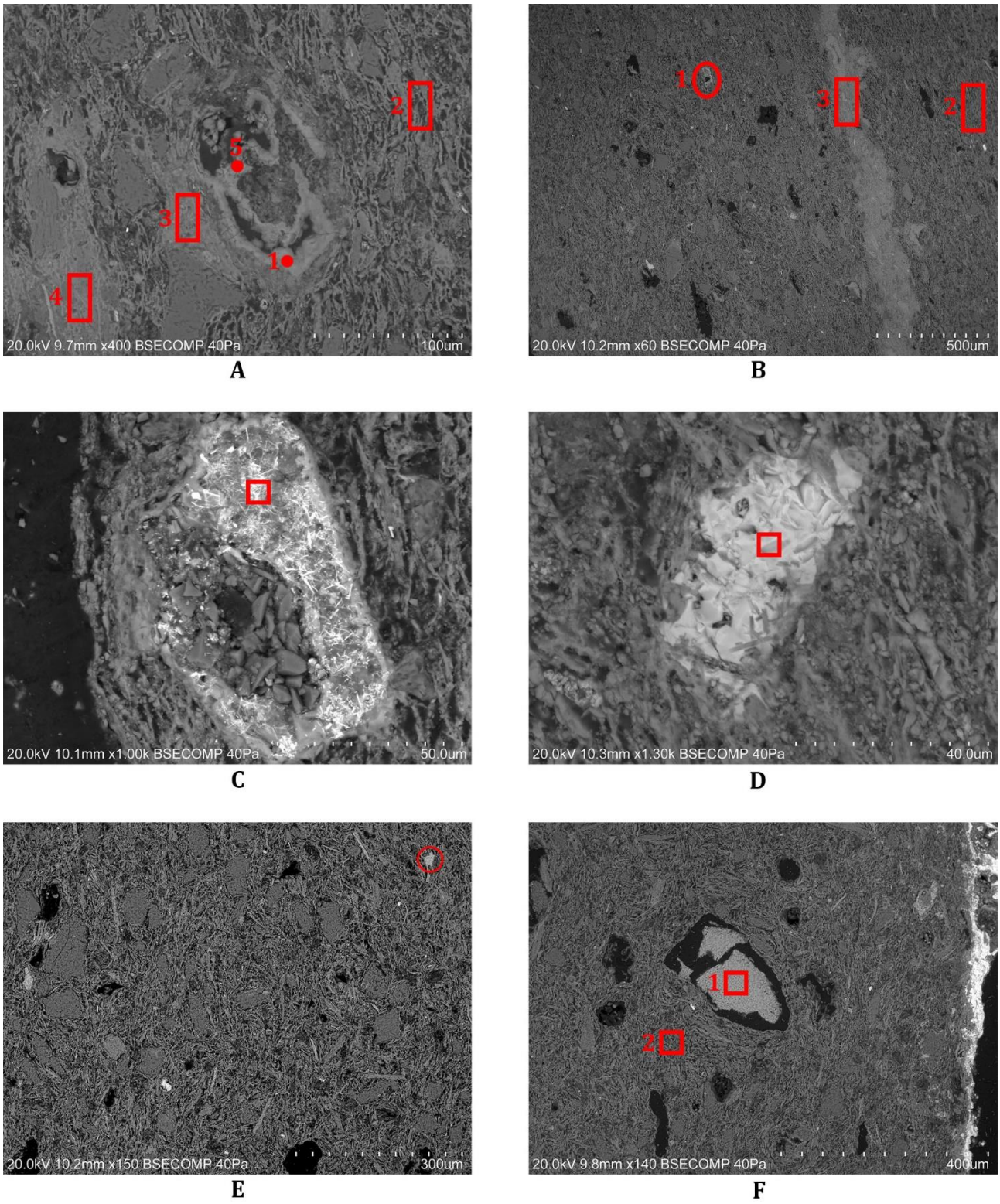

Image 10, annex 4. Features analysed by SEM-EDS on samples CRCSP-0021 (A, B, C, D) / 0027 (E, F)

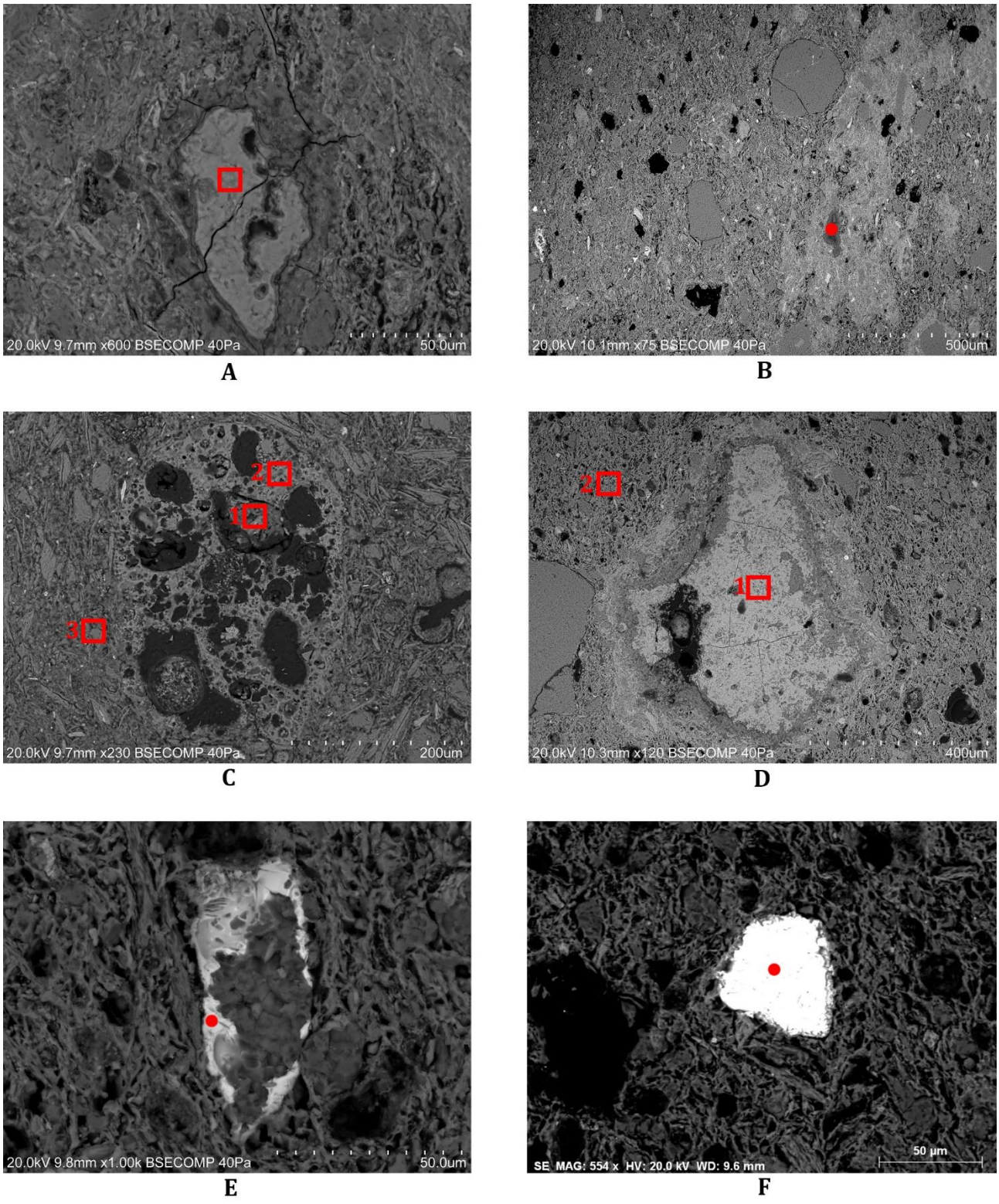

Image 11, annex 4. Features analysed by SEM-EDS on samples CRCSP-0028 (A, B) / 0030 (C) / 0031 (D, E, F).

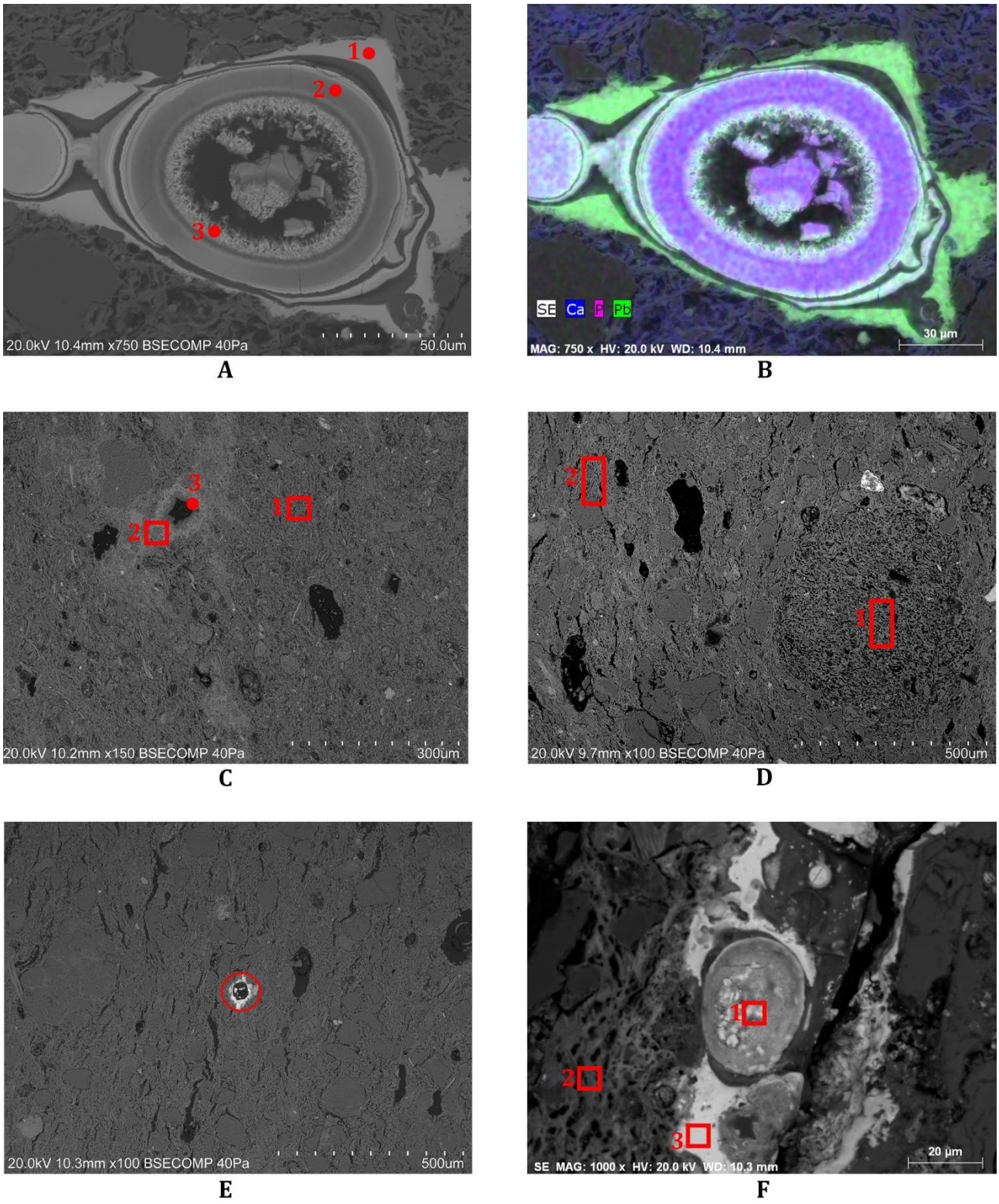

Imegae 12, annex 4. Features analysed by SEM-EDS on samples CRCSP-0031 (A, B), CRVF-0003 (C) and sample CRVM-0670 (D, E, F).

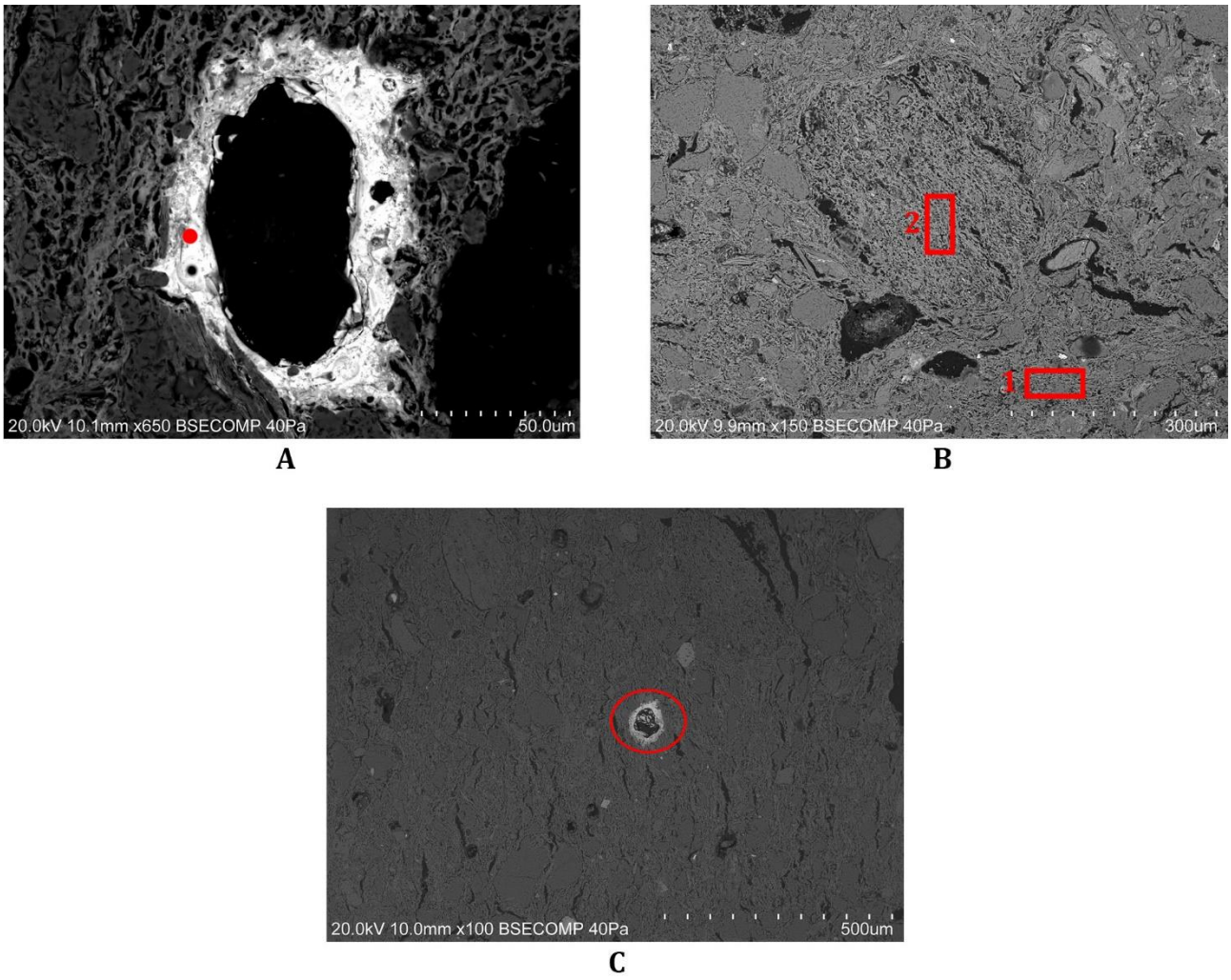

Image 13, annex 4. Features analysed by SEM-EDS on samples CRVM-223.

Table 14, annex 4. Chemical composition obtained by SEM-EDS of glass fragments and of the different features analysed (annexes 73 to 85) and identified on samples ceramic pastes. Results were normalized to 110% and uncertainty is 1 σ.

PLM Classification	Sample	Annex	Figure number	Feature classification	Specifics of the feature	Spot/area analysed	Na_2O	MgO	Al_2O_3	SiO_2	P_2O_5	K_2O	CaO	TiO_2	MnO	FeO	NiO	BaO	CuO	SnO_2	PbO
	CRVM-0357	74	A	Partially absorbed glass fragment, fr. 1	Residual glass	Spot	1.32	2.46	13.81	47.13		4.60	8.08	0.81	0.29	6.35					15.15
	CRVM-0357	74	B	Glass fragment Si and Pb, fr. 3	Glass	Spot	0.80	0.58	11.09	41.22	0.17	2.86	7.58	1.00		4.54					30.17
	CRVM-0357	74	C	Glass fragment Si and Pb, fr. 2	Glass	Area 1	1.72	1.26	8.48	38.78		1.43	4.49	1.84		3.26					38.73
	CRVM-0357	74	C	Glass fragment Si and Pb, fr. 2	Glass	Area 2	1.34	0.88	8.38	38.49		1.49	4.46	0.17		3.05		3.76			37.96
Glass	CRVM-0357	74	D	Vetrified bone	Raw material inside the inclusion	Spot 1	0.78	1.26	2.05	7.31	33.61	0.86	47.75	4.39		1.11					0.89
Glass	CRVM-0357	74	D	Vetrified bone	Raw material inside the inclusion	Spot 2	0.93	0.86	2.70	9.01	34.68	0.81	46.54	0.44		2.08					1.93
Glass	CRVM-0357	74	E	Glass fragment Si, Pb and Sn, fr. 1	Glass	Area 1	0.79	0.57	4.04	31.05	0.36	1.08	3.03			1.45				2.22	55.40
Glass	CRVM-0357	74	E	Glass fragment Si, Pb and Sn, fr. 1	Glass	Area 2	0.47	0.93	3.08	26.59		0.90	2.75			1.82				4.98	58.47
Glass	CRVM-0357	74	E	Glass fragment Si, Pb and Sn, fr. 1	Glass	Area 3	0.83	0.64	3.71	31.67		1.19	2.99			2.65				2.54	53.77
	CRVM-623	75	A	CaO and P_2O_5 rich area - wide, n. 2	Clay matrix	Area 1	1.26	3.52	16.79	49.30	0.92	2.70	17.31	1.41		5.90					0.89
	CRVM-623	75	A	CaO and P_2O_5 rich area - wide, n. 2	CaO and P_2O_5 rich raw material	Area 2	1.20	2.20	12.36	35.59	11.48	2.00	29.97	0.58		4.60					1.00
Glass	CRVM-623	75	B	Partially absorbed glass fragment, fr 3	Residual glass	Spot 1	0.89	0.56	2.80	20.65	0.53	0.66	4.76	1.17		4.33					63.64
	CRVM-623	75	B	Partially absorbed glass fragment, fr 4	Residual glass	Spot 2	0.65	0.89	2.50	9.69	24.85	0.36	29.32	0.00		1.55					30.18
	CRVM-642	75	D	Partially absorbed glass fragment, fr 5	Residual glass	Spot	1.11	1.36	6.13	49.34	0.37	4.68	4.70	0.55		2.63				1.80	27.33
	CRVM-642	75	C	CaO and P_2O_5 rich area - wide, n. 4	Clay matrix, P_2O_5 rich area	Area 1	0.90	2.49	16.41	43.01	5.57	2.44	21.91	0.64		5.72					0.90
	CRVM-642	75	C	CaO and P_2O_5 rich area - wide, n. 4	Clay matrix	Area 2	0.85	2.88	17.87	48.11	0.62	2.32	18.30	0.86		7.11					1.11
Glass	CRVM-666	75	E	CaO and P_2O_5 rich area - delimited, n. 5	Raw material inside the inclusion	Area 1	0.26	1.71	2.32	9.47	0.82	0.90	83.02			1.50					
	CRVM-666	75	E	CaO and P_2O_5 rich area - delimited, n. 5	Border of the inclusion	Area 2	0.76	3.20	11.93	41.55	3.27	1.72	21.78	0.59	1.57	5.70					7.93
	CRVM-666	75	E	CaO and P_2O_5 rich area - delimited, n. 5	Clay matrix	Area 3	0.77	4.40	16.00	43.34	0.28	1.90	24.07	1.23		5.53					2.48
Glass	CRVM-1097	76	A	CaO and P_2O_5 rich area - delimited, n. 7	Border of the inclusion	Area 1	0.73	2.26	11.05	33.32	14.22	1.11	32.39	0.39		4.53					
Glass	CRVM-1097	76	A	CaO and P_2O_5 rich area - delimited, n. 7	Clay matrix	Area 2	1.05	3.16	16.41	44.20	5.06	1.39	23.01	1.00		4.72					
	CRVM-1097	76	B	Partially absorbed glass fragment, fr 6	Residual glass	Area	3.24	0.90	7.87	40.88		3.40	3.95	1.03		4.17					34.56
Slip	CRVM-1659	76	C	Slip	Slip layer	Area	1.29	2.08	12.64	33.32	11.53	1.54	26.28	1.07		4.43					5.83
Slip	CRVM-1659	76	C	Slip	Slip layer	Area	1.20	2.09	11.44	38.53	11.09	1.67	24.07	0.99		3.59					5.34
Slip	CRVM-1659	76	C	Slip	Ceramic matrix under the slip	Area	1.30	2.69	15.00	47.11	4.64	1.53	18.55	1.06		5.64					2.47
Slip	CRVM-1659	76	C	Slip	Ceramic matrix under the slip	Area	1.23	2.82	15.85	46.64	2.70	2.07	18.92	0.85	0.44	6.57					1.91
Slip	CRVM-1659	76	Picture not included	Slip	Slip layer, back side	Area	1.46	2.64	12.08	32.08	12.98	1.78	28.08	0.75		3.89					4.26
Slip	CRVM-1659	76	Picture not included	Slip	Slip layer, back side	Area	1.18	2.34	13.95	48.86	5.94	1.66	16.37	0.80	0.38	5.30					3.23
Slip	CRVM-1659	76	Picture not included	Slip	Ceramic matrix under the slip, back side	Area	1.11	2.73	15.76	47.68	3.00	1.79	19.07	1.30		6.28					1.29

PLM Classification	Sample	Annex	Figure number	Feature classification	Specifics of the feature	Spot/area analysed	Na_2O	MgO	Al_2O_3	SiO_2	P_2O_5	K_2O	CaO	TiO_2	MnO	FeO	NiO	BaO	CuO	SnO_2	PbO
Slip	CRVM-1659	76	Picture not included	Slip	Ceramic matrix under the slip, back side	Area	0.68	2.49	15.17	43.51	2.27	1.31	18.79	1.21		6.42					8.15
Glass	CRVM-1659	76	D	CaO and P_2O_5 rich area - delimited, n. 11	Raw material inside the inclusion	Area 1	0.53	1.75	11.82	33.22	16.06	0.68	30.91	0.52		3.80					1.70
Glass	CRVM-1659	76	D	CaO and P_2O_5 rich area - delimited, n. 11	Clay matrix	Area 2	1.35	2.46	16.35	50.11	1.32	1.23	18.86	1.37		6.23					0.73
Glass	CRVM-1659	76	E	CaO and P_2O_5 rich area - wide, in. 11	Clay matrix	Spot 1	1.50	2.15	16.15	50.47	1.24	1.31	18.64	0.96		6.33					1.25
Glass	CRVM-1659	76	E	CaO and P_2O_5 rich area - wide, in. 11	Clay matrix, P_2O_5 rich area	Spot 2	0.75	2.02	11.69	33.60	15.23	0.82	30.43	0.71		3.59					1.14
Glass	CRVM-1659	76	E	CaO and P_2O_5 rich area - delimited, n. 11	Oval inclusion, quartz grain	Spot 3	0.17	0.17	1.63	90.57	1.49	0.26	3.21			2.51					0.00
Glass	CRVM-1659	76	E	CaO and P_2O_5 rich area - delimited, n. 11	Oval inclusion, CaO and P_2O_5 rich area	Spot 4	1.32	1.64	11.52	26.45	5.50	0.98	19.60	1.88		29.80					1.31
Glass	CRVM-1659	76	E	CaO and P_2O_5 rich area - delimited, n. 11	Oval inclusion, CaO and P_2O_5 rich area	Spot 5	0.71	0.42	1.86	6.62	37.60	0.46	49.00	0.93		1.87					0.52
Glass	CRVM-1659	77	F	CaO and P_2O_5 rich area - delimited, n. 11	Magnification oval inclusion, CaO and P_2O_5 and PbO rich area	Spot 1	0.70	0.97	2.85	7.60	35.31	0.47	44.30			2.14					5.66
Glass	CRVM-1659	77	F	CaO and P_2O_5 rich area - delimited, n. 11	Magnification oval inclusion, CaO and P_2O_5 rich area	Spot 2	0.36	1.85	9.89	24.74	3.22	0.53	19.81	0.83		37.40					1.35
Glass	CRVM-1659	77	F	CaO and P_2O_5 rich area - delimited, n. 11	Magnification oval inclusion, CaO and P_2O_5 rich area	Spot 3	0.52	5.42	18.74	30.93	2.94	0.59	22.63			17.63					0.60
	CRVM-1667	78	A	Type A lime rich inclusion	Raw material inside the inclusion	Area 1	0.67	2.21	15.18	51.88	0.95	3.07	21.24	1.01	0.28	3.51					
	CRVM-1667	78	A	Type A lime rich inclusion	Clay matrix	Area 2	0.87	2.39	17.17	55.09	0.47	3.18	14.07	1.13	0.24	5.40					
	CRVM-1667	78	B	Glass fragment Si and Pb, fr 4	Glass	Spot	0.72	0.73	7.06	40.53		1.93	5.24	0.70		2.39					40.72
	CRVM-1667	78	C	Glass fragment Si, Pb and Sn, fr. 3	Glass	Area 1	0.45	0.61	3.68	36.65		1.22	4.56	0.31		2.25				7.86	42.41
	CRVM-1667	78	C	Glass fragment Si, Pb and Sn, fr. 3	Glass	Spot 2	0.45	0.61	3.68	36.59	0.16	1.22	4.51	0.31		2.25				7.89	42.33
	CRVM-1667	78	C	Glass fragment Si, Pb and Sn, fr. 3	Glass	Spot 3	0.26	0.93	6.19	40.55		1.32	4.33	0.90		2.67				1.29	41.57
	CRVM-1667	78	D	Grog	Glaze	Area 1	0.21	1.03	7.81	42.63	0.18	2.05	6.78	0.74		5.62				0.63	32.32
	CRVM-1667	78	D	Grog	Glaze	Spot 2	0.32	0.76	7.76	42.64	0.12	2.00	6.13	0.49		6.33					33.45
	CRVM-1667	78	D	Grog	Clay matrix of the grog fragment	Area 3	0.26	3.23	17.03	61.67	0.37	4.82	2.57	0.43		7.87					1.75
	CRVM-1667	78	D	Grog	Clay matrix	Area 4	0.78	2.33	20.17	48.82	0.51	3.50	15.19	0.51		6.13					2.07
	CRVM-1668	79	A	Type C lime rich inclusion	CaO and P_2O_5 rich raw material	Area 1	0.51	0.81	2.23	8.21	35.11	0.86	50.68		0.29	0.78					0.52
	CRVM-1668	79	A	Type C lime rich inclusion	SiO_2 and Al_2O_3 rich raw material	Area 2	6.56	1.72	18.22	54.42	2.17	4.37	5.89	0.91	0.65	4.99					0.11
	CRVM-1668	79	A	Type C lime rich inclusion	CaO and P_2O_5 rich raw material	Area 3	0.75	0.61	2.23	7.57	34.77	0.87	49.55	0.70	0.88	1.24					0.82
	CRVM-1668	79	A	Type C lime rich inclusion	SiO_2 and Al_2O_3 rich raw material	Area 4	6.18	1.78	17.02	57.62	2.07	4.17	5.88	0.86		4.41					
	CRVM-1668	80	A	Type B lime rich inclusion	Raw material inside the inclusion	Spot	0.69	2.40	13.38	40.41	9.36	3.70	24.73	0.95		4.38					
	CRVM-1668	80	B	Partially absorbed glass fragment , fr. 9	Residual glass	Spot	0.57	1.04	4.89	46.68	0.33	3.39	5.42	0.63		2.80					34.25
Glass	CRVM-1668	80	C	Vetrified bone	Centre of the inclusion	Spot 1	0.86	0.67	2.02	6.66	36.49	0.69	47.29	0.65		2.05					2.62

PLM Classification	Sample	Annex	Figure number	Feature classification	Specifics of the feature	Spot/area analysed	Na_2O	MgO	Al_2O_3	SiO_2	P_2O_5	K_2O	CaO	TiO_2	MnO	FeO	NiO	BaO	CuO	SnO_2	PbO
Glass	CRVM-1668	80	C	Vetrified bone	Border of the inclusion	Spot 2	0.53	0.66	1.93	5.97	35.93	0.57	52.34	0.43	0.68	0.96					
Glass	CRVM-1668	80	D	Vetrified bone	Border of the inclusion	Spot	0.52	0.72	1.68	5.82	35.82	0.53	51.92			1.50					1.48
	CRVM-1669	80	E	Type B lime rich inclusion	Raw material inside the inclusion	Spot	0.29	1.74	3.63	11.83	0.55	1.28	77.79	1.04		1.85					
	CRVM-1669	80	Picture not included	Type B lime rich inclusion	Raw material inside the inclusion			2.04	3.27	11.61	0.45	0.82	79.06	0.56		1.75					1.44
	CRVM-1670	81	B	Silica-alkali-lime glass, fr.2	Glass	Area 1	3.46	4.66	6.74	63.13	1.12	6.69	8.57	0.80	0.23	3.49					1.11
	CRVM-1670	81	B	Silica-alkali-lime glass, fr.2	Glass	Area 2	4.47	4.05	6.81	64.02	1.08	7.81	5.71	0.96	0.52	2.60					1.99
	CRVM-1670	81	B	Silica-alkali-lime glass, fr.2	CaO and P_2O_5 rich glass	Spot 3	1.68	1.59	5.97	31.00	11.56	5.13	27.87	0.49	0.55	2.94					11.23
	CRVM-1670	81	B	Silica-alkali-lime glass, fr.2	CaO and P_2O_5 rich glass	Spot 4	1.39	5.87	3.90	49.24	3.92	2.95	17.20	1.15		3.24					11.14
	CRVM-1671	81	E	Type B lime rich inclusion	Raw material inside the inclusion	Spot	0.56	2.15	3.14	7.78	0.00	0.76	83.02			2.60					
	CRVM-1671	81	C	Type B lime rich inclusion	Inclusion limit	Area 1	0.16	8.34	12.46	51.58	0.78	1.49	19.72	1.57		3.91					
	CRVM-1671	81	C	Type B lime rich inclusion	Raw material outside the inclusion	Area 2	1.23	3.45	16.74	44.75	0.35	2.65	24.42	0.76		5.66					
	CRVM-1671	81	D	Partially absorbed glass fragment , fr. 11	Residual glass	Spot 1	1.21	0.80	6.74	48.34		4.77	5.11	0.77		4.01					28.26
	CRVM-1671	81	D	Partially absorbed glass fragment , fr. 11	Residual glass	Spot 2	0.39	1.59	12.76	67.84	0.61	2.60	5.18	0.75		2.86					5.41
	CRVM-1671	81	Picture not included	Partially absorbed glass fragment , fr. 11	Residual glass	Spot	0.79	0.76	12.73	56.90	1.24	5.98	4.89	0.97		6.40					9.34
	CRVM-1671	81	Picture not included	Partially absorbed glass fragment , fr. 11	Residual glass	Spot	0.74	1.03	9.42	47.69	0.33	3.82	5.21	0.92		5.75					25.08
	CRVM-1671	81	Picture not included	Glass fragment Si, Pb and Sn, fr. 4	Glass	Spot	0.34	1.04	3.56	15.87	8.14	0.26	11.47	0.79		2.87				0.79	55.86
Glass	LVG-02-SXVIII-187	82	A	Glass fragment Si, Pb and Sn, fr. 5	Glass	Area 1	0.97	1.31	4.14	41.49		3.80	4.39	0.44		2.57				1.91	38.98
Glass	LVG-02-SXVIII-187	82	A	Glass fragment Si, Pb and Sn, fr. 5	Glass	Area 2	0.91	0.49	3.76	14.29	14.06	0.81	12.88			2.16				3.36	47.30
	LVG-02-SXVIII-187	82	B	CaO and P_2O_5 rich area - wide, n. 14	CaO and P_2O_5 rich raw material	Area 1	1.03	2.24	12.04	32.45	13.39	2.17	30.63	0.77		4.51					0.77
	LVG-02-SXVIII-187	82	B	CaO and P_2O_5 rich area - wide, n. 14	Clay matrix	Area 2	1.14	2.89	16.61	46.04	1.30	2.22	20.88	0.96		6.33					1.64
	LVG-02-SXVIII-187	82	C	Bone fragment	Centre of the inclusion	Spot	0.57	0.86	2.11	5.55	31.92	0.75	56.92	0.69		0.64					
	LVG-02-SXVIII-187	82	D	Glass fragment Si and Pb, fr 5	Glass	Area 1	1.02	0.86	4.99	28.64	0.30	1.52	5.15	0.90	0.26	3.42					52.95
	LVG-02-SXVIII-187	82	D	Glass fragment Si and Pb, fr 5	Bone inclusion	Area 2	0.78	0.42	1.76	4.98	18.50	0.28	17.38			1.27					54.63
Glass	LVG-02-SXVIII-187	82	E	Glass fragment Si and Pb, fr 6	Glass	Area 1	0.54	1.45	4.82	26.57	1.66	0.94	6.04	0.70	0.56	4.06					52.66
Glass	LVG-02-SXVIII-187	82	E	Glass fragment Si and Pb, fr 6	Glass	Area 2	0.73	0.75	4.60	30.37	2.24	1.33	6.61	0.79	0.41	3.54					48.64
Glass	CSP-0021	83	A	CaO and P_2O_5 rich area - delimited, n. 15	Vetrified bone	Spot 1	1.07	0.92	5.07	11.94	34.28	1.02	39.79			1.49					5.42
Glass	CSP-0021	83	A	CaO and P_2O_5 rich area - delimited, n. 15	Clay matrix	Area 2	1.50	2.59	22.72	45.42	1.96	4.36	14.39	0.60		5.52					0.92
Glass	CSP-0021	83	A	CaO and P_2O_5 rich area - delimited, n. 15	Border of the inclusion	Area 3	1.52	1.95	14.56	29.86	17.05	1.39	27.23	0.41		4.02					2.00
Glass	CSP-0021	83	A	CaO and P_2O_5 rich area - delimited, n. 15	CaO and P_2O_5 rich raw material	Area 4	1.35	1.95	15.20	42.05	11.70	3.57	17.98	1.08		5.03					1.11

PLM Classification	Sample	Annex	Figure number	Feature classification	Specifics of the feature	Spot/area analysed	Na_2O	MgO	Al_2O_3	SiO_2	P_2O_5	K_2O	CaO	TiO_2	MnO	FeO	NiO	BaO	CuO	SnO_2	PbO
Glass	CSP-0021	83	A	CaO and P_2O_5 rich area - delimited, n. 15	Vetrified bone	Spot 5	1.23	0.91	5.58	6.27	36.21	0.76	42.39			1.52					5.12
	CSP-0021	83	B	CaO and P_2O_5 rich area - wide, n. 16	CaO and P_2O_5 rich raw material	Area 2	1.49	2.64	19.23	48.76	1.49	3.33	15.25	0.78		7.02					
	CSP-0021	83	B	CaO and P_2O_5 rich area - wide, n. 16	Clay matrix	Area 3	1.01	1.54	15.50	32.24	15.06	3.60	26.60	0.61		3.84					
	CSP-0021	83	B	Partially absorbed glass fragment, fr. 12	Residual glass	Spot 1	0.91	0.92	8.45	63.15	3.61	3.76	7.89			4.38				4.06	2.88
	CSP-0021	83	C	Partially absorbed glass fragment, fr. 13	Residual glass	Area	0.85	1.02	7.19	51.00	3.88	2.58	6.65	0.31		4.62				19.05	2.85
	CSP-0021	83	D	Partially absorbed glass fragment, fr. 14	Residual glass	Area	2.41	1.05	8.24	51.82	0.41	6.58	5.11	1.74		4.36					18.29
	CSP-0027	83	E	Vetrified bone	Centre of the inclusion	Spot	0.29	0.34	2.72	6.79	38.26	0.58	48.47		1.03	1.52					
Glass	CSP-0027	83	F	Vetrified bone	Centre of the inclusion	Area 1	0.58	0.36	1.70	5.19	38.61	0.57	52.02			0.98					
Glass	CSP-0027	83	F	Vetrified bone	Clay matrix	Area 2	1.82	2.99	19.36	48.57		2.80	18.03	0.88		5.56					
	CSP-0028	84	A	Vetrified bone	Centre of the inclusion	Spot	1.42	0.00	8.91	8.54	40.03	0.81	39.05			1.24					
	CSP-0028	84	B	Vetrified bone	Centre of the inclusion	Spot	0.67	0.67	20.19	11.87	40.07	2.04	22.55			1.94					
Glass	CSP-0030	84	C	Vetrified bone	Centre of the inclusion	Area 1	1.85	0.49	15.44	37.71	23.74	2.95	4.88	0.96		11.98					
Glass	CSP-0030	84	C	Vetrified bone	Border of the inclusion	Area 2	0.45	0.86	9.58	72.40	3.07	4.79	3.42	0.72		4.71					
Glass	CSP-0030	84	C	Vetrified bone	Clay matrix	Area 3	0.64	0.37	15.62	48.29	20.97	3.14	3.19	1.28		6.49					
	CSP-0031	84	D	Grey-yellow anhedral inclusion	Vetrified bone	Area 1	0.60	2.13	4.55	13.66	32.02	1.08	45.11			0.86					
	CSP-0031	84	D	Grey-yellow anhedral inclusion	Clay matrix	Area 2	1.59	2.61	18.23	55.13	0.67	3.65	11.77	1.76		5.59					
	CSP-0031	84	E	Glass fragment Si and Pb, fr 7	Glass	Spot	0.89	1.28	6.35	40.97	0.26	2.25	4.93	0.85		4.01					38.20
	CSP-0031	84	F	Partially absorbed glass fragment, fr. 15	Residual glass	Spot	1.03	0.67	6.41	51.39		2.84	3.89	1.00		2.56					30.21
	CSP-0031	85	A	Glass fragment Si and Pb, fr 9	Glass	Spot 1	1.25	0.63	5.87	45.38	0.79	2.38	3.43	0.73		2.48					37.05
	CSP-0031	85	A	Glass fragment Si and Pb, fr 9	Bone inclusion	Spot 2	0.29	0.61	2.21	8.97	29.75	0.56	38.23			1.07					18.33
	CSP-0031	85	A	Glass fragment Si and Pb, fr 9	Bone inclusion	Spot 3	0.44	0.77	1.96	7.61	25.23	0.29	26.32			1.23					36.16
	CRVF-0003	85	C	CaO and P_2O_5 rich area - wide, n. 18	Clay matrix	Area 1	0.95	2.58	19.45	57.63	2.14	3.92	4.69	1.94	0.67	6.04					
	CRVF-0003	85	C	CaO and P_2O_5 rich area - wide, n. 18	CaO and P_2O_5 rich raw material	Area 2	1.13	2.03	12.55	37.91	18.45	2.45	21.11	0.11	0.32	3.30		0.66			
Glass	CRVF-0003	85	C	CaO and P_2O_5 rich area - wide, n. 18	Vetrified bone	Spot 3	0.97	0.94	3.44	11.39	36.09	0.81	45.34		0.62	1.41					
	CRVM-0670	85	D	Type A lime rich inclusion	Raw material inside the inclusion	Area 1	0.53	2.32	17.01	52.52	0.60	2.83	19.16	0.90		4.12					
	CRVM-0670	85	D	Type A lime rich inclusion	Clay matrix	Area 2	0.63	2.00	18.83	54.60	0.62	3.41	12.73	0.98		6.19					
	CRVM-0670	85	E	Glass fragment Si and Pb, fr 8	Glass		1.17	2.68	4.73	45.86	0.69	0.74	21.01		0.53	1.95					20.63
	CRVM-0670	85	F	Glass fragment Si, Pb and Sn, fr. 6	Bone inclusion	Area 1	0.32	0.76	3.09	22.05	14.35	0.80	18.92	1.11		2.06					36.53
	CRVM-0670	85	F	Glass fragment Si, Pb and Sn, fr. 6	Clay matrix	Area 2	0.98	2.14	17.97	50.48	0.52	2.54	11.85	1.36		6.15					6.02
	CRVM-0670	85	F	Glass fragment Si, Pb and Sn, fr. 6	Glass	Area 3	0.65	0.51	5.54	37.86	0.17	1.13	4.13	0.68		2.83				2.02	44.47
	CRVM-223	86	A	Partially absorbed glass fragment, fr. 16	Residual glass	Spot	0.95	1.47	14.72	47.37	0.17	2.17	7.28	1.07		3.91					20.89

PLM Classification	Sample	Annex	Figure number	Feature classification	Specifics of the feature	Spot/area analysed	Na_2O	MgO	Al_2O_3	SiO_2	P_2O_5	K_2O	CaO	TiO_2	MnO	FeO	NiO	BaO	CuO	SnO_2	PbO
Type A lime rich inclusion	CRVM-223	86	B	Type A lime rich inclusion	Clay matrix	Area 1	0.55	1.74	17.59	58.95		2.89	11.37	0.67	0.30	5.94					
	CRVM-223	86	B	Type A lime rich inclusion	Raw material inside the inclusion	Area 2	0.35	2.32	16.32	50.24	0.54	2.45	21.54	0.72		5.53					
	CRVM-223	86	C	Glass fragment Si and Pb, fr 11	Glass	Spot	0.47	0.93	11.01	41.06	0.22	1.36	5.25	1.21		2.86					35.62

Table 15, annex 4. Glazes chemical composition table (normalized values). CuO, MnO, SnO_2 and PbO have been remouved and resulted values have been recasted to 100%.

Glazes chemical composition after the remouval of CuO, MnO, PbO and SnO_2. Data obtained by SEM-EDS											
Sample	**Glaze side**	**Na_2O**	**MgO**	**Al_2O_3**	**SiO_2**	**P_2O_5**	**K_2O**	**CaO**	**TiO_2**	**MnO**	**FeO**
CRVM-0357	Decorated side	3.75	1.07	2.80	82.56	0.23	1.91	4.33			3.34
CRVM-0357	Reverse side	3.39	1.28	3.72	76.49	1.72	3.56	7.03			2.80
CRVM-0357	Decorated side - slip	3.75	1.07	2.80	82.56	0.23	1.91	4.33			3.34
CRVM-623	Decorated side	3.63	1.64	6.44	72.86	0.39	4.77	5.91	2.29		2.09
CRVM-623	Reverse side	4.19	1.19	2.82	79.46	0.66	3.10	6.68	0.42		1.48
CRVM-666	Decorated side	3.43	1.62	7.05	72.16	0.44	4.33	6.53	0.97		3.46
CRVM-666	Reverse side	1.70	1.19	10.27	74.63		3.32	4.85	0.86		3.16
CRVM-642	Decorated side	1.52	1.24	9.72	66.68	0.45	4.52	8.98	1.74		5.14
CRVM-642	Reverse side	1.26	1.51	10.58	66.33	0.31	3.94	9.30	1.34		5.45
CRVM-1097	Decorated side	4.30	1.73	1.97	76.03	1.26	4.29	7.44	1.27		1.71
CRVM-1097	Reverse side	4.03	1.60	3.89	72.23	1.56	4.09	7.40	0.51	1.43	3.25
CRVM-1659	Decorated side	2.14	0.68	2.08	81.58	1.26	2.82	6.72	0.88		1.84
CRVM-1659	Reverse side	2.45	0.53	2.59	81.25	0.34	3.88	6.56	0.95		1.45
CRVM-1659	Decorated side - slip	2.14	0.68	2.08	81.58	1.26	2.82	6.72	0.88		1.84
CRVM-1659	Reverse side - slip	2.45	0.53	2.59	81.25	0.34	3.88	6.56	0.95		1.45
CRVM-1668	Decorated side	5.10	1.20	5.77	74.92	0.46	1.87	6.35	0.62	0.78	2.92
CRVM-1668	Reverse side	4.85	1.30	5.42	73.81	0.82	1.77	5.87	2.57		3.59
CRVM_1671	Decorated side	3.13	1.86	9.11	69.84	0.52	3.36	8.09	0.60	0.40	3.09
CRVM_1671	Reverse side	1.69	1.36	11.11	67.14	0.36	3.37	9.50	1.30		4.16
LVG-02-SXVIII-187	Decorated side	4.32	1.19	2.82	79.41	0.66	3.10	6.69	0.43		1.39
LVG-02-SXVIII-187	Reverse side	4.20	1.19	2.83	79.76	0.66	3.11	6.72	0.44		1.08
CRVM-1665	Decorated side	2.86	0.58	3.23	83.44		3.35	3.37	0.60		2.58
CRVM-1665	Reverse side	3.66	1.18	7.07	72.37	1.54	3.03	7.16	0.86		3.14
CRVM-1666	Decorated side	4.50	0.98	2.47	78.55	1.57	4.07	5.77			2.10
CRVM-1666	Reverse side	4.28	1.38	5.92	71.11	1.06	3.91	6.68	0.99	1.26	3.42
CRVM-1670	Turquoise	3.76	0.94	3.53	75.02		3.28	6.26	4.04		3.19
CRVM-1667	Decorated side	2.93	1.89	5.00	75.97		2.03	6.37	1.94		3.86

Glazes chemical composition after the remouval of CuO, MnO, PbO and SnO_2. Data obtained by SEM-EDS											
Sample	**Glaze side**	**Na_2O**	**MgO**	**Al_2O_3**	**SiO_2**	**P_2O_5**	**K_2O**	**CaO**	**TiO_2**	**MnO**	**FeO**
CRVM-1667	Reverse side	1.57	1.52	8.34	72.33		2.09	7.02	1.99		5.14
CRVM-1669	Decorated side	4.87	1.36	5.13	76.82	0.60	1.66	5.69			3.89
CRVM-1669	Reverse side	1.44	2.43	14.30	61.94	0.94	2.14	10.34	2.08		4.38
CRVM-223	Decorated side	4.08	1.42	4.05	80.06	0.51	1.48	3.46	1.35		3.59
CRVM-223	Reverse side	0.93	1.39	8.34	76.12		1.45	6.13	1.24		4.42
CRVM-0670	Decorated side	4.27	1.30	3.75	79.72	0.74	1.52	3.65	2.03		3.03
CRVM-0670	Reverse side	1.25	1.42	5.92	76.29	0.63	1.57	5.03	2.09		5.81
CRVF-0003	Decorated side	1.38	1.86	10.89	71.27		2.04	2.96	2.86	1.89	4.85
CRVF-0003	Reverse side	0.90	2.00	11.47	73.35		1.76	3.10	1.70	1.07	4.64
CRCSP-0030	Turquoise	6.42	1.36	2.55	78.11	0.72	3.86	3.95	0.80		2.22
CRCSP-0031	Turquoise	4.12	1.54	4.05	78.91	0.49	2.32	4.13	1.29		3.16
CRCSP-0028	Turquoise	5.66	1.37	3.34	78.58	0.93	2.06	3.32	3.00		1.74
CRCSP-0021	Turquoise	5.30	1.99	4.72	70.12	0.88	3.71	7.09	1.06		5.14
CRCSP-0027	Turquoise	5.47	1.51	3.84	75.75	0.52	3.24	5.45	1.23		2.99
CRCSP-0027	Honey	3.21	1.19	8.45	68.43	0.40	3.76	7.80	1.94	0.46	4.37
CRCSP-0021	Honey	3.22	1.20	8.65	64.91		4.30	9.48	1.67		6.56
CRCSP-0029	Honey	1.50	1.32	10.17	66.24	0.26	3.34	8.72	1.35		7.11
CRCSP-0031	Black	1.71	0.95	4.34	73.18		1.56	3.11	1.92		13.23
CRCSP-0027	Black	3.16	1.18	8.81	65.10	0.58	4.55	7.12	1.30	2.14	6.08

Table 16, annex 4. Ceramic paste chemical composition table (normalized values). Lead oxide have been remouved and resulted values have been recasted to 100%.

Ceramic paste chemical composition after the remouval of PbO, data obtained by SEM-EDS											
Sample	**Fragement side**	**Na_2O**	**MgO**	**Al_2O_3**	**SiO_2**	**P_2O_5**	**K_2O**	**CaO**	**TiO_2**	**MnO**	**FeO**
CRVM-0357	Decorated side	2.33	2.77	17.07	51.37	0.57	2.41	15.71	0.75		7.02
CRVM-0357	Reverse side	1.63	3.40	18.10	51.04	0.51	3.89	13.89	1.31		6.22
CRVM-0357	Decorated side-slip	1.66	2.32	15.74	37.55	8.16	2.56	24.72	0.59	0.67	6.03
CRVM-623	Decorated side	1.90	4.82	18.92	46.44	0.58	1.30	19.73	0.95		5.36
CRVM-623	Reverse side	1.51	3.14	19.82	46.04	0.50	2.17	19.83	1.05		5.95
CRVM-666	Decorated side	2.55	3.02	15.14	41.83	3.57	2.61	24.18	0.80		6.30
CRVM-666	Reverse side	1.24	3.07	15.19	40.54	2.51	3.11	25.88	1.06		7.40
CRVM-642	Decorated side	1.11	2.24	17.66	47.72	3.62	3.27	17.07	1.11	0.57	5.62
CRVM-642	Reverse side	0.76	3.30	18.73	49.02	0.30	2.59	17.12	1.11	0.29	6.77
CRVM-1097	Decorated side	2.97	3.47	18.18	47.94	1.10	1.63	17.43	1.19		6.11
CRVM-1097	Reverse side	1.64	3.65	17.47	51.71	0.68	1.43	16.59	1.02		5.80
CRVM-1659	Decorated side	1.29	2.81	15.73	47.81	3.76	1.84	19.11	0.97	0.45	6.23
CRVM-1659	Reverse side	0.94	2.74	16.23	47.85	2.78	1.63	19.86	1.32		6.66
CRVM-1659	Decorated side-slip	1.32	2.21	12.74	38.05	12.02	1.70	26.64	1.09		4.24
CRVM-1659	Reverse side-slip	1.37	2.58	13.49	41.94	9.85	1.78	23.04	0.80	0.39	4.76
CRVM-1668	Decorated side	2.36	3.03	15.17	43.70	2.59	2.31	22.01	0.96	0.41	7.46
CRVM-1668	Reverse side	1.55	2.85	15.77	41.44	3.57	1.95	25.64	1.33		5.90
CRVM_1671	Decorated side	1.88	3.26	17.59	44.59	1.58	2.76	19.88	1.00		7.46
CRVM_1671	Reverse side	1.13	3.54	16.49	49.70	0.80	2.42	17.93	0.92		7.08
LVG-02-SXVIII-187	Decorated side	1.96	2.68	16.75	50.42	0.86	1.95	17.37	0.94	0.42	6.64
LVG-02-SXVIII-187	Reverse side	1.68	2.72	16.88	51.70	1.00	1.82	16.03	1.00		7.17
CRVM-1665	Decorated side	1.99	2.10	17.61	52.24	0.58	1.85	15.67	1.04		6.92
CRVM-1665	Reverse side	1.99	2.10	17.61	52.24	0.58	1.85	15.67	1.04		6.92
CRVM-1666	Decorated side	1.65	2.79	17.28	43.24	8.33	2.12	15.65	0.96	0.64	7.34
CRVM-1666	Reverse side	1.81	2.75	16.36	44.34	4.68	2.36	17.09	1.15	3.46	6.00
CRVM-1670	Turquoise	1.83	2.25	19.94	50.42	0.48	1.46	15.71	1.18		6.73
CRVM-1667	Decorated side	1.87	2.44	18.28	52.67	0.67	2.24	14.39	1.04		6.40

Ceramic paste chemical composition after the remouval of PbO, data obtained by SEM-EDS											
Sample	**Fragement side**	**Na_2O**	**MgO**	**Al_2O_3**	**SiO_2**	**P_2O_5**	**K_2O**	**CaO**	**TiO_2**	**MnO**	**FeO**
CRVM-1667	Reverse side	0.79	1.98	17.93	52.04	0.73	3.23	14.96	0.99	0.47	6.89
CRVM-1669	Decorated side	1.78	4.28	14.97	46.36	0.65	2.04	23.62	1.60		4.71
CRVM-1669	Reverse side	0.64	3.03	17.07	46.83	0.59	2.72	21.51	1.05		6.54
CRVM-223	Decorated side	0.71	1.76	19.44	56.67	0.33	3.19	10.76	0.89	0.07	6.19
CRVM-223	Reverse side	0.80	2.27	19.36	53.47	0.39	2.93	12.85	1.06		6.86
CRVM-0670	Decorated side	0.79	1.89	18.53	57.26	0.26	3.15	10.51	1.23		6.37
CRVM-0670	Reverse side	0.52	2.13	19.55	53.00	0.43	3.27	13.95	0.88		6.27
CRVF-0003	Decorated side	1.19	2.77	20.47	58.20	1.25	4.28	3.59	1.25	0.41	6.61
CRVF-0003	Reverse side	1.19	2.77	20.47	58.20	1.25	4.28	3.59	1.25	0.41	6.61
CRCSP-0030	Turquase	0.94	0.69	17.19	45.19	20.49	3.19	4.24	0.92		7.16
CRCSP-0031	Turquase	1.27	2.93	17.64	56.87	0.47	2.96	10.91	0.86	0.17	5.93
CRCSP-0028	Turquase	1.18	1.93	21.05	53.43	5.11	3.91	5.77	0.94		6.67
CRCSP-0021	Turquase	1.48	2.34	18.08	49.31	2.73	2.22	16.95	1.08	0.11	5.72
CRCSP-0027	Turquase	2.38	3.21	19.37	48.45	0.37	2.23	16.45	1.11		6.43
CRCSP-0027	Honey	1.76	2.98	19.45	47.37	0.31	2.39	17.49	0.98	0.93	6.33
CRCSP-0021	Honey	1.48	2.34	18.08	49.31	2.73	2.22	16.95	1.08	0.11	5.72
CRCSP-0029	Honey	1.63	3.07	15.86	51.74	0.37	2.15	18.02	1.25		5.92
CRCSP-0031	Black	1.27	2.93	17.64	56.87	0.47	2.96	10.91	0.86	0.17	5.93
CRCSP-0027	Black	2.01	3.40	18.79	49.32	0.50	2.52	16.63	0.80		6.02